EMERGING INFECTIOUS DISEASES®

CDC
Centers for Disease Control and Prevention

Zoonotic Infections

October 2021

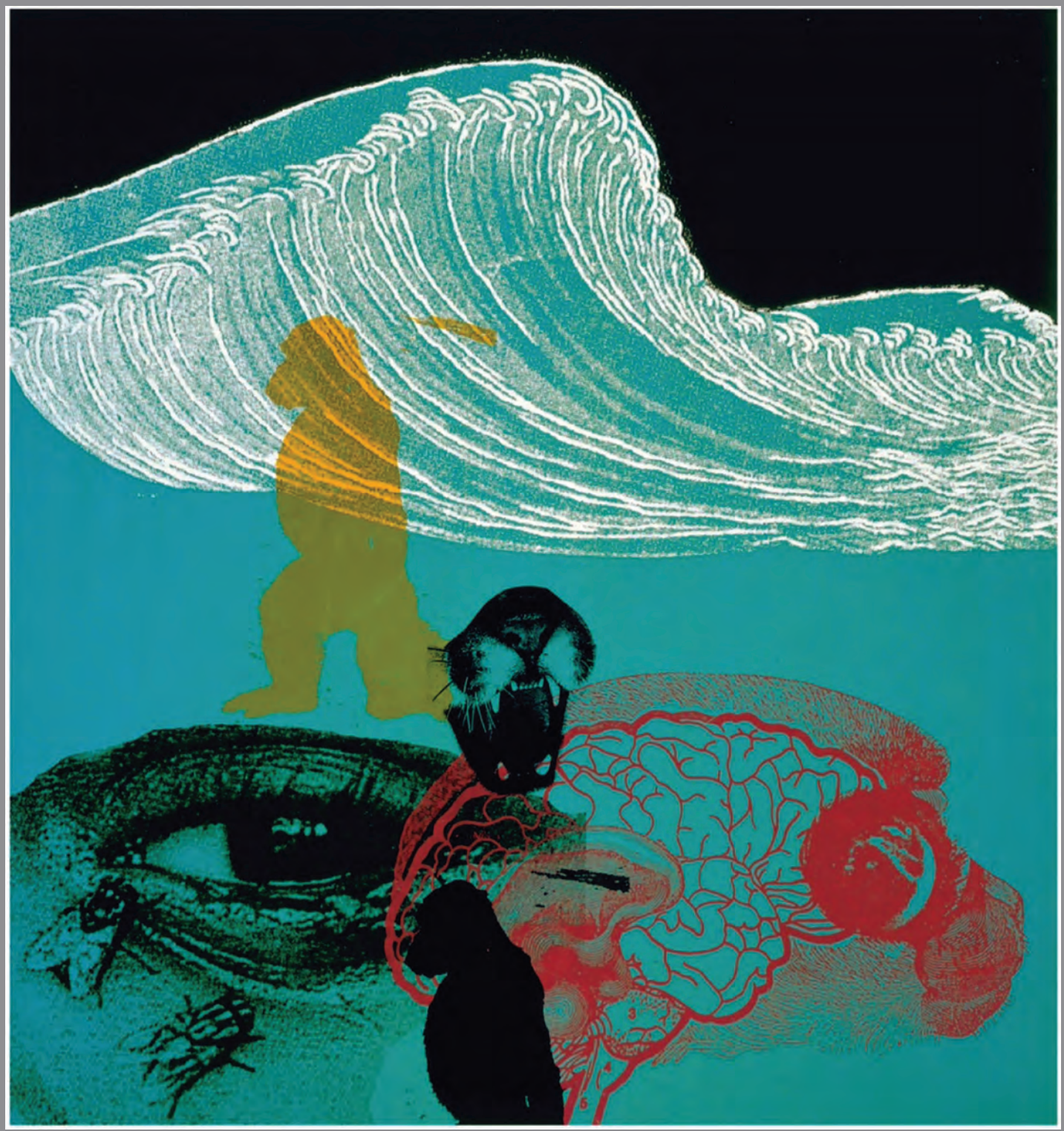

Kate Gibb (1972–), *The Island of Doctor Moreau*, 2006. Silkscreen by hand on paper, 19.7 in x 27.6 in/50 cm x 70 cm. Digital image used with permission of the artist. London, England.

EMERGING INFECTIOUS DISEASES®

Emerging Infectious Diseases is published monthly by the Centers for Disease Control and Prevention, 1600 Clifton Rd NE, Mailstop H16-2, Atlanta, GA 30329-4027, USA. Telephone 404-639-1960; email, eideditor@cdc.gov

EMERGING INFECTIOUS DISEASES®

Zoonotic Infections

October 2021

On the Cover

Kate Gibb (1972–), *The Island of Doctor Moreau*, 2006. Silkscreen by hand on paper, 19.7 in × 27.6 in/50 cm × 70 cm. Digital image used with permission of the artist. London, England.

About the Cover p. 2747

Perspective

Synopses

Research

Medscape EDUCATION ACTIVITY

Dispatches

EMERGING INFECTIOUS DISEASES®
October 2021

Research Letters

EMERGING INFECTIOUS DISEASES®
October 2021

Comment Letter

About the Cover

Online Report

Conference Summary

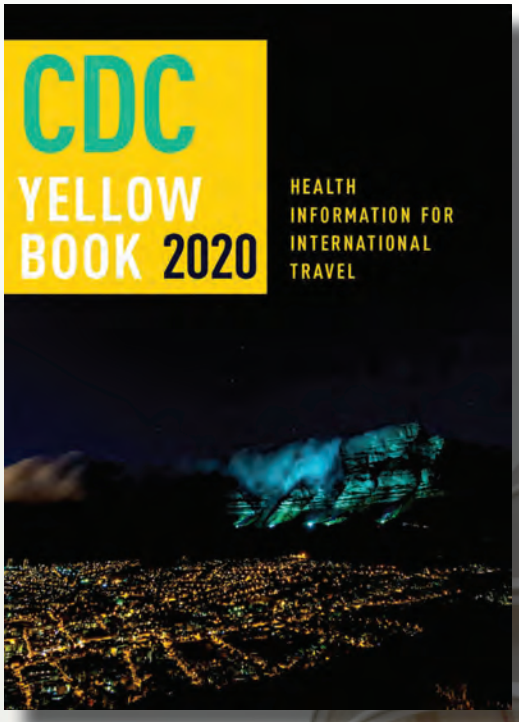

Available Now
Yellow Book 2020

The fully revised and updated CDC Yellow Book 2020: Health Information for International Travel codifies the US government's most current health guidelines and information for clinicians advising international travelers, including pretravel vaccine recommendations, destination-specific health advice, and easy-to-reference maps, tables, and charts.

ISBN: 978-0-19-006597-3 | $115.00 | May 2019 | Hardback | 720 pages

ISBN: 978-0-19-092893-3 | $55.00 | May 2019 | Paperback | 687 pages

Yellow Book 2020 includes important travel medicine updates

- **The latest information on emerging infectious disease threats, such as Zika, Ebola, and henipaviruses**
- **Considerations for treating infectious diseases in the face of increasing antimicrobial resistance**
- **Legal issues facing clinicians who provide travel health care**
- **Special considerations for unique types of travel, such as wilderness expeditions, work-related travel, and study abroad**

OXFORD
UNIVERSITY PRESS

Order your copy at:
www.oup.com/academic

Antimicrobial Resistance in Africa—How to Relieve the Burden on Family Farmers

Christian Ducrot, Alexandre Hobeika, Christian Lienhardt, Barbara Wieland, Charlotte Dehays, Alexis Delabouglise, Marion Bordier, Flavie Goutard, Ekta Patel, Muriel Figuié, Marisa Peyre, Arshnee Moodley, François Roger

Although currently available data indicate that Africa has the lowest usage of antimicrobials in animals in the world (adjusted by animal biomass), data show a high prevalence of antimicrobial resistance in foodborne pathogens isolated from animals and animal products. Apart from the lack of solid data on antimicrobial use in many countries in Africa, different hypotheses could explain this situation. Qualitative interviews of farmers show a lack of knowledge and uninformed use of antimicrobials. Considering the development of animal farming to meet an increasing demand for proteins, this deficiency represents a serious public health issue. We advocate for policies that consider the specific challenges faced by family farmers in Africa, to simultaneously improve access to veterinary drugs while strengthening the regulation of their use. We propose a global approach targeting the agri-food system, offering innovative social and technical interventions on antimicrobial usage, adapted to family farmers.

According to international official data, Africa seems to have the lowest usage of antimicrobials in animals in the world, adjusted by animal biomass (*1*), which would tend to indicate that antimicrobial resistance is not a question there. However, an extensive review by Van Boeckel et al. reports that a high prevalence of antimicrobial resistance (AMR) has been observed in foodborne pathogens isolated from animals and animal products in Africa (*2*). This article explores this apparent paradox, which, in fact, points to the quality of available data and the practices about antimicrobial use (AMU).

Antimicrobial Resistance in Animals in Africa

The literature review by Van Boeckel et al. shows that, in poultry, resistance rates to tetracycline reach 70% for *Escherichia coli* and 80% for *Campylobacter* in Africa, above the rates observed in Asia or the Americas (*2*). Resistance to sulfamethoxazole/trimethoprim and ampicillin is ≈60% for *E. coli*, again above the rates in other continents. The same trend was observed in studies on pigs, ruminants, and even wildlife (*3*), and resistance rates have been increasing over the years (*2*). Fortunately, lower rates of resistance are observed for antimicrobials considered critical to human medicine, such as cephalosporins, although

Author affiliations: Animals Health Territories Risks Ecosystems Research Unit (ASTRE), Univ Montpellier, Agricultural Research Center for International Development (CIRAD), Institut National de Recherche pour l'Agriculture, l'Alimentation et l'Environnement (INRAE), Montpellier, France (C. Ducrot, C. Dehays, A. Delabouglise, M. Bordier, F. Goutard, M. Peyre, F. Roger); CIRAD, Marché Organisations Institutions et Stratégies d'Acteurs Research Unit (MOISA), Montpellier (A. Hobeika); MOISA, Université de Montpellier, Centre International de Hautes Etudes Agronomiques Méditerranéennes–Institut Agronomique Méditerranéen de Montpellier, CIRAD, INRAE, Institut Agro, Montpellier (A. Hobeika, M. Figuié); Institut de Recherche pour le Développement (IRD), Recherches Translationnelles sur le VIH et les Maladies Infectieuses Research Unit (TransVIHMI), Montpellier (C. Lienhardt); TransVIHMI, Université de Montpellier, IRD, Institut National de la Santé et de la Recherche Médicale (INSERM), Montpellier (C. Lienhardt); International Livestock Research Institute, Addis Ababa, Ethiopia (B. Wieland); CIRAD, ASTRE, Montpellier (C. Dehays, A. Delabouglise, M. Peyre, F. Roger); Institut Sénégalais de Recherches Agricoles–Laboratoire National de l'Elevage et de Recherches Vétérinaires, Dakar-Hann, Senegal (M. Bordier); Kasetsart University Faculty of Veterinary Medicine, Bangkok, Thailand (F. Goutard); International Livestock Research Institute, Nairobi, Kenya (E. Patel, A. Moodley); Universidade Eduardo Mondlane Faculdade de Letras e Ciências Sociais, Maputo, Mozambique (M. Figuié); University of Copenhagen Department of Veterinary and Animal Sciences, Frederiksberg, Denmark (A. Moodley)

DOI: https://doi.org/10.3201/eid2710.210076

these rates are frequently above those observed globally. However, we should note that scientific data on AMR in animals and animal products was lacking in 10 of the 54 countries in Africa, and 11 of those that provided data experienced challenges because of a lack of experience in collecting data. Although solid data on AMR in different countries in Africa is lacking, the collection of data is improving rapidly.

The absence of national AMU surveillance programs in countries in Africa raises questions about the reliability of reported data, especially because some countries do not provide data to the World Organisation for Animal Health (OIE). Furthermore, data in certain countries probably do not fully capture actual AMU because of illegal sales and undocumented imports of antimicrobials (*1*). However, some studies indicate declining trends in AMU. Thus, Klein et al. mention that, during 2000–2015, antimicrobial consumption in low- and middle-income countries was approaching levels observed in high-income countries (*4*). However, regardless of whether antimicrobial consumption is underestimated in Africa or not, AMR in animal food products is at a high level. Hypotheses that could explain this situation need to be formulated and tested.

To help clarify smallholder farmers' motivations to use antimicrobials and the barriers they face, qualitative interviews of farmers, studies using participatory methods, and structured studies such as knowledge, attitudes, and practices analyses have been published in recent years. The results of these small-scale studies highlight low levels of AMU awareness and knowledge, AMU that appears to be far from informed or prudent, and AMR risk perceptions that are poor (*5*–*7*; Z.I. Kimera et al., unpub. data, https://doi.org/10.21203/rs.3.rs-33311/v1). Most farmers report using antimicrobials on individual animals to treat a disease but also on their entire flocks and herds to prevent disease and to promote growth (*8*). The prescribed dosage is often not respected (*9*–*11*). Farmers typically use antimicrobials without advice from an animal-health worker (*12*) and can easily purchase drugs without a prescription (*11*,*13*). Most farmers are not aware of the withdrawal period rule (*11*), which stipulates a period between drug administration and the slaughter or consumption of food from the treated animal; the period is defined for each drug to ensure that the food does not contain residue of that drug. Among farmers who report knowing about withdrawal periods, many do not always respect them (*12*,*14*), which sheds light on why various studies have found antimicrobial residues in animal food products (*15*,*16*). In addition, counterfeit and subquality drugs appear to be widespread in low-income countries; ≈60% of antimicrobials in Africa are of poor quality (*17*), which can select for antimicrobial-resistant pathogens. Together, those factors might be contributing to the high level of AMR rates in animals and animal food products in Africa. Additional factors might exist, such as a high burden of infections coupled with poor animal husbandry practices spreading the resistance genes (*18*), addition of antimicrobials to preserve animal products (*19*), weak enforcement of regulations (*20*), and use of antimicrobials in plant production (a practice that is poorly documented and possibly used on a great variety of crops) (*21*). Although the transmission routes of AMR from animals to humans and vice versa are insufficiently investigated in Africa, the situation is of public health concern because of the probability that resistance is being transmitted to farmers and consumers through animals and animal food products and through consumption of antimicrobial residues in animal products. This zoonotic contribution of AMR adds to the high level of AMR to commonly prescribed antimicrobial drugs that have already been observed in humans (*22*). Furthermore, the contribution of environmental contamination through the use of antimicrobials in animal husbandry is poorly documented in Africa, but it could play an important role in the acquisition of resistance in humans. In fact, 90% of antimicrobials administered orally are excreted in urine or manure in a very slightly degraded form and end up in water used for animal and vegetable production (*23*).

Animal farming, especially poultry, is expanding in Africa; meat production has increased by 64% since 2000, in response to an increasing demand for protein by the growing population (*2*,*24*). A major need exists to rationalize the use of antimicrobials for animals in Africa, keeping in mind 3 important aspects. First, and similar to what is observed in other continents, a large proportion of antimicrobial drugs are currently used without a relevant indication, so there is room for a substantial decrease of AMU without negatively affecting the productivity of the livestock industry. Second, antimicrobials remain essential in the treatment of livestock diseases for which no affordable alternative treatment exists; this point is particularly important because livestock provide a range of essential services to society, including income and savings for the rural poor, access to protein, transportation, and manure for fertilizer (*25*–*27*). Third, farming systems in Africa represent a wide continuum ranging from family farms (smallholders) to commercial

farms, which have very different levels of access to antimicrobials and support services. Although commercial farmers can adapt to evolving standards, adaptation is more difficult for the smallholder farmers (*28*). Therefore, policies must differentiate between commercial and family farms and be designed to minimize adverse health and socioeconomic effects on family farmers' standards of living, especially in the most vulnerable areas.

Antimicrobials have the double advantage of being relatively inexpensive and of having highly reliable effects on animal health. Substitutes for antimicrobials were evaluated in the context of large-scale commercial farming systems in high-income countries. These substitutes include investments in long-term prevention plans with vaccination and farm biosecurity enhancement aimed at reducing the probability of bacterial infections (*29*). However, implementing these measures involves training, specialization, and investment that are mostly incompatible with the economic rationale of small-scale farmers, who represent the bulk of the livestock production in Africa (*30*). In the context of most sub-Saharan Africa countries, where the availability of capital, credit, and government support is limited, livestock farming is favored precisely because it requires limited investment, and farmers often tend to diversify their activities to mitigate economic risks rather than specialize in a single product (*25*,*31*,*32*). Access to antimicrobials remains necessary to treat sick animals and thus maintain overall health. The annual cost of infectious animal diseases in Africa is estimated to be US $9.35 billion, and losses caused by lack of treatment far outweigh losses caused by AMR (*33*). Subsequently, in the absence of generalized improvement of access to veterinary services, drastically reducing the use of antimicrobials, which is necessary in the fight against AMR, will probably lead to an upsurge of diseases and a drop in production. This reduction will have an economic impact on small farmers and will reduce access to cheap meat for the most vulnerable groups, resulting in serious adverse effects on their nutrition (*34*). Therefore, the national regulations put in place to curb the emergence of resistance need to be reinforced, take into account the needs of family farmers and low-income populations, and address properly the ethical issues of social values and equal access (*34*).

The Way Forward

We advocate for policies that consider the specific challenges faced by family farms and commercial farms. On the one hand, the use of antimicrobials by commercial farms needs to be regulated. On the other hand, family farmers face severe difficulties in accessing veterinary drugs and professional veterinary advice (G. Jaime et al., unpub. data, https://doi.org/10.31730/osf.io/8vcj2), which hampers their capacity to change their animal health practices, adopt innovations, and cope with more demanding regulations and production standards. Policies designed to control AMR must meet the dual challenge of simultaneously improving access to veterinary drugs while strengthening the regulation of their use. Moreover, although antimicrobial use in farming is driven by the characteristics of individual farmers and farming systems, it also depends on the functioning of the antimicrobial value chain, existing regulations, and access to veterinary extension services. Consequently, policies should not stigmatize farmers and load them with a burden of measures against AMR but should modify the organization of international and national veterinary drug markets. We are arguing in favor of strong public policies that reinforce access to veterinary services for family farmers and a prudent use of antimicrobials. Efforts must be made to fill gaps in knowledge on the socioeconomic context that prompt farmers to misuse antimicrobials and increase the health risks for their families and consumers. We propose combining several complementary approaches at the farm and market value chain levels.

First, we urge using actions adapted to the complexity of agri-food systems (*35*), which entails assessing agricultural systems, identifying and understanding livestock farming networks and processing methods (with particular emphasis on practices linked to antimicrobials), developing programs of action aimed at rationalizing antimicrobial use on the basis of a participatory approach joining researchers with all the stakeholders involved, and targeting priority actions according to sectors and geographic areas.

Second, we advocate better regulation of farming practices that improves farmers' access to training (with special attention to sex) and advice (or support services) provided by trained veterinarians or paravets. Regulation should also be aimed at increasing biosecurity on farms (*36*), including better control of the introduction of animals, inputs, and drugs, notably the use of growth promoters; more effective management of contacts between animal species; closer monitoring of conditions in farm buildings; and vaccination against common infectious diseases to reduce the need for antimicrobials to treat preventable infections. We also recommend education and training programs for veterinarians

and paraveterinary and community-based animal health workers, in close collaboration with official authorities and nongovernment organizations such as Agronomes et Vétérinaires Sans Frontières, with the aim of promoting a reasoned use of antimicrobials and expanding the offer of veterinary services.

We recommend better structuring, regulation, and monitoring of the flows of veterinary drugs through improving farmers' access to medicines, especially in rural areas; improving information about drug quality from importation to local distribution; and overall monitoring of the flows of medicines. We also call for regulating and controlling the sale of illegal drugs, with the support of governing bodies such as OIE, as well as establishing appropriate, integrated, and multisectoral monitoring of AMU trends and resistance to antimicrobials in animals, food products, and the environment (*37*).

In practice, a major difficulty in fair public health reforms, which involve and affect a wide range of actors, is generally a lack of information about the political and social context in which they take place. Mapping antimicrobial supply chains could help overcome this problem by identifying target groups, their ability to block or support reform, and their ability to ally with and influence the political process (through power, leadership, or both) and to propose strategies to promote supportive actions and reduce counter actions (*38*). After this mapping, innovative social and technical interventions on AMU, adapted to the socioeconomic level of smallholders, could be co-constructed by using, for example, participatory modeling (*39*). The main idea of participatory modeling is to make explicit biological processes and the strategies and social relationships of the actors involved so that the actors themselves can deal with their own problems and identify mutually acceptable solutions that can lead to collective action plans. The efficacy of these co-constructed interventions could be assessed with randomized cluster trials to determine which measures have an impact, the magnitude of that impact, which strategies are most cost-effective, and which ones can be adopted quickly. Developing strong public–private partnerships within this process involving farmers, public and private veterinarians, public authorities, drug companies, and agro-industries, would be key to ensure the sustainability of the actions. Private organizations included in the partnership might support the process in the long run and ensure proper implementation of best practices for AMU as well as surveillance and control measures (e.g., vaccination and biosecurity) (*40*).

Conclusion

Reducing antimicrobial consumption and misuse is critical for reducing the threat of AMR in Africa. To that end, considering the complexity of social-ecologic systems, analyzing AMU drivers, monitoring AMR and AMU, and involving stakeholders in participatory approaches (in a One Health framework) will be key to ensuring the efficiency of action plans and regulations and to safeguarding family farming communities. Such reduction efforts must be linked with improved access to nonmedicated animal feed and better access and use of antimicrobials that are needed to treat sick animals. Similar to programs used in human health, antimicrobial stewardship programs geared around family farmers and involving all stakeholders should be developed and put in place in Africa (*41*), taking into account the specificities of the situation in each country.

Acknowledgments

We thank Grace Delobel for proofreading the text.

This article was developed from a CIRAD policy brief edited by R.F. and C.D. (*42*).

About the Author

Dr. Ducrot is senior researcher at France's National Research Institute for Agriculture, Food, and Environment. His current research focuses on the use of antimicrobials on farm animals, in close collaboration with sociologists.

References

1. World Organisation for Animal Health (OIE). OIE annual report on antimicrobial agents intended for use in animals—better understanding of the global situation. Fourth report. 2020 [cited 2021 Jun 2]. https://rr-africa.oie.int/wp-content/uploads/2019/09/annual_report_amr_3.pdf
2. Van Boeckel TP, Pires J, Silvester R, Zhao C, Song J. Global trends in antimicrobial resistance in animals in low- and middle-income countries. Science 2019;365(6459):eaaw1944. http://dx.doi.org/10.1126/science.aaw1944
3. Mercat M, Clermont O, Massot M, Ruppe E, de Garine-Wichatitsky M, Miguel E, et al. *Escherichia coli* population structure and antibiotic resistance at a buffalo/cattle interface in southern Africa. Appl Environ Microbiol. 2015;82:1459–67. https://doi.org/10.1128/AEM.03771-15
4. Klein EY, Van Boeckel TP, Martinez EM, Pant S, Gandra S, Levin SA, et al. Global increase and geographic convergence in antibiotic consumption between 2000 and 2015. Proc Natl Acad Sci U S A. 2018;115:E3463–70. https://doi.org/10.1073/pnas.1717295115
5. Alhaji NB, Haruna AE, Muhammad B, Lawan MK, Isola TO. Antimicrobials usage assessments in commercial poultry and local birds in north-central Nigeria: Associated pathways and factors for resistance emergence and spread. Prev Vet Med. 2018;154:139–47. https://doi.org/10.1016/j.prevetmed.2018.04.001

6. Alhaji NB, Aliyu MB, Ghali-Mohammed I, Odetokun IA. Survey on antimicrobial usage in local dairy cows in north-central Nigeria: drivers for misuse and public health threats. PLoS One. 2019;14:e0224949. https://doi.org/10.1371/journal.pone.0224949
7. Gemeda BA, Amenu K, Magnusson U, Dohoo I, Hallenberg GS, Alemayehu G, et al. Antimicrobial use in extensive smallholder livestock farming systems in Ethiopia: knowledge, attitudes, and practices of livestock keepers. Front Vet Sci. 2020;7:55. https://doi.org/10.3389/fvets.2020.00055
8. Donkor ES, Newman MJ, Yeboah-Manu D. Epidemiological aspects of non-human antibiotic usage and resistance: implications for the control of antibiotic resistance in Ghana. Trop Med Int Health. 2012;17:462–8. https://doi.org/10.1111/j.1365-3156.2012.02955.x
9. Vougat Ngom RRB, Tomdieu T, Ziébé R, Foyet HS, Moritz M, Vondou L, et al. Quality of veterinary pharmaceuticals and their use by pastoralists in the Far North Region of Cameroon. Pastoralism 2017;7:1,6. https://doi.org/10.1186/s13570-017-0081-5
10. Bâtie C, Kassie D, Randravatsilavo DNRM, Baril L, Waret Szkuta A, Goutard FL. Perception of drug vendors and pig and poultry farmers of Imerintsiatosika, in Madagascar, toward risks related to antibiotic usage: a q-method approach. Front Vet Sci. 2020;7:490. https://doi.org/10.3389/fvets.2020.00490
11. Gemeda BA, Amenu K, Magnusson U, Dohoo I, Hallenberg GS, Alemayehu G, et al. Antimicrobial use in extensive smallholder livestock farming systems in Ethiopia: knowledge, attitudes, and practices of livestock keepers. Front Vet Sci. 2020;7:55. https://doi.org/10.3389/fvets.2020.00055
12. Auta A, Hadi MA, Oga E, Adewuyi EO, Abdu-Aguye SN, Adeloye D, et al. Global access to antibiotics without prescription in community pharmacies: A systematic review and meta-analysis. J Infect. 2019;78:8–18. https://doi.org/10.1016/j.jinf.2018.07.001
13. Caudell MA, Dorado-Garcia A, Eckford S, Creese C, Byarugaba DK, Afakye K, et al. Towards a bottom-up understanding of antimicrobial use and resistance on the farm: A knowledge, attitudes, and practices survey across livestock systems in five African countries. PLoS One. 2020;15:e0220274. https://doi.org/10.1371/journal.pone.0220274
14. Olufemi O, Ojomo T, Adeseko Y. Antibiotics use and gentamicin residues in commercial poultry and chicken eggs from Oyo and Lagos states, Nigeria. Rev Élev Méd Vét Pays Trop. 2019;72:4. https://doi.org/10.19182/remvt.31510
15. Mensah SEP, Koudandé OD, Sanders P, Laurentie M, Mensah GA, Abiola FA. Antimicrobial residues in foods of animal origin in Africa: public health risks. Rev Sci Tech. 2014;33:987–96, 975–86. http://dx.doi.org/10.20506/rst.33.3.2335
16. Rakotoharinome M, Pognon D, Randriamparany T, Ming JC, Idoumbin JP, Cardinale E, et al. Prevalence of antimicrobial residues in pork meat in Madagascar. Trop Anim Health Prod. 2014;46:49–55. https://doi.org/10.1007/s11250-013-0445-9
17. Kelesidis T, Falagas ME. Substandard/counterfeit antimicrobial drugs. Clin Microbiol Rev. 2015;28:443–64. https://doi.org/10.1128/CMR.00072-14
18. Collignon P, Beggs JJ, Walsh TR, Gandra S, Laxminarayan R. Anthropological and socioeconomic factors contributing to global antimicrobial resistance: a univariate and multivariable analysis. Lancet Planet Health. 2018;2:e398–405. https://doi.org/10.1016/S2542-5196(18)30186-4
19. Carruth L, Roess AA, Terefe Y, Hosh FM, Salman MD. Antimicrobial resistance and food safety in Africa. Lancet Infect Dis. 2017;17:575–6. https://doi.org/10.1016/S1473-3099(17)30273-6
20. Grasswitz TR, Leyland TJ, Musiime JTSJ. O., Sones KR. The veterinary pharmaceutical industry in Africa: a study of Kenya, Uganda and South Africa. 2004 [cited 2021 Jan 12]. https://fic.tufts.edu/wp-content/uploads/Grasswitz-et-al.pdf
21. Taylor P, Reeder R. Antibiotic use on crops in low and middle-income countries based on recommendations made by agricultural advisors. CABI Agric Biosci. 2020;1:1. https://doi.org/10.1186/s43170-020-00001-y
22. Tadesse BT, Ashley EA, Ongarello S, Havumaki J, Wijegoonewardena M, González IJ, et al. Antimicrobial resistance in Africa: a systematic review. BMC Infect Dis. 2017;17:616. https://doi.org/10.1186/s12879-017-2713-1
23. Kumar K, Gupta SC, Chander Y, Singh AK. Antibiotic use in agriculture and its impact on the terrestrial environment. Adv Agron. 2005;87:1–54. https://doi.org/10.1016/S0065-2113(05)87001-4
24. Thornton PK. Livestock production: recent trends, future prospects. Philos Trans R Soc Lond B Biol Sci. 2010;365:2853–67. https://doi.org/10.1098/rstb.2010.0134
25. Herrero M, Grace D, Njuki J, Johnson N, Enahoro D, Silvestri S, et al. The roles of livestock in developing countries. Animal. 2013;7(Suppl 1):3–18. https://doi.org/10.1017/S1751731112001954
26. Alary V, Corniaux C, Gautier D. Livestock's contribution to poverty alleviation: how to measure it? World Dev. 2011;39:1638–48. https://doi.org/10.1016/j.worlddev. 2011.02.008
27. Guèye EF. The role of family poultry in poverty alleviation, food security and the promotion of gender equality in rural Africa. Outlook Agric. 2000;29:129–36. https://doi.org/10.5367/000000000101293130
28. Sourisseau JM. Family farming and the worlds to come. Springer Netherlands (Dordrecht, Netherlands) and Éditions Quæ (Versailles, France); 2015. http://dx.doi.org/10.1007/978-94-017-9358-2
29. Rojo-Gimeno C, Postma M, Dewulf J, Hogeveen H, Lauwers L, Wauters E. Farm-economic analysis of reducing antimicrobial use whilst adopting improved management strategies on farrow-to-finish pig farms. Prev Vet Med. 2016;129:74–87. https://doi.org/10.1016/j.prevetmed.2016.05.001
30. Obi TU, Olubukola A, Maina GA. Pro-poor HPAI risk reduction strategies in Nigeria. 2008 [cited 2020 Nov 12]. https://agris.fao.org/agris-search/search.do?recordID= GB2012111804
31. Leonard DK. Africa's changing markets for health and veterinary services: the new institutional issues. St. Martin's Press (New York); 2000.
32. Bowman MS, Zilberman D. Economic factors affecting diversified farming systems. Ecology and Society 2013;18:1,33 [cited 2021 Jan 12]. https://www.jstor.org/stable/pdf/26269286.pdf
33. Grace D. Review of evidence on antimicrobial resistance and animal agriculture in developing countries [cited 2020 Nov 12]. https://cgspace.cgiar.org/handle/10568/67092
34. Littmann J, Viens AM. The ethical significance of antimicrobial resistance. Public Health Ethics. 2015;8:209–24.
35. Lhermie G, Wernli D, Jørgensen PS, Kenkel D, Tauer LW, Gröhn YT. Global resistance to antimicrobials and their sustainable use in agriculture. Lancet Planet Health. 2019;3:e109–10. https://doi.org/10.1016/S2542-5196(18)30251-1

36. Conan A, Goutard FL, Sorn S, Vong S. Biosecurity measures for backyard poultry in developing countries: a systematic review. BMC Vet Res. 2012;8:240. https://doi.org/10.1186/1746-6148-8-240
37. Bordier M, Uea-Anuwong T, Binot A, Hendrikx P, Goutard FL. Characteristics of One Health surveillance systems: A systematic literature review. Prev Vet Med. 2020;181:104560. https://doi.org/10.1016/j.prevetmed. 2018.10.005
38. Schmeer K. Guidelines for conducting a stakeholder analysis. 1999 [cited 2020 Nov 12]. https://targeting.alnap.org/system/files/content/resource/files/main/hts3.pdf
39. Étienne M. Companion modelling: a participatory approach to support sustainable development. Springer: Heidelberg; 2013.
40. World Organisation for Animal Health (OIE). The OIE PPP handbook: guidelines for public-private partnerships in the veterinary domain. 2019 [cited 2020 Nov 12]. https://www.oie.int/fileadmin/Home/eng/Media_Center/docs/pdf/PPP/oie_ppp_handbook-20190419_ENint_BD.pdf
41. World Health Organization, Food and Agriculture Organization, World Organisation for Animal Health (OIE). Global framework for development and stewardship to combat antimicrobial resistance. 2018 [cited 2020 Nov 12]. https://www.who.int/publications/m/item/global-framework-for-development-stewardship-to-combat-antimicrobial-resistance-draft
42. Roger F, Ducrot C, editors. Antimicrobials in agriculture: reducing their use while limiting health and socioeconomic risks in the countries of the South. Perspective. 2017;39:1–4. https://doi.org/10.19182/agritrop/00014

Address for correspondence: Christian Ducrot, UMR ASTRE, CIRAD, Campus International de Baillarguet, 34980 Montferrier sur Lez, France; email: christian.ducrot@inrae.fr

Characteristics, Comorbidities, and Data Gaps for Coronavirus Disease Deaths, Tennessee, USA

John James Parker, Rany Octaria, Miranda D. Smith, Samantha J. Chao, Mary Beth Davis, Celia Goodson, Jon Warkentin, Denise Werner, Mary-Margaret A. Fill

As of March 2021, coronavirus disease (COVID-19) had led to >500,000 deaths in the United States, and the state of Tennessee had the fifth highest number of cases per capita. We reviewed the Tennessee Department of Health COVID-19 surveillance and chart-abstraction data during March 15–August 15, 2020. Patients who died from COVID-19 were more likely to be older, male, and Black and to have underlying conditions (hereafter comorbidities) than case-patients who survived. We found 30.4% of surviving case-patients and 20.3% of deceased patients had no comorbidity information recorded. Chart-abstraction captured a higher proportion of deceased case-patients with ≥1 comorbidity (96.3%) compared with standard surveillance deaths (79.0%). Chart-abstraction detected higher rates of each comorbidity except for diabetes, which had similar rates among standard surveillance and chart-abstraction. Investing in public health data collection infrastructure will be beneficial for the COVID-19 pandemic and future disease outbreaks.

As of March 5, 2021, the total of deaths from coronavirus disease (COVID-19) reached 2,564,560 worldwide, 515,013 in the United States (*1*), and 11,534 in Tennessee (*2*). Tennessee has been particularly affected by the pandemic; as of March 5, 2021, this state had the fifth highest number of cases per 100,000 residents in the United States (*3*). The mortality rate for COVID-19 infection varies greatly based on patient characteristics (*4*,*5*). Age and preexisting health conditions (hereafter comorbidities) have been associated with increased risk for death from COVID-19 (*5*–*7*). Cardiovascular disease (CVD), hypertension, diabetes, respiratory disease, cancer, kidney disease, and obesity have been associated with death; however, the strength of this association has differed among studies (*5*,*7*). Although worldwide racial and ethnic minorities account for a higher proportion of COVID-19 deaths, the independent impact of race and ethnicity is unclear (*8*).

Challenges with data collection and reporting have made it difficult to delineate some characteristics of COVID-19 deaths. According to an assessment of surveillance data reported to the Centers for Disease Control and Prevention (CDC), 58.9% of patients had missing comorbidity information (*6*). Because public health agencies gather their surveillance information from local laboratories and healthcare facilities; the completeness of their data are contingent on the local agencies obtaining and transmitting the information (*9*,*10*). Consequently, mortality rate studies often focus on medical record reviews from single institutions and urban centers (*11*–*13*).

To better distinguish the characteristics of COVID-19 deaths, during March 15, 2020–May 19, 2020, the Tennessee Department of Health (TDH) implemented a supplemental chart-abstraction process for COVID-19 deaths in Tennessee. This study reviews TDH COVID-19 surveillance data and the supplemental chart review data to describe the characteristics of COVID-19 deaths in Tennessee. In addition, this study evaluates the value of a supplemental chart review process during disease outbreak surveillance.

Methods

Our study describes TDH public health data that was collected as part of COVID-19 surveillance. Definitions and protocols in place were defined by the TDH, who used CDC guidelines for their definitions of confirmed cases, probable cases, and COVID-19 deaths (*14*). Confirmed case-patients in Tennessee were defined as persons who had SARS-CoV-2 detected by

Author affiliations: Tennessee Department of Health, Nashville, Tennessee, USA (J.J. Parker, R. Octaria, M.D. Smith, S.J. Chao, M.B. Davis, C. Goodson, J. Warkentin, D. Werner, M.-M.A. Fill); Vanderbilt University Medical Center, Nashville (J.J. Parker)

DOI: https://doi.org/10.3201/eid2710.211070

using real-time reverse transcription PCR. Probable case-patients were persons who had a positive antigen test result for a respiratory specimen or persons who had no positive PCR result but met the vital records criteria or clinical criteria and had close contact to a COVID-19 case-patient during the 14 days before illness onset (*15*). COVID-19 deaths were defined as case-patients whose death certificate lists COVID-19 or SARS-CoV-2 as an underlying cause of death or a major condition contributing to death (*16*).

The sample included confirmed and probable cases in Tennessee residents who had COVID-19. We conducted investigations during March 15, 2020–August 15, 2020. Data analysis began on September 15; we used a minimum 4-week lag time to best ensure that case-patients were categorized as alive or deceased. Our primary objective was to evaluate the baseline characteristics and comorbidities of persons who died from COVID-19 in Tennessee. A secondary objective was to compare the type and quantity of data obtained through standard disease surveillance and a supplemental chart review process. The TDH Institutional Review Board (TDH-IRB# 2020–0251) approved this study as minimal risk and waived the need for individualized consent.

Data Collection

As part of routine data entry for all COVID-19 cases, trained TDH employees completed the Human Infection with 2019 Novel Coronavirus Case Report Form (CRF) (https://www.cdc.gov/coronavirus/2019-ncov/downloads/pui-form.pdf) (*17*) and entered the information into the National Electronic Disease Surveillance System Base System (NBS; https://www.cdc.gov/nbs/index.html). Information gathered included patient characteristics, symptoms, comorbidities, and clinical course. (The terms preexisting condition and comorbidity were used by TDH to indicate medical conditions that were present before COVID-19 infection; these terms are used interchangeably in this article.) Data collected through the CRF was the TDH standard COVID-19 disease surveillance.

In addition, during the first few months of the pandemic, the TDH created a supplemental chart review process to better classify the comorbidities and characteristics of deceased patients. This chart-abstraction project began with a group of public health professionals creating a list of 20 comorbidities to supplement the information in the standard CRF (Appendix 1, https://wwwnc.cdc.gov/EID/article/27/10/21-1070-App1.pdf). The chart review process creates line items for additional comorbidities. However, the CRF has 2 free text items for other chronic diseases and other underlying conditions. Therefore, we believe there is value in comparing comorbidity frequencies between the data collection groups.

Next, we added the additional chart-abstraction comorbidities to NBS to enable data entry. We then requested the medical records of all COVID-19 patients who died before May 19, 2020; 5 physicians and 1 family medicine nurse practitioner reviewed the available medical records. The provider group only reviewed complete records that included at least a complete history and physical or complete death summary. This provider group abstracted the information from the charts and added comorbidities found in the medical records to the NBS database. If there was no mention of a comorbidity, we assumed that the person did not have an underlying condition. However, when charts had gaps in documentation, the medical providers included comorbidities if there was clear evidence that the patient had a condition. For example, if a patient's chart had minimal medical history documented but had chronic problems listed in a note's plans, those problems were recorded as preexisting conditions. The group met and decided on definitions of diseases, and if there was any question on how a disease should be categorized, the individual provider would consult the group. For haste of getting this information to public health leadership, the provider's chart-abstraction work was not reviewed by a second party. After completing their review, the providers updated the information from the CRF and added additional comorbidity data into NBS. Data from the supplemental chart review project were labeled as chart-abstracted. Preliminary data from the chart review project were presented to TDH leadership at the end of May 2020.

Data Characterization and Analysis

We grouped COVID-19 case-patients into 3 groups: alive (living) case-patients, standard surveillance COVID-19 deaths, and chart-abstracted COVID-19 deaths (Figure 1). All COVID-19 cases (n = 130,040) during the study period were included in demographic analysis (Table 1). The comorbidity analysis (Tables 2, 3; Appendix 2, https://wwwnc.cdc.gov/EID/article/27/10/21-1070-App2.pdf) excluded case-patients who had no comorbidity information recorded by only selecting cases with ≥1 answers completed in the comorbidity or preexisting condition sections (n = 89,270). In both the standard surveillance and the chart-abstraction process, if comorbidity data in the CRF was partially completed, blank items were listed as not having that condition. For race/ethnicity, we defined White as White race, non-Hispanic ethnicity,

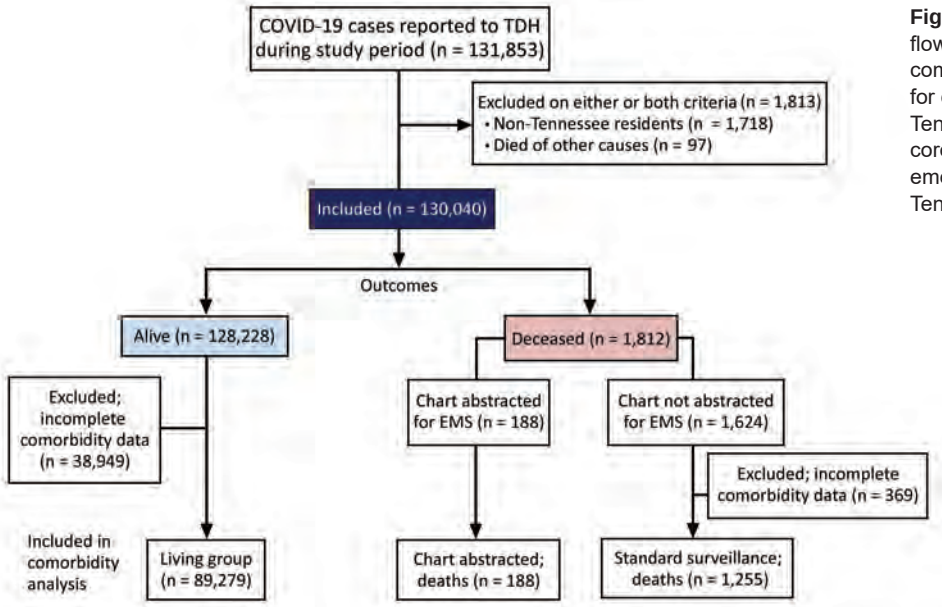

Figure 1. Data categorization flow diagram for characteristics, comorbidities, and data gaps for coronavirus disease deaths, Tennessee, USA. COVID-19, coronavirus disease; EMS, emergency medical services; TDH, Tennessee Department of Health.

and Black as Black race, non-Hispanic ethnicity. We defined Hispanic as all races that selected Hispanic ethnicity. For our race/ethnicity comorbidity analysis (Tables 2, 3; Appendix 2), we excluded all other races because there were only 6 case-patients in the chart-abstracted group who were not identified as White, Black, or Hispanic.

We converted comorbidities from CRFs and the chart-abstraction protocol into dichotomous variables for each condition. For the chart-abstracted deaths, we provided definitions of CVD and chronic lung disease (CLD) (Table 3) (*18*–*20*); for standard surveillance of COVID-19 deaths, we selected preexisting conditions, including CVD and CLD, on the basis of self-reports. Obesity was not included in the comorbidity analysis because the body mass index cutoffs differed between CRF and the chart-abstraction process. We calculated days to hospitalization by determining the difference in days between illness onset date and hospitalization admission date for patients who were hospitalized; we counted negative values (i.e., tested positive after hospitalization) as 0 and excluded probable cases from this calculation. We calculated days to specimen collection by determining the difference between the first specimen collection date for the PCR that had a positive result for SARS-CoV-2 and the illness onset date among for confirmed case-patients; probable case-patients were excluded from this calculation.

We report patient characteristics as frequencies and proportions for categorical variables and median and interquartile range for continuous variables. We compared characteristics between groups by using χ^2 or Fisher exact tests, as appropriate, for categorical variables and *t*-test for continuous variables and performed statistical analyses by using SAS version 9.4 (SAS Institute, https://www.sas.com).

Results

During the study period, we identified 131,854 COVID-19 case-patients. We excluded 1,813 case-patients because of either non-Tennessee residency or death from other causes. Of the 130,040 included case-patients, 1,812 (1.4%) died from COVID-19. Deaths of COVID-19 case-patients were more likely to be in older, male, and Black case-patients than living case-patients (Table 1). The prevalence of ≥1 underlying condition was higher for deceased patients (64.8%) than for living patients (22.6%), and this trend was true for all age groups. There were 38,949 (30.4%) living case-patients and 369 (20.3%) deceased case-patients who did not have any comorbidity information recorded. Therefore, for the comorbidity analysis (Tables 2, 3; Appendix 2), we excluded case-patients who did not have comorbidity data (Figure 1).

We found a difference in the case-fatality rate (CFR) for COVID-19 by race and ethnicity (White 1.9%, Black 2.6%, and Hispanic 0.5%) (Table 2). The mean age of living and deceased patients also differed by race; for deceased patients the average age was 75.6 years for White patients, 69.5 years for Black patients, and 61.3 years for Hispanic patients. After stratifying by age, we found that Black patients continued to have the highest CFR. However, Hispanic case-patients >65 years of age had a CFR similar to or

Table 1. Characteristics of coronavirus disease patients in Tennessee, USA, March 15–August 15, 2020

Characteristic	Living, n = 128,228	Deceased, n = 1,812
Race and ethnicity, no. (%)		
White, non-Hispanic	56,271 (43.9)	1,093 (60.3)
Black, non-Hispanic	26,697 (20.8)	540 (29.8)
Hispanic (all races)	21,390 (16.7)	126 (7.0)
All other races	8,155 (6.4)	49 (2.7)
Unknown	15,715 (12.3)	4 (0.2)
Sex, no. (%)		
F	64,966 (50.7)	789 (43.5)
M	62,100 (48.4)	1,023 (56.5)
Unknown	1,162 (0.9)	0
Age group, y, no. (%)		
0–20	21,703 (16.9)	4 (0.2)
21–64	93,486 (72.9)	451 (24.9)
65−80	10,080 (7.9)	706 (39.0)
≥81	2,820 (2.2)	651 (35.9)
Unknown	139 (0.1)	0
Age group, y, has any comorbidity, no. (%)*		
21–64†	20,844 (22.3)	252 (55.9)
65–80	5,043 (50.0)	467 (66.2)
≥81	1441 (51.1)	454(69.7)
All age groups	28,925 (22.6)	1,174 (64.8)
Incomplete comorbidity data, no. (%)‡	38,949 (30.4)	369 (20.3)
Mean (SD) days to hospitalization§	3.9 (5.4)	3.2 (5.8)
Mean (SD) days for obtaining specimen	1.8 (3.7)	1.8 (4.1)

*Includes persons who have incomplete comorbidity; data counted as having no comorbidity.
†Cell percent is the percentage within that age group (i.e., for living case-patients 21–64 years of age, the percentage is 20,844/94,486).
‡Incomplete comorbidity data were defined as any chart without a single recorded response for any preexisting condition or comorbidity.
§Days to hospitalization for living patients are only calculated for case-patients hospitalized because of coronavirus disease (n = 5,379).

higher than that for White patients (Table 2). Hispanic patients had the lowest rate of underlying medical conditions (64.3%) compared with White patients (85.7%) and Black patients (91.3%). However, Hispanic case-patients had the highest percent increase in number of comorbidities when comparing standard surveillance and chart-abstraction (Figure 2).

During March 15, 2020–May 19, 2020, there were 355 deaths; 188 of these patients who died had complete medical records available for chart abstraction. Standard surveillance and chart abstraction had comparable frequencies of race/ethnicity, proportion of females, and age (Table 3). Chart abstraction detected a higher proportion of case-patients with >1 comorbidity (96.3%) compared with standard surveillance deaths (79.0%) (Table 3). After stratifying by race and age, we found that chart abstraction still found more comorbidities in each age group and race group (Figure 2; Appendix 2). Compared with standard surveillance, chart-abstracted deaths had a higher proportion of hypertension (76.6% vs. 50.2%), CVDs (54.3% vs. 40.6%), CLD (29.8% vs. 20.5%), cancer (10.6% vs. 4.3%), and chronic renal disease (27.1% vs. 19.0%). However, there was minimal difference in proportion of case-patients who had diabetes (39.9% vs. 36.6%). Data for chart-abstracted deaths showed a higher proportion of current/former smoking (30.3% vs. 15.3%) when compared with the standard surveillance group.

Discussion

Our findings demonstrate that Tennessee has similar COVID-19 demographic trends to those that have been found throughout the United States (*21*,*22*). In our sample, the average age of case-patients who died was 72.9 years compared with 38.4 years for the surviving cases. Black patients were disproportionately affected by COVID-19; at the time of our analysis, 29.8% of deaths were in Black persons , but only 17.1% of the population of Tennessee identifies as Black (*23*). Hispanic patients accounted for 7.0% of deaths and 5.7% of the population in Tennessee; White patients represented 60.3% of the deaths but 73.5% of the population (*23*).

Table 2. Case-fatality rate stratified by race and age for characteristics, comorbidities, and data gaps for coronavirus disease deaths, Tennessee, USA

Characteristic	White, non-Hispanic, n = 46,677	Black, non-Hispanic, n = 16,669	Hispanic, n = 17,084
Mean age, y (interquartile range)	40 (25–57)	37 (25–52)	32 (21–45)
Age group, y, case-fatality rate, no. (%)*	896 (1.9)	428 (2.6)	84 (0.5)
21–64†	145 (0.4)	140 (1.1)	42 (0.3)
65–80	344 (5.9)	176 (12.1)	31 (9.0)
≥81	406 (19.6)	112 (28.6)	10 (18.2)

*There was 1 death for a White patient (<1–21 year age group) and 1 death for a Hispanic patient (<1–21 year age group).
†Cell percent is the case-fatality percentage for that age and race group.

Table 3. Characteristics and comorbidities for patients with coronavirus disease, Tennessee, USA*

Characteristic	Coronavirus disease deaths	
	Standard surveillance, n = 1,255	Chart-abstracted, n = 188
Race and ethnicity, no. (%)†		
White, non-Hispanic	787 (62.7)	109 (58.0)
Black, non-Hispanic	365 (29.1)	63 (33.6)
Hispanic (all races)	74 (5.9)	10 (5.3)
Sex, no. (%)		
F	549 (43.7)	79 (42.0)
M	706 (56.3)	109 (58.0)
Mean age, y, (SD)	73.6 (13.9)	72.7 (14.4)
Current/former smoker, no. (%)	192 (15.3)	57 (30.3)
Mean no. (SD) comorbidities	2.0 (1.5)	2.9 (1.6)
Age group, y, has any comorbidity, no. (%)†		
21–64: Nss = 284; Nca = 50	205 (72.2)	47 (94.0)
65–80: Nss = 505; Nca = 63	404 (80)	62 (98.4)
≥81: Nss = 465; Nca = 74	382 (82.2)	72 (97.3)
All ages: Nss = 1,254; Nca = 188	991 (79.0)	181 (96.3)
Comorbidities, no. (%)		
Hypertension	630 (50.2)	144 (76.6)
Cardiovascular disease‡	509 (40.6)	102 (54.3)
Chronic lung disease§	257 (20.5)	56 (29.8)
Diabetes mellitus	459 (36.6)	75 (39.9)
Obesity	156 (12.4)	42 (22.3)
Cancer	54 (4.3)	20 (10.6)
Chronic renal disease	238 (19.0)	51 (27.1)
Chronic liver disease	34 (2.7)	6 (2.7)
Immunocompromised	76 (6.1)	18 (9.6)
Autoimmune diseases	21 (1.7)	8 (4.3)
HIV/AIDS	5 (0.4)	1 (0.5)

*Nca, no. patients who had chart abstraction for that age group; Nss, no. patients who had standard surveillance for that age group.
†Cell percent is the percentage in that age group (i.e., for standard surveillance case-patients 21–64 years of age, the percentage is 205/284).
‡Defined as coronary artery disease, cerebrovascular, peripheral artery disease, heart failure, cardiomyopathies, valvular disease, myocarditis, and arrythmias. Hypertension is listed separately.
§Defined as asthma, chronic obstructive pulmonary disease, emphysema, pulmonary hypertension, interstitial fibrosis, or sarcoidosis.

We also found major differences in CFRs for race/ethnicity: Hispanic patients had the lowest CFR (0.5%) compared with that for White patients (1.9%) and Black patients (2.6%). The lower CFR for Hispanic patients differs from US aggregate data, in which Hispanic patients have a 2.8 times higher rate of death than do White patients (*24*). In Tennessee, Hispanic patients were younger than Black and White patients, and because age is the strongest predictor of death from COVID-19 (*5*,*11*,*25*), the age difference might explain this difference in CFR for Hispanic patients in Tennessee. After stratifying by age, we found that Hispanic case-patients had CFRs similar to those for White case-patients, but Black case-patients maintained the highest CFR. In a similar fashion, CDC data have demonstrated that Hispanic patients had the largest increase in CFR once adjusted for age (*21*). Studies have demonstrated that race and ethnicity are associated with COVID-19 infection and death (*8*,*26*). However, several reviews of in-hospital death data have demonstrated that race/ethnicity is not an independent risk factor for death after admission to the hospital (*11*,*26*,*27*). Taken together, these data suggest that the disproportionate burden of COVID-19 deaths among racial and ethnic minorities is secondary to systemic health and social inequities that have limited access to chronic disease management and increased the rate of COVID infection for these populations, rather than inherent difference between races and ethnicities (*28*).

The trend in Tennessee for comorbidities for COVID-19 patients who died also mirrors the rest of the nation (*29*); 22.6% of surviving case-patients had comorbidities, compared with 64.8% of those who died. After stratifying by age, we found that a higher percentage of deceased case-patients still had an underlying condition than did living case-patients. Hypertension, CVD, CLD, cancer, chronic renal disease, diabetes, and a history of smoking were more common among deceased case-patients (Appendix 1). These correlations have been found in other studies and systemic reviews in the United States and worldwide, which have had major implications for public health messaging and vaccine allocation (*29*).

The chart review process detected higher numbers of comorbidities than standard surveillance. In the standard surveillance group, 79.0% had a comorbidity, compared with 96.3% in the chart-abstracted group. The difference between the standard surveillance and chart-abstracted group probably

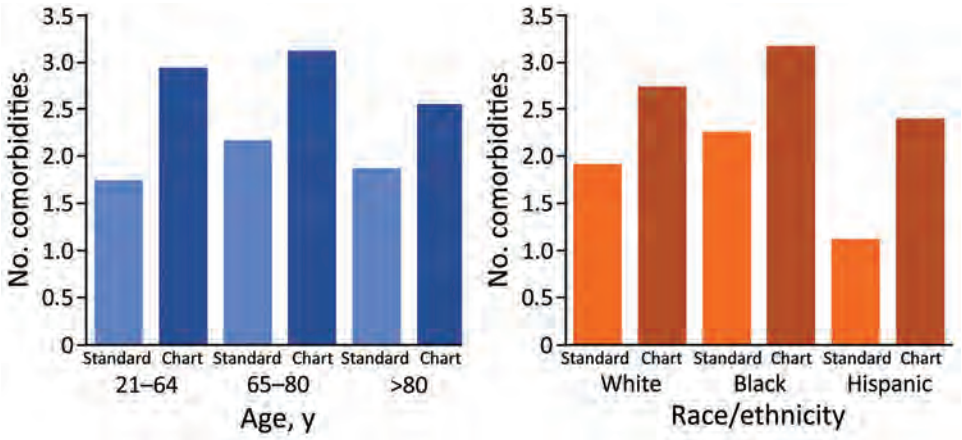

Figure 2. Number of comorbidities by age, race, and type of review for characteristics, comorbidities, and data gaps for coronavirus disease deaths, Tennessee, USA.

reflects issues with self-reporting and data collection. In a CDC review of COVID-19 deaths during February 12–May 18, 2020, a total of 58.9% of patients had missing comorbidity information according to CRF-based surveillance data (*6*). In our study, 30.4% of living case-patients and 20.3% of deceased case-patients had no comorbidity data recorded. The prevalence of deceased patients who had an underlying condition in our chart-abstracted group (96.3%) is similar to that for CDC COVID-19 hospitalization records (COVID-NET), which found 405 (96.4%) of 420 deaths had an underlying medical condition (*25*). This finding emphasizes that medical chart-abstraction data collects higher rates of comorbidity data than does standard public health surveillance and is a more comprehensive representation of baseline characteristics among COVID-19 patients.

For each race and age group, we found a higher number of comorbidities recorded with chart abstraction than with standard surveillance (Figure 2). In the standard surveillance group, Hispanic patients had a lower number of comorbidities than White and Black patients. Other studies have reported mixed results; Hispanic COVID-19 patients who died had more or fewer comorbidities than non-Hispanic patients (*25*,*27*). In our chart-abstracted group, the total number of comorbidities for Hispanic patients was twice that of the standard surveillance group, which was the largest increase for race/ethnicity (Appendix 2). For the standard surveillance group, information was gathered by in person or telephone conversations. Therefore, language barriers and concerns about disclosure of information are 2 possible explanations for the lower number of comorbidities recorded. It has been shown that non-English–speaking patients are more likely to have inaccurate medical information, to receive lower quality care, and are at a higher risk for medical errors that result in harm (*30*,*31*). Taken together, our findings demonstrate the value of chart abstractions to obtain accurate information for Hispanic and non–English speaking patients during disease surveillance.

We observed notable trends in the prevalence of certain comorbidities in the standard surveillance deaths compared with the chart-abstracted deaths. For example, hypertension, CVD, and CLD were detected in higher frequencies in the chart-abstracted group, and diabetes had similar rates in chart-abstraction and standard surveillance. Similarly, in multiple studies worldwide comparing self-reports and medical records, diabetes was the disease with the highest concordance (*32*–*34*); hypertension and CVD are frequently underreported in self-reports (*32*,*35*). Therefore, diabetes is probably better captured by standard interview-based surveillance than other comorbidities. A meta-analysis of 87 studies determined that diabetes was the comorbidity that had the highest association with COVID-19 deaths (*36*). Diabetes certainly increases risk for COVID-19 deaths, but it is possible that the high accuracy of diabetes disease reporting could disproportionately increase the association between diabetes and COVID-19 death compared with other comorbidities. In addition, there is mixed evidence about whether hypertension is an independent risk factor for death (*29*); part of this difference could be explained by data collection and inaccurate reporting by patients.

One limitation of our study is that we used a convenience sample of COVID-19 cases collected by the TDH, which led to collection biases. For our comorbidity analysis, we excluded cases without any comorbidity information, which led to selection bias. Our chart-abstracted study occurred at the beginning of the pandemic and does not capture the burden of COVID-19 for certain ethnic and geographic groups who had more cases later in the pandemic. For example, there were 126 deaths in Hispanic COVID-19 patients and only 10 patients in the Hispanic chart-abstracted group. Furthermore, our chart-abstracted

study relied on medical charts, which created selection bias and missed patients who died outside hospitals. There might be certain groups who are more likely to have out-of-hospital deaths, but these deaths were not evaluated in our study. The data collection process was different for the standard surveillance deaths and the chart-abstracted deaths, which limited the validity of comparing the frequencies of characteristics and comorbidities. Despite these limitations, we analyzed a large number of patients, and analyzed COVID-19 demographic trends for Tennessee for comparison to other states. In addition, our chart-abstraction analysis is a description of a public health study that met its goal to capture additional information compared with standard surveillance.

Our chart-based analysis showed that comorbidities related to COVID-19 deaths are more prevalent than those identified by standard public health disease surveillance. Furthermore, certain patient information tends to be reported less accurately in standard surveillance than in chart-based analysis. However, chart-based reviews are labor and time intensive, and the COVID-19 pandemic has highlighted how public health agencies are understaffed and underfunded (*9*). One solution for the challenges of data collection in public health disease surveillance is expansion of electronic case reporting. This type of reporting uses an interoperable, shared service infrastructure to enable automated real-time exchange of information from electronic medical records to public health agencies (*37*). In traditional case reporting, the most cases are reported from laboratories who lack detailed information on case demographics and often send their reports by paper copy. Therefore, public health departments receive incomplete information, which creates data gaps and distorted data, which is also apparent in our findings. In contrast, electronic case reporting provides faster and more complete data from healthcare institutions while decreasing the burden on reporters and public health departments (*37*). During the COVID-19 pandemic, there has been increased uptake in electronic case reporting, and continuing this trend is essential for effective disease surveillance (*38*).

Throughout the COVID-19 pandemic, data collected by public health agencies have been integral in identifying trends and providing information to health agencies (*39*). The surveillance data from Tennessee demonstrate trends in age, comorbidities, and race/ethnicity that mirror the rest of the country, and this data been used to protect those at highest risk for severe COVID-19 disease. Our study showed that chart abstraction collects more comorbidity data than standard public health disease surveillance. In addition, certain diseases and patient groups are frequently underreported in standard surveillance, which skews public health data. These data gaps can miss at risk groups and can lead to unadvised public health action. Investment in data collection infrastructure that collects more timely and complete data will equip public health institutions, governmental organizations, and the scientific community with accurate information required to mitigate disease burden in COVID-19 and future outbreaks.

Acknowledgments

We thank members of the Division of Communicable and Environmental Disease and Emergency Preparedness, Tennessee Department of Health for their support in data collection and storage.

About the Author

Dr. Parker is an internal medicine and pediatric resident at Vanderbilt University Medical Center, Nashville, TN. His primary research interest is COVID-19.

References

1. World Health Organization. Coronavirus disease, 2020 [cited 2021 Mar 5]. https://covid19.who.int
2. Tennessee Department of Health. Data dashboard, Jan 10, 2020 [cited 2021 Mar 5]. https://www.tn.gov/health/cedep/ncov/data.html
3. Johns Hopkins Coronavirus Resource Center. All state comparison of testing efforts, Jul 6, 2021 [cited 2021 Mar 5]. https://coronavirus.jhu.edu/testing/states-comparison
4. Jin J, Agarwala N, Kundu P, Harvey B, Zhang Y, Wallace E, et al. Individual and community-level risk for COVID-19 mortality in the United States. Nat Med. 2021;27:264–9. https://doi.org/10.1038/s41591-020-01191-8
5. Williamson EJ, Walker AJ, Bhaskaran K, Bacon S, Bates C, Morton CE, et al. Factors associated with COVID-19-related death using OpenSAFELY. Nature. 2020;584:430–6. https://doi.org/10.1038/s41586-020-2521-4
6. Wortham JM, Lee JT, Althomsons S, Latash J, Davidson A, Guerra K, et al. Characteristics of persons who died with COVID-19—United States, February 12–May 18, 2020. MMWR Morb Mortal Wkly Rep. 2020;69:923–9. https://doi.org/10.15585/mmwr.mm6928e1
7. Deng G, Yin M, Chen X, Zeng F. Clinical determinants for fatality of 44,672 patients with COVID-19. Crit Care. 2020;24:179. https://doi.org/10.1186/s13054-020-02902-w
8. Pan D, Sze S, Minhas JS, Bangash MN, Pareek N, Divall P, et al. The impact of ethnicity on clinical outcomes in COVID-19: a systematic review. EClinicalMedicine. 2020;23:100404. https://doi.org/10.1016/j.eclinm.2020.100404
9. Dixon BE, Caine VA, Halverson PK. Deficient response to COVID-19 makes the case for evolving the public health system. Am J Prev Med. 2020;59:887–91. https://doi.org/10.1016/j.amepre.2020.07.024
10. Centers for Disease Control and Prevention. Improving public health Surveillance, 2020 [cited 2021 Jun 2]. https://www.cdc.gov/surveillance/improving-surveillance/index.html

11. Price-Haywood EG, Burton J, Fort D, Seoane L. Hospitalization and mortality among black patients and white patients with COVID-19. N Engl J Med. 2020;382:2534–43. https://doi.org/10.1056/NEJMsa2011686
12. Richardson S, Hirsch JS, Narasimhan M, Crawford JM, McGinn T, Davidson KW, et al.; Northwell COVID-19 Research Consortium. Presenting characteristics, comorbidities, and outcomes among 5,700 patients hospitalized with COVID-19 in the New York City area. JAMA. 2020;323:2052–9. https://doi.org/10.1001/jama.2020.6775
13. Mueller JT, McConnell K, Burow PB, Pofahl K, Merdjanoff AA, Farrell J. Impacts of the COVID-19 pandemic on rural America. Proc Natl Acad Sci U S A. 2021;118:2019378118. https://doi.org/10.1073/pnas.2019378118
14. Centers for Disease Control and Prevention. Coronavirus disease 2019 (COVID-19), 2020. Interim case definition, approved August 5, 2020 [cited 2021 Feb 13]. https://ndc.services.cdc.gov/case-definitions/coronavirus-disease -2019-2020-08-05
15. Council of State and Editorial Epidemiologists. Interim-20-ID-02_COVID-19. [cited 2020 Sep 8]. https://cdn.ymaws.com/www.cste.org/resource/resmgr/ps/positionstatement2020/Interim-20-ID-02_COVID-19.pdf
16. Tennessee Department of Health. COVID-19 case definition [cited 2021 Jul 6]. https://www.tn.gov/content/dam/tn/health/documents/cedep/novel-coronavirus/COVID-Case-Definition.pdf
17. Centers for Disease Control and Prevention. pui-form [cited 2020 Jun 6]. https://www.cdc.gov/coronavirus/2019-ncov/downloads/pui-form.pdf
18. American Heart Association. What is cardiovascular disease? [cited 2020 Dec 14]. https://www.heart.org/en/health-topics/consumer-healthcare/what-is-cardiovascular-disease
19. World Health Organization. About cardiovascular diseases [cited 2020 Dec 14]. https://www.who.int/cardiovascular_diseases/about_cvd/en/
20. World Health Organization. Chronic respiratory diseases [cited 2020 Dec 14]. https://www.who.int/westernpacific/health-topics/chronic-respiratory-diseases
21. Centers for Disease Control and Prevention. COVID-19 provisional counts: health disparities, 2020 [cited 2020 Dec 13]. https://www.cdc.gov/nchs/nvss/vsrr/covid19/health_disparities.htm
22. Centers for Disease Control and Prevention. COVID-19 provisional counts: weekly updates by select demographic and geographic characteristics, 2020 [cited 2020 Dec 13]. https://www.cdc.gov/nchs/nvss/vsrr/covid_weekly/index.htm
23. US Census Bureau. Quick Facts Tennessee [cited 2020 Dec 12]. https://www.census.gov/quickfacts/TN
24. Centers for Disease Control and Prevention. COVID-19 hospitalization and death by race/ethnicity, 2020 [cited 2020 Dec 23]. https://www.cdc.gov/coronavirus/2019-ncov/covid-data/investigations-discovery/hospitalization-death-by-race-ethnicity.html
25. Kim L, Garg S, O'Halloran A, Whitaker M, Pham H, Anderson EJ, et al. Risk Factors for intensive care unit admission and in-hospital mortality among hospitalized adults identified through the U.S. coronavirus disease 2019 (COVID-19)–associated Hospitalization Surveillance Network (COVID-NET). Clin Infect Dis. 2021;72:e206–14. https://doi.org/10.1093/cid/ciaa1012
26. Golestaneh L, Neugarten J, Fisher M, Billett HH, Gil MR, Johns T, et al. The association of race and COVID-19 mortality. EClinicalMedicine. 2020;25:100455. https://doi.org/10.1016/j.eclinm.2020.100455
27. xKabarriti R, Brodin NP, Maron MI, Guha C, Kalnicki S, Garg MK, et al. Association of race and ethnicity with comorbidities and survival among patients with COVID-19 at an urban medical center in New York. JAMA Netw Open. 2020;3:e2019795. https://doi.org/10.1001/jamanetworkopen.2020.19795
28. Centers for Disease Control and Prevention. Communities, schools, workplaces, and events, 2020 [cited 2020 Dec 13]. https://www.cdc.gov/coronavirus/2019-ncov/community/health-equity/race-ethnicity.html
29. Centers for Disease Control and Prevention. COVID-19 and your health, 2020 [cited 2020 Dec 12]. https://www.cdc.gov/coronavirus/2019-ncov/need-extra-precautions/evidence-table.html
30. Divi C, Koss RG, Schmaltz SP, Loeb JM. Language proficiency and adverse events in US hospitals: a pilot study. Int J Qual Health Care. 2007;19:60–7. https://doi.org/10.1093/intqhc/mzl069
31. Green AR, Nze C. Language-based Inequity in health care: who is the "poor historian"? AMA J Ethics. 2017;19:263–71. https://doi.org/10.1001/journalofethics.2017.19.3.medu1-1703
32. Frost M, Wraae K, Gudex C, Nielsen T, Brixen K, Hagen C, et al. Chronic diseases in elderly men: underreporting and underdiagnosis. Age Ageing. 2012;41:177–83. https://doi.org/10.1093/ageing/afr153
33. van den Akker M, van Steenkiste B, Krutwagen E, Metsemakers JFM. Disease or no disease? Disagreement on diagnoses between self-reports and medical records of adult patients. Eur J Gen Pract. 2015;21:45–51. https://doi.org/10.3109/13814788.2014.907266
34. Kriegsman DM, Penninx BW, van Eijk JT, Boeke AJ, Deeg DJ. Self-reports and general practitioner information on the presence of chronic diseases in community dwelling elderly. A study on the accuracy of patients' self-reports and on determinants of inaccuracy. J Clin Epidemiol. 1996;49:1407–17. https://doi.org/10.1016/S0895-4356(96)00274-0
35. Peterson KL, Jacobs JP, Allender S, Alston LV, Nichols M. Characterising the extent of misreporting of high blood pressure, high cholesterol, and diabetes using the Australian Health Survey. BMC Public Health. 2016;16:695. https://doi.org/10.1186/s12889-016-3389-y
36. Corona G, Pizzocaro A, Vena W, Rastrelli G, Semeraro F, Isidori AM, et al. Diabetes is most important cause for mortality in COVID-19 hospitalized patients: systematic review and meta-analysis. Rev Endocr Metab Disord. 2021;22:275–96. https://doi.org/10.1007/s11154-021-09630-8
37. Centers for Disease Control and Prevention. How does electronic case reporting work? 2020 [cited 2021 Feb 15]. https://www.cdc.gov/ecr/index.html
38. American Medical Association. Why it's essential to improve data collection and reporting [cited 2021 Feb 15]. https://www.ama-assn.org/delivering-care/public-health/why-it-s-essential-improve-data-collection-and-reporting
39. Centers for Disease Control and Prevention. Coronavirus disease 2019 (COVID-19): transmission, 2020 [cited 2020 Dec 26]. https://www.cdc.gov/coronavirus/2019-ncov/covid-data/faq-surveillance.html

Address for correspondence: J.J. Parker, Attn: Mary-Margaret Fill, 710 James Robertson Pkwy, 4th Fl, Andrew Johnson Tower, Communicable and Environmental Diseases and Emergency Preparedness, Nashville, TN 37243, USA; email: jjparker847@gmail.com

Fatal Exacerbations of Systemic Capillary Leak Syndrome Complicating Coronavirus Disease

Patricia C. Cheung, A. Robin Eisch, Noble Maleque, Derek M. Polly, Sara C. Auld, Kirk M. Druey

We report 2 fatal exacerbations of systemic capillary leak syndrome (SCLS), also known as Clarkson disease, associated with coronavirus disease (COVID-19) in the United States. One patient carried an established diagnosis of SCLS and the other sought treatment for new-onset hypotensive shock, hemoconcentration, and anasarca, classic symptoms indicative of an SCLS flare. Both patients had only mild-to-moderate symptoms of COVID-19. This clinical picture suggests that these patients succumbed to complications of SCLS induced by infection with severe acute respiratory syndrome coronavirus 2. Persons with known or suspected SCLS may be at increased risk for developing a disease flare in the setting of mild-to-moderate COVID-19 infection.

Systemic capillary leak syndrome (SCLS), also known as Clarkson disease, is a rare disease of unknown etiology that most commonly develops in adults 50–70 years of age (*1*). Since SCLS was first characterized in 1960, <500 cases have been described in the medical literature. The current prevalence of SCLS is estimated to be <250 cases worldwide (*1*), although the disease is likely underdiagnosed.

SCLS is diagnosed clinically on the basis of a characteristic symptomatic triad of hypotension, hemoconcentration (elevated hemoglobin or hematocrit), and serum hypoalbuminemia resulting from fluid extravasation. Patients with SCLS experience transient and reversible episodes of plasma leakage into peripheral tissues, which lead to the acute onset of hypotensive shock and the development of anasarca after intravenous (IV) fluid resuscitation. Severe SCLS flares commonly result in multisystem organ failure and peripheral compartment syndromes (*2*). Between episodes, patients are typically asymptomatic.

Minor infections, typically of the upper respiratory tract, are common triggers for SCLS, although an infection-related prodrome is identified in only 44%–65% of cases (*2*,*3*). Although >80% of SCLS patients have a monoclonal gammopathy of unknown significance (MGUS), the role of this finding in disease pathogenesis remains unclear; the absence of MGUS does not exclude a diagnosis of SCLS (*4*). Interventions for acute SCLS episodes are limited to supportive measures, but monthly prophylaxis with high dose (1–2 g/kg patient weight) IV immunoglobulin (IVIg) prevents attacks among >90% of patients and provides them with a statistically significant survival advantage compared with those patients who were not treated with IVIg (*5*,*6*). Here we report the cases of 2 patients who died of severe SCLS soon after seeking treatment for mild-to-moderate symptoms of COVID-19; neither of them had been receiving IVIg prophylaxis beforehand.

Methods

Patients were referred to the National Institutes of Health (NIH) for evaluation of suspected SCLS. Where applicable, patients provided written informed consent to participate in a natural history protocol (09-I-0184) approved by the NIH institutional review board. We followed the CARE guidelines for writing medical case reports in the preparation of this manuscript.

Case Reports

Case 1

A 59-year-old woman with a history of hypertension but no known history of SCLS or prior episodes of peripheral edema was admitted to a hospital in January 2021 with a 6-day history of cough, shortness of breath, and lower extremity pain. She was hypotensive,

Author affiliations: Emory University School of Medicine and Rollins School of Public Health, Atlanta, Georgia, USA (P.C. Cheung, N. Maleque, S.C. Auld); National Institute of Allergy and Infectious Diseases/National Institutes of Health, Bethesda, Maryland, USA (A.R. Eisch, K.M. Druey); Emory University Hospital Midtown Department of Pharmacy, Atlanta (D.M. Polly)

DOI: https://doi.org/10.3201/eid2710.211155

with a blood pressure of 96/70 mm Hg, but her initial physical exam was otherwise unremarkable and included normal results for a pulmonary examination. Laboratory examination revealed hemoconcentration (hemoglobin 17.1 g/dL, hematocrit of 52%) and a lactic acid level of 3.7 mmol/L. Despite resuscitation with 5.5 L Ringer's lactate and 2.5 L normal saline IV fluids over the first 3 days of admission, serum lactate levels remained elevated at 5.7 mmol/L on day 4 of hospitalization (Table 1). Lower extremity pain worsened, and anasarca without hypoxemia developed. SARS-CoV-2 PCR testing of a nasal swab specimen taken at the time of admission returned positive results; daily treatment with 6 mg dexamethasone and 40 mg enoxaparin was initiated. Remdesivir was not administered because of a developing acute kidney injury. The patient's lung examination results remained unremarkable, but she became intermittently hypoxemic (SpO_2 of 88% on 2L nasal cannula), requiring ongoing nasal cannula support. A chest computed tomography revealed bilateral scattered ground glass opacities consistent with mild-to-moderate SARS-CoV-2 infection (Figure). A transthoracic echocardiogram performed on day 3 of hospitalization showed a normal left ventricular ejection fraction (70%–75%), no left ventricular dilation or geometric changes, and no wall motion abnormalities. Other laboratory abnormalities included increased creatinine phosphokinase levels, peaking at 15,094 units/L; elevated lactate at 6.3 mmol/L; and hypoalbuminemia at 2.4 g/dL, which raised concerns for SCLS.

The patient was transferred to the intensive care unit for further monitoring on day 4 of hospitalization. Pain increased in her extremities and tense anasarca developed; however, because compartment pressures were 18 mm Hg in her right arm and 15 mm Hg in her left arm, she did not meet criteria for a diagnosis of compartment syndrome. Apart from edema and tachypnea while on 2 L nasal cannula, her cardiopulmonary examination was otherwise normal. On hospitalization day 5, she suffered a cardiac arrest; spontaneous circulation returned after 2 rounds of cardiopulmonary resuscitation. She was intubated at the time of cardiac arrest and empirically started on vancomycin and cefepime. Because of concern for microvascular thrombi in the setting of SARS-CoV-2 infection, an argatroban infusion was started. Although the patient had remained afebrile and hemodynamically stable up to this point, shock rapidly developed, and she required vasopressor support with norepinephrine, vasopressin, epinephrine, and stress-doses of hydrocortisone. Continuous renal replacement therapy was initiated for oliguric renal failure.

The next day, edema in the extremities intensified, and creatinine phosphokinase levels increased further to >45,000 units/L, but compartment pressures were 17 mm Hg in her right arm and 16 mm Hg in her left arm, suggestive of rhabdomyolysis without compartment syndrome. No MGUS was detected. Serum SARS-CoV-2 IgG was not detected, prompting treatment with convalescent plasma. Given the patient's grave condition and lack of proven interventions for acute SCLS, empiric treatments were also administered, including IVIg; methylene blue, an agent that suppresses downstream effects of nitric oxide (*7*); and icatibant, a bradykinin receptor antagonist used to treat vascular leakage associated

Table 1. Laboratory values during hospitalization for case-patient 1 with systemic capillary leak syndrome and coronavirus disease*

Test	Reference range	Admission, 2021 Jan 31	Hospital floor, 2021 Feb 2	Hospital floor/ ICU, 2021 Feb 3	ICU, 2021 Feb 4	ICU, 2021 Feb 5
Albumin	3.5–5.7 g/dL	3.8	3.2	2.4	2.1	2.3
Hemoglobin	11.4–14.4 g/dL	17.1	20.3	17.4	14.5	8.7
Hematocrit	33.3%–41.4%	52.0	61.0	52.6	44.8	26.7
Creatinine	0.6–1.2 mg/dL	0.95	1.2	1.42	1.80	0.85[a]
Sodium	136–145 mmol/L	132	129	126	129	129
Potassium	3.5–5.1 mmol/L	4.3	4.7	5.6	6.1	6.5
Phosphate	2.5–5.0 mg/dL	NA	6.1	5.1	6.9	8.0
Alanine transaminase	7–52 unit/L	32	26	92	299	7,928
Troponin	≤0.04 ng/mL	0.04	<0.03	NA	0.23	0.50
Creatine kinase	30–223 unit/L	NA	1,851	15,094	41,696	>45,000
C-reactive protein	≤10 mg/L	NA	12.8	42.2	41.8	58.1
Leukocytes	4.0–10.0 10^3/μL	7.0	9.7	19.5	25.3	12.6
Platelets	150–400 10^3/μL	184	158	145	170	71
Lactate	0.5–2.2 mmol/L	4.6	6.3	5.7	8.2	10.5
D-dimer	≤574 ng/mL	475	NA	1,016	1,271	9,536
International normalized ratio	Not applicable	NA	0.97	NA	1.23	3.29
Activated partial thromboplastin time	26.5–36.5 s	NA	NA	NA	NA	148.9
Complement C3	81–157 mg/dL	NA	NA	NA	74	NA
Complement C4	13–39 mg/dL	NA	NA	NA	22	NA

*ICU, intensive care unit; NA, not available

Figure. Chest computed tomography from hospital day 3 for a 59-year-old woman (case-patient 1) with new-onset systemic capillary leak syndrome and coronavirus disease showing A) the upper and B) lower lung fields in axial plane and C) the coronal plane. The scans showed bilateral scattered ground glass opacities consistent with mild-to-moderate infection with severe acute respiratory syndrome coronavirus 2.

with hantavirus infection (*8*). Bradycardia developed and ultimately required transvenous pacing. Within hours, her hemoglobin decreased to 6.8 g/dL although there was no obvious source of hemorrhage. Because she was anticoagulated with argatroban and had a prolonged activated partial thromboplastin time in the setting of acute liver failure, the patient was transfused with packed erythrocytes. She suffered cardiac arrest, and ventricular fibrillation deteriorated into pulseless electrical activity. Transthoracic echocardiography performed during ACLS revealed no pericardial effusion. The patient received additional units of erythrocytes, IV fluids, fresh frozen plasma, and prothrombin complex concentrate during the cardiac arrest. However, spontaneous circulation was not restored, and the patient died on day 6 of her hospitalization.

Case 2

A 36-year-old man with no notable medical history first sought treatment in 2015 for transient hypotension and severe bilateral lower-extremity edema; laboratory testing showed hemoconcentration (hemoglobin 20.2 g/dL, hemocrit 59.4%) and a serum hypoalbuminemia level of 2.2 g/dL after several days of fevers and upper respiratory symptoms. SCLS was diagnosed on the basis of characteristic clinical presentation and an IgG lambda MGUS. His course was complicated by acute kidney injury and compartment syndromes in both legs, which required bilateral fasciotomies. He also had deep vein thromboses in the right internal jugular and left cephalic veins. He was treated transiently with anticoagulants, but a full evaluation for hypercoagulability was negative. Muscle biopsies taken at the time of fasciotomies provided no evidence of inflammatory myositis. All symptoms resolved before he was discharged from the hospital, although a bilateral sensorimotor neuropathy developed, presumably as a residual effect of compartment syndrome.

The patient was treated with IVIg (2 g/kg) within 24 hours of the 2015 hospitalization and monthly thereafter with no recurrence of his SCLS-related symptoms. In November 2016, IVIg prophylaxis was discontinued at the patient's request. In 2017 and 2018, the patient experienced 2 episodes of bilateral lower extremity swelling, in both cases after several days of upper respiratory symptoms. Blood pressure and laboratory tests were normal at the time of these episodes, and swelling resolved without further treatment.

In February 2020, the patient sought treatment for a several-day history of fevers (40°C) and productive cough. He was noted to be hypoxemic (SpO_2 of 87% on room air). *Mycoplasma* pneumonia was diagnosed on the basis of chest radiographic evidence of lung infiltrates and positive *Mycoplasma* serologic testing. He was hospitalized and treated with IV antimicrobial drugs and fluids (10.5 L total). Although the fevers and respiratory symptoms resolved, bilateral leg swelling and serum hypoalbuminemia developed, prompting treatment with 1 dose of IVIg (2 g/kg) for empirically presumed SCLS-related edema in the absence of any other proven treatment options. He ultimately recovered and experienced no residual symptoms.

In January 2021, the patient was transported to the emergency department because of disorientation after several days of upper respiratory symptoms, fever (40.6°C), and back pain. Upon arrival, he was hypotensive, with a blood pressure of 94/20 mm Hg, and tachycardic at 140 beats/min. Upon initial examination, he showed no signs of apparent dyspnea (respiratory rate of 19 breaths/min) or respiratory distress (SpO_2 of 99% on room air). A PCR nasal swab test for SARS-CoV-2 performed on the day

Table 2. Clinical characteristics of acute SCLS compared with severe COVID-19*

Parameter	SCLS	COVID-19
Blood pressure	Low/undetectable, vasopressor-resistant	Normal/high
Hgb/Hct	Very elevated	Normal/low
Serum albumin	Very low	Normal/low
Pulmonary findings	Absent	Lung infiltrates, tachypnea, hypoxemia
Edema	Anasarca, compartment syndrome	Pulmonary edema; no peripheral edema
Creatine kinase	Very elevated	Normal/elevated
Creatinine	Elevated, acute kidney injury common	Normal

*COVID-19, coronavirus disease; Hgb/Hct, hemoglobin/hematocrit ratio; SCLS, systemic capillary leak syndrome.

before he sought treatment was reported by the family to be positive. Laboratory tests taken at the time of hospital admission revealed severe hemoconcentration (hemoglobin >25 g/dL, 75% hemocrit), leukocytosis (leukocyte count 43.3K/μL blood), and lactic acidosis (lactate level 9.2 mmol/L). Other laboratory values included brain natriuretic peptide at 12 pg/mL, troponin at <0.02 ng/mL, and a fingerstick glucose level of 197 mg/dL. There was no ST elevation suggesting myocardial infarction or dysrhythmia on his electrocardiogram.

In the emergency department, his condition deteriorated rapidly. His blood pressure became unobtainable manually, and he exhibited an $Sp0_2$ of 73% on a 15-L nonrebreather mask. A bedside echocardiogram revealed a flat inferior vena cava, intact bilateral ventricular function, and pericardial effusion with no evidence of right heart strain or tamponade. He was intubated emergently but ultimately experienced cardiac arrest with pulseless electrical activity. Despite aggressive cardiopulmonary resuscitation and pharmacological interventions including boluses of epinephrine, bicarbonate, calcium, and magnesium, refractory ventricular tachycardia developed, followed by Torsade de Pointes, and he died shortly thereafter.

Discussion

We report 2 cases of SCLS associated with mild-to-moderate COVID-19 infection. Case-patient 1 exhibited the clinical diagnostic triad for SCLS: hypotension, hemoconcentration, and hypoalbuminemia. Case-patient 2 carried a prior diagnosis of SCLS. These findings suggest that patients with SCLS may be at high risk for exacerbations or even death if they contract COVID-19.

Information from our studies complements the findings of several recent case reports of severe SCLS attacks associated with mild-to-moderate SARS-CoV-2 infection (*9*–*12*). In each of the cases in those studies, patients exhibited all the hallmarks of severe SCLS exacerbations after experiencing mild-to-moderate symptoms of COVID-19; 2 of 3 patients died from SCLS-related complications.

Because COVID-19 had not previously been associated with secondary capillary leak syndrome and there were no other obvious triggers for the episode in case-patient 1 in our study, it is highly likely that she carried latent SCLS even though MGUS was not detected at the time of the episode. Although MGUS is an important clue, it is not detected in all patients with SCLS. In the most recent comprehensive reviews of the literature, which included 290 cases reported during 1960–2016, MGUS was detected in only ≈75% of case-patients (*3*). Although MGUS was detected in 34 (91%) of 37 patients in a 2017 study (*2*), the authors emphasized that "the three monoclonal gammopathy-negative patients had typical severe SCLS flares." Several studies failed to establish any functional role for these monoclonal paraproteins in disease pathogenesis (*13*–*15*). Finally, immunofixation may be negative during acute SCLS flares because of IgG extravasation and transient hypogammaglobulinemia (*15*,*16*).

Several unique clinical and laboratory features of SCLS can be used to differentiate disease flares from the sequelae of severe COVID-19 (Table 2). Most notably, edema of the trunk and extremities is a prominent feature of acute SCLS and can lead to the development of compartment syndromes. Edema in COVID-19 infection is typically peripheral and frequently confined to the fingers and toes in association with chilblains, painful erythematous lesions (*17*). Pulmonary edema is a feature of SCLS rarely noted at initial observation but is a frequent characteristic of acute COVID-19–associated acute respiratory distress syndrome (*18*). Furthermore, both patients exhibited severe hemoconcentration despite aggressive fluid resuscitation. Patients who are critically ill with COVID-19 typically exhibit anemia, which is a predictor of a poor clinical outcome (*19*). Finally, although mildly decreased serum albumin levels of ≈3 g/dL have been reported in patients with severe COVID-19 (*20*), hypoalbuminemia is typically much more severe in SCLS flares, with an albumin level usually <2 g/dL.

Of note, SCLS had not previously been diagnosed in case-patient 1, and neither patient was receiving IVIg prophylaxis at the time of COVID-19 infection.

Fortunately, we observed no COVID-19–associated SCLS flares in any of the >70 patients in the study cohort who were receiving IVIg prophylaxis (range 0.75–2.00 g/kg/mo). However, a previously published report (*11*) documented the case of a patient whose disease had been well-controlled by IVIg prophylaxis (0.5 g/kg/mo) but who died of refractory SCLS soon after COVID-19 infection. Nonetheless, in agreement with the authors of that study, we strongly recommend that SCLS patients receive IVIg prophylaxis indefinitely, at the highest recommended dose (2 g/kg/month), until the COVID-19 pandemic is under better control. Because no treatments for acute SCLS flares, including IVIg, have been proven effective, interventions are limited to supportive measures such as IV fluids and albumin, vasopressors, renal replacement therapy, and intubation. However, as noted in recent surveys of critically ill SCLS patients (*2*), fluid administration must be limited to avoid development of compartment syndromes and limb ischemia. Although case-patient 1 received several empiric treatments, including IVIg, icatibant, and methylene blue, the treatments appeared to have had no effect on her intermediate clinical outcomes.

Although the genetic basis of SCLS is not well understood (*21*,*22*), our work has provided evidence that patients with SCLS experience intrinsically exaggerated endothelial barrier dysfunction in response to otherwise mundane proinflammatory mediators (*23*,*24*). Severe COVID-19 and acute SCLS are both characterized by transient increases in the levels of proinflammatory cytokines in circulation; some of these cytokines, including C-X-C motif chemokine ligand 10, C-C motif chemokine ligand 2 and 3, interleukin -6, and tumor necrosis factor–α (Table 3), directly provoke endothelial barrier disruption (*25*–*27*). These results suggest that the cytokine storm associated with mild-to-moderate COVID-19 may lead to an SCLS flare. Alternatively, as suggested elsewhere (*9*), it is also possible that SARS-CoV-2 may be directly toxic to endothelial cells. This hypothesis suggests that viral factors synergize with host-intrinsic mechanisms to provoke severe SCLS flares. Endothelial cell infection, diffuse inflammatory endothelitis, and microvascular thrombosis are common in COVID-19, although these responses are typically associated with prominent lung involvement (*28*). Because neither of these patients exhibited prominent pulmonary abnormalities, these mechanisms may not be substantial components of COVID-19–associated SCLS.

Further characterization of the immune and inflammatory responses to SARS-CoV-2 will be needed to elucidate its effects on SCLS pathophysiology at the molecular level. However, clinicians should be aware that patients carrying a diagnosis of SCLS or another relapsing-remitting and inflammation-related disease (e.g., autoimmune or autoinflammatory rheumatological diseases) may be at increased risk for severe disease and require increased vigilance for this rare but potentially fatal potential complication of COVID-19 as the pandemic continues.

Table 3. Typical serum cytokine profiles for acute SCLS compared with severe COVID-19*

Cytokine	SCLS	COVID-19
IL-2	Normal	Elevated
IL-4	Normal	Elevated
IL-6	Elevated	Elevated
IL-7	Normal	Elevated
IL-10	Normal	Elevated
CXCL10	Elevated	Elevated
CCL2	Elevated	Elevated
TNF-α	Variable	Elevated
IFN-γ	Elevated	Elevated

*COVID-19, coronavirus disease; CCL, C-C motif chemokine ligand; CXCL, C-X-C motif chemokine ligand; IFN, interferon; IL, interleukin; SCLS, systemic capillary leak syndrome; TNF, tumor necrosis factor.

Acknowledgments

We thank Helene F. Rosenberg for critical review of the manuscript.

We dedicate this paper to Kathy Messina, who had SCLS.

Funding for this study was provided by the National Institute of Allergy and Infectious Diseases/National Institutes of Health Intramural Program (Z01-AI-001083).

The content of this publication does not necessarily reflect the views or policies of the US Department of Health and Human Services, nor does the mention of trade names, commercial products, or organizations imply endorsement by the US government.

About the Author

Dr. Cheung is an internal medicine resident at Emory University, Atlanta, Georgia, USA. Her research interests include epidemiology and applying implementation science to improve hospitals and health systems.

References

1. Druey KM, Parikh SM. Idiopathic systemic capillary leak syndrome (Clarkson disease). J Allergy Clin Immunol. 2017;140:663–70. https://doi.org/10.1016/j.jaci.2016.10.042
2. Pineton de Chambrun M, Luyt CE, Beloncle F, Gousseff M, Mauhin W, Argaud L, et al.; EurêClark Study Group. The clinical picture of severe systemic capillary-leak syndrome episodes requiring ICU admission. Crit Care Med. 2017;45:1216–23. https://doi.org/10.1097/CCM.0000000000002496
3. Eo TS, Chun KJ, Hong SJ, Kim JY, Lee IR, Lee KH, et al. Clinical presentation, management, and prognostic factors of

idiopathic systemic capillary leak syndrome: a systematic review. J Allergy Clin Immunol Pract. 2018;6:609–18. https://doi.org/10.1016/j.jaip.2017.07.021
4. Kapoor P, Greipp PT, Schaefer EW, Mandrekar SJ, Kamal AH, Gonzalez-Paz NC, et al. Idiopathic systemic capillary leak syndrome (Clarkson's disease): the Mayo Clinic experience. Mayo Clin Proc. 2010;85:905–12. https://doi.org/10.4065/mcp.2010.0159
5. Xie Z, Chan EC, Long LM, Nelson C, Druey KM. High-dose intravenous immunoglobulin therapy for systemic capillary leak syndrome (Clarkson disease). Am J Med. 2015;128:91–5. https://doi.org/10.1016/j.amjmed.2014.08.015
6. Pineton de Chambrun M, Gousseff M, Mauhin W, Lega JC, Lambert M, Rivière S, et al.; EurêClark Study Group. Intravenous immunoglobulins improve survival in monoclonal gammopathy-associated systemic capillary-leak syndrome. Am J Med. 2017;130:1219.e19–27. https://doi.org/10.1016/j.amjmed.2017.05.023
7. Umbrello M, Gardinali M, Ottolina D, Zanforlin G, Iapichino G. Systemic capillary leak syndrome: is methylene blue the silver bullet? Case Rep Crit Care. 2014;2014:141670. https://doi.org/10.1155/2014/141670
8. Antonen J, Leppänen I, Tenhunen J, Arvola P, Mäkelä S, Vaheri A, et al. A severe case of Puumala hantavirus infection successfully treated with bradykinin receptor antagonist icatibant. Scand J Infect Dis. 2013;45:494–6. https://doi.org/10.3109/00365548.2012.755268
9. Lacout C, Rogez J, Orvain C, Nicot C, Rony L, Julien H, et al. A new diagnosis of systemic capillary leak syndrome in a patient with COVID-19. Rheumatology. 2021;60:e19–20. https://doi.org/10.1093/rheumatology/keaa606
10. Case R, Ramaniuk A, Martin P, Simpson PJ, Harden C, Ataya A. Systemic capillary leak syndrome secondary to coronavirus disease 2019. Chest. 2020;158:e267–8. https://doi.org/10.1016/j.chest.2020.06.049
11. Pineton de Chambrun M, Cohen-Aubart F, Donker DW, Cariou PL, Luyt CE, Combes A, et al. SARS-CoV-2 induces acute and refractory relapse of systemic capillary leak syndrome (Clarkson's disease). Am J Med. 2020;133:e663–4. https://doi.org/10.1016/j.amjmed.2020.03.057
12. Pineton de Chambrun M, Constantin JM, Mathian A, Quemeneur C, Lepere V, Combes A, et al. Clarkson's disease episode or secondary systemic capillary leak-syndrome: that is the question! Chest. 2021;159:441. https://doi.org/10.1016/j.chest.2020.07.084
13. Xie Z, Ghosh CC, Patel R, Iwaki S, Gaskins D, Nelson C, et al. Vascular endothelial hyperpermeability induces the clinical symptoms of Clarkson disease (the systemic capillary leak syndrome). Blood. 2012;119:4321–32. https://doi.org/10.1182/blood-2011-08-375816
14. Zhang W, Ewan PW, Lachmann PJ. The paraproteins in systemic capillary leak syndrome. Clin Exp Immunol. 1993;93:424–9. https://doi.org/10.1111/j.1365-2249.1993.tb08195.x
15. Atkinson JP, Waldmann TA, Stein SF, Gelfand JA, MacDonald WJ, Heck LW, et al. Systemic capillary leak syndrome and monoclonal IgG gammopathy; studies in a sixth patient and a review of the literature. Medicine (Baltimore). 1977;56:225–39. https://doi.org/10.1097/00005792-197705000-00004
16. Matheny M, Maleque N, Channell N, Eisch AR, Auld SC, Banerji A, et al. Severe exacerbations of systemic capillary leak syndrome after COVID-19 vaccination: a case series. Ann Intern Med. 2021 Jun 15 [Epub ahead of print]. https://doi.org/10.7326/L21-0250
17. Wollina U, Karadağ AS, Rowland-Payne C, Chiriac A, Lotti T. Cutaneous signs in COVID-19 patients: a review. Dermatol Ther. 2020;33:e13549. https://doi.org/10.1111/dth.13549
18. Virot E, Mathien C, Pointurier V, Poidevin A, Labro G, Pinto L, et al. Characterization of pulmonary impairment associated with COVID-19 in patients requiring mechanical ventilation. Rev Bras Ter Intensiva. 2021;33:75–81.
19. Faghih Dinevari M, Somi MH, Sadeghi Majd E, Abbasalizad Farhangi M, Nikniaz Z. Anemia predicts poor outcomes of COVID-19 in hospitalized patients: a prospective study in Iran. BMC Infect Dis. 2021;21:170. https://doi.org/10.1186/s12879-021-05868-4
20. Huang J, Cheng A, Kumar R, Fang Y, Chen G, Zhu Y, et al. Hypoalbuminemia predicts the outcome of COVID-19 independent of age and co-morbidity. J Med Virol. 2020;92:2152–8. https://doi.org/10.1002/jmv.26003
21. Pierce R, Ji W, Chan EC, Xie Z, Long LM, Khokha M, et al. Whole exome sequencing of adult and pediatric cohorts of the rare vascular disorder systemic capillary leak syndrome. Shock. 2019;52:183–90. https://doi.org/10.1097/SHK.0000000000001254
22. Xie Z, Nagarajan V, Sturdevant DE, Iwaki S, Chan E, Wisch L, et al. Genome-wide SNP analysis of the systemic capillary leak syndrome (Clarkson disease). Rare Dis. 2013;1:e27445. https://doi.org/10.4161/rdis.27445
23. Sek AC, Xie Z, Terai K, Long LM, Nelson C, Dudek AZ, et al. Endothelial expression of endothelin receptor A in the systemic capillary leak syndrome. PLoS One. 2015;10:e0133266. [Erratum in PLoS One. 2015;10:e0137373.] https://doi.org/10.1371/journal.pone.0133266
24. Raza A, Xie Z, Chan EC, Chen WS, Scott LM, Robin Eisch A, et al. A natural mouse model reveals genetic determinants of systemic capillary leak syndrome (Clarkson disease). Commun Biol. 2019;2:398. https://doi.org/10.1038/s42003-019-0647-4 [Erratum in Commun Biol. 2019;2:439.]
25. Hu B, Huang S, Yin L. The cytokine storm and COVID-19. J Med Virol. 2021;93:250–6. https://doi.org/10.1002/jmv.26232
26. Xie Z, Ghosh CC, Parikh SM, Druey KM. Mechanistic classification of the systemic capillary leak syndrome: Clarkson disease. Am J Respir Crit Care Med. 2014;189:1145–7. https://doi.org/10.1164/rccm.201310-1746LE
27. Xie Z, Chan E, Yin Y, Ghosh CC, Wisch L, Nelson C, et al. Inflammatory markers of the systemic capillary leak syndrome (Clarkson disease). J Clin Cell Immunol. 2014;5:1000213.
28. Pons S, Fodil S, Azoulay E, Zafrani L. The vascular endothelium: the cornerstone of organ dysfunction in severe SARS-CoV-2 infection. Crit Care. 2020;24:353. https://doi.org/10.1186/s13054-020-03062-7

Address for correspondence: Kirk Druey, National Institute of Allergy and Infectious Diseases/National Institutes of Health, 10 Center Dr, Rm 11N238A, Bethesda, MD 20892, USA; email: kdruey@niaid.nih.gov

Severe Acute Respiratory Syndrome Coronavirus 2 and Pregnancy Outcomes According to Gestational Age at Time of Infection

Dominique A. Badr, Olivier Picone, Elisa Bevilacqua, Andrew Carlin, Federica Meli, Jeanne Sibiude, Jérémie Mattern, Jean-François Fils, Laurent Mandelbrot, Antonio Lanzone, Danièle De Luca, Jacques C. Jani, Alexandre J. Vivanti

We conducted an international multicenter retrospective cohort study, PregOuTCOV, to examine the effect of gestational age at time of infection with severe acute respiratory syndrome coronavirus 2 (SARS-CoV-2) on obstetric and neonatal outcomes. We included all singleton pregnancies with a live fetus at 10 weeks' gestation in which pregnancy outcomes were known. The exposed group consisted of patients infected with SARS-CoV-2, whereas the unexposed group consisted of all remaining patients during the same period. Primary outcomes were defined as composite adverse obstetric outcomes and composite adverse neonatal outcomes. Of 10,925 pregnant women, 393 (3.60%) were infected with SARS-CoV-2 (exposed group). After matching for possible confounders, we identified statistically significant increases in the exposed group of composite adverse obstetric outcomes at ≥20 weeks' gestation and of composite adverse neonatal outcomes at ≥26 weeks' gestation (p<0.001). Vaccination programs should target women early in pregnancy or before conception, if possible.

In early 2020, a new coronavirus, called severe acute respiratory syndrome coronavirus 2 (SARS-CoV-2), arrived in Europe. It infected millions of persons and led to the deaths of thousands by coronavirus disease (COVID-19) by May 2020, when numbers of infections per week in Europe decreased substantially. However, after a summer respite, the number of infections began to escalate again in September 2020, and several new variants were reported (*1*,*2*). Hundreds of articles published during this period reported the virus's relationship with and effect on pregnancy and attempted to determine adverse neonatal and obstetric outcomes after infection. Meanwhile, mother-to-child transmission of SARS-CoV-2 has been established, and the World Health Organization recognized the virus as part of the TORCH (toxoplasmosis, other viruses, rubella, cytomegalovirus, and herpes simplex) family of infections (of which Zika virus was the most recent new member) (*3*,*4*), adding yet more interest to the possible perinatal consequences of SARS-CoV-2.

In a cohort study using propensity score-matching at the level of age, body mass index (BMI), and underlying conditions (e.g., diabetes, hypertension, asthma), Badr et al. demonstrated that pregnant women at >20 weeks of gestation (WG) infected with SARS-CoV-2 had a significantly higher risk for intensive care unit admission, endotracheal intubation, hospitalization for disease-related symptoms, and need for oxygen therapy (*5*). A systematic review demonstrated an increased risk for intensive care unit

Author affiliations: University Hospital Brugmann, Brussels, Belgium (D.A. Badr, A. Carlin, J.C. Jani); Université Libre de Bruxelles, Brussels (D.A. Badr, A. Carlin, J.C. Jani); Louis Mourier Hospital, AP-HP, Colombes, France (O. Picone, J. Sibuide, L. Mandelbrot); Université de Paris, Paris, France (O. Picone, J. Sibuide, L. Mandelbrot); Inserm IAME-U1137, Paris (O. Picone, J. Sibuide, L. Mandelbrot); Groupe de Recherche sur les Infections pendant la Grossesse (GRIG), Velizy, France (O. Picone, J. Sibuide, L. Mandelbrot, A.J. Vivanti); Gemelli University Polyclinic Foundation, Rome, Italy (E. Bevilacqua, F. Melli, A. Lanzone); Antoine Béclère Hospital, AP-HP, Clamart, France (J. Mattern, A.J. Vivanti, D. De Luca); Paris Saclay University, Paris (J. Mattern, D. De Luca, A.J. Vivanti); Ars Statistica, Nivelles, Belgium (J.-F. Fils); Catholic University Sacro Cuore, Rome (A. Lanzone)

DOI: https://doi.org/10.3201/eid2710.211394

admission in infected pregnant women compared with infected nonpregnant women and noninfected pregnant women (*6*).

Many researchers have focused on the obstetric and neonatal outcomes of infected pregnant women. Some reports have demonstrated that rates of preterm and cesarean delivery have increased (*6*–*10*), whereas others have reported a close association between SARS-CoV-2 infection and preeclampsia or preeclampsia-like syndromes (*11*). Enormous effort has been made to learn more about adverse outcomes related to SARS-CoV-2 infection, but most studies investigated patients in the late second or third trimester. Very few studies have stratified the adverse outcomes of patients according to the gestational age at which infection occurred (*12*). The objective of our study was to measure the prevalence of obstetric and neonatal outcomes in patients infected with SARS-CoV-2 and to examine the effect of gestational age at infection on each outcome.

Methods

This international multicenter retrospective cohort study, PregOuTCOV, was conducted in 4 university hospitals in Europe that follow similar guidelines and protocols for antenatal and intrapartum care. The study population consisted of all pregnant women with a viable fetus from the 10th WG and a known pregnancy outcome during February 1–November 30, 2020. The exposed group included pregnant patients in whom nasopharyngeal swab specimens tested positive for SARS-CoV-2 by reverse transcription PCR (RT-PCR) during this period; the unexposed group consisted of the remaining cohort of patients followed in the 4 hospitals during the same period. These patients were either not tested (because there was no indication) or tested negative. We excluded multiple pregnancies, patients with ongoing pregnancies and hence no birth outcomes, those with unknown pregnancy outcomes, those with medical or voluntary pregnancy termination, and patients in whom spontaneous abortion occurred before the 10th WG. None of the centers involved in this study performed regular (by month or by trimester) systematic screening of pregnant women by RT-PCR during the study period; all testing was performed on the basis of clinical symptoms or before planned admissions (regular hospital admission or admission for labor and delivery).

The study was approved by the appropriate ethical board for each recruiting center (approval nos. CE2020/206, CEROG 2020-OBST-1104, and IST DIPUSVSP-24-02-217), and informed consent was obtained when required by the relevant local regulations. Clinical data were routinely collected in real time in the patient's electronic medical records. Data were then extracted retrospectively for the study and merged into a dedicated, secured, and anonymized database based at the coordinating center. A data control was performed before analysis and, if data were inaccurate or missing, the recruiting centers were contacted to correct the identified issues. All relevant local and Europe privacy regulations were respected.

The collated data included maternal age, geographic origin, prepregnancy BMI, parity, smoking status, chronic arterial hypertension, diabetes mellitus type I or II, preexisting pulmonary diseases (such as asthma, tuberculosis, and previous pulmonary embolism [PE]), and preexisting renal or liver diseases (such as renal or hepatic insufficiency, polycystic kidney disease, single kidney, previous nephrectomy, viral hepatitis, and kidney or liver transplant). For SARS-CoV-2–positive patients, we also collected data on date of positive RT-PCR test, gestational age at the time of RT-PCR, reason for performing RT-PCR (symptoms or screening), hospital admission related to SARS-CoV-2 infection, and disease severity according to the National Institutes of Health (*13*). We also recorded the occurrence of SARS-CoV-2 pneumonia, acute respiratory distress syndrome (*14*), invasive ventilation, oxygen support, and extracorporeal membrane oxygenation.

Primary outcomes of the study were a composite adverse obstetric outcome (CAOO) and a composite adverse neonatal outcome (CANO). CAOO was defined as preterm delivery (<37 WG), preeclampsia, eclampsia, HELLP (hemolysis, elevated liver enzymes, low platelet count) syndrome, unscheduled cesarean delivery, deep venous thrombosis (DVT), PE, pregnancy loss at <24 WG, intrauterine fetal demise (≥24 WG), or maternal death. CANO was defined as low birthweight (<2,500 g), neonatal intensive care unit (NICU) admission, APGAR score of <7 at 5 minutes of life, respiratory distress, or neonatal death. The criteria for NICU admission were gestational age at birth of ≤32 WG, birthweight of ≤1,500 g, signs of respiratory distress, hemodynamic instability, metabolic problems needing central venous access placement and intensive care, perinatal asphyxia defined according to American College of Obstetricians and Gynecologists and American Academy of Pediatrics criteria, and need for exchange-transfusion (*15*). Neonates of SARS-CoV-2–positive mothers were not systematically admitted to the NICU for monitoring for reasons outside these listed criteria. Secondary outcomes of the study included each outcome of the composite

variables, as well as delivery at <32 WG, spontaneous delivery at <37 WG, suspected fetal distress (such as fetal bradycardia or recurrent late or variable decelerations on antepartum or intrapartum cardiotocography), cesarean delivery, postpartum hemorrhage (defined as blood loss of >500 mL in normal vaginal delivery and >1,000 mL in cesarean delivery), umbilical artery pH abnormalities, small for gestational age (defined as estimated fetal weight <10th percentile), and large for gestational age (defined as estimated fetal weight >95th percentile) (*16*).

We performed 2 propensity scores on 2 groups: the maternal population (unexposed group [n = 10,532] and exposed group [n = 393]) and the neonatal population (unexposed group [n = 10,370] and exposed group [n = 388]). After we performed 15 multiple imputations of missing data of the original datasets by using the mice package in R software (R Project for Statistical Computing, https://www.r-project.org/), we used the CBPS R package to perform the propensity score, estimating an average treatment effect using covariate balancing and requesting an exact match, which has been shown to be superior to traditional logistic regression approaches and boosted classification and regression trees (*17*). We considered an absolute standardized difference (ASD) of <10%–15% to support the assumption of balance between the groups because it is not affected by sample size, unlike p values, and it can be used to compare the relative balance of variables measured in different units (*18*). We calculated the mean and SD obtained after matching for continuous variables and the percentage for categorical variables. After performing the propensity score, we used the survey R package to perform logistic regressions for the binary outcome variables, which included the treatment group effect, the weight resulting from the matching, and variables present in the propensity score to obtain a doubly robust estimator, which corrected the last remaining possible imbalance between the covariates and produced an unbiased treatment effect (*19*). The survey R package included the Huber-White corrected SEs, which maintained the SEs unbiased even under heterogeneity of the residuals (*20*). Finally, the advantage of a doubly robust estimator is that it needs only 1 of the 2 models (propensity score and logistic regression after the propensity score) to be correctly specified. We used R software version 3.4.3 (to produce the results. Before matching of covariates, a p value of <0.05 was considered statistically significant. Nevertheless, we had to correct for multiple testing with a Bonferroni correction. For the secondary outcomes, 10 comparisons were performed twice; therefore, we divided the p value by the number of comparisons to obtain the p value at which we considered a result significant (0.05/10 = 0.005). All secondary outcomes with a p value <0.005 after matching were therefore considered significant.

We used the coxme R package to estimate Cox proportional hazards models using the center as random effect on a subset of the data, for which the gestational age at the time of SARS-CoV-2 RT-PCR was collected (for maternal population, unexposed group [n = 2,343] and exposed group [n = 393]; for neonatal population, unexposed group [n = 2,308] and exposed group [n = 383]). This subgroup was representative of the study population (Appendix Table 1, https://wwwnc.cdc.gov/EID/article/27/10/21-1394-App1.pdf). One random effect Cox model with a censor at 41 WG was drawn per outcome, including the outcome of interest and the covariates included in the propensity score. A p value <0.05 was considered significant.

Results

Baseline Characteristics

In total, we identified 10,925 singleton pregnancies that were eligible for final analysis (Table 1). A total of 393 patients tested positive for SARS-CoV-2 (3.60%). Among them, 196 (49.87%) were symptomatic (8 critical, 12 severe, 34 moderate, 135 mild, and 7 not classified). Of these, 46 patients had pneumonia (11.70%) and 16 had acute respiratory distress syndrome (4.07%). A total of 37 patients (9.41%) needed oxygen therapy, whereas 9 (2.29%) needed invasive ventilation. No patients required extracorporeal membrane oxygenation. Among the 10,925 women, 167 had a pregnancy loss and 10,758 delivered a live neonate (Table 2; Figure 1).

Primary Outcomes

The rates of CAOOs and CANOs were significantly higher in SARS-CoV-2–positive patients. CAOOs occurred in 22.75% of exposed persons versus 19.25% of unexposed persons (p<0.001; ASD = 8.62%). CANOs occurred in 17.86% of exposed persons versus 14.28% of the unexposed (p<0.001; ASD = 9.76%) (Tables 3, 4).

Secondary Outcomes

SARS-CoV-2 infection was associated with an increase of many obstetric and neonatal outcomes, such as preeclampsia, eclampsia, or HELLP syndrome (2.44% vs. 1.89%; p = 0.004, ASD = 3.78%); delivery at <37 weeks (12.22% vs. 8.90%; p<0.001, ASD = 11.71%); cesarean delivery (26.63% vs. 24.68%;

Table 1. Baseline characteristics before and after covariate matching of 10,925 pregnant women in Europe included in final analysis in PregOutCOV study of pregnancy outcomes according to gestational age at time of infection with severe acute respiratory syndrome coronavirus 2*

	Before matching			After matching		
Characteristic	Unexposed, n = 10,532	Exposed, n = 393	ASD†	Unexposed, n = 10,532	Exposed, n = 393	ASD‡
Mean age, y (SD)	33.05 (±5.43)	33.32 (±5.58)	4.93	33.06 (±5.43)	33.08 (±5.49)	0.34
Origin						
Europe, Middle East, North Africa	78.37	77.35	2.45	78.34	78.39	0.13
Sub-Saharan Africa, Caribbean	13.79	17.56	10.39	13.93	13.94	0.02
Not mentioned by the patient	6.71	3.82	13.00	6.60	6.56	0.14
Not available	1.13	1.27	1.31	1.14	1.10	0.36
Prepregnancy BMI, kg/m^2 (SD)	25.16 (±5.09)	26.34 (±5.39)	22.50	25.21 (±5.12)	25.24 (±4.96)	0.55
Multiparity	54.12	58.78	9.40	54.26	54.44	0.36
Smoking	11.18	11.20	0.06	11.19	11.13	0.19
Chronic hypertension	1.35	1.27	0.67	1.34	1.33	0.14

*Values are % pregnant women except as indicated. ASD, absolute standardized difference; BMI, body mass index.
†ASDs before matching show heterogeneity between the exposed and unexposed groups.
‡ASDs after matching show a balance between the exposed and unexposed groups.

p = 0.002, ASD = 4.17%); unscheduled cesarean delivery (13.87% vs. 12.27%; p<0.001, ASD = 4.73%); postpartum hemorrhage (12.57% vs. 9.23%; p<0.001, ASD = 10.74%); DVT or PE (0.53% vs. 0.06%; p<0.001, ASD = 8.77%); fetal distress (10.95% vs. 8.74%; p<0.001, ASD = 7.44%); NICU admission (13.09% vs. 7.76%; p<0.001, ASD = 17.49%); and APGAR of <7 at 5 minutes (4.01% vs. 2.58%; p<0.001, ASD = 8.03%). Neonates in the exposed group also had significantly lower birthweight (mean ±SD 3,128.90 g ±602.93 g vs. 3,228.00 g ±579.34 g; p<0.001, ASD = 16.76%); however, z-scores of birthweight were similar to the unexposed group (Tables 3, 4).

Effect of Gestational Age at SARS-CoV-2 Infection on Primary and Secondary Outcomes

Cox regression models demonstrated that patients with CAOOs were more likely to be infected with SARS-CoV-2 than patients without this composite outcome. This difference was seen in patients infected at >20 WG (p<0.001). Similarly, patients with CANOs were more likely to be SARS-CoV-2–positive than patients without this composite outcome. The difference was seen in infected patients at >26 WG (p<0.001) (Figure 2).

Furthermore, when the infection started beyond a defined WG for selected secondary outcomes, the incidence of this outcome increased significantly. These included preeclampsia, eclampsia, or HELLP syndrome (p = 0.002, ≥15 WG at time of infection); delivery at <37 WG (p<0.001, ≥24 WG); spontaneous delivery at <37 WG (p<0.001, ≥26 WG); delivery at <32 WG (p<0.001, ≥26 WG); NICU admission (p<0.001, ≥28 WG); and respiratory distress (p<0.001, ≥28 WG) (Appendix Tables 2, 3, Figures 1, 2).

Discussion

This study reports the prevalence of adverse obstetric and neonatal outcomes in women infected with SARS-CoV-2 relative to the timing of infection during pregnancy. SARS-CoV-2–positive patients have an increased incidence of adverse obstetric and neonatal

Table 2. Baseline characteristics before and after covariate matching of the mothers of the 10,758 live neonates in Europe included in final analysis (after removing 167 patients with pregnancy losses) in PregOutCOV study of pregnancy outcomes according to gestational age at time of infection with severe acute respiratory syndrome coronavirus 2*

	Before matching			After matching		
Characteristic	Unexposed, n = 1,0370	Exposed, n = 388	ASD†	Unexposed, n = 10,370	Exposed, n = 388	ASD‡
Mean age, y (SD)	33.11 (±5.43)	33.31 (±5.61)	3.67	33.11 (±5.42)	33.13 (±5.55)	0.44
Origin						
Europe, Middle East, North Africa	78.52	77.58	2.29	78.49	78.51	0.07
Sub-Saharan Africa, Caribbean	13.63	17.27	10.08	13.76	13.75	0.04
Not mentioned by the patient	6.85	3.87	13.29	6.73	6.76	0.11
Not available	1.00	1.29	2.75	1.02	0.98	0.41
Prepregnancy BMI, kg/m^2 (SD)	25.65 (±5.99)	26.72 (±5.92)	17.83	25.71 (±6.05)	25.70 (±5.31)	0.11
Multiparity	53.78	59.28	11.10	53.96	53.96	0.01
Smoking	12.10	11.34	2.36	12.10	12.06	0.12
Chronic hypertension	1.26	1.29	0.24	1.26	1.27	0.10

*Values are % pregnant women except as indicated. ASD, absolute standardized difference; BMI, body mass index.
†ASDs before matching show heterogeneity between the exposed and unexposed groups.
‡ASDs after matching show a balance between the exposed and unexposed groups.

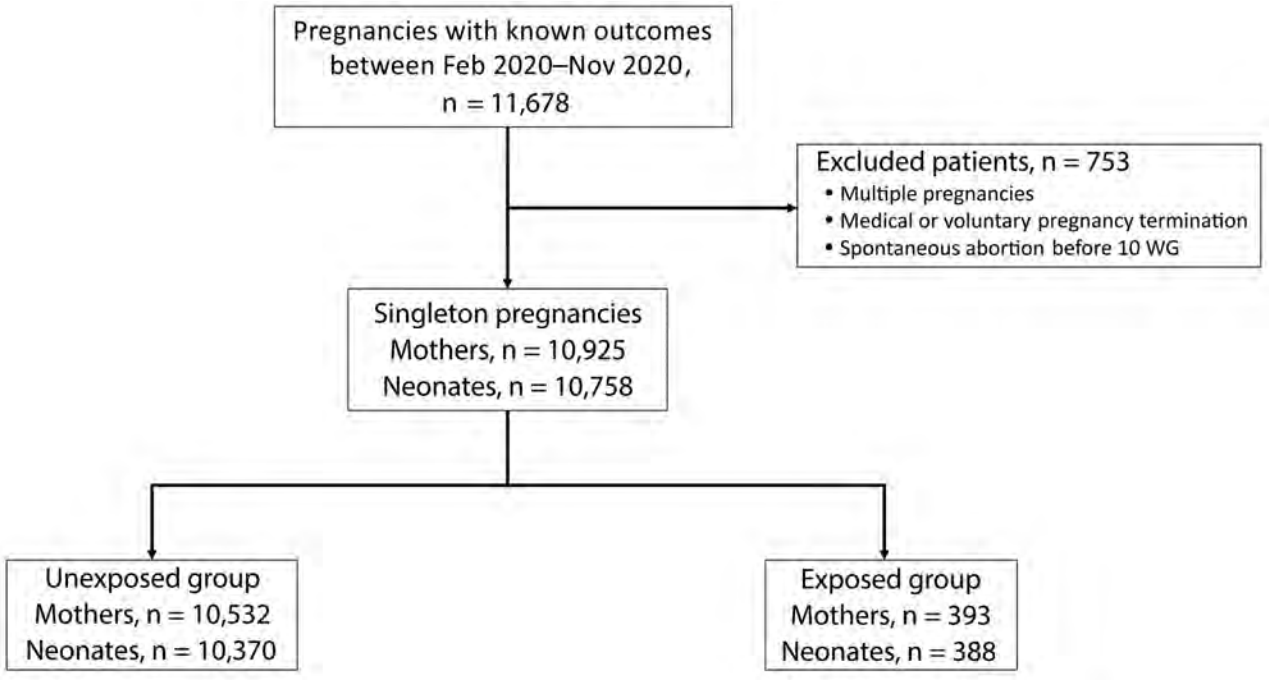

Figure 1. Flowchart of the study population in PregOutCOV study of pregnancy outcomes in Europe according to gestational age at time of infection with severe acute respiratory syndrome coronavirus 2. Pregnancy losses before delivery were excluded from the neonatal population. WG, weeks of gestation.

outcomes. It appears that pregnant women are more susceptible to the adverse effects of SARS-CoV-2 infection during the late second and early third trimesters.

The effects of SARS-CoV-2 on obstetric and neonatal outcomes has become more evident with time because of the growing body of literature in this area. However, the association between these outcomes and the timing of infection during pregnancy remains unclear. Most studies have reported the obstetric and neonatal outcomes of patients infected in the late second or third trimester. In our study, we included patients who were infected at the beginning of their pregnancies. We demonstrated that gestational age at the time of infection had a critical effect on the incidence of adverse obstetric and neonatal outcomes. SARS-CoV-2 infections after 20 WG significantly increased CAOOs, and infection after 26 WG significantly increased CANOs.

Adverse obstetric and neonatal outcomes, such as preeclampsia, preterm delivery, cesarean delivery, postpartum hemorrhage, and DVT or PE, significantly increased in pregnant women who were infected with SARS-CoV-2. In a meta-analysis published in September 2020 and updated in February 2021

Table 3. Obstetric outcomes in PregOutCOV study of pregnancy outcomes in Europe according to gestational age at time of infection with severe acute respiratory syndrome coronavirus 2*

Outcome	Unexposed, n = 10,532	Exposed, n = 393	p value	ASD
Primary outcome†				
Composite adverse obstetric outcome	19.25	22.75	<0.001	8.62
Secondary outcome‡				
Preeclampsia, eclampsia, or HELLP syndrome	1.89	2.44	0.004	3.78
Pregnancy loss at <24 weeks	1.06	0.71	0.034	3.73
Pregnancy loss at >24 weeks	1.54	1.19	0.060	2.97
Delivery at <32 weeks	3.18	3.63	0.052	2.51
Delivery at <37 weeks	8.90	12.22	<0.001	10.71
Spontaneous delivery at <37 weeks	5.65	4.96	0.056	2.86
Caesarean delivery	24.68	26.63	0.002	4.17
Unscheduled caesarean delivery	12.27	13.87	<0.001	4.73
Postpartum hemorrhage	9.23	12.57	<0.001	10.74
DVT or PE	0.06	0.53	<0.001	8.77

*Values are % pregnant women except as indicated. ASD, absolute standardized difference; DVT, deep vein thrombosis; HELLP, hemolysis, elevated liver enzymes, low platelet count; PE, pulmonary embolism.
†Significant statistical difference: $p < 0.05$.
‡Significant statistical difference: $p < 0.005$ (Bonferroni correction).

Table 4. Neonatal outcomes in PregOutCOV study of pregnancy outcomes in Europe according to gestational age at time of infection with severe acute respiratory syndrome coronavirus 2*

Outcome	Unexposed, n = 10,370	Exposed, n = 388	p value	ASD
Primary outcome†				
Composite adverse neonatal outcome	14.28	17.86	<0.001	9.76
Secondary outcome†				
Small for gestational age	10.89	9.39	<0.001	4.98
Large for gestational age	6.53	5.60	0.0029	3.87
Fetal distress	8.74	10.95	<0.001	7.44
Neonatal death	0.32	0.14	<0.001	3.66
Birthweight, g (SD)	3228.00 (±579.34)	3128.90 (±602.93)	<0.001	16.76
NICU admission	7.76	13.09	<0.001	17.49
Respiratory distress	7.10	7.86	0.0297	2.89
APGAR <7 at 5 min	2.58	4.01	<0.001	8.03
Umbilical artery pH	7.25 ± 0.08	7.25 ± 0.07	<0.001	11.12

*Values are % pregnant women except as indicated. ASD, absolute standardized difference; NICU, neonatal intensive care unit.
†Statistically significant difference: p<0.05.
‡Statistically significant difference: p<0.005 (Bonferroni correction).

examining 18 studies including 8,549 women, the rate of preterm birth in infected patients was higher than in noninfected patients (odds ratio 1.47, 95% CI 1.14–1.91) (*6*). A systematic review by Wei et al. also confirmed this finding (*21*).

With regard to the incidence of DVT or PE, our findings corresponded to early reports that highlighted the importance of thromboprophylaxis for SARS-CoV-2–positive patients. Most infected hospitalized patients in the 4 institutions in this study received some form of treatment to reduce their risk for DVT and PE (*22*,*23*). Several previous studies have demonstrated an association between preeclampsia and SARS-CoV-2 (*11*,*21*). In a new large observational study, Metz et al. (*24*) grouped 1,219 infected patients according to disease severity. Compared with asymptomatic patients, those with mild to moderate disease had similar rates of cesarean delivery, hypertensive disorders of pregnancy, and preterm birth. Nevertheless, patients with severe to critical disease were at higher risk for these perinatal outcomes. Our study was not designed to compare patients according to disease severity.

Fetal distress during labor, admission of live neonates to the NICU, APGAR scores of <7 at 5 minutes, and umbilical artery pH abnormalities were significantly higher and birthweight was significantly lower in infected patients than in matched unexposed

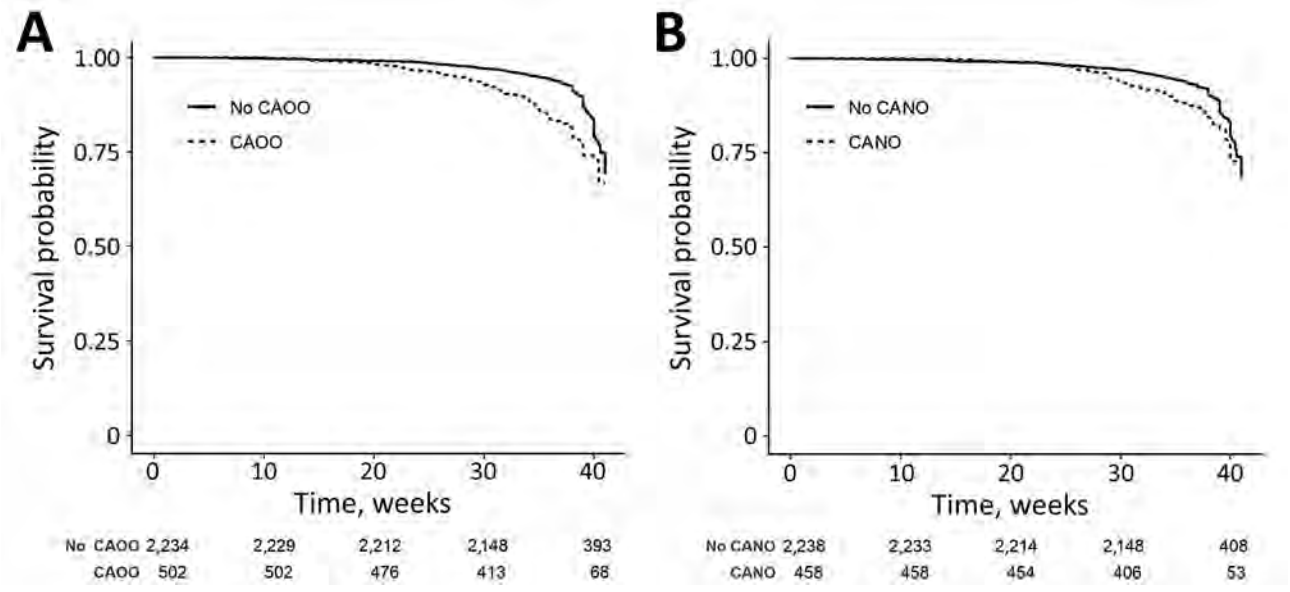

Figure 2. Kaplan-Meier curves demonstrating the effect of gestational age at the time of infection with severe acute respiratory syndrome coronavirus 2 (SARS-CoV-2) on pregnancy outcomes in Europe. A) Compared with patients without CAOO, patients with CAOO were more often infected with SARS-CoV-2. The difference was seen when patients were infected at ≥20 weeks of gestation. B) Compared with patients without CANO, patients with CANO were more often infected with SARS-CoV-2. The difference was seen when patients were infected at ≥26 weeks of gestation. Numbers below x-axis indicate number of persons at risk for each time point. CANO, composite adverse neonatal outcome; CAOO, composite adverse obstetric outcome.

patients. Placental abnormalities, among other factors, might play a role in the occurrence of these elevated risks. Patberg et al. (*25*) compared 77 placentae of infected patients with 56 placentae of noninfected patients and found an increased prevalence of histopathologic abnormalities, such as villitis of unknown etiology and fetal vascular underperfusion, in the SARS-CoV-2–positive group. Shanes et al. reported similar findings (*26*). In addition, Schwartz et al. studied 6 placentae from SARS-CoV-2–positive patients and found that all of them showed chronic histiocytic intervillositis and syncytiotrophoblast necrosis (*27*). These histopathologic abnormalities might interfere with the normal function of the maternal–fetal interface and thereby contribute to the observed adverse neonatal outcomes.

Rates of the remaining outcomes in our study, such as pregnancy loss, neonatal death, small size for gestational age, and large size for gestational age, were either similar or lower in SARS-CoV-2–positive women compared to rates in unexposed pregnant women. In a cohort study of 266 infected pregnant women, Di Mascio et al. estimated pregnancy loss and perinatal death at 6.4% and demonstrated that early gestational age at infection, maternal ventilator supports, and low birthweight were major risk factors for adverse outcomes (*28*). In contrast, in a case-control study of 225 women, Cosma et al. demonstrated that infection during the first trimester might not have a direct effect on spontaneous abortions (*12*). Similarly, a recent study from Denmark found no association between pregnancy loss and SARS-CoV-2 infection during the first trimester (*29*).

Pregnancy is an independent risk factor for respiratory deterioration in patients infected with SARS-CoV-2. Large studies that measure the effect of gestational age at time of infection on obstetric and neonatal outcomes are still lacking. Our study could aid in the counseling of pregnant patients and the organization of antenatal and perinatal care after SARS-CoV-2 infection. Furthermore, this study will help clinicians target pregnant women for SARS-CoV-2 vaccination early enough to provide protection before the crucial threshold of 20 WG. After this gestational age, SARS-CoV-2 infection significantly increases the risk for adverse outcomes.

Prospective studies are needed to examine the effect of the timing of SARS-CoV-2 infection during pregnancy on obstetric and neonatal outcomes. In addition, the possible harmful effects of the virus on placental function, such as chronic histiocytic intervillositis, villitis, and decidual arteriopathy, are still unclear. These placentopathies may be involved in the pathophysiology of adverse obstetric and neonatal outcomes even when the fetus is not directly infected by the virus. More investigations should be targeted at the placental level to learn more about the potentially pathologic and deleterious interactions between the virus and placenta.

This study compares the obstetric and neonatal outcomes of SARS-CoV-2–positive patients according to gestational age at time of infection. Data concerning pregnancy outcomes of patients infected before 20 WG are limited in the current literature. Patients who were infected at the beginning of the pandemic during their first weeks of pregnancy have recently begun to deliver. With this study, we have attempted to address this knowledge gap.

Because it is neither possible nor ethical to expose patients to SARS-CoV-2 infection, the use of propensity score-matching in such situations minimizes selection bias and balances confounding covariates (i.e., age, BMI, parity, and underlying conditions) that could alter between-group differences in obstetric or neonatal outcomes, leaving SARS-CoV-2 infection as the only exposure that could affect these outcomes. Moreover, the inclusion of 4 university hospitals that follow similar guidelines and protocols for antenatal and intrapartum care endorses the findings of this study. None of the recruiting centers used NICU admission to isolate neonates who were born to SARS-CoV-2-positive mothers but had no other need of neonatal critical care. This practice has been discouraged because of a lack of evidence demonstrating a clinical advantage, as well as to avoid unnecessary parent-child separation and NICU bed shortages (*30*).

Nevertheless, these results should be interpreted with caution. The unexposed group will inevitably have included patients who had false-negative SARS-CoV-2 test results or those who were SARS-CoV-2–positive but asymptomatic and not tested. Our chosen methodology means that there will also have been some false-positive results in the infected groups; overall, these small and unavoidable discrepancies would probably have been balanced out by chance. In addition, a single negative result does not exclude an asymptomatic infection that developed later during pregnancy. However, the choice of a contemporaneous unexposed group was the best of the various options available at the time because of various issues relating to the sensitivity, specificity, and the use of the RT-PCR platform in clinical practice (*31*). The exclusion of asymptomatic patients who were not tested for infection also might falsely modify the incidence of obstetric and neonatal outcomes. The selection of an unexposed group before the onset of pandemic

might be seen as a reasonable compromise to avoid some of these practical issues. However, this methodology could erroneously modify the incidence of certain outcomes that have also been observed to have changed during the pandemic, even in noninfected women (*7*,*32*).

In conclusion, SARS-CoV-2 infection in pregnant women during the late second and early third trimesters increases the risk for adverse obstetric and neonatal outcomes. However, there is no evidence that infection before 20 WG increases these risks, except for risk for preeclampsia. These findings have implications for public health policy and suggest that vaccination programs should target women either before pregnancy or early in pregnancy to ensure adequate protection when they will be most vulnerable.

Acknowledgments

We thank Giulia Bonanni, who actively participated in data collection.

About the Author

Dr. Badr is a practitioner in the department of obstetrics and gynecology at CHU Brugmann, Université Libre de Bruxelles. He manages a wide range of maternal and fetal high-risk conditions. His clinical and research interests include all aspects of these 2 fields.

References

1. World Health Organization. WHO coronavirus disease (COVID-19) dashboard [cited 2020 Nov 19]. https://covid19.who.int
2. Fontanet A, Autran B, Lina B, Kieny MP, Karim SSA, Sridhar D. SARS-CoV-2 variants and ending the COVID-19 pandemic. Lancet. 2021;397:952–4. https://doi.org/10.1016/S0140-6736(21)00370-6
3. Vivanti AJ, Vauloup-Fellous C, Prevot S, Zupan V, Suffee C, Do Cao J, et al. Transplacental transmission of SARS-CoV-2 infection. Nat Commun. 2020;11:3572. https://doi.org/10.1038/s41467-020-17436-6
4. World Health Organization. Definition and categorization of the timing of mother-to-child transmission of SARS-CoV-2 [cited 2021 Mar 2]. https://www.who.int/publications/i/item/WHO-2019-nCoV-mother-to-child-transmission-2021.1
5. Badr DA, Mattern J, Carlin A, Cordier AG, Maillart E, El Hachem L, et al. Are clinical outcomes worse for pregnant women at ≥20 weeks' gestation infected with coronavirus disease 2019? A multicenter case-control study with propensity score matching. Am J Obstet Gynecol. 2020;223:764–8. https://doi.org/10.1016/j.ajog.2020.07.045
6. Allotey J, Stallings E, Bonet M, Yap M, Chatterjee S, Kew T, et al.; for PregCOV-19 Living Systematic Review Consortium. Clinical manifestations, risk factors, and maternal and perinatal outcomes of coronavirus disease 2019 in pregnancy: living systematic review and meta-analysis. BMJ. 2020;370:m3320. https://doi.org/10.1136/bmj.m3320
7. Khalil A, von Dadelszen P, Draycott T, Ugwumadu A, O'Brien P, Magee L. Change in the incidence of stillbirth and preterm delivery during the COVID-19 pandemic. JAMA. 2020;324:705–6. https://doi.org/10.1001/jama.2020.12746
8. Prabhu M, Cagino K, Matthews KC, Friedlander RL, Glynn SM, Kubiak JM, et al. Pregnancy and postpartum outcomes in a universally tested population for SARS-CoV-2 in New York City: a prospective cohort study. BJOG. 2020;127:1548–56. https://doi.org/10.1111/1471-0528.16403
9. Berghella V, Boelig R, Roman A, Burd J, Anderson K. Decreased incidence of preterm birth during coronavirus disease 2019 pandemic. Am J Obstet Gynecol MFM. 2020;2:100258. https://doi.org/10.1016/j.ajogmf.2020.100258
10. Saccone G, Sen C, Di Mascio D, Galindo A, Grünebaum A, Yoshimatsu J, et al. WAPM (World Association of Perinatal Medicine) Working Group on COVID-19. Maternal and perinatal outcomes of pregnant women with SARS-CoV-2 infection. Ultrasound Obstet Gynecol. 2021;57:232–41. https://doi.org/10.1002/uog.23107
11. Mendoza M, Garcia-Ruiz I, Maiz N, Rodo C, Garcia-Manau P, Serrano B, et al. Pre-eclampsia-like syndrome induced by severe COVID-19: a prospective observational study. BJOG. 2020;127:1374–80. https://doi.org/10.1111/1471-0528.16339
12. Cosma S, Carosso AR, Cusato J, Borella F, Carosso M, Bovetti M, et al. Coronavirus disease 2019 and first-trimester spontaneous abortion: a case-control study of 225 pregnant patients. Am J Obstet Gynecol. 2021;224:391.e1–7. https://doi.org/10.1016/j.ajog.2020.10.005
13. National Institutes of Health. COVID-19 treatment guidelines [cited 2020 Oct 12]. https://www.covid19treatmentguidelines.nih.gov/overview/clinical-presentation/
14. Ranieri VM, Rubenfeld GD, Thompson BT, Ferguson ND, Caldwell E, Fan E, et al.; ARDS Definition Task Force. Acute respiratory distress syndrome: the Berlin Definition. JAMA. 2012;307:2526–33.
15. American College of Obstetricians and Gynecologists (ACOG). Neonatal encephalopathy and cerebral palsy: executive summary. Obstet Gynecol. 2004;103:780–1. https://doi.org/10.1097/01.AOG.0000120142.83093.30
16. Stirnemann J, Villar J, Salomon LJ, Ohuma E, Ruyan P, Altman DG, et al.; International Fetal and Newborn Growth Consortium for the 21st Century (INTERGROWTH-21st); Scientific Advisory Committee; Steering Committees; INTERGROWTH-21st; INTERBIO-21st; Executive Committee; In addition for INTERBIO 21st; Project Coordinating Unit; Data Analysis Group; Data Management Group; In addition for INTERBIO 21st; Ultrasound Group; In addition for INTERBIO-21st; Anthropometry Group; In addition for INTERBIO-21st; Laboratory Processing Group; Neonatal Group; Environmental Health Group; Neurodevelopment Group; Participating countries and local investigators; In addition for INTERBIO-21st; In addition for INTERBIO-21st. International estimated fetal weight standards of the INTERGROWTH-21st Project. Ultrasound Obstet Gynecol. 2017;49:478–86. https://doi.org/10.1002/uog.17347
17. Imai K, Ratkovic M. Robust estimation of inverse probability weights for marginal structural models. J Am Stat Assoc. 2014;110:1013–23. https://doi.org/10.1080/01621459.2014.956872
18. Austin PC. An introduction to propensity score methods for reducing the effects of confounding in observational studies. Multivariate Behav Res. 2011;46:399–424. https://doi.org/10.1080/00273171.2011.568786
19. Funk MJ, Westreich D, Wiesen C, Stürmer T, Brookhart MA, Davidian M. Doubly robust estimation of causal effects. Am J Epidemiol. 2011;173:761–7. https://doi.org/10.1093/aje/kwq439

20. Lin W. Agnostic notes on regression adjustments to experimental data: reexamining Freedman's critique. Ann Appl Stat. 2013;7:295–318. https://doi.org/10.1214/12-AOAS583
21. Wei SQ, Bilodeau-Bertrand M, Liu S, Auger N. The impact of COVID-19 on pregnancy outcomes: a systematic review and meta-analysis. CMAJ. 2021;193:E540–8. https://doi.org/10.1503/cmaj.202604
22. Thachil J, Tang N, Gando S, Falanga A, Cattaneo M, Levi M, et al. ISTH interim guidance on recognition and management of coagulopathy in COVID-19. J Thromb Haemost. 2020;18:1023–6. https://doi.org/10.1111/jth.14810
23. Di Renzo GC, Giardina I. Coronavirus disease 2019 in pregnancy: consider thromboembolic disorders and thromboprophylaxis. Am J Obstet Gynecol. 2020;223:135. https://doi.org/10.1016/j.ajog.2020.04.017
24. Metz TD, Clifton RG, Hughes BL, Sandoval G, Saade GR, Grobman WA, et al.; Eunice Kennedy Shriver National Institute of Child Health and Human Development (NICHD) Maternal-Fetal Medicine Units (MFMU) Network. Disease severity and perinatal outcomes of pregnant patients with coronavirus disease 2019 (COVID-19). Obstet Gynecol. 2021;137:571–80. https://doi.org/10.1097/AOG.0000000000004339
25. Patberg ET, Adams T, Rekawek P, Vahanian SA, Akerman M, Hernandez A, et al. Coronavirus disease 2019 infection and placental histopathology in women delivering at term. Am J Obstet Gynecol. 2021;224:382.e1–18. https://doi.org/10.1016/j.ajog.2020.10.020
26. Shanes ED, Mithal LB, Otero S, Azad HA, Miller ES, Goldstein JA. Placental Pathology in COVID-19. Am J Clin Pathol. 2020;154:23–32. https://doi.org/10.1093/ajcp/aqaa089
27. Schwartz DA, Baldewijns M, Benachi A, Bugatti M, Collins RRJ, De Luca D, et al. Chronic histiocytic intervillositis with trophoblast necrosis are risk factors associated with placental infection from coronavirus disease 2019 (COVID-19) and intrauterine maternal-fetal severe acute respiratory syndrome coronavirus 2 (SARS-CoV-2) transmission in liveborn and stillborn infants. Arch Pathol Lab Med. 2021;145:517–28. https://doi.org/10.5858/arpa.2020-0771-SA
28. Di Mascio D, Sen C, Saccone G, Galindo A, Grünebaum A, Yoshimatsu J, et al. Risk factors associated with adverse fetal outcomes in pregnancies affected by Coronavirus disease 2019 (COVID-19): a secondary analysis of the WAPM study on COVID-19. J Perinat Med. 2020;48:950–8. https://doi.org/10.1515/jpm-2020-0355
29. la Cour Freiesleben N, Egerup P, Hviid KVR, Severinsen ER, Kolte AM, Westergaard D, et al. SARS-CoV-2 in first trimester pregnancy: a cohort study. Hum Reprod. 2021;36:40–7.
30. De Luca D. Managing neonates with respiratory failure due to SARS-CoV-2. Lancet Child Adolesc Health. 2020;4:e8. https://doi.org/10.1016/S2352-4642(20)30073-0
31. Kucirka LM, Lauer SA, Laeyendecker O, Boon D, Lessler J. Variation in false-negative rate of reverse transcriptase polymerase chain reaction-based SARS-CoV-2 tests by time since exposure. Ann Intern Med. 2020;173:262–7. https://doi.org/10.7326/M20-1495
32. Kumari V, Mehta K, Choudhary R. COVID-19 outbreak and decreased hospitalisation of pregnant women in labour. Lancet Glob Health. 2020;8:e1116–7. https://doi.org/10.1016/S2214-109X(20)30319-3

Address for correspondence: Jacques Jani, Department of Obstetrics and Gynecology, University Hospital Brugmann, Place A. Van Gehuchten 4, 1020 Brussels, Belgium; email: jackjani@hotmail.com

Distribution and Characteristics of Human Plague Cases and *Yersinia pestis* Isolates from 4 *Marmota* Plague Foci, China, 1950–2019

Zhaokai He,[1] Baiqing Wei,[1] Yujiang Zhang,[1] Jun Liu,[1] Jinxiao Xi,[1] Dunzhu Ciren,[1] Teng Qi,[1] Junrong Liang, Ran Duan, Shuai Qin, Dongyue Lv, Yuhuang Chen, Meng Xiao, Rong Fan, Zhizhong Song, Huaiqi Jing, Xin Wang

We analyzed epidemiologic characteristics and distribution of 1,067 human plague cases and 5,958 *Yersinia pestis* isolates collected from humans, host animals, and insect vectors during 1950–2019 in 4 *Marmota* plague foci in China. The case-fatality rate for plague in humans was 68.88%; the overall trend slowly decreased over time but fluctuated greatly. Most human cases (98.31%) and isolates (82.06%) identified from any source were from the *Marmota himalayana* plague focus. The tendency among human cases could be divided into 3 stages: 1950–1969, 1970–2003, and 2004–2019. The *Marmota sibirica* plague focus has not had identified human cases nor isolates since 1926. However, in the other 3 foci, *Y. pestis* continues to circulate among animal hosts; ecologic factors might affect local *Y. pestis* activity. *Marmota* plague foci are active in China, and the epidemic boundary is constantly expanding, posing a potential threat to domestic and global public health.

Author affiliations: National Institute for Communicable Disease Control and Prevention, Beijing, China (Z. He, J. Liang, R. Duan, S. Qin, D. Lv, M. Xiao, R. Fan, H. Jing, X. Wang); Qinghai Institute for Endemic Disease Control and Prevention, Xining, China (B. Wei); Center for Disease Control and Prevention of Xinjiang Uygur Autonomous Region, Urumqi, China (Y. Zhang); Inner Mongolia Autonomous Region Comprehensive Center for Disease Control and Prevention, Hohhot, China (J. Liu); Gansu Provincial Centre for Disease Control and Prevention, Lanzhou, China (J. Xi); Center for Disease Control and Prevention of Tibet Autonomous Region, Lhasa, China (D. Ciren); Sichuan Center for Disease Control and Prevention, Chengdu, China (T. Qi); Shenzhen Nanshan Maternity and Child Healthcare Hospital, Shenzhen, China (Y. Chen); Yunnan Center for Disease Control and Prevention, Kunming, China (Z. Song)

DOI: https://doi.org/10.3201/eid2710.202239

Plague is a highly virulent fleaborne zoonotic disease caused by the bacterium *Yersinia pestis* (*1*,*2*). Humans can acquire plague through contact with infectious animal tissues or through inhalation. Human contact with infectious animal tissues usually occurs when hunting, trapping, skinning, or handling meat of infected animals. Humans infected through animal contact can develop pneumonic plague and, if not treated, spread their infections to other persons by coughing infectious respiratory droplets. Over the course of human history, plague pandemics have caused hundreds of millions of deaths around the world (*3*–*5*). Currently, the Democratic Republic of the Congo and Madagascar in Africa are the most severe plague epidemic areas; human cases are reported in Madagascar almost every year (*6*–*10*). Plague outbreaks also have caused major public health crises in China. In the first half of the 20th Century, *Y. pestis* caused several large epidemics and nearly 1 million deaths (*11*–*17*).

Plague foci in China are divided into 12 types on the basis of geographic landscape, host, vector, and *Y. pestis* ecotype characteristics (*18*). Among these, 4 are *Marmota* (marmot) foci: the *Marmota himalayana* (Himalayan marmot) plague focus, located in the Qinghai-Tibet Plateau; the *Marmota baibacina*–*Spermophilus undulatus* (gray marmot–long-tailed ground squirrel) plague focus, in the Tianshan Mountains; the *Marmota caudata* (red marmot) plague focus, in the Pamir Plateau; and the *Marmota sibirica* (Tarbagan marmot) plague focus, in the Hulun Buir Plateau of Inner Mongolia.

[1]These authors contributed equally to this article.

The *Marmota himalayana* plague focus is the largest and the most active foci in China. This focus covers >443,290 km^2 and, before the 1990s, most human cases occurred here. Since the 1990s, rat-associated plague epidemics have erupted in southern China, but beginning in 2004, the *Marmota himalayana* plague focus re-emerged as the main source of human cases. Outbreaks have occurred every few years in this focus.

Ecologic factors, including relevant environmental variables, have strong impacts on the shift between periods of inactivity, when plague is maintained at low levels of transmission among its animal reservoirs, and periods of activity, when rates of transmission greatly increase and cause widespread die-offs among susceptible rodents and increased numbers of human cases (*19*–*22*). Because of limitations of experimental technology and economic conditions, plague cases before 1958 were confirmed only by clinical symptoms, such as sudden high fever and lymphadenopathy; human cases usually were accompanied by increased rates of rodent deaths in the area before or at the early stage of human illnesses. Since the 1950s, China has strengthened plague surveillance and control and the number of human cases has decreased rapidly. Cases in the *Marmota* plague foci have continued to slowly decline; nevertheless, the combined numbers of cases from these foci during 1950–2019 exceeded the total number of plague cases in the United States during 1900–2012 (*23*).

Currently, most human cases in China occur in the *Marmota* plague foci. We investigated the distribution and characteristics of human plague cases and *Y. pestis* isolates recovered from animal hosts (mainly marmots) and insect vectors (mainly fleas) during 1950–2019. We describe the prevalence of *Y. pestis* in humans, animal hosts, and insect vectors of China.

Methods

Data Sources and Analyses

We included human cases and *Y. pestis* isolates from *Marmota* plague foci in China collected during 1950–2019. We applied descriptive statistics to analyze the distribution of isolates and human cases for each year (Figure 1–4) and for 5-year intervals (Figure 5). The main sources of data were 2 texts on the history of plague in China (*24*,*25*) and surveillance data of plague obtained from the regions comprising the *Marmota* plague foci, namely Qinghai Province (Qinghai), Gansu Province (Gansu), Tibet Autonomous Region (Tibet), Sichuan Province (Sichuan), Xinjiang Uygur Autonomous Region (Xinjiang), and Inner Mongolia Autonomous Region (Inner Mongolia) (*26*). These foci contain vast lands away from human habitation and surveillance efforts over time have gradually focused more intensely on the spots within these foci where plague is prevalent in marmots and found near human habitations.

The sources of *Y. pestis* isolates in *Marmota* plague foci were animals found dead in the environment, plague patients, insect vectors, and a few live animals. Samples collected from animals found dead in the environment showed most animals died of plague.

Diagnosis of Human Plague Cases

Human cases before 1958 included in the study mainly were confirmed by clinical and epidemiologic investigation based on symptoms, as stated. Human cases after 1958 included in the study had been confirmed by microbiological or serologic diagnosis.

Results

Landscape, Host, Vector, and Other Ecologic Features

The *Marmota himalayana* plague focus, identified in 1954, covers Qinghai, Gansu, Tibet, Sichuan, and Xinjiang

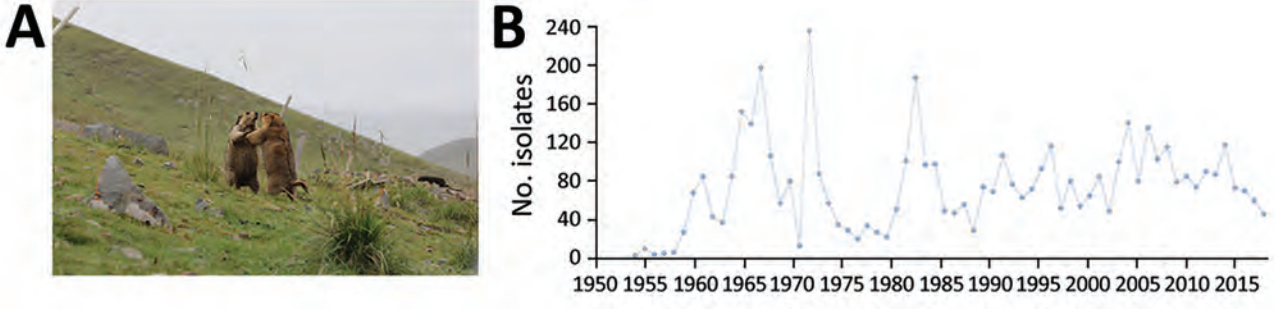

Figure 1. Plague ecology and surveillance of *Yersinia pestis* in the *Marmota himalayana* plague focus, Qinghai-Tibet Plateau, China, 1950–2019. This focus area encompasses Qinghai Province, Gansu Province, Tibet Autonomous Region, Sichuan Province, and Xinjiang Uygur Autonomous Region. A) The Himalayan marmot (*M. himalayana*), the predominant marmot species in this focus. Photograph by Xin Wang. B) Number of *Y. pestis* isolates collected from humans, animal hosts, and insect vectors (mostly *Callopsylla dolabris* and *Oropsylla silantiewi* fleas) in the focus.

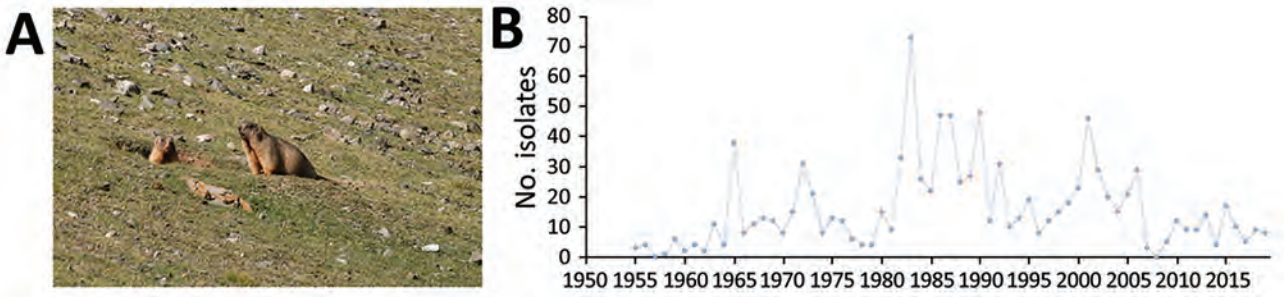

Figure 2. Plague ecology and surveillance of *Yersinia pestis* in the *Marmota baibacina–Spermophilus undulatus* plague focus of the Tianshan Mountains, Xinjiang Uygur Autonomous Region, China, 1950–2019. A) The gray marmot (*M. baibacina*), the predominant marmot species in this focus. Photograph by Yujiang Zhang. The long-tailed ground squirrel (*S. undulatus*) also is an *Y. pestis* host in the focus. B) Number of *Y. pestis* isolates collected from humans, animal hosts, and insect vectors (mostly *Oropsylla silantiewi* and *Citellophilus tesquorum* fleas) in the focus.

(Figure 6). The main host is the Himalayan marmot (Figure 1, panel A), which inhabits high-frigid shrub habitats and meadow-steppe zone at altitudes of 2,700–5,450 m. *Callopsylla dolabris* and *Oropsylla silantiewi* fleas are the main insect vectors (Table 1).

The *Marmota baibacina–Spermophilus undulatus* plague focus was identified in 1955 and is in Xinjiang (Figure 6). The main animal hosts are the gray marmot (Figure 2, panel A) and long-tailed ground squirrel, both of which inhabit forest meadow-steppe and alpine meadow-steppe zones at altitudes of 1,600–4,000 m. *O. silantiewi* fleas and *Citellophilus tesquorum* fleas are the main vectors.

The *Marmota caudata* plague focus was identified in 1956 and is located in Xinjiang (Figure 6). The main host is the red marmot, also known as the golden or long-tailed marmot (Figure 3, panel A), which inhabits the alpine steppe zone at altitudes of 2,800–5,000 m, but most live in the higher end of the range at 3,800–5,000 m. *O. silantiewi* fleas are the main insect vector.

The *Marmota sibirica* plague focus is located at the border of China, Mongolia, and Russia. The focus, located in Inner Mongolia (Figure 6), was identified in 1923. The main animal host is the Tarbagan marmot (Figure 7, panel A), which inhabits low mountains and hills and the meadow-steppe zone at altitudes of 600–800 m. *O. silantiewi* fleas are the main insect vector in this focus. No *Y. pestis* strains have been isolated from the *Marmota sibirica* plague focus since 1926; we only measured host surveillance in this focus. Surveillance of the Tarbagan marmot population density was started in 1978 (Figure 7, panel B). Professionals from the local Chinese Center for Disease Control and Prevention office conduct surveillance by counting the number of marmots observed along survey routes, then calculate density by dividing the number of marmots observed by the size of area. During 1978–2019, the density of *M. sibirica* in the focus area was highest in 2004, 1.274 marmots/hectare (10,000 m^2) and lowest in 1989 (0 per hectare) (Figure 7, panel B).

Distribution Characteristics of *Y. pestis* Isolates

During 1950–2019, a total of 5,958 *Y. pestis* isolates were recovered from *Marmota* plague foci in China. On average, 85.11 *Y. pestis* isolates were recovered each year. The years with the most isolates were 1967

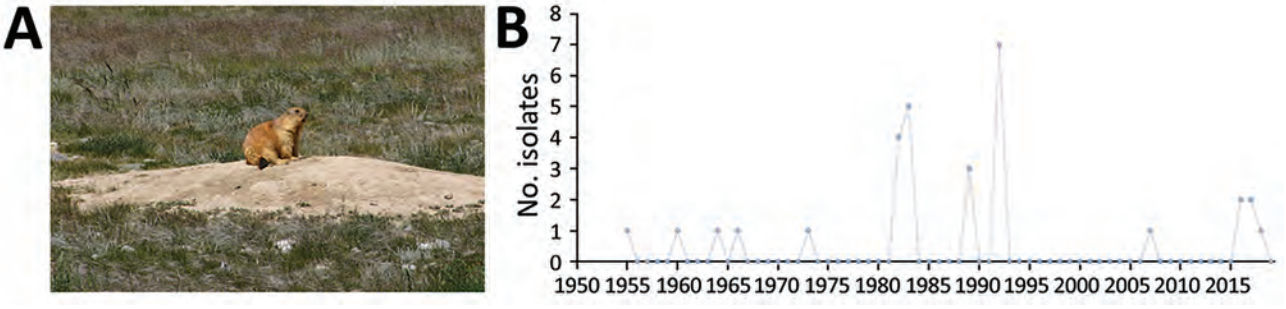

Figure 3. Plague ecology and surveillance of *Yersinia pestis* in the *Marmota caudata* plague focus of the Pamir Plateau, Xinjiang Uygur Autonomous Region, China, 1950–2019. A) The red marmot (*M. caudata*), the predominant marmot species in this focus. Photograph by Yujiang Zhang. B) Number of *Y. pestis* isolates collected from humans, animal hosts, and insect vectors (mostly *Oropsylla silantiewi* fleas) in the focus.

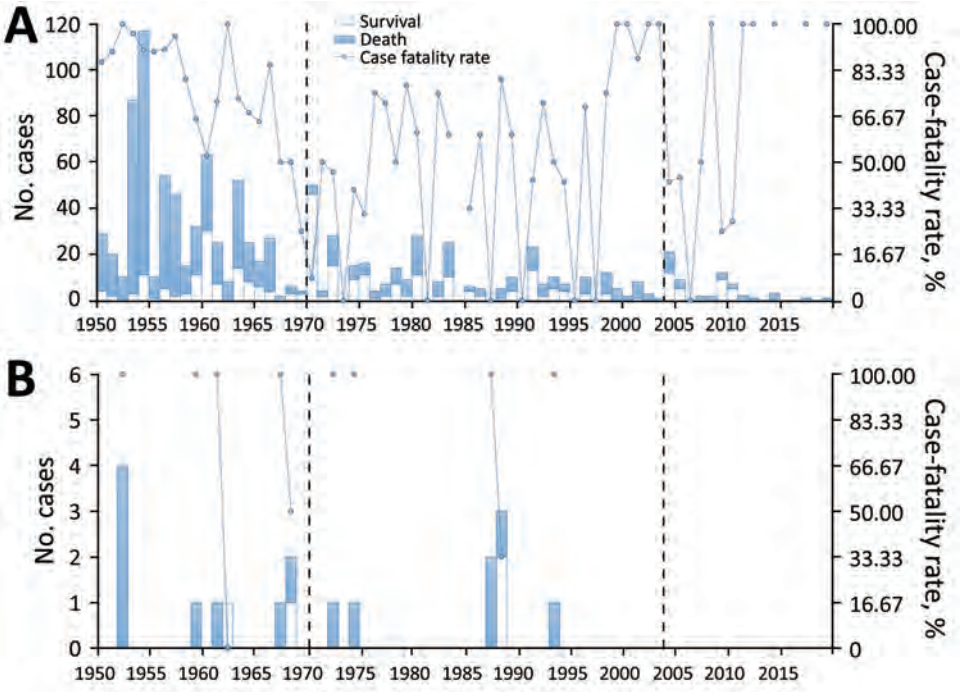

Figure 4. Frequency of human plague cases and case-fatality rates in 2 *Marmota* plague foci, China, 1950–2019. A) *Marmota himalayana* plague focus of the Qinghai-Tibet Plateau, which includes Qinghai Province, Gansu Province, Tibet Autonomous Region, Sichuan Province, and Xinjiang Uygur Autonomous Region. B) *Marmota baibacina–Spermophilus undulatus* plague focus includes Xinjiang Uygur Autonomous Region.

(208 isolates), 1983 (265 isolates), and 1972 (267 isolates). No *Y. pestis* isolates were recovered from the *Marmota sibirica* plague focus during this period.

Y. pestis has been isolated in the *Marmota himalayana* plague focus every year since the first isolate was recovered in 1954. During 1954–2019, 4,889 isolates were collected from the focus. In the *Marmota baibacina–Spermophilus undulatus* plague focus, *Y. pestis* isolates were first recovered in 1955 and a total of 1,039 isolates were collected by 2019. In the *Marmota caudata* plague focus, *Y. pestis* was first isolated in 1956 and 30 isolates were collected by 2019.

Epidemiologic Characteristics of Human Plague Cases

During 1950–2019, total of 1,067 human plague cases have occurred in the 4 *Marmota* plague foci in China, including 735 deaths. The average case-fatality rate was 68.88%, 15.24 cases annually. Among all plague

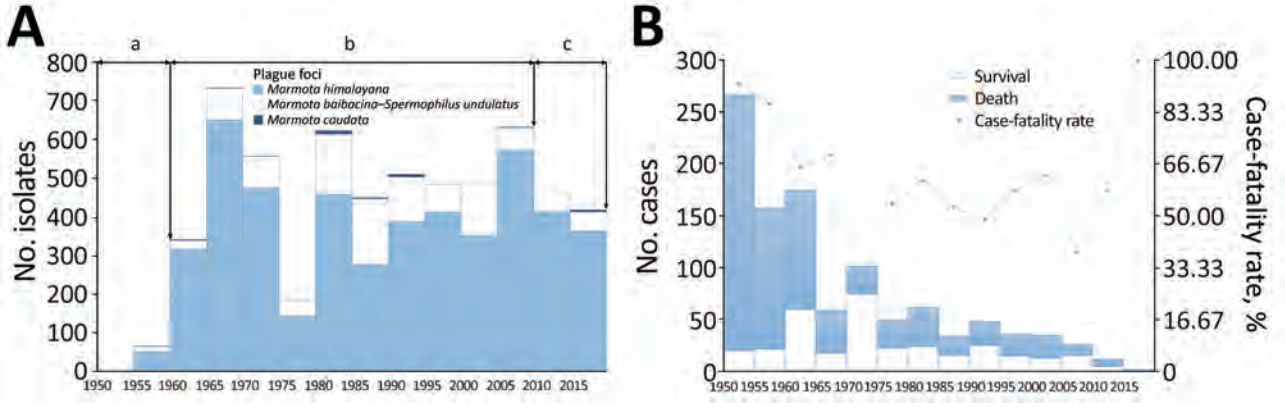

Figure 5. Number of *Yersinia pestis* isolates and human plague cases in *Marmota* plague foci, China, 1950–2019. Columns represent 5-year intervals. The 3 plague foci from which *Y. pestis* isolates have been collected are the *Marmota himalayana* plague focus of the Qinghai-Tibet Plateau, which includes Qinghai Province, Gansu Province, Tibet Autonomous Region, Sichuan Province, and Xinjiang Uygur Autonomous Region; the *Marmota baibacina–Spermophilus undulatus* plague focus of the Tianshan Mountains, Xinjiang Uygur Autonomous Region; and the *Marmota caudata* plague focus of the Pamir Plateau, Xinjiang Uygur Autonomous Region. A) Number of *Y. pestis* isolates collected from humans, animal hosts, and insect vectors. Lowercase letters at top indicate periods of isolate collection: a) early attempts during 1950–1959; b) increased diagnosis and animal plague surveillance increased number isolates collected during 1960–2009; and c) decrease in isolates likely due to decreasing numbers of dead marmot species found around active *Y. pestis* areas during 2010–2019. B) Number of human plague cases and case-fatality rates.

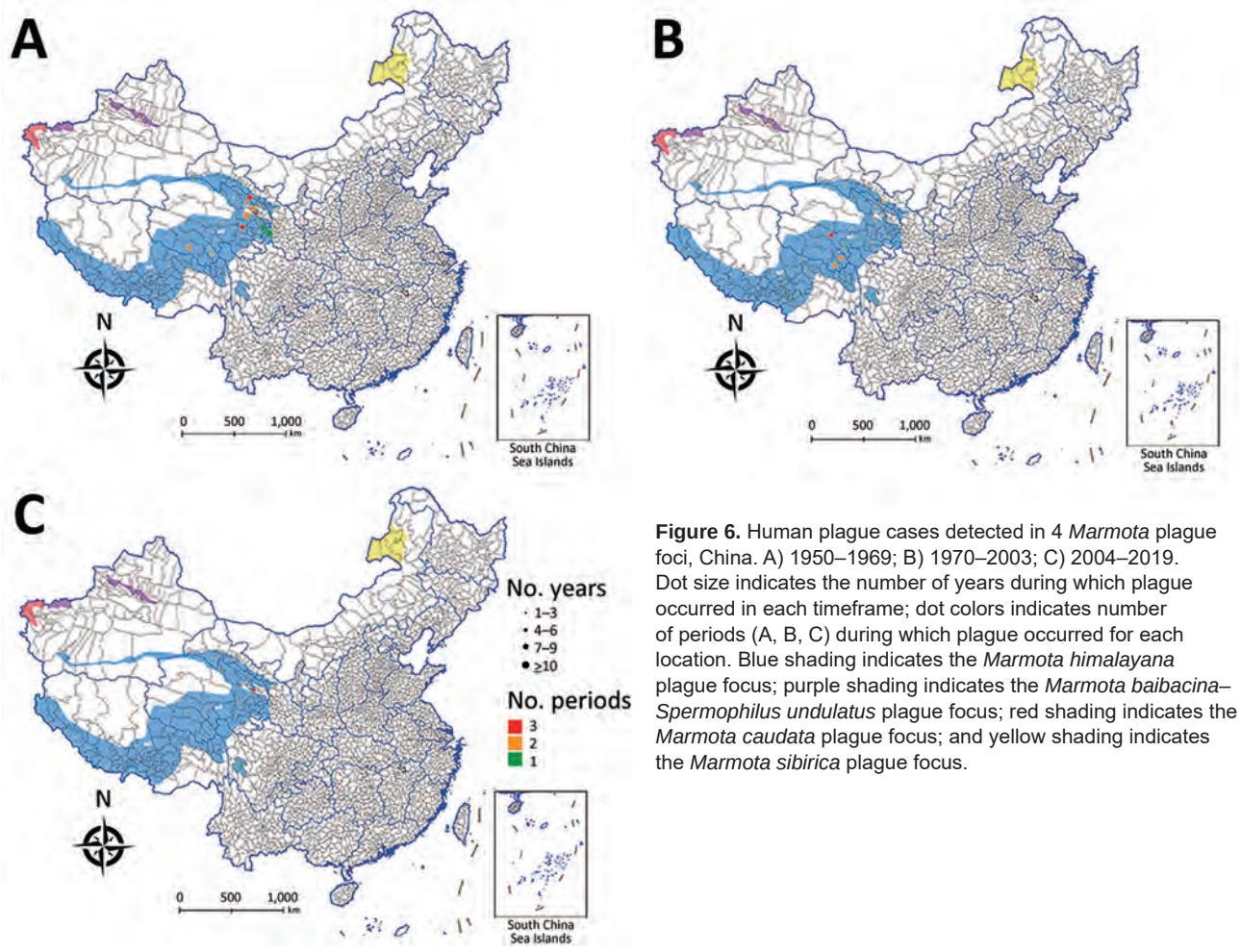

Figure 6. Human plague cases detected in 4 *Marmota* plague foci, China. A) 1950–1969; B) 1970–2003; C) 2004–2019. Dot size indicates the number of years during which plague occurred in each timeframe; dot colors indicates number of periods (A, B, C) during which plague occurred for each location. Blue shading indicates the *Marmota himalayana* plague focus; purple shading indicates the *Marmota baibacina–Spermophilus undulatus* plague focus; red shading indicates the *Marmota caudata* plague focus; and yellow shading indicates the *Marmota sibirica* plague focus.

cases, 690 were confirmed by laboratory or serologic diagnosis; 377 were diagnosed by clinical and epidemiologic investigations. Most cases occurred in 1953 (87 cases), 1954 (117 cases), and 1960 (63 cases).

During 1950–2019, the *Marmota himalayana* plague focus had the most (1,049) human cases (Figure 4, panel A); only 18 cases have occurred in the *Marmota baibacina–Spermophilus undulatus* plague focus (Figure 4, panel B). No human cases have been reported in the *Marmota caudata* or *Marmota sibirica* plague foci during 1950–2019.

Human case counts during 5-year intervals show the highest number of cases (267) occurred during 1950–1954 and the lowest (2 cases) during 2015–2019. Mortality rates were highest (92.51%) during 1950–1954 and 2015–2019 (100%) and lowest (26.47%) during 1970–1974 (Figure 5, panel B).

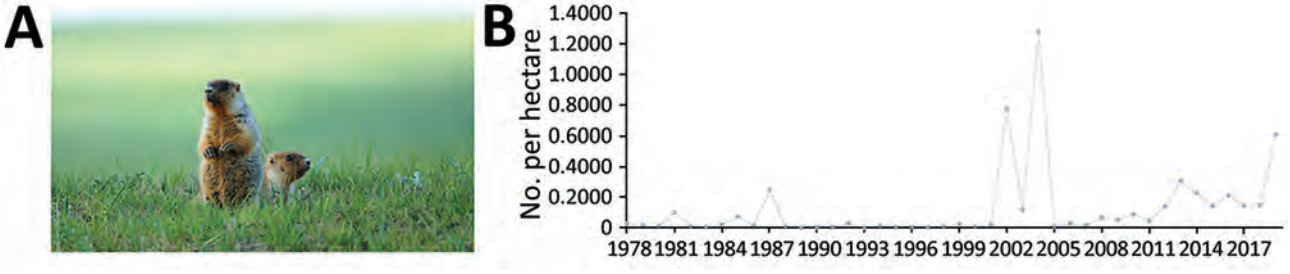

Figure 7. Ecology and surveillance of marmots in the *Marmota sibirica* plague focus of the Hulun Buir Plateau, Inner Mongolia, 1950–2019. A) Tarbagan marmot (*M. sibirica*), the predominant marmot species in this focus. Photograph by Jun Liu. B) Average density of this species in the focus area. Tarbagan marmots host *Oropsylla silantiewi* fleas, a known vector of *Yersinia pestis*, but no *Y. pestis* isolate has been collected from humans, animal hosts, or insect vectors in this focus since 1926.

Table 1. Ecologic characteristics of *Marmota* plague foci, China, 1950–2019

Characteristics	*Marmota himalayana**	*Marmota baibacina–Spermophilus undulatus*†	*Marmota caudata*‡	*Marmota sibirica*§
Year *Yersinia pestis* first isolated	1954	1955	1956	1923
Regions	Qinghai Province, Gansu Province, Tibet Autonomous Region, Sichuan Province, Xinjiang Uygur Autonomous Region	Xinjiang Uygur Autonomous Region	Xinjiang Uygur Autonomous Region	Inner Mongolia Autonomous Region
Hosts	Himalayan marmot	Gray marmot, long-tailed ground squirrel	Red marmot	Tarbagan marmot
Vectors	*Callopsylla dolabris*, *Oropsylla silantiewi* fleas	*O. silantiewi*, *Citellophilus tesquorum* fleas	*O. silantiewi* fleas	*O. silantiewi* fleas
Altitude	2,700–5,450 m	1,600–4,000 m	2,800–5,000 m	600–800 m
Hibernation				
Start	September–October	September	Mid-September	Late September–early October
End	Late March–mid-April	Early- to mid-April	Early April	Late March–early April
Animal plague season	April–October	May-September	May–August	NA¶
Peak	June–July	July	July	NA¶
Habitat	High-frigid shrubs, meadow-steppe	Forest-meadow-steppe, alpine meadow-steppe	Alpine steppe	Low mountains and hills, meadow-steppe

*Qinghai-Tibet Plateau.
†Tianshan Mountains.
‡Pamirs Plateau.
§Hulun Buir Plateau of Inner Mongolia.
¶No *Y. pestis* isolated since 1926.

The patterns of decline for human cases are different in the 2 most active foci (Figure 4). In the *Marmota himalayana* plague focus, the number of cases was relatively high and periodically fluctuated, but both the number and frequency of peaks declined over time (Figure 4, panel A). During 1950–1969, the number of cases was high and the peak interval was short; during 1970–2003, the number of cases decreased sharply and the interval was longer; after 2004, the number of cases declined further and in some years no cases were reported. In contrast, the pattern of decline in human cases in the *Marmota baibacina–Spermophilus undulatus* plague focus has had longer intervals. In several years ≤4 human cases occurred and no case has been reported since 1994 (Figure 4, panel B). During 1950–2019, primary and secondary pneumonic plague accounted for 69.26% (739/1,067) of cases, among which the case-fatality rate was 75.10% (555/739) (Table 2). The rate of other plague types, such as bubonic and septicemic, was 54.88% (180/328) (Table 2).

Discussion

Four *Marmota* plague foci have been identified and classified in China. Each focus is characterized by the marmot species that serves as the primary *Y. pestis* host in the region, but other animals in these areas also can be infected, usually with highly virulent *Y. pestis* strains (*27*). The 4 foci are active areas where animal and human plague epidemics continue in China. Except for the *Marmota sibirica* plague focus, most foci are in western China (Figure 6). Climatic conditions, such as long winters with heavy snow, are characteristic of these foci, as are unique geographic features, such as frozen glacial soils, cold desert plateaus, alpine grasslands, and river wetlands. Many rare wild animals inhabit these plateaus, and the human population is sparse. Little human disturbance and rela-

Table 2. Case-fatality rates for pneumonic and other types of plague, by *Marmota* plague focus, China, 1950–2019*

Focus	Pneumonic plague	Other plague types†	Total
Marmota himalayana‡	75.03 (544/725)	54.63 (177/324)	68.73 (721/1,049)
Marmota baibacina–Spermophilus undulatus§	78.57 (11/14)	75.00 (3/4)	77.78 (14/18)
Marmota caudata¶	0	0	0
Marmota sibirica#	0	0	0
Total case-fatality rate	75.10 (555/739)	54.88 (180/328)	68.88 (735/1,067)

*Data are reported as case-fatality rate, % (no. deaths/no. cases).
†Including bubonic, septicemic, and other types.
‡Qinghai-Tibet Plateau.
§Tianshan Mountains.
¶Pamirs Plateau.
#Hulun Buir Plateau of Inner Mongolia.

tively stable plague ecology could be conducive to maintaining the ecologic balance and active plague status of these foci (*21*).

The *Marmota sibirica* plague focus is located at the junction of China, Mongolia, and Russia, and 2 plague epidemics occurred in this focus in the early 20th Century. Of note, no human case has been reported in this part of China since 1923, and *Y. pestis* has not been isolated from there since 1926. However, cases of animal and human plague from this focus are reported in Mongolia and Russia (*11*–*17*,*28*–*35*). The main reason for the lack of human cases in this focus in China is the considerable decrease in Tarbagan marmot populations, which are believed to be due to ecologic changes and increased human activity. The development of animal husbandry, such as raising sheep that graze in marmot habitats in the region, and environmental disruption due to transportation and farming activities, have caused irreversible damage to the Tarbagan marmot habitat. In addition, sale of marmot skins and meat have depleted the population; ≈2,500,000 marmot skins were purchased in 1910, the peak year. In addition, a large fire in 1987 caused devastating damage to the Tarbagan marmot habitat and killed ≈200,000 marmots (*36*).

When the existing ecologic balance is disrupted, for instance due to habitat damage, the number of *Y. pestis* hosts and the host density changes, thus affecting the survival of the bacterium. *Y. pestis* circulates among animal and vector hosts within a limited range and with discrete distribution where it seldom causes human plague and is rarely detected by regular surveillance. The interactions between host, pathogen, and environment seem to be gradually settling into a period of relative inactivity in all *Marmota* plague foci (*19*,*21*).

China began attempts to isolate *Y. pestis* during 1950–1959 and the number of isolates recovered was relatively low (Figure 5). During 1960–2009, the number of collected isolates greatly increased, mainly due to improved case diagnosis and animal plague surveillance and plague diagnosis is confirmed through pathogen isolation or other laboratory evidence. During 2010–2019, the number of *Y. pestis* isolates decreased in China, which seems to be related to the decrease of marmots found dead around active plague locations and human cases. In 1953, China established specialized plague investigation agencies for the *Marmota* plague foci. Many unsuccessful attempts at eradicating *Y. pestis* in these foci have demonstrated that plague is inherent in these areas and cannot be eliminated by large scale attempts to kill rodent hosts (*21*,*27*,*37*).

After these unsuccessful attempts to reduce the possibility of human exposure to plague, *Y. pestis* elimination efforts have focused more on key locations and key seasons, particularly in locations with epidemic activity and during the peak marmot and flea breeding seasons (*38*). Long-term training and education among clinicians has resulted in more timely diagnosis, treatment, and reporting of human plague cases (*39*). Improving humans' awareness about plague and their ability to protect themselves seems to have reduced their exposure to marmots and infected fleas. For future surveillance, appropriate typing methods for tracking the spread of certain *Y. pestis* strains are needed. The *Y. pestis* genome remains stable in *Marmota* plague foci, enabling *Y. pestis* to maintain its high pathogenicity and virulence, and most *Y. pestis* strains in the *Marmota* plague foci are highly virulent (*27*). Single-nucleotide polymorphism typing and other phylogenic studies have shown that *Y. pestis* clusters geographically in China; it could take years to accumulate several mutations within the same focus or region (*40*).

During 1950–2019, human cases in the *Marmota* plague foci of China were mainly concentrated in the *Marmota himalayana* focus, which has remained active since it was identified in 1954 (*41*,*42*). Only 18 human cases have been reported in the *Marmota baibacina*–*Spermophilus undulatus* plague focus. No human case has ever been reported in the *Marmota caudata* plague focus since it was identified in 1956, which can be attributed to limited human habitation and limited exposure to infected animals. No human cases have been reported in the *Marmota sibirica* plague focus since 1923; marmot density in this region generally is low but has been reported as being abnormally high for several years (Figure 7, panel B), perhaps because earlier sampling was not representative of the whole because survey areas were limited. Recent ecologic protection measures in this region might raise the Tarbagan marmot density, which could increase the numbers of *Y. pestis*–infected marmots. Previously scattered pockets of *Y. pestis* infection might enlarge and eventually merge with other pockets, leading to a threat of increased spread among marmots and heightened human plague risk (*19*,*21*).

Human cases in the *Marmota* plague foci have shown a decreasing trend, but a slower decrease than in other plague foci of China. *Marmota* plague foci had a relatively high average case-fatality rate of 68.88% during 1950–2019 because of a higher proportion of pneumonic cases, which had a much higher average case-fatality rate (75.10%) than other plague types. In contrast, bubonic and septicemic plague had a com-

bined case-fatality rate of 54.88%. Because pneumonic plague can be transmitted directly between humans without vector involvement (*37*,*43*), it can spread rapidly in densely populated areas, as has occurred in several pandemics (*3*–*5*,*44*). In China, human cases before 1958 were pneumonic plague and had an extremely high fatality rate of 92.57% (Figure 5, panel B). Delayed medical treatment and misdiagnosis might contribute to high fatality rates. For instance, when horses were the main form of transportation, most human cases progressed to pneumonic plague because timely access to treatment was not possible; large-scale outbreaks with human-to-human transmission and high case-fatality rates were reported. At the same time, some sporadic or bubonic cases might have been missed. Nevertheless, the possibility of misdiagnosis in the past is estimated to be low because of high case-fatality rates, obvious clinical features, and epidemiologic evidence of rodent deaths before or at the early stage of illness and, in some cases, human-to-human transmission.

In recent years, the most active region of the *Marmota himalayana* plague focus has been Subei County in Gansu, where animal plague is extremely epizootic and the case-fatality rate is high. However, the area is sparsely populated, only ≈15,100 residents in 66,700 km^2, and improvements in early detection, diagnosis, and treatment have been achieved. Although the case-fatality rate is high, the disease is unlikely to spread to other areas because few persons travel outside Subei and because timely diagnosis and control help prevent further spread. Plague in the area mainly is limited to family groups, occasionally affecting neighbors or medical staff. In some years, the area had a high number of cases, but the case-fatality rate was low compared with the extremely high case-fatality rate of most years (Figure 5). Despite multiple pneumonic plague outbreaks in these epidemic spots, doctors and the public are highly vigilant and timely and effective antimicrobial drug treatment has improved patient prognoses. In 2009, for example, when an index case was identified in the county, a national medical team of experts from Beijing and Qinghai arrived at the scene to treat human plague cases and mitigate further spread (*41*).

The main transmission route of plague in the *Marmota* plague foci in China is through wounds incurred during marmot skinning, bites from infected fleas, or human-to-human transmission by pneumonic patients. In rare cases, shepherd dogs with pneumonic plague have transmitted plague to herders (*41*,*42*). In addition, Tibetan sheep (*Ovis aries*) are a host species unique to the *Marmota himalayana* plague focus and the number of human cases caused by sheep infections in this foci is second only to those caused by marmots. During 1950–2019, a total of 80 related human plague cases were reported, most caused by skinning and eating infected sheep. Tibetan sheep become infected through consuming animals that have died of plague or via bites from infected fleas. The sheep especially like chewing bone remains, which leads to oral mucosa damage and *Y. pestis* infection (*45*,*46*). Human cases have major occupational characteristics; most victims are marmot poachers, local herdsmen, and hired herders (*42*). Because of prohibitions on hunting, trafficking, and sales of marmots and related laws and education on self-protection, the number of poachers and herdsmen infection has decreased sharply. Recently, hired herders have become the most likely to be infected because they received less education on avoiding plague and engaged in skinning and eating marmots. In addition, transportation to *Marmota* plague foci has become convenient, greatly increasing the risk for long-distance transmission when persons leave foci plague infected with *Y. pestis* or carrying *Y. pestis* infected flea vectors. Illegal hunting and trading of marmots for their meat and skins also occasionally has occurred and live marmots are being shipped to densely populated cities, especially to some southern cities, where eating game animals is popular. Because of their unique geographic location and environment, *Marmota* plague foci have become excellent areas for scientific research, exploration, and tourism. Global tourists can easily reach these foci, which increases the risk for *Y. pestis* infection. Moreover, herdsmen from plague foci also can reach domestic and foreign cities within a day; thus, the increasing trend of plague transmission in densely populated areas (*47*). For example, in 2019, two patients with respiratory symptoms in the *Meriones unguiculatus* plague focus of Inner Mongolia were transferred to Chaoyang Hospital in Beijing where pneumonic plague later was diagnosed (*48*). This example demonstrates that human plague is a rare but serious infectious disease that still poses a public health risk in China and worldwide.

In summary, most human plague cases and *Y. pestis* isolates originating in the *Marmota* plague foci of China since 1950 have been concentrated in the *Marmota himalayana* plague focus. Cases from this region exhibit 3 major characteristics: the frequency of human cases during 1950–2019 slowly declined but fluctuated greatly, in sharp contrast to the rapid declines in other plague foci in China; human cases are primarily distributed in the Qinghai-Tibet Plateau and Tianshan Mountains of China; and index case-patients were mainly infected through wounds

incurred while skinning infected marmots. The Qinghai-Tibet Plateau and Tianshan Mountain regions have large land areas but sparse human populations and poor or no medical facilities. Most *Y. pestis* strains derived from marmots are highly virulent (*27*), which results in outbreaks of pneumonic plague, often with higher case-fatality rates. The number of dormant foci have increased and active foci are greatly reduced in China, especially in some southern regions where one of the largest plague outbreaks occurred and primarily associated with exposure of humans to rat flea bites (*21*). In sharp contrast, the *Marmota himalayana* plague focus is sparsely populated, and the interaction between the environment, host, and *Y. pestis* is relatively balanced, which is conductive to the sustained prevalence of plague. As was the case for the 2017 outbreak in Madagascar (*8*), the outcome of human plague in the *Marmota* plague foci of China is uncertain, and risk for long-distance transmission continues, which could have worldwide public health effects. Therefore, plague prevention and control remain a strong priority in China.

Acknowledgments

We thank American Journal Experts (submission no. 47MMS9GB) and Charlesworth author services (paper no. 75168) for their critical editing and helpful comments regarding our manuscript.

This work was supported by the National Sci-Tech Key Project (grant nos. 2018ZX10713-003-002 and 2018ZX10713-001-002).

About the Author

Dr. He is an epidemiologist at the Chinese Center for Disease Control and Prevention. Her research interests include pathogenic *Yersinia* and emerging infectious diseases.

References

1. Pollitzer R. Plague. World Health Organization monograph series no. 22. Geneva: The Organization;; 1954 [cited 2021 Aug 11]. http://apps.who.int/iris/bitstream/10665/41628/1/WHO_MONO_22.pdf
2. Dennis DT, Mead PS. *Yersinia* species, including plague. In: Mandell GL, Bennet JE, Dolin R, editors. Principles and practice of infectious diseases, 7th ed. Philadelphia: Elsevier; 2010. p. 2943–53.
3. Perry RD, Fetherston JD. *Yersinia pestis*—etiologic agent of plague. Clin Microbiol Rev. 1997;10:35–66. https://doi.org/10.1128/CMR.10.1.35
4. Drancourt M, Raoult D. Molecular history of plague. Clin Microbiol Infect. 2016;22:911–5. https://doi.org/10.1016/j.cmi.2016.08.031
5. Wagner DM, Klunk J, Harbeck M, Devault A, Waglechner N, Sahl JW, et al. *Yersinia pestis* and the plague of Justinian 541–543 AD: a genomic analysis. Lancet Infect Dis. 2014;14:319–26. https://doi.org/10.1016/S1473-3099 (13)70323-2
6. Boisier P, Rahalison L, Rasolomaharo M, Ratsitorahina M, Mahafaly M, Razafimahefa M, et al. Epidemiologic features of four successive annual outbreaks of bubonic plague in Mahajanga, Madagascar. Emerg Infect Dis. 2002;8:311–6. https://doi.org/10.3201/eid0803.010250
7. Abedi AA, Shako JC, Gaudart J, Sudre B, Ilunga BK, Shamamba SKB, et al. Ecologic features of plague outbreak areas, Democratic Republic of the Congo, 2004–2014. Emerg Infect Dis. 2018;24:210–20. https://doi.org/10.3201/eid2402.160122
8. Randremanana R, Andrianaivoarimanana V, Nikolay B, Ramasindrazana B, Paireau J, Ten Bosch QA, et al. Epidemiological characteristics of an urban plague epidemic in Madagascar, August–November, 2017: an outbreak report. Lancet Infect Dis. 2019;19:537–45. https://doi.org/10.1016/S1473-3099(18)30730-8
9. Mead PS. Plague in Madagascar—a tragic opportunity for improving public health. N Engl J Med. 2018;378:106–8. https://doi.org/10.1056/NEJMp1713881
10. Andrianaivoarimanana V, Piola P, Wagner DM, Rakotomanana F, Maheriniaina V, Andrianalimanana S, et al. Trends of human plague, Madagascar, 1998–2016. Emerg Infect Dis. 2019;25:220–8. https://doi.org/10.3201/eid2502.171974
11. Lien Teh W, Han CW, Pollitzer R. Plague in Manchuria: I. Observations made during and after the second Manchurian plague epidemic of 1920–21. II. The role of the Tarabagan in the epidemiology of plague. J Hyg (Lond). 1923;21:307–58. https://doi.org/10.1017/S0022172400031521
12. Lien Teh W, Tuck GL, Han CW, Pollitzer R. The second pneumonic plague epidemic in Manchuria, 1920–21: I. A general survey of the outbreak and its course. J Hyg (Lond). 1923;21:262–88. https://doi.org/10.1017/S0022172400031508
13. Lien Teh W, Tuck GL. Investigations into the relationship of the Tarbagan (Mongolian marmot) to plague. Lancet. 1913;182:529–35. https://doi.org/10.1016/S0140-6736(01)76466-5
14. Lien Teh W, Tuck GL. First report of the north Manchurian plague prevention service. J Hyg (Lond). 1913;13:237–90.21. PubMed https://doi.org/10.1017/s0022172400005404
15. Teh WL. Plague in the orient with special reference to the Manchurian outbreaks. J Hyg (Lond). 1922;21:62–76. https://doi.org/10.1017/S0022172400031223
16. Lien-Teh W. A further note on natural and experimental plague in Tarbagans. J Hyg (Lond). 1924;22:329–34. https://doi.org/10.1017/S0022172400008263
17. Teh WL, Chun JWH, Pollitzer R. Clinical observations upon the Manchurian plague epidemic, 1920–21. J Hyg (Lond). 1923;21:289–306. https://doi.org/10.1017/S002217240003151X
18. Ben-Ari T, Neerinckx S, Agier L, Cazelles B, Xu L, Zhang Z, et al. Identification of Chinese plague foci from long-term epidemiological data. Proc Natl Acad Sci U S A. 2012;109:8196–201. https://doi.org/10.1073/pnas.1110585109
19. Heier L, Storvik GO, Davis SA, Viljugrein H, Ageyev VS, Klassovskaya E, et al. Emergence, spread, persistence and fade-out of sylvatic plague in Kazakhstan. Proc Biol Sci. 2011;278:2915–23. https://doi.org/10.1098/rspb.2010.2614
20. Davis S, Begon M, De Bruyn L, Ageyev VS, Klassovskiy NL, Pole SB, et al. Predictive thresholds for plague in Kazakhstan. Science. 2004;304:736–8. https://doi.org/10.1126/science.1095854
21. Wang X, Wei X, Song Z, Wang M, Xi J, Liang J, et al. Mechanism study on a plague outbreak driven by the

construction of a large reservoir in southwest china (surveillance from 2000–2015). PLoS Negl Trop Dis. 2017; 11:e0005425. https://doi.org/10.1371/journal.pntd.0005425
22. Stenseth NC, Samia NI, Viljugrein H, Kausrud KL, Begon M, Davis S, et al. Plague dynamics are driven by climate variation. Proc Natl Acad Sci U S A. 2006;103:13110–5. https://doi.org/10.1073/pnas.0602447103
23. Kugeler KJ, Staples JE, Hinckley AF, Gage KL, Mead PS. Epidemiology of human plague in the United States, 1900–2012. Emerg Infect Dis. 2015;21:16–22. https://doi.org/10.3201/eid2101.140564
24. Institute of Epidemiology and Microbiology, Chinese Academy of Medical Sciences. The history of spread of plague in China [in Chinese]. Beijing: People's Medical Publishing House; 1981. p. 33–1794.
25. Xian W. History of plague epidemics [in Chinese]. Guangzhou (China): Epidemic Prevention Center of Guangdong Province Press; 1988.
26. Liu Y, Tan J, Shen E. The atlas of plague and its environment in People's Republic of China [in Chinese]. Beijing: Science Press; 2000.
27. Wang Z, Li C. Qinghai plague [in Chinese]. Beijing: People's Medical Publishing House Press; 2016.
28. Dubyanskiy VM, Yeszhanov AB. Ecology of *Yersinia pestis* and the epidemiology of plague. In: Yang R, Anisimov A, editors: *Yersinia pestis*: retrospective and perspective. Advances in experimental medicine and biology, volume 918. Dordrecht: Springer: 2016. https://doi.org/10.1007/978-94-024-0890-4_5
29. Pastukhov BN. The epizootic and epidemic situation in the natural foci of plague in the USSR and the prophylactic measures taken. Bull World Health Organ. 1960;23:401–4.
30. Popov NV, Bezsmertny VE, Toporkov VP, Matrosov AN, Knyazeva TV, Kuznetsov AA, et al. Epizootic activity of natural plague foci in the Russian Federation in 2013 and prognosis for the year of 2014 [in Russian]. Problems of Particularly Dangerous Infections. 2014:2;13–8. https://doi.org/10.21055/0370-1069-2014-2-13-18
31. Galdan B, Baatar U, Molotov B, Dashdavaa O. Plague in Mongolia. Vector Borne Zoonotic Dis. 2010;10:69–75. https://doi.org/10.1089/vbz.2009.0047
32. Riehm JM, Tserennorov D, Kiefer D, Stuermer IW, Tomaso H, Zöller L, et al. *Yersinia pestis* in small rodents, Mongolia. Emerg Infect Dis. 2011;17:1320–2. https://doi.org/10.3201/eid1707.100740
33. Riehm JM, Vergnaud G, Kiefer D, Damdindorj T, Dashdavaa O, Khurelsukh T, et al. *Yersinia pestis* lineages in Mongolia. PLoS One. 2012;7:e30624. https://doi.org/10.1371/journal.pone.0030624
34. Jones SD, Amramina AA. Entangled histories of plague ecology in Russia and the USSR. Hist Philos Life Sci. 2018;40:49. https://doi.org/10.1007/s40656-018-0220-3
35. Popov NV, Kuznetsov AA, Matrosov AN, Korzun VM, Verzhutsky DB, Vershinin SA, et al. Epizootic activity of natural plague foci of the Russian Federation in 2008–2017 and forecast for 2018 [in Russian]. Problems of Particularly Dangerous Infections. 2018;4:50–5. https://doi.org/10.21055/0370-1069-2018-1-50-55
36. Liu S, Wang Y, Bao S, Bai Y, De Q. The decrease factors of Marmota sibirica in Hulun Buir League [in Chinese]. Neimenggu Preventive Medicine. 1995;20:59–61. http://qikan.cqvip.com/Qikan/Article/Detail?id=67877898950246004
37. Ji S. Plague [in Chinese]. Beijing: People's Medical Publishing House Press; 1988.
38. National Health Commission of the People's Republic of China. National plague monitoring scheme 2005 [in Chinese] [cited 2021 Aug 11]. http://www.nhc.gov.cn/wjw/zcjd/201304/96300482f5e14a7094d74a9238bf76f2.shtml
39. National Health Commission of the People's Republic of China. Diagnostic criteria for plague 2008 [in Chinese] [cited 2021 Aug 11]. http://www.nhc.gov.cn/wjw/s9491/200802/38803.shtml
40. Cui Y, Yu C, Yan Y, Li D, Li Y, Jombart T, et al. Historical variations in mutation rate in an epidemic pathogen, *Yersinia pestis*. Proc Natl Acad Sci U S A. 2013;110:577–82. https://doi.org/10.1073/pnas.1205750110
41. Wang H, Cui Y, Wang Z, Wang X, Guo Z, Yan Y, et al. A dog-associated primary pneumonic plague in Qinghai Province, China. Clin Infect Dis. 2011;52:185–90. https://doi.org/10.1093/cid/ciq107
42. Ge P, Xi J, Ding J, Jin F, Zhang H, Guo L, et al. Primary case of human pneumonic plague occurring in a Himalayan marmot natural focus area Gansu Province, China. Int J Infect Dis. 2015;33:67–70. https://doi.org/10.1016/j.ijid.2014.12.044
43. Pechous RD, Sivaraman V, Stasulli NM, Goldman WE. Pneumonic plague: the darker side of *Yersinia pestis*. Trends Microbiol. 2016;24:190–7. https://doi.org/10.1016/j.tim.2015.11.008
44. Walløe L. Medieval and modern bubonic plague: some clinical continuities. Med Hist Suppl. 2008;52(S27):59–73. https://doi.org/10.1017/S0025727300072094
45. He J, Xiong H, Qi M, Yang H, Yang X, Jin Y, et al. Epidemic analysis of human plague caused by Tibetan sheep in Qinghai Province [in Chinese]. Chinese Journal of Epidemiology. 2016;35:354–6 http://www.wanfangdata.com.cn/details/detail.do?_type=perio&id=zgdfbxzz201605010
46. Ma Z, Jiang Z. Epidemiological analysis of human plague in Tibet from 1966 to 2012 [in Chinese]. Chinese Journal of Control of Endemic Diseases. 2013;28:119–22 [cited 2021 Aug 11]. http://www.cnki.com.cn/Article/CJFDTotal-DYBF201302016.htm
47. Bogoch II, Maxim T, Acosta H, Bhatia D, Chen S, Huber C, et al. Potential plague exportation from Madagascar via international air travel. Lancet Infect Dis. 2018;18:247–8. https://doi.org/10.1016/S1473-3099(18)30077-X
48. Health Commission of Xilinguole League Inner Mongolia. Two plague cases from Xilinguole League have been confirmed 2019 Nov 12 [cited 2021 Aug 11]. http://wjw.xlgl.gov.cn/zwgk_1/dtxx/201911/t20191112_2267734.htm

Address for correspondence: Xin Wang, National Institute for Communicable Disease Control and Prevention, Chinese Center for Disease Control and Prevention, No.155, Changbai Road, Changping, Beijing 102206, China; email: wangxin@icdc.cn

Novel Outbreak-Associated Food Vehicles, United States

Hilary K. Whitham, Preethi Sundararaman, Daniel Dewey-Mattia, Karunya Manikonda, Katherine E. Marshall, Patricia M. Griffin, Brigette L. Gleason, Sanjana Subramhanya, Samuel J. Crowe

Novel outbreak-associated food vehicles (i.e., foods not implicated in past outbreaks) can emerge as a result of evolving pathogens and changing consumption trends. To identify these foods, we examined data from the Centers for Disease Control and Prevention Foodborne Disease Outbreak Surveillance System and found 14,216 reported outbreaks with information on implicated foods. We compared foods implicated in outbreaks during 2007–2016 with those implicated in outbreaks during 1973–2006. We identified 28 novel food vehicles, of which the most common types were fish, nuts, fruits, and vegetables; one third were imported. Compared with other outbreaks, those associated with novel food vehicles were more likely to involve illnesses in multiple states and food recalls and were larger in terms of cases, hospitalizations, and deaths. Two thirds of novel foods did not require cooking after purchase. Prevention efforts targeting novel foods cannot rely solely on consumer education but require industry preventive measures.

Foodborne illness is a major public health issue in the United States; millions of persons become ill from contaminated food every year (*1*). Most cases are sporadic (i.e., not associated with a disease outbreak) (*2*), and the responsible food(s) is often undetermined. Outbreaks provide an opportunity for public health agencies to determine shared exposures and the source of infection. Many food safety laws and regulations, industry practices, and consumer education efforts have been implemented to make foods safer. Nevertheless, evolving foodborne pathogens and changing consumption trends provide continued opportunities for contamination and illness (*3*–*7*). Within these changing conditions, novel outbreak-associated food vehicles (i.e., foods not implicated in prior outbreaks) can emerge. Identifying these novel food vehicles provides an opportunity to determine emerging sources of illness and to inform prevention policies. To identify novel food vehicles reported during 2007–2016, we examined data from the Centers for Disease Control and Prevention (CDC) Foodborne Disease Outbreak Surveillance System (FDOSS).

Author affiliations: Centers for Disease Control and Prevention, Atlanta, Georgia, USA (H.K. Whitham, P. Sundararaman, D. Dewey-Mattia, K. Manikonda, K.E. Marshall, P.M Griffin, B.L. Gleason, S. Subramhanya, S.J. Crowe); Oak Ridge Institute for Science and Education, Oak Ridge, Tennessee, USA (S. Subramhanya)

DOI: https://doi.org/10.3201/eid2710.204080

Methods

FDOSS is a passive surveillance system that collects reports of foodborne disease outbreaks from federal, state, local, and territorial health departments in the United States. It is the primary source of data for outbreak-associated illnesses, hospitalizations, and deaths; etiologic agents; implicated foods; contributing factors; and preparation and consumption settings. Foodborne outbreaks are nationally notifiable and defined as ≥2 cases of a similar illness resulting from ingestion of the same food (*8*). When exposure occurs in 1 state, the outbreak is classified as a single-state outbreak; when exposure occurs in ≥2 states, the outbreak is classified as a multistate outbreak. Foods or specific ingredients are identified as sources by using epidemiologic, laboratory, traceback, and environmental assessment data. On the basis of this evidence, a sole food (e.g., apple) or a specific ingredient that is part of a complex food (e.g., beef in a sandwich) is reported as the source of an outbreak. A complex food is reported as the source when no specific ingredient is implicated. When an investigation does not identify a source, the food vehicle is reported as undetermined. CDC uses a hierarchical scheme to categorize reported foods (*9*,*10*). For simplicity and ease of interpretation, for this analysis we collapsed some categories (e.g., seeded and row crop vegetables are reported generically as vegetables).

Using FDOSS data from 1973–2016 (accessed December 11, 2017), we reviewed all 14,216 reported

outbreaks with an implicated food or ingredient (henceforth, collectively referred to as food). We compared reported foods from outbreaks with a year of first illness onset during 2007–2016 with those during 1973–2006 by using a 3-stage process to identify novel outbreak-associated food vehicles. First, foods that were reported identically in both time frames were identified and removed by using SAS version 9.4 (SAS Institute Inc., https://www.sas.com). Second, 2 independent reviewers manually compared the remaining 878 food items and flagged any foods that seemed to be novel in 2007–2016. Third, a 5-member panel reviewed all foods initially identified as novel. For the second and third steps, we excluded foods if they were reported in a prior outbreak by using a different term (e.g., rice, wild vs. wild rice), a more general term (e.g., cheddar vs. white cheddar), or a different spelling or an abbreviation (e.g., brat vs. bratwurst) or if a specific contaminated ingredient(s) was not implicated for a newly reported complex food. We adopted this final exclusion criterion when reviewing complex foods in which no specific ingredient was implicated because it could not be determined what ingredients were included in the food itself, much less which ingredient was actually contaminated and could be novel (i.e., direct comparison between 1973–2006 and 2007–2016 was impossible).

We then conducted a secondary check of additional sources for all foods initially identified as novel (PubMed, online forums [e.g., Food Safety News, Food Poison Journal, and MarlerClark], and media reports). This check served to identify false-positive results from 2 scenarios: 1) the food had been implicated in an outbreak during 1973–2006, but the outbreak had not been reported to FDOSS; or 2) the food had been reported as part of an outbreak occurring during 1973–2006 with a more generic term. We reclassified foods only if the available information was sufficient to follow our criteria (i.e., there were $\geq$2 confirmed cases and an identified implicated food).

Novel food vehicles are presented along with key outbreak characteristics, including etiology and various measures of burden (e.g., case counts, deaths) in addition to statistical comparisons of these characteristics for outbreaks associated with food vehicles that are novel or not novel. Specifically, we used nonparametric Wilcoxon tests to assess difference in means and χ^2 tests to assess differences in percentages. Statistical analyses were completed in R version 3.3.3 (R Foundation for Statistical Computing, https://www.r-project.org).

Results

Novel Food Vehicles

By comparing outbreaks from 2007–2016 with those from 1973–2006, we identified 28 novel food vehicles (Table 1); the most common were fish (6), nuts (6), fruits (4), vegetables (3), and meats (3). Two thirds of novel foods did not require cooking after they were purchased (e.g., blueberries, kale, various nuts), and half did not require refrigeration after purchase.

Outbreaks Associated with Novel Food Vehicles

A total of 36 outbreaks were linked to the 28 novel food vehicles during 2007–2016, and 7 foods were implicated in >1 outbreak (bison meat, blueberries, hazelnuts, kale, papaya, pepper, and pistachios). These 36 outbreaks resulted in 1,294 illnesses, 263 hospitalizations, 14 deaths, and 17 recalls. An average of 3.6 (range 0–8) outbreaks associated with a novel food vehicle were reported each year. Among outbreaks linked to a novel food vehicle, 22 (61%) occurred in multiple states; the largest multistate outbreak resulted from ground pepper in salami, involving 45 states and 272 illnesses (*11*). Etiologies included bacteria (27 [75%] outbreaks), toxins (5 [14%]), viruses (1 [3%]), and parasites (1 [3%]). The most commonly reported etiologic agent was *Salmonella* (19 [53%] outbreaks), followed by Shiga toxin–producing *Escherichia coli* (5 [14%]). Among outbreaks linked to novel food vehicles, 33% resulted from foods imported from another country.

Outbreaks associated with novel food vehicles differed from other outbreaks (i.e., those not associated with a novel food vehicle) in several ways (Table 2). First, 61.1% of outbreaks associated with a novel food vehicle involved exposure in multiple states, compared with 5.7% of other outbreaks ($p<0.001$). Second, 48.6% of outbreaks associated with a novel food vehicle resulted in a food recall, compared with 5.2% of other outbreaks ($p<0.001$). Third, the mean numbers of reported primary cases, hospitalizations, and deaths were greater among outbreaks linked to novel food vehicles than among other outbreaks ($p = 0.04$, $p<0.001$, and $p<0.001$, respectively). Fourth, the percentage of cases that resulted in hospitalization and the percentage of cases that resulted in death were significantly greater among outbreaks linked to novel food vehicles than among other outbreaks. Last, outbreaks associated with a novel food vehicle were more likely than other outbreaks to be caused by *Salmonella* contamination ($p<0.001$). Two potential confounding effects were a disproportionate number of *Salmonella* outbreaks linked to novel foods and

Table 1. Novel food vehicles implicated in outbreaks that occurred during 2007–2016, United States*

Food	Category	State (no. states)	Year of first illness	Etiology	No. illnesses	No. hosp.	No. deaths	Recall	Imported
Almaco jack	Fish	Florida	2014	Ciguatoxin	2	0	0	No	Yes
Apple†	Fruit	Multistate (12)	2014	*Listeria monocytogenes*	35	34	7	Yes	No
Bison	Meat	Tennessee	2008	STEC O157:H7	12	2	0	No	No
		Multistate (5)	2010	STEC O157:H7	10	NR	NR	Yes	No
Blueberries	Fruit	Multistate (6)	2009	*Salmonella enterica* serovar Muenchen	14	NR	0	No	No
		Minnesota	2010	*Salmonella* Newport	6	1	0	No	No
Carp	Fish	New York	2012	Other chemical or toxin, Haff disease‡	2	2	1	No	No
Cashews§	Nut/seed	Multistate (6)	2014	*Salmonella* Stanley	18	4	0	No	Yes
Chia seed¶	Nut/seed	Multistate (19)	2014	*Salmonella,* multiple serotypes#	45	7	0	Yes	Yes
Flour (wheat)	Grain	Multistate (24)	2015	STEC, multiple serogroups**	56	16	0	Yes	No
Frog††	Meat	Arizona	2015	*Salmonella* Javiana	5	1	0	No	No
Goose‡‡	Meat	New York	2013	*Campylobacter jejuni*	57	1	0	No	No
Hazelnuts	Nut/seed	Multistate (3)	2010	STEC O157:H7	8	3	0	Yes	No
		Multistate (2)	2016	*Salmonella* Typhimurium	6	1	0	Yes	No
Kale	Vegetable	Florida	2013	STEC O157:H7	7	5	0	No	No
		Wisconsin	2014	*Cryptosporidium parvum*	8	0	0	No	No
Lima beans	Vegetable	Florida	2009	Unknown	13	0	0	No	No
Lionfish	Fish	South Carolina	2013	Ciguatoxin	4	1	0	NR	NR
Mini peppers	Vegetable	Multistate (10)	2014	*Salmonella* Paratyphi B	21	5	0	No	Yes
Monchong	Fish	Hawaii	2013	Scombroid toxin	2	0	0	No	No
Moringa leaf¶	Herb/spice	Multistate (24)	2015	*Salmonella* Virchow	35	6	0	Yes	Yes
Papaya	Fruit	Multistate (25)	2011	*Salmonella* Agona	106	10	0	Yes	Yes
		Multistate (4)	2013	*Salmonella* Thompson	13	6	1	No	No
Pepper¶	Herb/spice	Multistate (4)	2008	*Salmonella* Rissen	87	NR	NR	Yes	No
		Multistate (45)	2009	*Salmonella* Montevideo	272	52	0	Yes	Yes
Pine nuts	Nut/seed	Multistate (6)	2011	*Salmonella* Enteritidis	53	2	0	Yes	Yes
Pistachios	Nut/seed	Multistate (21)	2008	*Salmonella*, multiple serovars§§	83	NR	0	Yes	No
		Multistate (6)	2013	*Salmonella* Senftenberg	8	1	0	Yes	No
		Multistate (9)	2016	*Salmonella*, multiple serovars¶¶	11	2	0	Yes	No
Pomegranate	Fruit	Multistate (10)	2013	Hepatitis A virus	157	70	0	No	Yes
Sheep milk##	Dairy	Multistate (14)	2012	*Listeria monocytogenes*	23	21	5	Yes	Yes
Skate	Fish	New York	2008	Scombroid toxin	3	0	0	No	No
Sprouted nut butter***	Nut/seed	Multistate (10)	2015	*Salmonella* Paratyphi B variant L(+) tartrate (+)	13	0	0	Yes	No
Sugar cane	Sugar	Multistate (3)	2013	*Salmonella* Virchow	7	1	0	No	Yes
Swai	Fish	New York	2014	Unknown	3	1	0	No	Yes
Tempeh†††	Grain	North Carolina	2012	*Salmonella* Paratyphi B var. L(+) tartrate (+)	89	8	0	Yes	No

*Data from Centers for Disease Control and Prevention Foodborne Disease Outbreak Surveillance System (FDOSS), 1973–2016. Five of the 6 outbreaks linked to fish were caused by naturally occurring toxins that cannot be destroyed through cooking or freezing. Hosp., hospitalization; NR, not reported; STEC, Shiga toxin–producing *Escherichia coli*.
†Apples were the contaminated ingredient in an outbreak associated with caramel apples. Prior apple cider outbreaks have been reported to FDOSS with no specific ingredient identified.
‡Haff disease is a syndrome of unexplained rhabdomyolysis caused by consumption of an unidentified toxin (rhabdomyolysis is a clinical syndrome caused by injury to skeletal muscle that results in the release of muscle cell contents into the circulation).
§Cashews were processed into raw cashew cheese.
¶Product was processed and sold as a ground powder.
#*Salmonella* Gaminara, Harford, Oranienburg, and Newport
**STEC O26:NM and O121
††Frog legs were from a noncommercial source.
‡‡Goose liver was the implicated ingredient of foie gras. Prior foie gras outbreaks have been reported to FDOSS with either no specific ingredient identified or a different implicated ingredient.
§§*Salmonella* Montevideo, Newport, and Senftenberg.
¶¶*Salmonella* Senftenberg and Montevideo.
##Pasteurized sheep milk, the only dairy food vehicle identified, was used in making ricotta salata cheese, which was later contaminated.
***Multiple nut butters from 1 company were implicated (cashew, almond, and hazelnut).
†††Tempeh was unpasteurized.

Table 2. Features of outbreaks associated with novel and other food vehicles, United States, 2007–2016*

	Food vehicle type								
	Novel				Other				
		Statistic				Statistic			
Feature	Outbreaks	Mean	Median	Range	Outbreaks	Mean	Median	Range	p value†
No. cases per outbreak									
Primary	36	35.9	13.0	2–272	3,722	21.4	9.0	2–1,939	0.04
Hospitalized	32	8.2	2.0	0–70	3,502	1.6	0.0	0–308	<0.001
Died	34	0.4	0.0	0–7	3,520	0	0.0	0–33	<0.001
% Cases per outbreak									
Hospitalized	32	25.4	16.9	0–100	3,502	9.9	0.0	0–100	<0.001
Died	34	2.9	0.0	0–50	3,520	0.4	0.0	0–100	<0.001
Outbreaks, no. (%)									
Multistate	36 (61.1)				3,722 (5.7)				<0.001
Had recall	35 (48.6)				3,567 (5.2)				<0.001
Etiology *Salmonella*‡	34 (55.9)				2,226 (28.3)				<0.001

*Data from Centers for Disease Control and Prevention Foodborne Disease Outbreak Surveillance System, 2007–2016. Analysis limited to outbreaks with an implicated food. This analysis included outbreaks resulting from a range of contributing factors, including contamination from ill food workers (and not resulting from more upstream processes). None of the outbreaks associated with a novel food vehicle were linked to an ill food worker. As a sensitivity analysis, 584 outbreaks linked to ill food workers were excluded from the comparison group, leaving 3,138 outbreaks. Among these, the median number of primary cases was 8.0; hospitalizations, percent of cases hospitalized, and deaths, and percent of cases resulting in death were all 0; 6.8% of outbreaks were multistate, 6.1% had a recall, and 31.6% had an etiology of *Salmonella*. All statistical results remained robust with p<0.05.
†Nonparametric Wilcoxon testing was used to assess statistical difference in means. χ^2 testing was used to assess statistical differences in percentages.
‡Limited to single-etiology outbreaks that met confirmation guidelines. Outbreaks associated with a novel food vehicle were more likely to be caused by *Salmonella* contamination. These outbreaks are more likely to result in large, multistate outbreaks leading to public health investigations. As a sensitivity analysis, we restricted the sample to outbreaks with an etiologic agent of *Salmonella* leaving 649 outbreaks (19 linked to novel food vehicles and 630 linked to other outbreaks). Case effects did not remain significant (i.e., when comparing novel and other outbreaks, we found no statistically significant differences in primary cases, hospitalization, deaths, as well as percent of cases hospitalized and percent of cases resulting in death). However, outbreaks associated with a novel food were more likely than other outbreaks to have cases exposed in multiple states (84.2% for novel and 17.8% for other outbreaks, p<0.001) and result in a recall (63.2% for novel and 8.9% for other outbreaks, p<0.001).

potential effects of contamination from ill food workers (sensitivity analyses in Table 2).

Discussion

We identified 28 novel foods linked to outbreaks that occurred during 2007–2016 in the United States. Compared with other outbreaks, those linked to novel foods were more likely to involve illnesses in multiple states; result in a food recall; and to be associated with, on average, larger numbers of cases, hospitalizations, and deaths. Investigating large and complex outbreaks requires considerable government resources and major costs to the public and industry. Moreover, two thirds of novel outbreak-associated food vehicles did not require cooking after purchase, and roughly half of novel foods did not require refrigeration. These factors highlight the need for targeted industry efforts to reduce contamination before point of purchase to protect consumers.

Food consumption patterns are dynamic, influenced by dietary trends, public health messaging, food accessibility, advertising, and affordability (*6*,*7*). Increased consumption of a food results in more opportunities for exposure and potentially larger outbreaks. Importing of foods and beverages into the United States has increased; average annual growth in economic value from 2007–2017 was 5.9% (*12*). As a result, access has expanded to a broader range of foods from diverse areas. One third of outbreaks linked to novel foods resulted from imported foods, whereas the overall percentage of outbreaks reported to CDC with an imported food implicated is relatively small (5% during the period 2009–2014) (*13*).

Identifying novel outbreak-associated foods highlights the need for improvements in public health. The 3 key areas are outbreak investigation, prevention, and communications.

First, identifying the source of an outbreak can be difficult. Especially in multistate outbreaks, investigators typically use standardized food history questionnaires to identify common foods among a sample of patients. Investigators develop questionnaires largely on the basis of trends in previous outbreaks and are influenced by common—rather than novel—food vehicles. However, identifying novel foods may require a detailed investigation of everything consumed by patients during the exposure period. A targeted questionnaire can be developed on the basis of data from these in-depth, hypothesis-generating interviews and administered to a larger group of patients and controls. Barriers to this approach include limited resources, reluctance of investigators to allow investigators from other areas to interview patients in their jurisdiction, lack of training with regard to conducting hypothesis-generating interviews, and the assumption that more interviews with the stan-

dardized questionnaire will eventually reveal the underlying food vehicle(s). Efforts to further engage, fund, and support states in investigating and reporting outbreaks are needed to effectively identify novel food vehicles.

Second, identifying novel food vehicles provides opportunities for new prevention measures. The occurrence of ≥2 outbreaks linked to novel foods (we identified 7 instances) may serve as a warning signal for public health authorities indicating gaps in food safety practices, regulatory oversight, or both. Targeted outreach to industry may be pursued when a novel food is identified. Focused, collaborative prevention efforts undertaken by industry in collaboration with academic institutions, regulatory agencies, consumer advocacy groups, and other nonprofit public health organizations have been successful in the past and should become standard practice.

Third, communications regarding novel food vehicles to the public, industry, and regulatory agencies could be improved. Intensive public health messaging may be needed to notify the public, industry, and public health partners of newly discovered risks to prevent additional illnesses. This type of communication is regularly performed by public health and regulatory agencies, but greater emphasis on the novelty of the food source could attract additional media attention and, in turn, lead to greater awareness.

The first limitation of our analysis is that it encompasses reported outbreaks with data on implicated foods representing both a subset of foodborne outbreaks occurring in the United States and of outbreaks reported to FDOSS. As a result, these novel outbreak-associated food vehicles may not actually be novel; rather, previous outbreaks associated with these vehicles may not have been detected or reported. The second limitation is that only a small percentage of foodborne illnesses are linked to recognized outbreaks (outbreak-associated cases are estimated to range from 0.5% of laboratory-diagnosed *Campylobacter* cases to 19.0% of Shiga toxin–producing *E. coli* O157 cases) (*2*), and it is possible that outbreak-associated novel foods differ from those linked to sporadic foodborne illnesses. The third limitation is the possibility that novel food vehicles were misclassified. Considerable efforts were made to reduce false-positive identifications by searching for different spellings, alternative names, and shared ingredients, as well as by using a team of independent reviewers. We also checked secondary sources for foods identified as novel from FDOSS data. This effort identified 2 food vehicles (mamey fruit and jalapeño peppers) that incorrectly initially seemed to be novel because of the use of more generic food terms in reports before 2007.

In summary, identifying novel food vehicles for foodborne illness provides opportunities for early interventions that should not go unheeded. This analysis highlights the need for expanded food safety measures to reduce opportunities for contamination as foods are grown, harvested, and processed and to prevent illness from both novel and other food sources in the United States and abroad. Greater investment in public health outbreak investigation capacity may increase and expedite identification of novel food vehicles, which is vital because novel foods may serve as signals for emerging threats.

Acknowledgments

We thank our local, state, and territorial health department colleagues who investigate and report foodborne outbreaks to FDOSS.

Funding for FDOSS is provided by CDC.

About the Author

Dr. Whitham is an epidemiologist with the Division of Foodborne, Waterborne, and Environmental Disease, National Center for Emerging and Zoonotic Infectious Diseases, CDC. Her research is focused on prevention and policy topics related to enteric and mycotic illnesses.

References

1. Scallan E, Hoekstra RM, Angulo FJ, Tauxe RV, Widdowson MA, Roy SL, et al. Foodborne illness acquired in the United States—major pathogens. Emerg Infect Dis. 2011;17:7–15. https://doi.org/10.3201/eid1701.P11101
2. Ebel ED, Williams MS, Cole D, Travis CC, Klontz KC, Golden NJ, et al. Comparing characteristics of sporadic and outbreak-associated foodborne illnesses, United States, 2004–2011. Emerg Infect Dis. 2016;22:1193–200. https://doi.org/10.3201/eid2207.150833
3. Nielsen Company. Total consumer report [cited 2020 Aug 1]. https://www.nielsen.com/wp-content/uploads/sites/3/2019/04/december-2018-total-consumer-report.pdf
4. Todd JE. Changes in eating patterns and diet quality among working-age adults, 2005–2010 [cited 2020 Aug 1]. https://www.ers.usda.gov/publications/pub-details/?pubid=45175
5. Nielsen Company. How America will eat [cited 2020 Aug 1]. https://www.nielsen.com/us/en/insights/report/2019/how-america-will-eat
6. Rehm CD, Peñalvo JL, Afshin A, Mozaffarian D. Dietary intake among US adults, 1999-2012. JAMA. 2016;315:2542–53. https://doi.org/10.1001/jama.2016.7491
7. Kearney J. Food consumption trends and drivers. Philos Trans R Soc Lond B Biol Sci. 2010;365:2793–807. https://doi.org/10.1098/rstb.2010.0149
8. Thomas K, Jajosky R, Coates RJ, Calvert GM, Dewey-Mattia D, Raymond J, et al. Summary of notifiable noninfectious

conditions and disease outbreaks: surveillance data published between April 1, 2016 and January 31, 2017—United States. MMWR Morb Mortal Wkly Rep. 2017;64:1–6. https://doi.org/10.15585/mmwr.mm6454a1
9. Centers for Disease Control and Prevention. Interagency Food Safety Analytics Collaboration (IFSAC) food categorization scheme [cited 2020 Aug 1]. https://www.cdc.gov/foodsafety/ifsac/projects/food-categorization-scheme.html
10. Richardson LC, Bazaco MC, Parker CC, Dewey-Mattia D, Golden N, Jones K, et al. An updated scheme for categorizing foods implicated in foodborne disease outbreaks: a tri-agency collaboration. Foodborne Pathog Dis. 2017;14:701–10. https://doi.org/10.1089/fpd.2017.2324
11. Gieraltowski L, Julian E, Pringle J, Macdonald K, Quilliam D, Marsden-Haug N, et al. Nationwide outbreak of *Salmonella* Montevideo infections associated with contaminated imported black and red pepper: warehouse membership cards provide critical clues to identify the source. Epidemiol Infect. 2013;141:1244–52. https://doi.org/10.1017/S0950268812001859
12. US Department of Agriculture. U.S. food imports [cited 2020 Jul 22]. https://www.ers.usda.gov/data-products/us-food-imports/us-food-imports
13. Gould LH, Kline J, Monahan C, Vierk K. Outbreaks of disease associated with food imported into the United States, 1996–2014(1). Emerg Infect Dis. 2017;23:525–8. https://doi.org/10.3201/eid2303.161462

Address for correspondence: Hilary K. Whitham, Centers for Disease Control and Prevention, Mailstop H24-9, Atlanta, GA 30329-4027, USA; email: hwhitham@cdc.gov

Population-Based Study of Bloodstream Infection Incidence and Mortality Rates, Finland, 2004–2018

Keiju S.K. Kontula, Kirsi Skogberg, Jukka Ollgren, Asko Järvinen, Outi Lyytikäinen

Medscape EDUCATION ACTIVITY

In support of improving patient care, this activity has been planned and implemented by Medscape, LLC and Emerging Infectious Diseases. Medscape, LLC is jointly accredited by the Accreditation Council for Continuing Medical Education (ACCME), the Accreditation Council for Pharmacy Education (ACPE), and the American Nurses Credentialing Center (ANCC), to provide continuing education for the healthcare team.

Medscape, LLC designates this Journal-based CME activity for a maximum of 1.00 ***AMA PRA Category 1 Credit(s)™***. Physicians should claim only the credit commensurate with the extent of their participation in the activity.

Successful completion of this CME activity, which includes participation in the evaluation component, enables the participant to earn up to 1.0 MOC points in the American Board of Internal Medicine's (ABIM) Maintenance of Certification (MOC) program. Participants will earn MOC points equivalent to the amount of CME credits claimed for the activity. It is the CME activity provider's responsibility to submit participant completion information to ACCME for the purpose of granting ABIM MOC credit.

All other clinicians completing this activity will be issued a certificate of participation. To participate in this journal CME activity: (1) review the learning objectives and author disclosures; (2) study the education content; (3) take the post-test with a 75% minimum passing score and complete the evaluation at http://www.medscape.org/journal/eid; and (4) view/print certificate. For CME questions, see page 2749.

Release date: September 15, 2021; Expiration date: September 15, 2022

Learning Objectives

Upon completion of this activity, participants will be able to:

- Describe incidence and outcome of bloodstream infections (BSIs) in Finland during 2004 to 2018, according to an analysis of national, laboratory-based surveillance data
- Identify causative agents of BSIs in Finland during 2004-2018, according to an analysis of national, laboratory-based surveillance data
- Determine clinical and public health implications of incidence, outcome, causative agents, and trends of BSIs in Finland during 2004-2018, according to an analysis of national, laboratory-based surveillance data

CME Editor

Amy J. Guinn, BA, MA, Copyeditor, Emerging Infectious Diseases. *Disclosure: Amy J. Guinn, BA, MA, has disclosed no relevant financial relationships.*

CME Author

Laurie Barclay, MD, freelance writer and reviewer, Medscape, LLC. *Disclosure: Laurie Barclay, MD, has disclosed no relevant financial relationships.*

Authors

Disclosures: ***Keiju S.K. Kontula, MD; Jukka Ollgren, MS;*** *and* ***Outi Lyytikäinen, MD, PhD,*** *have disclosed no relevant financial relationships.* ***Kirsi Skogberg, MD,*** *has disclosed the following relevant financial relationships: owns stock, stock options, or bonds from Nordea; Oriola; Orion Corporation.* ***Asko Järvinen, MD,*** *has disclosed the following relevant financial relationships: served as an advisor or consultant for Gilead Sciences, Inc.; GlaxoSmithKline; Sanofi; served as a speaker or member of a speakers bureau for: Astellas Pharma, Inc.; Gilead Sciences, Inc.*

Author affiliations: Helsinki University Hospital, Helsinki, Finland (K.S.K. Kontula, K. Skogberg, A. Järvinen); Finnish Institute for Health and Welfare, Helsinki (J. Ollgren, O. Lyytikäinen)

DOI: https://doi.org/10.3201/eid2710.204826

We evaluated the incidence, outcomes, and causative agents of bloodstream infections (BSI) in Finland during 2004–2018 by using data from the national registries. We identified a total of 173,715 BSIs; annual incidence increased from 150 to 309 cases/100,000 population. BSI incidence rose most sharply among persons ≥80 years of age. The 1-month case-fatality rate decreased from 13.0% to 12.6%, but the 1-month all-cause mortality rate rose from 20 to 39 deaths/100,000 population. BSIs caused by *Escherichia coli* increased from 26% to 30% of all BSIs. BSIs caused by multidrug-resistant microbes rose from 0.4% to 2.8%, mostly caused by extended-spectrum β-lactamase-producing *E. coli.* We observed an increase in community-acquired BSIs, from 67% to 78%. The proportion of patients with severe underlying conditions rose from 14% to 23%. Additional public health and healthcare prevention efforts are needed to curb the increasing trend in community-acquired BSIs and antimicrobial drug–resistant *E. coli*.

Bloodstream infections (BSIs) are a major cause of illness and death worldwide. The incidence of BSIs has increased over time and reported BSI rates range from 122 to 220 cases/100,000 population (*1*–*7*). Rising incidence is probably related to an aging population and an increasing prevalence of underlying conditions and invasive procedures.

Despite advances in antimicrobial drug therapy, intensive care, and prevention strategies, BSIs cause an estimated 250,000 deaths annually in North America and Europe combined (*8*). Recent studies have reported BSI mortality rates of 21–32 deaths/100,000 population (*3*,*6*) and 1-month case-fatality rates of ≈17%–28% for nosocomial BSIs and 10%–19% for community-acquired BSIs (*9*–*12*). Higher mortality rates of 40%–50% have been observed in surveys of patients with BSIs or septic shock in hospital intensive care units (*13*,*14*). However, only limited population-based data are available concerning the incidence and outcome of BSIs (*1*,*3*,*4*,*6*,*10*,*12*,*15*). Most other reports mainly focus on selected hospitals or hospital units, a specific causative agent, or either healthcare-associated or community-acquired BSIs, and thus those studies represent select patient populations.

We used data from the national, laboratory-based surveillance system in Finland to analyze the annual incidence, causative agents, and outcomes of all BSIs in the country during 2004–2018. Our objective was to assess the burden and temporal trends of BSIs in Finland and identify targets for preventive interventions.

Materials and Methods

Study Setting and Population

Finland had a population of 5.2 million in 2004 and 5.5 million in 2018. The country's healthcare system is organized into 20 healthcare districts; there are 5 tertiary care hospitals and 15 secondary care hospitals, and the number of primary care hospitals varies by district. All clinical microbiology laboratories in Finland report all bacterial and fungal isolates from blood samples to the National Infectious Disease Register (NIDR) (*16*). These notifications are sent electronically and comprise specimen date; type of microbe; and the patient's date of birth, sex, place of residence, and national identity code, a unique number given to each resident in Finland. NIDR merges multiple notifications of the same microbe from the same national identity code, indicating samples came from same person, and creates a single case if notifications occur within 3 months of each other.

In this retrospective study, we used NIDR data to identify all BSIs in Finland during 2004–2018. We included 187,553 BSIs with valid national identity codes in the study; we excluded 155 duplicate notifications, that is, those with same specimen date, microbe, and identity code (Figure 1). We retrieved date of death from the Population Information System (https://dvv.fi/en/population-information-system) by linking the patient's national identity code with database information. We obtained information on patient hospitalization, including origin of the infection, and current and prior (1 year) diagnosis codes by linking to the National Hospital Discharge Register (HILMO).

The Ethics Committee of the Finnish Institute for Health and Welfare granted permission to analyze and link data from the NIDR and HILMO (approval no. THL/1349/6.02.00/2019). Because the data were already anonymized, patient informed consent was waived.

Definitions

We defined the presence of BSI as occurrence of viable bacteria or fungi in bloodstream evidenced by positive blood cultures. We defined polymicrobial BSI as isolation of >1 bacterial or fungal species in blood cultures collected within 2 days (*16*).

We classified BSI as healthcare-associated when the first blood culture was obtained >2 days after admission to hospital or within 2 days after discharge (*17*). We also classified cases as healthcare-associated for patients who came from another healthcare facility. We classified cases as community-acquired when patients had no prior hospitalization and

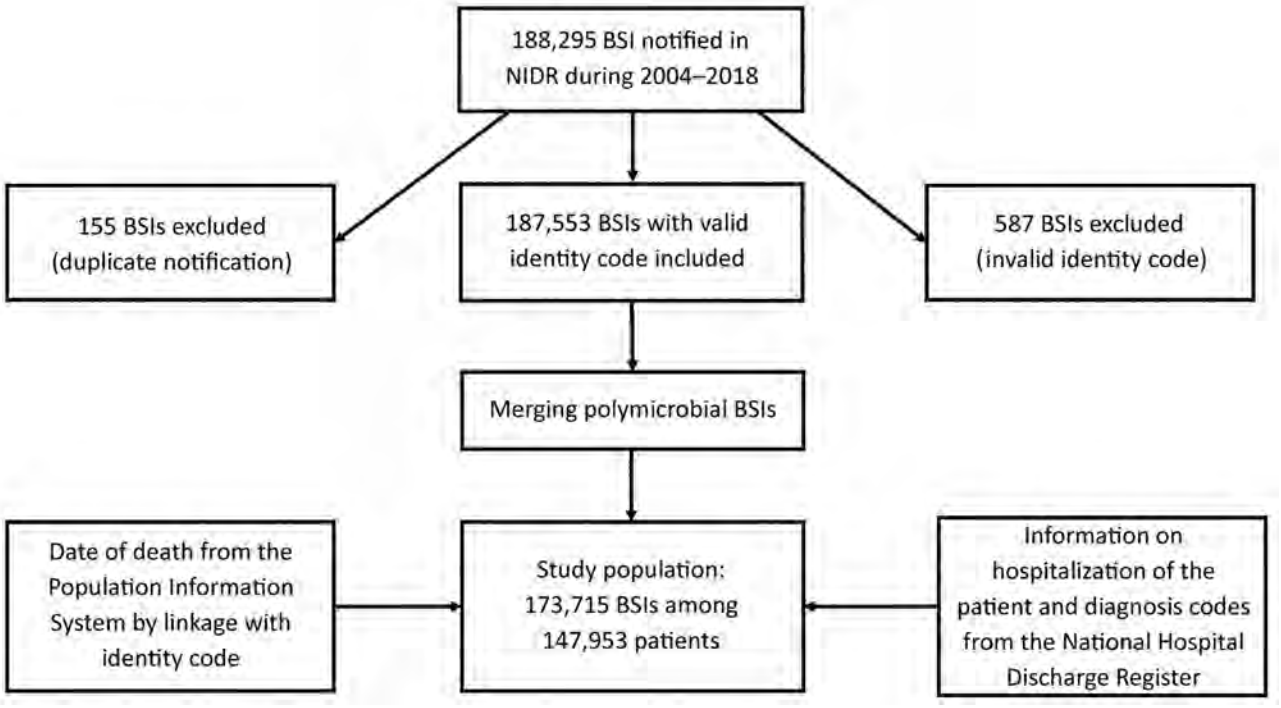

Figure 1. Flowchart of the data reviewed for inclusion in a study of the incidence of BSIs, Finland, 2004–2018. BSI, bloodstream infections; NIDR, National Infectious Disease Register.

blood culture specimens were collected ≤2 days after hospital admission.

We defined underlying illness by using a validated algorithm for the Charlson comorbidity index (CCI) based on the International Classification of Diseases, 10th Revision (*18*,*19*). We scored underlying illness on 3 levels: low (CCI score of 0) for patients with no reported underlying diseases, medium (CCI score 1–2), or high (CCI score ≥3) (*10*). We defined all-cause mortality and case-fatality as death of a particular patient ≤30 days after the first positive blood culture.

We defined the following bacteria as multidrug-resistant (MDR) microbes: extended-spectrum β-lactamase-producing (ESBL) *Escherichia coli* and *Klebsiella pneumoniae*, methicillin-resistant *Staphylococcus aureus* (MRSA), vancomycin-resistant *Enterococcus* (VRE) and carbapenemase-producing *Enterobacteriaceae* (CPE). We defined ESBL–*E. coli* and ESBL–*K. pneumoniae* as resistant or intermediately susceptible to third-generation cephalosporins. We defined CPE as *E. coli*, *K. pneumoniae*, and *Enterobacter* sp. resistant or intermediately susceptible to carbapenems.

Analyses and Statistics

We used population data from Statistics Finland (https://www.stat.fi/index_en.html) as denominators to calculate age- and sex-specific BSI incidence and mortality rates. We determined average annual incidence and mortality rates according to the total number of BSI episodes, BSI deaths, and population during 2004–2018. We applied a Poisson regression model, or negative binomial regression model in case of overdispersion, to compare the observed trends in annual incidence and mortality rates and used a log-linear binomial regression model for case-fatality proportions. We analyzed the data by using SPSS Statistics 25 (IBM, https://www.ibm.com) and Stata 16 (StataCorp LLC, https://www.stata.com).

Results

During 2004−2018, we identified a total of 173,715 BSIs among 147,953 patients in the NIDR (Figure 1). Median age among BSI patients was 70 (range 0–110) years; 52% were male and 48% female. Among all BSIs, 7,568 (4.4%) occurred in children <16 years of age, including 3,734 BSIs in infants <1 year of age. The average annual incidence was 216 BSI episodes/100,000 population and was higher among male (228 episodes/100,000 population) than female (203 episodes/100,000 population) patients. Overall BSI incidence was highest among patients ≥60 years of age (618 cases/100,000 population) and patients <1 year of age (431 cases/100,000 population). Among infants <1 year and persons ≥40 years of age, BSI

incidence rates were higher in male than in female patients; only among persons 20–29 years of age was BSI incidence higher in female patients.

During 2004–2018, the annual BSI incidence rose from 150 to 309 cases/100,000 population, an average annual increase of 5.2% (95% CI 4.8%–5.5%; p<0.01). BSI incidence increased in both sexes; among male persons, incidence increased from 155 to 327 cases/100,000 population, an average annual increase of 5.3% (95% CI 4.9%–5.7%; p<0.01); among female persons, incidence increased from 145 to 291 cases/100,000 population, an average annual increase of 5.0% (95% CI 4.6%–5.4%; p<0.01) (Figure 2). The increase in the annual incidence was most prominent among persons ≥90 years of age, from 1,155 to 3,005 cases/100,000 population, an average annual increase of 8.6% (95% CI 8.0%–9.1%; p<0.01). We observed a decreasing incidence only among infants <1 year of age, from 528 to 317 cases/100,000 population, an average annual decrease of 3.3% (p<0.01). We also noted a decreasing incidence in children <10 years of age, from 37 to 28 cases/100,000 population, an average annual decrease of 4.0% (p<0.01).

Among all reported BSI cases, 22,474 (13%) were fatal within 1 month; case-fatality rate was higher among male (13.7%) than female (12.1%) patients (relative risk 1.14, 95% CI 1.11–1.17; p<0.01). During 2004–2018, we noted a minor decrease in the 1-month case-fatality rate, from 13.0% to 12.6%, an average annual relative reduction of 0.4% (95% CI 0.1%–0.7%; p<0.01) (Figure 3). Among children and adolescents 1–19 years of age and among persons ≥90 years of age, the case-fatality rate increased slightly, but in other age groups we observed a descending rate. The average annual BSI mortality rate was 28 deaths/100,000 population during the study period. The mortality rate was higher for male patients in all age groups; among persons ≥20 years of age, mortality rates were >1.5-fold higher among male than female patients. The mortality rate increased with age; among persons ≥70 years of age, the rate was 148 deaths/100,000 population. The annual BSI mortality rate rose from 20 to 39 deaths/100,000 population during 2004–2018, and the overall average annual increase was 4.8% (95% CI 4.5%–5.1%; p<0.01) (Figure 4); the increase was 4.5% (p<0.01) among male patients and 5.2% (p<0.01) among female patients. The increase in mortality rate was most notable among persons ≥90 years of age, an average increase of 8.1% (p<0.01).

Among all BSIs, gram-positive bacteria caused 46% of infections, gram-negative bacteria 46%, fungi 1.5%, and other unclassified bacteria 0.2%. Polymicrobial BSIs accounted for 7% of all BSIs. *E. coli* was the most common causative pathogen (29% of all BSIs), but other identified pathogens included *S. aureus* (13%), coagulase-negative staphylococcus (CNS) (8%), β-hemolytic streptococci (8%), *Streptococcus pneumoniae* (7%), *Klebsiella* sp. (5%), and enterococci (4%). Gram-positive bacteria were the most common cause of BSIs in male patients (52% vs. 40% for female patients), whereas gram-negative bacteria were more prevalent in female patients (53% vs. 39% for male patients). Polymicrobial BSIs were more frequently noted in male patients than in female patients (7.4% vs. 5.6%), as were BSIs caused by fungi (1.7% vs. 1.2%). Altogether, 3,150 (1.8%) BSIs were caused by 3,168 MDR microbes; 2,503 (1.4%) BSIs were caused by ESBL–*E. coli* or ESBL–*K. pneumoniae*, 562 (0.3%) by MRSA, 66 (0.04%) by VRE, and 37 (0.02%) by CPE. Among 18 BSIs, 2 different MDR microbes were identified.

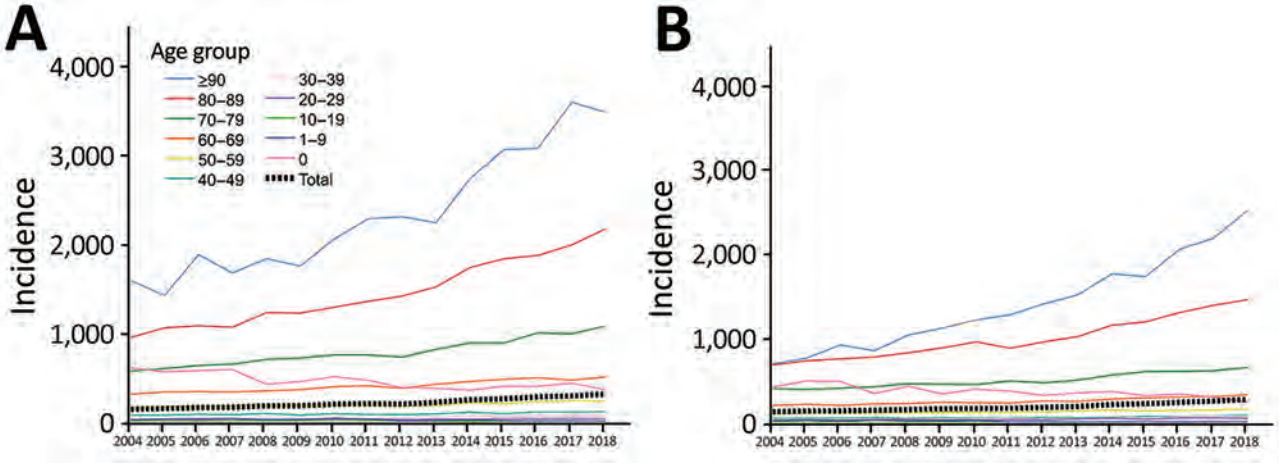

Figure 2. Annual incidence (cases/100,000 population) of bloodstream infections, by sex and age group, Finland, 2004–2018. A) Male patients; B) female patients.

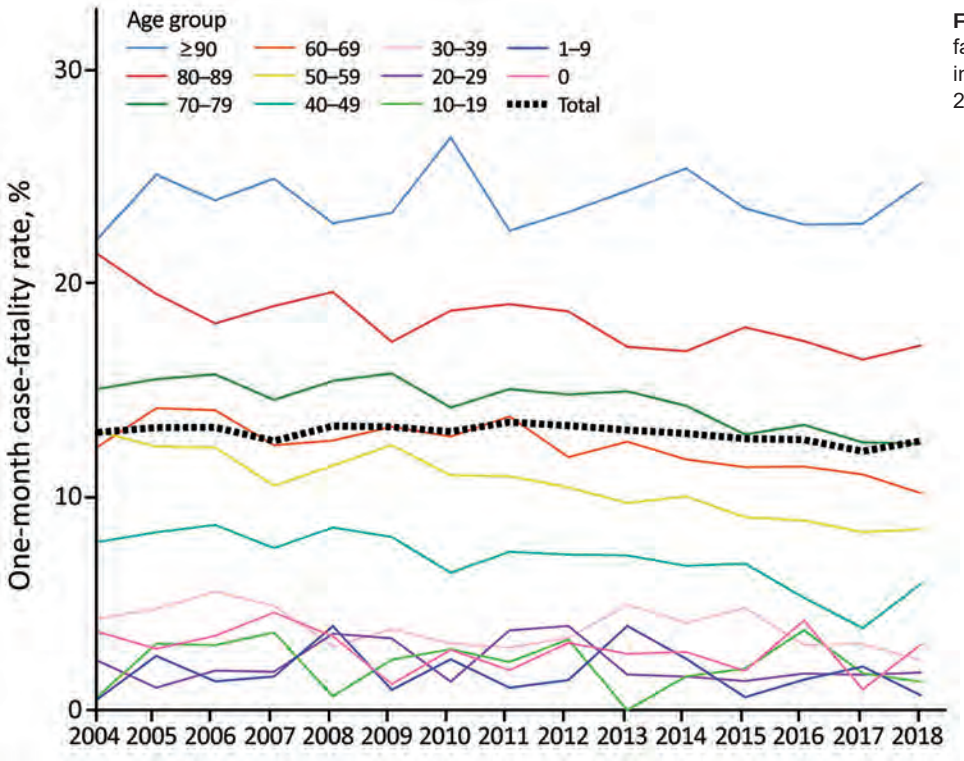

Figure 3. Annual 1-month case-fatality rates for bloodstream infections, by age group, Finland, 2004–2018.

During 2004–2018, the proportion of BSIs caused by gram-negative bacteria rose from 42% to 48%, whereas BSIs caused by gram-positive bacteria decreased from 50% to 43% (Figure 5). Polymicrobial BSIs increased slightly from 6.5% to 7.1%, and BSIs caused by fungi decreased from 1.7% to 1.1% (Figure 5). Among the most common pathogens, the proportion of *E. coli* BSIs rose from 26% to 30%, whereas no change was noted in *S. aureus* BSIs (13%), and we observed a decline in BSIs caused by CNS (from 11% to 7%) and *S. pneumoniae* (9% to 4%). *Candida albicans* was the most common fungus, causing 0.9% of all BSIs and 63% of fungal BSIs, but the proportion of fungemia caused by other *Candida* species increased from 34% to 47%.

The annual incidence of *E. coli*, *S. aureus*, β-hemolytic streptococci, and *Klebsiella* BSIs rose >2-fold. In particular, *E. coli* BSIs rose from 39 to 91 cases/100,000 population and *S. aureus* from 19 to 39 cases/100,000 population. We noted a similar increase in the incidence of *E. coli* and *S. aureus* BSIs in both sexes and the most prominent increase occurred among persons ≥80 years of age. The incidence of *S. pneumoniae* BSIs rose during 2004–2008, from 13 cases/100,000 population to 17 cases/100,000 population, and then decreased to 13 cases/100,000 population in 2018. We observed this decline in all age groups, but we noted the steepest reduction among persons <30 years of age, including infants <1 year of age.

The proportion of BSIs caused by MDR microbes rose from 0.4% in 2004 to 2.8% in 2018, mostly because of the increase in ESBL–*E. coli* BSIs, from 0 to 7% of all *E. coli* BSIs, an increase from 0 to 10% among male patients and from 0 to 6% in female patients. On the other hand, MRSA BSIs decreased from 3.1% to 2.0% of all *S. aureus* BSIs, and the annual number of MRSA BSIs ranged from 27 to 49 during 2004–2018. MDR microbes were causative agents in more BSIs leading to death within 30 days compared with other BSIs (2.4% vs. 1.7%).

Of the 173,715 BSI cases, 123,232 (71%) were community-acquired and 50,483 (29%) were healthcare-associated. During 2004–2018, the proportion of community-acquired BSIs rose from 67% to 78%, whereas healthcare-associated BSIs declined from 33% to 22%. The median CCI of all BSI patients was 1 (range 0–15); 38% had a low score (CCI 0) and 21% had a high score (CCI ≥3). During 2004–2018, the proportion of patients with a high CCI increased from 14% to 23%, but the proportion of patients with a low CCI decreased from 45% to 35%.

Discussion

In our nationwide population-based study, BSI incidence and mortality rates increased 2-fold during

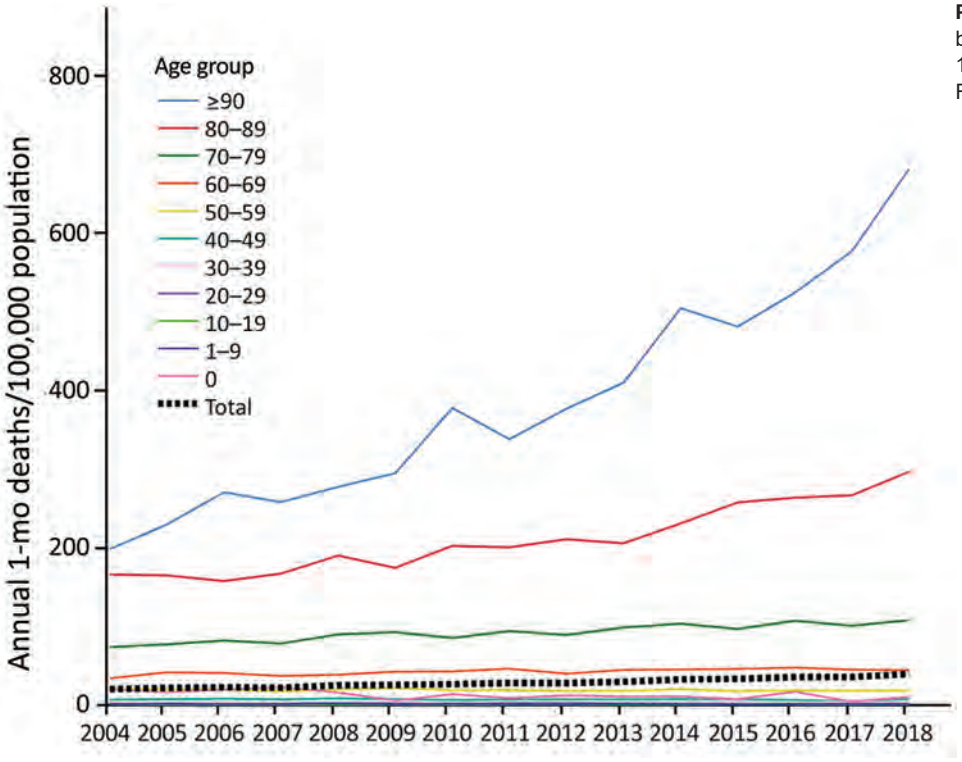

Figure 4. Annual average 1-month bloodstream infection deaths per 100,000 population, by age group, Finland, 2004–2018.

2004–2018 with the sharpest rise among persons ≥80 years of age. Community-acquired BSIs contributed to the rising incidence more than healthcare-associated BSIs did. The 1-month case fatality rate was 13% and remained rather stable over time despite the growing proportion of patients with high CCI scores. We noted a considerable, >2-fold, increase in the incidence of *E. coli* BSIs. The proportion of BSIs caused by MDR microbes was low, but we observed an ascending trend, mainly because of the increase in ESBL–*E. coli* BSIs.

During 2004–2018, the annual incidence of BSIs in Finland rose from 150 to 309 cases/100,000 population with an average annual rate of 216 BSI episodes/100,000 population. In 2 previous nationwide studies from Finland based on the same laboratory surveillance data, the average annual incidence rates were considerably lower than in our study, 125 cases/100,000 population during 1995–2002 and 159 cases/100,000 population during 2004–2007 (*3*,*20*). Similar increasing incidence rates have also been noted in other population-based surveys from Europe; from 114 to 166 cases/100,000 person-years during 1992–2006 in northern Denmark (*10*) and from 190 to 257 cases/100,000 person-years during 2002–2013 in mid-Norway (*6*). One recent population-based study, a report from Funen County, Denmark, during 2000–2008, demonstrated a decreasing overall incidence of BSIs (*15*).

We observed a marked, nearly 2-fold increase in all-cause mortality during 2004–2018; however, at the same time, the 1-month case-fatality rate decreased slightly, which might reflect advances in treatment for BSIs. A study from Norway during 2002–2013 demonstrated a similar mortality rate (32 cases/100,000 population) as in our study (28 cases/100,000 population) and showed higher rates in male than in female patients, comparable to our results (*6*). In that study, case-fatality rates decreased from 17.2% to 13.1% between 2002–2007 and 2008–2013 concurrent with an increasing incidence of BSIs and rising rates of blood culture sampling (*6*). A higher 30-day mortality rate was observed among hospitalized patients with bacteremia in Denmark, but that study also noted decreasing rates from 22.7% to 20.6% between 1992–1996 and 2002–2006 (*10*). A recent study from Sweden during 2000–2013 showed a 1-month case-fatality rate of 12.8%, similar to our results (*12*).

In our study, the proportion of BSI patients with a low CCI declined during 2004–2018 from 45% to 35%, but the proportion of those with a high CCI increased from 14% to 23%. Similarly, in a report from Denmark during 1992–2006, the proportion of BSI patients with a low CCI decreased from 42% to 33%, and the proportion of those with a high CCI rose from 20% to

30% (*10*). Furthermore, in a survey of BSIs from a county in Sweden, the proportion of patients with ≥1 underlying condition increased from 21% to 55% during 2000–2013 (*12*).

The average annual incidence of BSIs in our study was highest among older persons, as demonstrated in previous studies (*1*–*4*,*6*,*21*). In addition, we noted that the increase in the incidence over time was most notable among the oldest persons, those ≥90 years of age. Researchers widely recognize that the risk for BSIs increases as the population ages and as the life expectancy rises in industrialized countries. It is likely that the considerable rise in BSI incidence over time is also associated with increasing prevalence of underlying conditions, advanced treatments of chronic diseases, and implementation of invasive procedures. We noted a higher average annual BSI incidence among male patients, which aligns with results from previous reports (*1*–*3*,*6*,*21*), and is presumably related to higher prevalence of chronic diseases and predisposing factors among male persons.

In our study, healthcare-associated BSIs accounted for 29% of all BSIs and community-acquired BSIs for 71%; the proportion of healthcare-associated BSIs decreased during 2004–2018, but community-acquired BSIs increased. Similarly, a study in Sweden noted that hospital-acquired BSIs accounted for 33% and community-onset BSIs for 67% of all BSIs (*12*). In a survey from Denmark that reported 3 categories of BSIs by origin, the portion of nosocomial and community-acquired BSIs declined during 1992–2006, but healthcare-associated BSIs increased by >2-fold during the same time (*10*). The 2-day timeframe for our definition of healthcare-associated BSI was rather strict and might have led to underestimating these BSIs. Some healthcare-associated BSIs possibly were inaccurately interpreted as community-acquired because the data on the origin of the infection were obtained from HILMO. The HILMO hospital discharge registry does not cover long-term care facilities, does not include information on possible outpatient invasive procedures before the BSI, and does not provide data on regular patient hospital visits for chronic hemodialysis or chemotherapy.

E. coli and *S. aureus* were the most common causative pathogens of all BSIs in our study, and in similar

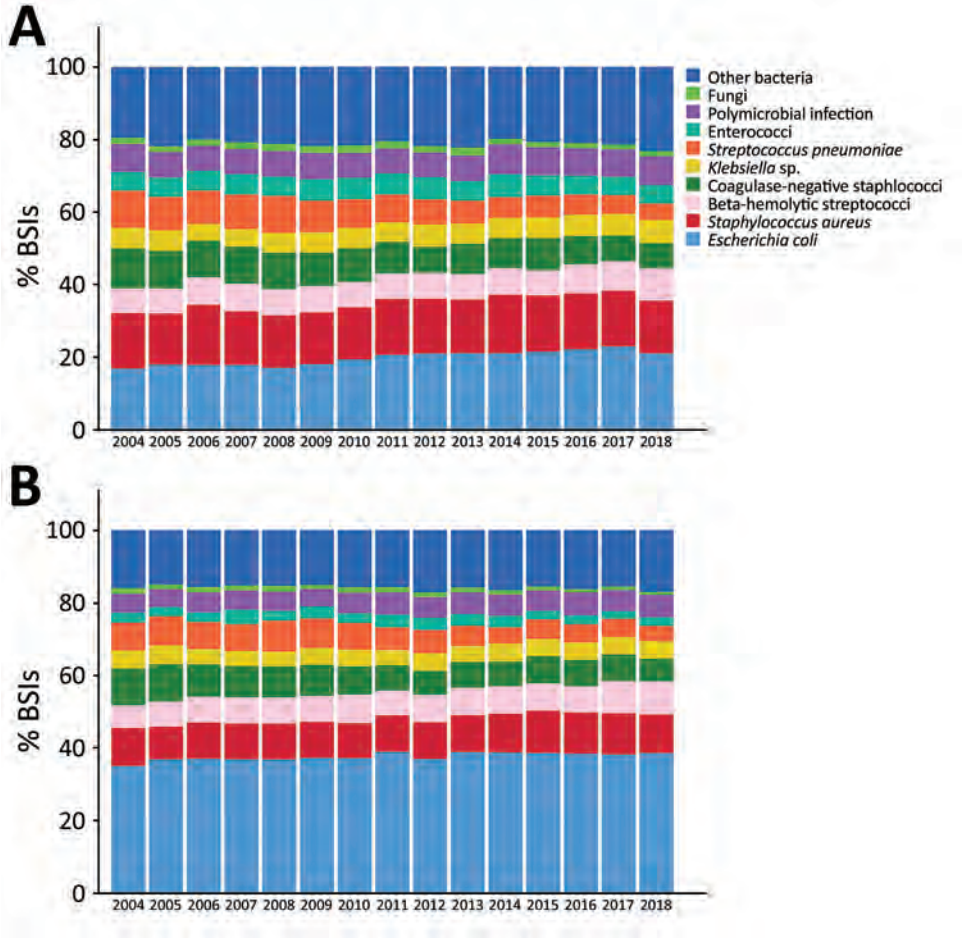

Figure 5. Frequency distribution of the most common causative agents of BSIs, by sex, Finland, 2004–2018. A) Male patients; B) female patients. BSI, bloodstream infections.

proportions as have been reported from Europe and North America (*1*,*3*,*12*,*15*,*21*). Our findings show the proportion of *E. coli* BSIs increased from 26% to 30% during 2004–2018, but no change was noted in *S. aureus* BSIs (13%). Similarly, in a report of BSIs in England during 2004–2008, the proportion of *E. coli* BSIs rose from 19% to 23%, but *S. aureus* BSIs decreased from 17% to 12% because of reduction in methicillin-resistant strains (*2*). A considerable increase in the proportion of *E. coli* BSIs also has been observed in Sweden (*12*), and in 2 other reports from countries in Scandinavia, the prevalence of bacteremia with urinary tract foci increased concurrently with rising rates of *E. coli* BSIs (*6*,*10*). In our study, the annual incidence of both *E. coli* and *S. aureus* rose by >2-fold during 2004–2018, which is comparable to results from previous population-based surveys (*22*,*23*). On the contrary, we noted that the incidence of *S. pneumoniae* BSIs decreased after 2008, which most likely is associated with the implementation of pneumococcal vaccines in Finland (*24*). This finding is in line with studies from Norway during 2002–2013 and England during 2004–2008 showing reduction in the incidence of *S. pneumoniae* BSIs after introduction of the conjugate vaccine to the childhood immunization schedule in 2006 (*2*,*6*).

In our study, the proportion of BSIs caused by MDR microbes was low (1.8%), but we observed a distinct ascending trend during 2004–2018; ESBL–*E. coli* BSIs increased the most. On the other hand, the proportion of MRSA BSIs decreased over time. In Finland, as in other Nordic countries, the proportion of MDR BSIs is typically low (*6*,*25*,*26*), whereas North America and most of Europe have considerably higher proportions of MDR BSIs, as shown in previous surveillance studies (*27*–*29*). These surveys also demonstrate a rising trend in MDR BSIs over time, as noted in our results.

Our study's first limitation was that we did not have exact numbers of blood cultures performed during the study period. However, in a previous report from Finland the annual national blood culturing rate increased by one third during 1995–2002, from 2,752 to 3,667 cultures/100,000 population (*30*). Also, estimates from the Finnish Hospital Infection Program suggest that the median number of blood cultures among hospitalized patients in Finland increased by 25% during 2014–2018, from ≈120 to 150 blood culture sets/1,000 patient-days (*28*; O. Lyytikäinen, unpub. data). Recent reports from other countries have shown that increasing blood culture rates might influence the rising BSI incidence (*6*,*7*). Thus, higher culturing rates lead to improved detection of milder BSIs, which might contribute to the slightly decreasing case-fatality rates noted in our study. The rising incidence of BSIs also might reflect changes in the healthcare delivery system, such as centralized healthcare services in which patients with acute infections are treated at hospital emergency departments instead of in community healthcare centers, and blood cultures possibly are taken before patient conditions progress to severe BSI or when patients have milder infections and milder symptoms. Second, because the study was based on surveillance data, we did not have information on the focus of the infection, on possible delays in recognition and treatment of the infection, nor data on the appropriateness of antimicrobial therapy, which might have affected the outcome of BSIs. Third, we did not have information on the main cause of death of the patients, but presumably BSI was a contributing factor. Finally, we did not have data on patients' underlying medical conditions other than those included in the CCI, nor did we have information on possible do-not-resuscitate orders for patients, which likely have influenced patient outcome, as we observed in our previous population-based case series of BSIs leading to early death (*31*).

Our population-based study of >170,000 BSIs in Finland during 15 consecutive years offers a comprehensive assessment of temporal trends and outcome of BSIs. We noted a 2-fold rise in the incidence and BSI mortality rates during 2004–2018. The proportion of BSIs caused by resistant microbes, mostly by ESBL–*E. coli*, rose over time, which could complicate antimicrobial therapy in the future and increase the risk for fatal BSI outcomes. Further research is required to assess the possible predisposing factors for BSI mortality. Overall, issues related to the increasing BSI incidence and death raised in our study ought to be evaluated separately in cases of community-acquired and healthcare-associated BSI in the future. Nonetheless, our data serve as a valuable point of reference for industrialized countries when estimating the effects of changes in the epidemiology of BSIs among an aging population and increasing antimicrobial resistance. Continuous BSI surveillance is needed to compose local recommendations for empiric antimicrobial treatment. Our findings underscore the necessity for substantial BSI prevention efforts and increased public and healthcare system awareness of severe infections.

K.K. received grants from the Finnish Cultural Foundation (no. 00190532), from the Finnish Society for Study of Infectious Diseases (no. 04/09/2019), from the HUS Inflammation Center Research Fund (no. Y1209INF01, Y1209TUTKK), and from state funding for the Finnish University Hospitals (no. TYH2018108).

About the Author

Dr. Kontula is a specialist in infectious diseases at the Helsinki University Hospital. Her research interests include the epidemiology and outcome of bloodstream infections.

References

1. Uslan DZ, Crane SJ, Steckelberg JM, Cockerill FR III, St Sauver JL, Wilson WR, et al. Age- and sex-associated trends in bloodstream infection: a population-based study in Olmsted County, Minnesota. Arch Intern Med. 2007;167:834–9. https://doi.org/10.1001/archinte.167.8.834
2. Wilson J, Elgohari S, Livermore DM, Cookson B, Johnson A, Lamagni T, et al. Trends among pathogens reported as causing bacteraemia in England, 2004–2008. Clin Microbiol Infect. 2011;17:451–8. https://doi.org/10.1111/j.1469-0691.2010.03262.x
3. Skogberg K, Lyytikäinen O, Ollgren J, Nuorti JP, Ruutu P. Population-based burden of bloodstream infections in Finland. Clin Microbiol Infect. 2012;18:E170–6. https://doi.org/10.1111/j.1469-0691.2012.03845.x
4. Laupland KB. Defining the epidemiology of bloodstream infections: the 'gold standard' of population-based assessment. Epidemiol Infect. 2013;141:2149–57. https://doi.org/10.1017/S0950268812002725
5. Buetti N, Atkinson A, Marschall J, Kronenberg A; Swiss Centre for Antibiotic Resistance (ANRESIS). Incidence of bloodstream infections: a nationwide surveillance of acute care hospitals in Switzerland 2008–2014. BMJ Open. 2017;7:e013665. https://doi.org/10.1136/bmjopen-2016-013665
6. Mehl A, Åsvold BO, Lydersen S, Paulsen J, Solligård E, Damås JK, et al. Burden of bloodstream infection in an area of mid-Norway 2002–2013: a prospective population-based observational study. BMC Infect Dis. 2017;17:205. https://doi.org/10.1186/s12879-017-2291-2
7. Laupland KB, Niven DJ, Pasquill K, Parfitt EC, Steele L. Culturing rate and the surveillance of bloodstream infections: a population-based assessment. Clin Microbiol Infect. 2018;24:910.e1–4. https://doi.org/10.1016/j.cmi.2017.12.021
8. Goto M, Al-Hasan MN. Overall burden of bloodstream infection and nosocomial bloodstream infection in North America and Europe. Clin Microbiol Infect. 2013;19:501–9. https://doi.org/10.1111/1469-0691.12195
9. Rodríguez-Baño J, López-Prieto MD, Portillo MM, Retamar P, Natera C, Nuño E, et al.; SAEI/SAMPAC Bacteraemia Group. Epidemiology and clinical features of community-acquired, healthcare-associated and nosocomial bloodstream infections in tertiary-care and community hospitals. Clin Microbiol Infect. 2010;16:1408–13. https://doi.org/10.1111/j.1469-0691.2010.03089.x
10. Søgaard M, Nørgaard M, Dethlefsen C, Schønheyder HC. Temporal changes in the incidence and 30-day mortality associated with bacteremia in hospitalized patients from 1992 through 2006: a population-based cohort study. Clin Infect Dis. 2011;52:61–9. https://doi.org/10.1093/cid/ciq069
11. Lenz R, Leal JR, Church DL, Gregson DB, Ross T, Laupland KB. The distinct category of healthcare associated bloodstream infections. BMC Infect Dis. 2012;12:85. https://doi.org/10.1186/1471-2334-12-85
12. Holmbom M, Giske CG, Fredrikson M, Östholm Balkhed Å, Claesson C, Nilsson LE, et al. 14-year survey in a Swedish county reveals a pronounced increase in bloodstream infections (BSI). Comorbidity—an independent risk factor for both BSI and mortality. PLoS One. 2016;11:e0166527. https://doi.org/10.1371/journal.pone.0166527
13. Laupland KB, Davies HD, Church DL, Louie TJ, Dool JS, Zygun DA, et al. Bloodstream infection-associated sepsis and septic shock in critically ill adults: a population-based study. Infection. 2004;32:59–64. https://doi.org/10.1007/s15010-004-3064-6
14. Prowle JR, Echeverri JE, Ligabo EV, Sherry N, Taori GC, Crozier TM, et al. Acquired bloodstream infection in the intensive care unit: incidence and attributable mortality. Crit Care. 2011;15:R100. https://doi.org/10.1186/cc10114
15. Nielsen SL, Pedersen C, Jensen TG, Gradel KO, Kolmos HJ, Lassen AT. Decreasing incidence rates of bacteremia: a 9-year population-based study. J Infect. 2014;69:51–9. https://doi.org/10.1016/j.jinf.2014.01.014
16. Laupland KB, Church DL. Population-based epidemiology and microbiology of community-onset bloodstream infections. Clin Microbiol Rev. 2014;27:647–64. https://doi.org/10.1128/CMR.00002-14
17. Laupland KB, Lyytikäinen O, Søgaard M, Kennedy KJ, Knudsen JD, Ostergaard C, et al.; International Bacteremia Surveillance Collaborative. The changing epidemiology of *Staphylococcus aureus* bloodstream infection: a multinational population-based surveillance study. Clin Microbiol Infect. 2013;19:465–71. https://doi.org/10.1111/j.1469-0691.2012.03903.x
18. Charlson ME, Pompei P, Ales KL, MacKenzie CR. A new method of classifying prognostic comorbidity in longitudinal studies: development and validation. J Chronic Dis. 1987;40:373–83. https://doi.org/10.1016/0021-9681(87)90171-8
19. Quan H, Sundararajan V, Halfon P, Fong A, Burnand B, Luthi JC, et al. Coding algorithms for defining comorbidities in ICD-9-CM and ICD-10 administrative data. Med Care. 2005;43:1130–9. https://doi.org/10.1097/01.mlr.0000182534.19832.83
20. Skogberg K, Lyytikäinen O, Ruutu P, Ollgren J, Nuorti JP. Increase in bloodstream infections in Finland, 1995-2002. Epidemiol Infect. 2008;136:108–14. https://doi.org/10.1017/S0950268807008138
21. Laupland KB, Pasquill K, Parfitt EC, Naidu P, Steele L. Burden of community-onset bloodstream infections, Western Interior, British Columbia, Canada. Epidemiol Infect. 2016;144:2440–6. https://doi.org/10.1017/S0950268816000613
22. Williamson DA, Lim A, Wiles S, Roberts SA, Freeman JT. Population-based incidence and comparative demographics of community-associated and healthcare-associated *Escherichia coli* bloodstream infection in Auckland, New Zealand, 2005–2011. BMC Infect Dis. 2013;13:385. https://doi.org/10.1186/1471-2334-13-385
23. Thorlacius-Ussing L, Sandholdt H, Larsen AR, Petersen A, Benfield T. Age-dependent increase in incidence of *Staphylococcus aureus* bacteremia, Denmark, 2008–2015. Emerg Infect Dis. 2019;25:875–82. https://doi.org/10.3201/eid2505.181733
24. Rinta-Kokko H, Palmu AA, Auranen K, Nuorti JP, Toropainen M, Siira L, et al. Long-term impact of 10-valent pneumococcal conjugate vaccination on invasive pneumococcal disease among children in Finland. Vaccine. 2018;36:1934–40. https://doi.org/10.1016/j.vaccine.2018.03.001
25. European Centre for Disease Prevention and Control (ECDC). Surveillance of antimicrobial resistance in Europe 2018. Annual report of the European Antimicrobial Resistance Surveillance Network (EARS-Net). Stockholm: ECDC. Nov 2019 [cited 2020 Nov 10]. https://www.ecdc.europa.eu/sites/default/files/documents/surveillance-antimicrobial-resistance-Europe-2018.pdf

26. Holmbom M, Möller V, Nilsson LE, Giske CG, Rashid MU, Fredrikson M, et al. Low incidence of antibiotic-resistant bacteria in south-east Sweden: an epidemiologic study on 9268 cases of bloodstream infection. PLoS One. 2020;15:e0230501. https://doi.org/10.1371/journal.pone.0230501
27. Wisplinghoff H, Bischoff T, Tallent SM, Seifert H, Wenzel RP, Edmond MB. Nosocomial bloodstream infections in US hospitals: analysis of 24,179 cases from a prospective nationwide surveillance study. Clin Infect Dis. 2004;39:309–17. https://doi.org/10.1086/421946
28. de Kraker ME, Jarlier V, Monen JC, Heuer OE, van de Sande N, Grundmann H. The changing epidemiology of bacteraemias in Europe: trends from the European Antimicrobial Resistance Surveillance System. Clin Microbiol Infect. 2013;19:860–8. https://doi.org/10.1111/1469-0691.12028
29. Diekema DJ, Hsueh PR, Mendes RE, Pfaller MA, Rolston KV, Sader HS, et al. The microbiology of bloodstream infection: 20-year trends from the SENTRY Antimicrobial Surveillance Program. Antimicrob Agents Chemother. 2019;63:e00355–19. https://doi.org/10.1128/AAC.00355-19
30. Klemets P, Lyytikäinen O, Ruutu P, Kaijalainen T, Leinonen M, Ollgren J, et al. Trends and geographical variation in invasive pneumococcal infections in Finland. Scand J Infect Dis. 2008;40:621–8. https://doi.org/10.1080/00365540801938931
31. Kontula KS, Skogberg K, Ollgren J, Järvinen A, Lyytikäinen O. Early deaths in bloodstream infections: a population-based case series. Infect Dis (Lond). 2016;48:379–85. https://doi.org/10.3109/23744235.2015.1131329

Address for correspondence: Keiju Kontula, Division of Infectious Diseases, Inflammation Center, Helsinki University Hospital, P.O. Box 340, 00029 HUS, Helsinki, Finland; email: keiju.kontula@hus.fi

Fatal Cowpox Virus Infection in Human Fetus, France, 2017

Audrey Ferrier,[1] Gaelle Frenois-Veyrat,[1] Evelyne Schvoerer, Sandrine Henard, Fanny Jarjaval, Isabelle Drouet, Hawa Timera, Laetitia Boutin, Estelle Mosca, Christophe Peyrefitte, Olivier Ferraris

Cowpox virus (CPXV) has an animal reservoir and is typically transmitted to humans by contact with infected animals. In 2017, CPXV infection of a pregnant woman in France led to the death of her fetus. Fetal death after maternal orthopoxvirus (smallpox) vaccination has been reported; however, this patient had not been vaccinated. Investigation of the patient's domestic animals failed to demonstrate prevalence of CPXV infection among them. The patient's diagnosis was confirmed by identifying CPXV DNA in all fetal and maternal biopsy samples and infectious CPXV in biopsy but not plasma samples. This case of fetal death highlights the risk for complications of orthopoxvirus infection during pregnancy. Among orthopoxviruses, fetal infection has been reported for variola virus and vaccinia virus; our findings suggest that CPXV poses the same threats for infection complications as vaccinia virus.

Cowpox virus (CPXV) is a member of the genus *Orthopoxvirus* in the family *Poxviridae*. CPXV is assumed to be the causative agent of cowpox, mainly associated with lesions on the udders of dairy cows and the hands of dairy workers. This zoonotic disease has a broad range of hosts (*1*), so spillover infections to accidental hosts (e.g., rats, cats, cattle, horses, llamas, zoo animals, and humans) are reported regularly; case numbers in Europe are increasing (*2*).

CPXV and all other orthopoxviruses that can infect humans (with the exception of variola virus) have an animal reservoir and are transmitted to humans by contact with infected animals. Wild rodents (voles) are considered the reservoir host species (*3*), but zoonotic transmissions of CPXV have been mainly caused by direct contact with infected pet rats (*4*–*7*), cats (*8*,*9*), or zoo animals (*10*,*11*).

Among orthopoxviruses, infection of the human fetus has been reported for variola virus and vaccinia virus (*12*–*15*). Congenital vaccinia is a rare complication of vaccination; <40 cases have been described in the literature (*16*), including serious consequences to the fetus of vaccinated women, such as death or premature birth (*16*,*17*). We describe a fatal case of CPXV infection in a human fetus.

Materials and Methods

The Case

On July 13, 2017, a 22-year-old pregnant woman (11 weeks of gestation, according to her last menstrual period) was admitted to Brabois University Hospital in Nancy, France. The patient arrived with multiple lesions on her right hand, 1 on the dorsal surface of a finger, and 2 on the palmar surface of the same finger (Figure 1, panels A, B). She also had a lesion on her chin (Figure 1, panel C), fever, ipsilateral axillary lymphadenopathy, and preexisting atopic dermatitis on her hands. The first lesion, on the dorsal surface of her right hand, seemed to have appeared on June 30, followed by the palmar lesions ≈3 days later. The patient stated that the lesion on her chin appeared later as a result of autoinoculation.

Since June 30, the patient had experienced 2 episodes of fever (38.5°C), on June 30 and July 12; she received antimicrobial therapy while hospitalized (July 13) to avoid superinfection. On July 18, the diagnosis of an orthopoxvirus-positive, smallpox virus–negative infection was confirmed by PCR at the hospital, and the National Reference Center–Expert Laboratory for Orthopoxvirus (Brétigny-sur-Orge, France) was contacted. DNA from a finger biopsy sample taken on July 18 was analyzed, as were cutaneous biopsy and plasma samples from July 19. The orthopoxvirus-positive, smallpox virus–negative

Author affiliations: Institut de Recherche Biomédicale des Armées, Brétigny-sur-Orge, France (A. Ferrier, G. Frenois-Veyrat, F. Jarjaval, I. Drouet, H. Timera, L. Boutin, E. Mosca, C. Peyrefitte, O. Ferraris); Centre Hospitalier Régional Universitaire, Nancy, France (E. Schvoerer, S. Henard)

DOI: https://doi.org/10.3201/eid2710.204818

[1]These authors are co–first authors.

Figure 1. Cowpox virus infection of a 22-year-old pregnant woman with atopic dermatitis, France, July 13, 2017. A) Cutaneous lesion on the dorsal surface of finger on right hand. B) Cutaneous lesion on the palmar surface of finger on right hand. C) Cutaneous lesion on the chin.

diagnosis was confirmed by identification of CPXV DNA in all samples. Infectious CPXV was detected in biopsy samples only, not in plasma. Fetal death was declared on July 20, after echography examination.

We identified CPXV DNA and infectious virus in fetal, placental, and cutaneous samples collected on July 21. On August 3, infectious CPXV was still detected in vaginal samples, whereas neither DNA nor infectious virus of CPXV was detected in the plasma. The last samples, collected on August 30, showed no infectious virus, only CPXV DNA, in vaginal samples; plasma was free of infectious virus and CPXV DNA (Table; Figure 2).

Because CPXV incubation time is 8–12 days (*5*), we determined the incubation time for this case to be a mean of 10 days. Beginning with the appearance of signs and symptoms on June 30, we estimated the day of infection to be June 20, which corresponded to the ninth week of pregnancy, 10 days before symptom onset.

The patient had preexisting atopic dermatitis on her hands. She lived near a farm and had 2 rabbits as well as 2 dogs and 3 cats that were free to roam outside the house. The patient declared that she had neither touched her animals nor cleaned their litter since the beginning of her pregnancy.

Virus Detection, Isolation, and Production

For virus detection, we extracted DNA from samples collected from pustular areas, blood, fetus, placenta, plasma, serum, and vaginal swabs in viral transport medium by using the QIAamp DNA Blood Mini Kit (QIAGEN, https://www.qiagen.com). We used 2 real-time quantitative PCR (qPCR) assays. The first assay detected orthopoxvirus on the basis of the A27L gene (*18*), by using the following primers: GF-5′-GCCAGAGATATCATAGCCGCTC, GR-5′-CAACGACTAACTAATTTGGAAAAAAAGAT, 14KD POX FAM/TAMRA-5′-TTTTCCAACCTAAATAGAACTTCATCGTTGCGTT and 14KD VAR FAM/TAMRA-5′-TTTTCCAACCTAAATAGAACGTCATCATTGCGTT. The second assay detected CPXV on the basis of the D8L and D11L genes by using the following primers: F-5′-GGTAGGTTCATGTTGGAAAATATC; R-5′-AAGATGTTATTAGTGGTATTAGAGAGAAAT, FAM/TAMRA-5-AAGTCATCTACTACATAGACCATGATCAACCAA (D8L gene) and F-5′-AAAACTCTCCACTTTCCATCTTCT; and R-5′-GCATTCAGATACGGATACTGATTC and FAM/TAMRA-5′-CCACAATCAGGATCTGTAAAGCGAGC(D11L gene). We conducted qPCR by using the iTaq Universal Probes Supermix (Bio-Rad, https://www.bio-rad.com).

To isolate competent virus, we used Vero cells maintained in Gibco Dulbecco's modified Eagle medium GlutaMAX (DMEM-GlutaMAX) supplemented with 10% inactivated fetal bovine serum (FBSi; Thermo Fisher Scientific, https://www.thermofisher.com.) We inoculated 24-well plates of Vero cells with plasma and with fetal, placental, and vaginal swab samples,

Table. Quantification of genomic or infectious CPXV in samples and CPXV-specific IgG detection in serum of mother and fetus, France, 2017*

	Jul 19, 29 dpi		Jul 21, 31 dpi			Aug 3, 44 dpi		Aug 30, 71 dpi	
Samples	Cutaneous biopsy	Plasma	Cutaneous biopsy	Fetus	Placenta	Vaginal swab	Plasma	Vaginal swab	Plasma
DNA, copies/µL	2.4×10^4	26.6	8.6×10^6	1.6×10^6	1.4×10^6	2.0×10^4	–	27	–
Infectious virus, $TCID_{50}$/mL	NT	–	1.86×10^7	2.32×10^7	9.74×10^7	1.95×10^8	–	–	–
CPXV-specific IgG	NA	++	NA	NA	NA	NA	++	NA	+++

*CPXV DNA was quantified by quantitative PCR. Infectious virus was titered on Vero cells. CPXV-specific IgG was detected by ELISA. The patient had domestic rabbits, cats and dogs at home. Given the probability of contamination of the animals, PCR was performed on claws and plasmas samples from the animals; all results were negative. CPXV, cowpox virus; dpi, days postinfection; NA, not applicable; NT, not tested; $TCID_{50}$, 50% tissue culture infectious dose; ++, medium level; +++, high level.

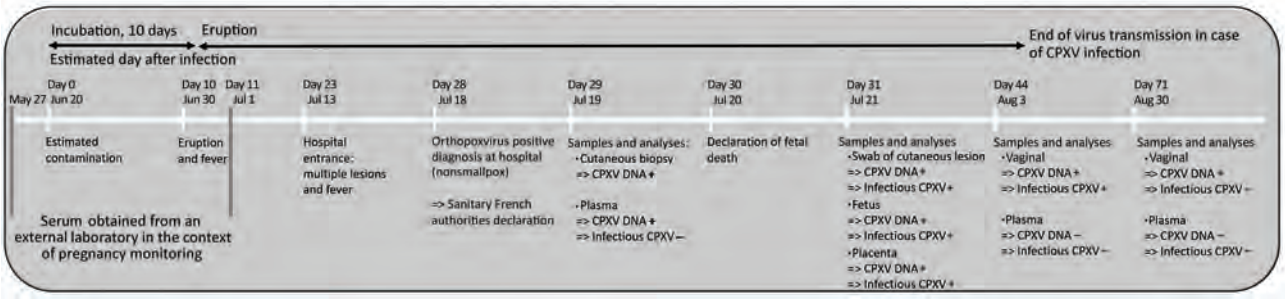

Figure 2. Chronology of CPXV infection of a 22-year-old pregnant woman, France, 2017, showing links between date of samples, detection of DNA or infectious CPXV, and course of the disease. Days after infection indicate the estimated day of infection based on the literature. CPXV, cowpox virus.

then placed the fetal, placental, and biopsy samples (from the mother's hands) in phosphate-buffered saline (PBS) and crushed for 4 min at 30 Hz (TissueLyser; QIAGEN). We diluted supernatant of centrifuged samples (5 min at 1,500 × *g*) from 10^{-2} to 10^{-6} in DMEM-GlutaMAX, 0.4% FBSi, and 0.5 mg/mL of streptomycin and penicillin (Gibco; Thermo Fisher Scientific). We inoculated cells in duplicate with 450 µL of each sample and incubated them for 1 h at 37°C and 5% CO_2. After incubation, we added 1.5 mL of DMEM-GlutaMAX, 0.4% FBSi, and 0.5 mg/mL of streptomycin and penicillin. After 8 days, we examined the cells for any cytopathic effects. For positive samples, we recovered the supernatants and stored them for amplification.

For virus amplification, we used Vero cells maintained in DMEM-GlutaMAX supplemented with 5% FBSi. After the cells reached 80% confluence, we removed the medium and inoculated the monolayer with 1 mL of viral suspension, which consisted of supernatant diluted to 1/10 in DMEM-GlutaMAX, 0.4% FBSi, and 0.5 mg/mL of streptomycin and penicillin. We incubated flasks at 37°C and 5% CO_2 for 1 h for adsorption; then we removed the viral suspension and added 5 mL of DMEM-GlutaMAX, 2% FBSi, and 0.5 mg/mL streptomycin and penicillin. We incubated cells at 37°C and 5% CO_2 for 3 d; on the third day, we freeze-thawed the flasks 3 times, then transferred the contents to 15-mL Falcon tubes and centrifuged at 1,200 × *g* for 10 min to pellet the cell debris. We removed the supernatant and aliquoted it for electronic microscopy and phylogenetic studies. We determined virus titers (expressed in terms of 50% tissue culture infectious dose [$TCID_{50}$] per milliliter) by plaque assay in 96-well plates on Vero cells according to the Reed-Muench method (*19*).

Transmission Electron Microscopy

For microscopy, we used BHK-21 cells maintained in Glasgow's minimum essential medium, 10% FBSi, and 0.5 mg/mL streptomycin and penicillin. To infect the cells, we used virus isolated from fetal and placental samples as well as vaginal swab samples. After cells reached 80% confluence, we inoculated them with virus at a multiplicity of infection of 0.5. Two days after infection, we fixed cells with 2.5% (vol/vol) glutaraldehyde in sodium cacodylate buffer (0.1 M; pH 7.4; 1 mM $CaCl_2$, 1 mM $MgCl_2$, and 2% sucrose) for 1 h at 4°C. After washing samples with a mixture of saccharose (0.2 M) and sodium cacodylate (0.1 M), we postfixed them with 1% (vol/vol) osmium tetraoxide in cacodylate buffer for 1 h at room temperature. Then, we stained them with 2% (vol/vol) uranyl acetate for 1 h at 4°C and gradually dehydrated them with increasing ethanol concentrations. We embedded samples in Epon LX112 resin (Ladd Research Industries, https://www.laddresearch.com) in embedding capsules and polymerized for 24 h at 60°C. We then cut ultrathin 80-nm sections with an UC6 ultramicrotome (Leica, https://www.leica-microsystems.com), placed them onto 300-mesh copper grids, stained sections with 2% uranyl acetate and lead citrate, and examined them under a Philips CM10 TEM microscope (https://www.philips.nl) operating at 100 kV and equipped with a Denka LaB6 cathode (https://www.denka.co.jp) and a CCD Erlanghsenn 1000 Gatan camera (https://www.gatan.com). We applied no filtering procedures to the images.

A56R Genome Sequencing

With regard to the ongoing case, we investigated 2 strains from our collection (CPXV-54-1716F1-France from the placenta specimen and CPXV-54-1716E1-France from the fetus specimen) and compared them with 7 CPXV strains from our strain collections (Cepad 332, Cepad 333, Cepad 336, Cepad 335, CPXV-85-1407-France, CPXV-35-1611-France, and CPXV-54-1405-France). We freeze-thawed infected cell cultures 3 times and extracted genomic DNA by using the QIAamp DNA Blood Mini Kit (QIAGEN). For molecular characterization, we amplified fragments containing the full A56R gene by PCR in a

reaction volume of 50 µL containing 500 nM forward primer, 500 nM reverse primer, Q5 High Fidelity 2X Master Mix (New England BioLabs, https://www.neb.com) at 1× concentration, and 5 µL template DNA. The cycling conditions for both genes corresponded to initial denaturation at 98°C for 30 s; followed by 30 cycles at 98°C for 10 s, 55°C for 20 s, and 72°C for 45 s; and by final extension at 72°C for 2 min. We purified the amplified product of the A56R gene by using QIAquick PCR Purification Kit (QIAGEN), and sequencing was performed by Eurofins at Cochin Institut (Paris, France).

We assembled and edited the sequences by using Clone Manager 7 (Sci Ed Software, https://www.scied.com) and aligned the full-length A56R gene sequences by using BioEdit software version 7.0.9 (https://bioedit.software.com). For phylogenetic reconstructions of the A56R tree, we aligned sequences with MUSCLE by using the aligned codon option of MEGA 6 (https://www.megasoftware.net). We inferred the evolutionary history by using the neighbor-joining method of MEGA 6.

IgG ELISA Data Processing and Normalization

For the IgG ELISA, we coated MaxiSorp microtiter plates (Dutscher, https://www.dutscher.com) with 4 µg/mL of purified vaccinia Copenhagen virus or noninfected cell lysate in carbonate buffer and incubated them overnight at 4°C. The plates were then blocked for 1 h at room temperature with Blocking Reagent (Roche France, https://www.roche.fr), followed by washing 3 times with PBS Tween (Fisher Scientific, https://fishersci.fr). We then added 2-fold serial dilutions in Antibody Diluent (HAMA Blocker) for ELISA (abcam, https://www.abcam.com), from 1:100 of orthopoxvirus-negative, orthopoxvirus-positive serum samples (human vaccinia Ig reference no. EDQM Y0000502), followed by patient serum samples and incubation for 2 h at 37°C. We washed the plates and added chicken anti-human IgG heavy and light chain horseradish peroxidase conjugate (abcam) at a 1:5,000 dilution (Antibody Diluent, abcam) for 1 h at 37°C. We then washed the plates again, added tetramethylbenzidine 1-component substrate (Sigma Aldrich, https://www.sigmaaldrich.com), and allowed development to colorimetric result to proceed for 15 min. We stopped the plate reactions by adding stop solution (H_3PO_4 1M), and we read the optical density at 450 nm on a spectrophotometer (Tecan Spark 10M, https://www.tecan.com).

On each ELISA plate, we included orthopoxvirus-negative, orthopoxvirus-positive serum for internal quality control and for data normalization. In brief, we calculated the optical density difference between infected and noninfected cell lysate for each serum sample and then subtracted the orthopoxvirus-negative values from those of the orthopoxvirus-positive serum and test serum. The level cutoff was determined by the mean $\pm$4.65 SD for 24 blanks tested. By using this normalization, we considered any resulting value above the cutoff value as positive.

Results

Characterization and Isolation of CPXV

The presence of CPXV DNA in different samples was confirmed by PCR amplification using primers for the A27L orthopoxvirus gene and CPXV-specific genes D8L and D11L. PCR showed positive results for the cutaneous biopsy samples from postinfection days 29 and 31, fetus and placental samples on postinfection day 31, and vaginal swab samples from postinfection days 44 and 71 (Table). PCR amplification of plasma showed positive results on postinfection day 29 and negative results on postinfection days 11, 44, and 71 (Table).

In parallel, Vero cells inoculated with each sample showed the typical cytopathic effect resulting from orthopoxvirus infection after 5 days of incubation at 37°C. Cytopathic effects on Vero cells were observed for cutaneous biopsy samples from postinfection days 29 and 31 and for fetal and placental samples from postinfection day 31. Cytopathic effects were still observed from the vaginal swab sample from postinfection day 44. Results were negative for plasma at each day tested and for the vaginal swab sample from postinfection day 71 (Table). Quantification of CPXV-specific IgG in plasma samples on days –23, 11, 29, 44, and 71 detected CPXV-specific IgG in plasma samples from postinfection days 11 (data not shown) through 71.

Serologic Results for the Patient's Animals

For each of the patient's animals, a veterinarian collected claw and plasma samples on August 24. Results of qPCR for CPXV DNA quantification were all negative. Serum samples analyzed by ELISA for CPXV-specific IgG detected no CPXV-specific IgG in serum from the rabbits and dogs but did detect CPXV-specific IgG in serum from 1 of the 3 cats (data not shown).

Electron Microscopic Features of CPXV

When exploring the morphologic features of this CPXV during its viral replicative stage, we examined virus from fetal (Figure 3), placental, and vaginal swab samples. Electron microscopy showed a typical A-type inclusion in the cytoplasm (Figure 3, panels

A, B), classifying this CPXV, named CPXV-54-1716-France, to the V+ subtype. We observed type B viral factories near the nucleus (Figure 3, panel C). We also observed extracellular enveloped viruses with a weight-shaped structure characteristic of CPXV, the nucleoside, containing genomic DNA and proteins involved in viral transcription (Figure 3, panel D).

Phylogenetic Analysis

We performed phylogenetic analysis of the sample against the available A56R gene (Figure 4). We observed that the novel isolate, CPXV-54-1716-France, belongs to clade E3 (CPXV-like 2), for which the reference strain is the Nancy 2001 isolate (GenBank accession no. HQ420894.1).

Discussion

CPXV represents a potential risk to human health, especially after the success of the worldwide smallpox vaccination campaign in 1979 and the subsequent cessation of vaccination. Smallpox vaccination is highly protective against other human-pathogenic orthopoxviruses, so stopping vaccination 40 years ago increased the probability of zoonotic orthopoxvirus infections in humans (*20*,*21*). In Europe, increasing numbers of documented infections with CPXV are being observed (*22*–*24*); lesions are usually localized to 1 extremity or body part (hands, face, neck, shoulders) (*25*). The case that we describe represents a rather atypical example of an orthopoxvirus infection of an orthopoxvirus-naive unvaccinated pregnant woman inducing fetal death. To date, the only mucous membrane–involved CPXV infections reported have been ocular (*5*,*26*,*27*), genital, or oral (*28*,*29*).

Historical studies have evaluated maternal outcomes in pregnancies complicated by smallpox. The overall case-fatality rate was estimated to be 34.3% (*30*). Because of the number of adverse events and the frequencies of complications after smallpox vaccination, maternal and fetal effects of smallpox vaccination during pregnancy were estimated. Despite the low incidence of fetal infection from the vaccinia virus (during smallpox vaccination) (*31*–*34*), some vaccinal complications, such as spontaneous abortion, congenital defects, stillbirth, preterm birth, or fetal vaccinia, have been described (*35*). Those studies have demonstrated that detection of infectious virus in fetal samples is consistent with the hypothesis that CXPVs are responsible for fetal death. The mechanisms governing the abortifacient activity of smallpox virus on gestating women has remained largely unexamined despite even acute maternal smallpox leading to spontaneous abortion, premature termination of pregnancy, and early postnatal infant death.

For the patient we report, CPXV was found in high titers in fetal and placental samples only 17 days after infection. The virus was still detectable in vaginal samples at postinfection day 57. The presence of CPXV in fetal and placental samples supports the hypothesis that the CPXV infection was responsible for the fetal death.

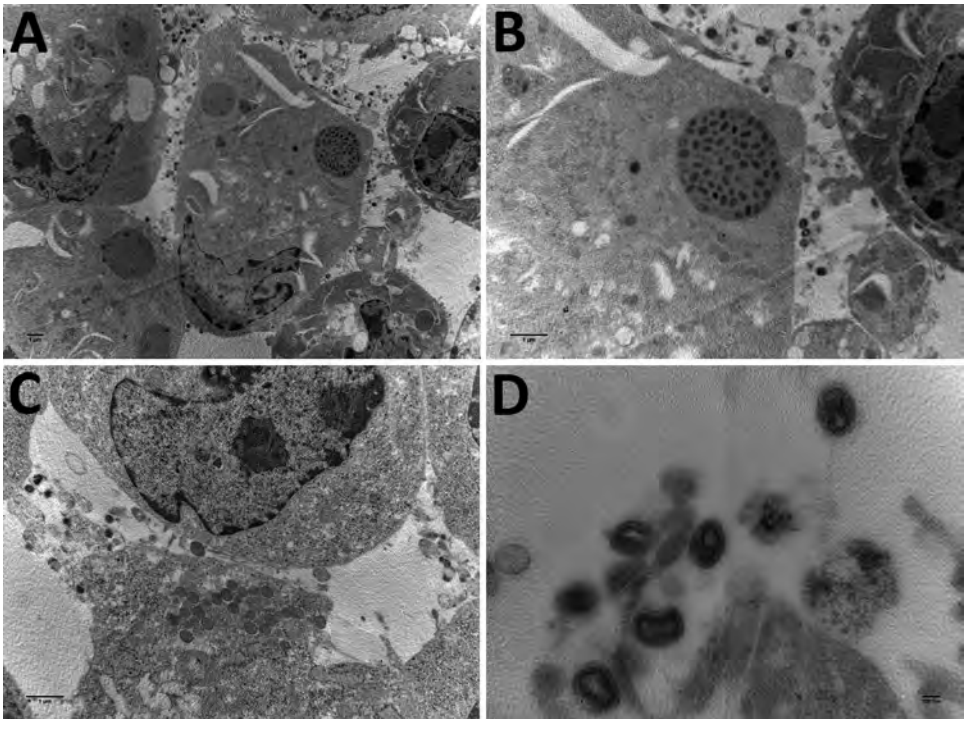

Figure 3. Electron microscopy images of cowpox virus CPXV-54-1716-France (CPXV-like 2), obtained from a pregnant woman in France, 2017. A) Ultrathin sections of BHK-21 cell at 42 hours after infection. Arrow indicates a typical inclusion in the cell cytoplasm. Original magnification ×4,600. B) Higher magnification of BHK-21 cell in panel A. Original magnification ×46,000. C) Ultrathin section of a BHK-21 cell with typical viral factories near the nucleus. Arrows indicate incomplete viruses. Original magnification ×10,500. D) Extracellular-enveloped viruses (arrow). Original magnification ×10,500.

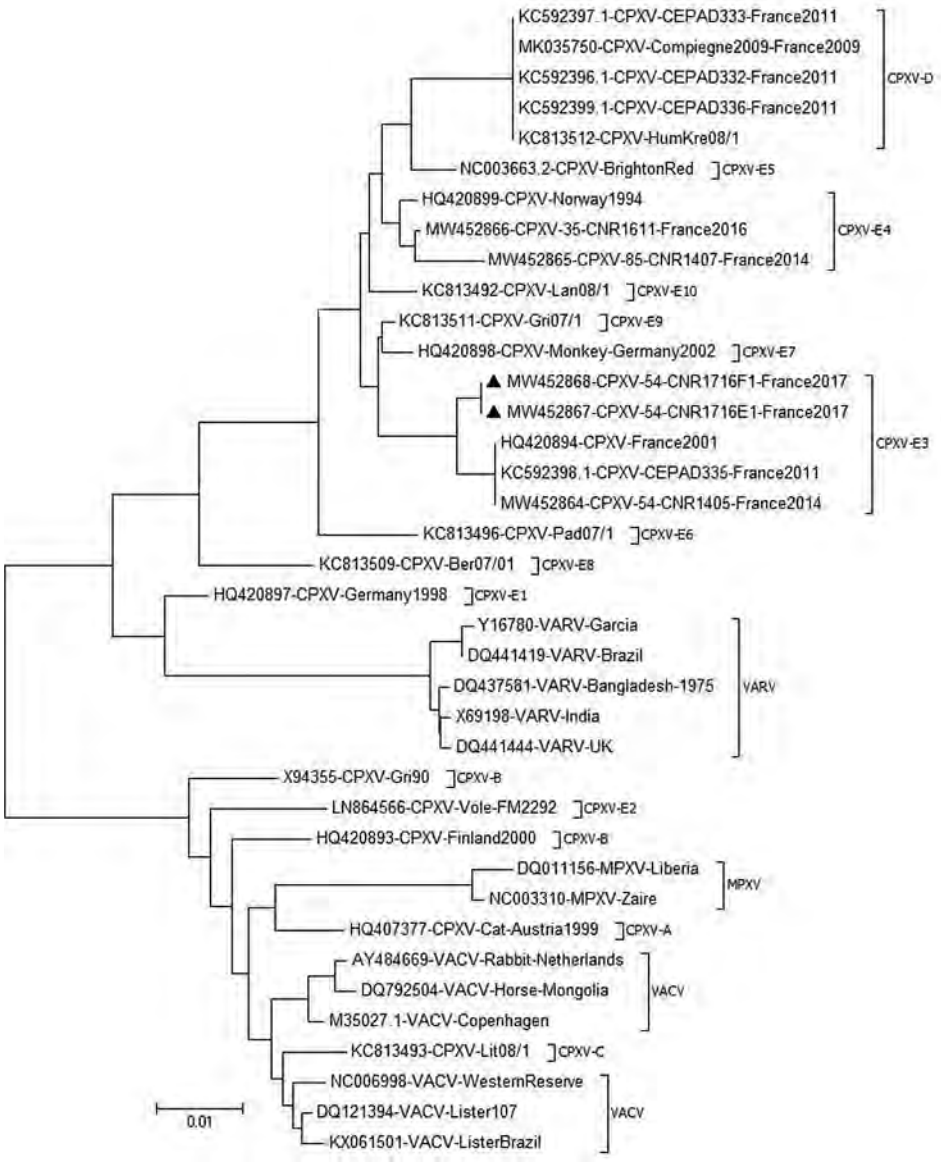

Figure 4. Phylogenic tree of CPXV collected from a woman in France (black triangles) and reference viruses. The tree was generated by using the maximum-likelihood method based on the nucleotide sequence of the A56R gene. The neighbor-joining algorithm was used to generate the initial tree. Evolutionary analyses were conducted in MEGA6 (https://www.megasoftware.net). GenBank accession numbers are provided. Scale bar indicates nucleotide substitutions/site. CPXV, cowpox virus; MPXV, monkeypox virus; VACV, vaccinia virus; VARV, varicella virus.

In cases of congenital vaccinia, viremia in vaccinated pregnant women was suspected to follow direct infection of the fetus or indirect infection of the fetus by placental or amniotic membrane infection (*17*). Although viremia has been demonstrated for variola virus (*36*), human CPXV infections have not been correlated with viremia (*37*). For vaccinia virus, it seems to be a very rare event (*38*) linked to adverse effects of vaccination, for which viremia was common (*17*). We hypothesized that CPXV viremia probably appeared between postinfection days 11 to 29, explaining the CPXV dissemination to the fetus from the blood, because we demonstrated DNA in plasma samples from those days despite the lack of viremia. The presence of specific antibodies in plasma samples could be responsible for the lack of viremia detection. Moreover, the lack of viremia detection could result from the fact that our samples were plasma only, whereas viremia was detected in erythrocytes from whole blood in the case of variola virus (*37*). Despite the lack of viremia, systemic or even fatal infection may affect patients with an immune deficiency or site of atopy (*27*,*29*,*40*,*41*). Atopic dermatitis combined with pregnancy could probably account for an immunodeficiency state inducing the patient's sensitivity to CPXV infection.

Rodents may serve as a natural reservoir for CPXV (*42*); however, transmission of CPXV to humans is mainly caused by direct contact with infected pet rats or cats. In this case, investigations of the patient's domestic rabbits, cats, and dogs failed to demonstrate

prevalence of CPXV infection among domestic pets. Because samples from pets arrive at the National Reference Center–Expert Laboratory for Orthopoxvirus months after the first samples from patients, it becomes difficult to retrace and investigate the route, initial host, or reservoir during the early stages of disease spread. The probable transmission of CPXV by 1 of the patient's likely infected cats, for which CPXV-specific IgG was found, may have occurred without direct contact. Rather, it may have occurred through contact with a contaminated surface or object because of her atopic dermatitis and the ability of robust orthopoxviruses to survive for an extended time in the environment (*43*,*44*).

To complete the description of this new isolate, we explored its morphologic features in the viral replicative stage. Electron microscopy showed a typical A-type inclusion in the cytoplasm, classifying the CPXV-54-1716-France virus in the V+ subtype (*45*). For viruses within the genus *Orthopoxvirus*, the formation of A-type inclusion bodies is a characteristic of pathogenic infection.

Taking the A56R sequence comparison into consideration, we believe that CPXV-54-1716-France virus branched off from the proposed E3 subclade cluster in Europe (*46*). We also found in this cluster E3, CPXV isolated in 2011, 2014, and 2016, all circulating in the same region in France (*6*,*47*). This result strengthens the observations of an endemic circulating CPXV subclade E3 or CPXV-like 2 clade in France (*46*).

We also find in this cluster E3, CPXV isolated in 2011, 2014 and 2016, all circulating in the same french region

In conclusion, this case of fetal death highlights the risk for complications of orthopoxvirus infection during pregnancy. The correlates of progressive vaccinia and eczema vaccinatum (and now fetal vaccinia) that have been observed with cowpox (*48*) suggest that CPXV poses the same threats for infection complications as vaccinia virus.

Acknowledgments

We thank Joseph Kononchik for grammatical corrections, Anne-Laure Favier and Cédric Castellarin for electronic microscopy, and Maël Bessaud for phylogenetic analyses.

This work was supported by the French Armed Forces Health Service, the Direction Générale pour l'Armement, and the National Reference Center–Expert Laboratory for Orthopoxvirus supported by "Santé Publique France."

About the Authors

Dr. Ferrier is a researcher for the Institut de Recherche Biomédicale des Armées, France. Her research interests are the development of new orthopoxvirus vaccine strategies. She participates in the diagnostic activity of the National Reference Center–Expert Laboratory for Orthopoxvirus.

References

1. Haller SL, Peng C, McFadden G, Rothenburg S. Poxviruses and the evolution of host range and virulence. Infect Genet Evol. 2014;21:15–40. https://doi.org/10.1016/j.meegid.2013.10.014
2. Vorou RM, Papavassiliou VG, Pierroutsakos IN. Cowpox virus infection: an emerging health threat. Curr Opin Infect Dis. 2008;21:153–6. https://doi.org/10.1097/QCO.0b013e3282f44c74
3. Chantrey J, Meyer H, Baxby D, Begon M, Bown KJ, Hazel SM, et al. Cowpox: reservoir hosts and geographic range. Epidemiol Infect. 1999;122:455–60. https://doi.org/10.1017/S0950268899002423
4. Vogel S, Sárdy M, Glos K, Korting HC, Ruzicka T, Wollenberg A. The Munich outbreak of cutaneous cowpox infection: transmission by infected pet rats. Acta Derm Venereol. 2012;92:126–31. https://doi.org/10.2340/00015555-1227
5. Becker C, Kurth A, Hessler F, Kramp H, Gokel M, Hoffmann R, et al. Cowpox virus infection in pet rat owners: not always immediately recognized. Dtsch Arztebl Int. 2009;106:329–34. https://doi.org/10.3238/arztebl.2009.0624
6. Ducournau C, Ferrier-Rembert A, Ferraris O, Joffre A, Favier AL, Flusin O, et al. Concomitant human infections with 2 cowpox virus strains in related cases, France, 2011. Emerg Infect Dis. 2013;19:1996–9. https://doi.org/10.3201/eid1912.130256
7. Favier AL, Flusin O, Lepreux S, Fleury H, Labrèze C, Georges A, et al. Necrotic ulcerated lesion in a young boy caused by cowpox virus infection. Case Rep Dermatol. 2011;3:186–94. https://doi.org/10.1159/000331426
8. Bonnekoh B, Falk K, Reckling K-F, Kenklies S, Nitsche A, Ghebremedhin B, et al. Cowpox infection transmitted from a domestic cat. J Dtsch Dermatol Ges. 2008;6:210–3. https://doi.org/10.1111/j.1610-0387.2007.06546.x
9. Świtaj K, Kajfasz P, Kurth A, Nitsche A. Cowpox after a cat scratch - case report from Poland. Ann Agric Environ Med. 2015;22:456–8. https://doi.org/10.5604/12321966.1167713
10. Hemmer CJ, Littmann M, Löbermann M, Meyer H, Petschaelis A, Reisinger EC. Human cowpox virus infection acquired from a circus elephant in Germany. Int J Infect Dis. 2010;14(Suppl 3):e338–40. https://doi.org/10.1016/j.ijid.2010.03.005
11. Kurth A, Straube M, Kuczka A, Dunsche AJ, Meyer H, Nitsche A. Cowpox virus outbreak in banded mongooses (*Mungos mungo*) and jaguarundis (*Herpailurus yagouaroundi*) with a time-delayed infection to humans. PLoS One. 2009;4:e6883. https://doi.org/10.1371/journal.pone.0006883
12. Macarthur P. Congenital vaccinia and vaccinia gravidarum. Lancet. 1952;2:1104–6. https://doi.org/10.1016/S0140-6736(52)90940-9
13. Garcia AGP. Fetal infection in chickenpox and alastrim, with histopathologic study of the placenta. Pediatrics. 1963;32:895–901.
14. MacDonald AM, Macarthur P. Foetal vaccinia. Arch Dis Child. 1953;28:311–5. https://doi.org/10.1136/adc.28.140.311

15. Dugeon JA. Viral infections. J Clin Path Suppl. (Roy. Coll. Path). 1976;10:99–106.
16. Fulginiti VA, Papier A, Lane JM, Neff JM, Henderson DA, Henderson DA, et al. Smallpox vaccination: a review, part II. Adverse events. Clin Infect Dis. 2003;37:251–71. https://doi.org/10.1086/375825
17. Centers for Disease Control and Prevention (CDC). Women with smallpox vaccine exposure during pregnancy reported to the National Smallpox Vaccine in Pregnancy Registry—United States, 2003. MMWR Morb Mortal Wkly Rep. 2003;52:386–8.
18. Scaramozzino N, Ferrier-Rembert A, Favier AL, Rothlisberger C, Richard S, Crance JM, et al. Real-time PCR to identify variola virus or other human pathogenic orthopox viruses. Clin Chem. 2007;53:606–13. https://doi.org/10.1373/clinchem.2006.068635
19. Reed LJ, Muench LH. A simple method of estimating fifty per cent end points. Am J Hyg. 1938;27:493–7.
20. Rimoin AW, Mulembakani PM, Johnston SC, Lloyd Smith JO, Kisalu NK, Kinkela TL, et al. Major increase in human monkeypox incidence 30 years after smallpox vaccination campaigns cease in the Democratic Republic of Congo. Proc Natl Acad Sci U S A. 2010;107:16262–7. https://doi.org/10.1073/pnas.1005769107
21. Shchelkunova GA, Shchelkunov SN. 40 Years without smallpox. Acta Naturae. 2017;9:4–12. https://doi.org/10.32607/20758251-2017-9-4-4-12
22. Popova AY, Maksyutov RA, Taranov OS, Tregubchak TV, Zaikovskaya AV, Sergeev AA, et al. Cowpox in a human, Russia, 2015. Epidemiol Infect. 2017;145:755–9. https://doi.org/10.1017/S0950268816002922
23. Nitsche A, Pauli G. Sporadic human cases of cowpox in Germany. Euro Surveill. 2007;12:E070419.3.
24. Campe H, Zimmermann P, Glos K, Bayer M, Bergemann H, Dreweck C, et al. Cowpox virus transmission from pet rats to humans, Germany. Emerg Infect Dis. 2009;15:777–80. https://doi.org/10.3201/eid1505.090159
25. Baxby D, Bennett M, Getty B. Human cowpox 1969-93: a review based on 54 cases. Br J Dermatol. 1994;131:598–607. https://doi.org/10.1111/j.1365-2133.1994.tb04969.x
26. Schwarzer H, Kurth A, Hermel M, Plange N. Severe ulcerative keratitis in ocular cowpox infection. Graefes Arch Clin Exp Ophthalmol. 2013;251:1451–2. https://doi.org/10.1007/s00417-012-2138-x
27. Kinnunen PM, Holopainen JM, Hemmilä H, Piiparinen H, Sironen T, Kivelä T, et al. Severe ocular cowpox in a human, Finland. Emerg Infect Dis. 2015;21:2261–3. https://doi.org/10.3201/eid2112.150621
28. Dina J, Lefeuvre PF, Bellot A, Dompmartin-Blanchère A, Lechapt-Zalcman E, Freymuth F, et al. Genital ulcerations due to a cowpox virus: a misleading diagnosis of herpes. J Clin Virol. 2011;50:345–7. https://doi.org/10.1016/j.jcv.2011.01.006
29. Pelkonen PM, Tarvainen K, Hynninen A, Kallio ER, Henttonen K, Palva A, et al. Cowpox with severe generalized eruption, Finland. Emerg Infect Dis. 2003;9:1458–61. https://doi.org/10.3201/eid0911.020814
30. Nishiura H. Smallpox during pregnancy and maternal outcomes. Emerg Infect Dis. 2006;12:1119–21. https://doi.org/10.3201/eid1207.051531
31. Ryan MAK, Gumbs GR, Conlin AMS, Sevick CJ, Jacobson IG, Snell KJ, et al. Evaluation of preterm births and birth defects in liveborn infants of us military women who received smallpox vaccine. Birth Defects Res A Clin Mol Teratol. 2008;82:533–9.
32. Cono J, Casey CG, Bell DM. Smallpox vaccination and adverse reactions. Guidance for clinicians. MMWR Recomm Rep. 2003;52(RR-4):1–28.
33. Green DM, Reid SM, Rhaney K. Generalised vaccinia in the human foetus. Lancet. 1966;1:1296–8. https://doi.org/10.1016/S0140-6736(66)91202-5
34. Harley JD, Gillespie AM. A complicated case of congenital vaccinia. Pediatrics. 1972;50:150–3.
35. Badell ML, Meaney-Delman D, Tuuli MG, Rasmussen SA, Petersen BW, Sheffield JS, et al. Risks associated with smallpox vaccination in pregnancy: a systematic review and meta-analysis. Obstet Gynecol. 2015;125:1439–51. https://doi.org/10.1097/AOG.0000000000000857
36. Downie AW, McCarthy K, MacDonald A. Viraemia in smallpox. Lancet. 1950;2:513–4. https://doi.org/10.1016/S0140-6736(50)91496-6
37. Nitsche A, Kurth A, Pauli G. Viremia in human cowpox virus infection. J Clin Virol. 2007;40:160–2. https://doi.org/10.1016/j.jcv.2007.07.014
38. Cummings JF, Polhemus ME, Hawkes C, Klote M, Ludwig GV, Wortmann G. Lack of vaccinia viremia after smallpox vaccination. Clin Infect Dis. 2004;38:456–8. https://doi.org/10.1086/381101
40. Czerny CP, Eis-Hübinger AM, Mayr A, Schneweis KE, Pfeiff B. Animal poxviruses transmitted from cat to man: current event with lethal end. Zentralbl Veterinärmed B. 1991;38:421–31. https://doi.org/10.1111/j.1439-0450.1991.tb00891.x
41. Fassbender P, Zange S, Ibrahim S, Zoeller G, Herbstreit F, Meyer H. Generalized cowpox virus infection in a patient with HIV, Germany, 2012. Emerg Infect Dis. 2016;22:553–5. https://doi.org/10.3201/eid2203.151158
42. Hazel SM, Bennett M, Chantrey J, Bown K, Cavanagh R, Jones TR, et al. A longitudinal study of an endemic disease in its wildlife reservoir: cowpox and wild rodents. Epidemiol Infect. 2000;124:551–62. https://doi.org/10.1017/S0950268899003799
43. Essbauer S, Meyer H, Porsch-Ozcürümez M, Pfeffer M. Long-lasting stability of vaccinia virus (orthopoxvirus) in food and environmental samples. Zoonoses Public Health. 2007;54:118–24. https://doi.org/10.1111/j.1863-2378.2007.01035.x
44. Sinclair R, Boone SA, Greenberg D, Keim P, Gerba CP. Persistence of category A select agents in the environment. Appl Environ Microbiol. 2008;74:555–63. https://doi.org/10.1128/AEM.02167-07
45. Hoffmann D, Franke A, Jenckel M, Tamošiūnaitė A, Schluckebier J, Granzow H, et al. Out of the reservoir: phenotypic and genotypic characterization of a novel cowpox virus isolated from a common vole. J Virol. 2015;89:10959–69. https://doi.org/10.1128/JVI.01195-15
46. Franke A, Pfaff F, Jenckel M, Hoffmann B, Höper D, Antwerpen M, et al. Classification of cowpox viruses into several distinct clades and identification of a novel lineage. Viruses. 2017;9:E142. https://doi.org/10.3390/v9060142
47. Andreani J, Arnault J-P, Bou Khalil JY, Abrahão J, Tomei E, Vial E, et al. Atypical cowpox virus infection in smallpox-vaccinated patient, France. Emerg Infect Dis. 2019;25:212–9. https://doi.org/10.3201/eid2502.171433
48. Belongia EA, Naleway AL. Smallpox vaccine: the good, the bad, and the ugly. Clin Med Res. 2003;1:87–92. https://doi.org/10.3121/cmr.1.2.87

Address for correspondence: Olivier Ferraris, IRBA, 1 Place Valérie André, Bretigny-sur-Orge 91223, France; email: olivier.ferraris@def.gouv.fr

Severe Acute Respiratory Syndrome Coronavirus 2 Transmission in Georgia, USA, February 1–July 13, 2020

Yuke Wang, Casey Siesel, Yangping Chen, Ben Lopman, Laura Edison, Michael Thomas, Carly Adams, Max Lau, Peter F.M. Teunis

The serial interval and effective reproduction number for coronavirus disease (COVID-19) are heterogenous, varying by demographic characteristics, region, and period. During February 1–July 13, 2020, we identified 4,080 transmission pairs in Georgia, USA, by using contact tracing information from COVID-19 cases reported to the Georgia Department of Public Health. We examined how various transmission characteristics were affected by symptoms, demographics, and period (during shelter-in-place and after subsequent reopening) and estimated the time course of reproduction numbers for all 159 Georgia counties. Transmission varied by time and place but also by persons' sex and race. The mean serial interval decreased from 5.97 days in February–April to 4.40 days in June–July. Younger adults (20–50 years of age) were involved in most transmission events occurring during or after reopening. The shelter-in-place period was not long enough to prevent sustained virus transmission in densely populated urban areas connected by major transportation links.

Coronavirus disease (COVID-19) is an infectious disease caused by severe acute respiratory syndrome coronavirus 2 (SARS-CoV-2). After it was first reported in Wuhan, China, in December 2019, COVID-19 spread rapidly across the world as an ongoing global pandemic. As of July 9, 2021, most confirmed COVID-19 cases (33,792,898 cases) and deaths (606,487) in the world were in the United States (*1*), and 906,136 confirmed cases and 18,544 deaths were in the state of Georgia (*2*).

Author affiliations: Rollins School of Public Health at Emory University, Atlanta, Georgia, USA (Y. Wang, C. Siesel, Y. Chen, B. Lopman, C. Adams, M. Lau, P.F.M. Teunis); Centers for Disease Control and Prevention, Atlanta (L. Edison); Georgia Department of Public Health, Atlanta (L. Edison, M. Thomas)

DOI: https://doi.org/10.3201/eid2710.210061

Transmission of COVID-19 varies by region (*3*,*4*), setting (long-term care facilities, prisons, and factories) (*5*), population demographics (age, sex, and race), and even among individual persons (physiologic and behavioral differences) (*6*). During the early phases of transmission in the United States, new cases were mainly imported by travelers and transmission was associated with human mobility (*7*). Local transmission was more intense in regions with high population density and in populations with frequent social contacts (*3*,*8*,*9*). When SARS-CoV-2 was introduced into high-risk settings (e.g., long-term care facilities), transmission rates were intense, and the outcomes were often fatal (*10*).

To study transmission of SARS-CoV-2, we examined the serial interval for symptom onset (defined as the time interval between symptom onset in a primary case-patient and symptom onset in a secondary case-patient infected by the primary case-patient) and the effective reproduction number R_t (the expected number of cases directly caused by any single infectious person). R_t has been shown to vary strongly; some case-patients have caused superspreading events (*11*,*12*). Such heterogeneity influences the spread as well as the control of COVID-19, as documented by studies of nonpharmaceutical interventions in China (*13*,*14*) and Europe (*15*) at the province and country levels.

After the first case of COVID-19 was reported in the state of Georgia on March 2, 2020, a series of events and interventions followed (Appendix Table 1, https://wwwnc.cdc.gov/EID/article/27/10/21-0061-App1.pdf). On April 3, state officials announced a shelter-in-place order, requiring all residents and visitors to remain in their residence and take every possible precaution to limit social interactions. On

April 24, officials allowed some businesses to reopen, and on April 30 the shelter-in-place order was lifted. On June 1, state officials further relaxed restrictions. During June–July 2020, as new COVID-19 cases continued to surge in Georgia and other states, knowing how shelter-in-place and the subsequent reopening events affected the transmission of SARS-CoV-2 in different regions became crucial.

Identifying a large number of the primary and secondary case-patient pairs enabled us to estimate the distribution of the serial interval for symptom onset. Using the serial interval distribution, we can estimate the time-varying R_t (*16*). With R_ts over time, we can study the spatial distribution of transmission across all 159 Georgia counties as well as the effects of shelter-in-place and subsequent gradual reopening.

The Georgia Department of Public Health (GDPH) Institutional Review Board determined that this analysis was exempt from the requirement for review and approval, and informed consent was not required. This activity was reviewed by the Centers for Disease Control and Prevention and was consistent with their applicable policy and with federal law.

Methods

Data Source

GDPH provided data for all 118,491 confirmed COVID-19 cases in all 159 counties of Georgia during February 1–July 13, 2020. Available data included demographic characteristics (age, sex, and race), clinical characteristics (dates of symptom onset, recorded symptoms, hospitalization, and ventilator use), and social contacts (contacts between confirmed case-patients and if cases were part of a confirmed outbreak) (Table; Appendix Table 2). Missing values in the data were common; large percentages of values for clinical characteristics were missing. With regard to events possibly driving transmission, periods were categorized as early transmission and shelter-in-place during February–April, after reopening (shelter-in-place order was lifted) in May, and further reopening (more restrictions were relaxed) during June–July (Appendix Table 1). For this study, we defined a COVID-19 case as SARS-CoV-2 infection confirmed by reverse transcription PCR irrespective of clinical signs and symptoms.

Tracked Pairs: Serial Intervals and Characteristics of Transmission

On the basis of reported contacts with confirmed case-patients, we identified pairs of primary and secondary case-patients by using the following procedure. First, most transmission pairs could be established as a unique close contact with a confirmed case-patient. We assumed that symptom onset for any primary case-patient in a confirmed pair occurred before symptom onset of the secondary case-patient. Second, when an outbreak involved multiple cases, we assigned primary case-patients according to review of the epidemiologic time lines. Usually, there was 1 case-patient whose symptom onset was several days earlier than that of the rest of the case-patients in the cluster, and this case-patient was designated as the primary case-patient. Thus, serial intervals were assumed to be always positive. To examine the influence of ignoring negative serial intervals on R_t estimation, we conducted a sensitivity analysis (Appendix Supplemental Material C). Transmission pairs with serial intervals >15 days were dropped because such long intervals are unlikely, as shown in previous studies (*17*,*18*). We modeled the serial interval as a gamma distribution and obtained maximum-likelihood estimators of shape and scale parameters. Furthermore, we explored whether the duration of the serial interval varied by demographic characteristics, various disease symptoms, and periods of symptom onset for primary case-patients. The large numbers of tracked case-patient pairs also enabled us to examine variation in transmission within and between different groups by age, sex, and race.

Confirmed Cases: Reproduction Numbers

We estimated probabilities of transmission between any pairs of case-patients in an outbreak by using a transmission probability matrix method (Appendix Supplemental Material B) (*16*). Using GDPH data for confirmed COVID-19 cases during February 1–July 13, 2020, we estimated R_ts by date, and we used dates of symptom onset and social contact information (wherever available) in each county independently by estimating the transmission probability matrix.

Among 118,491 confirmed cases, the date of symptom onset was missing for 48,893 (41.3%). These missing symptom-onset dates were imputed according to dates of first specimen collection if available or dates of laboratory report if not (Appendix Supplemental Material A).

The most recent data are incomplete because not all incident cases have been reported and not all persons have become symptomatic. Therefore, estimates of R_t approaching the present date are biased. Because one of our study goals was to examine the timing and magnitude of the first 2 waves of SARS-CoV-2 transmission in Georgia (and not to nowcast transmission), we removed R_t estimates of the most

recent 4 weeks (June 16–July 13) from the analysis. SARS-CoV-2 transmission in Georgia seemed to include multiple waves and varied considerably among counties. The time-varying average R_t estimates were smoothed by using LOESS regression, and local maximums/minimum were identified for each individual county. On the basis of our review of the epidemic curves and curves, we defined the following 5 transmission patterns:

- Consistent spreading: there was sustained transmission of SARS-CoV-2 (R_t >1) during the shelter-in-place period. Consequently, numbers of cases remained high and increased rapidly at reopening.
- Two strong waves: a first wave of early transmission was followed by a slowdown (R_t <1) during the shelter-in-place period and a new surge in cases ($1 \leq R_t < 2$) after reopening.
- Strong first wave: there was a considerable number of cases during the initial period of the outbreak. During the shelter-in-place period, spreading was controlled; after reopening no new surge in cases occurred (R_t <1).
- Strong second wave: there were few cases during the early transmission period, but new cases surged ($R_t \geq 2$) after reopening.
- Small case number (<200): SARS-CoV-2 transmission was rare.

Table. Demographic and clinical information for persons with confirmed coronavirus disease, Georgia, USA, during 3 periods, February 1–July 15, 2020

Variable	February–April, no. (%), n = 31,575*	May, no. (%), n = 19,270†	June–July, no. (%), n = 67,646‡	Total, no. (%), n = 118,491§
Sex				
M	13,770 (43.6)	9,142 (47.4)	30,247 (44.7)	53,159 (44.9)
F	17,308 (54.8)	9,747 (50.6)	33,828 (50)	60,883 (51.4)
Missing	497 (1.6)	381 (2.0)	3,571 (5.3)	4,449 (3.7)
Race				
Black	13,010 (41.2)	4,639 (24.1)	13,878 (20.5)	31,527 (26.6)
White	11,418 (36.2)	7,168 (37.2)	17,500 (25.9)	36,086 (30.5)
Other	2,818 (8.9)	2,029 (10.5)	6,158 (9.1)	11,005 (9.3)
Missing	4,329 (13.7)	5,434 (28.2)	30,110 (44.5)	39,873 (33.6)
Hospitalized				
Yes	6,714 (21.3)	2,099 (10.9)	4,523 (6.7)	13,336 (11.3)
No	15,627 (49.5)	10,729 (55.7)	27,926 (41.3)	54,282 (45.8)
Missing	9,234 (29.2)	6,442 (33.4)	35,197 (52)	50,873 (42.9)
Ventilator use				
Yes	1,046 (3.3)	184 (1.0)	258 (0.4)	1,488 (1.3)
No	12,188 (38.6)	8,404 (43.6)	19,313 (28.6)	39,905 (33.7)
Missing	18,341 (58.1)	10,682 (55.4)	48,075 (71.1)	77,098 (65.0)
Abnormal chest radiograph finding				
Yes	2,602 (8.2)	494 (2.6)	742 (1.1)	3,838 (3.2)
No	10,151 (32.1)	8,081 (41.9)	18,246 (27.0)	36,478 (30.8)
Missing	18,822 (59.6)	10,695 (55.5)	48,658 (71.9)	78,175 (66.0)
Death				
Yes	2,127 (6.7)	558 (2.9)	320 (0.5)	3,005 (2.5)
No	15,766 (49.9)	10,183 (52.8)	26,304 (38.9)	52,253 (44.1)
Missing	13,682 (43.3)	8,529 (44.3)	41,022 (60.6)	63,233 (53.4)
Fever				
Yes	10,094 (32.0)	4,005 (20.8)	11,787 (17.4)	25,886 (21.8)
No	8,489 (26.9)	7,951 (41.3)	19,655 (29.1)	36,095 (30.5)
Missing	12,992 (41.1)	7,314 (38)	36,204 (53.5)	56,510 (47.7)
Cough				
Yes	12,417 (39.3)	4,992 (25.9)	15,319 (22.6)	32,728 (27.6)
No	6,462 (20.5)	7,059 (36.6)	16,434 (24.3)	29,955 (25.3)
Missing	12,696 (40.2)	7,219 (37.5)	35,893 (53.1)	55,808 (47.1)
Shortness of breath				
Yes	8,504 (26.9)	2,952 (15.3)	7,325 (10.8)	18,781 (15.9)
No	9,807 (31.1)	8,960 (46.5)	23,542 (34.8)	42,309 (35.7)
Missing	13,264 (42)	7,358 (38.2)	36,779 (54.4)	57,401 (48.4)
Diarrhea				
Yes	4,410 (14)	1,971 (10.2)	6,072 (9.0)	12,453 (10.5)
No	12,718 (40.3)	9,589 (49.8)	23,936 (35.4)	46,243 (39.0)
Missing	14,447 (45.8)	7,710 (40.0)	37,638 (55.6)	59,795 (50.5)

*Median age (Q1–Q3) 51 (37–65) y.
†Median age (Q1–Q3) 43 (28–59) y.
‡Median age (Q1–Q3) 34 (23–50) y.
§Median age (Q1–Q3) 40 (26–56) y.

We generated maps to spatially examine the spreading of the COVID-19 first wave. We evaluated the effect of shelter-in-place, reopening, and further reopening by the trend of reproduction numbers before and after those events in different regions of Georgia.

Results

Tracked Pairs: Serial Intervals

On the basis of 4,080 tracked pairs of primary and linked secondary case-patients in Georgia (Appendix Table 3), we estimated the serial interval distribution as a gamma distribution with a mean (10th–90th percentile) of 4.99 (1.32–9.71) days. Generally, the serial interval was longer when outcomes for primary case-patients were severe, such as hospitalization, undergoing ventilation, having an abnormal chest radiograph result, or death as final outcome (Appendix Table 4). Specific signs/symptoms in primary case-patients (i.e., fever, cough, shortness of breath, or diarrhea) did not shorten serial intervals. Serial intervals did not differ across demographic categories (i.e., age, sex, race, or location). The mean (10th–90th percentile) serial interval was 5.97 (1.65–11.50) days in February–April, 5.03 (1.41–9.65) days in May, and 4.40 (1.18–8.52) days in June–July (Figure 1). The average serial interval became shorter over time: from 5.97 (1.65–11.50) days in February–April, to 5.03 (1.41–9.65) days in May, and then to 4.40 (1.18–8.52) days in June–July (Appendix Figure 1).

Tracked Pairs: Characteristics of Transmission

To study the variation in transmission by demographic characteristic (i.e., age, sex, and race), the observed frequencies in transmission pairs can be shown in a matrix (Figure 2, panels A, B). Male case-patients were twice as likely to transmit infection to a female than a male contact, whereas female case-patients were equally likely to transmit infection to a male or a female contact. Transmission between races was strongly assortative. White and Black persons were more likely to transmit infection to persons of their own races than to persons of other races; White persons were 4.4 times as likely to transmit infection to White persons, and Black persons were 5.6 times as likely to transmit infection to Black persons.

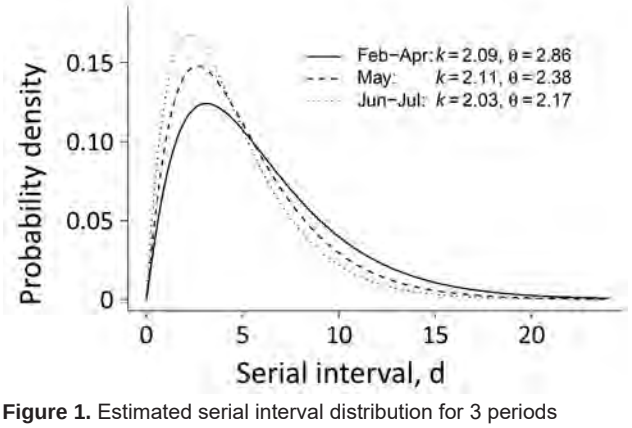

Figure 1. Estimated serial interval distribution for 3 periods in study of severe acute respiratory syndrome coronavirus 2 transmission in Georgia, USA: early transmission and shelter-in-place (February–April 2020); after reopening (May); and further reopening (June–July). *k* and θ indicate the scale and shape parameters for the gamma distribution. The y-axis represents the estimated probability density of having a certain serial interval.

SARS-CoV-2 seemed to mainly spread from adults 20–60 years of age during February–July 2020; transmission between children (<20 years) and elderly persons (>60 years) was observed less often, suggesting that transmission occurred more frequently between persons of similar ages (Figure 3, panels A–D). Transmission between persons of different sexes was mainly among those in the same age group. Cases in persons 10–30 years of age were associated with most transmission pairs of the same sex. Over the study period, most transmission pairs shifted from 40–70 years of age (median age for primary case-patients was 52 years and for secondary case-patients was 50 years) in February–April to 20–50 years of age (primary case-patient median age 36 years and secondary case-patient median age 34 years) in June–July (Figure 4).

Temporal and Spatial Patterns of Transmission

During February and March, R_ts were >1 and then decreased until late April and early May, considered the first wave in Georgia. R_t usually decreased to a (mathematical) local minimum during the shelter-in-place period and started to increase again as the second wave began. As during the first wave, R_ts peaked and then started to decrease again during the second wave (Figure 5). Although the number of reported cases was lower in first wave, R_t was much higher in the first wave (≈3.5) than in the second wave (≈1.7).

Although the general pattern of SARS-CoV-2 transmission was similar across all counties, the dates of local maximums/minimum (i.e., first peak, local minimum, and second peak) and the magnitude of R_t at these extremes varied among counties. The peak dates for the first wave in counties with cumulative case numbers was >200 cases by July 13, 2020 (Figure 6, panel A). At that time, counties with high numbers of COVID-19 cases were located around cities and along highways. Starting in early February, COVID-19 spread radially and along the interstate highway from Atlanta and Albany, the 2 initial outbreak sources. Outbreaks occurred later in other

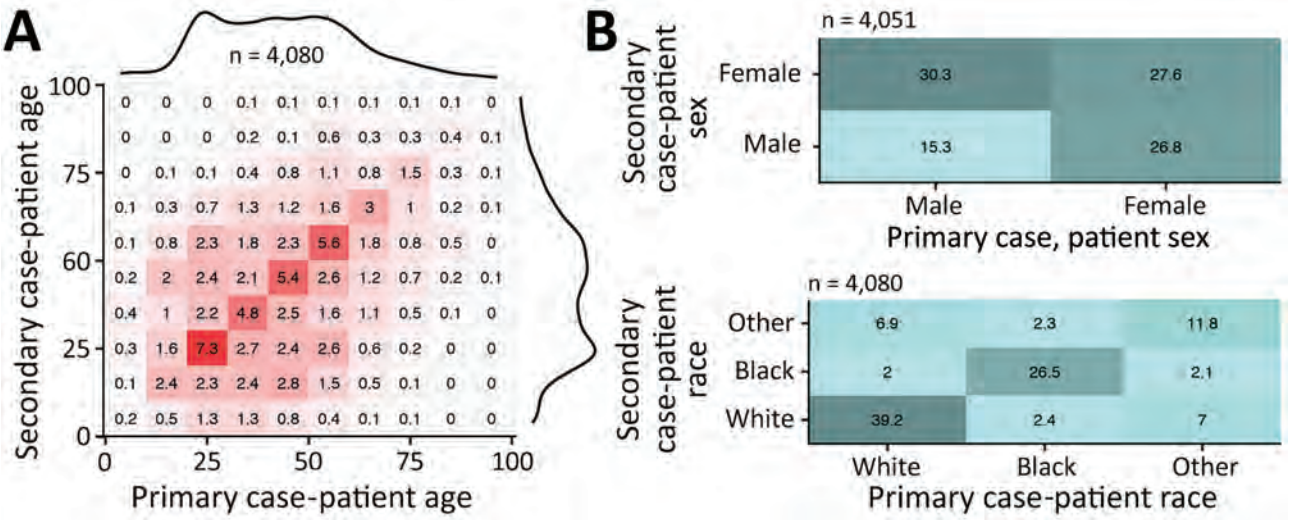

Figure 2. Patterns of severe acute respiratory syndrome coronavirus 2 transmission by patient age (A), sex (B), and race (B), based on 4,080 tracked pairs of coronavirus disease cases from Georgia, USA, during February–July 2020. The matrix graphs show numbers of transmission pairs as a percentage of the total, with primary case-patients as columns and their secondary case-patients as rows. Darker colors indicate a higher percentage of fraction of tracked pairs observed. In panel A, marginal totals are shown as density curves to illustrate the age distribution of case-patients.

cities, including Augusta and Savannah. A total of 65 (74.7%) of 87 counties with >200 cumulative cases by July 13th reached a local minimum in R_t during the shelter-in-place period (April 3–April 30) (Figure 7). After reopening, many counties experienced a second wave of COVID-19 and increased numbers of cases

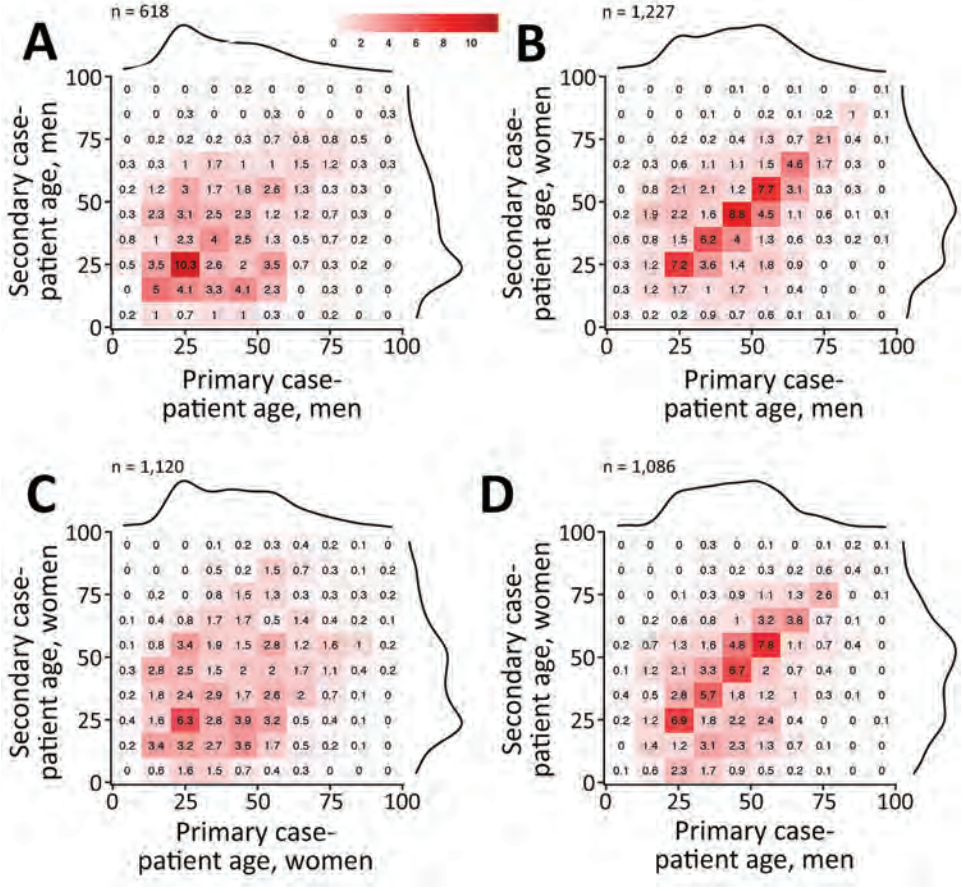

Figure 3. Patterns of severe acute respiratory syndrome coronavirus 2 transmission according to patient sex and age, based on 4,080 tracked pairs of coronavirus disease cases in Georgia, USA, February–July 2020. A) Male-to-male transmission; B) male-to-female transmission; C) female-to-female transmission; D) female-to-male transmission. The matrix graphs show numbers of transmission pairs as a percentage of the total, with primary case-patients as columns and their secondary case-patients as rows. Darker colors indicate a higher percentage of fraction of tracked pairs observed. Marginal totals are shown as density curves to illustrate the age distribution of case-patients.

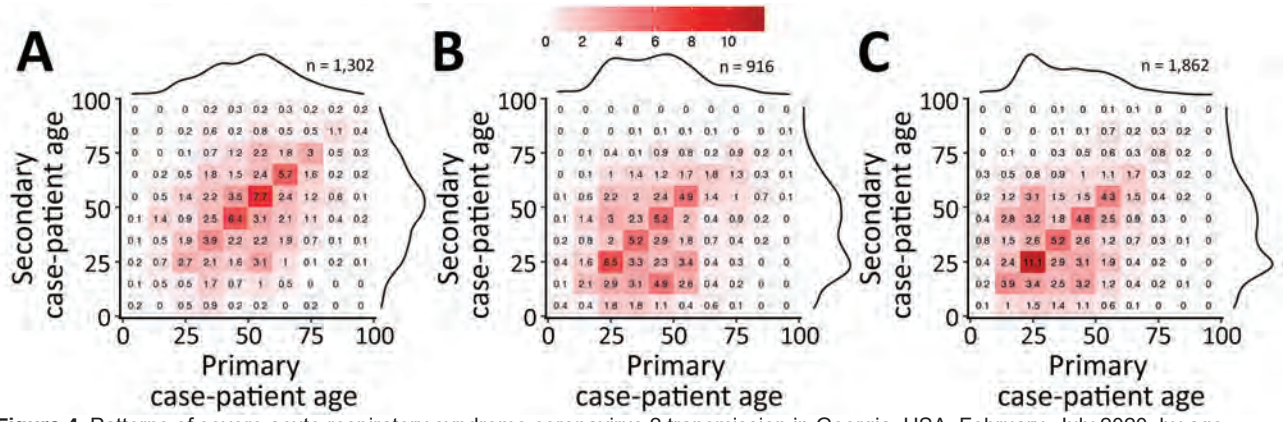

Figure 4. Patterns of severe acute respiratory syndrome coronavirus 2 transmission in Georgia, USA, February–July 2020, by age group, in 3 successive periods. A) Early transmission and shelter-in-place (February–April); B) after reopening (May); C) further reopening (June–July). The matrix graphs show numbers of transmission pairs as a percentage of the total, with primary case-patients as columns and their secondary case-patients as rows. Darker colors indicate a higher percentage of fraction of tracked pairs observed. Marginal totals are shown as density curves to illustrate the age distribution of case-patients.

were reported. On the basis of the magnitude of R_t at the first peak, local minimum, and second peak, we categorized case data into the 5 transmission patterns (Figure 5; Appendix Figures 11–169).

Consistent spreading occurred in Georgia counties around some major cities (e.g., Atlanta, Athens, Columbus, Savannah) and counties along interstate highways (Figure 6, panel B). In counties bordering other counties with consistent spreading, there were 2 strong waves or only a strong second wave. An early intense first wave but not a strong second wave occurred in counties around the city of Albany (Lee, Sumter, Terrell, Mitchell, Crisp, and Dooly Counties). Fewer cases occurred in counties not connected by interstate highways.

Discussion

During February–July, the estimated serial intervals for onset of COVID-19 symptoms in the state of Georgia seemed to become shorter (Figure 1). Such a phenomenon was also observed in mainland China during January–February 2020 (*19*). Shorter serial intervals imply more rapid transmission. During February–July, disease prevalence increased in Georgia; by August 25, Georgia had the fifth highest number of confirmed COVID-19 cases in the United States. One cause of contracting serial intervals could be that persons had more contacts after reopening; in particular, younger persons (20–50 years) might play a larger role in SARS-CoV-2 transmission. Also, Kenah et al. showed that increasingly more infectious case-patients are present in the local population, competing to infect susceptible persons, and the expected time until a new infection is shortened (*20*).

The serial interval estimation could also be affected by changing testing practices and contact tracing over the duration of the pandemic. COVID-19 testing capacity and contact tracing ability in Georgia were limited during earlier stages of the pandemic; thus, identification and isolation of COVID-19 case-patients and their close contacts were often delayed. With improved testing capacity, symptomatic case-patients were tested more promptly and isolated more quickly, which led to fewer exposures during their infectious periods. Rapid isolation and contact tracing could truncate transmission and lead to shorten serial intervals. More recent data collected when testing and contact tracing have improved are less likely to be affected by delayed testing and isolation. Contraction of serial intervals continued into May through early July, so the changes may still be explained at least partly by increased prevalence and increased contact rates (Figure 1).

Transmission of a respiratory infection such as COVID-19 depends on behavioral factors and in particular on social contacts. Studies of contact behavior have shown that persons tend to have social contact with peers of similar age and demographic backgrounds (*21*). The tracked transmission pairs in this study show that such assortative mixing also applies to SARS-CoV-2 transmission (Figure 2). The transmission pairs in this study were more likely to be tracked when case-patients knew each other (e.g., family members, friends, or colleagues), whereas transmission in public spaces (e.g., stores or restaurants) usually could not be tracked. Transmission occurs frequently among persons in the same age group and less frequently among those in different age

groups (Figure 3), although transmission may have been across generations (e.g., between parents and children, or grandparents and grandchildren) (22).

A primary case-patient who was male was more likely to transmit infection to a female contact than to a male contact. Female case-patients were infected by male case-patients across a wide range of ages (Figure 3, panel B), and male case-patients were mainly infected by young male case-patients (Figure 3, panel A). A possible explanation may be that female persons tend to be caregivers, taking care of sick persons in the household, and young male persons may be more likely to acquire infection outside the household.

Similar to the serial interval, transmission patterns also changed as the pandemic continued. The major contribution to spreading SARS-CoV-2 shifted over time to the younger generation. This shift could be caused by elderly persons becoming more careful to protect themselves from infection by taking measures such as staying at home, wearing face masks in public spaces, and observing good hand hygiene. At the same time, younger persons might have been less compliant with quarantine measures and more likely to attend indoor gatherings such as parties or to have visited bars, gyms, and clubs while not wearing face masks.

Previous pandemics, such as the 1918 influenza and the 2009 swine influenza (H1N1) pandemics,

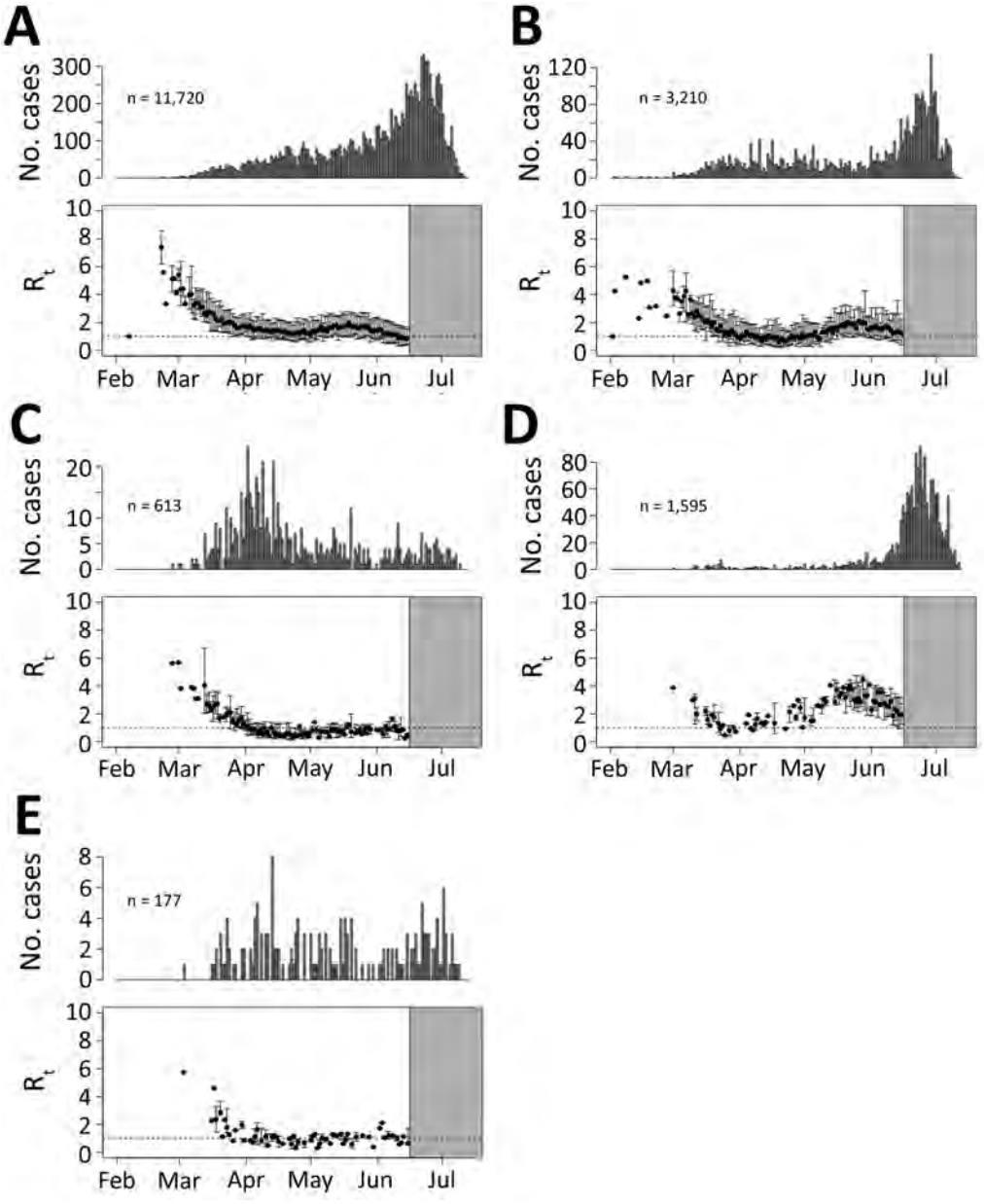

Figure 5. Examples of the 5 categories of severe acute respiratory syndrome coronavirus 2 spreading patterns in counties in Georgia, USA, February–July 2020. Shown are epidemic curves from the start of the outbreak until July 13, 2020, and effective reproduction number (R_t) estimates until June 15, in Gwinnett (A), Clayton (B), Sumter (C), Glynn (D), and Dawson (E) Counties. Tick marks indicate the first day of the month. The x-axis represents the date of symptom onset for patients with confirmed cases. The y-axis in the top plot shows the number of cases; the y-axis in the bottom plot shows the estimated median reproduction numbers. Error bars represent 2.5th–97.5th percentile ranges of R_ts. The gray area shows where R_t estimates were truncated on June 15.

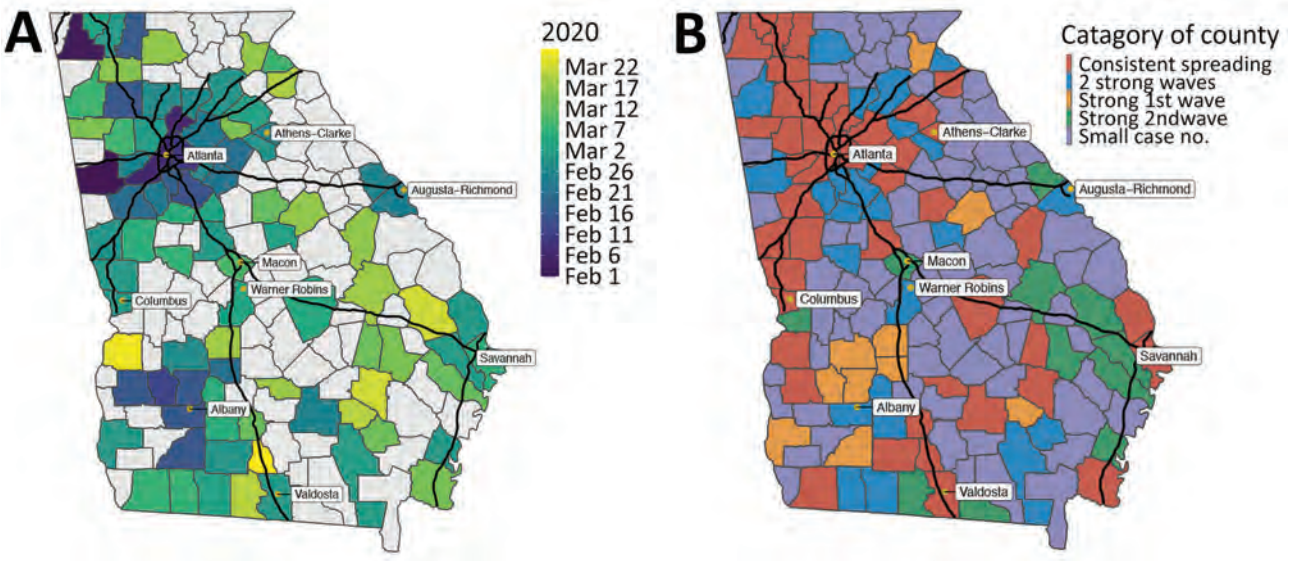

Figure 6. Spatial patterns of transmission of severe acute respiratory syndrome coronavirus 2 in Georgia, USA, February–July 2020. A) Date of reaching the peak (local maximum of effective reproduction number) for the first wave; B) spatial distribution of the 5 categories of virus transmission patterns by June 15, 2020. The black lines represent interstate highways.

caused multiple waves of infections (*23*). In Georgia, we have so far observed 2 waves of SARS-CoV-2 transmission separated by the shelter-in-place period. The COVID-19 cases of the first wave were first observed in Atlanta, the state capital with one of the busiest US airports, and Albany, the eighth largest city in Georgia. The outbreak in Albany resulted from 2 superspreading funeral events. However, the connectivity of these 2 cities differs: Atlanta is a transportation hub that connects multiple interstate highways, whereas Albany has no interstate highways. During the first wave, SARS-CoV-2 spread radially from both cities to the surrounding areas. For Atlanta, cases also started to appear along the interstate highways (Figure 6, panel A). Concentrations of increased transmission along highways, as links connecting population centers, suggest that commuter links might have been effective transmission links.

During the shelter-in-place period (April 3–April 30), SARS-CoV-2 transmission slowed and R_ts reached a local minimum in most counties. However, before reopening, R_ts were still >1 in many counties even at the local minimum, indicating continued disease spread (Figure 6, panel B). After reopening, transmission again increased across Georgia. These data suggest that the 3 or 4 weeks of shelter-in-place orders were not long enough to sufficiently suppress SARS-CoV-2 transmission (local and imported) in

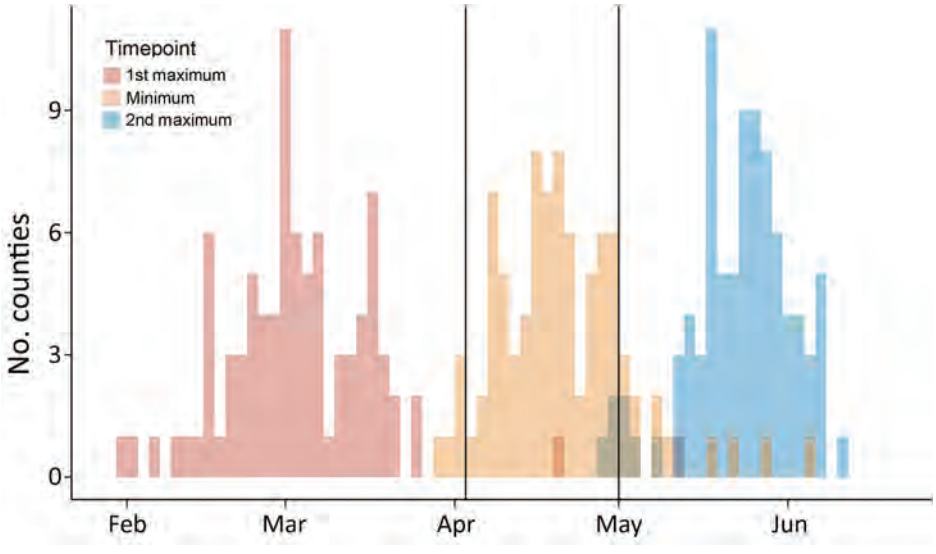

Figure 7. Distributions of estimated dates of first maximum, minimum, and second maximum in effective reproduction numbers for severe acute respiratory syndrome coronavirus 2 transmission in 87 counties in Georgia, USA, with 200 cumulative cases by July 13, 2020, and dates of key events possibly driving virus transmission.

densely populated urban areas connected by major transportation links.

Thus far, the second wave has been heterogenous in time and magnitude in different counties. Local prevalence was different at the time of reopening, and counties where prevalence was high (i.e., counties bordering cities and along interstate highways) experienced a stronger second wave. Counties not connected by major transportation links (e.g., around Albany) often also saw a second wave of COVID-19 but on a relatively small scale. Some counties that experienced an early and intense first wave (e.g., Lee, Sumter, Terrell, and Mitchell) did not experience a second wave. Possibly, inhabitants of those counties were more compliant with the prevention and control measures.

A limitation of our study is that although data were available for >100,000 cases, clinical information and contacts with a confirmed case-patient were missing on some records. Absence of clinical information may depend on several factors. For example, reporting rates tend to be lower and clinical information more frequently missing for case-patients with mild or no symptoms than for case-patients with severe symptoms. A subgroup analysis showed similar distributions of serial intervals for transmission pairs with complete clinical information and transmission pairs with missing clinical information. This finding lends credibility to the assumption that the absence of clinical information does not affect the overall serial interval.

Data on tracked pairs were not missing at random because contact tracing is voluntary and its capacity was limited during the early stages of the pandemic. Tracked pairs were more likely to be recorded when they involved known contacts. Identifying transmission links in public spaces or within clusters of cases remains challenging.

In this study, presymptomatic transmission leading to negative serial intervals was ignored because infectors could rarely be determined by exposure information or travel history. On the basis of the sensitivity analysis (Appendix Supplemental Material C), the influence of a small proportion of negative serial intervals on R_t estimates could safely be ignored.

When examining the time course of transmission of SARS-CoV-2 in Georgia, asymptomatic transmission was ignored. The observed numbers of case-patients thus underestimate the numbers of infected (infectious) persons, but this underestimation does not imply that R_t is underestimated by the same amount. Both the numbers of primary case-patients (transmitting infection) and the numbers of secondary case-patients (acquiring infection) are underestimated, so the estimated rate of increase is likely to be less affected (*24*).

In conclusion, transmission of SARS-CoV-2 in Georgia changed over time during February–July 2020. The mean serial interval decreased from 5.97 days in February–April to 4.40 days in June–July. The younger population (20–50 years of age) was involved in most transmission events during or after reopening subsequent to the shelter-in-place period. By mid-July, 2 waves of SARS-CoV-2 transmission were apparent, separated by the shelter-in-place period in Georgia. Transmission was more intense in counties around major cities and along interstate highways. These transmission patterns can be used to help predict and guide states in COVID-19 prevention and control according to population and region.

This article was preprinted at https://www.medrxiv.org/content/10.1101/2020.10.22.20217661v1.

Acknowledgments

We are grateful to Hannah Cooper and Laura Donnelly for their efforts in leading and coordinating the research partnership between GDPH and Emory University. We appreciate the support and critical discussions with Christine Moe, and we thank Michael Bryan for providing the data.

The raw data used in this study are available through the Public Health Information Portal data request process (https://dph.georgia.gov/phip-data-request).

This study was funded by the Emory Covid-19 Response Collaborative. The funder of this study had no role in study design, data collection, data analysis, data interpretation, or writing the report. All authors had full access to all data in the study, and the corresponding author had final responsibility for the decision to submit for publication.

Y.W. and P.T. conceived the study and developed the methods. Y.W., C.S., Y.C., and C.A. conducted literature reviews. Y.W., C.S., and Y.C. produced the estimates and created figures and tables. Y.W. and P.T. wrote the first draft of the manuscript and led the writing of subsequent drafts. B.L., L.E., M.T., C.S., C.A., and M.L. provided critical feedback on the first draft and contributed to the writing of subsequent drafts of the manuscript. M.L. and B.L. acquired the funding for the research.

About the Author

Mr. Wang is a senior biostatistician at the Center for Global Safe WASH (Water, Sanitation, and Hygiene),

Hubert Department of Global Health, Rollins School of Public Health at Emory University. His primary research interests focus on infectious disease transmission modeling, environmental surveillance, quantitative exposure assessment, WASH, and mathematical and statistical modeling.

References

1. Dong E, Du H, Gardner L. An interactive web-based dashboard to track COVID-19 in real time. Lancet Infect Dis. 2020;20:533–4. https://doi.org/10.1016/S1473-3099(20)30120-1
2. Georgia Department of Public Health. Georgia Department of Public Health daily status report, 2021 [cited 2021 Jul 9]. https://dph.georgia.gov/covid-19-daily-status-report
3. Wang Y, Teunis P. Strongly heterogeneous transmission of COVID-19 in mainland China: local and regional variation. Front Med (Lausanne). 2020;7:329. https://doi.org/10.3389/fmed.2020.00329
4. Rubin D, Huang J, Fisher BT, Gasparrini A, Tam V, Song L, et al. Association of social distancing, population density, and temperature with the instantaneous reproduction number of SARS-CoV-2 in counties across the United States. JAMA Netw Open. 2020;3:e2016099. https://doi.org/10.1001/jamanetworkopen.2020.16099
5. Althouse BM, Wenger EA, Miller JC, Scarpino SV, Allard A, Hébert-Dufresne L, et al. Superspreading events in the transmission dynamics of SARS-CoV-2: opportunities for interventions and control. PLoS Biol. 2020;18:e3000897. https://doi.org/10.1371/journal.pbio.3000897
6. Hou X, Gao S, Li Q, Kang Y, Chen N, Chen K, et al. Intracounty modeling of COVID-19 infection with human mobility: assessing spatial heterogeneity with business traffic, age, and race. Proc Natl Acad Sci U S A. 2021;118:e2020524118. https://doi.org/10.1073/pnas.2020524118
7. Kraemer MUG, Yang CH, Gutierrez B, Wu CH, Klein B, Pigott DM, et al.; Open COVID-19 Data Working Group. The effect of human mobility and control measures on the COVID-19 epidemic in China. Science. 2020;368:493–7. https://doi.org/10.1126/science.abb4218
8. Rocklöv J, Sjödin H. High population densities catalyse the spread of COVID-19. J Travel Med. 2020;27:taaa038. https://doi.org/10.1093/jtm/taaa038
9. Prem K, Liu Y, Russell TW, Kucharski AJ, Eggo RM, Davies N, et al.; Centre for the Mathematical Modelling of Infectious Diseases COVID-19 Working Group. The effect of control strategies to reduce social mixing on outcomes of the COVID-19 epidemic in Wuhan, China: a modelling study. Lancet Public Health. 2020;5:e261–70. https://doi.org/10.1016/S2468-2667(20)30073-6
10. McMichael TM, Currie DW, Clark S, Pogosjans S, Kay M, Schwartz NG, et al.; Public Health–Seattle and King County, EvergreenHealth, and CDC COVID-19 Investigation Team. Epidemiology of COVID-19 in a long-term care facility in King County, Washington. N Engl J Med. 2020;382:2005–11. https://doi.org/10.1056/NEJMoa2005412
11. Liu Y, Eggo RM, Kucharski AJ. Secondary attack rate and superspreading events for SARS-CoV-2. Lancet. 2020;395:e47. https://doi.org/10.1016/S0140-6736(20)30462-1
12. Lloyd-Smith JO, Schreiber SJ, Kopp PE, Getz WM. Superspreading and the effect of individual variation on disease emergence. Nature. 2005;438:355–9. https://doi.org/10.1038/nature04153
13. Lai S, Ruktanonchai NW, Zhou L, Prosper O, Luo W, Floyd JR, et al. Effect of non-pharmaceutical interventions to contain COVID-19 in China. Nature. 2020;585:410–3. https://doi.org/10.1038/s41586-020-2293-x
14. Cowling BJ, Ali ST, Ng TWY, Tsang TK, Li JCM, Fong MW, et al. Impact assessment of non-pharmaceutical interventions against coronavirus disease 2019 and influenza in Hong Kong: an observational study. Lancet Public Health. 2020;5:e279–88. https://doi.org/10.1016/S2468-2667(20)30090-6
15. Flaxman S, Mishra S, Gandy A, Unwin HJT, Mellan TA, Coupland H, et al.; Imperial College COVID-19 Response Team. Estimating the effects of non-pharmaceutical interventions on COVID-19 in Europe. Nature. 2020;584:257–61. https://doi.org/10.1038/s41586-020-2405-7
16. Teunis P, Heijne JC, Sukhrie F, van Eijkeren J, Koopmans M, Kretzschmar M. Infectious disease transmission as a forensic problem: who infected whom? J R Soc Interface. 2013;10:20120955. https://doi.org/10.1098/rsif.2012.0955
17. Nishiura H, Linton NM, Akhmetzhanov AR. Serial interval of novel coronavirus (COVID-19) infections. Int J Infect Dis. 2020;93:284–6. https://doi.org/10.1016/j.ijid.2020.02.060
18. Du Z, Xu X, Wu Y, Wang L, Cowling BJ, Meyers LA. Serial interval of COVID-19 among publicly reported confirmed cases. Emerg Infect Dis. 2020;26:1341–3. https://doi.org/10.3201/eid2606.200357
19. Ali ST, Wang L, Lau EHY, Xu XK, Du Z, Wu Y, et al. Serial interval of SARS-CoV-2 was shortened over time by nonpharmaceutical interventions. Science. 2020;369:1106–9. https://doi.org/10.1126/science.abc9004
20. Kenah E, Lipsitch M, Robins JM. Generation interval contraction and epidemic data analysis. Math Biosci. 2008;213:71–9. https://doi.org/10.1016/j.mbs.2008.02.007
21. Newman ME. Mixing patterns in networks. Phys Rev E Stat Nonlin Soft Matter Phys. 2003;67:026126. https://doi.org/10.1103/PhysRevE.67.026126
22. Mossong J, Hens N, Jit M, Beutels P, Auranen K, Mikolajczyk R, et al. Social contacts and mixing patterns relevant to the spread of infectious diseases. PLoS Med. 2008;5:e74. https://doi.org/10.1371/journal.pmed.0050074
23. Mummert A, Weiss H, Long LP, Amigó JM, Wan XF. A perspective on multiple waves of influenza pandemics. PLoS One. 2013;8:e60343. https://doi.org/10.1371/journal.pone.0060343
24. Wallinga J, Teunis P. Different epidemic curves for severe acute respiratory syndrome reveal similar impacts of control measures. Am J Epidemiol. 2004;160:509–16. https://doi.org/10.1093/aje/kwh255

Address for correspondence: Yuke Wang, Center for Global Safe WASH, Hubert Department of Global Health, Rollins School of Public Health, Emory University, 1518 Clifton Rd NE, CNR6040B, Atlanta, GA 30322, USA; email: yuke.wang@emory.edu

Bloodstream Infection Risk, Incidence, and Deaths for Hospitalized Patients during Coronavirus Disease Pandemic

Bhavarth S. Shukla, Prem R. Warde, Eric Knott, Sebastian Arenas, Darryl Pronty, Reinaldo Ramirez, Arely Rego, Miriam Levy, Martin Zak, Dipen J. Parekh, Tanira Ferreira, Hayley B. Gershengorn

Hospital-acquired infections are emerging major concurrent conditions during the coronavirus disease (COVID-19) pandemic. We conducted a retrospective review of hospitalizations during March–October 2020 of adults tested by reverse transcription PCR for severe acute respiratory syndrome coronavirus 2. We evaluated associations of COVID-19 diagnosis with risk for laboratory-confirmed bloodstream infections (LCBIs, primary outcome), time to LCBI, and risk for death by using logistic and competing risks regression with adjustment for relevant covariates. A total of 10,848 patients were included in the analysis: 918 (8.5%) were given a diagnosis of COVID-19, and 232 (2.1%) had LCBIs during their hospitalization. Of these patients, 58 (25%) were classified as having central line–associated bloodstream infections. After adjusting for covariates, COVID-19–positive status was associated with higher risk for LCBI and death. Reinforcement of infection control practices should be implemented in COVID-19 wards, and review of superiority and inferiority ranking methods by National Healthcare Safety Network criteria might be needed.

The incidence of co-infection with either bacterial or fungal pathogens in patients hospitalized because of coronavirus disease (COVID-19) during the ongoing pandemic has become a topic of great interest. Hospitalized COVID-19 patients have shown co-infection rates as low as 7% (*1*) and as high as 15%, and as many as 27% of those who ultimately die are co-infected (*1*–*5*). Although some COVID-19 patients have bacterial or fungal co-infections, it appears that nosocomial origins for co-infection might be a major factor. One study found that only 3.2% of hospitalized COVID-19 patients were co-infected at the time of hospital admission (*3*), and another study demonstrated a cumulative risk of 25% of developing a bloodstream infection in critically ill COVID-19 patients, but only after 48 hours in the intensive care unit (ICU) (*6*).

Sparse evidence exists that directly compares nosocomial incidence of bloodstream infection in those having COVID-19 with other hospitalized populations. A multicenter study in New York, New York, USA, found bloodstream infections in only 3.8% of hospitalized patients who had COVID-19 but in 8.0% of patients who did not have COVID-19 (*7*). When comparing with patients who had influenza, Hughes et al. found a 1.8-fold increased rate of bloodstream infection in COVID-19 patients (2.5% vs. 1.4%) hospitalized in the United Kingdom (*3*). However, differences in the types of case-patients by COVID-19 status were not considered in either study. Moreover, the generalizability of these differences by COVID-19 status to other geographic regions remains unknown.

Little evidence exists for risk factors for nosocomial infection in COVID-19. A single-center study from Wuhan, China, identified an association related to use of invasive devices and combination antimicrobial drugs, as well as having diabetes mellitus, with an increased risk for developing a hospital-acquired infection (HAI) (*8*). However, the external validity of these associations has not been explored.

In this study, we sought to investigate whether being infected with COVID-19 was independently associated with an increase in odds of developing a

Author affiliations: University of Miami Health System, Miami, Florida, USA (B.S. Shukla, P.R. Warde, S. Arenas, D. Pronty, R. Ramirez, A. Rego, M. Levy, D.J. Parekh, T. Ferreira, H.B. Gershengorn); University of Miami Miller School of Medicine, Miami (B.S. Shukla, E. Knott, M. Zak, D.J. Parekh, T. Ferreira, H.B. Gershengorn); Albert Einstein College of Medicine, Bronx, New York, USA (H.B. Gershengorn)

DOI: https://doi.org/10.3201/eid2710.210538

laboratory-confirmed bloodstream infection (LCBI). We also aimed to identify other potential risk factors for LCBI in hospitalized COVID-19 patients. We hypothesized that COVID-19 patients would have greater odds of acquiring an LCBI than hospitalized patients without COVID-19 after adjusting for relevant confounders, and that other risk factors might also be identified, which might serve as targets for interventions to reduce co-infection rates in this vulnerable group.

Methods

Study Design and Cohort

We conducted a retrospective cohort study of adult hospitalizations during March 25–October 27, 2020, at an academic, tertiary, acute-care facility in Miami, Florida, USA, which lacks capacity to give care with extracorporeal membrane oxygenation. Patients were included in the cohort if they had ≥1 reverse transcription PCR completed; patients could be included more than once if they were admitted to the hospital more than once over the study period. During the study period, all patients were screened by reverse transcription PCR before hospital admission. Although there were no specific exclusion criteria, the facility does not offer pediatric or obstetric services, so pregnant woman and patients <18 years of age were not included. A restricted cohort of patients that had central venous catheters at any point during their hospital stay was also considered.

Exposure and Outcomes

Our exposure of interest was COVID-19 positivity (determined by SARS-CoV-2 PCR testing) during the hospital stay. Patients who had ≥1 positive test result (from 7 days before admission up until discharge with or without preceding negative test results) were considered positive for COVID-19. Our primary outcome was LCBI. Secondary outcomes were death, time to LCBI (time from hospital admission to first positive blood culture per patient admission), and development of central line–associated bloodstream infection (CLABSI) evaluated by using the restricted cohort of patients who had a central venous catheter. We defined LCBIs and CLABSIs according to National Healthcare Safety Network (NHSN) 2020 criteria (*9*). In brief, LCBI is defined in these criteria as a single positive blood culture or molecular test result for a pathogen or 2 positive blood cultures for a commensal organism. CLABSI is defined as an LCBI associated with a central venous catheter in place for ≥2 calendar days (*9*).

Data Sources and Variables

We obtained information for each patient from the hospital system's electronic medical record by using EPIC software (https://www.epic.com). In addition to COVID-19 infection status and outcomes (including organism identification), we abstracted information on demographics (age, sex, race, primary insurance provider), organisms isolated from blood cultures, chronic health conditions, Elixhauser comorbidity conditions (*10*), body mass index, severity of acute illness (sequential organ failure assessment score [SOFA] during hospital day 1) (*11*), renal replacement therapy (either intermittent or continuous), invasive mechanical ventilation, care in the ICU, prone positioning (including persons using mechanical ventilation), central venous catheters, urinary catheters, systemic corticosteroids, tocilizumab, and remdesivir. For each of the resources other than prone positioning, we identified whether they were used and the total duration of use. For prone positioning, we were able to identify only use (not duration or timing of use). We also obtained data on hospital length of stay.

Statistical Analysis and Ethics

We described the cohort by using standard summary statistics. We made compared characteristics by outcome by using χ^2 and Kruskal-Wallis tests as appropriate. Our primary analysis was a risk for LCBI assessment by using multivariable logistic regression modeling with an exposure of COVID-19 status. We included all data elements except prone positioning, remdesivir, and tocilizumab as covariables, and resource elements were modeled as receipt/nonreceipt before development of LCBI (or hospital discharge if no LCBI). To ensure our results would not be confounded by deaths in hospitals, we recreated the same models for hospital survivors and decedents separately.

To consider secondary outcomes, we first used multivariable Cox proportional hazards modeling with censoring at hospital discharge and a competing risk for death to assess the association of COVID-19 positivity and time to LCBI. We then constructed a multivariable logistic regression model to assess the association of COVID-19 positivity with risk for death by hospital discharge. For this model, we included days of resource use as covariates.

We also constructed 3 models to evaluate for LCBI that developed ≥2 calendar days from admission, indicated as LCBI HAI. Next, we reconstructed the models (for our primary and 2 secondary outcomes) by using the restricted cohort of patients who had used central venous catheters to assess risk for and time to

CLABSI and death. Finally, to identify risk factors for infection among COVID-19 patients, we constructed 3 multivariable logistic regression models: for LCBI among all COVID-19 patients, for LCBI HAI among all COVID-19 patients, and for CLABSI among COVID-19 patients who had central venous catheters.

Because of a large number of patients who had missing data regarding calculation of SOFA, we imputed this score for each model (using multivariable regression modeling, including all covariates and outcome). We conducted 2 sensitivity analyses to assess the robustness of our primary analysis: only patients with an available SOFA score, and all patients but not including SOFA as a model covariate.

Study approval was obtained from the University of Miami Institutional Review Board (#20200739). We performed all analyses by using the programming language R (R Foundation for Statistical Computing, https://www.r-project.org). Results were considered significant if $p<0.05$. Because we did not adjust for multiple comparisons, we considered all nonprimary analyses to be hypothesis generating.

Table 1. Patients characteristics by outcome on bloodstream infection risk, incidence, and deaths for hospitalized patients during coronavirus disease pandemic, Miami, Florida, USA, March 25–October 27, 2020*

	Full cohort for LCBI analyses, no. (%)						Central line cohort for CLABSI analyses, no. (%)		
	NHSN LCBI			NHSN LCBI (HAI)					
Characteristic	No LCBI	LCBI	p value†	No LCBI	LCBI	p value†	No CLABSI	CLABSI	p value†
Patient admissions	10,616 (97.9)	232 (2.1)		10,694 (98.6)	154 (1.4)		2,840 (98.0)	58 (2.0)	
COVID-19 RT-PCR positive	854 (8.0)	64 (28)	<0.001	857 (8.0)	61 (40)	<0.001	365 (13)	32 (55)	<0.001
Age, y	63 (52–73)	66 (55–74)	0.093	63 (52–73)	66 (54–74)	0.4	66 (55–76)	66 (56–72)	0.3
Sex‡			0.094			0.001			0.016
M	5,479 (52)	134 (58)	0.094	5,512 (52)	101 (66)	0.001	1,343 (47)	37 (64)	0.016
F	5,136 (48)	98 (42)		5,181 (48)	53 (34)		1,497 (53)	21 (36)	
Race/ethnicity			0.041			0.053			<0.001
Non-Hispanic White	2,318 (22)	33 (14)		2,330 (22)	21 (14)		553 (19)	7 (12)	
Non-Hispanic Black	280 (2.6)	3 (1.3)		281 (2.6)	2 (1.3)		76 (2.7)	1 (1.7)	
Hispanic White	5,152 (49)	123 (53)		5,188 (49)	87 (56)		1,338 (47)	33 (57)	
Hispanic Black	1,952 (18)	49 (21)		1,976 (18)	25 (16)		647 (23)	4 (6.9)	
Other	577 (5.4)	17 (7.3)		581 (5.4)	13 (8.4)		154 (5.4)	8 (14)	
Unknown	337 (3.2)	7 (3.0)		338 (3.2)	6 (3.9)		72 (2.5)	5 (8.6)	
Payer			<0.001			<0.001			0.077
Commercial	3,849 (36)	59 (25)		3,869 (36)	39 (25)		741 (26)	15 (26)	
Government	73 (0.7)	4 (1.7)		74 (0.7)	3 (1.9)		17 (0.6)	2 (3.4)	
Medicaid	1,248 (12)	35 (15)		1,254 (12)	29 (19)		407 (14)	12 (21)	
Medicare	4,964 (47)	130 (56)		5,014 (47)	80 (52)		1,597 (56)	27 (47)	
Other	482 (4.5)	4 (1.7)		483 (4.5)	3 (1.9)		78 (2.7)	2 (3.4)	
BMI, kg/m^2§	27 (23–31)	26 (23–30)	0.2	27 (23–31)	27 (23–31)	0.7	26 (22–31)	28 (25–33)	0.028
Elixhauser comorbidity index	15 (4–29)	27 (15–40)	<0.001	15 (4–29)	26 (15–39)	<0.001	23 (11–36)	22 (12–34)	>0.9
Urethral catheter	3,406 (32)	126 (54)	<0.001	3,430 (32)	102 (66)	<0.001	1,249 (44)	45 (78)	<0.001
Central line	2,690 (25)	208 (90)	<0.001	2,754 (26)	144 (94)	<0.001	NA	NA	NA
Mechanical ventilation	750 (7.1)	97 (42)	<0.001	767 (7.2)	80 (52)	<0.001	569 (20)	39 (67)	<0.001
Steroid treatment	3,094 (29)	127 (55)	<0.001	3,119 (29)	102 (66)	<0.001	1,155 (41)	49 (84)	<0.001
ICU admission	2,043 (19)	135 (58)	<0.001	2,067 (19)	111 (72)	<0.001	1,118 (39)	48 (83)	<0.001
Dialysis	657 (6.2)	82 (35)	<0.001	682 (6.4)	57 (37)	<0.001	312 (11)	29 (50)	<0.001
SOFA score¶	1 (0–3)	3 (2–5)	<0.001	1 (0–3)	3 (2–5)	<0.001	2 (1–4)	3 (2–4)	0.055
Central line duration, d	0.0 (0.0–0.3)	14.2 (5.0–28.0)	<0.001	0.0 (0.0–0.4)	20.8 (10.2–34.3)	<0.001	5 (3–11)	28 (15–54)	<0.001
Hospital LOS, d	3.5 (1.9–6.9)	18.8 (9.4–30.9)	<0.001	3.5 (1.9–6.9)	24.9 (14.3–36.7)	<0.001	8 (5–14)	29 (20–50)	<0.001
Deaths in hospital	258 (2.4)	50 (22)	<0.001	267 (2.5)	41 (27)	<0.001	201 (7.1)	21 (36)	<0.001

*Values are no. (%) or median (IQR). BMI, body mass index; CLABSI, central line–associated bloodstream infection; COVID-19, coronavirus disease; HAI, healthcare associated infection; IQR, interquartile range; LCBI, laboratory-confirmed bloodstream infection; LOS, length of stay; NA, not applicable; NHSN, National Healthcare Safety Network; RT-PCR, reverse transcription PCR; SOFA. sequential organ failure assessment.
†Statistical tests performed: Fisher exact test; Wilcoxon rank-sum test; χ^2 test of independence.
‡One patient of an unknown sex in the full cohort (did not have an LCBI).
§Eight patients had missing BMIs in the full cohort (3 in the CLABSI cohort); none had a bloodstream infection.
¶Indicates patients who had missing SOFA scores: 4,815 (55%) of no LCBI full cohort, 104 (55%) of LCBI full cohort, 4,851 (55%) of no LCBI-HAI full cohort, 68 (56%) of LCBI-HAI full cohort, 1,355 (52%) of no CLABSI, and 25 (57%) of CLABSI patients.

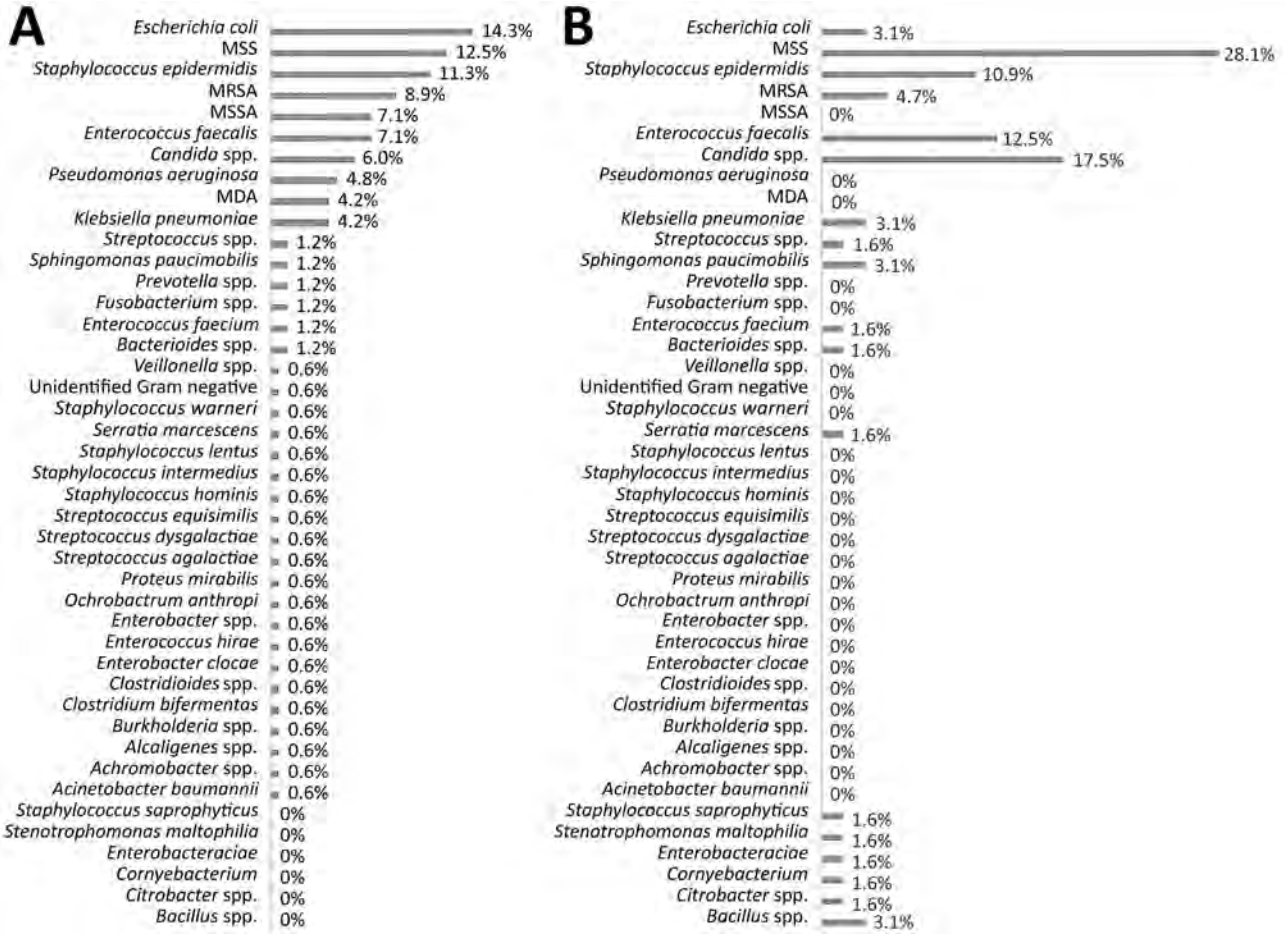

Figure. Organisms responsible for laboratory-confirmed bloodstream infections during COVID-19 pandemic, Miami, Florida, USA, March 25–October 27, 2020. A) COVID-19–negative patients (n = 168). B) COVID-19–positive patients (n = 64). COVID-19, coronavirus disease; MDA, organisms isolated during admission (defined as ≥2 organisms isolated from the bloodstream >48 hours apart during admission); MRSA, methicillin-resistant *Staphylococcus aureus*; MSSA, methicillin-sensitive *S. aureus*; MSS, multiple organisms isolated during bloodstream infection episode (defined ≥2 organisms isolated from the bloodstream within a 48-hour period from the index isolate).

Results

Our primary cohort consisted of 10,848 hospital admissions, of whom 918 (8.5%) were COVID-19 positive (Table 1; Appendix Figure 1, https://wwwnc.cdc.gov/EID/article/27/10/21-0538-App1.pdf). A total of 232 (2.1%) persons showed development of an LCBI: 64 (7.0%) of those who were COVID-19 positive and 168 (1.7%) of those who were COVID-19 negative. The subset of LCBIs acquired 2 calendar days after admission included 61 (95.3%) in the COVID-19–positive patient group and 93 (58.4%) in the COVID-19 negative patient group (Appendix Figure 1). Evaluation of baseline characteristics showed major differences by bivariate analysis of the cohort when divided by outcome (Table 1) or COVID-19 status (Appendix Table 1), including sex, payer, comorbidity index, and SOFA score.

Organisms most frequently cultured meeting NHSN definitions for LCBI among COVID-19 patients were *Candida* spp. (n = 11, 17.2%), *Enterococcus faecalis* (n = 8, 12.5%), and *Staphylococcus epidermidis* (7, 10.9%). These organisms were also found in the context of polymicrobial cultures (internally defined as ≥2 organisms isolated from the bloodstream within a 48-hour period). They constituted the largest percentage of the cohort of LCBI at 28.1% (n = 18) (Figure). Similar organisms were observed with cultures from COVID-19 patients meeting NHSN definition for CLABSI: *Candida* spp. 50.0% (n = 16), *E. faecalis* 25.0% (n = 8), and *S. epidermis* 12.5% (n = 4). The organisms identified on blood culture from COVID-19–positive versus COVID-19–negative patients for LCBI and CLABSI were comparatively different, but because of low numbers, no statistical analysis was performed (Appendix Figure 2).

Table 2. Adjusted association for virus positivity with outcomes for patients during the coronavirus disease pandemic, Miami, Florida, USA, March 25–October 27, 2020*

Cohort	Primary outcome	OR/HR (95% CI)
Full	Risk for LCBI†	3.88 (2.70–5.51)
	Time to LCBI‡	2.35 (1.77–3.13)
	Risk for death,§ adjusted for LCBI	6.68 (4.94–9.01)
	Risk for LCBI-HAI†	5.58 (3.67–8.43)
	Time to LCBI-HAI‡	2.73 (1.94–3.85)
	Risk for death,§ adjusted for LCBI-HAI	6.64 (4.91–8.96)
Central line	Risk for CLABSI†	5.68 (2.94–11.1)
	Time to CLABSI‡	2.86 (1.75–4.65)
	Risk for death§	5.30 (3.68–7.64)

*All p values were <0.001. BMI, body mass index; CLABSI: central line–associated bloodstream infection; HR, hazard ratio; ICU, intensive care unit; LCBI, laboratory-confirmed bloodstream infection; OR, odds ratio; SOFA, sequential organ failure assessment.
†Modeled with logistic regression including age, sex, race/ethnicity, payer, BMI, no. comorbidities, previous urethral catheter use, previous central line use, previous mechanical ventilation, previous steroid treatment, previous ICU admission, previous dialysis, previous prone positioning, previous remdesivir treatment, tocilizumab treatment, and imputed SOFA score as covariates. OR is reported.
‡Modeled with proportional hazards model including age, sex, race/ethnicity, payer, BMI, no. comorbidities, previous urethral catheter use, previous central line use, previous mechanical ventilation, previous steroid treatment, previous ICU admission, previous dialysis, and imputed SOFA score as covariates. HR is reported.
§Modeled with logistic regression including age, sex, race/ethnicity, payer, BMI, no. comorbidities, urethral catheter days, central line days, previous mechanical ventilation days, steroid treatment days, ICU days, dialysis days , imputed SOFA score, and LCBI as covariates; OR is reported.

Association of COVID-19 Status with Outcomes

After adjusting for potential confounders, we found that COVID-19 positivity was associated with an increase in odds of an LCBI developing (odds ratio [OR] 3.88, 95% CI 2.70–5.51; p<0.001 (Table 2; Appendix Table 2). COVID-19 was also significantly associated with LCBI developing for either hospital survivors (OR 3.50, 95% CI 2.28–5.27; p<0.001) or decedents (OR 3.14, 95% CI 1.33–7.72; p = 0.01) (Appendix Table 3) when considered separately. Our results were robust to sensitivity analyses aimed at addressing missing SOFA scores (Appendix Tables 4, 5).

We found significant associations with regards to time to LCBI (hazard ratio 2.35, 95% CI 1.77–3.13; p<0.001) (Table 2; Appendix Table 2, Figure 3). COVID-19 positivity was associated with an increased odds of hospital death (OR 6.68, 95% CI 4.94–9.01; p<0.001). After restricting the cohort to patients with positive cultures after 2 calendar days, we found that COVID-19 was associated with LCBI-HAI; after restricting the cohort to patients with central lines, we found that COVID-19 was associated with CLABSI (Table 2; Appendix Tables 6, 7).

Non–COVID-19 Risk Factors for LCBI, LCBI HAI, and CLABSI

In a subgroup analysis of only COVID-19 patients, we found that previous central line use was associated with an increased risk for LCBI (OR 8.11, 95% CI 2.40–37.3; p = 0.002) and LCBI HAI (OR 11.7, 95% CI 2.94–78.2; p = 0.002) (Table 3). We found no major associations with use of remdesivir, steroids, or tocilizumab. Another finding in the subgroup analysis was that prone positioning did not have any major associations with risk for outcomes in patients who had COVID-19.

Discussion

Before the COVID-19 pandemic, HAIs were well-recognized as a cause of death (*12*). To date, only a few studies have evaluated the effect of the COVID-19

Table 3. Subgroup analysis of clinical variables in patients who had COVID-19 and bloodstream infection risk, incidence, and deaths for hospitalized patients during coronavirus disease pandemic, Miami, Florida, USA, March 25–October 27, 2020*

	LCBI		LCBI HAI		CLABSI	
Characteristic	OR (95% CI)	p value	OR (95% CI)	p value	OR (95% CI)	p value
Sex						
M	1.84 (0.96–3.61)	0.068	2.09 (1.07–4.23)	0.034	3.50 (1.29–10.7)	0.019
F	0.54 (0.28–1.04)	0.068	0.48 (0.24–0.93)	0.034	0.29 (0.09–0.77)	0.019
Age, y	0.97 (0.94–1.00)	0.03	0.97 (0.94–1.00)	0.029	0.99 (0.94–1.03)	0.6
BMI, kg/m^2	0.99 (0.94–1.04)	0.7	0.99 (0.95–1.05)	0.8	0.98 (0.91–1.05)	0.5
Comorbidity index	1.00 (0.98–1.03)	0.9	1.00 (0.97–1.02)	0.8	0.97 (0.93–1.00)	0.094
Previous urethral catheter	1.96 (0.75–5.18)	0.2	1.99 (0.74–5.41)	0.2	1.60 (0.28–10.2)	0.6
Previous central line	8.11 (2.40–37.3)	0.002	11.7 (2.94–78.2)	0.002	NA	NA
Previous mechanical ventilation	2.82 (0.91–9.89)	0.086	2.18 (0.70–7.44)	0.2	∞ (0.00–∞)	>0.9
Previous steroid treatment	0.91 (0.40–2.14)	0.8	0.91 (0.39–2.21)	0.8	1.42 (0.35–6.73)	0.6
Previous ICU admission	2.47 (0.74–7.61)	0.12	3.56 (1.07–11.5)	0.034	0.00 (0.00–∞)	>0.9
Previous dialysis	1.01 (0.46–2.14)	>0.9	0.95 (0.43–2.07)	>0.9	0.59 (0.20–1.68)	0.3
Prone positioning	1.09 (0.49–2.37)	0.8	1.21 (0.55–2.69)	0.6	2.02 (0.64–6.97)	0.2
Remdesivir treatment	1.58 (0.78–3.24)	0.2	1.58 (0.76–3.32)	0.2	1.29 (0.45–3.77)	0.6
Tocilizumab treatment	1.29 (0.42–3.77)	0.6	1.23 (0.39–3.62)	0.7	1.10 (0.25–4.44)	0.9
SOFA score imputed	1.00 (0.86–1.14)	>0.9	0.96 (0.82–1.10)	0.6	0.083 (0.63–1.03)	0.12

*Model also adjusted for race/ethnicity and payer (these variables had no major association with outcomes). BMI, body mass index; CLABSI, central line–associated bloodstream infection; ICU, intensive care unit; LCBI, laboratory–confirmed bloodstream infection; NA, not applicable; SOFA, sequential organ failure assessment.

pandemic on HAIs and their outcomes, particularly LCBIs (*3*,*13*). Using data for >10,000 patients hospitalized after SARS-CoV-2 testing, we found that COVID-19 positivity was associated with a 3.88-fold increased odds of developing an LCBI. This finding might be related to COVID-19 itself or other variables not accounted for in our cohort, such as changes in supplementary nursing care or changes in infection control practices associated with the care of these patients. In addition, isolates responsible for LCBI and CLABSI in COVID-19 patients versus non–COVID-19 patients show major differences with regards to type and number of organisms.

Prone positioning has proven benefits for patients who have non-COVID-19–associated acute respiratory distress syndrome requiring invasive mechanical ventilation (*14*). Studies have noted increases in use of prone positioning as treatment for critical care patients who have influenza (*15*) and, in recent months, data have emerged suggesting benefits of prone positioning for ventilated patients (*16*–*20*) and nonventilated patients who have COVID-19 (*21*). Although potential adverse effects, such as pressure ulcers (*22*) and deep venous thromboses (*23*), have been observed with prone positioning, we did not find any statistical association with our primary outcomes.

The strengths of our study stem from detailed clinical data (including organism identification) and severity of illness information (both acute and chronic) available to us. Our study is limited by a high rate of missing SOFA score data. However, the robustness of our results to sensitivity analyses, in which we excluded patients who had missing SOFA data and excluded SOFA as a model covariate, suggests that this limitation had minimal effect on our findings. Although our sample included >10,000 patients (of whom 918 patients had COVID-19), we included only patients from a single hospital, which might limit the generalizability of our results. In addition, several of the factors included in our models occurred after COVID-19 testing (our exposure), making it plausible that these factors are mediators rather than confounders of the association of COVID-19 with outcomes.

Another limitation of the study was our inability to include admission symptoms or central venous catheter insertion sites in the analysis. This limitation was largely caused by inconsistent documentation of these data points in a nondiscrete format in our electronic medical record. We also were not able to address markers of hospital operational stressors that might have varied over the time period of our study and might effect patient outcomes. Collinearity of clinical variables included in the models was also a concern. However, our evaluation identified only 2 variables that had higher correlation coefficients (previous mechanical ventilation and ICU stay) (Appendix Figure 4). A final limitation was the difficulty in analyzing dose and type of steroids and antimicrobial drugs given before and after bloodstream infections, as well as timing and duration of prone positioning.

As more data emerge regarding increases in HAIs during the COVID-19 pandemic (*24*), we propose that these challenges warrant reevaluation of the NHSN SIR methods for LCBI and CLABSI in COVID-19–designated care areas. Further studies are needed to clarify the relationship between COVID-19 and non-LCBI infections to ascertain whether prone positioning, COVID-19-specific treatments, changes in adherence to infection control practices, or a combination of these variables might be associated with higher rates of other HAIs.

In conclusion, inpatient management of patients who have COVID-19 has brought many changes in treatment protocols and associated challenges, including adherence to infection control best practices. Established infection control best practices should be reemphasized among COVID-19 patients who might be at higher risk for LCBI, adding a concurrent condition to an already vulnerable population.

Acknowledgments

We thank members of the UHealth-Data Analytics Research Team for their support and feedback on this study.

About the Author

Dr. Shukla is an infectious diseases physician at the University of Miami Miller School of Medicine, Miami, FL. His primary research interest are infection control and hospital epidemiology with a focus on multidrug-resistant bacterial organisms.

References

1. Lansbury L, Lim B, Baskaran V, Lim WS. Co-infections in people with COVID-19: a systematic review and meta-analysis. J Infect. 2020;81:266–75. https://doi.org/10.1016/j.jinf.2020.05.046
2. Wang L, Amin AK, Khanna P, Aali A, McGregor A, Bassett P, et al. An observational cohort study of bacterial co-infection and implications for empirical antibiotic therapy in patients presenting with COVID-19 to hospitals in North West London. J Antimicrob Chemother. 2021;76:796–803.
3. Hughes S, Troise O, Donaldson H, Mughal N, Moore LS. Bacterial and fungal coinfection among hospitalized patients with COVID-19: a retrospective cohort study in a UK secondary-care setting. Clin Microbiol Infect. 2020;26:1395–9. https://doi.org/10.1016/j.cmi.2020.06.025
4. Verweij PE, Gangneux JP, Bassetti M, Brüggemann RJ, Cornely OA, Koehler P, et al.; European Confederation of

Medical Mycology; International Society for Human and Animal Mycology; European Society for Clinical Microbiology and Infectious Diseases Fungal Infection Study Group; ESCMID Study Group for Infections in Critically Ill Patients. Diagnosing COVID-19-associated pulmonary aspergillosis. Lancet Microbe. 2020;1:e53–5. https://doi.org/10.1016/S2666-5247(20)30027-6
5. Chen N, Zhou M, Dong X, Qu J, Gong F, Han Y, et al. Epidemiological and clinical characteristics of 99 cases of 2019 novel coronavirus pneumonia in Wuhan, China: a descriptive study. Lancet. 2020;395:507–13. https://doi.org/10.1016/S0140-6736(20)30211-7
6. Giacobbe DR, Battaglini D, Ball L, Brunetti I, Bruzzone B, Codda G, et al. Bloodstream infections in critically ill patients with COVID-19. Eur J Clin Invest. 2020;50:e13319. https://doi.org/10.1111/eci.13319
7. Sepulveda J, Westblade LF, Whittier S, Satlin MJ, Greendyke WG, Aaron JG, et al. Bacteremia and blood culture utilization during COVID-19 surge in New York City. J Clin Microbiol. 2020;58:e00875–20. https://doi.org/10.1128/JCM.00875-20
8. He Y, Li W, Wang Z, Chen H, Tian L, Liu D. Nosocomial infection among patients with COVID-19: A retrospective data analysis of 918 cases from a single center in Wuhan, China. Infect Control Hosp Epidemiol. 2020;41:982–3. https://doi.org/10.1017/ice.2020.126
9. National Healthcare Safety Network (NHSN). Patient safety component manual [cited2020 Oct 13]. https://www.cdc.gov/nhsn/pdfs/pscmanual/pcsmanual_current.pdf
10. Elixhauser A, Steiner C, Harris DR, Coffey RM. Comorbidity measures for use with administrative data. Med Care. 1998;36:8–27. https://doi.org/10.1097/00005650-199801000-00004
11. Vincent JL, Moreno R, Takala J, Willatts S, De Mendonça A, Bruining H, et al. The SOFA (sepsis-related organ failure assessment) score to describe organ dysfunction/failure. On behalf of the Working Group on Sepsis-Related Problems of the European Society of Intensive Care Medicine. Intensive Care Med. 1996;22:707–10. https://doi.org/10.1007/BF01709751
12. Umscheid CA, Mitchell MD, Doshi JA, Agarwal R, Williams K, Brennan PJ. Estimating the proportion of healthcare-associated infections that are reasonably preventable and the related mortality and costs. Infect Control Hosp Epidemiol. 2011;32:101–14. https://doi.org/10.1086/657912
13. Kokkoris S, Papachatzakis I, Gavrielatou E, Ntaidou T, Ischaki E, Malachias S, et al. ICU-acquired bloodstream infections in critically ill patients with COVID-19. J Hosp Infect. 2021;107:95–7. https://doi.org/10.1016/j.jhin.2020.11.009
14. Guérin C, Reignier J, Richard JC, Beuret P, Gacouin A, Boulain T, et al.; PROSEVA Study Group. Prone positioning in severe acute respiratory distress syndrome. N Engl J Med. 2013;368:2159–68. https://doi.org/10.1056/NEJMoa1214103
15. Marin-Corral J, Climent C, Muñoz R, Samper M, Dot I, Vilà C, et al.; en representacion del Grupo de Trabajo H1N1 GETGAG SEMICYUC. Patients with influenza A (H1N1) pdm09 admitted to the ICU. Impact of the recommendations of the SEMICYUC. Med Intensiva (Engl Ed). 2018;42:473–81. https://doi.org/10.1016/j.medine.2018.08.002
16. Weiss TT, Cerda F, Scott JB, Kaur R, Sungurlu S, Mirza SH, et al. Prone positioning for patients intubated for severe acute respiratory distress syndrome (ARDS) secondary to COVID-19: a retrospective observational cohort study. Br J Anaesth. 2021;126:48–55. https://doi.org/10.1016/j.bja.2020.09.042
17. Gleissman H, Forsgren A, Andersson E, Lindqvist E, Lipka Falck A, Cronhjort M, et al. Prone positioning in mechanically ventilated patients with severe acute respiratory distress syndrome and coronavirus disease 2019. Acta Anaesthesiol Scand. 2020.
18. Berrill M. Evaluation of oxygenation in 129 proning sessions in 34 mechanically ventilated COVID-19 patients. J Intensive Care Med. 2021;36:229–32. https://doi.org/10.1177/0885066620955137
19. Shelhamer MC, Wesson PD, Solari IL, Jensen DL, Steele WA, Dimitrov VG, et al. Prone positioning in moderate to severe acute respiratory distress syndrome due to COVID-19: a cohort study and analysis of physiology. J Intensive Care Med. 2021;36:241–52. https://doi.org/10.1177/0885066620980399
20. Khullar R, Shah S, Singh G, Bae J, Gattu R, Jain S, et al. Effects of prone ventilation on oxygenation, inflammation, and lung infiltrates in COVID-19 related acute respiratory distress syndrome: a retrospective cohort study. J Clin Med. 2020;9:4129. https://doi.org/10.3390/jcm9124129
21. Venus K, Munshi L, Fralick M. Prone positioning for patients with hypoxic respiratory failure related to COVID-19. CMAJ. 2020;192:E1532–7. https://doi.org/10.1503/cmaj.201201
22. Munshi L, Del Sorbo L, Adhikari NK, Hodgson CL, Wunsch H, Meade MO, et al. Prone position for acute respiratory distress syndrome. A systematic review and meta-analysis. Ann Am Thorac Soc. 2017;14(Suppl 4):S280–8. https://doi.org/10.1513/AnnalsATS.201704-343OT
23. Klok FA, Kruip MJ, van der Meer NJ, Arbous MS, Gommers DA, Kant KM, et al. Incidence of thrombotic complications in critically ill ICU patients with COVID-19. Thromb Res. 2020;191:145–7. https://doi.org/10.1016/j.thromres.2020.04.013
24. Patel PR, Weiner-Lastinger LM, Dudeck MA, Fike LV, Kuhar DT, Edwards JR, et al. Impact of COVID-19 pandemic on central-line-associated bloodstream infections during the early months of 2020, National Healthcare Safety Network. Infect Control Hosp Epidemiol. 2021;Mar 15:1–4.

Address for correspondence: Bhavarth S. Shukla, University of Miami Health System, 1321 NW 14th St, Ste 602, West Bldg, Miami, FL 33136, USA; email: bxs729@miami.edu

Direct and Indirect Effectiveness of mRNA Vaccination against Severe Acute Respiratory Syndrome Coronavirus 2 in Long-Term Care Facilities, Spain

Susana Monge, Carmen Olmedo, Belén Alejos, María Fé Lapeña, María José Sierra,[1] Aurora Limia;[1] COVID-19 Registries Study Group[2]

We conducted a registries-based cohort study of long-term care facility residents ≥65 years of age offered vaccination against severe acute respiratory syndrome coronavirus 2 before March 10, 2021, in Spain. Risk for infection in vaccinated and nonvaccinated persons was compared with risk in the same persons in a period before the vaccination campaign, adjusted by daily-varying incidence and reproduction number. We selected 299,209 persons; 99.0% had ≥1 dose, 92.6% had 2 doses, and 99.8% of vaccines were Pfizer/BioNTech (BNT162b2). For vaccinated persons with no previous infection, vaccine effectiveness was 81.8% (95% CI 81.0%–82.7%), and 11.6 (95% CI 11.3–11.9) cases were prevented per 10,000 vaccinated/day. In those with previous infection, effectiveness was 56.8% (95% CI 47.1%–67.7%). In nonvaccinated residents with no previous infection, risk decreased by up to 81.4% (95% CI 73.3%–90.3%). Our results confirm vaccine effectiveness in this population and suggest indirect protection in nonvaccinated persons.

From the beginning of the coronavirus disease (COVID-19) pandemic through March 7, 2021, a total of 18,927 residents in long-term care facilities (LTCF) in Spain died from confirmed COVID-19, resulting in a cumulative mortality rate of 67/1,000 residents. An additional 10,492 persons have died exhibiting symptoms compatible with COVID-19 (*1*). Dependent persons living in closed institutions are at higher risk for exposure. In addition, older age and underlying conditions are associated with more severe infection. Indeed, in the LTCF setting, death was the outcome of 1/5 cases of severe acute respiratory syndrome coronavirus 2 (SARS-CoV-2) infection (*1*).

In Spain, COVID-19 vaccination with the Pfizer/BioNTech (BNT162b2; https://www.pfizer.com) vaccine began on December 27, 2020; LTCF residents and workers were the first priority group (*2*). The vaccination campaign coincided with the third COVID-19 epidemic wave in Spain; national 14-day cumulative incidence increased from <250 cases/100,000 population at the end of 2020 to >1,000 by the end of January 2021 (*3*). Vaccination started in facilities considered at higher risk, such as those that had never experienced a COVID-19 outbreak, had higher numbers of residents, or had experienced more difficulties implementing prevention and control measures. Vaccination teams visited the facilities and vaccination was offered to all, including persons with previous SARS-CoV-2 infection. Vaccination was deferred only in persons with active infection. The recommendation was to vaccinate persons under quarantine, but this guidance was inconsistently followed by vaccination teams. Acceptance has been high; 97.8% of all LTCF residents received ≥1 vaccine dose, and 88.8% received 2 doses (*4*).

The Pfizer/BioNTech vaccine has shown an efficacy of 95% in preventing COVID-19 in randomized clinical trials (*5*). However, elderly persons in general, and those living in LTCF in particular, are not well represented in randomized studies (*6*). Therefore, interest in estimating vaccine effectiveness (VE) in this population after widespread vaccination is great. Moreover, because vaccination coverage was so high, nonvaccinated persons might be indirectly protected if vaccination reduces infection and transmissibility

Author affiliation: Ministry of Health, Madrid, Spain

DOI: https://doi.org/10.3201/eid2710.211184

[1]These senior authors contributed equally to this article.

[2]Group members are listed at the end of this article.

among vaccinated persons. A few observational studies focusing on the elderly have been published recently; 2 published and 1 preprint studies have specifically addressed effects of vaccination in LTCF residents (*7*,*8*; I.R. Moustsen-Helms et al., unpub. data, https://www.medrxiv.org/content/10.1101/2021.03.08.21252200v1). However, none have addressed indirect protection in nonvaccinated persons in this high-coverage setting. This study aims to estimate indirect and total (direct plus indirect) effects of vaccination in residents of LTCFs in Spain in a high-incidence context.

Methods

Data Sources

REGVACU (Registro de Vacunación COVID-19) is a nationwide registry of all COVID-19 vaccine doses administered and vaccine rejections in Spain. Administrative censoring was on March 10, 2021. We selected persons who were ≥65 years of age by December 27, 2020, with a valid postal code who were identified as residents in elderly homes according to REGVACU. SERLAB (Sistema Estatal de Resultados de Laboratorio) is a nationwide registry of all SARS-CoV-2 PCR and rapid antigen tests performed. We excluded positive tests within 60 days of a previous positive result, because they were more likely to correspond to prolonged PCR positivity than to reinfection, according to national guidelines (*9*). In LTCFs, tests were performed on symptomatic persons and at-risk contacts. Incoming residents were also routinely tested and periodic screenings were conducted. Therefore, documented infections registered in SERLAB reflect symptomatic and asymptomatic infections, although this distinction was not recorded. Residents in REGVACU were cross-matched with SERLAB by person identification number, birthdate, and sex.

Study Design

To estimate the effect of vaccination in vaccinated persons, we studied the risk for documented SARS-CoV-2 infection in the cohort of persons in whom the first dose was administered during December 27, 2020–March 10, 2021 (study period). We considered a before-after comparison more appropriate because of the possibility of indirect protection in nonvaccinated persons after the vaccination program began, because of the high vaccination coverage achieved at LTCFs. This effect would mean that nonvaccinated persons (after the start of the vaccination program) would not represent infection risk in the absence of vaccination. Therefore, for the comparison group, we included the same persons but in the period before the vaccination program started. Baseline infection risk, on the other hand, is heavily influenced by community incidence, and the study period coincided with the third epidemic wave in Spain. To minimize this effect, we chose as reference period the second epidemic wave. In particular, the most comparable period in terms of COVID-19 incidence was October 1–December 13; start dates for the reference period and study period were 87 days apart (Figure 1).

To estimate the indirect protection of vaccination in unvaccinated persons, we compared the risk for documented SARS-CoV-2 infection in the cohort of nonvaccinated persons in the study period with risk in the same persons during the reference period, similarly to the method explained previously for vaccinated persons. Because all residents of the same LTCF were offered vaccination on the same day, the follow-up period began on the date when the vaccine was first offered. Therefore, we could ensure that persons were included on the date that a first vaccine dose was administered to most coresidents and workers.

We also registered any previous documented SARS-CoV-2 infection on the first day of follow-up in the reference period or the study period for both analyses. Follow-up for all persons in the study period or reference period concluded if the person tested positive for SARS-CoV-2 or at administrative censoring (December 13 for the reference period or March 10 for the study period), whichever occurred first. Unfortunately, no information on deaths was available.

To monitor for possible design-associated bias, we created a bias-indicator cohort with nonvaccinated time-at-risk during the study period of persons who were later vaccinated, with follow-up beginning on December 27 and ending at date of first vaccine dose or date of positive SARS-CoV-2 test. We compared it to equivalent follow-up time in the reference period, similarly to the method explained previously. The study was approved by the research ethics committee at the Instituto de Salud Carlos III (approval no. CEI PI 98_2020).

Data Analysis

We performed analyses separately for the group with previously documented SARS-CoV-2 infection and the group with no previously documented infection. We computed the standardized cumulative risk for a documented SARS-CoV-2 infection under a causal inference approach (*10*). First, to estimate the probability of the event on each follow-up day, conditioned to remaining event-free up to that day

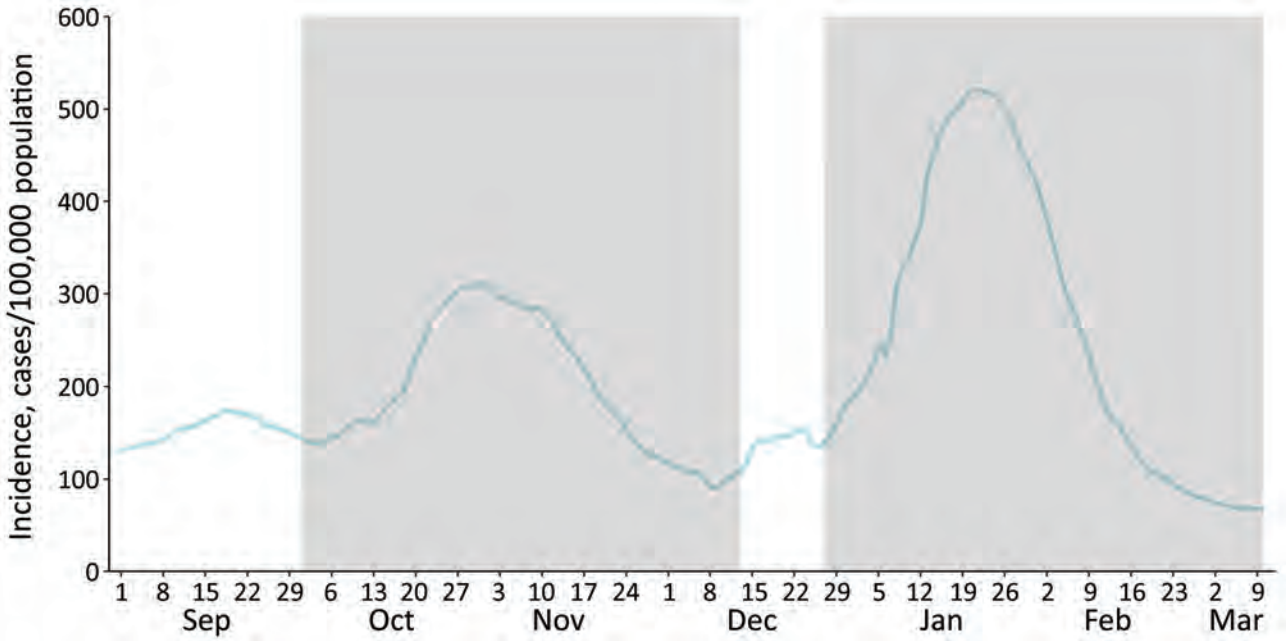

Figure 1. Seven-day cumulative incidence of diagnosis of severe acute respiratory syndrome coronavirus 2, Spain. Shadowed areas indicate the study period for the selected persons (December 27, 2020–March 10, 2021) and the reference period 87 days before (October 1–December 13, 2020).

and given the individual covariates, a pooled logistic regression was fitted adjusting by follow-up day, daily varying 7-day SARS-CoV-2 cumulative incidence specific to the province, its quadratic term, and the empirical reproduction number for that province on that date. An interaction between follow-up day and vaccination was introduced to allow for a time-varying effect of the vaccine. We built robust models by using individual identification as a clustering variable. We predicted the probability of the event by using this model for 2 contrafactual samples: one in which everyone was exposed, as defined for the study period (vaccinated persons or, for the indirect effect analysis, nonvaccinated persons indirectly protected) and one in which everyone was unexposed, as in the reference period. We then used the Kaplan-Meier method to derive standardized cumulative risk curves.

Risk ratios (RR) comparing the risk in the exposed and the unexposed, VE (VE = 1 – RR), and risk difference (RD) were estimated for the overall period and in 4 subperiods after the administration of the first dose to serve as proxies of different vaccine protection: 0–14 days, 15–21 days, 22–28 days (proxy of first 7 days after the second dose), and ≥29 days (proxy of fully vaccinated [i.e., >7 days after second vaccine dose]). We estimated normal distribution-based 95% CIs by using bootstrapping with 300 repetitions.

Results

Description of Participants

Out of 5,068,733 vaccination records from 3,615,403 persons in REGVACU before March 10, a total of 573,533 records from 299,209 persons were selected as being ≥65 years of age, having a valid postal code, and living in a LTCF. Of those, 296,093 (99.0%) had received ≥1 vaccine dose, of which 99.8% were Pfizer/BioNTech (BNT162b2) and 0.2% were Moderna (https://www.modernatx.com); 92.6% received a second vaccine dose within a median of 21 days (interquartile range [IQR] 21–21 days); 3,116 (1.0%) were not vaccinated (Appendix Figure 1, https://wwwnc.cdc.gov/EID/article/27/10/21-1184-App1.pdf). Mean (SD) age was 85.9 (±7.8) years and 70.9% were women. We cross-matched selected persons with SERLAB; 77,662 (26.0%) had ≥1 positive test during March 1, 2020–March 11, 2021.

A previous SARS-CoV-2 infection was identified in 12.7% of vaccinated participants at the beginning of the reference period and 22.3% at the beginning of the study period. The median time since the last positive SARS-CoV-2 test (PCR or rapid antigen test) was 173 (IQR 48–189) days at the beginning of the reference period and 106 (IQR 57–264) days in the study period. Similarly, in the indirect effects analysis, 27.7% of nonvaccinated persons had previous infection at the beginning of follow-up in the study period and 12.9% had previous infection

in the reference period. The median time since the last positive SARS-CoV-2 test in this group was 179 (IQR 62–191) days at the beginning of the reference period and 76 (IQR 44–264) days in the study period.

Estimation of VE in Persons with No Previous SARS-CoV-2 Infection

VE in vaccinated persons without evidence of previous SARS-CoV-2 infection was estimated on the basis of 230,195 persons vaccinated during the study period and 258,357 persons in the reference period. A total of 10,785 events occurred during the study period, and 19,244 events occurred during the reference period (Table 1; Appendix Table 1, Figure 2). Adjusted VE for the study period was 57.6% (95% CI 56.6%–58.6%), which increased after full vaccination to 81.8% (95% CI 81.0%–82.7%) (Table 1; Figure 2). The estimated number of SARS-CoV-2 infections averted by vaccination (RD) was greatest in the intermediate periods, which coincided with the peak of the epidemic waves at 11.6 cases/10,000 vaccinated persons per day.

We estimated indirect effects of vaccination in nonvaccinated persons without evidence of previous SARS-CoV-2 infection on the basis of 2,713 persons not vaccinated during the study period and 2,254 nonvaccinated persons in the reference period. Within these groups, 271 events occurred during the study period and 117 events occurred during the reference period (Appendix Table 1, Figure 2). Adjusted indirect protection was estimated at 58.7% (95% CI 49.4%–68.5%) for the whole study period. There was no statistically significant reduction in risk in the first 14 days of follow-up, but protection increased progressively thereafter, particularly after ≥29 days (as a proxy of full vaccination in LTCF residents), when VE reached 81.4% (95% CI 73.3%–90.3%) (Table 1; Figure 2). The estimated number of SARS-CoV-2 infections averted by vaccination was similar to that found in the vaccinated group.

Estimation of VE in Persons with Previous SARS-CoV-2 Infection

VE in vaccinated persons with previous SARS-CoV-2 infection was estimated on the basis of 65,898 persons vaccinated during the study period, and 37,736 persons in the reference period. A total of 519 events occurred during the study period, and 412 events occurred during the reference period (Table 2). Time since previous infection to the beginning of follow-up was similar for those in whom an event occurred (median 129 [IQR 72–187] days) or those who remained event-free (median 134 [IQR 55–208] days) (Appendix). Baseline risk in those with previous infection was 1.78 (95% CI 1.58–1.96) infections/10,000 persons/day, much lower than the baseline risk in those with no previous infection of 12.8 (95% CI 12.6–13.0)

Table 1. Standardized risk, risk ratio, vaccine effectiveness, and risk difference in elderly residents of long-term care facilities with no evidence of previous severe acute respiratory syndrome coronavirus 2 infection, by time since first vaccinated, Spain, December 27, 2020–March 10, 2021*

Time since vaccination	Events/persons at risk		Standardized risk† (95% CI)		RR (95% CI)	VE, % (95% CI)	RD (95% CI)
	Reference period	Study period	Unexposed	Exposed			
Effects in the vaccinated							
Full period	19,244/258,357	10,785/230,195	12.8 (12.61–12.98)	5.42 (5.32–5.52)	0.43 (0.41–0.42)	57.6 (56.6–58.6)	−7.37 (−7.58 to −7.16)
0–14 d	5,355/258,357	5,957/230,195	20.92 (20.49–21.33)	14.87 (14.56–15.16)	0.73 (0.69–0.71)	28.9 (26.9–31)	−6.05 (−6.56 to −5.54)
15–21 d	2,966/246,924	2,690/218,621	22.34 (21.97–22.72)	10.75 (10.55–10.95)	0.49 (0.47–0.48)	51.9 (50.7–53.1)	−11.59 (−12.01 to −11.19)
22–28 d	3,234/239,409	1,253/212,421	18.43 (18.14–18.72)	6.84 (6.67–7.0)	0.38 (0.36–0.37)	62.9 (61.9–64)	−11.59 (−11.92 to −11.28)
≥29 d‡	7,389/230,438	885/207,774	7.91 (7.73–8.09)	1.44 (1.37–1.49)	0.19 (0.17–0.18)	81.8 (81.0–82.7)	−6.47 (−6.66 to −6.28)
Indirect effects in the unvaccinated							
Full period	271/2,713	117/2,254	17.16 (15.07–19.21)	7.08 (5.79–8.35)	0.41 (0.32–0.51)	58.7 (49.4–68.5)	−10.08 (−12.62 to −7.52)
0–14 d	70/2,713	59/2,254	20.87 (17.54–24.02)	17.08 (13.68–20.48)	0.82 (0.6–1.03)	18.2 (−3.1 to 39.8)	−3.79 (−8.54 to 1.14)
15–21 d	37/2,565	22/2,128	24.51 (21.37–27.52)	13.48 (11.11–15.91)	0.55 (0.43–0.67)	45 (32.8–57.1)	−11.02 (−14.88 to −6.99)
22–28 d	38/2,473	16/2,056	22.16 (19.34–24.93)	9.35 (7.36–11.37)	0.42 (0.32–0.53)	57.8 (47.5–68.2)	−12.81 (−16.16 to −9.39)
≥29 d‡	126/2,350	20/1,997	14.09 (11.46–16.73)	2.63 (1.58–3.62)	0.19 (0.1–0.27)	81.4 (73.3–90.3)	−11.46 (−14.39 to −8.6)

*Time since first vaccinated was a proxy of number of vaccine doses and days since last dose. RD, risk difference; RR, risk ratio; VE, vaccine effectiveness.
†Per 10,000 population per day.
‡Full vaccination.

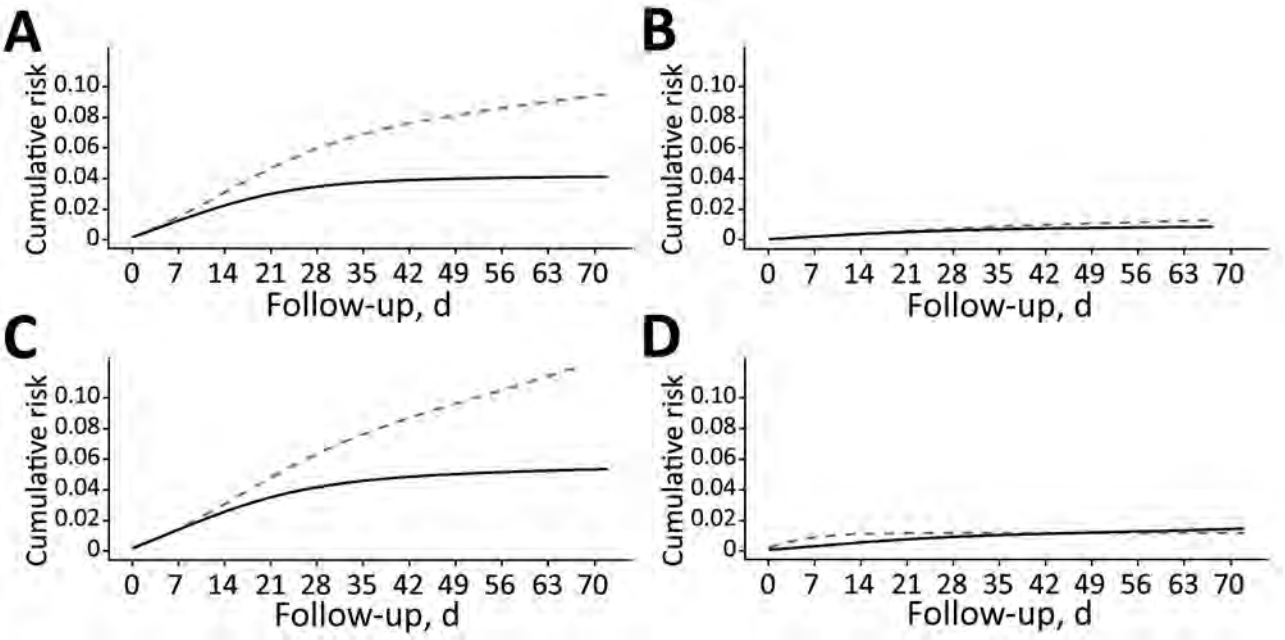

Figure 2. Cumulative incidence of documented severe acute respiratory syndrome coronavirus 2 infection in long-term care facilities estimated from adjusted hazards models, Spain, December 27, 2020–March 10, 2021. A) Standardized risk in the vaccinated with no previous infection and its reference group; B) standardized risk in the vaccinated with previous infection and its reference group; C) standardized risk in nonvaccinated (indirectly protected) with no previous infection and its reference group; D) standardized risk in nonvaccinated (indirectly protected) with previous infection and its reference group. Solid lines indicate study group; dotted lines indicate reference group.

infections/10,000 persons/day (Tables 1, 2). Consequently, VE was lower than that seen for those with no history of previous infection (Appendix Table 1, Figure 2). Adjusted VE for the whole study period was 36.3% (95% CI 27.9%–45.5%), which increased after full vaccination to 56.8% (95% CI 47.1%–67.7%) (Table 2; Figure 2); the number of infections averted was lower at ≈0.7/10,000 vaccinated persons/day. Estimating VE for indirect protection in the group with previous SARS-CoV-2 infection was not possible because only 14 events occurred (Table 2), 95% CIs virtually tended to infinite, and the model did not result in credible risk curves.

Bias-Indicator Analysis

In the bias-indicator analysis, crude risk for infection was much higher for the group in the study period (Appendix Figure 3); estimated crude RR was 1.71 (95% CI 1.62–1.81). This bias was mitigated but not eliminated after adjusting; RR of 1.36 (95% CI 1.27–1.46) showed a higher baseline risk in the study period compared with the reference period.

Discussion

This study on elderly residents of LTCFs confirms the high benefit of vaccination in this population, reducing the risk for infection by up to 81.8% and avoiding up to 11.6 cases/10,000 population/day in persons with no previous SARS-CoV-2 infection. The risk reduction was through direct protection of vaccinated persons but also through indirect protection of nonvaccinated persons. Those with previous infection also benefited from vaccination, despite an already lower baseline risk in this group.

Immunosenescence and factors related to chronic conditions, together with malnutrition, are known to impair the immunity required for an effective vaccine response (*11*), and lower neutralizing antibody response to Pfizer/BioNTech vaccine in persons ≥65 years of age has been reported (*12*,*13*). However, our estimates were similar to those of observational studies in younger adult populations. A cohort study of healthcare workers in the United Kingdom found a VE of 70% 21 days after the first dose and 85% 7 days after the second dose of the Pfizer/BioNTech vaccine (*14*). A slightly higher estimate of 94.1% was given in a study with data from Israel (*15*).

Other observational studies have explored VE in older age groups and have found a rate comparable to that seen in younger populations. In a registries-based study from Israel, in persons ≥70 years of age, VE was 44% at 14–20 days after vaccination, 64% at

Table 2. Standardized risk, risk ratio, vaccine effectiveness, and risk difference in residents of long-term care facilities with evidence of previous severe acute respiratory syndrome coronavirus 2 infection, by time since first vaccinated, Spain, December 27, 2020–March 10, 2021*

Time since vaccination	Events/persons at risk		Standardized risk† (95% CI)		RR (95% CI)	VE (95% CI)	RD (95% CI)
	Reference period	Study period	Unexposed	Exposed			
Effects in the vaccinated							
Full period	412/37,736	519/65,898	1.78 (1.58–1.96)	1.13 (1.02–1.23)	0.64 (0.54–0.72)	36.3 (27.9–45.5)	−0.64 (−0.86 to −0.44)
0–14 d	100/37,736	245/65,898	2.64 (2.22–3.03)	2.39 (2.13–2.63)	0.9 (0.73–1.07)	9.6 (−6.9 to 26.8)	−0.25 (−0.72–0.23)
15–21 d	72/37,440	104/64,988	2.58 (2.26–2.89)	1.92 (1.74–2.09)	0.74 (0.63–0.85)	25.5 (15.1–36.6)	−0.66 (−1.00 to −0.32)
22–28 d	77/36,840	55/63,236	2.2 (1.95–2.44)	1.44 (1.29–1.58)	0.65 (0.56–0.74)	34.6 (25.7–44.1)	−0.76 (−1.03 to −0.5)
≥29 d	163/36,288	115/60,176	1.31 (1.11–1.52)	0.57 (0.46–0.67)	0.43 (0.32–0.53)	56.8 (47.1–67.7)	−0.75 (−0.98 to −0.53)
Indirect effects in the unvaccinated							
Full period	5/403	9/862	1.32 (0.12–2.55)	1.89 (0.3–3.34)	NE	NE	NE
0–14 d	4/403	4/862	6.39 (0.64–12.47)	3.39 (0.63–6.05)	NE	NE	NE
15–21 d	1/394	2/842	0.76 (−0.63 to 2.08)	2.95 (0.97–5.19)	NE	NE	NE
22–28 d	0/386	1/827	0.16 (−0.4 to 0.6)	2.21 (0.72–3.95)	NE	NE	NE
≥29 d	0/381	2/778	0.01 (−0.04 to 0.04)	1.2 (−0.97 to 3.12)	NE	NE	NE

*Time since first vaccinated was a proxy of number of vaccine doses and days since last dose. NE, not estimated because of insufficient number of events; RD, risk difference; RR, risk ratio; VE, vaccine effectiveness.
†Per 10,000 population per day.
‡Full vaccination.

21–27 days after vaccination, and 98% at ≥27 days after the second vaccine dose, rates that were similar to those for younger age groups (*16*). Bernal et al. reported vaccine effects started 10–13 days after vaccination with Pfizer/BioNTech and, in persons ≥80 years of age, reached 70% ≥29 days after vaccination and 89% 14 days after the second dose (*17*).

Some studies have focused on LTCFs. A study of COVID-19 outbreaks in skilled nursing facilities in Connecticut, USA, found 63% protection after partial vaccination (14–28 days after the first dose), which is close to our estimates (*7*). A recently released report from the VIVALDI study in the United Kingdom found no protection conferred by the Pfizer/BioNTech vaccine in the first 28 days after the first dose among residents of LTCFs (*8*). Nevertheless, VE during days 29–47 was between 56% and 62%, similar to the range of effect in our study for the period 22–28 days (61.9%). In contrast with these studies, the study from Denmark of LTCFs (I.R. Moustsen-Helms et al., unpub. data) found no protective effect of a first vaccine dose, a 52% reduction of risk in days 0–7 after the second dose, and a 64% reduction after day 7, with a strong confounding effect by calendar time, although no details are provided on the methods for adjustment. An approximation of VE using the screening method in the same population of our study (*18*) also resulted in a reduced VE of 71%, although CIs were wide and compatible with our estimation.

A time-series analysis of surveillance data from Spain comparing SARS-CoV-2 incidence in persons ≥65 years of age living in LTCFs versus those not living in LTCFs (in whom vaccination did not begin until early February) (*19*) found an 85% (95% CI 81%–88%) reduction in incidence in residents of LTCFs after January 17, which provides further validation of the effect of vaccination in LTCFs. Of note, our work included both symptomatic and asymptomatic infections; risk was probably reduced for both, although to an unknown degree. In national COVID-19 surveillance, 39% of all notified infections since May 10, 2020, in persons ≥65 years of age were asymptomatic.

A considerable 22% of all participants in our study had a previous documented SARS-CoV-2 infection, although a high number of undocumented infections are possible, especially during the first epidemic wave in March–April 2020. Several studies have documented a high immune response to a first COVID-19 vaccine dose in persons with previous infection (*20*; S. Saadat et al., unpub. data, https://www.medrxiv.org/content/10.1101/2021.01.30.21250843v5; C. Camara et al., unpub. data, https://www.biorxiv.org/content/10.1101/2021.03.22.436441v1). The results of our study add to the literature on this subject by demonstrating that, even though the effect was greater in

persons naive to SARS-CoV-2, those with previous infection also benefited from a risk reduction of 57%, although it translated to <1 infection averted/10,000 population/day.

Results from the indirect protection analysis in nonvaccinated persons support the hypothesis that vaccination might reduce transmissibility of SARS-CoV-2 and result in herd immunity. Previous studies have shown decreased viral load in vaccinated persons, including those in LTCFs (*7*,*21*). A study from Scotland found a 30% lower risk for SARS-CoV-2 in household members of vaccinated healthcare workers, although the reduction in SARS-CoV-2 transmission from vaccinated persons could be double that estimate, since household members could also have been infected in the community (A.S. Shah et al., unpub. data, https://www.medrxiv.org/content/10.1101/2021.03.11.21253275v1). A recent ecologic study from Israel has shown that increasing vaccine coverage provides cross-protection to unvaccinated persons in the community (*22*). In our study, nonvaccinated persons living in facilities where most residents and staff had been vaccinated showed a risk reduction similar to persons who were actually vaccinated. However, the magnitude of protection might be overestimated, because nonvaccinated persons could be more likely to have had previous infection, even if not documented. Also, indirect protection was measured in a context of very high vaccine coverage, which is difficult to attain in a noninstitutional setting; therefore, our results might not apply to the community setting.

Some limitations to our study could relate to the before-after comparison. Although we tried to minimize it, the bias-indicator cohort showed residual confounding because of higher incidence during the study period, which coincided with the third epidemic wave. The high incidence could also be related to relaxed isolation in LTCFs during the Christmas season, when numbers of days out and visits were higher. Of note, SARS-CoV-2 testing policy did not change during the study period. This residual bias would be in the direction of underestimation of the protection of the vaccine. Another limitation is that, because the selection of participants was performed through the vaccination registry, we were able to include only persons who survived until the vaccination campaign. We observed a high incidence during the second epidemic wave (9.6% of study participants were infected between the beginning of the reference period and the beginning of the study period). Therefore, the group with previous infection in the study period had more recent infections compared with the group in the reference period; if this factor conferred greater protection, it could overestimate VE in this group. On the other hand, prolonged viral shedding (beyond 60 days) could be mistaken for a new infection and, if this factor was more frequent because of recent infections in the study period, it could decrease VE. However, discarding tests within 90 days (instead of 60) of a previous positive test did not substantially change results (analysis not shown). Finally, full vaccination was accounted for by a proxy of ≥29 days after the first dose. This assumption is reasonable in our study because uptake of a second dose was very high, and the number of days between doses was 21 for most persons.

A strength of our study was that it included virtually all residents of LTCFs in Spain. The number of included persons was slightly higher than the number of residents in the official LTCF census (299,209 vs. 281,428), which is expected because the census does not include a small number of LTCFs (e.g., those managed by the church).

In conclusion, our results confirm the effectiveness of vaccination in LTCF residents. Our findings endorse the policy of universal vaccination in this setting, including in persons with previous infection, and suggest that nonvaccinated persons benefit from indirect protection. Questions remain regarding the effects of age and previous infection on the duration of protection afforded by vaccination.

This article was preprinted at https://www.medrxiv.org/content/10.1101/2021.04.08.21255055v2.

COVID-19 Registries Study Group members: David Moreno, Manuel Méndez Díaz, Ismael Huerta González, Antònia Galmés Truyols, Ana Barreno Estévez, Valvanuz García Velasco, Mª Jesús Rodríguez Recio, José Sacristán, Montserrat Martínez Marcos, Eliseo Pastor Villalba, María José Macías Ortiz, Ana García Vallejo, Sara Santos Sanz, Rocío García Pina, Aurelio Barricarte, Rosa Sancho Martínez, Eva María Ochoa, Mauricio Vázquez Cantero, Atanasio Gómez Anés, María Jesús Pareja Megía, Yolanda Castán, Manuel Roberto Fonseca Álvarez, Antonia Salvà Fiol, Hilda Sánchez Janáriz, Luz López Arce, María Ángeles Cisneros Martín, José Sacristán, Frederic Jose Gibernau, Cesar Fernandez Buey, Katja Villatoro Bongiorno, Francisco Javier Rubio García, Fernando Santos Guerra, Jenaro Astray Mochales, Francisco Javier Francisco Verdu, Isabel García Romero, Rosa Oriza Bernal, Tomás Gómez Pérez, Salomé Hijano Villegas, Sergio Román Soto, Virgilio Yagüe Galaup, Mariano Martín García, Lucía Escapa Castro, Mercedes Alfaro Latorre, Marta Aguilera Guzmán, Belén Crespo Sánchez-Eznarriaga, Montserrat Neira León, Noemí Cívicos Villa, Amparo Larrauri, and Clara Mazagatos.

Acknowledgments

We thank the General Directorate of Digital Health and National Health Service Information Systems and the General Sub-Directorate for Health Information (Ministry of Health, Spain) for their work in managing the registries on which this study was based, as well as in providing all the necessary IT support. We especially thank Miguel Hernán for his methodologic advice and support in the design of the analysis, as well as Luis Sanguiao for his support in implementing parallel computing. We also acknowledge all the work of the professionals involved in the vaccination program and in managing the vaccination and laboratory registries from the Autonomous Communities.

S.M., C.O., M.J.S., and A.L. conceived the idea for the study. S.M. and C.O. designed the analysis, which was performed by S.M. with help from B.A., support from M.F.L. and under the supervision of M.J.S. and A.L. All authors participated in the interpretation of results and critically reviewed the content of the manuscript.

About the Author

Dr. Monge is a medical specialist in public health and preventive medicine and a graduate of the European Programme for Intervention Epidemiology Training with more than 10 years' experience in applied epidemiology and research in communicable diseases. Her primary research interests are HIV, tuberculosis and hepatitis, respiratory viruses, and vaccine-preventable diseases.

References

1. Instituto de Mayores y Servicios Sociales (Imserso). Second update: Coronavirus disease (COVID-19) in long-term care facilities (LTCF) [in Spanish]. 2021 Mar 7 [cited 2021 Mar 31]. https://www.imserso.es/InterPresent2/groups/imserso/documents/binario/inf_resid_20210312.pdf
2. Grupo de Trabajo Técnico de Vacunación COVID-19 de la Ponencia de Programa y Registro de Vacunaciones. Strategy for COVID-19 vaccination in Spain [in Spanish]. 2020 Dec 2 [cited 2021 Mar 31]. https://www.mscbs.gob.es/profesionales/saludPublica/prevPromocion/vacunaciones/covid19/docs/COVID-19_EstrategiaVacunacion.pdf
3. Centro de Coordinación de Alertas y Emergencias Sanitarias, Ministry of Health of Spain. Update 335: coronavirus disease (COVID-19) [in Spanish]. 2021 Mar 18 [cited 2021 Mar 31]. https://www.mscbs.gob.es/profesionales/saludPublica/ccayes/alertasActual/nCov/documentos/Actualizacion_335_COVID-19.pdf
4. GIV COVID-19, Ministry of Health of Spain. Integral management of COVID vaccination: activity report [in Spanish]. 2021 Mar 18 [cited 2021 Mar 31]. https://www.mscbs.gob.es/profesionales/saludPublica/ccayes/alertasActual/nCov/documentos/Informe_GIV_comunicacion_20210318.pdf
5. Polack FP, Thomas SJ, Kitchin N, Absalon J, Gurtman A, Lockhart S, et al.; C4591001 Clinical Trial Group. Safety and efficacy of the BNT162b2 mRNA Covid-19 vaccine. N Engl J Med. 2020;383:2603–15. https://doi.org/10.1056/NEJMoa2034577
6. Prendki V, Tau N, Avni T, Falcone M, Huttner A, Kaiser L, et al.; ESCMID Study Group for Infections in the Elderly (ESGIE). A systematic review assessing the under-representation of elderly adults in COVID-19 trials. BMC Geriatr. 2020;20:538. https://doi.org/10.1186/s12877-020-01954-5
7. Britton A, Jacobs Slifka KM, Edens C, Nanduri SA, Bart SM, Shang N, et al. Effectiveness of the Pfizer-BioNTech COVID-19 vaccine among residents of two skilled nursing facilities experiencing COVID-19 outbreaks—Connecticut, December 2020–February 2021. MMWR Morb Mortal Wkly Rep. 2021;70:396–401. https://doi.org/10.15585/mmwr.mm7011e3
8. Shrotri M, Krutikov M, Palmer T, Giddings R, Azmi B, Subbarao S, et al. Vaccine effectiveness of the first dose of ChAdOx1 nCoV-19 and BNT162b2 against SARS-CoV-2 infection in residents of long-term care facilities in England (VIVALDI): a prospective cohort study. Lancet Infect Dis. 2021 Jun 23 [Epub ahead of print].
9. Ministerio de Sanidad e Instituto de Salud Carlos III. Estrategia de detección precoz, vigilancia y control de COVID-19 [cited 2021 May 24]. https://www.mscbs.gob.es/profesionales/saludPublica/ccayes/alertasActual/nCov/documentos/COVID19_Estrategia_vigilancia_y_control_e_indicadores.pdf
10. Hernán MA, Robins JM. Causal inference: what if. Boca Raton (Florida): Chapman & Hall/CRC Press; 2020 [cited 2021 Mar 31]. https://www.hsph.harvard.edu/miguel-hernan/causal-inference-book/
11. Fulop T, Pawelec G, Castle S, Loeb M. Immunosenescence and vaccination in nursing home residents. Clin Infect Dis. 2009;48:443–8. https://doi.org/10.1086/596475
12. Müller L, Andrée M, Moskorz W, Drexler I, Walotka L, Grothmann R, et al. Age-dependent immune response to the Biontech/Pfizer BNT162b2 COVID-19 vaccination. Clin Infect Dis. 2021;ciab381; [Epub ahead of print].
13. Walsh EE, Frenck RW Jr, Falsey AR, Kitchin N, Absalon J, Gurtman A, et al. Safety and immunogenicity of two RNA-based Covid-19 vaccine candidates. N Engl J Med. 2020;383:2439–50. https://doi.org/10.1056/NEJMoa2027906
14. Hall VJ, Foulkes S, Saei A, Andrews N, Oguti B, Charlett A, et al.; SIREN Study Group. COVID-19 vaccine coverage in health-care workers in England and effectiveness of BNT162b2 mRNA vaccine against infection (SIREN): a prospective, multicentre, cohort study. Lancet. 2021;397:1725–35. https://doi.org/10.1016/S0140-6736(21)00790-X
15. Haas EJ, Angulo FJ, McLaughlin JM, Anis E, Singer SR, Khan F, et al. Impact and effectiveness of mRNA BNT162b2 vaccine against SARS-CoV-2 infections and COVID-19 cases, hospitalisations, and deaths following a nationwide vaccination campaign in Israel: an observational study using national surveillance data. Lancet. 2021;397:1819–29. https://doi.org/10.1016/S0140-6736(21)00947-8
16. Dagan N, Barda N, Kepten E, Miron O, Perchik S, Katz MA, et al. BNT162b2 mRNA Covid-19 vaccine in a nationwide mass vaccination setting. N Engl J Med. 2021;384:1412–23. https://doi.org/10.1056/NEJMoa2101765
17. Lopez Bernal J, Andrews N, Gower C, Robertson C, Stowe J, Tessier E, et al. Effectiveness of the Pfizer-BioNTech and Oxford-AstraZeneca vaccines on covid-19 related symptoms, hospital admissions, and mortality in older adults in England: test negative case-control study. BMJ. 2021;373:n1088. https://doi.org/10.1136/bmj.n1088

18. Mazagatos C, Monge S, Olmedo C, Vega L, Gallego P, Martín-Merino E, et al. Working Group for the surveillance and control of COVID-19 in Spain. Effectiveness of mRNA COVID-19 vaccines in preventing SARS-CoV-2 infections and COVID-19 hospitalisations and deaths in elderly long-term care facility residents, Spain, weeks 53 2020 to 13 2021. Euro Surveill. 2021;26:2100452. https://doi.org/10.2807/1560-7917.ES.2021.26.24.2100452
19. Ministry of Health and Institute of Health Carlos III. Effectiveness and impact of COVID-19 vaccination in residents of elderly long-term care facilities in Spain [in Spanish]. 2021 Apr 25 [cited 2021 Jul 19]. https://www.mscbs.gob.es/profesionales/saludPublica/prevPromocion/vacunaciones/covid19/docs/Efectividad_Residentes_Centros_Mayores_Informe.pdf
20. Manisty C, Otter AD, Treibel TA, McKnight Á, Altmann DM, Brooks T, et al. Antibody response to first BNT162b2 dose in previously SARS-CoV-2-infected individuals. Lancet. 2021;397:1057–8. https://doi.org/10.1016/S0140-6736(21)00501-8
21. Levine-Tiefenbrun M, Yelin I, Katz R, Herzel E, Golan Z, Schreiber L, et al. Initial report of decreased SARS-CoV-2 viral load after inoculation with the BNT162b2 vaccine. Nat Med. 2021;27:790–2. https://doi.org/10.1038/s41591-021-01316-7
22. Milman O, Yelin I, Aharony N, Katz R, Herzel E, Ben-Tov A, et al. Community-level evidence for SARS-CoV-2 vaccine protection of unvaccinated individuals. Nat Med. 2021; Epub ahead of print. https://doi.org/10.1038/s41591-021-01407-5

Address for correspondence: Susana Monge, Centro de Coordinación de Alertas y Emergencias Sanitarias (CCAES), Ministerio de Sanidad, Paseo del Prado, 18. 28014 Madrid, Spain; email: smonge@mscbs.es

Predictors of Test Positivity, Mortality, and Seropositivity during the Early Coronavirus Disease Epidemic, Orange County, California, USA

Daniel M. Parker, Tim Bruckner, Verónica M. Vieira, Catalina Medina, Vladimir N. Minin, Philip L. Felgner, Alissa Dratch, Matthew Zahn, Scott M. Bartell, Bernadette Boden-Albala

We conducted a detailed analysis of coronavirus disease in a large population center in southern California, USA (Orange County, population 3.2 million), to determine heterogeneity in risks for infection, test positivity, and death. We used a combination of datasets, including a population-representative seroprevalence survey, to assess the actual burden of disease and testing intensity, test positivity, and mortality. In the first month of the local epidemic (March 2020), case incidence clustered in high-income areas. This pattern quickly shifted, and cases next clustered in much higher rates in the north-central area of the county, which has a lower socioeconomic status. Beginning in April 2020, a concentration of reported cases, test positivity, testing intensity, and seropositivity in a north-central area persisted. At the individual level, several factors (e.g., age, race or ethnicity, and ZIP codes with low educational attainment) strongly affected risk for seropositivity and death.

In late 2019, an epidemic of coronavirus disease (COVID-19), a respiratory disease caused by a novel coronavirus, severe acute respiratory syndrome coronavirus 2 (SARS-CoV-2), emerged in Wuhan, China, and rapidly spread worldwide. COVID-19 has manifested in different ways across social, economic, and demographic groups, with regard to apparent risk for infection, disease severity, and death (*1*–*3*). The elderly and those with underlying conditions are at the highest risk for severe disease (*4*). Many hospitalized patients require supplemental oxygen or ventilators (*5*), and a high mortality rate occurs among those who are hospitalized (*6*). In many places, healthcare facilities have been overwhelmed by a surge in cases and have had an insufficient supply of needed ventilators and intensive care unit beds, resulting in massive illness and death (*7*,*8*). Availability of tests and operational barriers were limiting factors for diagnosis in parts of the United States during the early months of the pandemic (*9*).

California is the most populous state in the United States, and it has an estimated 39.5 million inhabitants. Orange County (OC) is a coastal county in California and the sixth most populous county in the country, with an estimated 3.2 million inhabitants. The first confirmed case in California (the third US case) was reported from OC on January 25 (*10*). On January 30, the World Health Organization declared a global health emergency (*11*), and on January 31, the United States likewise declared a public health emergency (*12*). On February 26, local (i.e., community) transmission was first confirmed in the United States in northern California (*13*). Several counties by this time had already declared local public health emergencies, including Santa Clara (*14*), San Diego (*15*), and Orange (*16*) Counties, as had the city of San Francisco (*17*). By mid-March, an apparent surge in locally transmitted cases was occurring in OC (Figure 1) and other counties in California, triggering emergency shelter-in-place orders by the governor and the county health officer at the Orange County Health Care Agency (OCHCA), prohibiting public or private gatherings and also leading to school and business closures (*18*). Although many businesses were closed

Author affiliations: University of California, Irvine, Irvine, California, USA (D.M. Parker, T. Bruckner, V.M. Vieira, C. Medina, V.N. Minin, P.L. Felgner, S.M. Bartell, B. Boden-Albala); Orange County Health Care Agency, Santa Ana, California, USA (A. Dratch, M. Zahn)

DOI: https://doi.org/10.3201/eid2710.210103

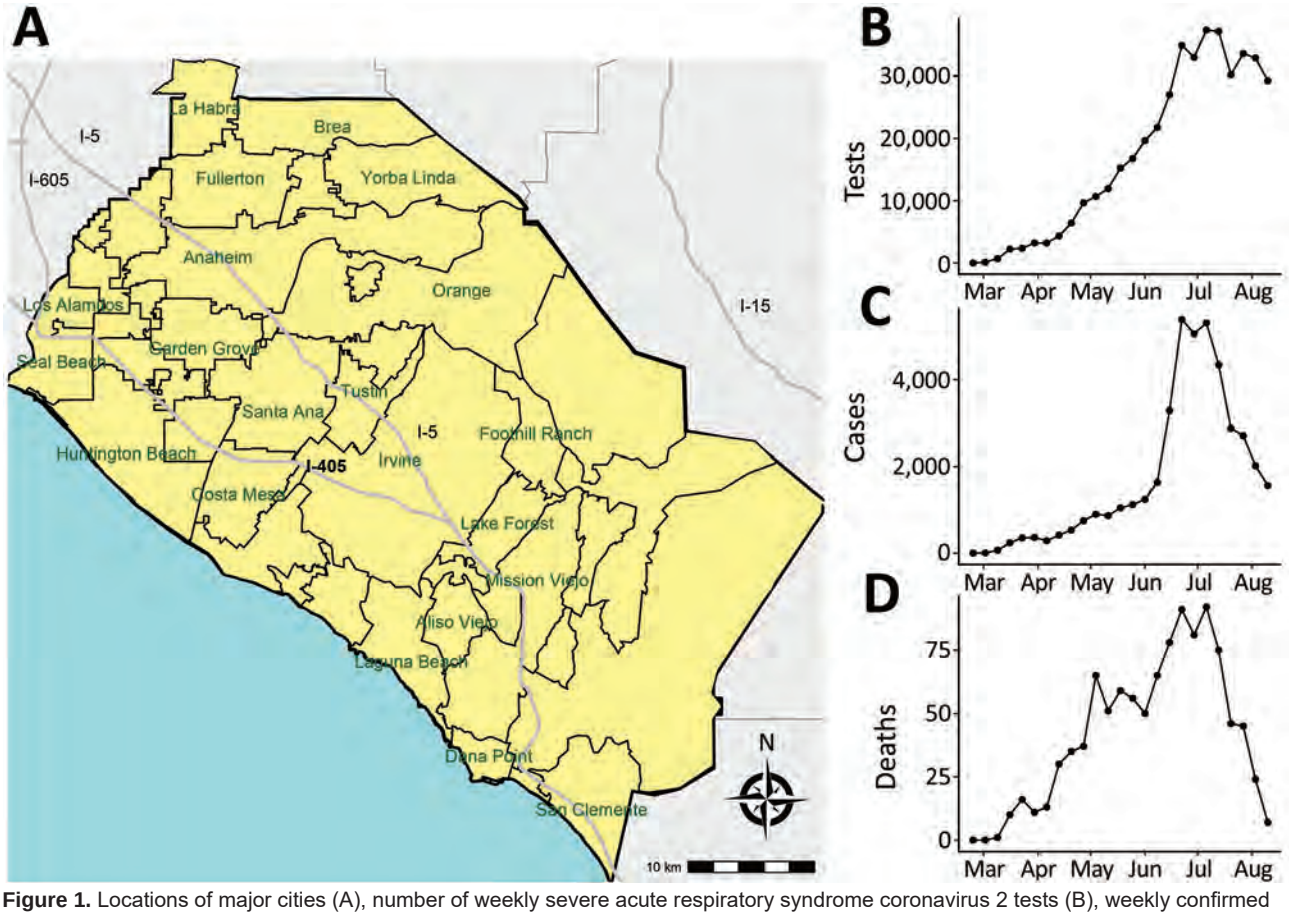

Figure 1. Locations of major cities (A), number of weekly severe acute respiratory syndrome coronavirus 2 tests (B), weekly confirmed coronavirus disease cases (C), and weekly coronavirus disease deaths (D), Orange County, California, USA, July–August 2020.

at this time, the mandated social distancing measures had exceptions in place for persons working in essential jobs, which was broadly defined and included medical professionals, food providers, delivery agencies, public officials, construction contractors, and building laborers (*19*). The social and economic characteristics of persons working essential jobs differs from the overall population (*20*).

Almost half of OC residents >5 years of age speak a language other than English at home. In addition, many within the Hispanic/Latinx and Asian communities of OC live below the poverty level (17.9% and 12.0%, respectively) and face challenges in education, household income, access to healthcare, health disparities, and life expectancy (*21*,*22*). The relatively small land area, high population density, and diverse population of OC provides a unique opportunity to explore potentially important social, economic, and demographic correlates of COVID-19 epidemiology.

Table 1. Global Moran's *I* statistics for reported coronavirus disease case incidence, test positivity, and testing intensity for each month of the study period, Orange County, California, USA, March–August 2020*

	Case incidence		Test positivity		Testing intensity	
Month	*I*	p value	*I*	p value	*I*	p value
March	0.238	0.002	0.059	0.150	0.448	0.001
April	0.168	0.012	0.271	0.001	0.022	0.257
May	0.558	0.001	0.492	0.001	0.345	0.001
June	0.606	0.001	0.552	0.001	0.469	0.001
July	0.591	0.001	0.500	0.001	0.408	0.001
August	0.603	0.001	0.472	0.001	0.185	0.002

*The Moran's *I* statistic indicates the degree of spatial clustering whereas the simulated p-value gives an indication of statistical significance. Moran's *I* values roughly range from −1 to 1, with 1 indicating complete spatial clustering (i.e., all areas with high values are neighboring other areas with high values) and −1 indicating complete spatial dispersion (with high value areas always neighboring low value areas).

We conducted a detailed spatiotemporal epidemiologic analysis of COVID-19 in OC during March 1–August 16, 2020. We drew from reported tests and mortality data from the county health agency. Given that passively detected cases are prone toward bias, in July 2020 we also conducted a seroprevalence

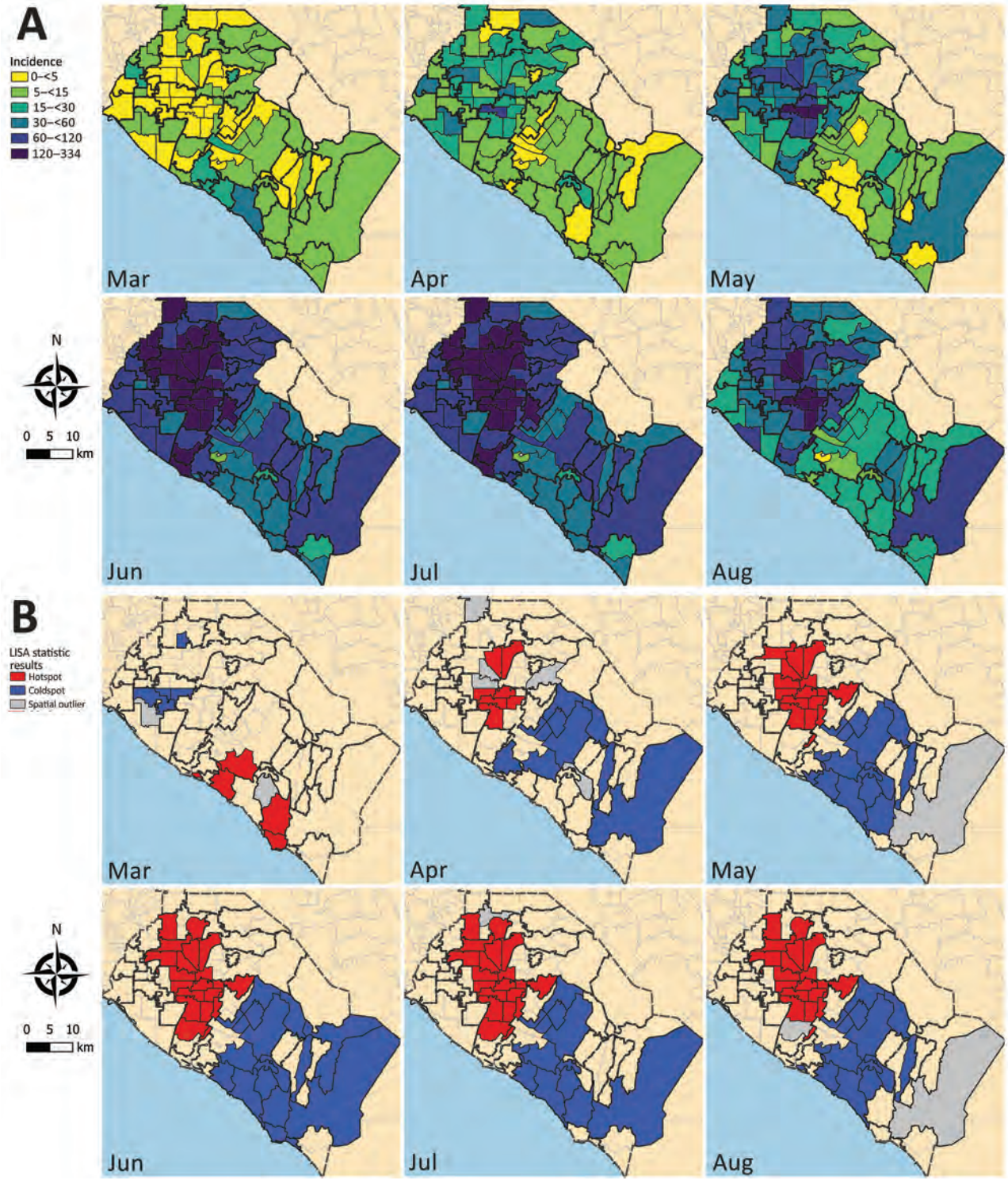

Figure 2. Coronavirus disease incidence, Orange County, California, USA, July–August 2020. A) Reported case incidence of coronavirus by month. Case incidence is calculated as the number of cases per 100,000 persons per week.B) Results from tests of statistical clustering (based on LISA statistics [*24*]). LISA, local indicators of spatial autocorrelation.

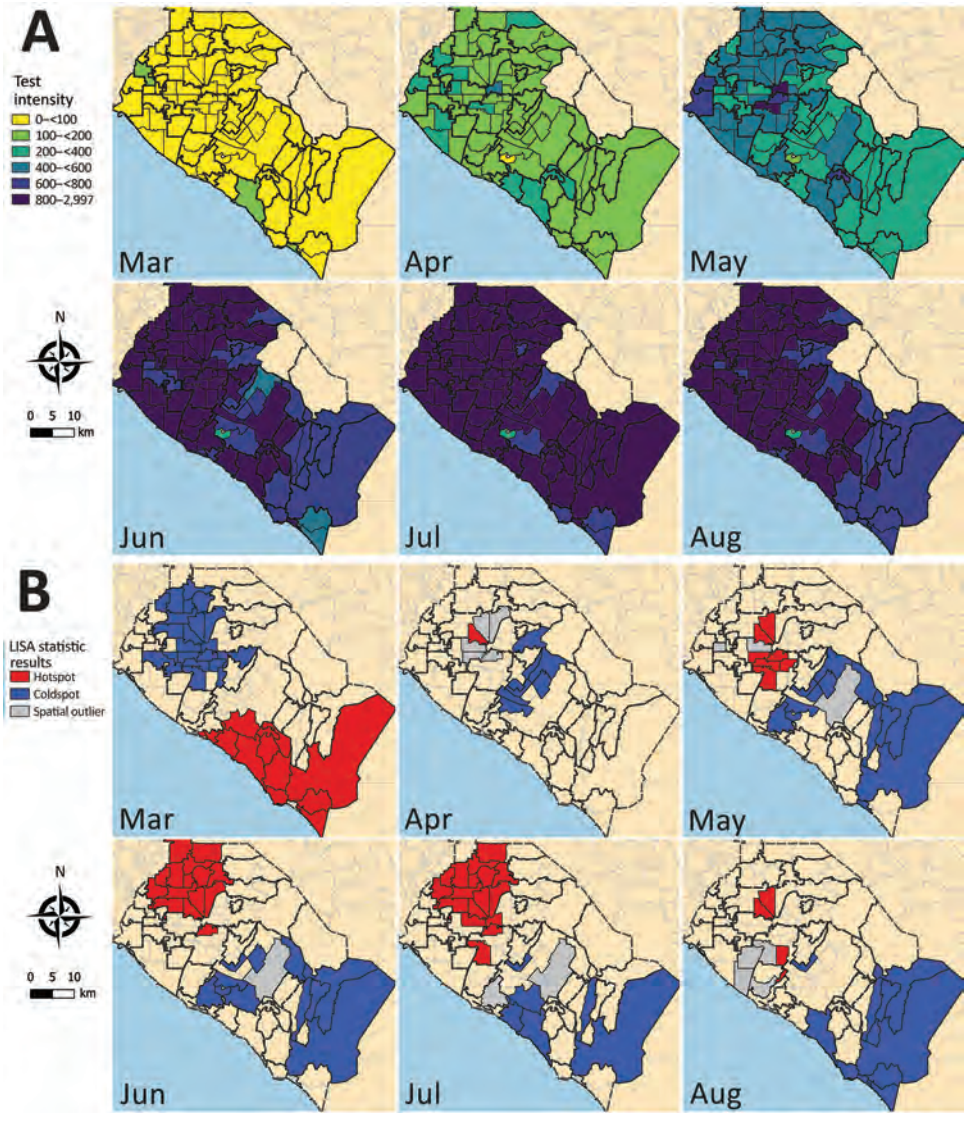

Figure 3. Severe acute respiratory syndrome coronavirus 2 test intensity, Orange County, California, USA, July–August 2020. A) Test intensity by month, calculated as the number of tests per 100,000 persons per week at the ZIP code level.. B) Results from tests of statistical clustering (based on LISA statistics [*24*]). LISA, local indicators of spatial autocorrelation.

survey to assess the actual burden of disease in the county. We use both datasets to compare predictors of test positivity, death, and seropositivity over the first 6 months of the epidemic.

Methods

Data

Case and Mortality Data

Case data were provided by OCHCA and consisted of individual-level records of all negative and positive PCR tests conducted throughout the county during March 1–August 16, 2020; this date aligns with our cross-sectional seroprevalence survey completed on August 16. OCHCA receives testing data from the California Reportable Disease Information Exchange (CalREDIE), an infectious disease surveillance system implemented by the California Department of Public Health (*14*). The data include test date, age, sex, race, ethnicity, and ZIP code of the person taking the test. For persons who had repeat PCR testing after testing positive, we included only the first positive diagnosis in our analyses; we retained multiple negative test results. Mortality data were also provided by OCHCA (also through CalREDIE) and consisted of individual-level records of deaths attributed to COVID-19. OCHCA likewise provided data on the number and percentage of hospital beds that were occupied by COVID-19 patients over time.

Seroprevalence Data

Participants in the serologic survey were recruited using a proprietary database (Appendix, https://wwwnc.cdc.gov/EID/article/27/10/21-0103-App1.

pdf), which is intended to be representative of the age, income, and racial and ethnic diversity of OC. We recruited 1 participant per household (by email or phone) to participate in a survey on their thoughts and opinions regarding COVID-19. The survey included questions on sociodemographics, occupation, social activities, any illness or symptoms in the past few months, and whether the person had been diagnosed with COVID-19. After completing this portion of the survey, each eligible participant was asked if they would be willing to participate in a drive-through blood test for SARS-CoV-2 antibodies. Eligibility for antibody testing was restricted to a quota sample designed to be demographically representative of the county as a whole. Recruitment to the antibody test was delayed to the end of the questionnaire to avoid biasing the serologic survey toward persons who believed that they were infected with SARS-CoV-2. A total of 10 field sites for drive-through blood tests were dispersed throughout OC to minimize driving distances for participants. This cross-sectional survey was conducted July 10–August 16, 2020. The seroprevalence study design and overall findings for OC have been described previously (*23*).

Serologic Test Data

We used a coronavirus antigen microarray to classify participants from the serologic survey as seropositive or seronegative. The array tests for IgG and IgM and contains 12 antigens from SARS-CoV-2 (R.R. de Assis et al., unpub. data, https://doi.org/10.1101/2020.04.15.043364).

ZIP Code–Level Sociodemographic Data

At the ZIP code level, we included median household income, the percentage of adults >25 years of

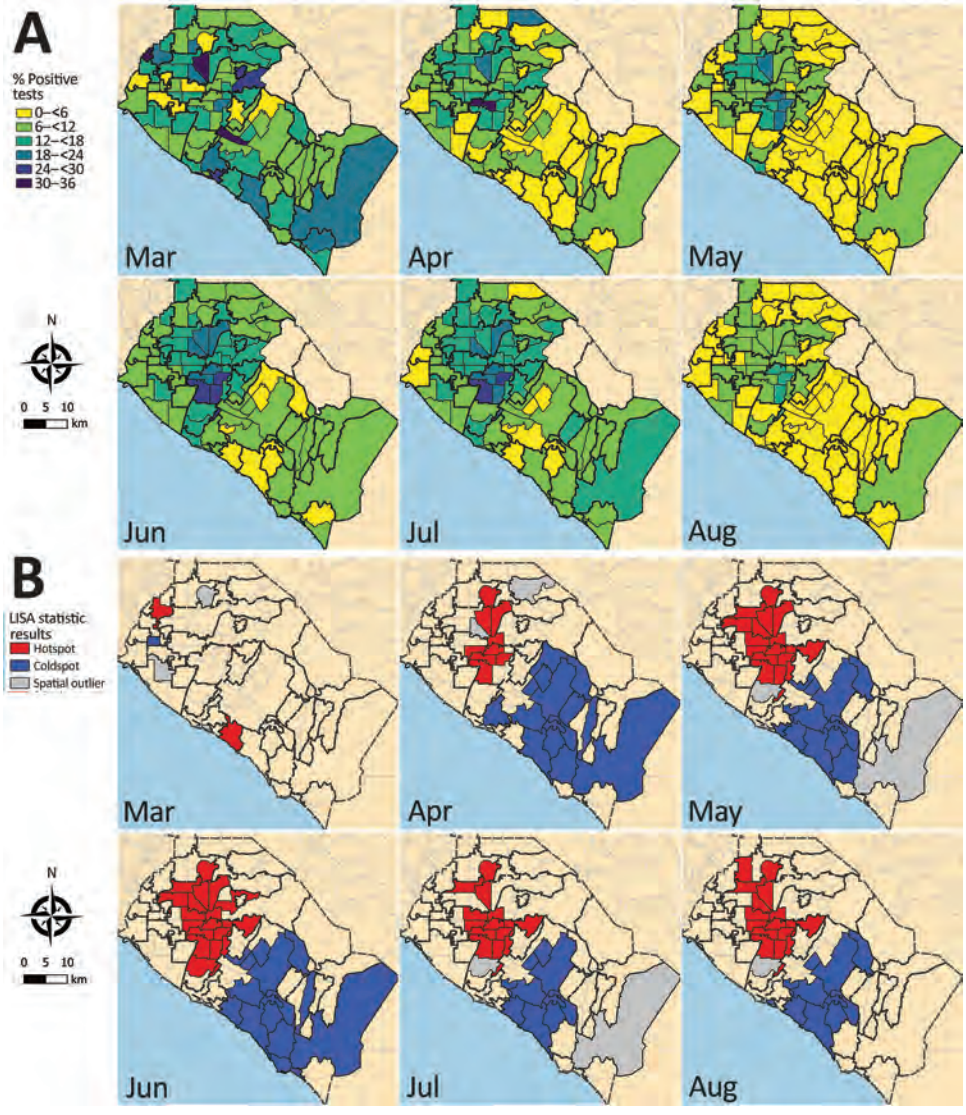

Figure 4. Severe acute respiratory syndrome coronavirus 2 test positivity, Orange County, California, USA, July–August 2020. A) Test positivity at ZIP code level by month. B) Results from tests of statistical clustering (based on LISA statistics [*24*]). LISA, local indicators of spatial autocorrelation.

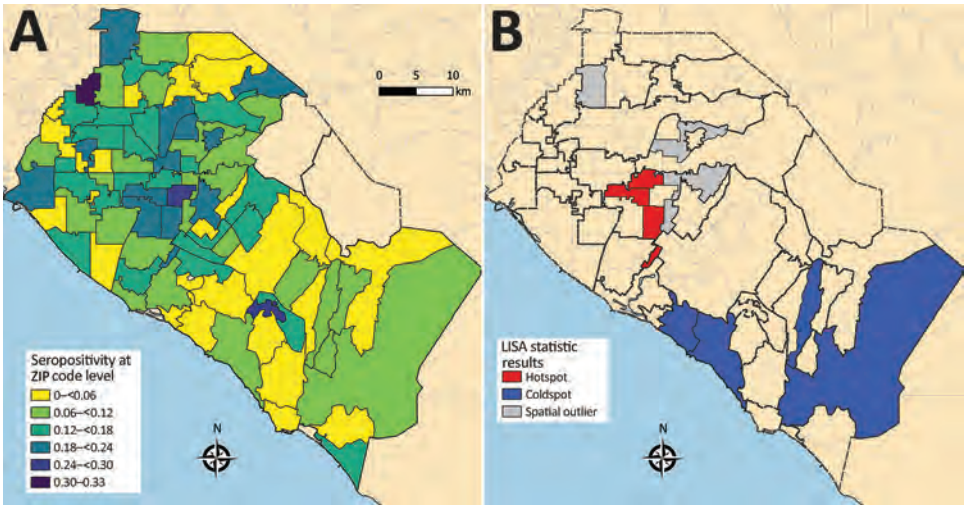

Figure 5. Severe acute respiratory syndrome coronavirus 2 seropositivity, Orange County, California, USA, July–August 2020. A) Seropositivity at ZIP code level. B) Results from tests of statistical clustering (based on LISA statistics [*24*]). LISA, local indicators of spatial autocorrelation.

age with at least a bachelor's degree, the percentage of adults who had health insurance in the previous 5 years, the number of persons per square kilometer, and the percentage of houses with >1 person per room. These data came from the 2018 American Community Survey (*21*).

Analysis

Descriptive Spatiotemporal Data Analysis

We aggregated reported cases and number of tests at the ZIP code level and by week. We included 86 ZIP codes in the analysis. For plotting cases on OC maps, we further aggregated the data by month (March–August). We calculated and mapped case incidence as positive cases per 100,000 population per week, testing intensity as total number of tests per 100,000 persons per week, and test positivity as the percentage of positive tests for each month.

We conducted formal testing of spatial autocorrelation by using the global Moran's *I* statistic and spatial correlograms. We then used local clustering statistics (local indicators of spatial autocorrelation [LISA] [*24*]) to visualize the location of clusters. We ran all tests for case incidence, test positivity, and test intensity. We also used LISA statistics to map and assess seropositivity.

Relational Analysis of COVID-19 Test Positivity, Risk for Death, and Seropositivity

We used logistic regressions to explore geographic, demographic, economic, and epidemiologic predictors of the odds of testing positive for COVID-19, of dying from COVID-19, and of being seropositive for SARS-CoV-2 antibodies. Predictors in our models were age group, sex, and race or ethnicity at the individual level (Appendix Table 1). ZIP code–level predictors were median household income, the percentage of adults >25 years of age with at least a bachelor's degree, the percentage of adults who had health insurance in the previous 5 years, population density (persons/km^2), and house crowding (the percentage of houses with >1 person per room).

We tested several specifications of the models. Through preliminary exploratory analyses, we noted that the first cases were reported from coastal ZIP codes but that this pattern had shifted inland over time. The best fitting model included a smoothed interaction term for time, coded by day (Appendix Table 1), and median household income at the ZIP code level.

We included the same predictors in the model for risk for death, except for the interaction between time and median household income, which did not improve model performance. Given reports of increased mortality rates related to hospital bed shortages, we also included as a predictor the number of intensive care unit beds occupied by suspected or confirmed COVID-19 patients on the day that any person tested positive for SARS-CoV-2. For all model results, we calculated model-adjusted odds ratios (aORs) with 95% CIs.

Software

We created maps by using QGIS 3.4.9 (https://qgis.org). We conducted tests for spatial autocorrelation by using GeoDa 1.14.0 (https://geodacenter.github.io) and all other analyses by using R statistical software 3.5.2 (R Project for Statistical Computing, https://www.r-project.org).

Table 2. Generalized additive logistic regression results for odds of testing positive for SARS-CoV-2, Orange County, California, USA, March–August 2020*

Characteristic	No. (%) SARS-CoV-2 positive	No. (%) Total tests	Adjusted odds ratio† (95% CI)
Age group, y			
0–4	487 (1.3)	4,835 (1.53)	Referent
5–9	490 (1.31)	3,855 (1.22)	1.62 (1.41–1.86)
10–14	855 (2.28)	5,064 (1.6)	2.26 (2.00–2.56)
15–19	2,124 (5.66)	13,814 (4.36)	2.32 (2.08–2.58)
20–24	4,646 (12.37)	31,727 (10.02)	2.04 (1.85–2.26)
25–29	4,640 (12.36)	34,695 (10.96)	1.74 (1.57–1.93)
30–34	3,791 (10.1)	29,900 (9.44)	1.62 (1.46–1.79)
35–39	3,291 (8.77)	25,776 (8.14)	1.67 (1.5–1.85)
40–49	5,950 (15.85)	44,835 (14.16)	1.75 (1.58–1.93)
50–59	5,747 (15.31)	48,502 (15.32)	1.54 (1.39–1.71)
60–69	3,045 (8.11)	36,294 (11.46)	1.04 (0.94–1.16)
70–79	1,404 (3.74)	22,190 (7.01)	0.77 (0.69–0.86)
≥80	1,076 (2.87)	15,139 (4.78)	0.80 (0.72–0.9)
Sex			
F	19,076 (50.81)	173,723 (54.87)	Referent
M	18,470 (49.19)	142,903 (45.13)	1.20 (1.18–1.23)
Race or ethnicity			
White	12,195 (32.48)	63,050 (19.91)	Referent
Asian	1,573 (4.19)	13,858 (4.38)	0.55 (0.52–0.58)
Black	289 (0.77)	2,058 (0.65)	0.58 (0.51–0.65)
Hispanic	3,473 (9.25)	9,147 (2.89)	1.68 (1.6–1.76)
Native American	56 (0.15)	314 (0.1)	0.82 (0.62–1.09)
Pacific Islander	127 (0.34)	1,600 (0.51)	0.35 (0.29–0.42)
Unknown	19,833 (52.82)	226,599 (71.57)	0.32 (0.31–0.33)
% Persons with college degree in ZIP code			
1st quartile	20,665 (55.04)	120,279 (37.99)	Referent
2nd quartile	9,484 (25.26)	87,802 (27.73)	0.89 (0.77–1.03)
3rd quartile	4,560 (12.15)	64,604 (20.4)	0.70 (0.58–0.84)
4th quartile	2,837 (7.56)	43,941 (13.88)	0.68 (0.56–0.83)
% Persons with insurance in ZIP code			
1st quartile	19,749 (52.6)	111,798 (35.31)	Referent
2nd quartile	10,371 (27.62)	93,431 (29.51)	0.83 (0.73–0.95)
3rd quartile	3,824 (10.18)	53,201 (16.8)	0.67 (0.56–0.8)
4th quartile	3,602 (9.59)	58,196 (18.38)	0.58 (0.48–0.7)
Population density, × 1,000 persons/km^2‡			0.97 (0.9–1.04)
House crowding			1.03 (1.02–1.04)

*Excludes the coefficients for ZIP code–level median income and time because of interaction between median income and time. A random intercept was included for ZIP code. The period covered in this analysis is March 1–August 16, 2020. SARS-CoV-2, severe acute respiratory syndrome coronavirus 2.
†Adjusted for all covariates listed plus ZIP code estimated median income and time of test in days. Model intercept represents odds of a White female in the 0–4-y age group in a ZIP code in the first quartile of college degree and insured with the average population density. The odds of this person testing positive for SARS-CoV-2 is estimated to be 0.19 (95% CI 0.16–0.22).
‡Estimated percentage of population density in a person's ZIP code.

Ethics Considerations

This analysis constitutes a retrospective analysis of deidentified, anonymized epidemiologic records. Therefore, it is exempt from ethics review.

Results

A total of 597,922 tests were reported to OCHCA through August 16, 2020. After excluding repeated tests and those with incomplete data, 316,626 (53.0% of all records) persons were included in the test positivity analysis; 37,546 (12.0%) persons tested positive for COVID-19. A total of 42,383 persons with positive COVID-19 tests were included in the mortality analysis; 1,038 (2.5%) died from the disease. In the separate population-based serologic survey, 2,979 persons participated and 350 tested seropositive.

Spatial Patterns in Reported COVID-19 Cases, Testing Intensity, and Seropositivity

The tests for spatial autocorrelation indicated significant clustering in reported cases and testing intensity in the first month (March) of the local epidemic (Table 1; Appendix Figures 1, 2). Conversely, no detectable clustering of test positivity occurred in March (Table 1; Appendix Figure 3). The highest reported case incidence in March was along the central coast and southern portion of the county (Figure 2, panel A). The LISA statistics indicated statistically significant clustering of high-incidence ZIP codes in the central coast area (Figure 2, panel B). This clustering of case incidence overlaps with clustering of test intensity in March (Figure 3, panels A, B).

Clustering of reported cases and test positivity increased in magnitude in May (Table 1; Appendix Figures 1, 3). Although clustering in test intensity was high in March (Table 1; Appendix Figure 2), it decreased in May as access to testing spread throughout much of the county. Clustering in testing intensity increased again in June and July (centered on the hotspots in the north-central part of the county) (Figure 2, 4). By April, case incidence, testing intensity, and test positivity had all shifted to the north-central part of the county. ZIP code–level seropositivity also revealed a cluster in the north-central part of OC (Figure 5), especially in the city of Santa Ana (Figure 1).

Results from Generalized Additive Model Logistic Regression Analysis

Factors Associated with Testing Positive for SARS-CoV-2 infection

Age was a strong predictor of testing positive. Persons in the 10–14- and 15–19-year age groups had the highest odds of testing positive (both with ≈2.30 times the odds of testing positive compared with the 0–4 year age group) (Table 2; Figure 6). Men and boys had 1.20 times the odds of testing positive than women and girls (95% 95% CI 1.18–1.23). Persons who identified as Hispanic or Latinx had 1.7 times the odds of testing positive (95% CI 1.60–1.76) than did non-Hispanic Whites, whereas Asian (aOR 0.55; 95% CI 0.52–0.58), Black (aOR 0.58; 95% CI 0.51–0.65), and Pacific Islander (aOR 0.35; 95% CI 0.29–0.42) persons had lower odds of testing positive than did non-Hispanic Whites. A large proportion of persons did not have attributable race or ethnicity data in the records (72% of all records through August 16). This unknown category includes persons who had no race or ethnicity categories recorded, those who had unknown or mixed listed for race or ethnicity, and those who listed multiple races.

ZIP code–level population density was not a significant predictor of testing positive (Table 2; Figure 6). However, education (percentage of adults >25 years

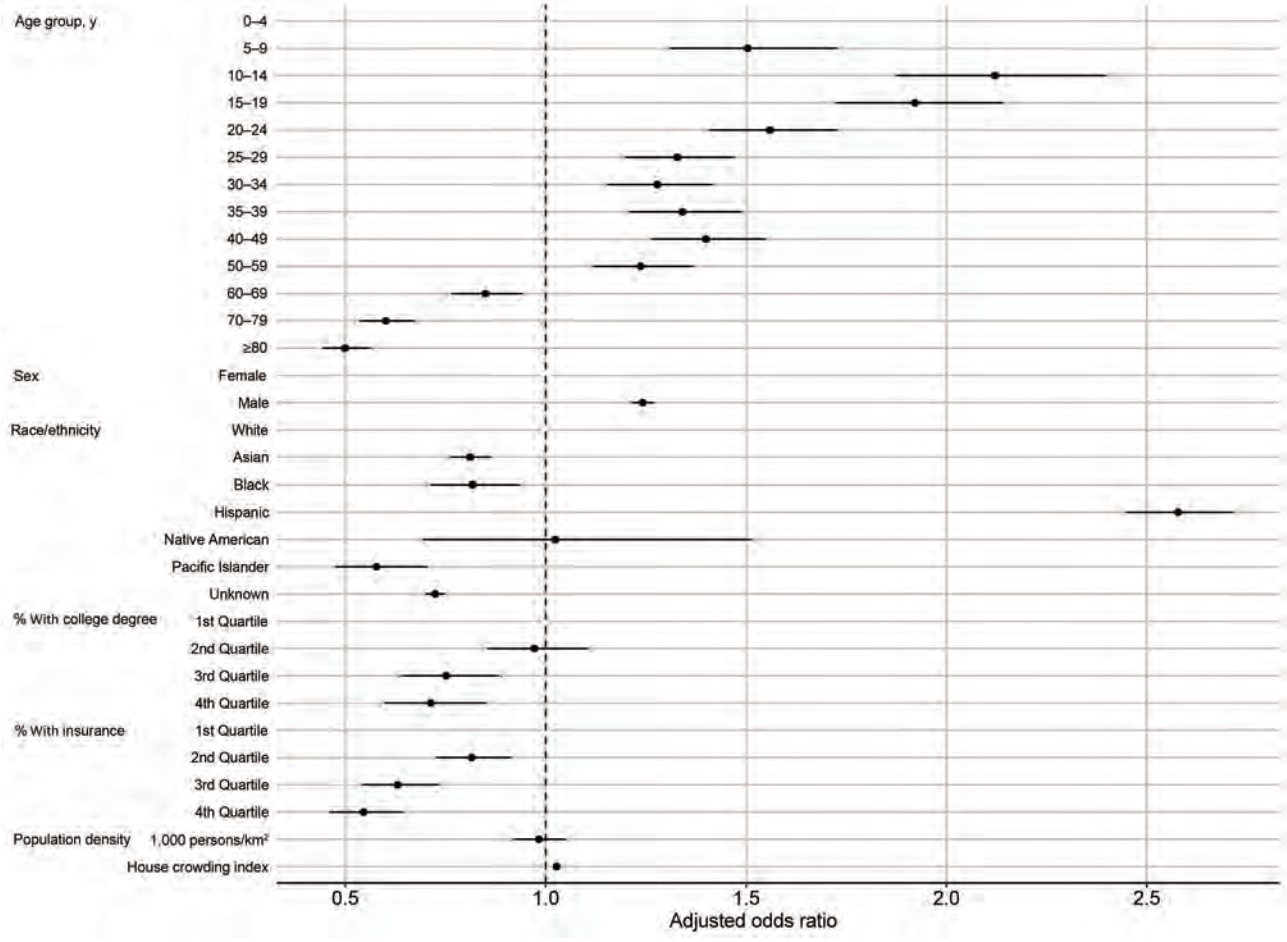

Figure 6. Model-adjusted odds ratios and 95% CIs from the logistic regression for odds of testing positive for severe acute respiratory syndrome coronavirus 2, Orange County, California, USA, July–August 2020. Corresponding data presented in Table 2.

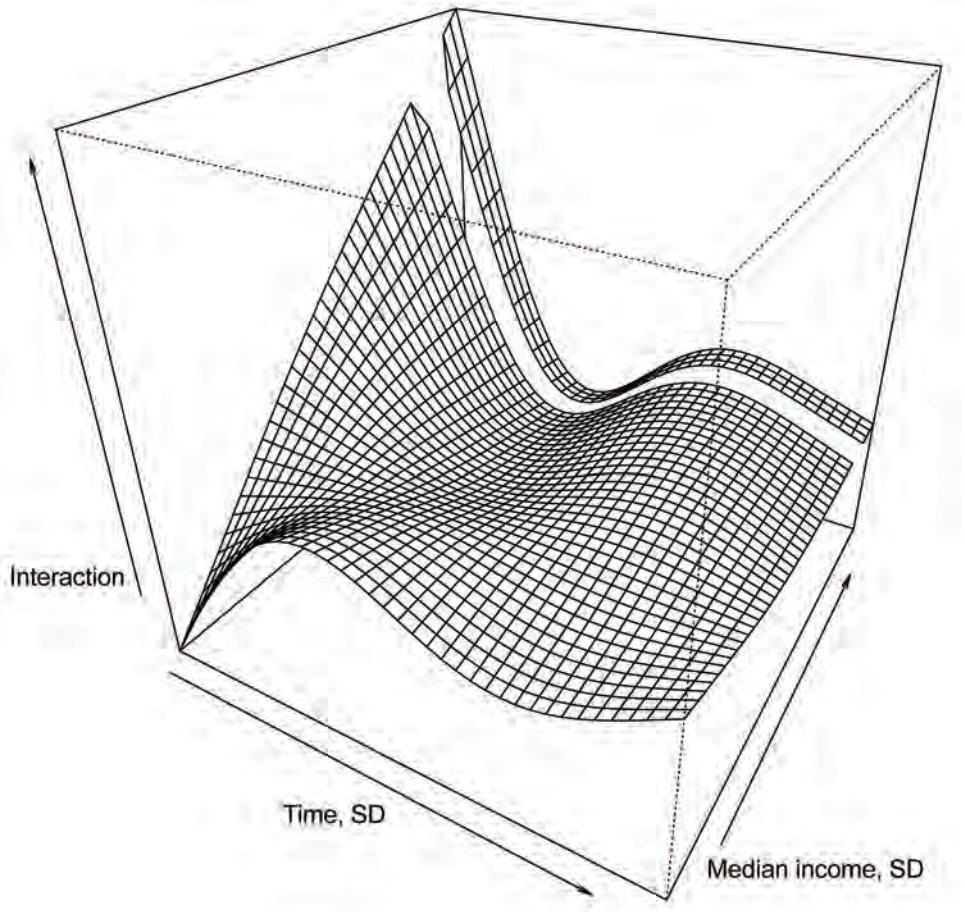

Figure 7. Three-dimensional plot of the smoothed interaction between ZIP code–level median household income and time as a predictor of testing positive for severe acute respiratory syndrome coronavirus 2, Orange County, California, USA, July–August 2020.

of age with at least a bachelor's degree), health insurance coverage (percentage of adults who had health insurance in the previous 5 years), median household income, and household crowding were all statistically significant predictors of testing positive. For example, persons who lived in ZIP codes with the highest education levels had 32% decreased odds of testing positive (aOR for the fourth quartile 0.68, 95% CI 0.56–0.83). In addition, the interaction between ZIP code–level median household income (Figure 7) indicates that persons from wealthier ZIP codes had increased risk for testing positive at the beginning of the epidemic in OC. However, this pattern quickly shifted, and persons from lower-income areas showed the highest odds of testing positive in subsequent months.

Factors Associated with Dying from COVID-19

For each increase in 10 years of age, we observed an associated 2.5-fold increase in the odds of death (aOR 2.56, 95% CI 2.45–2.67; Table 3; Figure 8). Infected men and boys were twice as likely to die from COVID-19 than were women and girls (aOR 2.00, 95% CI 1.73–2.31). Although persons who identified as Asian were less likely to test positive for SARS-CoV-2 infection (Table 2), those who did test positive had higher odds of death. Compared with non-Hispanic Whites, this group had 54% increased odds of dying from COVID-19 (aOR 1.54, 95% CI 1.23–1.93).

Living in ZIP codes with high education levels and health insurance coverage was also predictive of mortality outcomes (Table 3; Figure 8). Persons who tested positive for COVID-19 and lived in ZIP codes with the highest levels of educational attainment had 49% lower odds of dying from COVID-19 (aOR for the fourth quartile 0.51, 95% CI 0.31–0.84). Persons who lived in ZIP codes with the highest levels of health insurance coverage had 21% lower odds of dying from COVID-19. ZIP code–level household crowding and the number of COVID-19 patients in hospital beds were both significant predictors of death. Risk for death from COVID-19 decreased over the study period.

Factors Associated with SARS-CoV-2 Seropositivity

ZIP code–level cumulative incidence was a significant predictor of individual-level seropositivity in

the absence of other ZIP code–level predictors. Every increase in 10% of the ZIP code cumulative incidence resulted in an approximately 50% increase in the odds that a person would be seropositive (Appendix Table 2).

ZIP code–level cumulative incidence was no longer a statistically significant predictor of seropositivity when other ZIP code–level predictors were added to the model (Table 4; Figure 9). In the full model (including all ZIP code–level covariates), median household income had a protective effect; persons coming from ZIP codes with higher median household income had lower odds of being seropositive for SARS-CoV-2 antibodies (aOR for every 1 SD increase 0.75, 95% CI 0.57–1.00).

We found no difference in age groups with regard to seropositivity. Although men and boys were more likely to test positive or to die from SARS-CoV-2 infection, they were less likely than women and girls to be seropositive (aOR 0.75, 95% CI 0.59–0.94). Hispanic and Latinx persons had 54% increased odds of being seropositive (aOR 1.54, 95% CI 1.17–2.03). Pacific Islanders may also have had higher odds of being seropositive, but with small total numbers and broad 95% CIs (aOR 3.89, 95% CI 1.04–14.65); 3 of 12 Pacific Islanders tested were seropositive.

Discussion

Infectious disease data from passive case detection can be biased in various ways, including the well-documented challenge of uneven access to testing and diagnosis (*25*) and a general bias toward persons who are seeking clinical care for symptomatic disease. In our analysis of COVID-19 in OC, we used a rich set of complementary data that included those passively collected (e.g., reported cases and mortality records) and those from active screening (e.g., population-based serologic testing). Results indicate that, in the early days of the epidemic in OC, both testing intensity and test positivity were concentrated in wealthy and affluent areas along the central coast. After March, however, a large cluster of reported cases formed in lower-income north-central OC (especially the cities of Santa Ana and Anaheim)

Table 3. Logistic regression results for odds of dying from COVID-19 among persons who tested positive for SARS-CoV-2, Orange County, California, USA, March–August 2020*

Characteristic	No. (%) COVID-19 deaths, n = 1,038	No. (%) Total cases, n = 42,383	Adjusted odds ratio (95% CI)†
Age, decades			2.56 (2.45–2.67)
Sex			
F	450 (43.35)	21,694 (51.19)	Referent
M	588 (56.65)	20,689 (48.81)	2.00 (1.73–2.31)
Race or ethnicity			
White	345 (33.24)	6,390 (15.08)	Referent
Asian	186 (17.92)	1,963 (4.63)	1.54 (1.23–1.93)
Black	15 (1.45)	322 (0.76)	1.06 (0.56–2.02)
Hispanic	92 (8.86)	3,874 (9.14)	1.05 (0.79–1.38)
Native American	3 (0.29)	34 (0.08)	1.46 (0.46–4.58)
Pacific Islander	3 (0.29)	130 (0.31)	0.71 (0.22–2.26)
Unknown	394 (37.96)	29,670 (70)	0.47 (0.4–0.55)
% With college degree in ZIP code			
1st quartile	656 (63.2)	23,221 (54.79)	Referent
2nd quartile	190 (18.3)	10,223 (24.12)	0.67 (0.52–0.86)
3rd quartile	155 (14.93)	5,691 (13.43)	0.77 (0.54–1.08)
4th quartile	37 (3.56)	3,248 (7.66)	0.51 (0.31–0.84)
% With insurance in ZIP code			
1st quartile	566 (54.53)	21,989 (51.88)	Referent
2nd quartile	281 (27.07)	11,097 (26.18)	1.04 (0.83–1.29)
3rd quartile	123 (11.85)	5,185 (12.23)	1.36 (0.95–1.93)
4th quartile	68 (6.55)	4,112 (9.7)	0.79 (0.52–1.2)
Population density, × 1,000 persons/km^2‡			0.83 (0.71–0.96)
House crowding index			1.04 (1.02–1.05)
Median income (SD)			0.86 (0.7–1.05)
Time (SD)			0.68 (0.62–0.75)
COVID-19 ICU patients (SD)§			1.18 (1.05–1.34)

*Values are no. (%) except where indicated. A random intercept was included for ZIP code. The period covered in this analysis is March 1–August 16, 2020. Total numbers of positive cases are larger than the total number reported in Table 2 because of more extensive data curation for mortality data than for general test data. More rows of data were dropped because of missing information (e.g., on age or sex) in the test positivity data than in the mortality data. COVID-19, coronavirus disease; ICU, intensive care unit; SARS-CoV-2, severe acute respiratory syndrome coronavirus 2.
†Model intercept represents odds of death for a White female diagnosed with SARS-CoV-2 in the 0–4 years age group in a ZIP code in the first quartile of college degree and insured with the average population density in Orange County. The odds of this person testing dying from COVID-19 is estimated to be zero.
‡Estimated percentage of population density in a person's ZIP code.
§Percentage of hospital beds not being used by COVID-19 patients in Orange County.

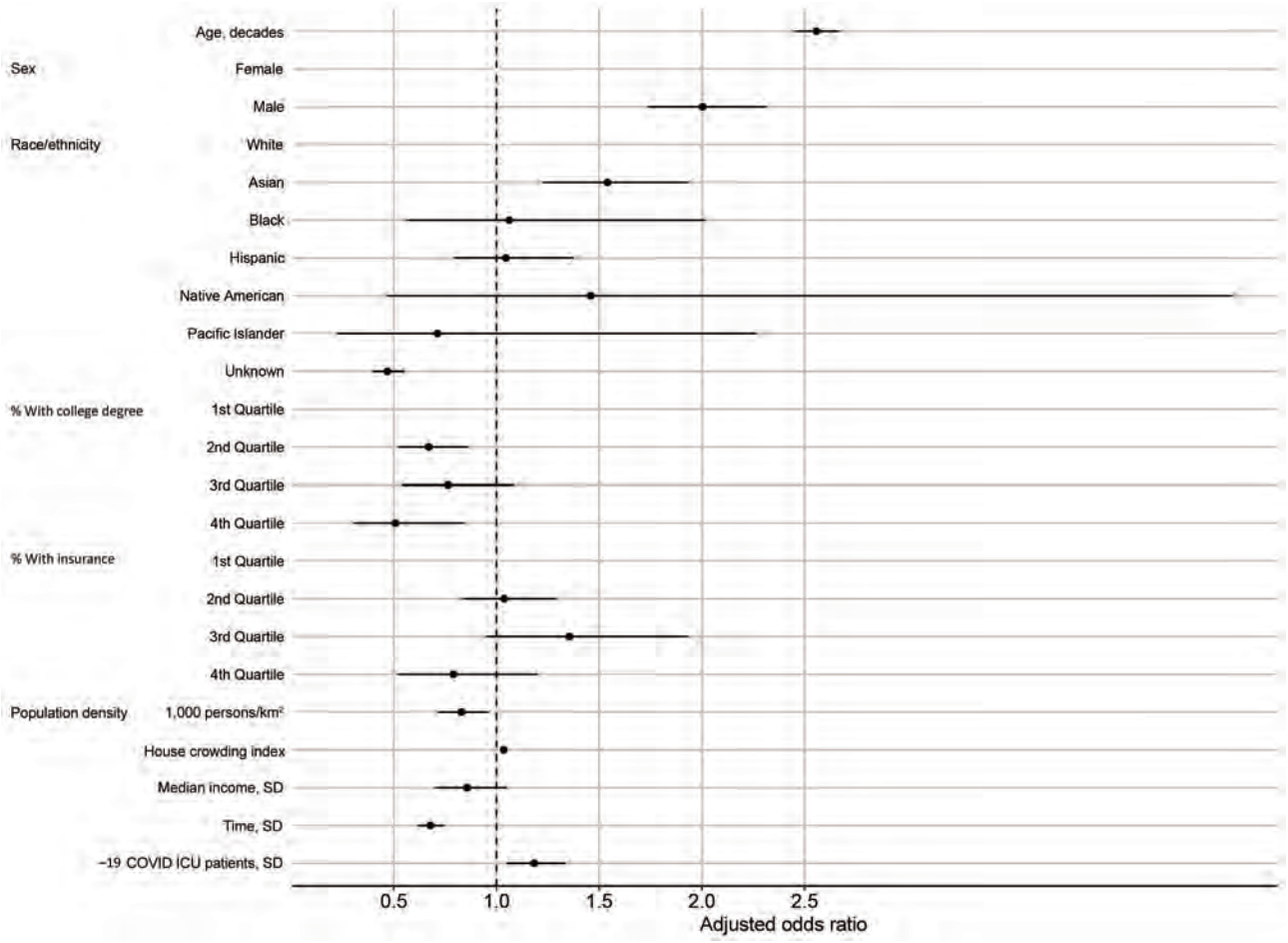

Figure 8. Model-adjusted odds ratios and 95% CIs from the logistic regression for the odds of dying from COVID-19, Orange County, California, USA, July–August 2020. Corresponding data presented in Table 3. COVID-19, coronavirus disease; ICU, intensive care unit.

(Figures 1, 2), growing in size in May and persisting over time. Testing intensity spread throughout the county during this same period.

Consistent with other reports, we also found that age and male sex strongly predict testing positive and COVID-19 associated death (*26*). Intriguingly, whereas older age groups and men and boys were more likely to have symptomatic disease, our population-based serologic survey found that women and girls were more likely than their male counterparts to be seropositive. Hispanic and Latinx persons had higher risk for infection and testing positive, even after controlling for several ZIP code–level socioeconomic factors. Given the consistency of this finding between the models for test positivity and seropositivity, the risk for being infected with SARS-CoV-2 rises above and beyond the risks of living in a ZIP code with high transmission or a ZIP code with low income and low levels of educational attainment. Other studies also note an increased risk for testing positive among Hispanic and Latinx persons (*27*–*29*). Our seroprevalence survey indicates that in OC, this finding is not an artifact of passive case detection but instead represents an actual true greater risk for infection for Hispanic and Latinx persons.

Although persons identifying as Asian were less likely to test positive for SARS-CoV-2, they were more likely to die when infected. This disparity is consistent with national data, though its cause is uncertain (*30*). This pattern may reflect discrepancies in outreach communication to these communities or other socioeconomic and cultural factors (*31*,*32*) and warrants further detailed investigation.

Social determinants of health, defined as "conditions in which people are born, grow, work, live, age, and the wider set of forces and systems," play a critical role in the creation of disparities related to illness, death, and quality of life (*33*). These social determinants include (among other factors) poverty, wealth, educational quality, household and neighborhood

conditions, childhood experience, and social support. Several speculative explanations have been proposed for these sociodemographic patterns related to COVID-19, including living in dense quarters (and this pattern is evident in our analyses). In addition, as the state and local shelter-in-place and social distancing policies were mandated, persons who are independently wealthy or who work in occupations where working from home was a viable option, were more capable of practicing social distancing. Persons from low socioeconomic status areas, by contrast, may have less ability to practice social distancing. Our analyses show that persons from ZIP codes with lower overall educational attainment and health insurance coverage and with higher housing density were more likely to test positive for and die from COVID-19. The association with median household income was more complex and changed over time with regard to test positivity. However, we also find that persons from ZIP codes with lower median household income were also more likely to be seropositive for SARS-CoV-2. These findings underscore the importance of understanding contextual factors surrounding infectious disease outbreaks.

Study limitations include that county-reported testing and mortality data did not include individual-level information on income, education, and insurance. These variables were only available at the ZIP

Table 4. Logistic regression results for odds ratio of testing seropositive for SARS-CoV-2, Orange County, California, USA, July–August 2020*

Characteristic	No. (%) SARS-CoV-2 seropositive, n = 350	No. (%) Total tested, n = 2,604	Adjusted odds ratio (95% CI)†
Age group, y			
18–24	19 (5.43)	158 (5.35)	Referent
25–29	31 (8.86)	234 (7.92)	1.09 (0.58–2.04)
30–34	33 (9.43)	275 (9.31)	0.97 (0.52–1.81)
35–39	35 (10)	328 (11.1)	0.85 (0.46–1.56)
40–49	83 (23.71)	651 (22.04)	1.08 (0.62–1.87)
50–59	82 (23.43)	659 (22.31)	1.09 (0.62–1.89)
60–69	46 (13.14)	418 (14.15)	1.02 (0.56–1.86)
70–79	18 (5.14)	188 (6.36)	0.93 (0.45–1.91)
≥80	3 (0.86)	43 (1.46)	0.64 (0.18–2.32)
Sex			
F	222 (63.43)	1,668 (56.47)	Referent
M	128 (36.57)	1,286 (43.53)	0.75 (0.59–0.94)
Race or ethnicity‡			
White	108 (30.86)	1,228 (41.57)	Referent
Asian	47 (13.43)	435 (14.73)	1.25 (0.85–1.82)
Black	5 (1.43)	42 (1.42)	1.28 (0.48–3.37)
Hispanic	162 (46.29)	1,010 (34.19)	1.54 (1.17–2.03)
Pacific Islander	3 (0.86)	12 (0.41)	3.89 (1.04–14.65)
Unknown	25 (7.14)	227 (7.68)	1.25 (0.78–2)
% With college degree in ZIP code			
1st quartile	158 (45.14)	937 (31.72)	Referent
2nd quartile	92 (26.29)	893 (30.23)	0.98 (0.65–1.46)
3rd quartile	59 (16.86)	644 (21.8)	1.15 (0.64–2.04)
4th quartile	41 (11.71)	480 (16.25)	1.15 (0.59–2.22)
% With insurance in ZIP code			
1st quartile	154 (44)	928 (31.42)	Referent
2nd quartile	91 (26)	812 (27.49)	0.98 (0.67–1.43)
3rd quartile	54 (15.43)	597 (20.21)	0.99 (0.56–1.76)
4th quartile	51 (14.57)	617 (20.89)	0.95 (0.51–1.76)
Population density, × 1,000 persons/km^2			1.02 (0.81–1.29)
House crowding index			1.00 (0.96–1.04)
Median income (SD)			0.76 (0.57–1.00)
% Persons in ZIP code SARS-CoV-2 positive >10%§			1.25 (0.80–1.96)

*This cross sectional survey was conducted July 10–August 16, 2020. SARS-CoV-2, severe acute respiratory syndrome coronavirus 2.
†Model intercept represents odds of testing seropositive for SARS-CoV-2 for a White female diagnosed with SARS-CoV2 in the 18–24 years age group in a ZIP code in the first quartile of college degree and insured with the average population density, and average percentage of SARS-CoV-2 positive persons in Orange County. The odds of this person testing seropositive is estimated to be 0.074 (95% CI 0.031–0.178). 95% CIs computed with robust SEs.
‡For comparison, the estimated race/ethnicity makeup of Orange County in 2021 is non-Hispanic White (38.6%, n = 1,223,157; Black/African American (1.6%, n = 52,696); American Indian or Alaskan Native (0.3%, n = 6,018); Asian (21.1%, n = 685,728); Native Hawaiian or Pacific Islander (0.3%, n = 8,885); other or multiple races (3.1%, n = 100,297); Hispanic or Latinx (35.0%, n = 1,115,740) (*21*). American Indian or Alaska Native race group not included in analysis because of lack of data; no person of this race group tested seropositive.
§Number of persons who tested positive in person's ZIP code reported to Orange County Public Health Department during March 1–August 16, 2020, divided by estimated population of ZIP code.

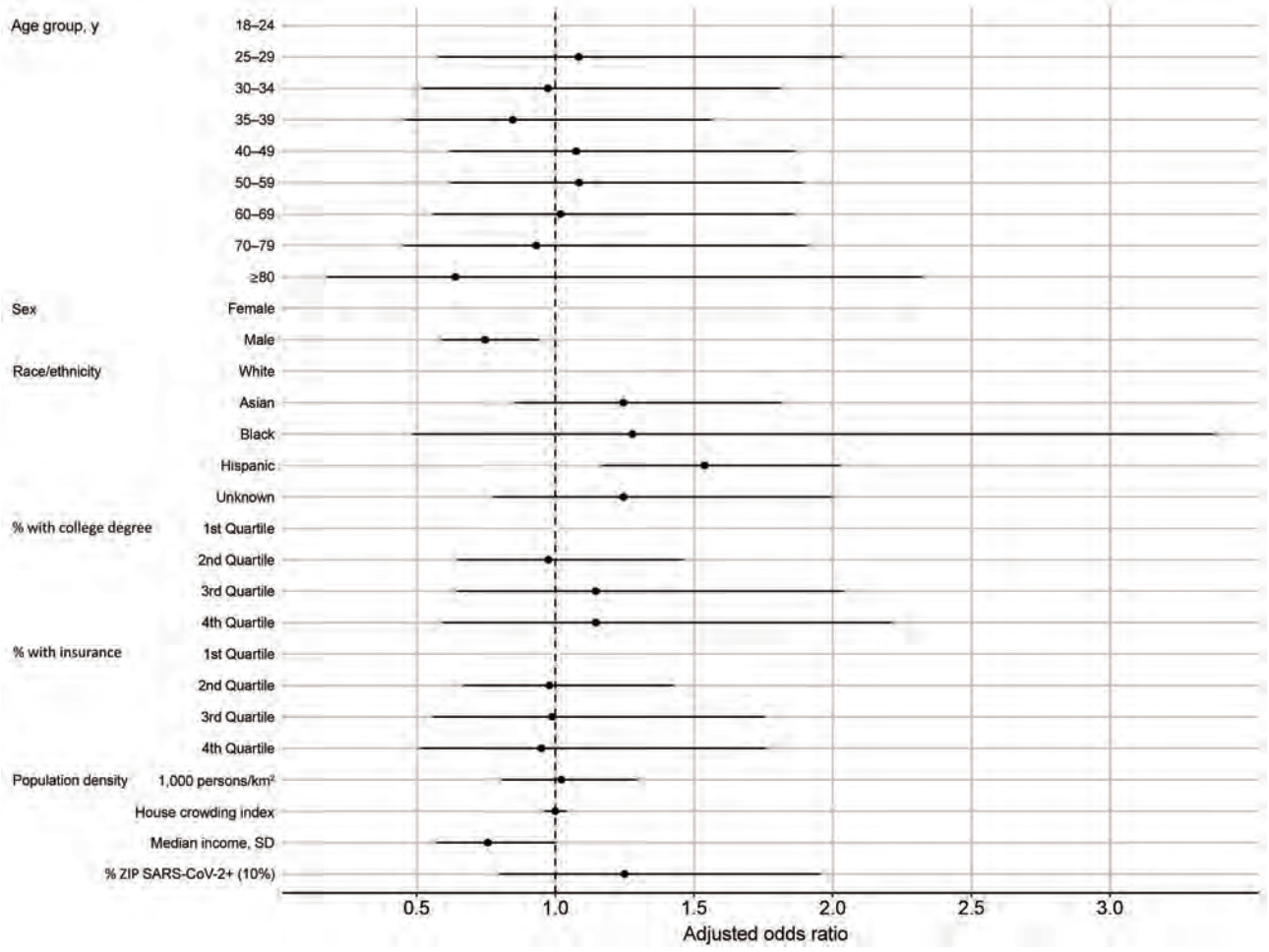

Figure 9. Model-adjusted odds ratios and 95% CIs from the logistic regression for the odds of being seropositive for severe acute respiratory syndrome coronavirus 2, Orange County, California, USA, July–August 2020. Corresponding data presented in Table 4. +, positive.

code–level, and ZIP codes are unlikely to adequately represent important spatial units. Our seroprevalence survey occurred during July 10–August 16, 2020. We limited our analyses of test positivity and risk for death to before August 16, to correspond with the end of the seroprevalence survey. However, the survey occurred over a period of just over a month, during which time the cumulative incidence was changing. Missing data on race and ethnicity (72% of all official test records) and small counts of some racial and ethnic groups may have affected our findings for groups with low counts in this analysis. Even when race or ethnicity data were available, they were broad categories (e.g., Asian rather than specific Asian ethnicities), which is a major limitation of these data, and efforts are being made to improve collection of race and ethnicity data. A major challenge over the course of this pandemic has been collecting data in a standardized format when test results are being reported from a wide variety of laboratories that are affiliated with many different private and governmental entities. We do not believe that the race and ethnicity data are missing at random but also are not able to assess the magnitude of bias that this possibility would introduce, especially given that race and ethnicity appear to be risk factors for infection.

Study strengths include the diversity of OC in terms of socioeconomic and demographic predictors, which provide sufficient power to investigate these factors in our analyses. California was also one of the first states to issue an executive order for residents to stay home, providing data for several months when only essential workers were permitted to work outside the home. Our analyses were able to identify temporal shifts in the demographics of COVID-19 test positivity that likely reflect disparities related to occupation type that are further amplified by household characteristics. Finally, we are able to assess differences in

risk for infection and test positivity by comparing our population-level serologic survey to routinely collected (passive) data from county statistics.

The reasons for the spatial, sociodemographic, and economic patterns we discovered are likely complex and broadly related to issues of accessing healthcare and general social determinants of health. The clear disparities in how this disease has manifested in OC point toward the need for approaches that are socio-culturally appropriate and have a focus on health equity. The large amount of missing data and the collection of only broad categories of race and ethnicity information highlight the need for improved data collection. Finally, measures that focus on the hardest-hit communities, including those that involve working with community-based organizations who have experience working with hard-hit demographic and geographic groups to ensure equitable access to health services, may serve as efficient points of intervention for COVID-19.

Acknowledgments

We acknowledge the actOC research manager, Emily Drum, and the logistical expertise of Bruce Albala, who set up and helped run the seroprevalence study. Many University of California–Irvine students and alumni were involved in collecting blood samples for the serologic survey, and we gratefully acknowledge their contributions. We are grateful to members of the Felgner Laboratory who made the serologic survey possible under sometimes trying conditions (especially Rie Nakajima, Aarti Jain, and Rafael Ramiro de Assis). Guiyun Yan and Xiaoming Wang provided space for cold storage. We also acknowledge conversations with colleagues and community leaders with regard to social determinants of health and health equity, including Sora Tanjasiri, Mary Anne Foo, Brittany Morey, Ahn Ellen, Tricia Nguyen, America Bracho, and many others.

The serologic survey was funded through a contract with OCHCA (contract no. MA-042-20011978).

T.B. and B.B.A. were both principal investigators for the serologic survey. B.B.A. also oversaw the data exchange between University of California, Irvine and Orange County Health Care Agency.

About the Author

Dr. Parker is an infectious disease epidemiologist with expertise in spatial epidemiology, demography, and biomedical anthropology. He is an assistant professor in public health at the University of California, Irvine, and the director of the Global Health Research, Education, and Translation Initiative.

References

1. Dowd JB, Andriano L, Brazel DM, Rotondi V, Block P, Ding X, et al. Demographic science aids in understanding the spread and fatality rates of COVID-19. Proc Natl Acad Sci U S A. 2020;117:9696–8. https://doi.org/10.1073/pnas.2004911117
2. Dorn AV, Cooney RE, Sabin ML. COVID-19 exacerbating inequalities in the US. Lancet. 2020;395:1243–4. https://doi.org/10.1016/S0140-6736(20)30893-X
3. Yancy CW. COVID-19 and African Americans. JAMA. 2020;323:1891–2. https://doi.org/10.1001/jama.2020.6548
4. Garg S, Kim L, Whitaker M, O'Halloran A, Cummings C, Holstein R, et al. Hospitalization rates and characteristics of patients hospitalized with laboratory-confirmed coronavirus disease 2019—COVID-NET, 14 states, March 1–30, 2020. MMWR Morb Mortal Wkly Rep. 2020;69:458–64. https://doi.org/10.15585/mmwr.mm6915e3
5. Dondorp AM, Hayat M, Aryal D, Beane A, Schultz MJ. Respiratory support in novel coronavirus disease (COVID-19) patients, with a focus on resource-limited settings. Am J Trop Med Hyg. 2020;102:1191–7. https://doi.org/10.4269/ajtmh.20-0283
6. Bhatraju PK, Ghassemieh BJ, Nichols M, Kim R, Jerome KR, Nalla AK, et al. Covid-19 in critically ill patients in the Seattle region—case series. N Engl J Med. 2020;382:2012–22. https://doi.org/10.1056/NEJMoa2004500
7. Yang X, Yu Y, Xu J, Shu H, Xia J, Liu H, et al. Clinical course and outcomes of critically ill patients with SARS-CoV-2 pneumonia in Wuhan, China: a single-centered, retrospective, observational study. Lancet Respir Med. 2020;8:475–81. https://doi.org/10.1016/S2213-2600(20)30079-5
8. Grasselli G, Pesenti A, Cecconi M. Critical care utilization for the COVID-19 outbreak in Lombardy, Italy: early experience and forecast during an emergency response. JAMA. 2020;323:1545–6. https://doi.org/10.1001/jama.2020.4031
9. Maxmen A. Thousands of coronavirus tests are going unused in US labs. Nature. 2020;580:312–3. https://doi.org/10.1038/d41586-020-01068-3
10. Orange County Health Care Agency. OC Health Care Agency confirms first case of novel coronavirus. 2020 Jan [cited 2021 Jun 3]. https://mailchi.mp/ochca/novelcoronavirus
11. World Health Organization. Statement on the second meeting of the International Health Regulations (2005) Emergency Committee regarding the outbreak of novel coronavirus (2019-nCoV) [cited 2021 Jun 3]. https://www.who.int/news/item/30-01-2020-statement-on-the-second-meeting-of-the-international-health-regulations-(2005)-emergency-committee-regarding-the-outbreak-of-novel-coronavirus-(2019-ncov)
12. US Department of Health and Human Services. Determination that a public health emergency exists. 2020 Jan [cited 2021 Jun 3]. https://www.phe.gov/emergency/news/healthactions/phe/Pages/2019-nCoV.aspx
13. California Department of Public Health. CDC confirms possible first instance of COVID-19 community transmission in California [cited 2021 Jun 3]. https://www.cdph.ca.gov/Programs/OPA/Pages/NR20-006.aspx
14. Villasanta A. Coronavirus USA update: Santa Clara County extends local health emergency over nCov. International Business Times. 2020 [cited 2021 Jun 3]. https://www.ibtimes.com/coronavirus-usa-update-santa-clara-county-extends-local-health-emergency-over-ncov-2919607
15. Sisson P. County declares local health emergency to aid coronavirus response. San Diego Union–Tribune [cited 2021 Jun 3]. https://www.sandiegouniontribune.com/news/

health/story/2020-02-14/county-declares-local-health-emergency-to-aid-coronavirus-response
16. Anderson P. Orange County declares emergency due to coronavirus. NBC Los Angeles [cited 2021 Jun 3]. https://www.nbclosangeles.com/news/local/orange-county-declares-emergency-due-to-coronavirus/2321434
17. Office of the Mayor of San Francisco. City of San Francisco moves proactively to prepare for possible novel coronavirus activity in the community. 2020 Feb 25 [cited 2021 Jan 19]. https://sfmayor.org/article/city-san-francisco-moves-proactively-prepare-possible-novel-coronavirus-activity-community
18. Orange County Operational Area Emergency Operations Center. Press release # 010: county issues amended health order and guidance. 2020 Mar 18 [cited 2020 Dec 18]. https://cms.ocgov.com/civicax/filebank/blobdload.aspx?BlobID=114421
19. State of California. Essential workforce [cited 2020 Dec 18]. https://covid19.ca.gov/essential-workforce
20. Rho HJ, Brown H. Fremstad S. A basic demographic profile of workers in frontline industries [cited 2021 Jan 19]. https://cepr.net/a-basic-demographic-profile-of-workers-in-frontline-industries
21. Orange County's Healthier Together. OC dashboard [cited 2020 Dec 18]. http://www.ochealthiertogether.org/indicators/index/dashboard?alias=ocdashboard&localeId=267&page=2&card=1
22. Transforming Orange County. Transforming Orange County: assets and needs of Asian Americans and Native Hawaiians and Pacific Islanders [cited 2020 Dec 18]. https://transformingoc.advancingjustice-oc.org
23. Bruckner TA, Parker DM, Bartell SM, Vieira VM, Khan S, Noymer A, et al. Estimated seroprevalence of SARS-CoV-2 antibodies among adults in Orange County, California. Sci Rep. 2021;11:3081. https://doi.org/10.1038/s41598-021-82662-x
24. Anselin L. Local indicators of spatial association. Geogr Anal. 1995;27:93–115. https://doi.org/10.1111/j.1538-4632.1995.tb00338.x
25. Zhou G, Afrane YA, Malla S, Githeko AK, Yan G. Active case surveillance, passive case surveillance and asymptomatic malaria parasite screening illustrate different age distribution, spatial clustering and seasonality in western Kenya. Malar J. 2015;14:41. https://doi.org/10.1186/s12936-015-0551-4
26. Mi J, Zhong W, Huang C, Zhang W, Tan L, Ding L. Gender, age and comorbidities as the main prognostic factors in patients with COVID-19 pneumonia. Am J Transl Res. 2020;12:6537–48.
27. Ogedegbe G, Ravenell J, Adhikari S, Butler M, Cook T, Francois F, et al. Assessment of racial/ethnic disparities in hospitalization and mortality in patients with COVID-19 in New York City. JAMA Netw Open. 2020;3:e2026881. https://doi.org/10.1001/jamanetworkopen.2020.26881
28. Rubin-Miller L, Alban C. COVID-19 racial disparities in testing, infection, hospitalization, and death: analysis of epic patient data. 2020 Sep 16 [cited 2021 Jan 8]. https://www.kff.org/coronavirus-covid-19/issue-brief/covid-19-racial-disparities-testing-infection-hospitalization-death-analysis-epic-patient-data
29. Webb Hooper M, Nápoles AM, Pérez-Stable EJ. COVID-19 and racial/ethnic disparities. JAMA. 2020;323:2466–7. https://doi.org/10.1001/jama.2020.8598
30. Centers for Disease Control and Prevention. Coronavirus disease 2019 (COVID-19). 2020 [cited 2021 Jan 9]. https://www.cdc.gov/coronavirus/2019-ncov/covid-data/investigations-discovery/hospitalization-death-by-race-ethnicity.html
31. Gover AR, Harper SB, Langton L. Anti-Asian hate crime during the COVID-19 pandemic: exploring the reproduction of inequality. Am J Crim Justice. 2020;45:1–21. https://doi.org/10.1007/s12103-020-09545-1
32. Ng E. The pandemic of hate is giving novel coronavirus disease (COVID-19) a helping hand. Am J Trop Med Hyg. 2020;102:1158–9. https://doi.org/10.4269/ajtmh.20-0285
33. World Health Organization. Social determinants of health [cited 2020 Dec 18]. https://www.who.int/westernpacific/health-topics/social-determinants-of-health

Address for correspondence: Daniel M. Parker, University of California, Irvine, 2070 Anteater Instruction and Research Bldg, Mail Code 3957, Irvine, CA 92697, USA; email: dparker1@hs.uci.edu

Risk Assessment for Highly Pathogenic Avian Influenza A(H5N6/H5N8) Clade 2.3.4.4 Viruses

Christine H.T. Bui,[1] Denise I.T. Kuok,[1] Hin Wo Yeung, Ka-Chun Ng, Daniel K.W. Chu, Richard J. Webby, John M. Nicholls, J.S. Malik Peiris, Kenrie P.Y. Hui, Michael C.W. Chan

The numerous global outbreaks and continuous reassortments of highly pathogenic avian influenza (HPAI) A(H5N6/H5N8) clade 2.3.4.4 viruses in birds pose a major risk to the public health. We investigated the tropism and innate host responses of 5 recent HPAI A(H5N6/H5N8) avian isolates of clades 2.3.4.4b, e, and h in human airway organoids and primary human alveolar epithelial cells. The HPAI A(H5N6/H5N8) avian isolates replicated productively but with lower competence than the influenza A(H1N1)pdm09, HPAI A(H5N1), and HPAI A(H5N6) isolates from humans in both or either models. They showed differential cellular tropism in human airway organoids; some infected all 4 major epithelial cell types: ciliated cells, club cells, goblet cells, and basal cells. Our results suggest zoonotic potential but low transmissibility of the HPAI A(H5N6/H5N8) avian isolates among humans. These viruses induced low levels of proinflammatory cytokines/chemokines, which are unlikely to contribute to the pathogenesis of severe disease.

The genetic evolution of the highly pathogenic avian influenza (HPAI) subtype H5N1 A/goose/Guangdong/1/1996 lineage has resulted in the divergence and generation of 10 distinct virus clades (0–9) and multiple subclades (*1*,*2*). Since early 2014, novel reassortant HPAI A(H5N6/H5N8) viruses of clade 2.3.4.4 have gained attention because of their rapid evolution and global spread. They have been widely distributed among regions of Asia, Europe, and Africa and have been reported in North America (mainly in the United States and Canada), accompanied by further evolution into subclades 2.3.4.4a–h (*3*). Many avian species, including wild aquatic birds, domestic poultry, and zoo birds, are susceptible to the infection or support transmission of clade 2.3.4.4 viruses, resulting in unprecedented panzootic waves accompanied by massive culling and major economic losses to the poultry industry (*1*,*2*). Detection of HPAI H5N6 clade 2.3.4.4 viruses in cats, pigs, and humans has also been reported (*4*–*6*). As of May 2021, there have been 29 laboratory-confirmed cases of human infection, including at least 16 deaths (*3*,*6*–*8*). The isolated viruses mainly belong to subclades 2.3.4.4a, b, d, g, and h. These cases in humans were mainly sporadic and linked to direct contact with poultry or contaminated poultry market environments (*7*). The initial clinical signs in hospitalized patients were influenza-like, followed by severe pneumonia, acute respiratory distress syndrome, and multiple organ failure in deceased patients (*7*,*8*). Natural infection of mammals by HPAI H5N8 clade 2.3.4.4 viruses is not as commonly reported.

In February 2021, the Russian Federation reported detecting 7 cases of asymptomatic human infection with HPAI H5N8 clade 2.3.4.4b viruses in poultry farm workers, linked to a poultry outbreak (*9*). However, a serologic study revealed the presence of antibodies to an HPAI H5N8 clade 2.3.4.4 virus in 61 of 760 serum samples from persons who had had contact with infected or deceased birds during the 2016–17 HPAI outbreaks in Russia (*10*), providing evidence of overlooked human infection.

The persistent circulation of clade 2.3.4.4 viruses among bird populations enables continuous reassortment with prevailing low pathogenicity avian influenza (LPAI) viruses. Together with intercontinental

Author affiliations: The University of Hong Kong, Hong Kong, China (C.H.T. Bui, D.I.T. Kuok, H.W. Yeung, K.-C. Ng, D.K.W. Chu, J.M. Nicholls, J.S.M. Peiris, K.P.Y. Hui, M.C.W. Chan); St. Jude Children's Research Hospital, Memphis, Tennessee, USA (R.J. Webby)

DOI: https://doi.org/10.3201/eid2710.210297

[1]These first authors contributed equally to this article.

dissemination through wild aquatic bird migration and potential interspecies transmission leading to mammalian adaptation, this circulation poses a major risk to human health should clade 2.3.4.4 viruses gain efficient human-to-human transmissibility, especially when immunity in the general population is lacking (*1*,*2*,*8*). Some HPAI H5N6/H5N8 clade 2.3.4.4 viruses have been shown to bind both α2,6- (human) and α2,3- (avian) linked sialic acid receptors, and more than half of HPAI H5N6 clade 2.3.4.4 isolates from humans found in GISAID acquired E627K or D701N substitutions in the polymerase basic (PB) 2 protein, which play prominent roles in mammalian adaptation of avian influenza viruses (*8*,*11*–*13*). An HPAI H5N8 clade 2.3.4.4 virus quickly acquired virulence markers, enhancing its virulence in mice and replication and polymerase activity in human cell lines within 5 murine passages (*14*), suggesting potential rapid adaptation after repeated virus introduction.

Surveillance efforts and characterization of clade 2.3.4.4 viruses provide insight into their pathogenicity and transmissibility, which can be used to prevent future outbreaks and assess zoonotic potential. Experimentally inoculated ferrets, mice, and guinea pigs displayed considerable variation in pathogenicity, and transmission by direct contact was demonstrated in guinea pig and ferret models (*8*,*11*–*13*,*15*,*16*). A few studies have also indicated efficient replication of HPAI H5N6 clade 2.3.4.4 viruses in human bronchus and lung explants and in primary human bronchial epithelial cells, which might have been linked to their respective successful infection of humans and direct-contact transmission among ferrets (*16*,*17*).

To further build on these findings, we used physiologically relevant 3-dimensional human airway organoids and primary human alveolar epithelial cells to investigate the tropism and innate host responses of 5 HPAI H5N6/H5N8 clades 2.3.4.4b, e, and h avian isolates from 2016–2018. We compared these responses to those of earlier human isolates of HPAI H5N1 clades 0 and 2.3.2.1b, HPAI H5N6 clade 2.3.4.4, an influenza A(H1N1)pdm09 virus (pH1N1), and an LPAI H5N8 virus.

Methods

Viruses

We used 3 HPAI H5N6 avian isolates: A/environment/Hong Kong/WCRB-01/2018 (avHPAI H5N6/DK01) of clade 2.3.4.4h, isolated from the outside of a chilled duck (GISAID accession no. EPI_ISL_885144); A/spoonbill/HK/17-18259/2017 (avHPAI H5N6/18259) of clade 2.3.4.4b, isolated from a trachea tissue sample of a dead black-faced spoonbill (GISAID accession no. EPI_ISL_885145); and A/northern pintail/HK/MP692/2016 (avHPAI H5N6/MP692) of clade 2.3.4.4e, isolated from a fecal sample of a northern pintail (GISAID accession no. EPI_ISL_885147). We also used 2 HPAI H5N8 clade 2.3.4.4b avian isolates: A/chicken/Egypt/F1366A/2017 (avHPAI H5N8/636099) (GISAID accession no. EPI_ISL_885148) and A/grey-headed gull/Uganda/200144/2017 (avHPAI H5N8/642613) (GISAID accession no. EPI_ISL_885149); 1 HPAI H5N6 clade 2.3.4.4 human isolate A/Guangzhou/39715/2014 (HPAI H5N6/39715) from the throat swab of a 59-year-old male patient on day 8 of illness (GenBank accession no. KP765785-KP765792); 2 HPAI H5N1 human isolates, A/Hong Kong/483/1997 (HPAI H5N1/483) of clade 0 isolated from a person with a fatal case (GenBank accession nos. GU052096-GU052104, AF258820, AF084277) and A/Shenzhen/1/2011 (HPAI H5N1/SZ1) of clade 2.3.2.1b (GISAID accession no. EPI_ISL_891209); LPAI H5N8 avian isolate A/northern pintail/Hong Kong/MP5883/2004 (avLPAI H5N8/MP5883) (GISAID accession no. EPI_ISL_885151); and pH1N1 virus A/Hong Kong/415742/2009.

We prepared virus stocks in MDCK cells with limited passages. To determine virus titers, we used 50% tissue culture infectious dose ($TCID_{50}$) assays.

Human Airway Organoids

We cultured human airway organoids from cells isolated from human lung tissue and infected in 6 log $TCID_{50}$/mL virus for 1 h at 37°C as previously described (*18*,*19*). We collected supernatant at 1, 24, 48, and 72 h after infection for virus titration by $TCID_{50}$ assay. We fixed organoids in 4% paraformaldehyde at postinfection hours 24 and 48 for immunohistochemical double staining and collected cell lysates at postinfection hour 24 for measurement of mRNA expression.

Primary Human Alveolar Epithelial Cells

We isolated alveolar epithelial cells from human lung tissues, cultured, and infected at multiplicities of infection (MOIs) of 0.01 and 2 for 1 h at 37°C as previously described (*17*,*18*). We collected supernatant at 1, 24, 48, and 72 h after infection for virus titration by $TCID_{50}$ assay and collected cell lysates at 24 h after infection to measure mRNA expression. We compiled a description of our detailed study methods (Appendix 1, https://wwwnc.cdc.gov/EID/article/27/10/21-0297-App1.pdf).

Results

Productive Replication

All 5 HPAI (H5N6/H5N8) avian isolates demonstrated productive replication in human airway organoids and alveolar epithelial cells (MOI 0.01); by 72 h after infection, mean peak titers were 3.7–5.1 log $TCID_{50}$/mL for human airway organoids and 4.6–7.0 log $TCID_{50}$/mL for alveolar epithelial cells (Figure, panels A, B). Mean peak titers of HPAI H5 isolates

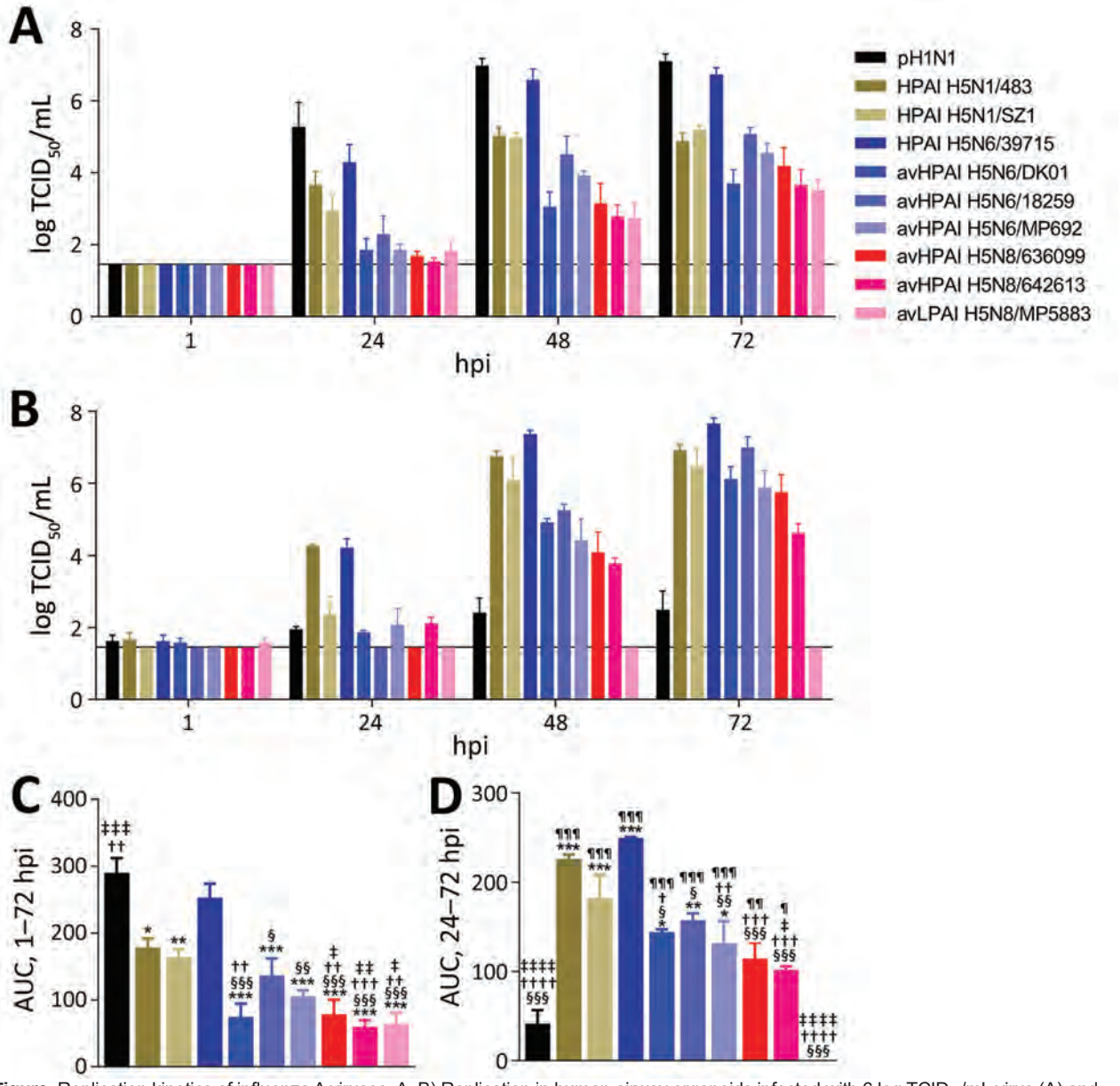

Figure. Replication kinetics of influenza A viruses. A, B) Replication in human airway organoids infected with 6 log $TCID_{50}$/mL virus (A) and primary human alveolar epithelial cells infected at multiplicity of infection 0.01 at 37°C (B). Virus titers in culture medium (mean ± SEM, n≥3) were determined by $TCID_{50}$ assays with a detection limit of 1.5 log $TCID_{50}$/mL, denoted by a solid line. Statistical significance between virus titers at each time point after infection is provided in Appendix 1 Figure 1 (https://wwwnc.cdc.gov/EID/article/27/10/21-0297-App1.pdf). C, D) The areas under the replication kinetic curves above the detection limit in human airway organoids from 1 to 72 hpi (C) and alveolar epithelial cells from 24 to 72 hpi (mean ± SEM, n ≥3) (D). Statistical significance between AUC values was analyzed by using 1-way analysis of variance with Bonferroni posttests. *p≤0.01; **p≤0.001; ***p≤0.0001 (compared with pH1N1); †p≤0.05; ††p≤0.01; †††p≤0.001; ††††p≤ 0.0001 (compared with HPAI H5N1/483); ‡p≤0.05; ‡‡p≤0.01; ‡‡‡p≤ 0.001; ‡‡‡‡p≤0.0001 (compared with HPAI H5N1/SZ1); §p≤0.01; §§p≤0.001; §§§ p≤0.0001 (compared with HPAI H5N6/39715); ¶p≤0.01; ¶¶p≤ 0.001; ¶¶¶p≤0.0001 (compared with avLPAI H5N8/MP5883). AUC, area under the curve; av, avian; HPAI, highly pathogenic avian influenza; hpi, hours postinfection; LPAI, low pathogenicity avian influenza; pH1N1, influenza A(H1N1)pdm09 virus; $TCID_{50}$, 50% tissue culture infectious dose.

from humans were 5.0–6.7 log $TCID_{50}$/mL for human airway organoids and 6.5–7.7 log $TCID_{50}$/mL for alveolar epithelial cells. As expected, pH1N1 replicated to the highest mean peak titer of 7.1 log $TCID_{50}$/mL in human airway organoids but reached only 2.5 log $TCID_{50}$/mL in alveolar epithelial cells. AvLPAI H5N8/MP5883 replicated to a mean peak titer of 3.5 log $TCID_{50}$/mL in human airway organoids but did not show any detectable replication in alveolar epithelial cells. When we compared the replication kinetic areas under the curve (AUCs), which estimated the total quantity of virus released, we found comparable AUC values among the HPAI H5N6/H5N8 avian isolates but lower AUC values for HPAI H5N6/H5N8 avian isolates than for the HPAI H5N6/39715 human isolate in human airway organoids and in alveolar epithelial cells (Figure, panels C, D). The AUC values of HPAI H5N6/H5N8 avian isolates were also lower than those of pH1N1 in human airway organoids and the HPAI H5N1/483 human isolate in alveolar epithelial cells, except for the statistically insignificant AUC values between avHPAI H5N6/18259 and HPAI H5N1/483 in alveolar epithelial cells.

Cellular Tropism

According to immunohistochemistry double staining, avHPAI H5N6/18259, avHPAI H5N6/MP692, and avHPAI H5N8/636099 infected acetyl-α-tubulin–positive ciliated cells, SCGB1A1–positive/CC10–positive secretory club cells, MUC5AC–positive secretory goblet cells, and p63-α–positive basal cells, similar to pH1N1, HPAI H5N1/483, HPAI H5N6/39715, and avLPAI H5N8/MP5883 (Appendix 2 Figure 1, https://wwwnc.cdc.gov/EID/article/27/10/21-0297-App2.pdf). avHPAI H5N6/DK01 and HPAI H5N1/SZ1 infected ciliated cells, club cells, and goblet cells. avHPAI H5N8/642613 infected only club cells.

Proinflammatory Cytokine and Chemokine Induction

We studied induction of proinflammatory cytokines and chemokines by using HPAI H5N1/483 as a high inducing virus control and pH1N1 as a low inducing virus control. At 24 h after infection, HPAI H5N1/483 tended to induce higher mRNA levels of IFN-β, IFN-λ1, CCL5, CXCL10, TNFα, IL-6, ISG15, and MX1 than most HPAI H5N6/H5N8 avian isolates in human airway organoids and in alveolar epithelial cells (MOI 2); we observed statistical significance for IFN-λ1, CXCL10, and MX1 in human airway organoids and IFN-β, IFN-λ1, CCL5, CXCL10, ISG15, and MX1 in alveolar epithelial cells (Appendix 2 Figure 2). We found no statistically significant differences in the mRNA levels of these genes between HPAI H5N6/H5N8 avian isolates, HPAI H5N6/39715, pH1N1, and avLPAI H5N8/MP5883 in human airway organoids. Similarly, we detected only a few differences between their IFN-β, TNFα, ISG15, and MX1 mRNA levels in alveolar epithelial cells.

Molecular Comparisons

Molecular analysis revealed that all 5 HPAI H5N6/H5N8 avian isolates and the 3 HPAI H5 human isolates contained a 5 to 6 basic residue polybasic cleavage site (Appendix 2 Table), characteristic of a highly pathogenic phenotype. We detected amino acid differences in the receptor-binding sites and glycosylation sites of the hemagglutinin (HA) proteins, which may contribute to altered receptor-binding preference among the 9 HPAI/LPAI H5 viruses. Of note, all H5 viruses possessed ≥1 of the 7 observed HA amino acid mutations previously reported to increase virus binding to α2,6-linked sialic acid receptors: 94N, 133A, 154D, 155N, 156A, 188I, and 189R (*20*–*23*). HPAI H5N6/H5N8 viruses and HPAI H5N1/SZ1 also contained a single or double HA amino acid mutation(s), 218Q and 223R, required for binding fucosylated α2,3-linked sialic acid receptors (*24*). Of the 29 molecular marker positions associated with virulence, transmission, replication efficiency, and adaptation in mammals, which were differentially expressed among the 9 H5 viruses in neuraminidase (NA), PB2, PB1, PB1-F2, polymerase acidic, nucleocapsid, matrix (M) 1, M2, nonstructural (NS) 1 and NS2 proteins (*11*,*17*,*25*–*34*), most (20) molecular markers were found in HPAI H5N1/483 viruses; 8–11 in HPAI H5N1/SZ1 and HPAI H5N6 viruses, except for avHPAI H5N6/18259, which contained only 2, and 4–6 in HPAI/LPAI H5N8 viruses. The well-known mammalian adaptation marker PB2 627K was detected in only 2 HPAI H5 human isolates, HPAI H5N1/483 and HPAI H5N6/39715; PB2 701N was not detected in any of the H5 viruses. The NA 96A and M2 31N mutations, which confer resistance, were observed in avHPAI H5N6/18259 (resistant to zanamivir and oseltamivir) and avHPAI H5N6/MP692 (resistant to amantadine and rimantadine) (*35*, *36*).

Receptor Binding

We used untreated and desialylated 0.5% turkey red blood cells (TRBCs) to determine the receptor-binding specificities of the HPAI H5N6/H5N8 avian isolates. Cleavage of α2,3-linked unbranched sialic acid by Glyko Sialidase S (Agilent, https://www.agilent.com) reduced the hemagglutination of avHPAI H5N6/18259 by 16-fold but did not affect

hemagglutination of avHPAI H5N6/DK01, avHPAI H5N6/MP692, avHPAI H5N8/636099, and avHPAI H5N8/642613 (Table). On the other hand, cleavage of both α2,3- and α2,6-linked unbranched sialic acid by Glyko Sialidase C (Agilent) resulted in 2- to 16-fold drops in hemagglutination of avHPAI H5N6/DK01, avHPAI H5N6/MP692, avHPAI H5N8/636099, and avHPAI H5N8/642613. However, there was no further reduction in the level of hemagglutination of avHPAI H5N6/18259 in Sialidase C–treated versus Sialidase S–treated TRBCs. These data suggest that avHPAI H5N6/18259 predominantly binds α2,3-linked sialic acid, but the other 4 HPAI H5N6/H5N8 avian isolates can bind to receptors with α2,6 linkage. Treatment of TRBCs with Sialidase S and Sialidase C similarly abolished the hemagglutination of predominantly α2,3-linked sialic acid binders HPAI H5N1/483 and HPAI H5N6/39715 (*17*, *18*) and partially prevented the hemagglutination of HPAI H5N1/SZ1 and avLPAI H5N8/MP5883. The hemagglutination of predominantly α2,6-linked sialic acid binder pH1N1 (*37*) was not affected by Sialidase S but was partly inhibited by Sialidase C. The ability of the tested viruses, apart from HPAI H5N1/483 and HPAI H5N6/39715, to maintain some hemagglutination to Sialidase C–treated TRBCs suggests their potential to bind to receptors other than sialic acid with α2,3 and α2,6 unbranched linkages.

Discussion

We demonstrated that the 5 HPAI H5N6/H5N8 clade 2.3.4.4b, e, and h avian isolates from 2016–2018 replicated productively and to similar competence in human airway organoids and alveolar epithelial cells. Replication was less efficient than that of pH1N1 and HPAI H5N6/39715 in human airway organoids and HPAI H5N1/483 and HPAI H5N6/39715 in alveolar epithelial cells. The isolates showed differential cellular tropism in human airway organoids; some infected all 4 major epithelial cell types, including ciliated cells, club cells, goblet cells, and basal cells, similar to pH1N1 and the HPAI H5 human isolates. Compared with HPAI H5N1/483, HPAI H5N6/H5N8 clade 2.3.4.4 viruses induced fewer proinflammatory cytokines and chemokines.

Tropism of influenza virus for the human conducting airways and lower lung epithelial cells is a useful parameter for assessing its zoonotic and pandemic threat in terms of receptor-binding capacity, and the World Health Organization has listed infection of human bronchus explants as a reliable risk-assessment platform (*38*). In addition, replication in the conducting airways has been suggested as a prerequisite for influenza virus acquisition of efficient human-to-human transmission (*38*, *39*). We have previously demonstrated that tropism and replication competence of influenza viruses in human airway organoids mimicked those found in human bronchus explants (*18*, *19*). However, human airway organoids are more readily available for studies because they can be easily rescued from long-term cryopreservation and expanded.

In this study, the productive but lower replication competence of HPAI H5N6/H5N8 clade 2.3.4.4b, e, and h avian isolates compared with that of pH1N1, HPAI H5N1/483, and HPAI H5N6/39715 in human airway organoids, alveolar epithelial cells, or both, suggests lower zoonotic potential and transmissibility of these avian isolates in humans. Knowing that pH1N1 was a successful pandemic virus that infected an estimated 20%–27% of the world population during the first year of circulation (*40*) and that HPAI subtypes H5N1 and H5N6 are able to cause zoonotic infection but lack efficient human-to-human transmission to cause a pandemic to date, we could extrapolate that the risk for human-to-human transmission of HPAI H5N6/H5N8 clade 2.3.4.4b, e, and h avian isolates in this study is low but that zoonotic infection caused by direct contact with infected poultry or contaminated environment is possible, as

Table. Effects of desialylation on influenza A virus hemagglutination of turkey red blood cells*

	0.5% Turkey red blood cells		
Virus	Untreated	Sialidase S†	Sialidase C†
Influenza A(H1N1)pdm09	64	64	8
HPAI H5N1/483	256	0	0
HPAI H5N1/SZ1	64	4	4
HPAI H5N6/39715	128	0	0
avHPAI H5N6/DK01	128	128	32
avHPAI H5N6/18259	64	4	4
avHPAI H5N6/MP692	64	64	32
avHPAI H5N8/636099	128	128	8
avHPAI H5N8/642613	256	256	64
avLPAI H5N8/MP5883	32	4	4

*Hemagglutination titers were calculated as the reciprocal of the highest dilution that gave hemagglutination. Experiments were performed in triplicate and led to identical results. Av, avian; HPAI, highly pathogenic avian influenza.
†Agilent (https://www.agilent.com).

in the case of HPAI H5N6/39715 and most previous human cases of HPAI H5N6/H5N8 clade 2.3.4.4 infection (*7*, *8*). Perhaps it would be best to confirm the virus transmissibility in animal models, such as ferrets and guinea pigs. However, the inability of HPAI H5N6/39715 to transmit among ferrets via respiratory droplets (*41*) makes it highly doubtful that the HPAI H5N6/H5N8 clade 2.3.4.4b, e, and h avian isolates in this study would transmit better. It has been shown that replication in human bronchus explants correlates with respiratory droplet transmission of swine influenza viruses in ferrets (*39*). Respiratory droplet transmission of HPAI H5N6/H5N8 clade 2.3.4.4 viruses has not been demonstrated in any animal model examined (*8*,*12*,*13*,*16*,*41*,*42*), which is consistent with their lack of human-to-human spread. However, direct contact transmission of some HPAI H5N6 clade 2.3.4.4 viruses was previously demonstrated in ferrets and guinea pigs (*8*,*12*,*13*,*16*), thus indicating potential risk.

Although transmissibility of the HPAI H5N6/H5N8 clade 2.3.4.4 viruses in humans seems to be low, persons with frequent exposure to poultry and wild birds should be educated to practice precautionary measures because of ongoing outbreaks among avian species. Repeated virus introductions provide a chance for adaptation to enhance virus replication efficiency, virulence, and transmissibility in humans (*14 43*). An avian influenza HPAI H5N1 virus became airborne transmissible among ferrets after acquiring mutations during passage in ferrets (*43*). Moreover, reassortments of viral gene segments in avian species are continuously associated with the evolution of H5Nx viruses (*1*,*2*,*8*).

The lower replication competence of avHPAI H5N6/18259, avHPAI H5N6/MP692, and avHPAI H5N8/636099 compared with that of HPAI H5N6/39715 in human airway organoids, despite being similarly able to infect all 4 major epithelial cell types, may partially be explained by their lack of the mammalian adaptation marker PB2 627K that is present in HPAI H5N6/39715. PB2 627K enhances polymerase activity and avian virus replication in mammalian cells. Likewise, the presence of PB2 627E instead of 627K and a higher preference for α2,6-linked sialic acid among the 5 HPAI H5N6/H5N8 avian isolates may partially be accounted for by their lower replication competence compared with that of HPAI H5N1/483 and HPAI H5N6/39715 in alveolar epithelial cells, which are predominantly lined with α2,3-linked sialic acid receptors (*44*).

Because human respiratory epithelium is the primary target for influenza viruses, knowledge of the innate host responses in the respiratory epithelium, especially that of the alveolar epithelium, on severe influenza infection, such as infection with HPAI H5N1, helps elucidate the pathogenesis of the dysregulated cytokine responses and severe pneumonia associated with the disease. In this study, HPAI H5N6/H5N8 clade 2.3.4.4 viruses, including the HPAI H5N6/39715 human isolate, were found to be low inducers of proinflammatory cytokines and chemokines in alveolar epithelial cells and in human airway organoids, which is unlikely to contribute to the pathogenesis of severe disease. In connection, we found fewer molecular markers associated with virulence in the tested clade 2.3.4.4 viruses compared with HPAI H5N1/483. Our data are consistent with those from previous studies that reported low cytokine/chemokine induction of HPAI H5N6 clade 2.3.4.4 viruses in alveolar epithelial cells and low virulence of clade 2.3.4.4 HPAI H5N8 viruses in humans, ferrets, and mice (*9*,*10*,*16*,*17*,*42*,*45*,*46*). However, those findings cannot help explain the high fatality rate of HPAI H5N6 clade 2.3.4.4 infection in humans and the high cytokine/chemokine levels in the serum of some patients infected with HPAI H5N6 clade 2.3.4.4, which are comparable to those infected with HPAI H5N1 (*7*). One possible explanation may be the differences in virus strains involved. Some studies have pointed out that HPAI H5N6 clade 2.3.4.4 viruses exhibited pronounced strain-specific heterogeneity regarding their capacity to cause severe and fatal disease (*11*,*13*). Another reason maybe the differences in the patients' health conditions, including their ages and underlying medical conditions, in naturally infected patients (*47*). Moreover, apart from innate host responses in the epithelium, other factors (e.g., responses from immune cells and viral tropism for deeper body cells/tissues) are likely to contribute to the final outcomes of the viral infection.

Previous studies that used different receptor-binding assays demonstrated both dual receptor-binding preference and preference to α2,3-linked sialic acid of H5 clade 2.3.4.4 viruses (*13*,*16*,*17*,*48*). Although avHPAI H5N6/18259 predominantly bound α2,3-linked sialic acid in our desialylation–hemagglutination assay, it showed comparable productive replication to the 4 α2,6-linked sialic acid–binding HPAI H5N6/H5N8 avian isolates in human airway organoids, which are predominantly lined with α2,6-linked sialic acid receptors (*19*). It also showed tropism for all 4 major epithelial cell types infected by the predominantly α2,6-linked sialic acid binder pH1N1 in human airway organoids.

Likewise, Kwon et al. showed efficient replication of 2 HPAI H5N6/H5N8 clade 2.3.4.4 avian viruses with strong preferential binding to α2,3-linked sialic acid in human bronchial epithelial cells (*16*). These data suggest that the α2,3/α2,6 linkage type alone may not be sufficient to successfully determine influenza virus tropism in the human respiratory tract. More comprehensive but focused glycan arrays that express the wide spectrum of relevant glycans in human airways are needed (*37*). Unfortunately, only a few glycans present in currently available glycan arrays are found in the human respiratory tract.

Because our desialylation–hemagglutination assay involved sialidases that cleaved only unbranched α2,3- and α2,6-linked sialic acid, binding of the H5 viruses to branched sialic acid could not be assessed, which might have contributed to the maintenance of hemagglutination titers in Sialidase S–treated and Sialidase C–treated TRBCs. Fucosylated α2,3-linked sialic acid is a potential branched receptor. It was shown to bind H5 HA clade 2.3.4.4 proteins with substitutions in K218Q, S223R, or both, which can be found in our tested HPAI H5N6/H5N8 clade 2.3.4.4 viruses (*24*). Complex glycans containing fucosylated structures with sialylation, including sialyl-Lewis X (NeuAcα2–3Galβ1–4[Fucα1–3]GlcNAc) and sialyl-Lewis A (NeuAcα2–3Galβ1–3[Fucα1–4]GlcNAc), have been detected in human lung tissues and the epithelium of small airways (*49*). Binding to these glycans might increase the infectivity and hence replication of clade 2.3.4.4 viruses in human airways. In contrast, earlier HPAI H5N1 viruses without the double HA amino acid substitutions have reduced binding to glycans that are fucosylated at the penultimate GlcNAc residue (*24*,*50*).

In conclusion, the productive viral replication and tropism for different cell types in human airway organoids and alveolar epithelial cells suggest zoonotic potential of the 5 HPAI H5N6/H5N8 clade 2.3.4.4b, e, and h avian isolates from 2016–2018. However, the risk for human-to-human transmission seems to be low. The low levels of proinflammatory cytokines and chemokines induced by these viruses in the human respiratory epithelium are unlikely to contribute to the pathogenesis of severe disease. However, the persistent circulation of clade 2.3.4.4 viruses among avian populations and periodic infection of human hosts enable ongoing evolution of the viruses with the possibility of acquiring better transmissibility, higher pathogenicity, or both, in humans. Therefore, education, vaccine development, surveillance, and risk assessment surrounding these viruses should continue.

Acknowledgments

We thank Kevin Fung for assistance with immunohistochemistry and Hung Sing Li, Rachel H.H. Ching, Amy W.Y. Tang, Samuel M.S. Chan, and Joe K.C. Tsun for technical support.

This work was supported by Theme Based Research Scheme (T11-705/14N, T11-712/19-N), Research Grants Council, Hong Kong SAR, China; and the US National Institute of Allergy and Infectious Diseases under Centers of Excellence for Influenza Research and Surveillance (HHSN272201400006C).

C.H.T.B. and D.I.T.K. designed and coordinated the study, planned and conducted the experiments, and analyzed the results. C.H.T.B. wrote the manuscript. H.W.Y., K-C.N., and D.K.W.C. conducted the experiments and analyzed the results. R.J.W. provided HPAI H5N8 viruses. J.M.N., J.S.M.P., and K.P.Y.H. designed the study and reviewed the manuscript. M.C.W.C. did the overall coordination and design of the study, analyzed the results, and reviewed the manuscript.

About the Author

Dr. Bui is a postdoctoral fellow in the School of Public Health, The University of Hong Kong, Hong Kong. Her primary research interests are influenza viruses and coronaviruses and their tropism and pathogenesis in the human respiratory tract.

References

1. Lee DH, Bertran K, Kwon JH, Swayne DE. Evolution, global spread, and pathogenicity of highly pathogenic avian influenza H5Nx clade 2.3.4.4. J Vet Sci. 2017;18(S1):269–80. https://doi.org/10.4142/jvs.2017.18.S1.269
2. Antigua KJC, Choi WS, Baek YH, Song MS. The emergence and decennary distribution of clade 2.3.4.4 HPAI H5Nx. Microorganisms. 2019;7:E156. https://doi.org/10.3390/microorganisms7060156
3. World Health Organization. Antigenic and genetic characteristics of zoonotic influenza A viruses and development of candidate vaccine viruses for pandemic preparedness. Weekly Epidemiological Record. Nos. 11,12,13,41,44. 2014–2021;89–96 [cited 2021 May 28]. https://www.who.int/publications/journals/weekly-epidemiological-record
4. Yu Z, Gao X, Wang T, Li Y, Li Y, Xu Y, et al. Fatal H5N6 avian influenza virus infection in a domestic cat and wild birds in China. Sci Rep. 2015;5:10704. https://doi.org/10.1038/srep10704
5. Li X, Fu Y, Yang J, Guo J, He J, Guo J, et al. Genetic and biological characterization of two novel reassortant H5N6 swine influenza viruses in mice and chickens. Infect Genet Evol. 2015;36:462–6. https://doi.org/10.1016/j.meegid.2015.08.017
6. World Health Organization. Avian influenza weekly update number 793, 21 May 2021. 2021 [cited 2021 May 28]. https://www.who.int/westernpacific/emergencies/surveillance/avian-influenza

7. Bi Y, Tan S, Yang Y, Wong G, Zhao M, Zhang Q, et al. Clinical and immunological characteristics of human infections with H5N6 avian influenza virus. Clin Infect Dis. 2019;68:1100–9. https://doi.org/10.1093/cid/ciy681
8. Yamaji R, Saad MD, Davis CT, Swayne DE, Wang D, Wong FYK, et al. Pandemic potential of highly pathogenic avian influenza clade 2.3.4.4 A(H5) viruses. Rev Med Virol. 2020;30:e2099. https://doi.org/10.1002/rmv.2099
9. Pyankova OG, Susloparov IM, Moiseeva AA, Kolosova NP, Onkhonova GS, Danilenko AV, et al. Isolation of clade 2.3.4.4b A(H5N8), a highly pathogenic avian influenza virus, from a worker during an outbreak on a poultry farm, Russia, December 2020. Euro Surveill. 2021;26:pii=2100439. https://doi.org/10.2807/1560-7917.ES.2021.26.24.2100439
10. Ilyicheva TN, Durymanov AG, Svyatchenko SV, Marchenko VY, Sobolev IA, Bakulina AY, et al. Humoral immunity to influenza in an at-risk population and severe influenza cases in Russia in 2016-2017. Arch Virol. 2018; 163:2675–85. https://doi.org/10.1007/s00705-018-3904-9
11. Pulit-Penaloza JA, Brock N, Pappas C, Sun X, Belser JA, Zeng H, et al. Characterization of highly pathogenic avian influenza H5Nx viruses in the ferret model. Sci Rep. 2020;10:12700. https://doi.org/10.1038/s41598-020-69535-5
12. Sun H, Pu J, Wei Y, Sun Y, Hu J, Liu L, et al. Highly pathogenic avian influenza H5N6 viruses exhibit enhanced affinity for human type sialic acid receptor and in-contact transmission in model ferrets. J Virol. 2016;90:6235–43. https://doi.org/10.1128/JVI.00127-16
13. Zhao Z, Guo Z, Zhang C, Liu L, Chen L, Zhang C, et al. Avian influenza H5N6 viruses exhibit differing pathogenicities and transmissibilities in mammals. Sci Rep. 2017;7:16280. https://doi.org/10.1038/s41598-017-16139-1
14. Choi WS, Baek YH, Kwon JJ, Jeong JH, Park SJ, Kim YI, et al. Rapid acquisition of polymorphic virulence markers during adaptation of highly pathogenic avian influenza H5N8 virus in the mouse. Sci Rep. 2017;7:40667. https://doi.org/10.1038/srep40667
15. Moatasim Y, Kandeil A, Aboulhoda BE, El-Shesheny R, Alkhazindar M, AbdElSalam ET, et al. Comparative virological and pathogenic characteristics of avian influenza H5N8 viruses detected in wild birds and domestic poultry in Egypt during the winter of 2016/2017. Viruses. 2019;11:E990. https://doi.org/10.3390/v11110990
16. Kwon HI, Kim EH, Kim YI, Park SJ, Si YJ, Lee IW, et al. Comparison of the pathogenic potential of highly pathogenic avian influenza (HPAI) H5N6, and H5N8 viruses isolated in South Korea during the 2016-2017 winter season. Emerg Microbes Infect. 2018;7:29. https://doi.org/10.1038/s41426-018-0029-x
17. Hui KP, Chan LL, Kuok DI, Mok CK, Yang ZF, Li RF, et al. Tropism and innate host responses of influenza A/H5N6 virus: an analysis of *ex vivo* and *in vitro* cultures of the human respiratory tract. Eur Respir J. 2017;49:1601710. https://doi.org/10.1183/13993003.01710-2016
18. Bui CHT, Chan RWY, Ng MMT, Cheung MC, Ng KC, Chan MPK, et al. Tropism of influenza B viruses in human respiratory tract explants and airway organoids. Eur Respir J. 2019;54:1900008. https://doi.org/10.1183/13993003.00008-2019
19. Hui KPY, Ching RHH, Chan SKH, Nicholls JM, Sachs N, Clevers H, et al. Tropism, replication competence, and innate immune responses of influenza virus: an analysis of human airway organoids and ex-vivo bronchus cultures. Lancet Respir Med. 2018;6:846–54. https://doi.org/10.1016/S2213-2600(18)30236-4
20. Su Y, Yang HY, Zhang BJ, Jia HL, Tien P. Analysis of a point mutation in H5N1 avian influenza virus hemagglutinin in relation to virus entry into live mammalian cells. Arch Virol. 2008;153:2253–61. https://doi.org/10.1007/s00705-008-0255-y
21. Yang ZY, Wei CJ, Kong WP, Wu L, Xu L, Smith DF, et al. Immunization by avian H5 influenza hemagglutinin mutants with altered receptor binding specificity. Science. 2007;317:825–8. https://doi.org/10.1126/science.1135165
22. Imai M, Watanabe T, Hatta M, Das SC, Ozawa M, Shinya K, et al. Experimental adaptation of an influenza H5 HA confers respiratory droplet transmission to a reassortant H5 HA/H1N1 virus in ferrets. Nature. 2012;486:420–8. https://doi.org/10.1038/nature10831
23. Wang W, Lu B, Zhou H, Suguitan AL Jr, Cheng X, Subbarao K, et al. Glycosylation at 158N of the hemagglutinin protein and receptor binding specificity synergistically affect the antigenicity and immunogenicity of a live attenuated H5N1 A/Vietnam/1203/2004 vaccine virus in ferrets. J Virol. 2010;84:6570–7. https://doi.org/10.1128/JVI.00221-10
24. Guo H, de Vries E, McBride R, Dekkers J, Peng W, Bouwman KM, et al. Highly pathogenic influenza A(H5Nx) viruses with altered H5 receptor-binding specificity. Emerg Infect Dis. 2017;23:220–31. https://doi.org/10.3201/eid2302.161072
25. Yu Y, Zhang Z, Li H, Wang X, Li B, Ren X, et al. Biological characterizations of H5Nx avian influenza viruses embodying different neuraminidases. Front Microbiol. 2017;8:1084. https://doi.org/10.3389/fmicb.2017.01084
26. Kamal RP, Alymova IV, York IA. Evolution and virulence of influenza A virus protein PB1-F2. Int J Mol Sci. 2017;19:E96. https://doi.org/10.3390/ijms19010096
27. Chen H, Bright RA, Subbarao K, Smith C, Cox NJ, Katz JM, et al. Polygenic virulence factors involved in pathogenesis of 1997 Hong Kong H5N1 influenza viruses in mice. Virus Res. 2007;128:159–63. https://doi.org/10.1016/j.virusres.2007.04.017
28. Long JX, Peng DX, Liu YL, Wu YT, Liu XF. Virulence of H5N1 avian influenza virus enhanced by a 15-nucleotide deletion in the viral nonstructural gene. Virus Genes. 2008;36:471–8. https://doi.org/10.1007/s11262-007-0187-8
29. Spesock A, Malur M, Hossain MJ, Chen LM, Njaa BL, Davis CT, et al. The virulence of 1997 H5N1 influenza viruses in the mouse model is increased by correcting a defect in their NS1 proteins. J Virol. 2011;85:7048–58. https://doi.org/10.1128/JVI.00417-11
30. Shaw M, Cooper L, Xu X, Thompson W, Krauss S, Guan Y, et al. Molecular changes associated with the transmission of avian influenza a H5N1 and H9N2 viruses to humans. J Med Virol. 2002;66:107–14. https://doi.org/10.1002/jmv.2118
31. Hiromoto Y, Yamazaki Y, Fukushima T, Saito T, Lindstrom SE, Omoe K, et al. Evolutionary characterization of the six internal genes of H5N1 human influenza A virus. J Gen Virol. 2000;81:1293–303.
32. Lycett SJ, Ward MJ, Lewis FI, Poon AF, Kosakovsky Pond SL, Brown AJ. Detection of mammalian virulence determinants in highly pathogenic avian influenza H5N1 viruses: multivariate analysis of published data. J Virol. 2009;83:9901–10. https://doi.org/10.1128/JVI.00608-09
33. Gabriel G, Herwig A, Klenk HD. Interaction of polymerase subunit PB2 and NP with importin alpha1 is a determinant of host range of influenza A virus. PLoS Pathog. 2008;4:e11. https://doi.org/10.1371/journal.ppat.0040011
34. Koçer ZA, Fan Y, Huether R, Obenauer J, Webby RJ, Zhang J, et al. Survival analysis of infected mice reveals pathogenic variations in the genome of avian H1N1 viruses. Sci Rep. 2014;4:7455. https://doi.org/10.1038/srep07455
35. Ilyushina NA, Seiler JP, Rehg JE, Webster RG, Govorkova EA.

Effect of neuraminidase inhibitor-resistant mutations on pathogenicity of clade 2.2 A/Turkey/15/06 (H5N1) influenza virus in ferrets. PLoS Pathog. 2010;6:e1000933. https://doi.org/10.1371/journal.ppat.1000933
36. Cheung CL, Rayner JM, Smith GJ, Wang P, Naipospos TS, Zhang J, et al. Distribution of amantadine-resistant H5N1 avian influenza variants in Asia. J Infect Dis. 2006;193:1626–9. https://doi.org/10.1086/504723
37. Walther T, Karamanska R, Chan RW, Chan MC, Jia N, Air G, et al. Glycomic analysis of human respiratory tract tissues and correlation with influenza virus infection. PLoS Pathog. 2013;9:e1003223. https://doi.org/10.1371/journal.ppat.1003223
38. World Health Organization. Tool for Influenza Pandemic Risk Assessment (TIPRA). 2016 [cited 2021 May 20]. https://apps.who.int/iris/bitstream/handle/10665/250130/WHO-OHE-PED-GIP-2016.2-eng.pdf
39. Chan RW, Kang SS, Yen HL, Li AC, Tang LL, Yu WC, et al. Tissue tropism of swine influenza viruses and reassortants in ex vivo cultures of the human respiratory tract and conjunctiva. J Virol. 2011;85:11581–7. https://doi.org/10.1128/JVI.05662-11
40. Van Kerkhove MD, Hirve S, Koukounari A, Mounts AW; H1N1pdm Serology Working Group. Estimating age-specific cumulative incidence for the 2009 influenza pandemic: a meta-analysis of A(H1N1)pdm09 serological studies from 19 countries. Influenza Other Respir Viruses. 2013;7:872–86. https://doi.org/10.1111/irv.12074
41. Herfst S, Mok CKP, van den Brand JMA, van der Vliet S, Rosu ME, Spronken MI, et al. Human clade 2.3.4.4 A/H5N6 influenza virus lacks mammalian adaptation markers and does not transmit via the airborne route between ferrets. MSphere. 2018;3:e00405-17. https://doi.org/10.1128/mSphere.00405-17
42. Richard M, Herfst S, van den Brand JM, Lexmond P, Bestebroer TM, Rimmelzwaan GF, et al. Low virulence and lack of airborne transmission of the Dutch highly pathogenic avian influenza virus H5N8 in ferrets. PLoS One. 2015;10:e0129827. https://doi.org/10.1371/journal.pone.0129827
43. Herfst S, Schrauwen EJ, Linster M, Chutinimitkul S, de Wit E, Munster VJ, et al. Airborne transmission of influenza A/H5N1 virus between ferrets. Science. 2012;336:1534–41. https://doi.org/10.1126/science.1213362
44. Chan RW, Chan MC, Nicholls JM, Malik Peiris JS. Use of ex vivo and in vitro cultures of the human respiratory tract to study the tropism and host responses of highly pathogenic avian influenza A (H5N1) and other influenza viruses. Virus Res. 2013;178:133–45. https://doi.org/10.1016/j.virusres.2013.03.003
45. Pulit-Penaloza JA, Sun X, Creager HM, Zeng H, Belser JA, Maines TR, et al. Pathogenesis and transmission of novel highly pathogenic avian influenza H5N2 and H5N8 viruses in ferrets and mice. J Virol. 2015;89:10286–93. https://doi.org/10.1128/JVI.01438-15
46. Kim YI, Pascua PN, Kwon HI, Lim GJ, Kim EH, Yoon SW, et al. Pathobiological features of a novel, highly pathogenic avian influenza A(H5N8) virus. Emerg Microbes Infect. 2014;3:e75. https://doi.org/10.1038/emi.2014.75
47. Jiang H, Wu P, Uyeki TM, He J, Deng Z, Xu W, et al. Preliminary epidemiologic assessment of human infections with highly pathogenic avian influenza A(H5N6) virus, China. Clin Infect Dis. 2017;65:383–8. https://doi.org/10.1093/cid/cix334
48. Liu K, Gu M, Hu S, Gao R, Li J, Shi L, et al. Genetic and biological characterization of three poultry-origin H5N6 avian influenza viruses with all internal genes from genotype S H9N2 viruses. Arch Virol. 2018;163:947–60. https://doi.org/10.1007/s00705-017-3695-4
49. Jia N, Byrd-Leotis L, Matsumoto Y, Gao C, Wein AN, Lobby JL, et al. The human lung glycome reveals novel glycan ligands for influenza A virus. Sci Rep. 2020;10:5320. https://doi.org/10.1038/s41598-020-62074-z
50. Crusat M, Liu J, Palma AS, Childs RA, Liu Y, Wharton SA, et al. Changes in the hemagglutinin of H5N1 viruses during human infection—influence on receptor binding. Virology. 2013;447:326–37. https://doi.org/10.1016/j.virol.2013.08.010

Address for correspondence: Michael C.W. Chan, L6-39, 6/F, Laboratory Block, Faculty of Medicine Building, 21 Sassoon Rd, Pokfulam, Hong Kong, China; email: mchan@hku.hk

New Delhi Metallo-β-Lactamase–Producing *Enterobacterales* Bacteria, Switzerland, 2019–2020

Jacqueline Findlay, Laurent Poirel, Julie Kessler, Andreas Kronenberg, Patrice Nordmann

Carbapenemase-producing *Enterobacterales* (CPE) bacteria are a critical global health concern; New Delhi metallo-β-lactamase (NDM) enzymes account for >25% of all CPE found in Switzerland. We characterized NDM-positive CPE submitted to the Swiss National Reference Center for Emerging Antibiotic Resistance during a 2-year period (January 2019–December 2020) phenotypically and by using whole-genome sequencing. Most isolates were either *Klebsiella pneumoniae* (59/141) or *Escherichia coli* (52/141), and >50% were obtained from screening swabs. Among the 108 sequenced isolates, NDM-1 was the most prevalent variant, occurring in 56 isolates, mostly *K. pneumoniae* (34/56); the next most prevalent was NDM-5, which occurred in 49 isolates, mostly *E. coli* (40/49). Fourteen isolates coproduced a second carbapenemase, predominantly an OXA-48-like enzyme, and almost one third of isolates produced a 16S rRNA methylase conferring panresistance to aminoglycosides. We identified successful plasmids and global lineages as major factors contributing to the increasing prevalence of NDMs in Switzerland.

Carbapenem-resistant *Enterobacterales* (CRE) bacteria are considered by the World Health Organization to be a critical global health concern; they were placed in the organization's critical-priority group of the priority pathogens list for the research and development of new antibiotics in 2017 (*1*). Among the Ambler class B β-lactamases, the New Delhi metallo-β-lactamases (NDM) were identified in 2008 in a patient from Sweden who had been hospitalized in India and upon return to Sweden had a carbapenem-resistant *Klebsiella pneumoniae* sequence type (ST) 14 strain isolated from his urine, leading to the identification of the bla_{NDM-1} gene (*2*). In a follow-up study in 2009, NDM enzymes were shown to be widespread in India, Pakistan, and Bangladesh; the bla_{NDM-1} gene was identified in multiple *Enterobacterales* species, predominantly in *Escherichia coli* and *K. pneumoniae* (*3*). Since those initial studies, NDM carbapenemases have been reported globally (*4*,*5*). The SMART global surveillance program analyzed *Enterobacterale* isolates in 55 countries from 2008–2014 and found that the prevalence of NDM carbapenemase producers was substantially higher in India, Egypt, the United Arab Emirates, and Serbia (*6*). In 2010, NDM-1-producing *Acinetobacter baumannii* bacteria were reported in India (*7*), and reports in other *Acinetobacter* spp. followed (*8*). In 2011, NDM-1 was reported in *Pseudomonas aeruginosa* in Serbia (*9*), illustrating a wide host range among gram-negative bacteria.

NDM enzymes are capable of conferring resistance to almost all β-lactam antimicrobial drugs (except aztreonam), including carbapenems which are often considered drugs of last resort for the treatment of serious infections (*2*). Treatment options for infections caused by NDM-producing bacteria are very limited, particularly because they often harbor multiple other resistance genes. For example, there are notable associations between bla_{NDM} genes and plasmid-borne extended-spectrum β-lactamases (ESBLs) and pAmpC encoding genes (most commonly bla_{CTX-M} and bla_{CMY}) that result in resistance to aztreonam (*10*); similarly, 16S rRNA methylases (RMTases), which can confer high-level resistance to all aminoglycosides, have also been strongly associated with NDM carriage (*11*). The recently approved β-lactamase inhibitors, diazabicyclooctanes (e.g., avibactam [AVI], relebactam [REL]) and cyclic boronates (e.g., vaborbactam [VAB]) have no activity against metallo-β-lactamases (MBLs) and subsequently new treatment options are urgently

Author affiliations: University of Fribourg, Fribourg, Switzerland (J. Findlay, L. Poirel, J. Kessler, P. Nordmann); University of Bern, Bern, Switzerland (A. Kronenberg); Institute for Microbiology, University of Lausanne and University Hospital Centre, Lausanne, Switzerland (P. Nordmann); Associate Editor, Emerging Infectious Diseases (P. Nordmann)

DOI: https://doi.org/10.3201/eid2710.211265

needed. Aztreonam (ATM)/AVI has been suggested as a treatment option for infections caused by NDM-producing bacteria because ATM is spared by MBL hydrolytic activities and AVI inhibits the activity of any co-produced ESBL or AmpC (*12*).

To date, a total of 32 NDM variants have been identified (https://www.ncbi.nlm.nih.gov/pathogens/beta-lactamase-data-resources); however, the NDM-1, NDM-4, NDM-5, and NDM-7 variants remain dominant globally with some exhibiting increased carbapenemase activity compared with NDM-1 (*3*–*5*,*10*). NDM encoding genes are highly transmissible, often located on plasmids of various replicon types harboring several antibiotic resistance genes. Outbreaks of NDM producers, either clonal or due to the dissemination of successful plasmids, have been increasingly reported (*13*–*15*).

In Switzerland, production of NDM enzymes was identified in 2011 in *E. coli*, *K. pneumoniae,* and *Proteus mirabilis* isolates obtained from Geneva University Hospitals (*16*) and since then have become one of the dominant carbapenemase types, just after oxacillin (OXA) 48 (*17*) in the country, accounting for >25% of all carbapenem-producing *Enterobacterales* (CPE) submitted to the Swiss National Reference Centre for Emerging Antibiotic Resistance (NARA) in 2020. In this study we describe the epidemiology of NDM-positive *Enterobacterales* submitted to NARA during January 2019–December 2020.

Materials and Methods

Bacterial Isolates, Identification, and Susceptibility Testing

The NARA reference laboratory received 532 CPE samples from hospitals and clinics throughout Switzerland over a 2-year period, January 2019–December 2020, after a mandatory request in January 2019 for carbapenemase producers. We obtained patient and isolation source data from the accompanying request forms sent by referring laboratories. Of the 532 samples, 141 were confirmed to be NDM-positive enterobacterial isolates. Species identification was confirmed using API-20E tests (bioMérieux, https://www.biomerieux.com) and UriSelect 4 agar (Bio-Rad, https://www.bio-rad.com). Susceptibility testing was performed by disk diffusion or by broth microdilution for the β-lactam/β-lactamase inhibitor combinations and results interpreted in accordance with EUCAST guidelines (*18*). For the ATM/AVI combination, AVI was used at a fixed concentration of 4 mg/L.

Detection of Carbapenemase Genes

All isolates were subject to the Rapidec Carba NP test (bioMérieux) and then to NG-Test CARBA 5 test (NG Biotech, https://ngbiotech.com), according to the manufacturer's instructions. Isolates testing positive by the Rapidec Carba NP test and the NG-Test CARBA 5 test or exhibiting resistance to ≥1 carbapenem (ertapenem, imipenem, or meropenem) were screened by PCR (*19*) for the presence of carbapenemase genes (bla_{KPC}, bla_{OXA-48}, bla_{NDM}, bla_{VIM}, and bla_{IMP}). Sanger sequencing of amplified carbapenemase genes was performed by Microsynth AG (Microsynth AG, https://www.microsynth.com) to identify the exact alleles.

Whole-Genome Sequencing and Analyses

Whole-genome sequencing (WGS) was performed on a subset of 108 nonduplicate isolates (by patient and species) on a MiSeq instrument (Illumina, https://www.illumina.com) using the Nextera sample preparation method with 2 × 150 bp paired end reads. Reads were assembled into contigs using the Shovill pipeline (https://github.com/tseemann/shovill), which is based on SPAdes version 3.13.0 (*20*). Sequence types, the presence of resistance genes, and speciation were confirmed, using MLST version 2.0, ResFinder version 4.1 (*21*), and KmerFinder version 3.2 (*22*) on the Center for Genomic Epidemiology platform (https://cge. cbs.dtu.dk/services); contigs were annotated using Prokka (*23*). A core genome single-nucleotide polymorphism (SNP) alignment was generated using Parsnp (*24*) and viewed using Interactive Tree of Life version 6.1.1 (*25*). *E. coli* MG1655 (GenBank accession no. NC_000913) and *K. pneumoniae* ATCC 700721/MGH78578 (GenBank accession no. NC_009648) were used as the reference sequences for each alignment.

Complete NDM-encoding plasmid sequences were downloaded from GenBank by using the search terms and filters "NDM" and "plasmid" and applying a minimum sequence length of 15 kb to generate an NDM plasmid reference database for mapping analyses. Reads were mapped to reference sequences using CLC Genomics Workbench (QIAGEN, https://www.qiagen.com) and then contigs mapped using progressive Mauve alignment software to manually mitigate against false positives (*26*). A ≥95% coverage and identity were used to assess relevant matches (Appendix Table, https://wwwnc.cdc.gov/EID/article/27/11/21-1265-App1.pdf). We have submitted sequence data from this study to the National Center for Biotechnology Information's Sequence Read Archive (BioProject no. PRJNA744003).

Results

Isolate Sources and Species Identification

More than half of isolates (82/141; 58.2%) were obtained from screening swab samples (fecal and rectal, and nonrectal) and the remaining isolates were from urine (34/141; 24.1%), tissue and fluid (14/141; 9.9%), respiratory (4/141; 2.8%), blood cultures (3/141; 2.1%), and 4 isolates were of unknown origin (Table 1). Isolates were *K. pneumoniae* (59/141; 41.8%), *E. coli* (52/141; 36.9%), *Enterobacter cloacae* complex (19/141; 13.5%), *Citrobacter freundii* (3/141; 2.1%), *Klebsiella aerogenes* (3/141; 2.1%), *Klebsiella quasipneumoniae* (2/141; 1.4%), *Klebsiella variicola* (2/141; 1.4%), and *Klebsiella oxytoca* (1/141; 0.7%). Isolates were obtained from 116 patients; 65 were male (56%), 47 female (41%), and 4 did not have sex stated.

All 7 main regions of Switzerland were represented in this study; 8–40 isolates were submitted from each (Figure 1). Approximately half of all isolates (71/141; 50.4%) were obtained from hospitals in either the Lake Geneva or Zurich region, 2 of the most populated areas of Switzerland, but just 8 isolates were received from central Switzerland, the region with the greatest population size (*27*). Sixty-six isolates were from 2019 and 75 from 2020, whereas 33 NDM-positive *Enterobacterales* isolates were submitted to NARA in 2018 (data not shown). Such a significant increase in numbers could indicate a trend of increased NDM prevalence in Switzerland, as has been observed previously during 2013–2018 (*17*). We selected 108 nonduplicate isolates for further investigation: 46 *E. coli*, 42 *K. pneumoniae*, 14 *Enterobacter cloacae* complex, 3 *K. quasipneumoniae*, 2 *K. aerogenes*, and 1 *K. pneumoniae variicola* isolate.

Susceptibility Testing

Susceptibility testing showed that most isolates were resistant to fluoroquinolones (93/108; 86.1%), and most (69/108; 63.9%) were resistant to >2 aminoglycosides, of which we tested kanamycin, tobramycin, gentamicin, and amikacin. No isolate was found resistant to tigecycline, 6 (5.6%) isolates exhibited resistance to colistin, and 1 isolate was resistant to fosfomycin. We also performed susceptibility testing against selected β-lactam and β-lactam/inhibitor combinations, namely imipenem (IPM), IPM/REL, meropenem (MEM), MEM/VAB, ceftazidime (CAZ), CAZ/AVI, ATM, and ATM/AVI (Table 2). All isolates were resistant to both CAZ and CAZ/AVI, as well as MEM; 17 (15.7%) isolates were susceptible to MEM/VAB. Ten (9.3%) isolates were susceptible to IPM and 2 (1.9%) to IPM/REL; of note, breakpoints for IPM and IPM/REL are different, which may explain the lower susceptibility rate for the combination. Most (97/108; 89.8%) isolates exhibited resistance to ATM, whereas 8 isolates (7 *E. coli* and 1 *K. pneumoniae*) were resistant to ATM/AVI with MICs of 8 mg/L (n = 4) and 16 mg/L (n = 4), based on breakpoint value of resistance for AZT/AVI taken from that of ATM. Among the drug combinations, AZT/AVI was the most effective, as expected.

AZT/AVI Resistance Mechanisms

Analysis of the ATM/AVI-resistant isolates revealed that 6/7 *E. coli* isolates harbored a bla_{CMY} allele: bla_{CMY-2} (n = 1), bla_{CMY-42} (n = 2), $bla_{CMY-145}$ (n = 2), and $bla_{CMY-148}$ (n = 1). All those isolates had an insertion of 4 amino acids within the PBP-3 encoding gene located after residue 333, which was YRIN in 5 isolates and YRIK in the other 2 isolates. Similar 4-aa insertions have been reported among NDM-5–producing *E. coli* as a cause of elevated MICs of ATM, related to impeding accessibility to the binding site of PBP-3, and therefore were involved in ATM/AVI resistance in addition to CMY production (*28*). Ma et al. reported that the insertion alone has a minor effect on ATM/AVI resistance levels (*29*), but resistance could be achieved when combined with CMY production (*29*). Other studies reported that CMY variants with a glycine residue at position 231 exhibited enhanced hydrolysis against ATM (*30*,*31*). Among the isolates we tested, CMY-42, CMY-145, and CMY-148 variants all harbored a Val231Ser substitution, suggesting that those

Table 1. Sources of 141 bla_{NDM}-positive isolates identified in *Enterobacterales* bacteria, Switzerland, 2019–2020

	No. from patient source							
Species	Urine	Blood culture	Tissue and fluid	Respiratory	Fecal and rectal swab	Nonrectal screening swab	Unknown	Total
Klebsiella pneumoniae	12	1	7	2	31	4	2	59
Escherichia coli	13	2	1	0	31	4	1	52
Enterobacter cloacae complex	6	0	5	1	6	0	1	19
K. aerogenes	1	0	0	0	2	0	0	3
Citrobacter freundii	1	0	0	0	1	1	0	3
K. quasipneumoniae	0	0	0	0	2	0	0	2
K. variicola	0	0	1	1	0	0	0	2
K. oxytoca	1	0	0	0	0	0	0	1
Total	34	3	14	4	73	9	4	141

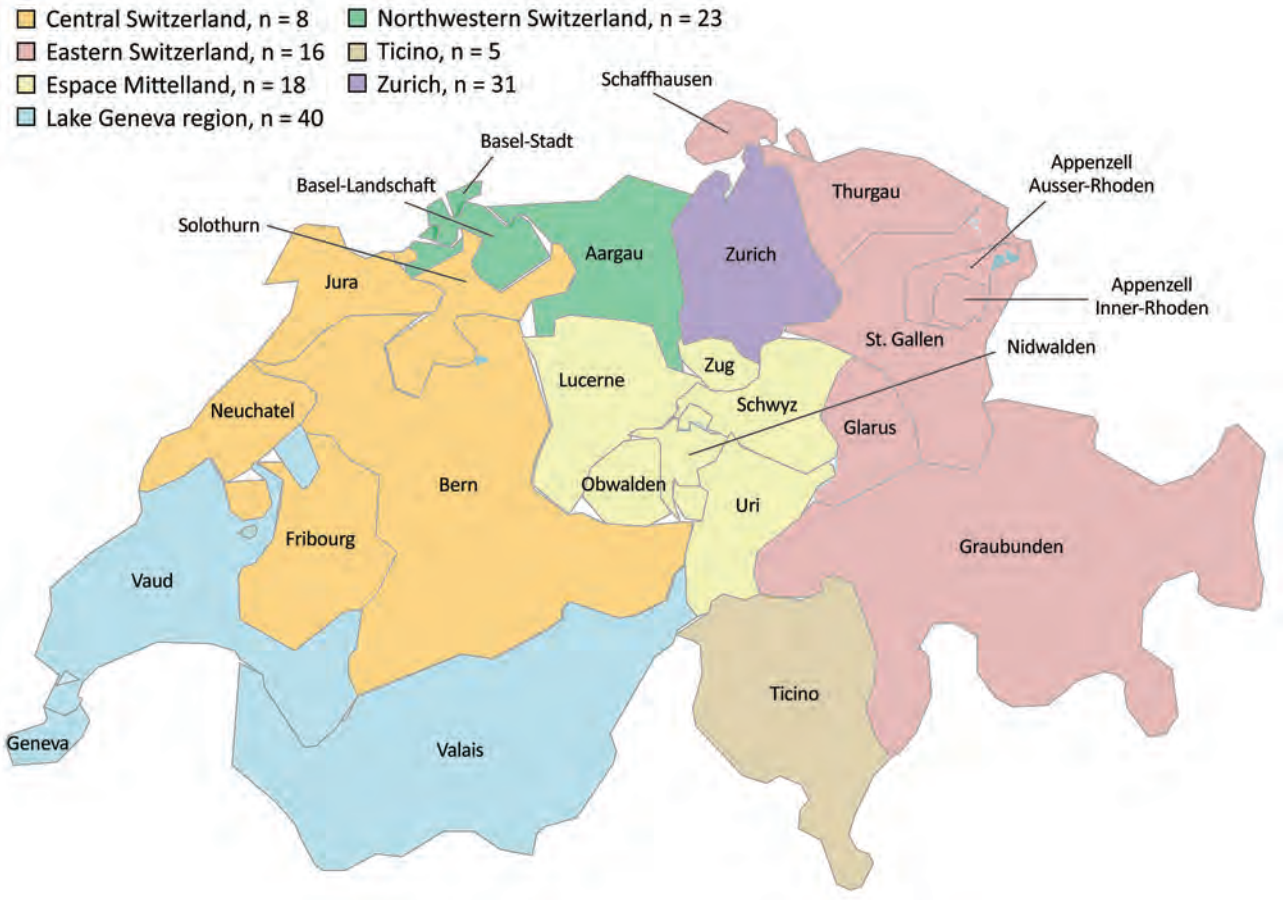

Figure 1. Regions of Switzerland from which *Enterobacterale* isolates positive for New Delhi metallo-β-lactamase were obtained, January 2019–December 2020.

enzymes affected the levels of ATM/AVI resistance, along with the PBP-3 modifications.

One ATM/AVI-resistant *K. pneumoniae* isolate exhibited an MIC of 8 mg/L; it neither carried a bla_{CMY} gene nor harbored any mutation within its PBP-3 encoding gene. However, it did harbor $bla_{CTX\text{-}M\text{-}15}$, and we identified a premature stop codon near the beginning of *ompK35*, which would render the porin nonfunctional. Although this does not explain the ATM/AVI MIC by itself, it might be a contributing factor.

Carbapenemase Alleles and Other Resistance Genes

Carbapenemase Alleles

Among the 108 sequenced isolates, we identified 4 bla_{NDM} allelic variants; $bla_{NDM\text{-}1}$ (n = 56), $bla_{NDM\text{-}4}$ (n = 2), $bla_{NDM\text{-}5}$ (n = 49), and $bla_{NDM\text{-}7}$ (n = 1). Most *E. coli* isolates harbored $bla_{NDM\text{-}5}$ (40/46 isolates) and the 6 remaining *E. coli* isolates had $bla_{NDM\text{-}1}$ (Table 3). This finding indicated that the spread of $bla_{NDM\text{-}5}$ gene in *E. coli* may be affected by the increased catalytic efficiency of NDM-5 against carbapenems compared with NDM-1 (*32*). Conversely, *K. pneumoniae* isolates predominantly carried $bla_{NDM\text{-}1}$ (34/42), and rarely $bla_{NDM\text{-}5}$ (6/42) and $bla_{NDM\text{-}4}$ (2/42). Most (12/14) *E. cloacae* complex isolates harbored $bla_{NDM\text{-}1}$; of the others, 1 harbored $bla_{NDM\text{-}5}$ and 1 $bla_{NDM\text{-}7}$. Multiple carbapenemase genes were found in 18 isolates, namely 11 *K. pneumoniae*, 6 *E. coli,* and 1 *E. cloacae* complex isolate. Sixteen of the 18 isolates harbored a $bla_{OXA\text{-}48}$-like gene ($bla_{OXA\text{-}48}$ [n = 5], $bla_{OXA\text{-}181}$ [n = 6], $bla_{OXA\text{-}232}$ [n = 3], $bla_{OXA\text{-}244}$ [n = 2]), and single *E. coli* and *K. pneumoniae* isolates harbored $bla_{KPC\text{-}3}$ genes. In addition to producing the various carbapenemases, most isolates also produced multiple other β-lactamases, including CTX-M–type ESBLs and CMY-type AmpC–encoding genes. We identified genes encoding RMTases conferring resistance to all clinically significant aminoglycosides in a total of 35 isolates (Figures 2, 3).

E. coli Isolates

We identified a total of 17 sequence types (STs) among the 46 *E. coli* isolates. Four dominant ST clusters or clonal complexes (CCs) were identified by performing

Table 2. MIC distributions for 108 bla_{NDM}-positive isolates identified in *Enterobacterales* bacteria, Switzerland, 2019–2020*

Antimicrobial drug	Breakpoint MIC, mg/L S	R	No. isolates at MIC ≤0.06	0.125	0.25	0.5	1	2	4	8	16	32	64	128	≥256	% Susceptible
Imipenem	≤2	>4						2	8	23	37	19	11	8		9.3
Imipenem/relebactam	≤2	>2						2	9	30	34	15	11	7		1.9
Meropenem	≤2	>2							8	9	15	27	25	20	4	0
Meropenem/vaborbactam	≤2	>8							8	9	19	27	25	19	1	15.7
Ceftazidime	≤1	>4													108†	0
Ceftazidime/avibactam	≤8	>8													108†	0
Aztreonam	≤1	>4		3	1	1	1	2	3	8	3	2	8	22	54	10.2
Aztreonam/avibactam‡	≤4	>4§	15¶	19	16	14	12	11	13	4	4					92.6

*Testing range for all drugs was 0.06–256 mg/L. Breakpoints from the European Committee on Antimicrobial Susceptibility Testing. Gray shading indicates resistant isolates. R, resistant; S, susceptible.
†MIC≥256 mg/L.
‡Avibactam used at a fixed concentration of 4 mg/L.
§Aztreonam/avibactam breakpoint selected arbitrarily based on the aztreonam breakpoints.
¶MIC≤0.06 mg/L.

core genome SNP analyses as follows: ST405 (n = 5), all producing NDM-5 and obtained from 4 regions of Switzerland; ST410 (n = 7), all producing NDM-5 and obtained from 3 regions; ST361 (n = 8), all producing NDM-5 and obtained from 4 regions; CC10 from 4 regions, comprising ST167 (n = 9) and single representatives of its single locus variants, ST617 and ST1284, all of which also produced NDM-5 (Figure 2). Six isolates co-produced another carbapenemase gene, namely $bla_{OXA-181}$ (n = 3), $bla_{OXA-244}$ (n = 2), or bla_{KPC-3} (n = 1). The core genome size in this analysis was 2.82 Mb.

K. pneumoniae Isolates

Within the 42 K. pneumoniae isolates, we identified 14 STs. A core-genome SNP analysis showed that 2 clonal clusters dominated; 1 contained CC258 isolates, comprising 10 ST11 and 3 ST437 isolates, and the other included 14 ST147 isolates (Figure 3). Among CC258 isolates, all produced NDM-1 with the exception of 1 that produced NDM-4 and 1 NDM-7, both belonging to ST11. Within ST147 isolates, 12 produced NDM-1 and 2 produced NDM-5. Isolates from both clusters were scattered geographically; we obtained CC258 isolates from hospitals in 4 regions and ST147 isolates from 6 regions in Switzerland. Eleven isolates coharbored >1 carbapenemase gene; the genes were bla_{OXA-48} (n = 4), $bla_{OXA-181}$ (n = 3), $bla_{OXA-232}$ (n = 3), and bla_{KPC-3} (n = 1). The core genome size in this analysis was 4.25 Mb.

E. cloacae Complex Isolates and Other Species

The 14 *E. cloacae* complex isolates represented 10 STs, indicating no dominant clone. Twelve isolates produced NDM-1, and the remaining 2 produced either NDM-5 or NDM-7. One ST91 *E. cloacae* isolate additionally carried a bla_{OXA-48} gene. The remaining isolates included 3 of *K. quasipneumoniae*, 2 of *K. aerogenes*, and 1 of *K. variicola*. The *K. quasipneumoniae* isolates were of ST4834, ST5330, and 1 novel ST. Both *K. aerogenes* isolates belonged to ST93. The *K. quasipneumoniae* and *K. variicola* isolates produced NDM-1, and the *K. aerogenes* isolates produced NDM-5.

16S RMTases

By screening our collection of NDM-producing isolates for RMTase encoding genes, we found a high positivity rate. Almost a third of isolates (35/108) harbored >1 RMTase gene, most commonly *armA* (16 isolates), followed by *rmtB* (13 isolates), *rmtC* (6 isolates), and *rmtF* (co-produced in 2 isolates

Table 3. Carbapenemase alleles harbored by isolates sequenced in study of *Enterobacterales* bacteria, Switzerland, 2019–2020

Species	Carbapenemase NDM-1	NDM-1 + OXA-48	NDM-1 + OXA-232	NDM-1 + KPC-3	NDM-4	NDM-4 + OXA-181	NDM-5	NDM-5 + OXA-48	NDM-5 + OXA-181	NDM-5 + OXA-232	NDM-1 + OXA-244	NDM-5 + KPC-3	NDM-7
Escherichia coli	6						34		3		2	1	
Klebsiella pneumoniae	28	3	2	1	1	1	2	1	2	1			
Enterobacter cloacae complex	11	1					1						1
K. aerogenes							2						
K. quasipneumoniae	3												
K. variicola	1												
Total	49	4	2	1	1	1	39	1	5	1	2	1	1

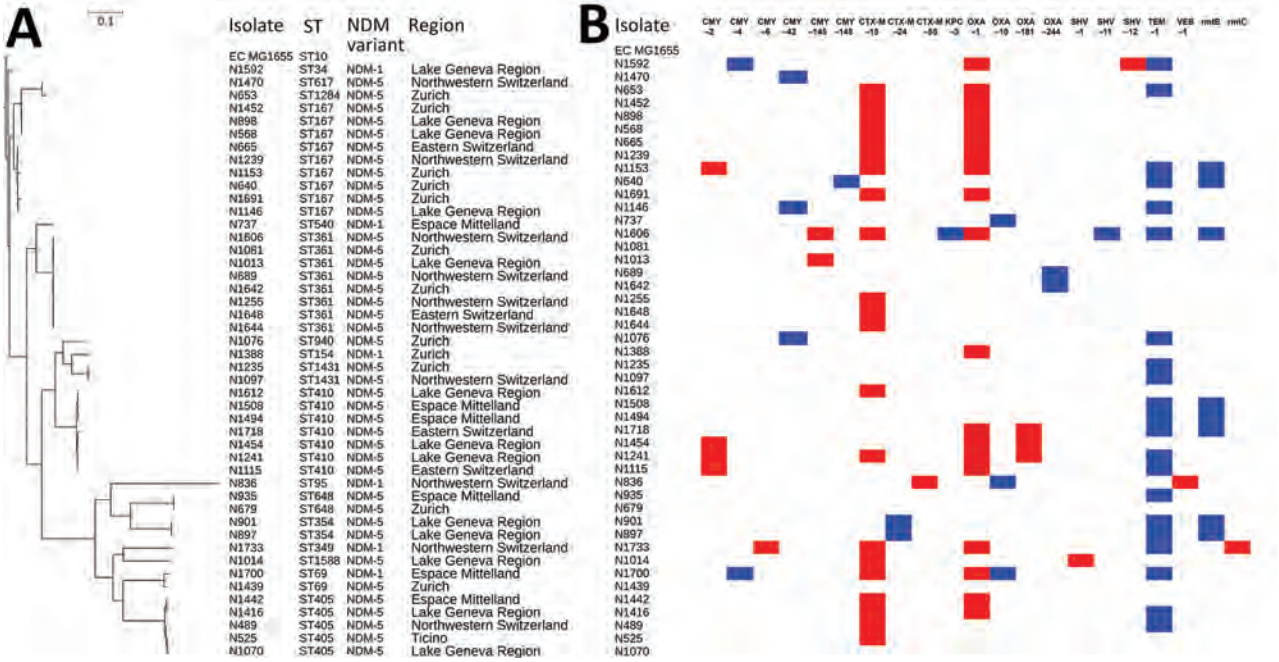

Figure 2. Clustering and gene content of 46 *Escherichia coli* isolates collected in Switzerland, January 2019–December 2020. A) Phylogenetic tree showing clustering and the respective ST, NDM variant, and region of Switzerland from which each isolate was obtained. B) Gene matrix showing β-lactamase and RMTase gene content of the isolates. NDM, New Delhi metallo-β-lactamase; ST, sequence type.

alongside *rmtB*). RMTases are capable of conferring high-level resistance to all clinically relevant aminoglycoside antimicrobial drugs including the recently approved urinary tract infection treatment plazomicin (33). RMTases have previously been shown to have a strong association with bla_{NDM}, particularly K. pneumoniae ST147 (34); in our study, 8 of the K. pneumoniae ST147 isolates carried RMTase genes. Of the 35 RMTase-positive isolates we identified, a highly similar plasmid could be identified for 24, and 10/24 harbored the same RMTase genes as the reference plasmid. This result could suggest that the RMTase genes in these isolates may be carried on the same plasmid as the blaNDM gene. The remaining 14 identified highly similar plasmids either did not encode an RMTase gene or encoded one different from that identified in our isolates. The strong association between blaNDM and RMTase gene carriage have been previously reported elsewhere (34) and has been associated with both the co-localization of blaNDM and RMTase gene types on the same plasmid, as well as encoded separately in diverse plasmid types (34). Such high level of association of carbapenemases to the NDM-5 and RMTase genes will further limit the choice of therapeutics available for treating infections because of those multidrug-resistant bacteria.

Typing of NDM Plasmids

By mapping sequencing reads against a database of known NDM-encoding plasmids and applying a stringent cutoff (≥95% coverage and identity), we identified plasmids highly similar to those in our study. We found plasmids with ≥95% coverage and identity for 69/108 (63.9%) of the sequenced isolates (Appendix Table). Most (50/69) of the identified plasmids harbored IncF replicons, albeit a diverse range. Plasmids with the IncF replicon types were the most common, among which the bla_{NDM-5} gene was dominant; the replicons IncFII (n = 14), IncFII/IncFIA (n = 11), IncFIB(pQIL) (n = 7), and IncF(pKPX1) (n = 6) were the most common. A total of 13/69 plasmids carrying a bla_{NDM} gene possessed an IncX3 replicon, and carried either bla_{NDM-5} (n = 9), bla_{NDM-1} (n = 3), and bla_{NDM-7} (n = 1) genes.

Within *E. coli* isolates, highly similar plasmids could be identified for 31/46 isolates, representing 7 different replicon types and combinations. Most (24/31) were IncF replicon variants, and 9 of these bla_{NDM}-bearing plasmids exhibited 95%–100% coverage and identity to pIncF, a ≈116 kb IncFII/IncFIA NDM-5–producing plasmid identified in *E. coli* ST617 from Italy (GenBank accession no. MW048884.1). The pIncF-like plasmids were identified in 4 STs, namely ST167 (n = 4), ST361 (n = 3), ST617 (n = 1), and ST1588

(n = 1). Highly similar IncX3 plasmids could be identified from 4 isolates, corresponding to the previously reported ≈46 kb pEsco-5256cz (GenBank accession no. MG252891.1) carrying the bla_{NDM-5} gene from Czech Republic, and 2 other highly similar bla_{NDM-5}-carrying IncX3 plasmids exhibited high similarity to a ≈35 kb pABC280-NDM-5 (GenBank accession no. MK372392) identified from the United Arab Emirates.

Within *K. pneumoniae* isolates, we identified similar plasmids for 28/42 isolates from 9 different replicon types or combinations. Similar to *E. coli* isolates, most plasmids (22/28) corresponded to IncF replicon variants. Seven isolates, all belonging to ST147, exhibited 99%–100% coverage and identity to pM321-NDM-1 (GenBank accession no. AP018834), a ≈54 kb bla_{NDM-1}-positive plasmid harboring the FIB(pQIL) replicon type and described in isolates from Myanmar (*35*). Six ST11 *K. pneumoniae* isolates also exhibited 100% coverage and similarity to pAR_0146 (GenBank accession no. CP021962), a ≈ 132 kb IncFII(pKPX1) plasmid identified in the United States. Of interest, within the 4 IncX3 plasmids that could be identified, 2 exhibited high similarity (100% coverage and identity) to pEsco-5256cz and 1 to pABC280-NDM-5; we found those 2 plasmids in *E. coli* isolates as well, which suggested interspecies plasmid sharing. We also detected the plasmid pEsco-5256cz in the *E. cloacae* complex isolates; 3 of those ST93 isolates harboring plasmids exhibited 99% coverage and identity to pEsco-5256cz.

Discussion

This study showed increasing prevalence of NDM-producing *Enterobacterales* bacteria in Switzerland. One cause appears to be successful lineages of both *E. coli* and *K. pneumoniae*.

The *E. coli* clusters we identified in this study are all considered as high-risk clones or correspond to CC that are frequently reported internationally (*36*–*40*). Multiple studies reported NDM-5–producing ST405 *E. coli* isolates circulating in Europe and particularly in isolates from Germany, Italy, and Spain (*39*–*40*). One study alluded to the cross-border transmission between Switzerland and Germany of NDM-5-producing ST405 isolates (*39*), and in our study this *E. coli* clone also appears widespread, found in multiple regions of Switzerland. *E. coli* ST410 is increasingly reported as a cause of hospital outbreaks and has been associated with the carriage of both ESBLs and various carbapenemase genes, including bla_{NDM-5}, in both Europe and Asia (*36*,*37*). CC10 members producing NDM-5, have been described in multiple countries, including China, the United States, and Switzerland (*39*,*41*). We found it in isolates across a wide geographical area. *E. coli* ST361 was most commonly described as an ESBL-producing clone in both human and animal populations, usually harboring the $bla_{CTX-M-15}$ gene, but more recently it has been described as harboring bla_{NDM-5} in several countries, including Germany and Switzerland (*39*,*42*–*45*). Similarly,

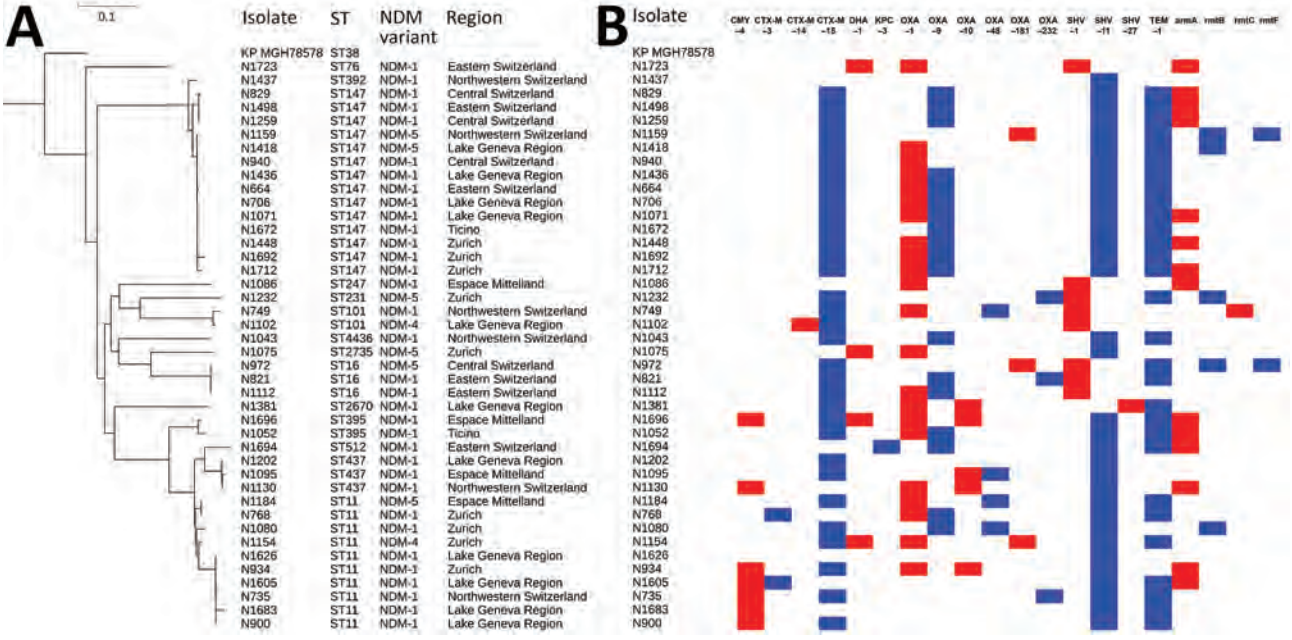

Figure 3. Clustering and gene content of 42 *Klebsiella pneumoniae* isolates collected in Switzerland, January 2019–December 2020. A) Phylogenetic tree showing clustering and the respective ST, NDM variant, and region of Switzerland from which each isolate was obtained. B) Gene matrix showing β-lactamase and RMTase gene content of the isolates. NDM, New Delhi metallo-β-lactamase; ST, sequence type.

ESBL-producing *E. coli* ST167 and ST410 isolates have been found in food products (meat and dairy) in Germany (*45*), indicating that these lineages may already be widespread, albeit without the bla_{NDM-5}–carrying plasmid. A recent study in Switzerland identified both ST167 and ST410 *E. coli* isolates harboring the NDM-5 encoding gene; genomic analysis showed that the isolates harbored bla_{NDM-5}–carrying plasmids with a high nucleotide identity to plasmids previously identified in a nosocomial outbreak in Myanmar (*38*).

Both *K. pneumoniae* clusters identified in this study encompass high-risk clones. *K. pneumoniae* ST147 has emerged as an important clone for the dissemination of various antimicrobial-resistance genes, given its wide global distribution and strong association with hospital outbreaks (*46*). Tavoschi et al. identified NDM-1-producing ST147 *K. pneumoniae* isolates as the dominant cause of a yearlong outbreak in hospitals in Tuscany, Italy (*42*); their finding might explain a dominance of ST147 isolates, considering the proximity of Italy and Switzerland. *K. pneumoniae* CC258 is most commonly associated with the global dissemination of bla_{KPC} through ST11 and ST258. *K. pneumoniae* ST11, however, seems amenable to the dissemination of a wide range of resistance genes; hospitals have reported outbreaks harboring various carbapenemase family genes including bla_{KPC}, bla_{NDM}, and bla_{VIM} (*47*,*48*). NDM-1–producing *K. pneumoniae* ST11 has long been reported throughout Europe and could be considered as endemic in some countries (*48*–*50*). *K. pneumoniae* ST11 might therefore be considered as a successful clone in Switzerland, as we observed. We detected pEsco-5256cz–like and pABC280-NDM-5–like IncX3 plasmids in complex isolates of all 3 species groups (*E. coli*, *K. pneumoniae,* and *E. cloacae*). Our findings suggest that the plasmids are highly capable of cross-species transmission, which has been observed for IncX3 plasmids generally and is a factor in their success.

The isolates in this study were multidrug resistant, and a substantial proportion exhibited resistance to aminoglycosides, largely resulting from the co-carriage of RMTases. The high level of association of carbapenemases to the NDM-5 and RMTase genes will limit the choice of therapeutics available for treating infections because of those multidrug-resistant bacteria. Several isolates were identified that were resistant to the β-lactam/inhibitor combination ATM/AVI, a potential future treatment for infections caused by NDM-producing bacteria (*28*,*29*). The transmission of successful plasmids, both within and between species, was identified as a major factor in the increasing prevalence of NDM-producing *Enterobacterales*. This 2-year study gives a snapshot of the epidemiology of NDM producers in Switzerland and illustrates how the use of WGS is both an essential and informative tool for surveillance and for monitoring emerging resistance. Our findings underpin the importance of the surveillance of NDM-producing bacteria and particularly the monitoring of successful clonal lineages and plasmids.

Acknowledgments

We thank the following colleagues from throughout Switzerland for providing us with the clinical strains used in our study: M. Oberle, C. Ottiger (Aargau); O. Dubuis, S. Garf (Basel-Landschaft); A. Egli, D. Goldenberger (Basel Stadt); K. Burren, C. Casanova, S. Droz, S. Thiermann, R. Troesch (Bern); D. Bandera, V. Deggim, S. Pfister (Fribourg); N. Liassine, G. Renzi (Geneva); C. Guler (Grisons); L. Monnerat (Jura); I. Dietrich, P. Friderich, I. Mitrovic, B. Suterbuser (Lucerne); K. Vidakovic (Schaffhausen); M. Ritzler, S. Sieffert (St Gallen); K. Herzog (Thurgau); V. Gaia (Ticino); S. Emonet, M. Eyer, L. Tissieres (Valais); C. Andreutti, M. Corthesy, M. Dessauges, M. Maitrejean, M. Rosselin, C. Vogne (Vaud); V. Bruderer, G. Eich, E. Gruner, M. Kuegler, K. Lucke, P. Minkova, S. Mancini (Zurich).

This work has been funded by the University of Fribourg, the Swiss National Reference Center for Emerging Antibiotic Resistance, and by the Swiss National Science Foundation (project FNS-31003A_163432).

About the Author

Dr. Findlay is a researcher at the University of Fribourg, Switzerland. Her primary research interests include the evolution of antimicrobial resistance and the molecular epidemiology of antimicrobial-resistant bacteria.

References

1. World Health Organization. Global priority list of antibiotic-resistant bacteria to guide research, discovery, and development of new antibiotics. 2017 [cited 2021 Aug 9]. https://www.who.int/medicines/publications/WHO-PPL-Short_Summary_25Feb-ET_NM_WHO.pdf
2. Yong D, Toleman MA, Giske CG, Cho HS, Sundman K, Lee K, et al. Characterization of a new metallo-β-lactamase gene, bla_{NDM-1}, and a novel erythromycin esterase gene carried on a unique genetic structure in *Klebsiella pneumoniae* sequence type 14 from India. Antimicrob Agents Chemother. 2009;53:5046–54. https://doi.org/10.1128/AAC.00774-09
3. Kumarasamy KK, Toleman MA, Walsh TR, Bagaria J, Butt F, Balakrishnan R, et al. Emergence of a new antibiotic resistance mechanism in India, Pakistan, and the UK: a molecular, biological, and epidemiological study. Lancet Infect Dis. 2010;10:597–602. https://doi.org/10.1016/S1473-3099(10)70143-2

4. Dortet L, Poirel L, Nordmann P. Worldwide dissemination of the NDM-type carbapenemases in gram-negative bacteria. BioMed Res Int. 2014;249856. https://doi.org/10.1155/2014/249856
5. van Duin D, Doi Y, The global epidemiology of carbapenemase-producing Enterobacteriaceae. Virulence. 2017; 19:460–9. https://doi.org/10.1080/21505594.2016.1222343
6. Karlowsky JA, Lob SH, Kazmierczak KM, Badal RE, Young K, Motyl MR, et al. In vitro activity of imipenem against carbapenemase-positive *Enterobactericeae* isolates collected by the SMART global surveillance program from 2008 to 2014. J Clin Microbiol. 2017;55:1638–49. https://doi.org/10.1128/JCM.02316-16
7. Karthikeyan K, Thirunarayan MA, Krishnan P. Coexistence of bla_{OXA-23} with bla_{NDM-1} and *armA* in clinical isolates of *Acinetobacter baumannii* from India. J Antimicrob Chemother. 2010;65:2253–4. https://doi.org/10.1093/jac/dkq273
8. Hu H, Hu Y, Pan Y, Liang H, Wang H, Wang X, et al. Novel plasmid and its variant harboring both a bla_{NDM-1} gene and type IV secretion system in clinical isolates of *Acinetobacter lwoffii*. Antimicrob Agents Chemother. 2012;56:1698–702. https://doi.org/10.1128/AAC.06199-11
9. Jovcic B, Lepsanovic Z, Suljagic V, Rackov G, Begovic J, Topisirovic L, et al. Emergence of NDM-1 metallo-β-lactamase in *Pseudomonas aeruginosa* clinical isolates from Serbia. Antimicrob Agents Chemother. 2011;55:3929–31. https://doi.org/10.1128/AAC.00226-11
10. Wu W, Feng Y, Tang G, Qiao F, McNally A, Zong Z. NDM metallo-β-lactamases and their bacterial producers in healthcare settings. Clin Microbiol Rev. 2019;32:e00115–8. https://doi.org/10.1128/CMR.00115-18
11. Doi Y, Wachino JI, Arakawa Y. Aminoglycoside resistance: the emergence of acquired 16S ribosomal RNA methyltransferases. Infect Dis Clin North Am. 2016;30:523–37. https://doi.org/10.1016/j.idc.2016.02.011
12. Shields RK, Doi Y. Aztreonam combination therapy: an answer to metallo-β-lactamase–producing gram-negative bacteria? Clin Infect Dis. 2020;71:1099–101. https://doi.org/10.1093/cid/ciz1159
13. Politi L, Gartzonika K, Spanakis N, Zarkotou O, Poulou A, Skoura L, et al. Emergence of NDM-1-producing *Klebsiella pneumoniae* in Greece: evidence of a widespread clonal outbreak. J Antimicrob Chemother. 2019;74:2197–202. https://doi.org/10.1093/jac/dkz176
14. Otter JA, Doumith M, Davies F, Mookerjee S, Dyakova E, Gilchrist M, et al. Emergence and clonal spread of colistin resistance due to multiple mutational mechanisms in carbapenemase-producing *Klebsiella pneumoniae* in London. Sci Rep. 2017;7:12711. https://doi.org/10.1038/s41598-017-12637-4
15. Wailan AM, Sidjabat HE, Yam WK, Alikhan N-F, Petty NK, Sartor AL, et al. Mechanisms involved in acquisition of bla_{NDM} genes by IncA/C2 and $IncFII_Y$ plasmids. Antimicrob Agents Chemother. 2016;60:4082–8. https://doi.org/10.1128/AAC.00368-16
16. Poirel L, Schrenzel J, Cherkaoui A, Bernabeu S, Renzi G, Nordmann P. Molecular analysis of NDM-1–producing enterobacterial isolates from Geneva, Switzerland. J Antimicrob Chemother. 2011;66:1730–3. https://doi.org/10.1093/jac/dkr174
17. Ramette A, Gasser M, Nordmann P, Zbinden R, Schrenzel J, Perisa D, et al. Temporal and regional incidence of carbapenemase-producing *Enterobacterales*, Switzerland, 2013 to 2018. Euro Surveill. 2021;26:1900760. https://doi.org/10.2807/1560-7917.ES.2021.26.15.1900760
18. European Committee on Antimicrobial Susceptibility Testing. Breakpoint tables for interpretation of MICs and zone diameters. Version 11.0. 2021 [cited 2021 Aug 9]. https://www.eucast.org/fileadmin/src/media/PDFs/EUCAST_files/Breakpoint_tables/v_11.0_Breakpoint_Tables.pdf
19. Poirel L, Walsh TR, Cuvillier V, Nordmann P. Multiplex PCR for detection of acquired carbapenemase genes. Diagn Microbiol Infect Dis. 2011;70:119–23. https://doi.org/10.1016/j.diagmicrobio.2010.12.002
20. Bankevich A, Nurk S, Antipov D, Gurevich AA, Dvorkin M, Kulikov AS, et al. SPAdes: a new genome assembly algorithm and its applications to single-cell sequencing. J Comput Biol. 2012;19:455–77. https://doi.org/10.1089/cmb.2012.0021
21. Zankari E, Hasman H, Cosentino S, Vestergaard M, Rasmussen S, Lund O, et al. Identification of acquired antimicrobial resistance genes. J Antimicrob Chemother. 2012;67:2640–4. https://doi.org/10.1093/jac/dks261
22. Larsen MV, Cosentino S, Lukjancenko O, Saputra D, Rasmussen S, Hasman H, et al. Benchmarking of methods for genomic taxonomy. J Clin Microbiol. 2014;52:1529–39. https://doi.org/10.1128/JCM.02981-13
23. Seemann T. Prokka: rapid prokaryotic genome annotation. Bioinformatics. 2014;30:2068–9. https://doi.org/10.1093/bioinformatics/btu153
24. Treangen TJ, Ondov BD, Koren S, Phillippy AM. The Harvest suite for rapid core-genome alignment and visualization of thousands of intraspecific microbial genomes. Genome Biol. 2014;15:524. https://doi.org/10.1186/s13059-014-0524-x
25. Letunic I, Bork P. Interactive Tree Of Life (iTOL) v4: recent updates and new developments. Nucleic Acids Res. 2019;47(W1):W256–9. https://doi.org/10.1093/nar/gkz239
26. Darling AE, Mau B, Perna NT. progressiveMauve: multiple genome alignment with gene gain, loss and rearrangement. PLoS One. 2010;5:e11147. https://doi.org/10.1371/journal.pone.0011147
27. Federal Statistical Office. Permanent resident population by age, canton, district, and commune, 2010–2019. 2020 [cited 2021 Aug 10]. https://www.bfs.admin.ch/bfs/en/home/statistics/population/effectif-change.assetdetail.13707298.html
28. Alm RA, Johnstone MR, Lahiri SD. Characterization of *Escherichia coli* NDM isolates with decreased susceptibility to aztreonam/avibactam: role of a novel insertion in PBP3. J Antimicrob Chemother. 2015;70:1420–8.
29. Ma K, Feng Y, McNally A, Zong Z. Struggle to survive: the choir of target alteration, hydrolyzing enzyme, and plasmid expression as a novel aztreonam-avibactam resistance mechanism. mSystems. 2020;5:e00821–20. https://doi.org/10.1128/mSystems.00821-20
30. Kotsakis SD, Papagiannitsis CC, Tzelepi E, Tzouvelekis LS, Miriagou V. Extended-spectrum properties of CMY-30, a Val211Gly mutant of CMY-2 *cephalosporinase*. Antimicrob Agents Chemother. 2009;53:3520–3. https://doi.org/10.1128/AAC.00219-09
31. Sadek M, Juhas M, Poirel L, Nordmann P. Genetic features leading to reduced susceptibility to aztreonam/avibactam among metallo-β-lactamase–producing *Escherichia coli* isolates. Antimicrob Agents Chemother. 2020;64:e01659–2. https://doi.org/10.1128/AAC.01659-20
32. Rogers BA, Sidjabat HE, Silvey A, Anderson TL, Perera S, Li J, et al. Treatment options for New Delhi metallo-β-lactamase–harboring *Enterobacteriaceae*. Microb Drug Resist. 2013;19:100–3. https://doi.org/10.1089/mdr.2012.0063
33. Taylor E, Sriskandan S, Woodford N, Hopkins KL. High prevalence of 16S rRNA methyltransferases among

carbapenemase-producing *Enterobacteriaceae* in the UK and Ireland. Int J Antimicrob Agents. 2018;52:278–82. https://doi.org/10.1016/j.ijantimicag.2018.03.016
34. Sugawara Y, Akeda Y, Hagiya H, Sakamoto N, Takeuchi D, Shanmugakani RK, et al. Spreading patterns of NDM-producing *Enterobacteriaceae* in clinical and environmental settings in Yangon, Myanmar. Antimicrob Agents Chemother. 2019;63:e01924–18. https://doi.org/10.1128/AAC.01924-18
35. Eljaaly K, Alharbi A, Alshehri S, Ortwine JK, Pogue JM. Plazomicin: a novel aminoglycoside for the treatment of resistant gram-negative bacterial infections. Drugs. 2019;79:243–69. https://doi.org/10.1007/s40265-019-1054-3
36. Roer L, Overballe-Petersen S, Hansen F, Schønning K, Wang M, Røder BL, et al. *Escherichia coli* sequence type 410 is causing new international high-risk clones. MSphere.2018;3:e00337–18. https://doi.org/10.1128/mSphere.00337-18
37. Li J, Yu T, Tao X-Y, Hu Y-M, Wang H-C, Liu J-L, et al. Emergence of an NDM-5-producing *Escherichia coli* sequence type 410 clone in infants in a children's hospital in China. Infect Drug Resist. 2020;13:703–10. https://doi.org/10.2147/IDR.S244874
38. Bleichenbacher S, Stevens MJA, Zurfluh K, Perreten V, Endimiani A, Stephan R, et al. Environmental dissemination of carbapenemase-producing *Enterobacteriaceae* in rivers in Switzerland. Environ Pollut. 2020;265(Pt B):115081. https://doi.org/10.1016/j.envpol.2020.115081
39. Chakraborty T, Sadek M, Yao Y, Imirzalioglu C, Stephan R, Poirel L, et al. Cross-border emergence of *Escherichia coli* producing the carbapenemase NDM-5 in Switzerland and Germany. J Clin Microbiol. 2021;59:e02238–20. https://doi.org/10.1128/JCM.02238-20
40. Bitar I, Piazza A, Gaiarsa S, Villa L, Pedroni P, Oliva E, et al. ST405 NDM-5 producing *Escherichia coli* in northern Italy: the first two clinical cases. Clin Microbiol Infect. 2017;23:489–90. https://doi.org/10.1016/j.cmi.2017.01.020
41. Garcia-Fernandez A, Villa L, Bibbolino G, Bressan A, Trancassini M, Pietropaolo V, et al. Novel insights and features of the NDM-5–producing *Escherichia coli* sequence type 167 high-risk clone. MSphere. 2020;5:e00269–20. https://doi.org/10.1128/mSphere.00269-20
42. Tavoschi L, Forni S, Porretta A, Righi L, Pieralli F, Menichetti F, et al. The Tuscan Clinical Microbiology Laboratory Network. Prolonged outbreak of New Delhi metallo-β-lactamase–producing carbapenem-resistant *Enterobacterales* (NDM-CRE), Tuscany, Italy, 2018 to 2019. Euro Surveill. 2020;25:2000085. https://doi.org/10.2807/1560-7917.ES.2020.25.6.2000085
43. Park Y, Choi Q, Kwon GC, Koo SH. Emergence and transmission of New Delhi metallo-β-lactamase-5–producing *Escherichia coli* sequence type 361 in a tertiary hospital in South Korea. J Clin Lab Anal. 2020;34:e23041. https://doi.org/10.1002/jcla.23041
44. Ali T, Rahman SU, Zhang L, Shahid M, Han D, Gao J, et al. Characteristics and genetic diversity of multidrug resistant extended-spectrum β-lactamase (ESBL)–producing *Escherichia coli* isolated from bovine mastitis. Oncotarget. 2017;8:90144–63. https://doi.org/10.18632/oncotarget.21496
45. Irrgang A, Falgenhauer L, Fischer J, Ghosh H, Guiral E, Guerra B, et al. CTX-M-15-producing *E. coli* isolates from food products in Germany are mainly associated with an IncF-type plasmid and belong to two predominant clonal *E. coli* lineages. Front Microbiol. 2017;8:2318. 10.3389/fmicb.2017.02318 https://doi.org/10.3389/fmicb.2017.02318
46. Peirano G, Chen L, Kreiswirth BN, Pitout JDD. Emerging antimicrobial-resistant high-risk *Klebsiella pneumoniae* clones ST307 and ST147. Antimicrob Agents Chemother. 2020;64:e01148–20. https://doi.org/10.1128/AAC.01148-20
47. Liao W, Liu Y, Zhang W. Virulence evolution, molecular mechanisms of resistance and prevalence of ST11 carbapenem-resistant *Klebsiella pneumoniae* in China: a review over the last 10 years. J Glob Antimicrob Resist. 2020;23:174–80. https://doi.org/10.1016/j.jgar.2020.09.004
48. Zhao J, Liu C, Liu Y, Zhang Y, Xiong Z, Fan Y, et al. Genomic characteristics of clinically important ST11 *Klebsiella pneumoniae* strains worldwide. J Glob Antimicrob Resist. 2020;22:519–26. https://doi.org/10.1016/j.jgar.2020.03.023
49. Baraniak A, Machulska M, Żabicka D, Literacka E, Izdebski R, Urbanowicz P, et al.; NDM-PL Study Group. Towards endemicity: large-scale expansion of the NDM-1-producing *Klebsiella pneumoniae* ST11 lineage in Poland, 2015–16. J Antimicrob Chemother. 2019;74:3199–204. https://doi.org/10.1093/jac/dkz315
50. Voulgari E, Gartzonika C, Vrioni G, Politi L, Priavali E, Levidiotou-Stefanou S, et al. The Balkan region: NDM-1-producing *Klebsiella pneumoniae* ST11 clonal strain causing outbreaks in Greece. J Antimicrob Chemother. 2014;69:2091–7. https://doi.org/10.1093/jac/dku105

Address for correspondence: Laurent Poirel, Medical and Molecular Microbiology Unit, Department of Medicine, Faculty of Science, University of Fribourg, Chemin du Musée 18, CH-1700 Fribourg, Switzerland; email: laurent.poirel@unifr.ch

New Perspective on the Geographic Distribution and Evolution of Lymphocytic Choriomeningitis Virus, Central Europe

Alena Fornůsková, Zuzana Hiadlovská, Miloš Macholán, Jaroslav Piálek, Joëlle Goüy de Bellocq

Lymphocytic choriomeningitis virus (LCMV) is an Old World mammarenavirus found worldwide because of its association with the house mouse. When LCMV spills over to immunocompetent humans, the virus can cause aseptic meningitis; in immunocompromised persons, systemic infection and death can occur. Central Europe is a strategic location for the study of LCMV evolutionary history and host specificity because of the presence of a hybrid zone (genetic barrier) between 2 house mouse subspecies, *Mus musculus musculus* and *M. musculus domesticus*. We report LCMV prevalence in natural mouse populations from a Czech Republic–Germany transect and genomic characterization of 2 new LCMV variants from the Czech Republic. We demonstrate that the main division in the LCMV phylogenetic tree corresponds to mouse host subspecies and, when the virus is found in human hosts, the mouse subspecies found at the spillover location. Therefore, LCMV strains infecting humans can be predicted by the genetic structure of house mice.

Lymphocytic choriomeningitis virus (LCMV) is the prototype of the family Arenaviridae. Its genus *Mammarenavirus* is associated with rodent-transmitted diseases in humans, including agents of hemorrhagic fevers, such as Lassa virus and Junin virus (*1*). In immunocompetent persons, LCMV infection is typically asymptomatic but can cause nonspecific febrile illness or aseptic meningitis. However, LCMV infection can cause severe congenital disease, and it has been reported at the origin of 6 clusters of severe or fatal disease among solid organ recipients in the past 20 years (*2*).

All mammarenaviruses are enveloped ambisense RNA viruses. Their genome (≈11-kb) is composed of 2 segments, each encoding 2 proteins in nonoverlapping open reading frames (ORFs); the large 7.2-kb segment encodes the Z matrix and the large polymerase proteins, and the small 3.4-kb segment encodes the glycoprotein and nucleoprotein (*1*).

The primary host reservoirs of LCMV are house mice (*Mus musculus*), although the virus has been reported in other rodents, and experimental infections have been described in other mammals, such as rabbits, dogs, and pigs (*3*–*5*). The house mouse is a complex of several subspecies. The most widespread subspecies are *M. musculus musculus*, found from central and northern Europe to the Far East; *M. musculus domesticus*, which is found in western and southern Europe, northern Africa, the Middle East, and, more recently, in North and South America, southern Africa, Australia, and Oceania because of passive transport with humans; and *M. musculus castaneus,* which is found in central and southeastern Asia (*6*,*7*) (Figure 1). These subspecies are not reproductively isolated, and several regions of secondary contact hybridization exist, including a >2,500 km–long region in Europe extending from Scandinavia to the Black Sea in which *M. musculus musculus* and *M. musculus domesticus* mice have contact (Figure 1). In this region, the 2 subspecies form a hybrid zone with a barrier to gene flow between them (*6*,*9*,*10*). Recent studies have shown that such hybrid zones can also act as barriers for the organisms' pathogens (*11*–*14*). Hybrid zones are thus useful natural settings to study the limit of host specificity, which is pivotal to understanding the geographic distribution of pathogens and their potential for spillover. For example, 2 mammarenaviruses, Morogoro virus and Gairo virus, are each confined to

Author affiliations: Institute of Vertebrate Biology of the Czech Academy of Sciences, Brno, Czech Republic (A. Fornůsková, J. Piálek, J. Goüy de Bellocq); Institute of Animal Physiology and Genetics of the Czech Academy of Sciences (Z. Hiadlovská, M. Macholán); Czech University of Life Sciences Prague, Prague (J. Goüy de Bellocq)

DOI: https://doi.org/10.3201/eid2710.210224

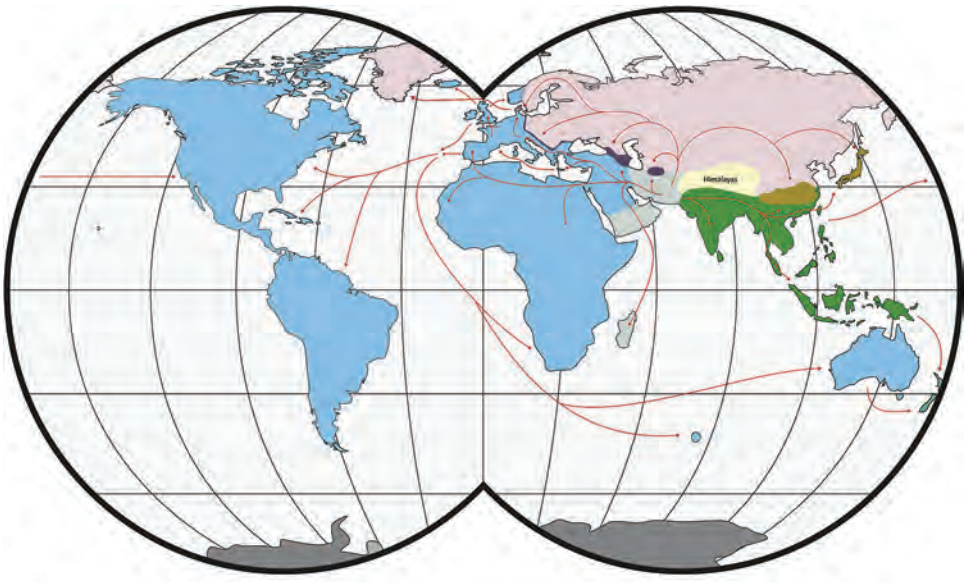

Figure 1. Worldwide distribution of *Mus musculus* mouse subspecies. Colors indicate subspecies ranges: green and tan, *M. musculus castaneus*; blue and purple, *M. musculus domesticus*; pink, *M. musculus musculus*; gray, central populations and *M. musculus gentilulus*. Note that house mice may not be found throughout the complete extent of some areas (e.g., subarctic regions, the Sahara Desert, and the Amazon rainforest). The tan, purple, and gray areas indicate regions of hybridization. Red arrows indicate inferred routes of historical migrations and recent movements in association with humans. Adapted from (*7*,*8*).

1 of the 2 subtaxa of their host, the Natal mulimammate mouse (*Mastomys natalensis*), even though the host hybridizes in Tanzania (*13*,*15*).

In 2010, Albariño et al. (*16*) investigated the genetic diversity and distribution of LCMV variants by analyzing 29 genomes. They demonstrated that LCMV is highly diverse and forms 4 distinct lineages (I–IV) but found little correlation of those lineages with time or place of isolation. From their dataset, only 3 strains (Marseille12-2004, Yale-1977, and Michigan-2005) originated from wild mice, but those strains were not assigned to subspecies. Furthermore, the place of isolation is a poor proxy for the origin of spillover to human hosts. For example, focusing on lineage II of Albariño et al., strains M1 and M2 were isolated in Japan in 2005, but came from a wild-derived strain originating from *M. musculus musculus* mice caught in Illmitz, Austria, in 1985 (*17*). Likewise, the Dandenong-Yugoslavia LCMV strain (*18*) was isolated in Australia from a human spillover, but that person returned from the former Yugoslavia before becoming ill and dying. The Bulgaria 1956 strain (*19*) was isolated from a human spillover, but geographic origin was not mentioned in the original study; a contact of that patient was treated for the same symptoms in a hospital in Vidin, Bulgaria, suggesting spillover origin in northwestern Bulgaria. Finally, the last LCMV strain in lineage II, LE-FRANCE (*20*), was isolated from a pregnant woman in France (i.e., within *M. musculus domesticus* mouse territory), but the person worked in a pet store, making strain origin uncertain because other rodent species, especially hamsters, are known to be LCMV carriers (*3*,*4*,*20*). In summary, for 3 of 4 LCMV strains in lineage II, the potential spillover origin is consistent with *M. musculus musculus* mouse territory despite diverse viral isolation locations. Similarly, in LCMV lineage I, strains were found in laboratory mice, essentially of *M. musculus domesticus* origin (*21*); wild mice; or in primate (including human) spillovers in the United States or western Europe, and were thus consistent with *M. musculus domesticus* mouse origin (*22*). LCMV lineage IV consists only of strains isolated from woodmice (*Apodemus sylvaticus*) from Spain. Given these observations, we hypothesized that host specificity could be a better predictor of LCMV genetics than the place or time of LCMV strain isolation.

In this study, we test the hypothesis that LCMV phylogenetic clustering reflects specificity to its host reservoirs by investigating the diversity of LCMV in central Europe across the house mouse hybrid zone (HMHZ). We also update the phylogenetic analysis of LCMV from Albariño et al. (*16*) by complementing their dataset with LCMV genomes sequenced in the last decade and with our data.

Material and Methods

Sampling and Mouse Genotyping

A total of 748 house mice (410 *M. musculus domesticus* and 338 *M. musculus musculus*) from 179 localities

(100 for *M. musculus domesticus* and 79 for *M. musculus musculus*) were trapped in farms during 2008–2019 across a 145-km by 110-km belt stretching from northeastern Bavaria (Germany) to western Bohemia (Czech Republic), a region in which these mouse subspecies meet and form the HMHZ (*23*) (Figure 2; Appendix 1 Table 1, https://wwwnc.cdc.gove/EID/article/27/10/21-0224-App1.xlsx). Tissue samples were preserved in liquid nitrogen and later stored at −80°C as described in Goüy de Bellocq et al. (*24*). Mice were identified on the basis of a set of diagnostic markers as in Macholán et al. (*23*) or on the basis of 1,401 single-nucleotide polymorphism (SNP) markers (*25*) or 0.62 million SNP markers (*26*) (Appendix 1 Table 1). Each individual mouse's hybrid index (HI) was estimated as the proportion of *M. musculus musculus* alleles. We considered all mice with HIs <0.5 as *M. musculus domesticus*–like and those with HIs >0.5 as *M. musculus musculus*–like.

LCMV Serologic and Molecular Screening

We screened 291 blood plasma samples collected from 100 localities during 2008–2011 for LCMV antibodies by using the ELISA kit IM-698 C-EB (XpressBio, https://xpressbio.com). We used 100 µL of 1:50 diluted serum for the reaction according to the manufacturer's instructions. In addition, we extracted RNA from 616 spleen or salivary gland samples by using RNeasy Mini kit (QIAGEN, https://www.qiagen.com). We reverse-transcribed the RNA samples collected in 2008–2013 by using the Applied Biosystems High-Capacity RNA-to-cDNA Kit (ThermoFisher Scientific, https://www.thermofisher.com) in 10 µL final volume. We screened for LCMV by targeting a 340-nt fragment of the large gene by using primers from Vieth et al. (*27*), because these primers detected LCMV in a previous study (*28*). Samples were screened with the Multiplex PCR kit (QIAGEN) in a final volume of 15 µL by using 2 µL of cDNA and following the manufacturer's instructions. To increase assay sensitivity, we also designed primers for a nested PCR assay on the basis of LCMV sequences available in GenBank and targeting 442 nt in a part of the large gene partially overlapping with the region described previously. We tested 96 samples with both assays and results showed the same number of positive samples. However, the first assay (i.e., Vieth et al. primers) showed higher sensitivity (stronger band in 1.5% agarose gels); therefore, we selected that assay to screen the complete dataset. However, we used the second assay for Sanger sequencing of all positive samples to obtain longer final large fragment (659–665 nt resulting from merging both assay outputs). We screened the 2019 RNA samples with Vieth et al. primers by using Invitrogen SuperScript IV One-Step RT-PCR System (ThermoFisher Scientific) in a final volume of 20 µL and using 3 µL of extracted RNA. We attempted additional amplifications in positive samples to sequence parts of the glycoprotein and nucleoprotein

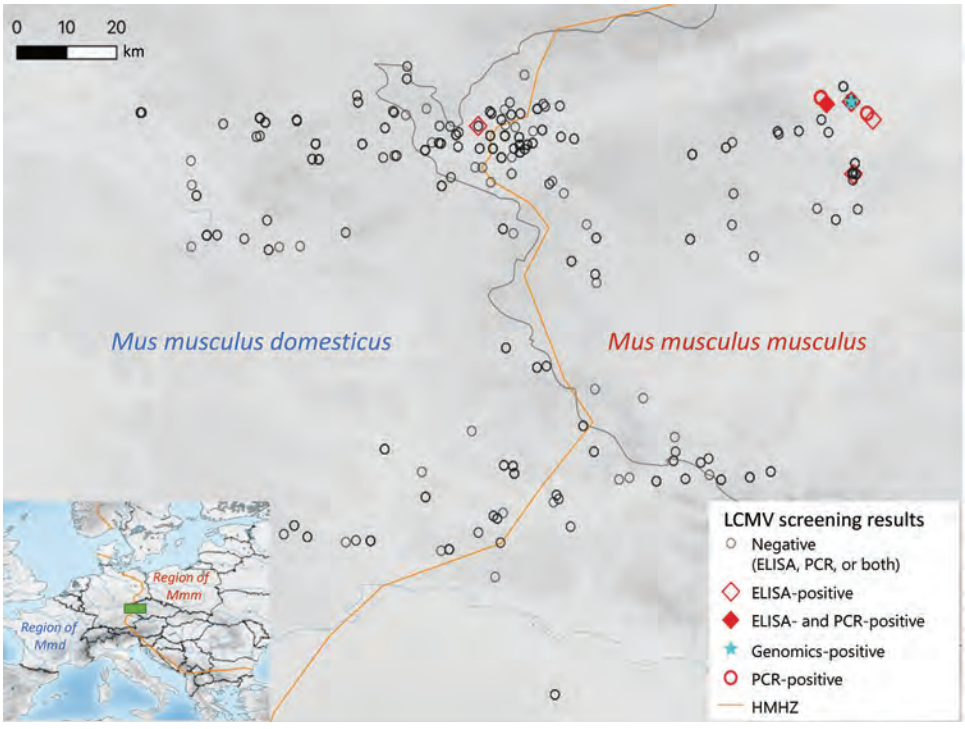

Figure 2. Tested localities for LCMV, Central Europe. The center of the HMHZ is represented by the orange line. The green rectangle in the inset map shows the sampling area, located in the center of the HMHZ. HMHZ, house mouse hybrid zone; LCMV, lymphocytic choriomeningitis virus.

genes (Appendix 2 Table, https://wwwnc.cdc.gov/EID/article/27/10/21-0224-App2.pdf). We purified PCR products and Sanger sequenced in both directions by using Eurofins Genomics (https://eurofinsgenomics.com).

Whole-Genome Sequencing and Assembly of LCMV Viruses

We selected 2 positive samples from localities 10 km apart: sample SK1042 from Kryry, Czech Republic (KRY1) and sample SK1194 from Nepomyšl, Czech Republic (NEPO1), for whole-genome sequencing. We extracted RNA from lung and liver specimens by using the viral enrichment protocol described in Goüy de Bellocq et al. (*29*). The cDNA synthesis, library preparation, and sequencing (BGI Genomics, https://www.bgi.com) were carried out as described in Goüy de Bellocq et al. (*30*). After read demultiplexing, quality filtering, and trimming, 48,209,592 paired-end reads were available for SK1042, and 39,228,040 paired-end reads were available for SK1194. We used only 10,000,000 paired-end reads for a de novo assembly by iterative mapping with Geneious Mapper in Geneious 11 (Geneious, https://www.geneious.com). We enriched for LCMV reads in silico by removing all reads that mapped to mouse reference genome GRCm38. The LCMV iterative mapping was seeded with the 340 nt of the large gene obtained by Sanger sequencing and a 74-nt sequence conserved among LCMV strains for the Z gene. For the small segment, we generated 2 small seed reference sequences of ≈150 nt in the glycoprotein and nucleoprotein by first mapping the paired-end reads to LCMV strain Traub (from *M. musculus domesticus* mice). We confirmed the sequence of the intergenic region of the large segment by Sanger sequencing designing primers in the neighboring coding regions (Appendix 2 Table). After assembly, we ensured the seeding had not influenced the output. Finally, as part of a viral metagenomic study of digestive tract samples taken from mice in the HMHZ (J. Goüy de Belloq, unpub. data), we detected 229-nt and 458-nt contigs that matched via BLAST (https://blast.ncbi.nlm.nih.gov/Blast.cgi) with the large and glycoprotein gene of LCMV and Dandenong virus in a pooled sample of 3 mice coming from Buškovice (BUS2) collected in 2014. We included these 2 sequences in the current study.

Phylogenetic Analyses

LCMV nucleotide sequences were aligned with the sequence coding parts of the nucleoprotein, glycoprotein, and large genes of other strains available in GenBank (Appendix 1 Table 2). We included all strains analyzed in Albariño et al. (*16*), augmented with 11 recently published genome sequences that included LCMV variants of *M. musculus domesticus* mouse origin from France, Gabon, and French Guiana (*28*,*31*,*32*). Nucleotide alignment was based on amino acid sequences in Geneious Prime 2019.2 (Geneious) by using the ClustalW algorithm. We used the Bayesian Information Criterion in MEGA X (*33*) to evaluate models of nucleotide and amino acid substitution. The best-fit model was general time reversible plus invariate sites plus gamma distribution for all 3 genes on the basis of the nucleic acid dataset, Jones-Taylor-Thornton plus invariate sites plus gamma for large and nucleoprotein genes, and Le Gascuel plus gamma for the glycoprotein gene for the amino acid dataset. We performed phylogenetic analyses on nucleic acid and amino acid sequences by using Bayesian inference using MrBayes version 3.2.7 (*34*). For the amino acid sequence dataset, we only included LCMV sequences in which a large proportion of the coding genes were sequenced. We conducted default priors for all parameters and 2 independent runs with 10 million generations per run and sampled trees and parameters every 500 generations, discarding the first 25% of sampled trees as burn-in. We used Bayesian posterior probabilities (PP) to assess node support and the complete genome of Lunk virus from African *Mus minutoides* as an outgroup. We prepared tree figures in FigTree version 1.4.4 (http://tree.bio.ed.ac.uk/software/figtree).

Results

Rodent Sampling and LCMV Detection

We found 7 positive samples among the 291 samples (160 *M. musculus domesticus* and 131 *M. musculus musculus*) tested with ELISA for a prevalence of 2.4%. A total of 6 positives were revealed in *M. musculus musculus* mouse territory: 3 in Buškovice (BUS2, 2008), 1 in Nepomyšl (NEPO1, 2009), 1 in Kryry (KRY1, 2009), and 1 in Žihle (2010). All these specimens had HI >0.96, indicating almost pure *M. musculus musculus*. The single positive specimen from *M. musculus domesticus* territory mouse (HI = 0.20) was captured in locality Starý Rybník Vepřín (SRYV) (2009), 3.7 km from the center of the HMHZ. By using the molecular LCMV screening, we found 5 positive samples out of 616 analyzed (prevalence = 0.8%) (Table 1). All were from *M. musculus musculus* mouse territory with HI >0.97: 4 specimens from NEPO1 (2008 and 2009) and 1 specimen from KRY1 (2009). One specimen from NEPO1 (SK1042; HI = 0.98) was found positive by both serologic and molecular screening approaches.

Table 1. Overview of sampled localities and tested mice in study of geographic distribution and evolution of lymphocytic choriomeningitis virus, central Europe

Subspecies	No. sampled localities	No. tested by PCR/no. positive	No. tested by ELISA/no. positive	No. genomic sequences	Total positive samples
Mus musculus domesticus	100	335/0	160/1	0	1
M. musculus musculus	79	281/5	131/6	3	11
Total	179	616/5	291/7	3	12

All the positive localities confirmed genetically were located within a 12-km^2 area. The detection of RNA-positive samples in 2009 and 2010 in NEPO1 and the repeated finding of positive specimens in BUS2 by ELISA in 2008 and 2014 (J. Goüy de Belloq, unpub. data) suggest that LCMV is locally endemic in *M. musculus musculus* mouse territory, persisting within farms over several years.

Characterization of the Full Genomes of LCMV from the Czech Republic

We obtained LCMV whole-genome sequences from 2 mice samples. Because the partial large sequences of the 4 samples from NEPO1 were identical, we characterized the genome of only 1 LCMV sample (SK1194). The other sample (SK1042) was from the locality KRY1, 10 km from NEPO1. At the 3′ end of the large segment of the variant SK1194, ≈19 noncoding nucleotides were missing. Each of the 2 segments showed the 2 ORFs typical for mammarenavirus separated by typical stem-loop structures. The complete large segment was 7232 nt (for strain SK1042) and contained 2 ORFs: the Z ORF (270 nt) encodes a 90-aa zinc-finger protein, whereas the large ORF (6627 nt) encodes a 2209-aa RNA-dependent RNA polymerase. The complete small segment was 3380 nt for SK1194 and 3381 nt for SK1042 and contained 2 ORFs: the glycoprotein ORF (1494 nt) coding for a 498-aa glycoprotein precursor and the nucleoprotein ORF (1674 nt) encoding a 558-aa nucleoprotein. The pairwise nucleotide divergence between the 2 variants was 8.4% for the small segment and 9.6% for the large segment.

Phylogenetic Analysis

We analyzed the large, glycoprotein, and nucleoprotein genes separately and highlighted the position of the new LCMV variants found in *M. musculus musculus* mice from the Czech Republic and of the variants known to have been isolated from wild *M. musculus domesticus* mice. For the large nucleotide tree (Figure 3), the topology of the phylogeny is similar to that of Albariño et al. (*16*); 2 lineages are highly supported (PP = 0.99): I (harboring 24 LCMV strains) and II (10 LCMV strains). Lineage III, which consisted of a single sequence isolated from a human in Georgia (USA), has a highly supported basal position (PP = 1). All sequences from Czech Republic *M. musculus musculus* mice form a sister clade to Dandenong virus within lineage II, the lineage we hypothesized to originate from *M. musculus musculus* mice. The 3 variants from *M. musculus domesticus* mice are found scattered within the highly supported lineage I (PP = 0.99). The internal topology of lineage I is not resolved and consists of sequences originating from various hosts and regions. Among these clades, a subset was isolated from primate spillovers, likely from local mice in the United States, Spain, France, and Germany (i.e., within *M. musculus domesticus* mouse territory). The other strains that do not overlap with the range of *M. musculus domesticus* mice have either been isolated from cell culture (strains from Japan or Slovakia) or ticks (strains from China). In the phylogenetic tree constructed on the basis of large amino acid sequences, the position of lineage III is again well supported but is basal to lineages I and II, both with highly supported monophyly (PP = 1) (Appendix 2 Figure, panel A).

The phylogenetic position of the sequences from Czech Republic *M. musculus musculus* and wild *M. musculus domesticus* mice in our nucleoprotein and glycoprotein gene trees corresponds to that in the large gene tree. An additional clade, clade IV, is composed of strains isolated from the woodmouse (*Apodemus sylvaticus*). All 4 glycoprotein lineages based on amino acid sequences were highly supported (PP = 1) (Appendix 2 Figure, panel B), whereas the phylogenetic signal at the nucleotide level seems to be compromised by homoplasy, resulting in trichotomy between lineages I, II, and III (Figure 4). A similar pattern can be seen in the phylogenetic trees based on the nucleoprotein gene but with low support. Phylogenetic relationships between lineages are not resolved, demonstrating differences with regard to the type of data. The basal position of lineage IV (woodmouse) to other lineages is well supported (PP = 1) on the basis of amino acid sequences (Appendix 2 Figure, panel C). By contrast, nucleotide sequences show lineage IV as sister group to lineage I (PP = 0.92) and lineage III clustering with lineage II (PP = 1), whereas the strain from Bulgaria is basal to all other ingroup lineages (PP = 1), suggesting that homoplasy at the nucleic acid level affects the phylogenetic signal (Figure 5).

Discussion

We found LCMV at low prevalence in wild mice in central Europe, and all genetically confirmed cases clustered within a small geographic region in the *M. musculus musculus* mouse side of the HMHZ. This low prevalence prevents direct inference of the zone as a barrier to LCMV exchange between the mouse subspecies in nature. However, our phylogenetic analyses, which included new LCMV variants from the Czech Republic, 3 variants sequenced from wild *M. musculus domesticus* mice, other LCMV variants sequenced during the last decade, and supplemented with published data, support the hypothesis that LCMV lineage I harbors viruses originating from *M. musculus domesticus* mice and lineage II includes viruses primarily found in *M. musculus musculus* mice.

The low prevalence of LCMV observed in central Europe is not uncommon. In wild mice, this prevalence has been shown to be variable, ranging from 0 to 25% (*2*), but most studies have reported low prevalence and patchy distribution. For example, Ackermann et al. (*34*) found an overall prevalence of 3% in wild mice from Germany, with 65 LCMV-positive specimens from 44 localities, but despite extensive sampling efforts in Bavaria as a whole (380 mouse samples over 70,000 km^2), no LCMV-positive mice were found there (*35*). We also failed to detect any positive LCMV samples in Bavaria (*M. musculus domesticus* mouse region). The low prevalence of LCMV is comparable to other mammarenaviruses (e.g., Gairo virus and Morogoro virus in *Mastomys natalensis* mice in Tanzania) (*13*,*15*).

We reported LCMV infection in Buškovice in 2008 and 2014; however, we were unable to demonstrate genetic turnover during that period. Commensal mouse populations are usually structured to local

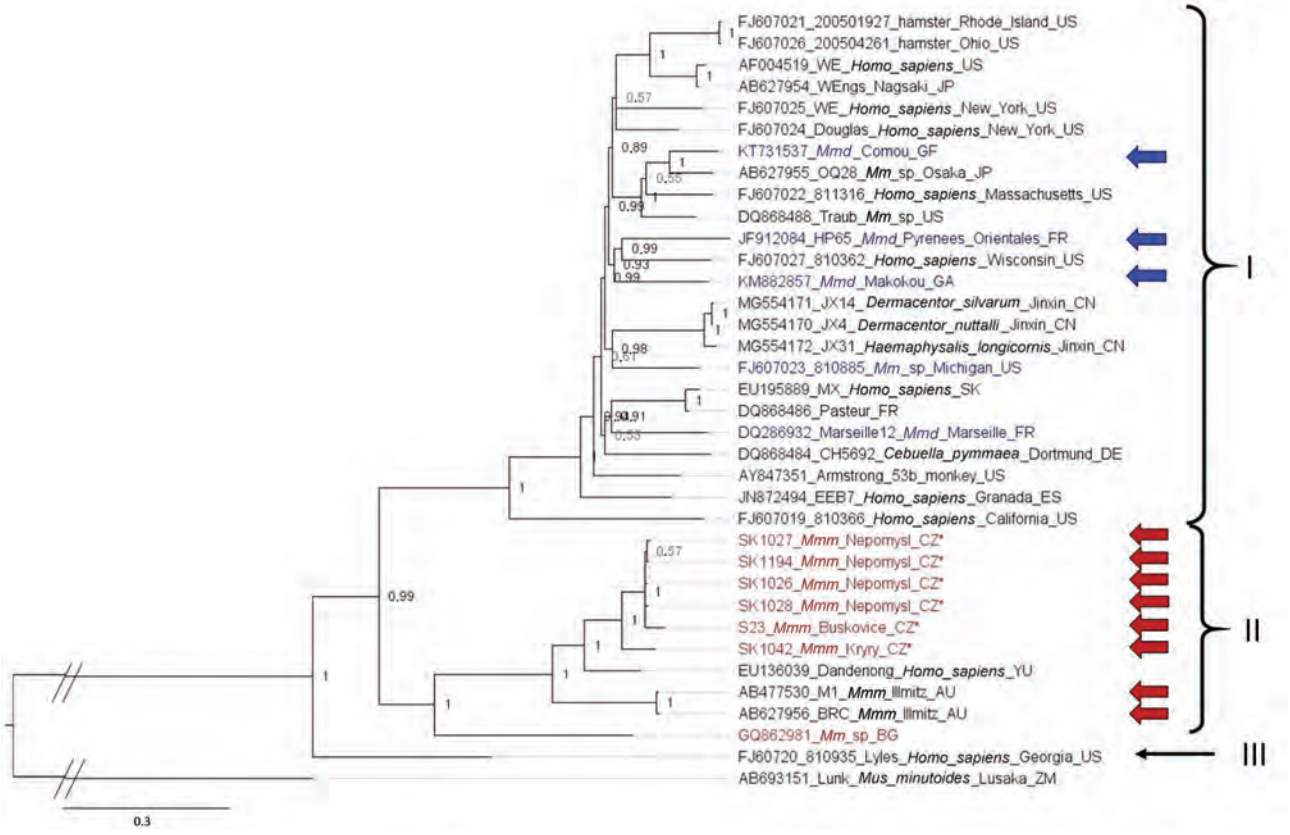

Figure 3. Phylogenetic analysis performed on nucleic acid sequences of large gene of lymphocytic choriomeningitis virus (LCMV) sequences using Bayesian inference. Bayesian posterior probabilities were used to assess node support. Lunk virus from *Mus minutoides* (Africa) was used as outgroup. All sequences obtained in this study were submitted to GenBank (accession nos. MZ568450–7, MZ558311–3, MZ568449). Names of LCMV strains are composed of GenBank accession number, strain name, host species, and place and country of origin (if known) or isolation. Country code is defined as ISO code (https://countrycode.org). Colors indicate LCMV strains isolated from wild rodents where there is a match between expected mouse subspecies on the basis of geographic region and sampling area: blue, *Mus musculus domesticus*; red, *M. musculus musculus*. Arrows indicate known origin of mice subspecies on the basis of genetic data, asterisks (*) indicate LCMV strains from this study, and lineages are indicated by roman numerals. Scale bar indicates nucleotide substitutions per site. Mmd, *M. musculus domesticus*; Mmm, *M. musculus musculus*; Mmm_lab, laboratory mouse strain derived from *M. musculus musculus*; Mm_lab, laboratory mouse strain; Mm_sp, *Mus musculus* spp.

subpopulations or demes, with a dispersal scale of ≈1 km² (*36*,*37*). Because LCMV can spread both horizontally and vertically, maintenance of the virus within a deme over several years seems plausible. Whether LCMV variants are still present in the 12 km² area is not certain. If so, targeted rodent control measures could feasibly decrease or eliminate LCMV risk for humans in this geographic area.

Albariño et al. (*16*) described 4 main LCMV lineages. Our results suggest that ≥3 of these lineages correspond to different host subspecies: lineage I to *M. musculus domesticus*, lineage II to *M. musculus musculus*, and lineage IV to *Apodemus sylvaticus*. We make no claim regarding the origin of lineage III, a single isolate from a human in Georgia (USA) (i.e., theoretically *M. musculus domesticus* mouse territory). We suggest more highly divergent lineages are likely to be discovered corresponding to rodent species, subspecies, and cryptic taxa. A new LCMV strain was recently reported from human serum in southern Iraq (*38*), but its phylogenetic position cannot be resolved; only a short fragment of the large gene (395 nt) is available in GenBank. This new LCMV strain is likely to cluster in clade I because *M. musculus domesticus* is the expected house mouse subspecies in southern Iraq (*39*–*41*). Uncertainty persists with respect to 4 LCMV strains clustered within lineage I of expected *M. musculus domesticus* mouse origin; JX14, JX4, and JX31 were isolated from ticks in 2015 from a coastal area in Jinxin, Jilin Province, northeastern China, and strain OQ28 was sequenced in 1990 from a wild mouse (*M. musculus*) captured in Osaka, Japan (*42*,*43*). In both regions, mice of subspecies other than *M. musculus domesticus* were reported. *M. musculus musculus* mice occur in northern China (*44*), whereas in Japan, mice are generally identified as *M. musculus castaneus* or *M. musculus molossinus* (*45*). However, the *M. musculus domesticus* mouse is known to be a

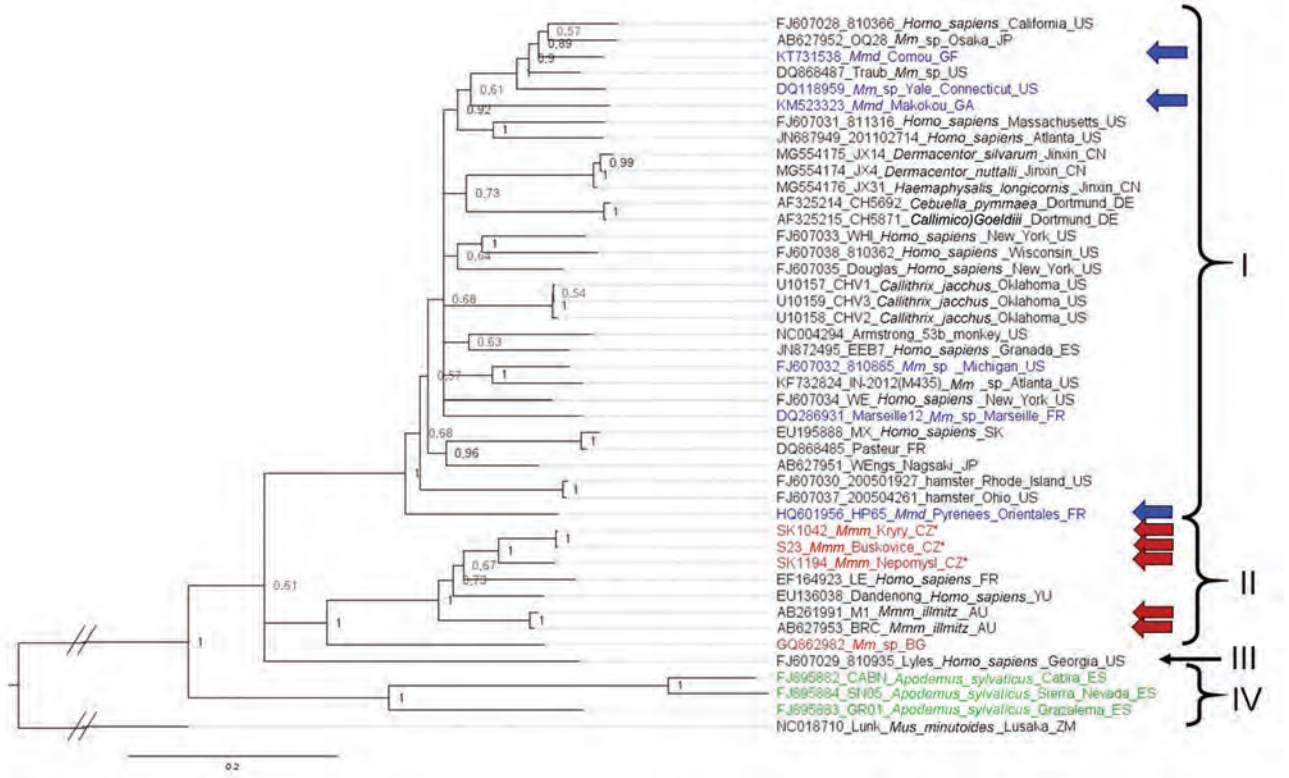

Figure 4. Phylogenetic analysis performed on nucleic acid sequences of glycoprotein gene of lymphocytic choriomeningitis virus (LCMV) sequences using Bayesian inference. Bayesian posterior probabilities were used to assess node support. Lunk virus from *Mus minutoides* (Africa) was used as outgroup. All sequences obtained in this study were submitted to GenBank (accession nos. MZ568450–7, MZ558311–3, MZ568449). Names of LCMV strains are composed of GenBank accession number, strain name, host species, and place and country of origin (if known) or isolation. Country code is defined as ISO code (https://countrycode.org). Colors indicate LCMV strains isolated from wild rodents where there is a match between expected mouse subspecies on the basis of geographic region and sampling area: blue, *Mus musculus domesticus*; red, *M. musculus musculus*. Arrows indicate known origin of mouse subspecies on the basis of genetic data, asterisks (*) indicates LCMV strains from this study, and lineages are indicated by roman numerals. LCMV strains isolated from *Apodemus sylvaticus* are indicated in green (lineage IV). Scale bar indicates nucleotide substitutions per site. Mmd, *M. musculus domesticus*; Mmm, *M. musculus musculus*; Mmm_lab, laboratory mouse strain derived from *M. musculus musculus*; Mm_lab, laboratory mouse strain; Mm_sp, *Mus musculus* spp.

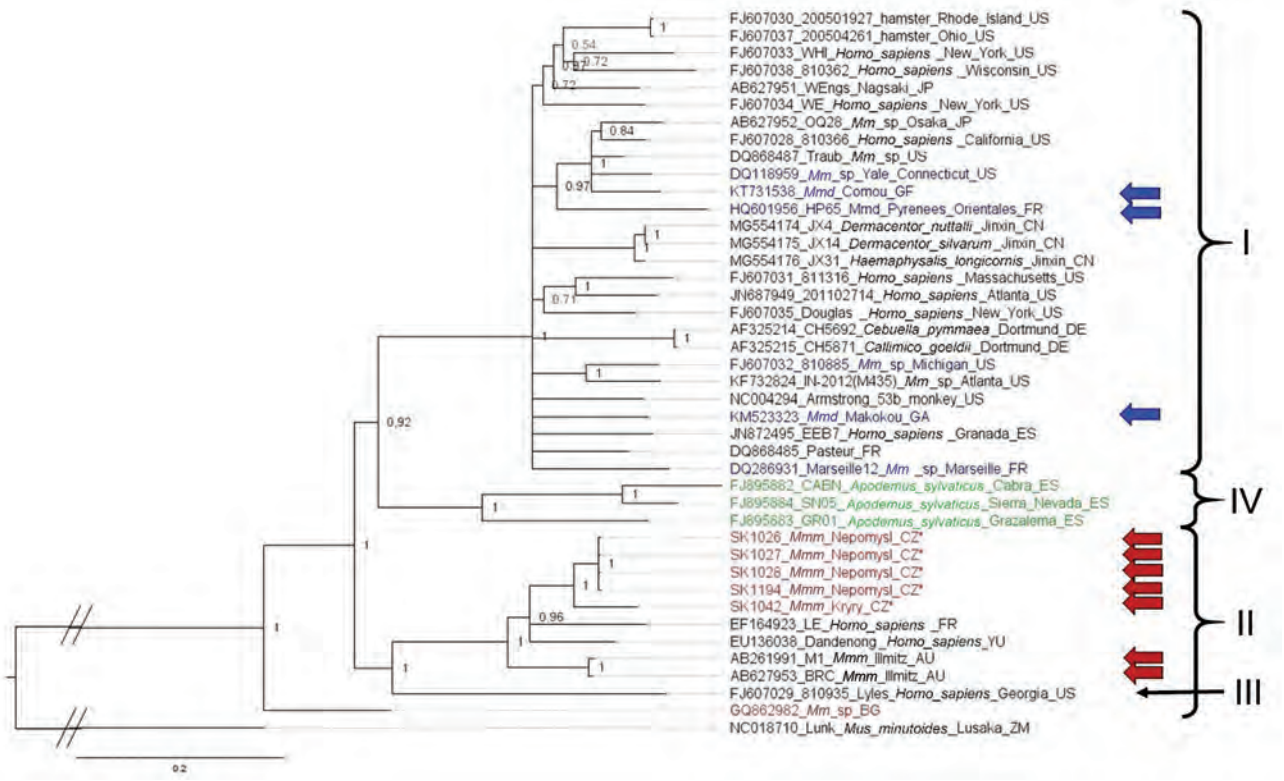

Figure 5. Phylogenetic analysis performed on nucleic acid sequences of nucleoprotein gene of lymphocytic choriomeningitis virus (LCMV) sequences using Bayesian inference. Bayesian posterior probabilities were used to assess node support. Lunk virus from *Mus minutoides* (Africa) was used as outgroup. All sequences obtained in this study were submitted to GenBank (accession numbers: MZ568450–7, MZ558311–3, MZ568449). Names of LCMV strains are composed of GenBank number, strain name, host species, and place and country of origin (if known) or isolation. Country code is defined as ISO code (https://countrycode.org). Colors indicate LCMV strains isolated from wild rodents where there is a match between expected mouse subspecies on the basis of geographic region and sampling area: blue, *Mus musculus domesticus*; red, *M. musculus musculus*. Arrows indicate known origin of mice subspecies on the basis of genetic data, asterix indicates LCMV strains from this study, and lineages are indicated by roman numerals. LCMV strains isolated from *Apodemus sylvaticus* are indicated in green (lineage IV). Scale bar indicates nucleotide substitutions per site. Mmd, *M. musculus domesticus*; Mmm, *M. musculus musculus*; Mmm_lab, laboratory mouse strain derived from *M. musculus musculus*; Mm_lab, laboratory mouse strain; Mm_sp, *Mus musculus* spp.

successful invasive species because of ancient and recent human mobility, and its introduction to new areas is regularly reported, particularly in port cities, coastal areas, and islands (*6*). This expansion might explain the presence of *M. musculus domesticus* LCMV strains in Osaka and Jinxin, both coastal areas.

LCMV can take a severe toll on human health, particularly in immunosuppressed persons. Cases of death after organ transplant have been reported involving strains from both lineages I and II (*3*,*18*,*46*). Takagi et al. (*41*) showed that 3 LCMV strains—OQ28, WE, and BRC—differ in pathogenicity in mice, concluding that strains OQ28 and BRC were genetically classified within the same cluster but exhibited very different pathogenicity. In this study, we demonstrate that the OQ28 strain clusters to *M. musculus domesticus* lineage I and the BRC strain clusters to *M. musculus musculus* lineage II; thus, we propose the 2 lineages have different host origins. From this perspective, the differences observed in strain pathogenicity by Takagi et al. (*41*) seem less surprising. Nevertheless, the variation of pathogenicity of LCMV strains corresponding to other host taxa is currently unknown.

In conclusion, our results suggest that the evolutionary diversity of LCMV might reflect rodent expansion history. When a human LCMV infection is diagnosed, sampling efforts should be applied to any synanthropic rodents. This effort could help clarify LCMV evolutionary history and elucidate whether different lineages differ in their spillover ability.

Acknowledgments

We thank Stuart J.E. Baird for English proofreading and final improvement of the article, and many colleagues and local farmers for their help trapping mice. We are grateful to Mark Blaxter, Konrad Lohse, Kamil Jaroň, and Jordan

Asworth for the warm welcoming of A. Fornuskova at the University of Edinburgh during her internship and introducing her to the world of genomic analyses. We are indebted to Anne Lavergne for providing us genetic information of positive mouse samples from French Guiana and to Vladislav Vergilov for his assistance with translating a Bulgarian article and hence with locating the geographic origin of LCMV-Bulgaria.

This work was supported by the Czech Science Foundation (grant no. 16-20049S) and the Program of the Czech Academy of Science to support the international cooperation of early-stage researchers (grant no. MSM200931901). The European Society for Evolutionary Biology awarded A. Fornuskova the Godfrey Hewitt Mobility Award, which enabled her to combine scientific work and family life during her stay in the United Kingdom. Computational resources were supplied by the project e-Infrastruktura CZ (e-INFRA LM2018140) provided within the program Projects of Large Research, Development and Innovations Infrastructures. Samples were collected with the support of the project 16-23773S of the Czech Science Foundation and the project 39022/2018-1 of the Ministry of Education, Youth, and Sports.

About the Author

Dr. Fornůsková is a research assistant at the Institute of Vertebrate Biology, Czech Academy of Sciences, Czech Republic. Her research is focused on host-pathogen interactions with special attention on small mammals as reservoir hosts.

References

1. Radoshitzky SR, Buchmeier MJ, Charrel RN, Clegg JCS, Gonzalez JJ, Günther S, et al.; Ictv Report Consortium. ICTV virus taxonomy profile: Arenaviridae. J Gen Virol. 2019;100:1200–1. https://doi.org/10.1099/jgv.0.001280
2. Childs JE, Klein SL, Glass GE. A case study of two rodent-borne viruses: not always the same old suspects. Front Ecol Evol. 2019;7:35. https://doi.org/10.3389/fevo.2019.00035
3. Amman BR, Pavlin BI, Albariño CG, Comer JA, Erickson BR, Oliver JB, et al. Pet rodents and fatal lymphocytic choriomeningitis in transplant patients. Emerg Infect Dis. 2007;13:719–25. https://doi.org/10.3201/eid1305.061269
4. Parker JC, Igel HJ, Reynolds RK, Lewis AM Jr, Rowe WP. Lymphocytic choriomeningitis virus infection in fetal, newborn, and young adult Syrian hamsters (*Mesocricetus auratus*). Infect Immun. 1976;13:967–81. https://doi.org/10.1128/iai.13.3.967-981.1976
5. Skinner HH, Knight EH. The potential role of Syrian hamsters and other small animals as reservoirs of lymphocytic choriomeningitis virus. J Small Anim Pract. 1979;20:145–61. https://doi.org/10.1111/j.1748-5827.1979.tb07023.x
6. Boursot P, Auffray JC, Britton-Davidian J, Bonhomme F. The evolution of house mice. Annu Rev Ecol Syst. 1993;24:119–52. https://doi.org/10.1146/annurev.es.24.110193.001003
7. Didion JP, de Villena FP-M. Deconstructing *Mus gemischus*: advances in understanding ancestry, structure, and variation in the genome of the laboratory mouse. Mamm Genome. 2013;24:1–20. https://doi.org/10.1007/s00335-012-9441-z
8. Phifer-Rixey M, Nachman MW. Insights into mammalian biology from the wild house mouse Mus musculus. eLife. 2015;4:e05959. https://doi.org/10.7554/eLife.05959
9. Baird S, Macholán M. What can the *Mus musculus musculus/M. m. domesticus* hybrid zone tell us about speciation. In: Macholán M, Baird S, Munclinger P, Piálek J, editors. Evolution of the house mouse. Cambridge: Cambridge University Press; 2012. p. 334–72.
10. Ďureje L, Macholán M, Baird SJE, Piálek J. The mouse hybrid zone in Central Europe: from morphology to molecules. Folia Zool (Brno). 2012;61:308–18. https://doi.org/10.25225/fozo.v61.i3.a13.2012
11. Goüy de Bellocq J, Wasimuddin, Ribas A, Bryja J, Piálek J, Baird SJE. Wasimuddin, Ribas A, Bryja J, Piálek J, Baird SJE. Holobiont suture zones: Parasite evidence across the European house mouse hybrid zone. Mol Ecol. 2018;27:5214–27. https://doi.org/10.1111/mec.14938
12. Čížková D, Baird SJE, Těšíková J, Voigt S, Ľudovít Ď, Piálek J, et al. Host subspecific viral strains in European house mice: Murine cytomegalovirus in the Eastern (*Mus musculus musculus*) and Western house mouse (*Mus musculus domesticus*). Virology. 2018;521:92–8. https://doi.org/10.1016/j.virol.2018.05.023
13. Gryseels S, Baird SJE, Borremans B, Makundi R, Leirs H, Goüy de Bellocq J. When viruses don't go viral: the importance of host phylogeographic structure in the spatial spread of Arenaviruses. PLoS Pathog. 2017;13:e1006073. https://doi.org/10.1371/journal.ppat.1006073
14. Kváč M, McEvoy J, Loudová M, Stenger B, Sak B, Květoňová D, et al. Coevolution of *Cryptosporidium tyzzeri* and the house mouse (*Mus musculus*). Int J Parasitol. 2013;43:805–17. https://doi.org/10.1016/j.ijpara.2013.04.007
15. Cuypers LN, Baird SJE, Hánová A, Locus T, Katakweba AS, Gryseels S, et al. Three arenaviruses in three subspecific natal multimammate mouse taxa in Tanzania: same host specificity, but different spatial genetic structure? Virus Evol. 2020 May 19 [Epub ahead of print]. https://doi.org/10.1093/ve/veaa039
16. Albariño CG, Palacios G, Khristova ML, Erickson BR, Carroll SA, Comer JA, et al. High diversity and ancient common ancestry of lymphocytic choriomeningitis virus. Emerg Infect Dis. 2010;16:1093–100. https://doi.org/10.3201/eid1607.091902
17. Ike F, Bourgade F, Ohsawa K, Sato H, Morikawa S, Saijo M, et al. Lymphocytic choriomeningitis infection undetected by dirty-bedding sentinel monitoring and revealed after embryo transfer of an inbred strain derived from wild mice. Comp Med. 2007;57:272–81.
18. Palacios G, Druce J, Du L, Tran T, Birch C, Briese T, et al. A new arenavirus in a cluster of fatal transplant-associated diseases. N Engl J Med. 2008;358:991–8. https://doi.org/10.1056/NEJMoa073785
19. Bozhinov S, Shindarov L, Makedonska D. Clinical and virologic examination of lymphocytic choriomeningitis [in Bulgarian]. Suvr Med (Sofiia). 1956;7:49–59.
20. Meritet JF, Krivine A, Lewin F, Poissonnier MH, Poizat R, Loget P, et al. A case of congenital lymphocytic choriomeningitis virus (LCMV) infection revealed by hydrops fetalis. Prenat Diagn. 2009;29:626–7. https://doi.org/10.1002/pd.2240
21. Lilue J, Doran AG, Fiddes IT, Abrudan M, Armstrong J, Bennett R, et al. Sixteen diverse laboratory mouse reference

genomes define strain-specific haplotypes and novel functional loci. Nat Genet. 2018;50:1574–83. https://doi.org/10.1038/s41588-018-0223-8
22. Tichy H, Zaleska-Rutczynska Z, O'Huigin C, Figueroa F, Klein J. Origin of the North American house mouse. Folia Biol (Praha). 1994;40:483–96.
23. Macholán M, Baird SJE, Dufková P, Munclinger P, Bímová BV, Piálek J. Assessing multilocus introgression patterns: a case study on the mouse X chromosome in central Europe. Evolution. 2011;65:1428–46. https://doi.org/10.1111/j.1558-5646.2011.01228.x
24. Goüy de Bellocq J, Baird SJE, Albrechtová J, Sobeková K, Piálek J. Murine cytomegalovirus is not restricted to the house mouse *Mus musculus domesticus*: prevalence and genetic diversity in the European house mouse hybrid zone. J Virol. 2015;89:406–14. https://doi.org/10.1128/JVI.02466-14
25. Wang L, Luzynski K, Pool JE, Janoušek V, Dufková P, Vyskočilová MM, et al. Measures of linkage disequilibrium among neighbouring SNPs indicate asymmetries across the house mouse hybrid zone. Mol Ecol. 2011;20:2985–3000. https://doi.org/10.1111/j.1365-294X.2011.05148.x
26. Yang H, Wang JR, Didion JP, Buus RJ, Bell TA, Welsh CE, et al. Subspecific origin and haplotype diversity in the laboratory mouse. Nat Genet. 2011;43:648–55. https://doi.org/10.1038/ng.847
27. Vieth S, Drosten C, Lenz O, Vincent M, Omilabu S, Hass M, et al. RT-PCR assay for detection of Lassa virus and related Old World arenaviruses targeting the L gene. Trans R Soc Trop Med Hyg. 2007;101:1253–64. https://doi.org/10.1016/j.trstmh.2005.03.018
28. Yama IN, Cazaux B, Britton-Davidian J, Moureau G, Thirion L, de Lamballerie X, et al. Isolation and characterization of a new strain of lymphocytic choriomeningitis virus from rodents in southwestern France. Vector Borne Zoonotic Dis. 2012;12:893–903. https://doi.org/10.1089/vbz.2011.0892
29. Goüy de Bellocq J, Těšíková J, Meheretu Y, Čížková D, Bryjová A, Leirs H, et al. Complete genome characterisation and phylogenetic position of Tigray hantavirus from the Ethiopian white-footed mouse, *Stenocephalemys albipes*. Infect Genet Evol. 2016;45:242–5. https://doi.org/10.1016/j.meegid.2016.09.009
30. Goüy de Bellocq J, Bryjová A, Martynov AA, Lavrenchenko LA. Dhati Welel virus, the missing mammarenavirus of the widespread *Mastomys natalensis*. J Vertebr Biol. 2020;69:20018.1–11.
31. Lavergne A, de Thoisy B, Tirera S, Donato D, Bouchier C, Catzeflis F, et al. Identification of lymphocytic choriomeningitis mammarenavirus in house mouse (*Mus musculus*, Rodentia) in French Guiana. Infect Genet Evol. 2016;37:225–30. https://doi.org/10.1016/j.meegid.2015.11.023
32. N'Dilimabaka N, Berthet N, Rougeron V, Mangombi JB, Durand P, Maganga GD, et al. Evidence of lymphocytic choriomeningitis virus (LCMV) in domestic mice in Gabon: risk of emergence of LCMV encephalitis in Central Africa. J Virol. 2014;89:1456–60.
33. Kumar S, Stecher G, Li M, Knyaz C, Tamura K. MEGA X: molecular evolutionary genetics analysis across computing platforms. Mol Biol Evol. 2018;35:1547–9. https://doi.org/10.1093/molbev/msy096
34. Ronquist F, Teslenko M, van der Mark P, Ayres DL, Darling A, Höhna S, et al. MrBayes 3.2: efficient Bayesian phylogenetic inference and model choice across a large model space. Syst Biol. 2012;61:539–42. https://doi.org/10.1093/sysbio/sys029
35. Ackermann R, Bloedhorn H, Küpper B, Winkens I, Scheid W. Spread of the lymphocytic choriomeningitis virus among West German mice. I. Investigations mostly on domestic mice (Mus musculus) [in German]. Zentralbl Bakteriol Orig. 1964;194:407–30.
36. Macholán M, Munclinger P, Sugerková M, Dufková P, Bímová B, Bozíková E, et al. Genetic analysis of autosomal and X-linked markers across a mouse hybrid zone. Evolution. 2007;61:746–71. https://doi.org/10.1111/j.1558-5646.2007.00065.x
37. Pocock MJO, Hauffe HC, Searle JB. Dispersal in house mice. Biol J Linn Soc Lond. 2005;84:565–83. https://doi.org/10.1111/j.1095-8312.2005.00455.x
38. Alburkat H, Jääskeläinen AJ, Barakat AM, Hasony HJ, Sironen T, Al-Hello H, et al. Lymphocytic choriomeningitis virus infection, Southern Iraq. Emerg Infect Dis. 2020;26:3002–6. https://doi.org/10.3201/eid2612.201792
39. Carleton M, Musser GG. Order Rodentia. In: Wilson DE, Reeder DM, editors. Mammal species of the world: a taxonomic and geographic reference. 3rd ed. Baltimore: The Johns Hopkins University Press; 2005. p. 745–52.
40. Hardouin EA, Orth A, Teschke M, Darvish J, Tautz D, Bonhomme F. Eurasian house mouse (*Mus musculus* L.) differentiation at microsatellite loci identifies the Iranian plateau as a phylogeographic hotspot. BMC Evol Biol. 2015;15:26. https://doi.org/10.1186/s12862-015-0306-4
41. Shad H, Darvish J, Rastegar Pouyani E, Mahmoudi A. Subspecies differentiation of the house mouse *Mus musculus* Linnaeus, 1758 in the center and east of the Iranian plateau and Afghanistan. Mammalia. 2016;81:147–68.
42. Takagi T, Ohsawa M, Morita C, Sato H, Ohsawa K. Genomic analysis and pathogenic characteristics of lymphocytic choriomeningitis virus strains isolated in Japan. Comp Med. 2012;62:185–92.
43 Zhang L, Li S, Huang S-J, Wang Z-D, Wei F, Feng X-M, et al. Isolation and genomic characterization of lymphocytic choriomeningitis virus in ticks from northeastern China. Transbound Emerg Dis. 2018;65:1733–9. https://doi.org/10.1111/tbed.12946
44. Jing M, Yu H-T, Bi X, Lai Y-C, Jiang W, Huang L. Phylogeography of Chinese house mice (*Mus musculus musculus/castaneus*): distribution, routes of colonization and geographic regions of hybridization. Mol Ecol. 2014;23:4387–405. https://doi.org/10.1111/mec.12873
45. Yonekawa H, Moriwaki K, Gotoh O, Miyashita N, Matsushima Y, Shi LM, et al. Hybrid origin of Japanese mice "*Mus musculus molossinus*": evidence from restriction analysis of mitochondrial DNA. Mol Biol Evol. 1988;5:63–78.
46. Fischer SA, Graham MB, Kuehnert MJ, Kotton CN, Srinivasan A, Marty FM, et al.; LCMV in Transplant Recipients Investigation Team. Transmission of lymphocytic choriomeningitis virus by organ transplantation. N Engl J Med. 2006;354:2235–49. https://doi.org/10.1056/NEJMoa053240

Address for correspondence: Alena Fornůsková, Institute of Vertebrate Biology of the Czech Academy of Sciences, Květná 170/8, 603 65 Brno, Czech Republic; email: afornuskova@gmail.com

Burden of Influenza-Associated Respiratory Hospitalizations, Vietnam, 2014–2016

Nguyen Cong Khanh,[1] Ashley L. Fowlkes,[1] Ngu Duy Nghia, Tran Nhu Duong, Ngo Huy Tu, Tran Anh Tu, Jeffrey W. McFarland, Thoa Thi Minh Nguyen, Nga Thu Ha, Philip L. Gould, Pham Ngoc Thanh, Nguyen Thi Huyen Trang, Vien Quang Mai, Phuc Nguyen Thi, Satoko Otsu, Eduardo Azziz-Baumgartner, Dang Duc Anh, A. Danielle Iuliano

Influenza burden estimates are essential to informing prevention and control policies. To complement recent influenza vaccine production capacity in Vietnam, we used acute respiratory infection (ARI) hospitalization data, severe acute respiratory infection (SARI) surveillance data, and provincial population data from 4 provinces representing Vietnam's major regions during 2014–2016 to calculate provincial and national influenza-associated ARI and SARI hospitalization rates. We determined the proportion of ARI admissions meeting the World Health Organization SARI case definition through medical record review. The mean influenza-associated hospitalization rates per 100,000 population were 218 (95% uncertainty interval [UI] 197–238) for ARI and 134 (95% UI 119–149) for SARI. Influenza-associated SARI hospitalization rates per 100,000 population were highest among children <5 years of age (1,123; 95% UI 946–1,301) and adults ≥65 years of age (207; 95% UI 186–227), underscoring the need for prevention and control measures, such as vaccination, in these at-risk populations.

Annual circulation of influenza viruses causes substantial disease and death worldwide, disproportionately affecting young children and older adults (*1*,*2*). Globally, influenza causes ≈9.4 million hospitalizations each year (*3*) but remains an underrecognized contributor to hospitalizations in many countries (*4*). In 2014, the World Health Organization (WHO) published a manual to guide countries to estimate influenza disease burden using influenza surveillance data (*5*–*10*). Such estimates have been instrumental in demonstrating influenza as a common cause of hospitalization in tropical and low- and middle-income countries (*11*), including Southeast Asia countries (*8*,*10*,*12*), and have provided a platform for evaluating the cost-effectiveness of influenza vaccines. Country-specific burden estimates can inform decisions to invest resources in influenza prevention and control programs (*4*,*13*), whereas studies from other countries may not be sufficiently compelling among national leaders to guide policy or investments (*14*).

During the past 40 years, Vietnam has experienced rapid economic growth, shifting from a low-income to a lower middle-income classification (*15*). Correspondingly, government spending on national health programs has increased, including efforts to address public health threats from human and zoonotic influenza (*14*). Vietnam has had sustained influenza surveillance programs since 2006, generating data about influenza virus circulation through influenza-like illness (ILI) and severe acute respiratory infection (SARI) surveillance. In 2019, the Institute of Vaccines and Medical Biologicals successfully licensed the first locally manufactured seasonal influenza vaccine (*16*). To sustain Vietnam's influenza prevention and control programs, information about the annual disease burden and value of averting costly hospitalizations is useful. Building on the established SARI sentinel surveillance, we conducted a hospital admission survey

Author affiliations: National Institute of Hygiene and Epidemiology, Hanoi, Vietnam (K.C. Nguyen, N.D. Ngu, D.N. Tran, T.H. Ngo, T.A. Tran, A.D. Dang); US Centers for Disease Control and Prevention, Atlanta, Georgia, USA (A.L. Fowlkes, J.W. McFarland, E. Azziz-Baumgartner, A.D. Iuliano); US Centers for Disease Control and Prevention, Hanoi, Vietnam (T.T.M. Nguyen, N.T. Ha, P.L. Gould); Tay Nguyen Institute of Hygiene and Epidemiology, Buon Ma Thuot, Vietnam (T.N. Pham); Pasteur Institute Ho Chi Minh, Ho Chi Minh City, Vietnam (T.T.H. Nguyen); Pasteur Institute Nha Trang, Nha Trang, Vietnam (M.Q. Vien); World Health Organization Vietnam Country Office, Hanoi (N.T. Phuc, S. Otsu)

DOI: https://doi.org/10.3201/eid2710.204765

[1]These authors contributed equally to this article.

(HAS) to estimate the national disease burden of influenza-associated hospitalization.

Methods

Vietnam's 63 provinces are divided into the north, central, highlands, and south major health regions. The healthcare system includes both public and private hospitals, but public hospitals are most commonly used (*17*). In 2011, the Vietnam Ministry of Health began adopting electronic medical records (EMRs) in all public hospitals (*18*,*19*). For the HAS, we selected 1 province per region that had all public hospitals using EMRs, a nearby provincial-level hospital enrolled in SARI surveillance using trained surveillance officers, and no private hospitals routinely admitting acute respiratory infection (ARI) patients.

To estimate the influenza-associated respiratory hospitalization rate in Vietnam for comparison with other countries, we combined existing virologic data from SARI sentinel surveillance (*20*), EMR data, and a medical record review of a random set of ARI hospitalizations (*5*). Influenza burden data were interpreted in conjunction with influenza seasonality to inform vaccine formulation considerations for maximizing population benefit.

Data Sources

ARI Hospitalizations

We defined an ARI hospitalization as a hospitalization with an admission code from the International Classification of Diseases, 10th Revision (ICD-10), for either acute upper respiratory infection (J06) or codes to approximate SARI (influenza, J09–11; pneumonia, J12–18; or other acute lower respiratory infections, J20–J22) (*5*). An overnight stay was not required because of variability in thresholds for admission, cultural practice of taking the most severely ill patients home, minimum availability of precise admission and discharge times, and possible patient transfer. Using the EMR system, public hospitals provided a list of patients with an ARI admission code during 2014–2016 with the following data: admission and discharge ICD-10 codes; hospital admission and discharge dates; patient residential province, age, and sex; and outcome of hospitalization at discharge.

Medical Record Review to Identify SARI Proportion

From ARI hospitalizations for each hospital, a random selection of medical records was reviewed by health officers and clinical data collected to evaluate both the 2011 and 2014 WHO SARI case definitions. The 2011 definition was sudden onset of fever ≥38°C, with cough or sore throat, and with shortness of breath or difficulty breathing, and illness requiring hospitalization; the revised 2014 definition was temperature of ≥38°C or history of fever, cough of duration ≤10 days, and illness requiring hospitalization. We assumed that 50% of ARI hospitalizations would meet SARI case criteria and assigned 80 records per hospital to reach a sufficient sample size with a 5% margin of error.

Influenza Test Results from SARI Sentinel Surveillance

In 2011, Vietnam initiated SARI surveillance in sentinel hospitals representing the 4 major regions of Vietnam; 6–14 hospitals participated per year. Each week, sentinel hospitals reported the total number of SARI admissions. Surveillance staff collected nasopharyngeal and oropharyngeal swabs from 8 SARI patients per week (protocols varied by hospital and ward). Demographic and clinical information also were collected. The National Influenza Center conducted real-time reverse transcription PCR to detect influenza A (subtypes A(H1N1) pdm09, A/H3, A/H5, and A/H7) and B (*20*). Influenza virologic surveillance data were obtained from all SARI sentinel hospitals participating in surveillance during 2014–2016.

Population Data

A national census survey was conducted in 2009 with annual population projections (*21*). To calculate population-based rates of ARI and SARI, we used 2014–2016 provincial and national population projections for 4 age groups: <5 years, 5–49 years, 50–64 years, and ≥65 years. Evaluation of 14 demographic, health, and healthcare characteristics in each province within the 4 regions demonstrated that provinces selected for the HAS were representative and could be combined for a national estimate of ARI and SARI rates in Vietnam (Appendix, https://wwwnc.cdc.gov/EID/article/27/10/20-4765-App1.pdf).

Data Analysis

ARI and SARI Hospitalizations

We reviewed the reported ARI hospitalizations and excluded patients with non-ARI ICD-10 codes and those residing outside of the province. Eight hospitals in 2014 and 7 in 2015 reported zero or near-zero ARI hospitalizations during the introduction of the EMR system. To compensate for underreporting, we used the individual hospital's 2016 ARI counts to estimate the expected number of hospitalizations in 2014 and

2015. We further adjusted for patients with missing age information by using the distribution of patients with known ages (Appendix Figure 1). We assessed the percentage of ARI hospitalizations meeting the SARI case definition by province, hospital, year, age group, and ICD-10 code.

Estimating the Rate of Influenza-Associated Hospitalizations

We estimated the influenza-attributable proportion of ARI and SARI hospitalizations by using 2014–2016 SARI sentinel surveillance data. We calculated influenza-associated ARI and SARI hospitalization rates by multiplying the age- and month-specific number of hospitalizations and percentage of SARI surveillance patients positive for influenza, then dividing by the age-specific census population estimates for each province. We summed the monthly rate estimates to calculate the annual age-adjusted rates. We calculated the 95% uncertainty intervals (UI) for estimated rates by using 1,000 Monte Carlo simulation iterations, assuming a Poisson distribution for the number of hospitalizations and a binomial distribution for the proportion of SARI patients positive for influenza. We used the same method to calculate influenza-associated SARI hospitalization rates, but first we multiplied ARI hospitalization totals by the percentage of ARI hospitalizations meeting SARI criteria to obtain the age- and month-specific number of influenza-associated SARI hospitalizations. The 95% UIs assumed a binomial distribution for the proportion meeting the SARI case definition. We extrapolated the number of influenza-associated ARI and SARI hospitalizations by multiplying age-specific influenza rates by the provincial census population.

To estimate national rates, we summed age- and month-specific provincial counts of all-cause ARI and SARI and influenza-associated ARI and SARI across the provinces, and then divided the sum by the total population of the 4 provinces. We obtained the 95% UIs by calculating the upper and lower 2.5% percentiles from the distribution of provincial rate estimates.

We used χ^2 tests of proportions to assess statistical differences and calculate 95% CIs by using the observed data when appropriate. We performed all analyses using SAS 9.4 (SAS Institute, https://www.sas.com).

This activity was reviewed by the US Centers for Disease Control and Prevention and the ethics committee and scientific committee of the National Institute of Hygiene and Epidemiology (Hanoi, Vietnam). The data are considered nonresearch; therefore, Institutional Review Board review was not required.

Results

Reported ARI Hospitalizations

The provinces identified for the HAS included Quang Ninh (14 hospitals) in the north region, Khanh Hoa (10 hospitals) in the central region, Dak Lak (15 hospitals) in the highlands region, and Dong Thap (12 hospitals) in the south region (Figure 1). During January 2014–December 2016, a total of 220,217 ARI hospitalizations were reported, excluding 2,781 patients living outside of the province and 4,960 patients who did not have qualifying ARI ICD-10 codes. We identified 8 hospitals with clear underreporting during EMR implementation in 2014 and 2015 and imputed the expected number of ARI hospitalizations by using the 2016 percentage distribution of patient counts across hospitals, giving an overall estimated 4.1% underreporting of ARI hospitalizations and an adjusted total of 229,144 ARI hospitalizations included in analysis.

Among patients with known age, 61% were <5 years, 15% were 5–49 years, 7.4% were 50–64 years, and 17% were ≥65 years (Table 1). The median length of hospitalization was 6 days (interquartile range 4–6 days). Among 180,316 ARI hospitalizations with a known discharge disposition, 482 (0.3%) patients died and 4,376 (2.4%) were sent home as too severely ill to be cured.

Estimated SARI Hospitalizations

Of 3,626 medical record reviews from ARI hospitalizations, 61% met the SARI case definition, whereas 27% did not have documented fever, 8% did not have cough, and 4% had neither. SARI accounted for 75% of ARI hospitalizations among children <5 years of age, compared with patients 5–49 years of age (59%), 50–64 years of age (38%), and ≥65 years of age (34%) ($p<0.001$) (Table 1). The ICD-10 codes most commonly listed for patients with illness meeting SARI criteria were acute bronchiolitis (J21 [72%]) and acute upper respiratory tract infection (J06 [71%]) among codes reported for ≥10 patients. Influenza codes were reported infrequently, and significantly less frequently among patients with illness meeting the SARI criteria (37%) compared with other diagnoses ($p<0.001$) (Table 1).

Influenza Detection

The SARI sentinel surveillance collected specimens from 6,647 patients. Influenza detection varied significantly by age ($p<0.001$), and was less frequent among children <5 years of age (13% [95% CI 12%–14%]) and patients ≥65 years of age (16% [95% CI 14%–18%])

compared with patients 5–49 years of age (23% [95% CI 21%–24%]) and patients 50–64 years of age (23% [95% CI 20%–25%]). The age-weighted proportion of samples testing positive for influenza was 22% (95% CI 21%–23%), varying by year (20% in 2014, 18% in 2015, and 23% in 2016). Influenza detections did not vary substantially by region (Appendix Figure 2); therefore, we combined data to allow stratification by age and month.

Across all years, ≈74.4% of influenza detections occurred during March–July (Figure 2). Influenza A viruses predominated in 2014 and 2015; subtype H1N1 made up 44% of viruses detected in 2014 and subtype H3N2 65% of viruses detected in 2015. In 2016, influenza viruses cocirculated; 36% were A(H1N1), 28% A(H3N2), and 35% B, but H1N1 and B co-circulated during March–June, whereas most H3N2 detections occurred during June–November (Figure 2).

Rates of Influenza-Associated ARI and SARI Hospitalizations

Provincial Rates of Influenza-Associated ARI and SARI Hospitalizations

During 2014–2016, the mean annual influenza-associated ARI hospitalization rates ranged by province from 183 (95% UI 159–206) to 284 (95% UI 256–312) per 100,000 population (Table 2). The provincial influenza-associated ARI hospitalization rates were lower in 2014, when influenza viruses were primarily detected during January–June, compared with 2016, when influenza was detected throughout the year and all 3 viruses circulated.

National Rates of ARI Hospitalizations and Influenza-Associated ARI Hospitalizations

Across the 4 provinces, the mean annual ARI hospitalization rate was 1,263 (95% UI 1,248–1,278)/100,000 population and the influenza-associated ARI hospitalization rate was 218 (95% UI 197–238)/100,000 population (Table 3). The age-adjusted rate of influenza-associated ARI was higher in 2016 (295 [95% UI 273–318]/100,000 population) compared with 2014 (142 [95% UI 128–157]/100,000 population). After extrapolating provincial rates to Vietnam's population of ≈93 million during 2014–2016, we estimated that 129,019 influenza-associated ARI hospitalizations occurred in 2014, 195,795 in 2015, and 273,357 in 2016. Using the extrapolated counts, we found that the mean influenza-associated ARI hospitalizations during April–September, when Southern Hemisphere influenza vaccines typically are available, was 116,324 compared with 69,493 during October–March, when Northern Hemisphere influenza vaccines typically are available (Appendix Figure 3).

National Rates of Influenza-Associated SARI

We estimated age-adjusted influenza-associated SARI rates per 100,000 population of 87 in 2014, 134 in 2015, and 180 in 2016. The mean age-adjusted annual rate was 134 (95% UI 119–149)/100,000 population. Children <5 years of age had the highest rates of influenza-associated SARI (1,123 [95% UI 946–1,301]/100,000 population), followed by adults aged ≥65 years (207 [95% UI 186–227]/100,000 population).

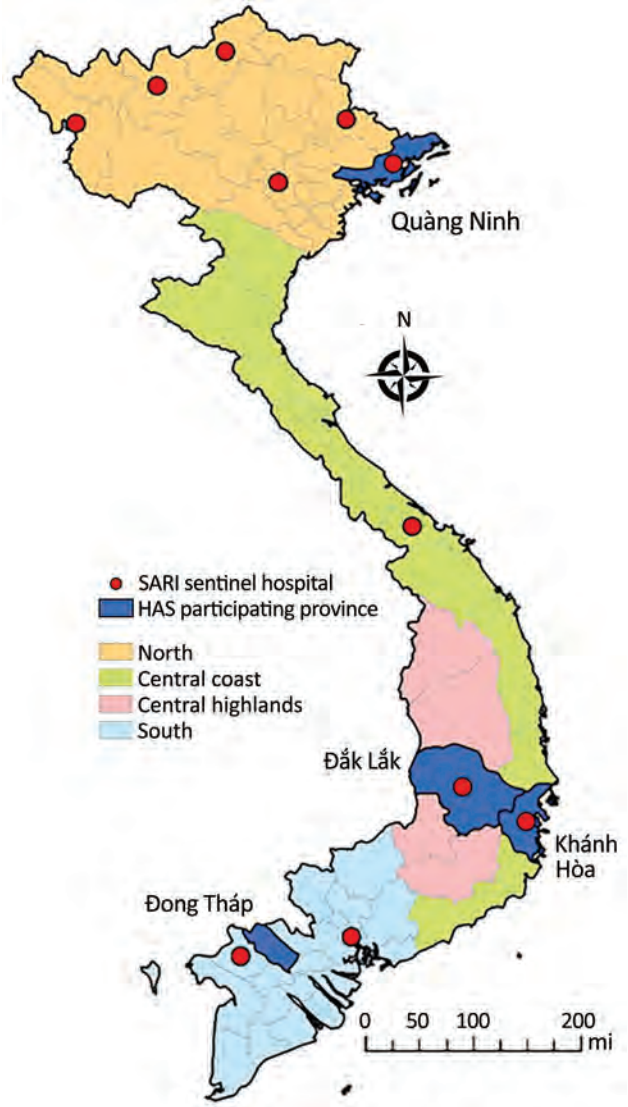

Figure 1. Locations of sentinel hospitals conducting surveillance for severe acute respiratory infection and provinces with all hospitals participating in the hospital admission survey, Vietnam, 2014–2016. HAS, hospital admission survey; SARI, severe acute respiratory infection.

Table 1. Percentages of ARI hospitalizations that met SARI case criteria from medical chart review, by age group, qualifying admission code, and province, Vietnam, 2014–2016*

Category	No. (%) hospitalization		
	All ARI hospitalizations†	Medical record reviewed	Met SARI criteria‡
Overall	220,217 (100)	3,626 (100)	2,205 (60.8)
Age group, y§			
<5	132,076 (61.0)	1,934 (53.4)	1,443 (74.6)
5–49	32,112 (14.8)	716 (19.8)	421 (58.8)
50–64	16,030 (7.4)	324 (8.9)	123 (38.0)
≥65	36,329 (16.8)	647 (17.9)	217 (33.5)
Diagnosis, ICD-10 code			
Acute upper respiratory infections, J06	37,957 (17.2)	459 (12.7)	325 (70.8)
Influenza	4,278 (1.9)	82 (2.3)	30 (36.6)
Influenza caused by other identified influenza virus, J10	963 (0.4)	36 (1.0)	9 (25.0)
Influenza caused by unidentified influenza virus, J11	3,315 (1.5)	46 (1.3)	21 (45.7)
Pneumonia	117,890 (53.5)	1,946 (53.7)	271 (13.9)
Viral pneumonia, not elsewhere classified, J12	470 (0.2)	10 (0.3)	7 (70.0)
Pneumonia caused by *Streptococcus pneumoniae*, J13	82 (0)	9 (0.2)	7 (77.8)
Pneumonia caused by *Hemophilus influenzae*, J14	51 (0)	0 (0)	0 (0)
Bacterial pneumonia, not elsewhere classified, J15	22,252 (10.1)	399 (11.0)	257 (64.4)
Pneumonia caused by other infectious organisms, J16	10,629 (4.8)	40 (1.1)	28 (70.0)
Pneumonia in diseases classified elsewhere, J17	65 (0)	3 (0.1)	3 (100.0)
Pneumonia, unspecified organism, J18	84,341 (38.3)	1,485 (41.0)	970 (65.3)
Other acute lower respiratory infections¶	60,092 (27.3)	1139 (31.4)	578 (50.7)
Acute bronchitis, J20	55,492 (25.2)	1,096 (30.2)	547 (49.9)
Acute bronchiolitis, J21	4,563 (2.1)	43 (1.2)	31 (72.1)
Unspecified acute lower respiratory infection, J22	37 (0)	0 (0)	0 (0)
Province			
Dak Lak, 15 hospitals	60,805 (27.6)	853 (23.5)	567 (66.5)
Dong Thap, 12 hospitals	67,746 (30.8)	828 (22.8)	495 (59.8)
Khanh Hoa, 10 hospitals	56,187 (25.5)	854 (23.6)	522 (61.1)
Quang Ninh, 14 hospitals	35,479 (16.1)	1,091 (30.1)	612 (56.1)

*ARI, acute respiratory infection; ICD-10, International Classification of Diseases, 10th Revision; SARI, severe acute respiratory infection.
†Percentages show the overall proportion of patients in the listed category (column percentage).
‡Percentages show the proportion of patients with illness meeting SARI criteria (row percentage), defined as temperature of ≥38°C or history of fever, cough of duration ≤10 d, and illness requiring hospitalization; all proportions varied substantially within categories.
§Age data were missing for 3,670 ARI and 5 patients with medical record review.
¶Admission ICD codes J14 and J22 were not identified among reviewed patient records; J09 was not identified among any patients.

Discussion

Using HAS methodology in 4 of Vietnam's provinces during 2014–2016, we estimated influenza virus infections were associated with 123,000–200,000 respiratory hospitalizations each year and demonstrated influenza as a common cause of hospitalization in young children and older adults. We estimated the influenza-associated hospitalization rate using both an expanded set of ICD-10 codes to define our ARI case definition (218/100,000 population) and a medical chart review to establish rates with the commonly used SARI case definition (134/100,000 population). Among age groups specifically recommended by WHO for vaccination (*22*), we estimated higher rates of hospitalization among children <5 years of age (ARI, 1,508/100,000 population; SARI, 1,123/100,000 population) and adults ≥65 years of age (ARI, 600/100,000 population; SARI, 207/100,000 population). We also found in any year that 74% of influenza detections were identified during March–July, when Southern Hemisphere influenza vaccines typically are available.

In Vietnam, influenza viruses were detected among 18%–23% of SARI patients, a finding that is consistent with assessments of influenza detection among SARI patients conducted in New Zealand and Hong Kong (*23*,*24*) but higher than those reported in systematic reviews that focus specifically on acute lower respiratory tract infections (*2*,*3*). Our influenza-associated SARI hospitalization rates were similar to those found in a study in the Philippines that used comparable methods (*25*) and other studies in Bhutan, Korea, Thailand, and China that reported a comparable percentage of cases positive for influenza (*10*,*26*–*28*). Our estimates among children <5 years of age (1,123/100,000 population) were 5–35 times higher than the other age groups, potentially reflecting differences in healthcare utilization. The government of Vietnam pays all medical costs for children <5 years of age, thus removing important barriers to healthcare access. Conversely, among adults ≥65 years of age, our estimated influenza-associated SARI hospitalization rate (207/100,000) was

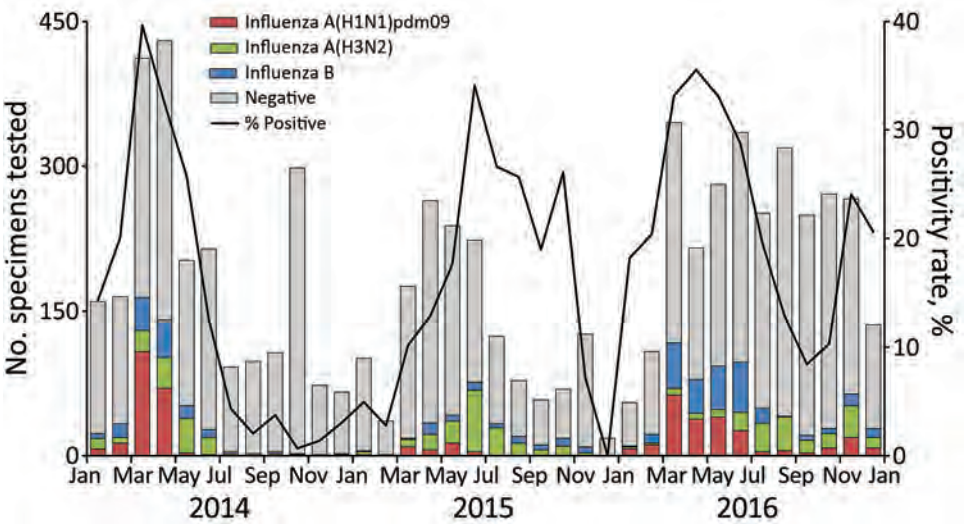

Figure 2. Number of specimens tested and percentage testing positive for influenza viruses among severe acute respiratory infection sentinel surveillance system patients, by month, Vietnam, 2014–2016.

lower than those reported from the United States and Hong Kong (*29*,*30*).

Influenza burden estimates specific to Vietnam support local decision making and targeted risk communications for subpopulations at higher risk for influenza-associated complications and clinicians for targeted use of treatment and nonpharmaceutical interventions. In supporting decision-making for governmental leaders, burden estimates can provide evidence to sustain influenza surveillance programs and investments in pandemic planning, influenza treatment, and vaccination programs. The government of Vietnam has supported influenza virus surveillance and supported the development of the first licensed, locally produced influenza vaccine. Vaccination remains the best way to prevent influenza (*29*), and establishing a strong seasonal vaccine program may also be useful in providing the necessary infrastructure required for pandemic vaccines in the event of an emergent influenza virus or other pandemic respiratory viruses, such as severe acute respiratory syndrome coronavirus 2 (*31*). Burden estimates also can help in understanding the potential impact of a possible future vaccination program.

Table 2. Provincial estimates of influenza-associated ARI and SARI hospitalizations and rates for all ages, Vietnam, 2014–2016*

	ARI Hospitalizations			Estimated SARI Hospitalizations		
		No. (95% UI)		No. (95% UI)		
Year and province	No.	Rate	Influenza-associated rate	No.	Rate	Influenza-associated rate
Mean annual						
Dak Lak	20,746	1,107 (1,091–1,122)	183 (159–206)	14,093 (13,861–14,308)	752 (739–763)	121 (104–139)
Dong Thap	22,582	1,314 (1,297–1,330)	224 (200–247)	13,561 (13,352–13,772)	789 (777–801)	133 (118–148)
Khanh Hoa	20,433	1,665 (1,645–1,686)	284 (256–312)	12,760 (12,558–12,957)	1,040 (1,023–1,056)	177 (157–197)
Quang Ninh	12,620	1,030 (1,011–1,046)	197 (180–215)	7,423 (7,280–7,553)	606 (594–616)	113 (103–124)
2014						
Dak Lak	18,592	1,004 (988–1,021)	103 (90–116)	12,711 (12,487–12,929)	687 (675–698)	66 (57–75)
Dong Thap	22,188	1,299 (1,281–1,319)	151 (134–171)	13,403 (13,178–13,647)	785 (772–799)	90 (80–102)
Khanh Hoa	18,788	1,546 (1,523–1,570)	195 (174–219)	11,793 (11,578–12,003)	971 (953–988)	119 (105–135)
Quang Ninh	11,171	921 (902–938)	137 (122–153)	6,877 (6,714–7,037)	567 (553–580)	83 (73–94)
2015						
Dak Lak	19,605	1,046 (1,030–1,061)	192 (145–243)	13,346 (13,116–13,572)	712 (700–724)	133 (96–173)
Dong Thap	20,655	1,202 (1,185–1,219)	219 (171–269)	12,384 (12,168–12,597)	720 (708–733)	131 (100–163)
Khanh Hoa	20,919	1,705 (1,682–1,728)	292 (239–344)	13,055 (12,837–13,273)	1,064 (1,046–1,082)	184 (148–220)
Quang Ninh	11,216	915 (893–935)	161 (136–188)	6,614 (6,450–6,768)	540 (526–552)	93 (76–111)
2016						
Dak Lak	24,041	1,266 (1249–1,283)	251 (228–272)	16,220 (15,974–16,467)	854 (841–867)	164 (149–178)
Dong Thap	24,903	1,440 (1422–1,459)	299 (273–324)	14,896 (14,660–15,134)	861 (847–875)	177 (161–193)
Khanh Hoa	21,593	1,743 (1720–1,768)	363 (332–397)	13,434 (13,196–13,651)	1,084 (1,065–1,102)	226 (205–250)
Quang Ninh	15,473	1,251 (1227–1,273)	291 (264–321)	8,776 (8,579–8,956)	709 (693–724)	162 (149–177)

*Rates are given per 100,000 population and age-adjusted. Rates were calculated regionally using reported ARI hospitalizations multiplied by the percentage of patients meeting the SARI criteria upon medical chart review. Regional hospitalization counts were multiplied by the national percentage of specimens testing influenza-positive from SARI sentinel surveillance, adjusted by age and month, and then divided by the combined population of the regions. ARI, acute respiratory infection; SARI, severe acute respiratory infection; UI, uncertainty interval.

Table 3. National influenza-associated acute respiratory infection (ARI) and severe acute respiratory infection (SARI) hospitalization and rate estimates, Vietnam, 2014–2016

Year and age group, y	ARI hospitalizations, no. (95% UI)			SARI hospitalizations, no. (95% UI)		
	Mean regional rate	Mean regional influenza-associated rate	Extrapolated national influenza-associated cases	Mean regional rate	Mean regional influenza-associated rate	Extrapolated national influenza-associated cases
Mean annual						
All	1,263 (1,248–1,278)	218 (197–238)	199,368 (180,126–217,895)	791 (779–803)	134 (119–149)	122,832 (109,263–136,377)
<5	9,530 (9,372–9,693)	1,508 (1,272–1,745)	114,338 (96,479–132,357)	7,103 (6,966–7,236)	1,123 (946–1,301)	85,191 (71,749–98,623)
5–49	257 (253–260)	56 (53–60)	36,738 (34,767–39,225)	146 (143–148)	32 (30–34)	20,876 (19,660–22,312)
50–64	690 (658–717)	155 (132–181)	20,150 (17,093–23,480)	272 (253–291)	61 (51–72)	7912 (6,654–9,354)
≥65	3,776 (3,730–3,820)	600 (545–656)	34,527 (31,367–37,757)	1,301 (1,275–1,326)	207 (186–227)	11,883 (10,729–13,064)
2014						
All	1,181 (1,167–1,196)	142 (128–157)	129,019 (116,354–142,617)	748 (737–759)	87 (77–97)	78,905 (70,212–88,261)
<5	9,201 (9,051–9,358)	942 (792–1105)	71,035 (59,718–83,357)	6,843 (6,714–6,970)	698 (587–818)	52,663 (44,230–61,689)
5–49	223 (218–228)	41 (38–44)	26,821 (24,830–28,928)	127 (123–131)	24 (22–26)	15,326 (14,149–16,601)
50–64	606 (582–629)	91 (74–113)	11,341 (9,219–13,987)	242 (226–258)	37 (29–46)	4,553 (3,587–5,681)
≥65	3,446 (3,380–3,519)	427 (355–504)	24,073 (20,032–28,429)	1,195 (1,154–1,236)	147 (120–177)	8,307 (6,781–9,969)
2015						
All	1,197 (1,182–1,212)	214 (175–254)	195,795 (160,673–232,667)	751 (739–762)	134 (107–164)	123,124 (98,168–149,830)
<5	9,114 (8,961–9,270)	1,642 (1,183–2,115)	124,690 (89,882–160,624)	6,798 (6,666–6,927)	1,226 (886–1,583)	93,111 (67,328–120,261)
5–49	233 (228–238)	40 (36–46)	26,219 (23,210–30,057)	131 (128–135)	23 (20–26)	14,803 (13,087–17,042)
50–64	655 (619–686)	128 (96–160)	16,572 (12,422–20,720)	260 (239–282)	50 (37–64)	6,514 (4,811–8,362)
≥65	3,594 (3,524–3,661)	613 (506–722)	35,180 (29,065–41,434)	1,233 (1,195–1,268)	210 (173–250)	12,073 (9916–14,337)
2016						
All	1,409 (1,391–1,426)	295 (273–318)	273,357 (252,921–294,062)	874 (860–887)	180 (165–195)	166,505 (152,831–180,715)
<5	10,271 (10,095–10,450)	1,935 (1,705–2,185)	147,341 (129,794–166,383)	7,664 (7,507–7,810)	1,443 (1,267–1,625)	109,840 (96,439–123,710)
5–49	314 (308–319)	87 (81–94)	57,237 (53,188–61,587)	178 (174–182)	50 (46–54)	32,533 (30,011–35,101)
50–64	799 (763–831)	240 (196–283)	32,395 (26,510–38,173)	312 (291–332)	93 (77–111)	12,613 (10,375–15,037)
≥65	4,264 (4,193–4,332)	752 (657–867)	44,234 (38,629–51,022)	1,468 (1,426–1,506)	259 (225–299)	15,238 (13,251–17,595)

*Rates are given per 100,000 population and age-adjusted unless shown for a single age group. Rates were calculated regionally using reported ARI hospitalizations multiplied by the percentage of patients meeting the SARI criteria upon medical chart review. Regional hospitalization counts were multiplied by the national percentage of specimens testing influenza-positive from SARI sentinel surveillance, adjusted by age and month, and then divided by the combined population of the regions. ARI, acute respiratory infection; SARI, severe acute respiratory infection; UI, uncertainty interval.

The seasonal distribution of influenza detections suggested circulation in Vietnam occurred primarily during January–July. We demonstrated that 75% of influenza detections were observed during March–July, which was consistent when evaluating all available years of SARI sentinel surveillance data, including data published previously from 2011–2014 (*20*). Nguyen et al. demonstrated variable timing of peaks for influenza A and B viruses; 76% of influenza A viruses were detected in May–October, and little pattern was observed for influenza B viruses (*32*). Our findings are similar to those in neighboring Thailand (*27*) and Cambodia (*33*), suggesting that most influenza circulation occurs during the rainiest months (April–August) (*34*) and that a Southern Hemisphere vaccine formulation is appropriate for use in Vietnam.

To align our work with existing literature and evaluate the broad potential burden of influenza, we studied influenza in patients with illness meeting

the SARI and ARI case definitions. Previous studies have demonstrated that the SARI case definition is less sensitive and more specific (*35*), ensuring more efficient use of resources for virologic surveillance; however, the actual influenza hospitalization burden may be underestimated. A more sensitive case definition is needed to encompass the entirety of influenza disease burden. Furthermore, a recent review of influenza-associated hospitalization rates underscored the effect of heterogeneity in methods and case definitions on burden estimates (*36*). A strength of our study is the use of a medical chart review to identify SARI in ≈60% of hospitalized patients with ARI, which is consistent with a previous study evaluating the sensitivity of administrative codes to identify SARI (*37*) and enabled us to provide burden estimates that may contribute to pooled estimates in studies using different case definitions. Additional research is needed to understand the relationship between diagnostic codes indicative of ARI, the SARI case definition, and influenza detection.

The first limitation of our study is that we were only able to perform the HAS in 4 of Vietnam's 63 provinces. Although our comparison of provincial characteristics demonstrated minimal variation within each region from the HAS referent provinces, we could not account for many characteristics that might lead to differences in influenza hospitalization rates, such as healthcare-seeking behaviors. Second, the EMR transition was delayed in some hospitals during 2014 and 2015, resulting in underestimation of the number of respiratory hospitalizations recorded. We imputed an expected number of hospitalizations for hospitals with known delays and increased the total ARI hospitalization accordingly, but other hospitals may have had unidentified implementation challenges that were not captured. Third, in accordance with reporting procedures in Vietnam, only the primary reason for a hospitalization was listed in the EMR for each patient (*37*). Although this practice serves to indicate the primary reason for a hospitalization, patients with other conditions in conjunction with a respiratory illness may be missed (*38*). Fourth, participation in SARI surveillance was not continuous for all hospitals, potentially underrepresenting the central and highlands regions and resulting in insufficient sample size to calculate both age- and region-specific influenza detection percentage positives. However, we identified minimal variability in region-specific influenza circulation and thus stratified analyses by age only (Appendix).

Our results highlight the burden of influenza-associated hospitalizations in Vietnam during 2014–2016 and underscore the value of country-specific disease burden studies. As Vietnam undertakes the production of influenza vaccine locally, influenza prevention and control investments and well-timed public health interventions such as vaccination campaigns and empiric antiviral use during epidemics may be supported through burden estimates like ours. Systematic testing of SARI patients can be used to identify the prevalent influenza subtypes and strains that inform vaccine strain selection for in-country influenza vaccines being produced. Our methods largely used existing hospitalization and surveillance data, which will be helpful to efforts to replicate or update the results. These and future efforts to better quantify influenza disease burden can be used with vaccine effectiveness and coverage data to estimate potential averted illnesses with vaccination, inform cost-effectiveness analyses, and direct communications to vulnerable populations.

Acknowledgments

We thank our colleagues at provincial Centers for Disease Control and at hospitals in Quang Ninh, Khanh Hoa, Dak Lak, and Dong Thap provinces for their generous support and expertise. We also thank James Kile, Carrie Reed, Melissa Rolfes, Michael Daugherty, and Hien Do for their contributions.

About the Author

Dr. Nguyen is an epidemiologist at the Department of Communicable Diseases Control, National Institute of Hygiene and Epidemiology, Vietnam. His research interest includes epidemiology of viral and bacterial respiratory infectious diseases and zoonotic diseases including COVID-19, SARS, avian influenza H5N1, and seasonal influenza.

References

1. Iuliano AD, Roguski KM, Chang HH, Muscatello DJ, Palekar R, Tempia S, et al.; Global Seasonal Influenza-associated Mortality Collaborator Network. Estimates of global seasonal influenza-associated respiratory mortality: a modelling study. Lancet. 2018;391:1285–300. https://doi.org/10.1016/S0140-6736(17)33293-2
2. Lafond KE, Nair H, Rasooly MH, Valente F, Booy R, Rahman M, et al.; Global Respiratory Hospitalizations—Influenza Proportion Positive (GRIPP) Working Group. Global role and burden of influenza in pediatric respiratory hospitalizations, 1982–2012: a systematic analysis. PLoS Med. 2016;13:e1001977. https://doi.org/10.1371/journal.pmed.1001977

3. Troeger CE, Blacker BF, Khalil IA, Zimsen SRM, Albertson SB, Abate D, et al.; GBD 2017 Influenza Collaborators. Mortality, morbidity, and hospitalisations due to influenza lower respiratory tract infections, 2017: an analysis for the Global Burden of Disease Study 2017. Lancet Respir Med. 2019;7:69–89. https://doi.org/10.1016/S2213-2600(18)30496-X
4. Lee VJ, Ho ZJM, Goh EH, Campbell H, Cohen C, Cozza V, et al.; WHO Working Group on Influenza Burden of Disease. Advances in measuring influenza burden of disease. Influenza Other Respir Viruses. 2018;12:3–9. https://doi.org/10.1111/irv.12533
5. World Health Organization. A manual for estimating disease burden associated with seasonal influenza [cited 2018 Feb 3]. https://www.who.int/influenza/resources/publications/manual_burden_of_disease/en
6. Gefenaite G, Pistol A, Popescu R, Popovici O, Ciurea D, Dolk C, et al. Estimating burden of influenza-associated influenza-like illness and severe acute respiratory infection at public healthcare facilities in Romania during the 2011/12–2015/16 influenza seasons. Influenza Other Respir Viruses. 2018;12:183–92. https://doi.org/10.1111/irv.12525
7. Niang MN, Barry MA, Talla C, Mbengue A, Sarr FD, Ba IO, et al.; 4S Network Group. Estimation of the burden of flu-association influenza-like illness visits on total clinic visits through the sentinel influenza monitoring system in Senegal during the 2013–2015 influenza seasons. Epidemiol Infect. 2018;146:2049–55. https://doi.org/10.1017/S0950268818002418
8. Stewart RJ, Ly S, Sar B, Ieng V, Heng S, Sim K, et al. Using a hospital admission survey to estimate the burden of influenza-associated severe acute respiratory infection in one province of Cambodia—methods used and lessons learned. Influenza Other Respir Viruses. 2018;12:104–12. https://doi.org/10.1111/irv.12489
9. Emukule GO, Namagambo B, Owor N, Bakamutumaho B, Kayiwa JT, Namulondo J, et al. Influenza-associated pneumonia hospitalizations in Uganda, 2013–2016. PLoS One. 2019;14:e0219012. https://doi.org/10.1371/journal.pone.0219012
10. Thapa B, Roguski K, Azziz-Baumgartner E, Siener K, Gould P, Jamtsho T, et al. The burden of influenza-associated respiratory hospitalizations in Bhutan, 2015–2016. Influenza Other Respir Viruses. 2019;13:28–35. https://doi.org/10.1111/irv.12605
11. Cheung DH, Tsang TK, Fang VJ, Xu J, Chan KH, Ip DKM, et al. Association of oseltamivir treatment with virus shedding, illness, and household transmission of influenza viruses. J Infect Dis. 2015;212:391–6. https://doi.org/10.1093/infdis/jiv058
12. Chittaganpitch M, Waicharoen S, Yingyong T, Praphasiri P, Sangkitporn S, Olsen SJ, et al. Viral etiologies of influenza-like illness and severe acute respiratory infections in Thailand. Influenza Other Respir Viruses. 2018;12:482–9. https://doi.org/10.1111/irv.12554
13. de Francisco Shapovalova N, Donadel M, Jit M, Hutubessy R. A systematic review of the social and economic burden of influenza in low- and middle-income countries. Vaccine. 2015;33:6537–44. https://doi.org/10.1016/j.vaccine.2015.10.066
14. World Health Organization. Made in Viet Nam vaccines: efforts to develop sustainable in-country manufacturing for seasonal and pandemic influenza vaccines: consultation held in Viet Nam, April–June 2016 [cited 2018 Feb 7]. https://apps.who.int/iris/handle/10665/254184
15. World Bank. World development indicators. Vietnam. 2019 [cited 2019 Oct 23]. https://data.worldbank.org/country/vietnam
16. Lan PT, Toan NT, Thang HA, Thang TC, Be LV, Thai DH, et al. A phase 2/3 double-blind, randomized, placebo-controlled study to evaluate the safety and immunogenicity of a seasonal trivalent inactivated split-virion influenza vaccine (IVACFLU-S) in healthy adults in Vietnam. Hum Vaccin Immunother. 2019;15:2933–9. https://doi.org/10.1080/21645515.2019.1613127
17. Vietnam Ministry of Health. Statistical yearbook of Vietnam 2015. 2017 [cited 2018 Feb 7]. https://www.gso.gov.vn/en/data-and-statistics/2019/10/statistical-yearbook-of-vietnam-2015-2
18. Tran PD, Vu LN, Nguyen HT, Phan LT, Lowe W, McConnell MS, et al.; Centers for Disease Control and Prevention (CDC). Strengthening global health security capacity—Vietnam demonstration project, 2013. MMWR Morb Mortal Wkly Rep. 2014;63:77–80.
19. Hochwarter S, Cuong DD, Chuc NT, Larsson M. Towards an electronic health record system in Vietnam: a core readiness assessment. J Health Inform Dev Ctries. 2014;8:93–103.
20. Nguyen HKL, Nguyen SV, Nguyen AP, Hoang PMV, Le TT, Nguyen TC, et al. Surveillance of severe acute respiratory infection (SARI) for hospitalized patients in northern Vietnam, 2011–2014. Jpn J Infect Dis. 2017;70:522–7. https://doi.org/10.7883/yoken.JJID.2016.463
21. Government of Vietnam. Population projections for Vietnam, 2009–2049. 2011 [cited 2019 Jun 30]. http://portal.thongke.gov.vn/khodulieudanso2009/Tailieu/AnPham/DuBaoDanSo/4_Population-Projections.pdf
22. World Health Organization. Vaccines against influenza WHO position paper—November 2012. Wkly Epidemiol Rec. 2012;87:461–76.
23. Huang QS, Baker M, McArthur C, Roberts S, Williamson D, Grant C, et al. Implementing hospital-based surveillance for severe acute respiratory infections caused by influenza and other respiratory pathogens in New Zealand. Western Pac Surveill Response J. 2014;5:23–30. https://doi.org/10.5365/wpsar.2014.5.1.004
24. Chiu SS, Lo JYC, Chan K-H, Chan ELY, So L-Y, Wu P, et al. Population-based hospitalization burden of influenza a virus subtypes and antigenic drift variants in children in Hong Kong (2004–2011). PLoS One. 2014;9:e92914. https://doi.org/10.1371/journal.pone.0092914
25. Tallo VL, Kamigaki T, Tan AG, Pamaran RR, Alday PP, Mercado ES, et al. Estimating influenza outpatients' and inpatients' incidences from 2009 to 2011 in a tropical urban setting in the Philippines. Influenza Other Respir Viruses. 2014;8:159–68. https://doi.org/10.1111/irv.12223
26. Choi WS, Cowling BJ, Noh JY, Song JY, Wie SH, Lee JS, et al. Disease burden of 2013–2014 seasonal influenza in adults in Korea. PLoS One. 2017;12:e0172012. https://doi.org/10.1371/journal.pone.0172012
27. Simmerman JM, Chittaganpitch M, Levy J, Chantra S, Maloney S, Uyeki T, et al. Incidence, seasonality and mortality associated with influenza pneumonia in Thailand: 2005–2008. PLoS One. 2009;4:e7776. https://doi.org/10.1371/journal.pone.0007776
28. Yu H, Huang J, Huai Y, Guan X, Klena J, Liu S, et al. The substantial hospitalization burden of influenza in central China: surveillance for severe, acute respiratory infection, and influenza viruses, 2010–2012. Influenza Other Respir Viruses. 2014;8:53–65. https://doi.org/10.1111/irv.12205
29. Rolfes MA, Foppa IM, Garg S, Flannery B, Brammer L, Singleton JA, et al. Annual estimates of the burden of seasonal influenza in the United States: a tool for strengthening influenza surveillance and preparedness. Influenza Other Respir Viruses. 2018;12:132–7. https://doi.org/10.1111/irv.12486

30. Wu P, Presanis AM, Bond HS, Lau EHY, Fang VJ, Cowling BJ. A joint analysis of influenza-associated hospitalizations and mortality in Hong Kong, 1998–2013. Sci Rep. 2017;7:929. https://doi.org/10.1038/s41598-017-01021-x
31. Porter RM, Goldin S, Lafond KE, Hedman L, Ungkuldee M, Kurzum J, et al. Does having a seasonal influenza program facilitate pandemic preparedness? An analysis of vaccine deployment during the 2009 pandemic. Vaccine. 2020; 38:1152–9. https://doi.org/10.1016/j.vaccine.2019.11.025
32. Nguyen YT, Graitcer SB, Nguyen TH, Tran DN, Pham TD, Le MTQ, et al. National surveillance for influenza and influenza-like illness in Vietnam, 2006–2010. Vaccine. 2013; 31:4368–74. https://doi.org/10.1016/j.vaccine.2013.07.018
33. Leng V, Tek B, Sar B, Sim K, Seng H, Thy M, et al. National burden of influenza-associated hospitalizations in Cambodia, 2015 and 2016. Western Pac Surveill Response J. 2018;9(Suppl 1):44–52.
34. Schuit M, Gardner S, Wood S, Bower K, Williams G, Freeburger D, et al. The influence of simulated sunlight on the inactivation of influenza virus in aerosols. J Infect Dis. 2020;221:372–8. https://doi.org/10.1093/infdis/jiz582
35. Makokha C, Mott J, Njuguna HN, Khagayi S, Verani JR, Nyawanda B, et al. Comparison of severe acute respiratory illness (SARI) and clinical pneumonia case definitions for the detection of influenza virus infections among hospitalized patients, western Kenya, 2009–2013. Influenza Other Respir Viruses. 2016;10:333–9. https://doi.org/10.1111/irv.12382
36. Roguski KM, Rolfes MA, Reich JS, Owens Z, Patel N, Fitzner J, et al. Variability in published rates of influenza-associated hospitalizations: a systematic review, 2007–2018. J Glob Health. 2020;10:020430. https://doi.org/10.7189/jogh.10.020430
37. Vietnam Ministry of Health. Regulations on standards and format of output data used in management, evaluation, and payment of expenses for medical examination and treatment. 2017 [cited 2020 June 23]. https://thuvienphapluat.vn/van-ban/Bao-hiem/Quyet-dinh-4210-QD-BYT-2017-du-lieu-dau-ra-trong-thanh-toan-chi-phi-kham-chua-benh-y-te-361955.aspx
38. Steffens AF, Friedlander H, Como-Sabetti K, Boxrud D, Bistodeau S, Strain A, et al. ICD-9 code reporting among patients from the Minnesota SARI surveillance program. Online J Public Health Inform. 2017;9:e105. https://doi.org/10.5210/ojphi.v9i1.7688

Address for correspondence: Nguyen Cong Khanh, National Institute of Hygiene and Epidemiology, Department of Communicable Diseases Control, 1 Yersin, Hanoi 10000, Vietnam; email: nck@nihe.org.vn; Ashley L. Fowlkes, Centers for Disease Control and Prevention, 1600 Clifton Rd NE, Mailstop H24-7, Atlanta, GA 30329-4027, USA; email: afowlkes@cdc.gov

Recurrence of Human Babesiosis Caused by Reinfection

Jonathan Ho,[1] Erin Carey, Dennis E. Carey, Peter J. Krause

Medscape ACTIVITY EDUCATION

In support of improving patient care, this activity has been planned and implemented by Medscape, LLC and Emerging Infectious Diseases. Medscape, LLC is jointly accredited by the Accreditation Council for Continuing Medical Education (ACCME), the Accreditation Council for Pharmacy Education (ACPE), and the American Nurses Credentialing Center (ANCC), to provide continuing education for the healthcare team.

Medscape, LLC designates this Journal-based CME activity for a maximum of 1.00 ***AMA PRA Category 1 Credit(s)™***. Physicians should claim only the credit commensurate with the extent of their participation in the activity.

Successful completion of this CME activity, which includes participation in the evaluation component, enables the participant to earn up to 1.0 MOC points in the American Board of Internal Medicine's (ABIM) Maintenance of Certification (MOC) program. Participants will earn MOC points equivalent to the amount of CME credits claimed for the activity. It is the CME activity provider's responsibility to submit participant completion information to ACCME for the purpose of granting ABIM MOC credit.

All other clinicians completing this activity will be issued a certificate of participation. To participate in this journal CME activity: (1) review the learning objectives and author disclosures; (2) study the education content; (3) take the post-test with a 75% minimum passing score and complete the evaluation at http://www.medscape.org/journal/eid; and (4) view/print certificate. For CME questions, see page 2750.

Release date: September 17, 2021; Expiration date: September 17, 2022

Learning Objectives

Upon completion of this activity, participants will be able to:

- Describe clinical findings and course in a previously healthy patient who experienced a second episode of babesiosis 3 years after an initial episode
- Determine laboratory findings in a previously healthy patient who experienced a second episode of babesiosis 3 years after an initial episode
- Identify clinical implications of a case of babesiosis in a previously healthy patient who experienced a second episode of babesiosis 3 years after an initial episode

CME Editor

Thomas J. Gryczan, MS, Technical Writer/Editor, Emerging Infectious Diseases. *Disclosure: Thomas J. Gryczan, MS, has disclosed no relevant financial relationships.*

CME Author

Laurie Barclay, MD, freelance writer and reviewer, Medscape, LLC. *Disclosure: Laurie Barclay, MD, has disclosed no relevant financial relationships.*

Authors

Disclosures: ***Jonathan Ho, MD; Erin E. Carey, MS;*** *and* ***Dennis E. Carey, MD,*** *have disclosed no relevant financial relationships.* ***Peter J. Krause, MD,*** *has disclosed the following relevant financial relationships: received grants for clinical research from Gold Standard Diagnostics.*

Author affiliations: Yale School of Public Health, New Haven, Connecticut, USA (J. Ho, P.J. Krause); University of Bridgeport, Bridgeport, Connecticut, USA (E. Carey); Zucker School of Medicine at Hofstra/Northwell, Hempstead, New York, USA (D.E. Carey); Yale School of Medicine, New Haven (P.J. Krause)

DOI: https://doi.org/10.3201/eid2720.211240

[1]Current affiliation: Brown University, Providence, Rhode Island, USA.

Babesiosis developed in a 62-year-old immunocompetent physician, who had an uneventful recovery after receiving atovaquone and azithromycin. Three years later, babesiosis developed again, and he was again successfully given treatment. Clinical and laboratory evidence were highly supportive of *Babesia* reinfection. Healthcare professionals should be aware that reinfection might occur in babesiosis.

Babesia microti, the primary cause of human babesiosis, is an intraerythrocytic protozoan that is transmitted by hard-bodied ticks to mammalian hosts and occasionally to humans (*1*). White-footed mice are the primary host and once infected may remain so for life. Parasitemia also persists in humans, even after antimicrobial drug therapy (*2*–*7*). Immunocompetent human hosts can experience asymptomatic infection for as long as 1 year after antimicrobial drug therapy, although most patients clear infection within several months. Patients who are immunocompromised generally have a longer duration of infection and may experience relapsing symptoms. These patients might remain parasitemic for as long as 2 years, despite antimicrobial drug therapy (*5*,*7*). Most patients recover without long-term complications, although babesiosis can result in fatal illness (*1*,*6*).

We report a case of babesiosis in a previously healthy patient who experienced a second episode of babesiosis 3 years after an initial episode. He was given a standard course of antimicrobial drugs for *Babesia* infection for each episode.

The Study

A 62-year-old physician living in Huntington, Long Island, New York, USA, was in good health until June 9, 2013, when he felt unwell and fever, chills, headache, myalgias, fatigue, sweats, joint pain, poor appetite, and conjunctivitis developed. On the third day of illness, he noted dark urine that lasted for several days. On June 13, he was seen by his family physician, who noted fever but no other abnormality.

A complete blood count (CBC) showed a hemoglobin level of 13.9 g/dL (reference range 13 g/dL–18 g/dL); a hematocrit of 40.8% (40%–54%); a leukocyte count of 4,700 cells/μL (4,500 cells/μL–11,000 cells/μL) with 55% neutrophils (54%–62%) and 28% lymphocytes (25%–33%); a platelet count of 68,000 cells/μL (150,000 cells/μL–400,00 cells/μL); an aspartate aminotransferase level of 65 U/L (1 U/L–36 U/L); and an alanine aminotransferase level of ALT 70 U/L (1 U/L–45 U/L). He was told to return for reevaluation if symptoms did not resolve and was seen again on June 16. At that time, he had a fever (temperature 103°F). He was given doxycycline (100 mg orally every 12 h) but did not improve.

Laboratory results on June 16 showed that a *B. microti* IgM result was strongly positive (IgM titer ≥1:1,024, IgG titer ≤1:16), but *Anaplasma phagocytophilum* antibody was absent (Table). He was then given atovaquone (750 mg, 2×/d for 2 wks) and azithromycin (500 mg, 1×/d for 2 wks). He recovered completely 3 weeks after symptoms began.

Subsequent attempts to perform *Babesia* whole-genome sequencing on a residual blood sample obtained 3 days after the start of treatment identified *B. microti* DNA, but it was insufficient to perform full-genomic sequencing. At a follow-up visit to his physician on July 5, a CBC and tests for aspartate and alanine aminotransferase levels showed results within references ranges.

Three years later, on June 19, 2016, the patient had fever (temperature 100°F), chills, sweats, headache, myalgias, anorexia, and difficulty concentrating develop. He also noted dark urine for several days. On June 22, he was seen by his physician, who obtained a CBC, which showed a hemoglobin level of 12.6 g/dL and hematocrit of 38.3%; a leukocyte count of 4,700 cells/μL with 55% neutrophils and 30% lymphocytes; and a platelet count of 41,000 cells/μL. A blood smear showed a *Babesia* parasitemia level of 1%. We amplified *B. microti* DNA by using PCR. Results for *B. microti* antibody were positive (IgM titer 1:256, IgG titer ≥1;1,024) (Table). He was then given atovaquone (750 mg every 12 h) and azithromycin (500 mg on day 1 and then 250 mg 1×/d) for 10 days, at which time symptoms had resolved. A repeat blood smear did not show any parasites. The patient has subsequently been in good health.

Conclusions

This patient had 2 separate episodes of *B. microti* babesiosis 3 years apart. He lived in an area where *B. microti* was hyperendemic and showed typical symptoms of *Babesia* infection during each episode, including dark urine that is indicative of hemoglobinuria (*8*). In the first episode, he did not have a blood smear or PCR performed, but a high *B. microti* IgM response was suggestive of *B. microti* infection (*1*,*9*). *B. microti* infection was subsequently confirmed by identification of *B. microti* DNA. In the second episode, *B. microti* infection was confirmed by blood smear and PCR.

Both clinical and laboratory evidence support reinfection rather than relapse of infection for this patient. He was repeatedly exposed to ticks in an area

Table. *Babesia microti* indirect fluorescent antibody test results for patient who had babesiosis 2 times, New York, USA

B. microti test date	Days after onset of symptoms	*B. microti* IgM titer	*B. microti* IgG titer
Episode 1, 2013 Jun 16	7	≥1:1,024	<1:16
Episode 2, 2016 Jun 22	4	1:256	≥1:1,024

where babesiosis is commonly reported (*1*). He was in good general health without evidence of immunosuppression, whereas all cases of relapsing babesiosis have been reported in immunocompromised persons. After the first episode of babesiosis, he had complete clinical recovery 2 weeks after the onset of infection and did not experience the second episode until 3 years later. In contrast, those persons who have had relapsed *B. microti* infection have all been immunocompromised, experienced relapses of infection 2 weeks to 3 months after the previous episode, and usually lack full clinical recovery between relapses (*3*–*7*). Finally, our patient had a robust *B. microti* IgM response 2 weeks after the onset of his first infection and an anamnestic antibody response with a high IgG titer on day 4 of the second infection, which is characteristic of reinfection rather than relapse. Patients who have experienced relapse have conditions that impair antibody response (e.g., B cell lymphoma, rituximab therapy, HIV/AIDS). A minimal or absent *B. microti* antibody response has been demonstrated in patients who have had relapsing babesiosis and have been tested for *B. microti* antibody (*5*,*7*).

Previous studies describe the persistence of human *B. microti* infection and clinical immunity. In a prospective study of babesiosis patients who were tested for *B. microti* DNA by PCR every 3 months after acute illness until infection cleared, parasitemia persisted up to 13 months in 22 antimicrobial drug–treated patients and up to 27 months in 23 untreated patients (*2*). In another study, a patient was reported as having relapsing infection that persisted for 27 months (*5*). The immediate host response to *B. microti* infection is provided by innate immune elements that include the spleen, macrophages, and neutrophils. In contrast, long-term clearance of *B. microti* parasites depends in large part on antibody (*2*–*7*). Studies of the duration of *B. microti* antibody have demonstrated persistence for as little as 6 months and as long as 6 years (*2*,*6*,*10*–*11*).

Although there is strong evidence that our patient experienced reinfection, we do not have absolute confirmation, and it is possible that he could have had persistent *B. microti* infection that relapsed after 3 years. No *B. microti* PCR (or blood smear) was obtained after the initial infection. We attempted to further distinguish between relapse and reinfection by genetic sequencing of *B. microti* DNA from blood samples obtained from both episodes of infection. Unfortunately, we were unable to obtain sufficient DNA from the first episode for sequencing because a blood sample was only available 3 days after antimicrobial drug therapy was initiated, leaving few viable parasites.

In summary, our study shows evidence of reinfection after successful treatment of a *B. microti* infection. Although the evidence is highly supportive, it is not definitive. Whether our patient experienced reinfection or relapse 3 years after the initial infection, investigation of similar patients could provide useful information about the immune response to *B. microti* infection. Patients who have experienced babesiosis, and their healthcare professionals, need to be aware that babesiosis reinfection might occur, as for Lyme disease (*12*,*13*). Tickborne disease preventive measures should be maintained for patients with or without a history of babesiosis (*14*).

This study was supported in part by the Gordon and Llura Gund Foundation.

About the Author

Dr. Ho is a resident of internal medicine at Rhode Island Hospital/Warren Alpert Medical School, Brown University, Providence, RI. His research interests include antimicrobial drug resistance and quality care in gastroenterology.

References

1. Vannier E, Krause PJ. Human babesiosis. N Engl J Med. 2012;366:2397–407. https://doi.org/10.1056/NEJMra1202018
2. Krause PJ, Spielman A, Telford SR III, Sikand VK, McKay K, Christianson D, et al. Persistent parasitemia after acute babesiosis. N Engl J Med. 1998;339:160–5. https://doi.org/10.1056/NEJM199807163390304
3. Lemieux JE, Tran AD, Freimark L, Schaffner SF, Goethert H, Andersen KG, et al. A global map of genetic diversity in Babesia microti reveals strong population structure and identifies variants associated with clinical relapse. Nat Microbiol. 2016;1:16079. https://doi.org/10.1038/nmicrobiol.2016.79
4. Simon MS, Westblade LF, Dziedziech A, Visone JE, Furman RR, Jenkins SG, et al. Clinical and molecular evidence of atovaquone and azithromycin resistance in relapsed *Babesia microti* infection associated with rituximab and chronic lymphocytic leukemia. Clin Infect Dis. 2017;65:1222–5. https://doi.org/10.1093/cid/cix477
5. Raffalli J, Wormser GP. Persistence of babesiosis for >2 years in a patient on rituximab for rheumatoid arthritis. Diagn

Microbiol Infect Dis. 2016;85:231–2. https://doi.org/10.1016/j.diagmicrobio.2016.02.016
6. Bloch EM, Kumar S, Krause PJ. Persistence of *Babesia microti* infection in humans. Pathogens. 2019;8:102. https://doi.org/10.3390/pathogens8030102
7. Krause PJ, Gewurz BE, Hill D, Marty FM, Vannier E, Foppa IM, et al. Persistent and relapsing babesiosis in immunocompromised patients. Clin Infect Dis. 2008;46:370–6. https://doi.org/10.1086/525852
8. Hunfeld KP, Hildebrandt A, Gray JS. Babesiosis: recent insights into an ancient disease. Int J Parasitol. 2008;38:1219–37. https://doi.org/10.1016/j.ijpara.2008.03.001
9. Krause PJ, Ryan R, Telford S III, Persing D, Spielman A. Efficacy of immunoglobulin M serodiagnostic test for rapid diagnosis of acute babesiosis. J Clin Microbiol. 1996;34:2014–6. https://doi.org/10.1128/jcm.34.8.2014-2016.1996
10. Ruebush TK II, Chisholm ES, Sulzer AJ, Healy GR. Development and persistence of antibody in persons infected with *Babesia microti.* Am J Trop Med Hyg. 1981;30:291–2. https://doi.org/10.4269/ajtmh.1981.30.291
11. Moritz ED, Winton CS, Tonnetti L, Townsend RL, Berardi VP, Hewins ME, et al. Screening for *Babesia microti* in the U.S. blood supply. N Engl J Med. 2016;375:2236–45. https://doi.org/10.1056/NEJMoa1600897
12. Nadelman RB, Hanincová K, Mukherjee P, Liveris D, Nowakowski J, McKenna D, et al. Differentiation of reinfection from relapse in recurrent Lyme disease. N Engl J Med. 2012;367:1883–90. https://doi.org/10.1056/NEJMoa1114362
13. Krause PJ, Foley DT, Burke GS, Christianson D, Closter L, Spielman A; Tick-Borne Disease Study Group. Reinfection and relapse in early Lyme disease. Am J Trop Med Hyg. 2006;75:1090–4. https://doi.org/10.4269/ajtmh.2006.75.1090
14. Piesman J, Beard CB. Prevention of tick-borne diseases. J Environ Health. 2012;74:30–2.

Address for correspondence: Peter J. Krause, Yale University, 60 College St, New Haven, CT 06510; USA; email: peter.krause@yale.edu

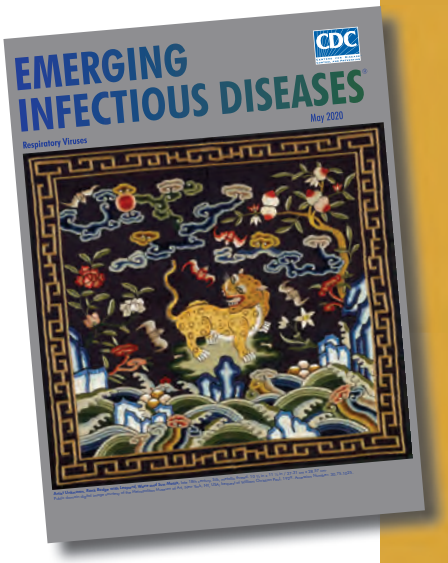

Originally published in May 2020

etymologia revisited

Coronavirus

The first coronavirus, avian infectious bronchitis virus, was discovered in 1937 by Fred Beaudette and Charles Hudson. In 1967, June Almeida and David Tyrrell performed electron microscopy on specimens from cultures of viruses known to cause colds in humans and identified particles that resembled avian infectious bronchitis virus. Almeida coined the term "coronavirus," from the Latin *corona* ("crown"), because the glycoprotein spikes of these viruses created an image similar to a solar corona. Strains that infect humans generally cause mild symptoms. However, more recently, animal coronaviruses have caused outbreaks of severe respiratory disease in humans, including severe acute respiratory syndrome (SARS), Middle East respiratory syndrome (MERS), and 2019 novel coronavirus disease (COVID-19).

Sources:

1. Almeida JD, Tyrrell DA. The morphology of three previously uncharacterized human respiratory viruses that grow in organ culture. J Gen Virol. 1967;1:175–8. https://doi.org/10.1099/0022-1317-1-2-175
2. Beaudette FR, Hudson CB. Cultivation of the virus of infectious bronchitis. J Am Vet Med Assoc. 1937;90:51–8.
3. Estola T. Coronaviruses, a new group of animal RNA viruses. Avian Dis. 1970;14:330–6. https://doi.org/10.2307/1588476
4. Groupe V. Demonstration of an interference phenomenon associated with infectious bronchitis virus of chickens. J Bacteriol. 1949;58:23–32. https://doi.org/10.1128/JB.58.1.23-32.1949

https://wwwnc.cdc.gov/eid/article/26/5/et-2605_article

Point-of-Care Antigen Test for SARS-CoV-2 in Asymptomatic College Students

Sarah C. Tinker, Christine M. Szablewski, Anastasia P. Litvintseva, Cherie Drenzek, Gary E. Voccio, Melissa A. Hunter, Stephen Briggs, Debbie E. Heida, Jennifer Folster, Patricia L. Shewmaker, Magdalena Medrzycki, Michael D. Bowen, Caitlin Bohannon, Dennis Bagarozzi Jr., Marla Petway, Paul A. Rota, Wendi Kuhnert-Tallman, Natalie Thornburg, Jessica L. Prince-Guerra, Lisa C. Barrios, Azaibi Tamin, Jennifer L. Harcourt, Margaret A. Honein, CDC Sample Collection Team,[1] CDC Surge Laboratory Group[1]

We used the BinaxNOW COVID-19 Ag Card to screen 1,540 asymptomatic college students for severe acute respiratory syndrome coronavirus 2 in a low-prevalence setting. Compared with reverse transcription PCR, BinaxNOW showed 20% overall sensitivity; among participants with culturable virus, sensitivity was 60%. BinaxNOW provides point-of-care screening but misses many infections.

Point-of-care antigen testing provides results more quickly than real-time reverse transcription PCR (rRT-PCR). In August 2020, the US Food and Drug Administration granted emergency use authorization to the BinaxNOW COVID-19 Ag Card (BinaxNOW; Abbott Laboratories, https://www.abbott.com) for the detection of severe acute respiratory syndrome 2 (SARS-CoV-2) infection in persons with signs or symptoms of coronavirus disease (COVID-19) (*1*). However, administrative discretion permits the screening of asymptomatic persons, thereby enabling the rapid identification and isolation of infectious persons (*2*). To assess the abilities of BinaxNOW to screen asymptomatic persons for SARS-CoV-2 in a low-prevalence setting, we compared the performance of BinaxNOW and rRT-PCR using paired samples collected from students at a residential college in the United States.

Author affiliations: Centers for Disease Control and Prevention, Atlanta, Georgia, USA (S.C. Tinker, C.M. Szablewski, A.P. Litvintseva, J. Folster, P.L. Shewmaker, M. Medrzycki, M.D. Bowen, C. Bohannon, D. Bagarozzi Jr., M. Petway, P.A. Rota, W. Kuhnert-Tallman, N. Thornburg, J.L. Prince-Guerra, L.C. Barrios, A. Tamin, J.L. Harcourt, M.A. Honein); Georgia Department of Public Health, Atlanta (C.M. Szablewski, C. Drenzek); Georgia Department of Public Health Northwest Health District, Rome, Georgia, USA (G.E. Voccio, M.A. Hunter); Berry College, Mount Berry, Georgia, USA (S. Briggs, D.E. Heida)

DOI: https://doi.org/10.3201/eid2710.210080

The Study

During November 2020, the county in which the college is located reported 467 RT-PCR–positive cases/100,000 persons and a 13.7% positivity rate (*3*). The school instituted COVID-19 mitigation policies, including mask mandates, social distancing in classrooms, enhanced cleaning measures, limited campus access, and encouragement of small, mutually exclusive social bubbles. Most (87%) students lived on-campus, and the COVID-19 prevalence among students was 0.6%.

In total, 1,827 students were eligible for SARS-CoV-2 testing on campus, excluding 162 students who had tested positive during the previous 90 days. Students who reported signs or symptoms of COVID-19 in the school's daily online tracking system were directed to the campus health center for testing.

All students at the testing event, which was conducted over 4 days in November 2020, were asymptomatic. We obtained student demographic data from college records. This activity was reviewed by the institutional review boards of the Georgia Department of Public Health, Centers for Disease Control and Prevention (CDC; Atlanta, GA, USA), and college; the study was conducted in accordance with applicable federal law and CDC policy.

Project staff directed students to self-collect 2 anterior nasal swab samples by inserting 1 swab into each nostril and then switching the swabs to obtain sample secretions from the other nostril. We tested

[1]Members are listed at the end of this article.

1 swab immediately using BinaxNOW and sent the other swab to CDC for rRT-PCR.

We conducted BinaxNOW assays on-site in accordance with manufacturer instructions (*4*). Students received BinaxNOW results after 15–30 minutes. Those who tested positive were counseled to isolate for 10 days and interviewed for contact tracing.

Swab samples collected for rRT-PCR were stored using Remel R12587 viral transport media (Thermo Fisher Scientific, https://www.thermofisher.com) with cold packs; samples were transported daily to CDC and refrigerated at 4°C. We isolated nucleic acid from the specimens using the MagNA Pure 96 Instrument (Roche Molecular Systems, Inc., https://lifescience.roche.com) within 48 hours of collection, then analyzed the nucleic acid using the CDC Influenza SARS-CoV-2 (Flu SC2) Multiplex Assay (*5*). Results were reported as SARS-CoV-2–positive (cycle threshold [C_t] <40 for the SARS-CoV-2 target), SARS-CoV-2–negative, or invalid (C_t value ≥40 for all viral targets and C_t ≥35 for human RNase P reference gene on repeat testing, according to the manufacturer's guidelines).

We cultured residual frozen SARS-CoV-2–positive samples in 100 μL viral transport media. We limited dilution in Vero CCL-81 cells and monitored 96-well plates daily for cytopathic effects (J. Harcourt, unpub. data, https://www.biorxiv.org/content/10.1101/2020.03.02.972935v2). We extracted nucleic acid from the wells exhibiting cytopathic effects and confirmed the presence of SARS-CoV-2 by rRT-PCR. We considered a specimen to be culture-positive if the first viral passage had a C_t value ≥2 less than the clinical sample.

Conclusions

In total, 1,540 asymptomatic students provided paired samples (Table). Forty (2.6%) samples tested positive by rRT-PCR; of these, 8 (20%) also tested positive by BinaxNOW. We did not observe any false-positive BinaxNOW results (100% specificity). Concordant samples had a lower median C_t value than discordant samples (21.9 vs. 34.9). Students received rRT-PCR results within 72 hours. No specimens tested positive for influenza A or B viruses. All 8 persons who tested positive by BinaxNOW and rRT-PCR later reported symptom onset. Among the 32 students who provided samples that tested negative by BinaxNOW and positive by rRT-PCR, 10 (31.3%) later reported symptom onset (median C_t 34.9), 16 (50.0%) later reported no symptoms (median C_t 35.1), and 6 (18.8%) did not report information on symptoms (median C_t 34.9).

Table. Characteristics of asymptomatic college students participating in study on point-of-care antigen test for severe acute respiratory syndrome coronavirus 2, 2020

Characteristic	No. (%)
Total	1,540
Age, y	
≤18	362 (23.5)
19–20	733 (47.6)
21–22	418 (27.1)
23–24	18 (1.2)
≥25	9 (0.6)
Sex	
M	549 (35.6)
F	991 (64.4)
Race/ethnicity*	
Non-Hispanic White	1,157 (75.4)
Non-Hispanic Black	112 (7.3)
Hispanic	133 (8.7)
Asian	43 (2.8)
Other†	89 (5.8)
Not available	6
Housing	
On-campus	1,379 (89.5)
Off-campus	161 (10.5)

*Percentages do not include the 6 persons whose race/ethnicity was not available.
†Includes persons of ≥2 races.

We detected culturable virus in 5 (12.5%) samples that tested positive by rRT-PCR, including 3 (60%) that also tested positive by BinaxNOW (Figure). One person provided a sample (C_t 28.9) that tested negative by BinaxNOW but was culture-positive; symptoms later developed in this person, who tested positive by a different antigen test (BD Veritor System; Becton, Dickinson and Company, https://www.bd.com) the next day. Symptoms did not develop in the other person who provided a sample that tested negative by BinaxNOW and positive by culture (C_t 37.3).

BinaxNOW provides rapid, point-of-care results; students received BinaxNOW results 3 days earlier than rRT-PCR results. However, BinaxNOW had low sensitivity, especially among persons with higher C_t values, which suggest lower viral load. BinaxNOW did not identify 32 persons who tested positive by rRT-PCR.

Our data are consistent with those of Prince-Guerra et al. (*6*), which found low overall BinaxNOW sensitivity (35.8%; 44/123) compared with RT-PCR among asymptomatic persons. Prince-Guerra et al. (*6*) found that concordant samples had a lower mean C_t value than discordant samples (22.5 vs. 33.9); we observed 88.9% (8/9) sensitivity among samples with C_t values <32. However, Prince-Guerra et al. (*6*) collected samples using disparate methods (nasopharyngeal swab for RT-PCR and anterior nasal swab for BinaxNOW), precluding direct comparison of samples. Our results are

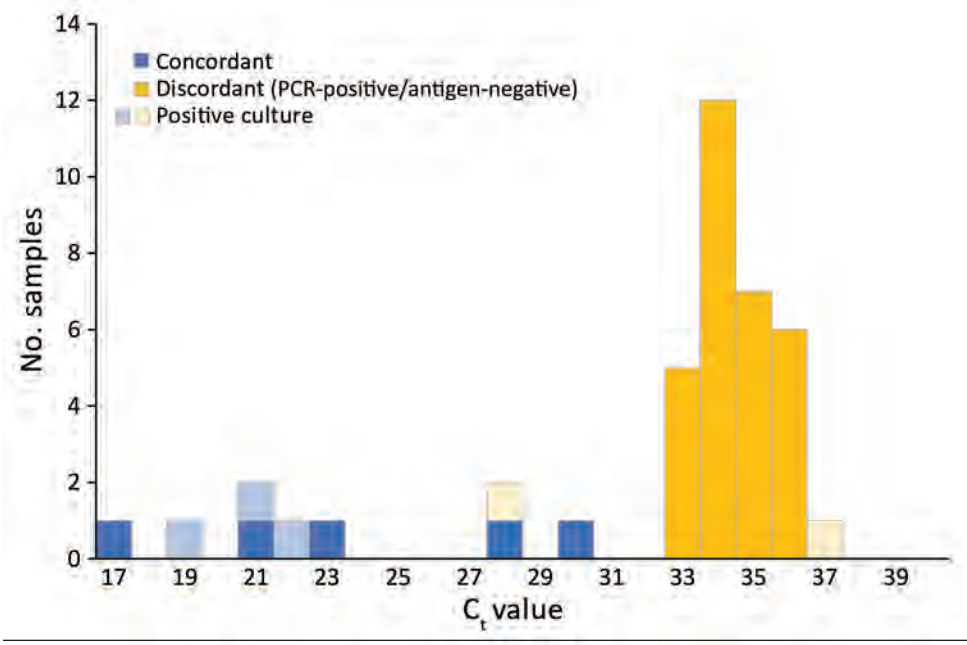

Figure. C_t values of severe acute respiratory syndrome coronavirus 2–positive samples tested by reverse transcription PCR, the BinaxNOW COVID-19 Ag Card (BinaxNOW; Abbott Laboratories, https://www.abbott.com), and viral culturing. C_t, cycle threshold.

inconsistent with those of Pilarowski et al. (*7*), which showed 81.4% sensitivity among 102 persons who were asymptomatic or had symptom onset >1 week previously. We observed high specificity, consistent with results of both investigations (*6*,*7*). Unlike the community investigations of Prince-Guerra et al. (*6*) and Pilarowski et al. (*7*), in which testing was offered to persons who might have had specific reasons for seeking testing, our investigation was conducted in a closed, defined population, among persons with no known exposures or symptoms, providing more generalizable performance data for similar institutions.

CDC provided guidance on expanded screening testing of asymptomatic individuals to reduce spread of SARS-CoV-2 and for interpretation of antigen tests (*8*,*9*). Test performance among asymptomatic persons probably varies for different antigen tests. For example, an assessment of the Sofia SARS Antigen Fluorescent Immunoassay (Quidel Corporation, https://www.quidel.com) reported 41.2% sensitivity and 98.4% specificity among 871 asymptomatic college students (*10*).

Isolation of SARS-CoV-2 in cell culture demonstrates viral replication. However, because many factors affect the culture performance, lack of culturable virus does not necessarily indicate a lack of infectious virus. The presence of culturable virus in samples that test negative for SARS-CoV-2 antigens suggests that BinaxNOW does not identify some persons with infectious virus. However, the speed of BinaxNOW enabled the immediate identification of 8 SARS-CoV-2–positive persons, thereby limiting transmission that might have occurred during the additional 2 days that students waited for rRT-PCR results.

Although rRT-PCR tests remain standard for SARS-CoV-2 detection, point-of-care antigen tests such as BinaxNOW could increase access to serial screening, enabling the rapid identification and isolation of infectious persons. Because presymptomatic and asymptomatic persons can transmit SARS-CoV-2 (*11*), screening of asymptomatic persons is a key strategy for interrupting SARS-CoV-2 transmission. Although messaging must clearly communicate the low sensitivity of the test, positive results enable immediate public health action.

Members of the CDC Sample Collection Team: Melissa M. Arons, Ellen O. Boundy, Kevin Chatham-Stephens, Michele B. Daly, Jennifer Driggers, Alicia Dunajcik, Brian Emerson, Mary E. Evans, Jenna R. Gettings, Collette Fitzgerald Leaumont, Martha Marquesen, Jasmine Nakayama, Kim Newsome, Glenn P. Niemeyer, Kelly Regan, Catherine Smith, Kenneth D. Swanson, and Malania Wilson.

Members of the CDC Surge Laboratory Group: Baoming Jiang, Jan Vinjé, Hannah Browne, Amy Hopkins, Eric Katz, Kenny Nguyen, Leslie Barclay, Mathew D. Esona, Rashi Gautam, Slavica Mijatovic-Rustempasic, Sung-Sil Moon, Theresa Bessey, Preeti Chhabra, Leeann Smart, Lalitha Gade, Claire Hartloge, Shilpi Jain, Kashif Sahibzada, Alexandra Tejada-Strop, and Phili Wong. This investigation was financially supported by the Centers for Disease Control and Prevention, Berry College, and the Georgia Department of Public Health.

About the Author

Dr. Tinker is a senior scientist in the Human Development and Disability Division, National Center on Birth Defects and Developmental Disabilities, Centers for Disease Control and Prevention in Atlanta, Georgia, USA. Her research interests include epidemiology and developmental disabilities.

References

1. US Food and Drug Administration. BinaxNOW COVID-19 Ag Card emergency use authorization. 2020 [cited 2021 Jun 28]. https://www.fda.gov/media/147264/download
2. Centers for Medicare and Medicaid Services. Updated CLIA SARS-CoV-2 molecular and antigen point of care test enforcement discretion. 2020 [cited 2021 Jun 28]. https://www.cms.gov/files/document/clia-sars-cov-2-point-care-test-enforcement-discretion.pdf
3. Georgia Department of Public Health. Covid-19 daily status report, by county (Floyd County, November 16th). 2020 [cited 2021 Feb 28]. https://dph.georgia.gov/covid-19-daily-status-report
4. US Food and Drug Administration. BinaxNOW COVID-19 Ag Card—instructions for use. 2020 [cited 2021 Jun 28]. https://www.fda.gov/media/141570/download
5. US Food and Drug Administration. Influenza SARS-CoV-2 (Flu SC2) Multiplex Assay emergency use authorization. 2020 [cited 2021 Jun 28]. https://www.fda.gov/media/139744/download
6. Prince-Guerra JL, Almendares O, Nolen LD, Gunn JKL, Dale AP, Buono SA, et al. Evaluation of Abbott BinaxNOW rapid antigen test for SARS-CoV-2 infection at two community-based testing sites—Pima County, Arizona, November 3–17, 2020 [Erratum in: MMWR Morb Mortal Wkly Rep. 2021; 70:144]. MMWR Morb Mortal Wkly Rep. 2021;70:100–5. https://doi.org/10.15585/mmwr.mm7003e3
7. Pilarowski G, Marquez C, Rubio L, Peng J, Martinez J, Black D, et al. Field performance and public health response using the BinaxNOW rapid severe acute respiratory syndrome coronavirus 2 (SARS-CoV-2) antigen detection assay during community-based testing. Clin Infect Dis. 2020 Dec 26 [Epub ahead of print]. https://doi.org/10.1093/cid/ciaa1890
8. Centers for Disease Control and Prevention. Overview of testing for SARS-CoV-2 (COVID-19). 2021 Jun 14 [cited 2021 Jun 28]. https://www.cdc.gov/coronavirus/2019-ncov/hcp/testing-overview.html
9. Centers for Disease Control and Prevention. Interim guidance for antigen testing for SARS-CoV-2. 2021 Jun 14 [cited 2021 Jun 28]. https://www.cdc.gov/coronavirus/2019-ncov/lab/resources/antigen-tests-guidelines.html
10. Pray IW, Ford L, Cole D, Lee C, Bigoutee JP, Abedi G, et al. Performance of an antigen-based test for asymptomatic and symptomatic SARS-CoV-2 testing at two university campuses—Wisconsin, September–October 2020. MMWR Morb Mortal Wkly Rep. 2021;69:1642–7.
11. Arons MM, Hatfield KM, Reddy SC, Kimball A, James A, Jacobs JR, et al.; Public Health—Seattle and King County and CDC COVID-19 Investigation Team. Presymptomatic SARS-CoV-2 infections and transmission in a skilled nursing facility. N Engl J Med. 2020;382:2081–90. https://doi.org/10.1056/NEJMoa2008457

Address for correspondence: Sarah C. Tinker, Centers for Disease Control and Prevention, 1600 Clifton Rd NE, Mailstop S106-4, Atlanta GA 30329-4027, USA; email: zzu9@cdc.gov

Genetic Diversity of SARS-CoV-2 among Travelers Arriving in Hong Kong

Haogao Gu,[1] Daniel K.W. Chu,[1] Lydia D.J. Chang, Sammi S.Y. Cheuk, Shreya Gurung, Pavithra Krishnan, Daisy Y.M. Ng, Gigi Y.Z. Liu, Carrie K.C. Wan, Ruopeng Xie, Samuel S.M. Cheng, Benjamin J. Cowling, Dominic N.C. Tsang, Malik Peiris, Vijaykrishna Dhanasekaran, Leo L.M. Poon

We sequenced 10% of imported severe acute respiratory syndrome coronavirus 2 infections detected in travelers to Hong Kong and revealed the genomic diversity of regions of origin, including lineages not previously reported from those countries. Our results suggest that international or regional travel hubs might be useful surveillance sites to monitor sequence diversity.

Hong Kong uses an elimination strategy to control coronavirus disease (COVID-19) that includes stringent travel restrictions to reduce the risk of introducing severe acute respiratory syndrome coronavirus 2 (SARS-CoV-2) into local communities (*1*). COVID-19 testing was mandated on departure and arrival for all inbound travelers. Compulsory 14-day home quarantine was put in place for all arrivals beginning March 19, 2020. Nonresidents were banned from entry after March 25. In subsequent months, persons arriving from high-risk locations were required to quarantine in hotels; by November, all arrivals had to quarantine in hotels. On December 25, the quarantine period was extended to 21 days. Predeparture COVID-19 testing was mandated for travelers inbound from high-risk locations. Furthermore, daily health declarations were required from all quarantined travelers and respiratory samples were collected on arrival, day 12, and day 19 (for 21-day quarantine) for reverse transcription PCR (RT-PCR) testing. As of April 25, 2021, authorities had recorded 11,731 RT-PCR–positive COVID-19 cases in Hong Kong. About 20% (2,350) of the laboratory-confirmed COVID-19 cases were considered imported, detected in persons thought to have been infected outside of Hong Kong. Here, we report the analyses of 10% of these imported cases through genome sequencing.

The Study

A total of 2,192 COVID-19–positive travelers arrived in Hong Kong during January 2020–March 2021 (Appendix 1 Figure 1, https://wwwnc.cdc.gov/EID/article/27/10/21-1028-App1.pdf). Stratifying cases by departure location (Appendix 1 Table 1) showed that 10 countries accounted for 77.8% of all imported cases during this period: United Kingdom (406), Philippines (318), India (309), Pakistan (245), Indonesia (149), United States (131), Nepal (75), Russia (40), France (33), and United Arab Emirates (25). After compulsory COVID-19 RT-PCR screening on arrival at the airport began on April 7, 2020, authorities detected 1,102 cases; 80% (886) of case-patients were asymptomatic at the time of testing. Of 491 case-patients testing SARS-CoV-2–positive during quarantine, 69% were asymptomatic and cases were detected a mean (± SD) of 11.3 ±4.32 days after arrival. This finding indicates that many COVID-19 cases from quarantined travelers were only identified during the first compulsory testing on day 12. These findings support Hong Kong's stringent follow-up measures for inbound travelers to prevent introduction of SARS-CoV-2 into communities.

To estimate the viral sequence diversity among these imported cases, we performed next-generation

Author affiliations: School of Public Health, University of Hong Kong, Hong Kong, China (H. Gu, D.K.W. Chu, L.D.J. Chang, S.S.Y. Cheuk, S. Gurung, P. Krishnan, D.Y.M. Ng, G.Y.Z. Liu, C.K.C. Wan, R. Xie, S.S.M. Cheng, B.J. Cowling, M. Peiris, V. Dhanasekaran, L.L.M. Poon); Department of Health Centre for Health Protection, Government of Hong Kong Special Administrative Region, Hong Kong (D.N.C. Tsang); HKU-Pasteur Research Pole, University of Hong Kong, Hong Kong (M. Peiris, V. Dhanasekaran, L.L.M. Poon)

DOI: https://doi.org/10.3201/eid2710.211028

[1]These first authors contributed equally to this article.

sequencing on 10% (221) of clinical samples collected (*2*,*3*) (Appendix). We selected a greater proportion of samples (204) beginning in June 2020 when greater genetic diversity began to appear globally. The number of samples we sequenced by country of origin was proportional to all cases detected in travelers from that country (R = 0.91).

Using the Pangolin classification system (https://github.com/hCoV-2019/pangolin), we detected 58 different SARS-CoV-2 lineages; the most common were B.1.1.7 (39), B.1.1.63 (21), B.1.36 (18), B.1 (17), and B.1.1 (17) (Figure; Appendix 1 Table 2). We detected 2 variants of concern (VOC) and 3 variants of interest (VOI; Table 1) (*5*). VOC B.1.1.7 (Alpha variant), which began spreading rapidly in the United Kingdom in November 2020 (*6*,*7*), was the most common VOC (39) in our study. We first detected this lineage in a passenger arriving from the United Kingdom on December 13, 2020, and we subsequently detected it in another 38 travelers from other countries, predominantly from the Philippines and Pakistan (Table 1). This finding corresponds with data from global surveillance that indicate this lineage has been circulating over a wide geographic range beginning in December 2020. The second VOC, B.1.351 (Beta), which was first reported to circulate widely in South Africa beginning in November 2020 (*8*), we first detected on December 16 in an arriving passenger with a recent travel history in the United Kingdom and South Africa (*1*). Subsequent cases caused by this variant were detected only in March 2021 in travelers from the Philippines (*5*) and Bangladesh (*1*). All 3 of the VOI we detected were imported from the countries where they were first reported to have emerged: B.1.526 (Iota) from the United States, B.1.617 (Kappa) from India, and P.3 (Theta) from the Philippines (M.K. Annavajhala et al., unpub data, https://doi.org/10.1101/2021.02.23.21252259; S. Cherian et al., unpub data, https://doi.org/10.1101/2021.04.22.440932; F.A. Tablizo et al., unpub data, https://doi.org/10.1101/2021.03.03.21252812). Based on sequences detected in samples from case-patients, B.1.526 was imported on March 20, B.1.617 on March 25, and P.3 on January 21, 2021. These variants were first reported to spread rapidly in these countries during February (B1.526 and B.1.617) and March 2021 (P.3), indicating that testing arrivals from outside of Hong Kong and sequencing positive samples might enable us to capture information about variants circulating in other geographic locations.

Fifty percent of our cases were imported from 5 middle-income countries in Asia: India, Indonesia, Nepal, Pakistan, and the Philippines (https://databank.worldbank.org/data/download/site-content/CLASS.xls; Appendix Table 1). We wanted to compare the genomic diversity of SARS-CoV-2 imported from these countries with those reported in the GISAID database (https://www.gisaid.org). However, the Philippines, Nepal, and Pakistan had limited SARS-CoV-2 sequence information in the GISAID database (Table 2) (*9*). Of the 3 VOC or VOI we identified in travelers from the Philippines (Table 2), B.1.351 was not among sequences the Philippines submitted to GISAID, but the March 6–20, 2021, arrival dates of the 5 case-patients with B.1.351 suggest unreported domestic circulation of that lineage. Similarly, Nepal had reported to GISAID only 15 of the 20 viral sequences from 8 lineages we had identified. Other countries also had not previously reported several lineages we identified to GISAID, including 3 from India and 1 each from Pakistan and Indonesia. We did not analyze samples from travelers from some countries, either because they had their own extensive domestic sequencing efforts or we had few samples from these countries (<5 per country).

We further compared GISAID data with our data from the Philippines, Nepal, and Pakistan. We retrieved the earliest collection date for each lineage we detected that these countries had also reported to GISAID; some of those dates were close to the first dates of arrival for case-patients with those lineages in our study. In fact, in over half of those lineages reported in both sources, we identified the lineage either before or <1 month after it was reported by the country (Appendix Table 3), highlighting the potential use of this method of surveillance to assess genomic diversity in regions with limited sequence information.

The emergence of VOC and VOI in different geographic locations highlights the need for global-level genomic surveillance of SARS-CoV-2 (*10*), but genomic sequencing information from some regions remains incomplete. Our findings suggest that

Table 1. Severe acute respiratory syndrome coronavirus 2 variants of concern and variants of interest identified in imported cases in Hong Kong, January 2020–March 2021

Pango lineage	Total cases	Country (no. cases)
B.1.1.7*	39	Pakistan (13), Philippines (8), United Kingdom (7), United Arab Emirates (3), India (2), Netherlands (2), Canada (1), Ireland (1), South Korea (1), Switzerland (1)
B.1.351*	7	Philippines (5), Bangladesh (1), United Kingdom/South Africa (1)
B.1.526†	1	United States (1)
B.1.617†	1	India (1)
P.3†	6	Philippines (6)

*Variant of concern.
†Variant of interest.

Table 2. Severe acute respiratory syndrome coronavirus 2 lineages imported from different countries in Asia into Hong Kong, January 2020–March 2021

Country	No. sequences from GISAID*	No. sequences in this study	Lineages found in this study
India	11,435	32	B.1, B.1.1, B.1.1.1, B.1.1.306, B.1.1.7, B.1.210, B.1.36, B.1.36.18, B.1.36.29, B.1.36.36,† B.1.36.8, B.1.369, B.1.562,† B.1.589,† B.1.617
Indonesia	1,170	18	B.1.1, B.1.1.272,† B.1.1.398, B.1.36.19, B.1.459, B.1.468, B.1.470
Philippines	188	47	B.1.1, B.1.1.263, B.1.1.63, B.1.1.7, B.1.351,† B.6, P.3
Pakistan	136	21	A.21,† B.1, B.1.1.1, B.1.1.7, B.1.36, B.1.471
Nepal	15	20	B.1.1, B.1.1.214,† B.1.1.216, B.1.36, B.1.36.18,† B.1.36.22,† B.1.36.27,† B.1.468†

*GISAID, https://www.gisaid.org.
†Lineage not reported by the corresponding country.

travel hubs such as Hong Kong can be used as surveillance sites to identify infected travelers from regions with widespread circulation of lineages of interest. Such indirect surveillance might provide useful data to partially reveal virus diversity in countries with limited sequence information, leading to better preparedness for and response to newly emerging SARS-CoV-2 variants. However, findings from these indirect analyses are likely to be only partial and skewed by the level of passenger traffic to destination countries from various points of departure. Also, the extent of different virus lineages circulating in a country of departure may have affected our observations; lineages that circulate at a low level in a country of interest might be missed by our current strategy. Optimizing this approach, such as by directing sequencing efforts toward travelers departing from targeted countries or regions rather than at the points of arrival, might help overcome those limitations.

Acknowledgments

We gratefully acknowledge the efforts of the staff of the laboratories responsible for obtaining the specimens and the laboratories receiving submissions where genomic data were generated and shared via GISAID (Appendix 2, https://wwwnc.cdc.gov/EID/article/27/10/21-1028-App2.xlsx). We acknowledge the technical support provided by colleagues from the Centre for PanorOmic Sciences of the University of Hong Kong.

This work was supported by grants from the National Institute of Allergy and Infectious Diseases (U01AI151810, HHSN272201400006C), the Health and Medical Research Fund (COVID190205), and the Collaborative Research Fund, RGC (C7123-20G). We also acknowledge the Centre for Health Protection of the Department of Health for providing epidemiologic data for the study.

Virus sequences reported in this study are available from GISAID. The epidemiological data for these imported cases can be accessed in a public database (https://data.gov.hk/en-data/dataset/hk-dh-chpsebcddr-novel-infectious-agent).

About the Author

Dr. Gu is a postdoctoral fellow at the University of Hong Kong. His interests focus on bioinformatics and virus evolution.

References

1. Xue W, Lam C, Yeung HH, Wong CS, Chan VLY, Wong YS. Travel restrictions in the rising COVID-19 pandemic. Hong Kong Med J. 2020;26:255–7.
2. Choi EM, Chu DKW, Cheng PKC, Tsang DNC, Peiris M, Bausch DG, et al. In-flight transmission of SARS-CoV-2. Emerg Infect Dis. 2020;26:2713–6. https://doi.org/10.3201/eid2611.203254
3. Sit THC, Brackman CJ, Ip SM, Tam KWS, Law PYT, To EMW, et al. Infection of dogs with SARS-CoV-2. Nature. 2020;586:776–8. https://doi.org/10.1038/s41586-020-2334-5
4. Rambaut A, Holmes EC, O'Toole Á, Hill V, McCrone JT, Ruis C, et al. A dynamic nomenclature proposal for SARS-CoV-2 lineages to assist genomic epidemiology. Nat Microbiol. 2020;5:1403–7. https://doi.org/10.1038/s41564-020-0770-5
5. CDC. SARS-CoV-2 Variant classifications and definitions.2021 [cited 2021 Apr 30] https://www.cdc.gov/coronavirus/2019-ncov/cases-updates/variant-surveillance/variant-info.html
6. Leung K, Shum MH, Leung GM, Lam TT, Wu JT. Early transmissibility assessment of the N501Y mutant strains of SARS-CoV-2 in the United Kingdom, October to November 2020. Euro Surveill. 2021;26:2002106. https://doi.org/10.2807/1560-7917.ES.2020.26.1.2002106
7. Davies NG, Abbott S, Barnard RC, Jarvis CI, Kucharski AJ, Munday JD, et al.; CMMID COVID-19 Working Group; COVID-19 Genomics UK (COG-UK) Consortium. Estimated transmissibility and impact of SARS-CoV-2 lineage B.1.1.7 in England. Science. 2021;372:eabg3055. https://doi.org/10.1126/science.abg3055
8. Tegally H, Wilkinson E, Giovanetti M, Iranzadeh A, Fonseca V, Giandhari J, et al. Detection of a SARS-CoV-2 variant of concern in South Africa. Nature. 2021;592:438–43. https://doi.org/10.1038/s41586-021-03402-9
9. Elbe S, Buckland-Merrett G. Data, disease and diplomacy: GISAID's innovative contribution to global health. Glob Chall. 2017;1:33–46. https://doi.org/10.1002/gch2.1018
10. The Lancet. Genomic sequencing in pandemics. Lancet. 2021;397:445. https://doi.org/10.1016/S0140-6736(21)00257-9

Address for correspondence: Leo Poon, School of Public Health, University of Hong Kong, 21 Sassoon Rd, Pokfulam, Hong Kong; email: llmpoon@hku.hk

Multiple Transmission Chains within COVID-19 Cluster, Connecticut, USA, 2020[1]

Stephen M. Bart, Eileen Flaherty, Tara Alpert, Sherry Carlson, Lisa Fasulo, Rebecca Earnest, Elizabeth B. White, Noel Dickens, Anderson F. Brito, Nathan D. Grubaugh, James L. Hadler, Lynn E. Sosa

In fall 2020, a coronavirus disease cluster comprising 16 cases occurred in Connecticut, USA. Epidemiologic and genomic evidence supported transmission among persons at a school and fitness center but not a workplace. The multiple transmission chains identified within this cluster highlight the necessity of a combined investigatory approach.

During widespread community transmission of severe acute respiratory syndrome coronavirus 2 (SARS-CoV-2), transmission chains are sometimes unclear. Although often unavailable, viral genome sequencing can complement epidemiologic investigations.

In fall 2020, the Connecticut Department of Public Health analyzed date from contact tracing interviews and initially identified 5 cases of coronavirus disease (COVID-19), the illness caused by SARS-CoV-2, in employees of a single workplace within 1 week. One employee also worked at an elementary school and fitness center; in those settings, several contacts of this employee later tested positive for SARS-CoV-2. At the time, the weekly community case rate in this county was 141 cases/100,000 persons (https://portal.ct.gov/Coronavirus/COVID-19-Data-Tracker), reflecting high community transmission according to thresholds set by the Centers for Disease Control and Prevention (CDC) (*1*). To better characterize this cluster, we investigated its scope, phylogenetic relationships, and factors associated with transmission.

Author affiliations: Centers for Disease Control and Prevention, Atlanta, Georgia, USA (S.M. Bart); Connecticut Department of Public Health, Hartford, Connecticut, USA (S.M. Bart, E. Flaherty, L.E. Sosa); Yale School of Public Health, New Haven, Connecticut, USA (T. Alpert, R. Earnest, E.B. White, N. Dickens, A.F. Brito, N.D. Grubaugh, J.L. Hadler); local health departments, Connecticut, USA (S. Carlson, L. Fasulo)

DOI: https://doi.org/10.3201/eid2710.211196

The Study

We defined a cluster-associated case as COVID-19 in a coworker, primary contact, or secondary contact of the initial 5 employees; all cases were diagnosed by a viral test (i.e., antigen or nucleic acid amplification tests) authorized for emergency use by the Food and Drug Administration (*2*). We defined the investigation period as starting 1 week before symptom onset of the earliest workplace case and ending 2 weeks after symptom onset of the last workplace case. We assessed symptoms, onset dates, adherence to prevention strategies, and potential exposures. This activity was reviewed by CDC and was conducted in accordance with applicable federal law and CDC policy (e.g. 45 C.F.R. part 46.102(l) [2], 21 C.F.R. part 56; 42 U.S.C. 241(d); 5 U.S.C. 552a; 44 U.S.C. 3501 et seq.).

We extracted SARS-CoV-2 RNA from clinical nasopharyngeal specimens and conducted genomic sequencing using an amplicon-based approach with the MinION (Oxford Nanopore Technologies, https://nanoporetech.com) (*3*). We reconstructed maximum-likelihood phylogenetic trees using IQ-Tree with a general time-reversible nucleotide substitution model (*4*) (Appendix 1, https://wwwnc.cdc.gov/EID/article/27/10/21-1196-App1.pdf; Appendix 2 Table, https://wwwnc.cdc.gov/EID/article/27/10/21-1196-App2.xlsx).

Overall, we identified 16 cluster-associated cases in 6 workplace employees, 3 school staff members and students, 2 fitness center attendees, and 5 household contacts. Symptom onset was generally earlier among workplace employees than among school and fitness center contacts (Figure 1).

The workplace employed 35 persons and provided in-person customer service. After the first

[1]Preliminary results from this study were presented at the 2021 Council of State and Territorial Epidemiologists Annual Conference; June 13–17, 2021; https://www.csteconference.org.

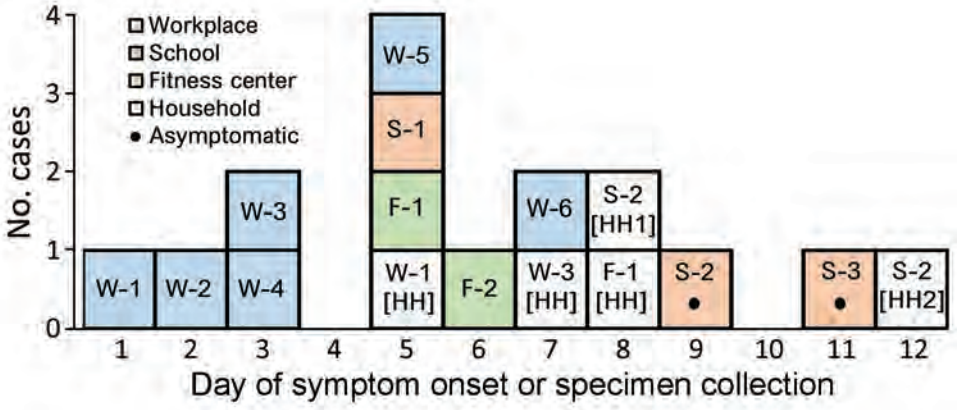

Figure 1. Epidemic curve for coronavirus disease cluster, Connecticut, USA, 2020. Symptomatic cases are plotted by day of symptom onset; asymptomatic cases are plotted by specimen collection day. Workplace employee W-3 had contacts in the school and fitness center. W, workplace; S, school; F, fitness center; [HH], household.

employee (W-1) experienced symptoms on day 1 and tested positive for SARS-CoV-2, the workplace closed and recommended SARS-CoV-2 screening for other employees. In addition to the 5 initial cases, we identified 1 other case in a workplace employee (Figure 1). All 6 employees worked during the week before their symptoms began (Appendix 1 Figure 1).

In total, 4 of the 6 employees agreed to be interviewed (Appendix 1 Table 1). W-1 reported a potential exposure outside the workplace during the week before symptom onset. Two employees (W-2 and W-5) had contact with each other outside of work. No other employees reported contact with coworkers or members of coworkers' households outside the workplace. Some employees were unable to maintain 6 feet of distance from coworkers and occasionally removed masks near coworkers. To increase air circulation, ventilation system fans were run continuously. Customers were not required to wear masks, and customer visits lasted 45–60 minutes.

One employee (W-3) also worked at an elementary school that offered in-person education 5 days a week. W-3 worked at the school on outbreak days 1–3; W-3's symptoms developed on day 3. Three school contacts of W-3 subsequently tested positive for SARS-CoV-2 infection: a staff member (S-1) and 2 students (S-2 and S-3). S-1, a staff member, spent most of their time in a neighboring classroom but had brief contact with W-3 while substituting for W-3's classroom. W-3 and S-1 reported strict adherence to prevention measures, including masking and social distancing, and did not have contact outside of school. To improve ventilation, the classroom windows were kept open. Among ≈15 students in W-3's classroom, 2 asymptomatic students (S-2 and S-3) tested positive for SARS-CoV-2. S-2 was tested after a family member (S-2 [HH1]) had COVID-19 symptoms; another family member (S-2 [HH2]) later experienced symptoms as well. S-3 was tested after being notified that another person in the classroom tested positive for SARS-CoV-2.

W-3 taught an indoor fitness class on day 2, the day before their symptom onset. Approximately 6 clients attended the 1-hour class. Attendee F-1 experienced symptoms on day 5; attendee F-2 experienced symptoms on day 7. A household contact of F-2 (F-2 [HH]) later tested positive for SARS-CoV-2. W-3 and F-1 reported that attendees wore masks before and after the class but removed them during distanced (i.e., >6 feet) exercise. Information regarding facility ventilation was unavailable.

We acquired 13 specimens for viral genome sequencing. Specimens were unavailable for 2 workplace employees (W-2 and W-5) and 1 student household contact (S-2 [HH2]). The resulting genomes clustered into 2 separate lineages (Appendix 1 Figure 2). Cluster 1 comprised 11 genomes, of which 9 were identical or differed by 1 mutation. These 9 genomes were extracted from samples from W-3, W-3's household contact, the school staff and students, the fitness center attendees, and household contacts of persons at the school and fitness center (Figure 2). The other 2 genomes in cluster 1 were isolated from W-1 and W-6. W-1 was the only employee to work during the infectious period (defined as beginning 2 days before symptom onset); however, sequences for W-3 and W-6 differed from W-1's sequence by ≥3 mutations. Cluster 2 comprised genomes isolated from a workplace employee and the household contact of another employee (Figure 2); there was no known epidemiologic link between these 2 persons.

Conclusions

We found that the 16 members of a single COVID-19 cluster were involved in multiple transmission chains.

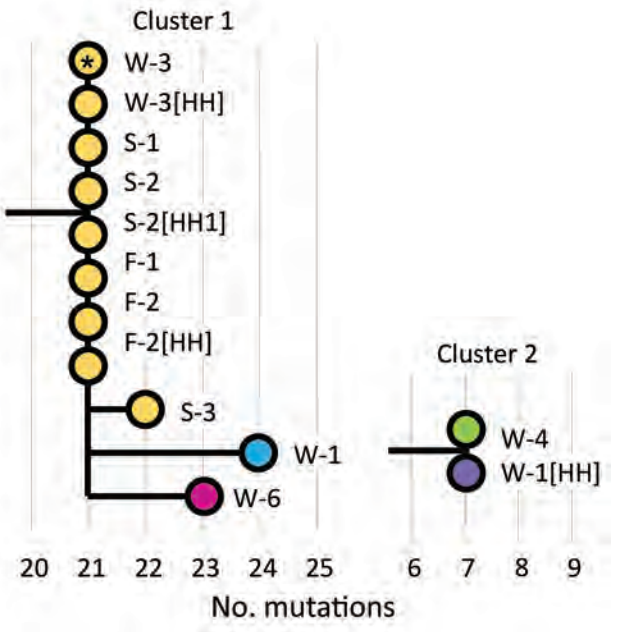

Figure 2. Maximum-likelihood phylogenetic tree for coronavirus disease cluster, Connecticut, USA, 2020. Wuhan/Hu-1/2019 (GISAID accession no. EPI_ISL_402125; https://www.gisaid.org) and Wuhan/WH01/2019 (accession no. EPI_ISL_406798) were used as reference genomes. Workplace employee W-3 (asterisk) had contacts in the school and fitness center. Colors correspond with presumed transmission chains based on epidemiologic and genomic data. W, workplace; S, school; F, fitness center; [HH], household.

Epidemiologic and genomic evidence supported transmission in the school and fitness center but not the workplace. These findings highlight challenges in accurate delineation of SARS-CoV-2 transmission chains and emphasize the benefits of combined epidemiologic and genomic investigation.

Although diagnostic specimens are often discarded by laboratories soon after testing, rapid identification of this cluster enabled the acquisition of specimens from 13 of the 16 cases. Our results suggest that infection was directly transmitted from W-3 to ≥6 other persons within their household, school, and fitness center. Classroom transmission of SARS-CoV-2 is uncommon in the context of prevention strategies such as masking and distancing; previous studies have suggested that most school-associated cases are acquired outside of school (*5*,*6*). However, our results suggest that staff-to-staff and staff-to-student transmission occurred in this classroom. This investigation also adds to evidence that indoor exercise without masks can facilitate SARS-CoV-2 transmission (*7*,*8*). Fitness centers might consider moving high-exertion exercise outdoors, improving ventilation, and promoting mask use during indoor exercise. Mask use during indoor exercise was mandated in Connecticut later in November 2020 (*9*).

Genomic data did not indicate SARS-CoV-2 transmission among workplace employees. Divergence among viral sequences of workplace employees and the SARS-CoV-2 evolutionary rate of ≈1 mutation per 2 weeks (*10*) suggest that the 4 other workplace cases were each acquired independently. However, workplace transmission from unidentified employees or customers remains possible. In addition, a workplace employee and household contact had unrelated sequences, suggesting that they also were infected independently (Figure 2). This apparent workplace cluster, disproven by sequencing, highlights challenges in defining transmission chains during widespread SARS-CoV-2 community transmission. These findings highlight the crucial role of genomic sequencing in clarifying transmission chains.

Acknowledgments

We thank Matthew L. Cartter, Kristine M. Bisgard, Trent Joseph, Zachary Faiella, and Matthew Payne for their helpful discussions.

T.A. was funded by Clinical and Translational Science Awards Program (grant no. TL1 TR001864) and N.D.G. was funded by the Fast Grant program from Emergent Ventures at the Mercatus Center at George Mason University. N.D.G. received consulting fees from Tempus Laboratories (https://www.tempus.com) related to infectious disease genomics.

About the Author

Dr. Bart is an Epidemic Intelligence Service Officer with the Center for Surveillance, Epidemiology, and Laboratory Services, Centers for Disease Control and Prevention, stationed at the Connecticut Department of Public Health, Hartford, Connecticut, USA. His interests include infectious disease epidemiology and virology.

References

1. Centers for Disease Control and Prevention. Operational strategy for K-12 schools through phased mitigation. 2021 [cited 2021 Feb 25]. https://www.cdc.gov/coronavirus/2019-ncov/community/schools-childcare/operation-strategy.html#indicators
2. Council of State and Territorial Epidemiologists. Update to the standardized surveillance case definition and national notification for 2019 novel coronavirus disease (COVID-19). 2020 [cited 2021 Jun 16]. https://cdn.ymaws.com/www.cste.org/resource/resmgr/ps/positionstatement2020/Interim-20-ID-02_COVID-19.pdf
3. Quick J, Grubaugh ND, Pullan ST, Claro IM, Smith AD, Gangavarapu K, et al. Multiplex PCR method for MinION and Illumina sequencing of Zika and other virus genomes

directly from clinical samples. Nat Protoc. 2017;12:1261–76. https://doi.org/10.1038/nprot.2017.066
4. Nguyen L-T, Schmidt HA, von Haeseler A, Minh BQ. IQ-TREE: a fast and effective stochastic algorithm for estimating maximum-likelihood phylogenies. Mol Biol Evol. 2015;32:268–74. https://doi.org/10.1093/molbev/msu300
5. Falk A, Benda A, Falk P, Steffen S, Wallace Z, Høeg TB. COVID-19 cases and transmission in 17 K-12 schools—Wood County, Wisconsin, August 31–November 29, 2020. MMWR Morb Mortal Wkly Rep. 2021;70:136–40. https://doi.org/10.15585/mmwr.mm7004e3
6. Zimmerman KO, Akinboyo IC, Brookhart MA, Boutzoukas AE, McGann KA, Smith MJ, et al.; ABC SCIENCE COLLABORATIVE. Incidence and secondary transmission of SARS-CoV-2 infections in schools. Pediatrics. 2021;147:e2020048090. https://doi.org/10.1542/peds.2020-048090
7. Jang S, Han SH, Rhee J-Y. Cluster of coronavirus disease associated with fitness dance classes, South Korea. Emerg Infect Dis. 2020;26:1917–20. https://doi.org/10.3201/eid2608.200633
8. Lendacki FR, Teran RA, Gretsch S, Fricchione MJ, Kerins JL. COVID-19 outbreak among attendees of an exercise facility—Chicago, Illinois, August–September 2020. MMWR Morb Mortal Wkly Rep. 2021;70:321–5. https://doi.org/10.15585/mmwr.mm7009e2
9. Reopen Connecticut. Sector rules for reopening. 2021 Feb 9 [cited 2021 Feb 25]. https://portal.ct.gov/-/media/DECD/Covid_Business_Recovery-Phase-2-1/CTReopens21_Sports_FitnessCentersFeb.pdf
10. Rambaut A. Phylogenetic analysis of nCoV-2019 genomes. 2020 [cited 2021 Feb 20]. https://virological.org/t/phylodynamic-analysis-176-genomes-6-mar-2020/356

Address for correspondence: Stephen M. Bart, Connecticut Department of Public Health, 410 Capitol Avenue, Hartford, CT 06134, USA; email: sbart@cdc.gov

Breakthrough Infections of SARS-CoV-2 Gamma Variant in Fully Vaccinated Gold Miners, French Guiana, 2021

Nicolas Vignier,[1] Vincent Bérot,[1] Nathalie Bonnave, Sandrine Peugny, Mathilde Ballet, Estelle Jacoud, Céline Michaud, Mélanie Gaillet, Félix Djossou, Denis Blanchet, Anne Lavergne, Magalie Demar, Mathieu Nacher, Dominique Rousset, Loïc Epelboin

An outbreak of severe acute respiratory syndrome coronavirus 2 caused by the Gamma variant of concern infected 24/44 (55%) employees of a gold mine in French Guiana (87% symptomatic, no severe forms). The attack rate was 60% (15/25) among fully vaccinated miners and 75% (3/4) among unvaccinated miners without a history of infection.

On May 31, 2021, a gold miner tested positive for severe acute respiratory syndrome coronavirus 2 (SARS-CoV-2) at the Cacao health center, French Guiana. He worked in a legal gold mine located 72 km from Cayenne (including 13 km of forest trail) in the Amazon Forest. Other workers from the same site were reported as symptomatic, although a large part of this specific population had benefited from complete coronavirus disease (COVID-19) vaccination in the previous month. A medical team went on site to investigate, examine, and screen the 44 employees of the mine. We describe results of the outbreak investigation.

The Study

We collected data by completing standardized forms with data gathered through interviews and medical examination of all gold miners and by reviewing the health center records. All employees of the mine were examined by a physician and screened by nasopharyngeal Panbio COVID-19 Ag Rapid Test device (Abbott Laboratories, https://www.abbott.com) if they were symptomatic; all miners underwent SARS-CoV-2 PCR EurobioPlex SARS-CoV-2 Multiplex (Eurobio Scientific, https://www.eurobio-scientific.com) testing on June 2, 2021. All employees were reassessed on June 8 and 15, 2021; those with negative results were rescreened by PCR. We performed serologic tests on blood specimens collected from 39 gold miners whether PCR was negative or positive. Serum samples were initially tested with anti–SARS-CoV-2 ELISA IgG (Euroimmun, https://www.euroimmun.com). We used descriptive statistics to analyze the variables and performed univariate analyses. Intervention was a public health response as part of activities of Cayenne Hospital. All gold miners gave their verbal informed consent for recording and processing of information during interviews and for the use of their biologic results for research purposes, and physicians completed a nonobjection form in accordance with laws of France.

Mine workers were mostly men (42/44); median age was 53.3 years. Eighteen of the workers had risk factors for severe COVID-19: high blood pressure (11/44), diabetes mellitus (4/44), or obesity (4/44). Miners lived onsite in separate rooms but shared face-to-face meals and machine cabins. They also worked outside without masks. Twenty-one workers reported contacts outside the mining site during the previous 2 weeks.

The first symptomatic cases occurred on May 29 among 3 machine operators and 1 miner. Their antigen tests and PCR results were positive on June 2. The

Author affiliations: Institut Pierre Louis d'Épidémiologie et de Santé Publique Inserm UMR1136, Paris, France (N. Vignier); Université Sorbonne Paris Nord, Bobigny, France (N. Vignier); Centre Hospitalier de Cayenne, Cayenne, French Guiana (N. Vignier, V. Bérot, N. Bonnave, S. Peugny, E. Jacoud, C. Michaud, M. Gaillet, F. Djossou, D. Blanchet, M. Demar, M. Nacher, L. Epelboin); Centre d'Investigation Clinique Antilles Guyane Inserm 1424, Cayenne (N. Vignier, M. Nacher, L. Epelboin); Centre Hospitalier Ouest Guyanais, Saint Laurent du Maroni, French Guiana (V. Bérot); Agence Régionale de la Santé de Guyane, Cayenne (M. Ballet); Institut Pasteur de la Guyane, Cayenne (A. Lavergne, D. Rousset)

DOI: https://doi.org/10.3201/eid2710.211427

[1]These first authors contributed equally to this article.

peak of the outbreak occurred 2 days after the early cases, on May 31 (Figure). Five asymptomatic miners who tested negative moved to a separate open housing for quarantine. Among them, 4 became symptomatic during June 6–8 and tested positive on June 8.

The overall attack rate was 54.5% (24/44); 87% were symptomatic, 65% with fever, and 22.6% with dyspnea. No clinically severe COVID-19 (*1*) was observed, and no patient was hospitalized. Among infected miners, 18/23 (78.2%) had a cycle threshold (C_t) <28 (Appendix Table 1, https://wwwnc.cdc.gov/EID/article/27/10/21-1427-App1.pdf). The variant of concern (VOC) gamma (P.1 lineage), also known as 20J/501Y.V3, was identified in 9/9 viruses sequenced by the Pasteur Institute (Appendix Table 2), without any new mutation. Of the 4 persons who tested negative and were not vaccinated, 3 had a positive SARS-CoV-2 IgG. Patient 40 could be the index case-patient; he reported visiting his family the previous week and had an asymptomatic SARS-CoV-2 infection with C_t of 33–35.

Regarding immune status, 25/44 (56.8%) were fully vaccinated with BNT162b2 vaccine (Pfizer-BioNTech, https://www.pfizer.com); 3/6 workers who had a history of COVID-19 were vaccinated with a single injection, according to the guidelines of France (*2*) (Table). Several BNT162b2 batch numbers were involved. Vaccine temperature had been monitored and electronically recorded by LogTag Analyzer (LogTag Recorders, http://www.logtag-recorders.com) without any break in the cold chain. The attack rate was 15/25 (60.0%) in fully vaccinated miners, 6/15 (40.0%) in those partially vaccinated or with a history of COVID-19, and 3/4 (75%) in those not vaccinated. Attack rate was 0/6 among persons with a previous history of COVID-19 versus 63.2% among those with no previous history (Table). No other factors were found to be associated with the risk for infection.

Among the mine workers were recorded 14/28 vaccine clinical failures (COVID-19 onset >14 days after the second dose, or after a single dose for patients with history of COVID-19); none had serious infections. Twelve (42.3%) of the 28 fully vaccinated reported vaccine reactogenicity. Among the fully vaccinated, the SARS-CoV-2 IgG ratio was high for most (mean 9.22, SD 1.5). We performed serologic testing a median of 4 (interquartile range [IQR] 2–5.5) days after the onset of symptoms in symptomatic patients and 58 (IQR 46–62) days after vaccination.

mRNA vaccines such as BNT162b2 demonstrated high effectiveness both in clinical trials and in real-world situations against wild-type SARS-CoV-2 and its Alpha variant infections (*3*,*4*). However, other VOC, such as Beta or Gamma, harbor mutations conferring potential escape from humoral response induced either by prior infection or vaccination, as proven by both decreased seroneutralization in vitro (*5*–*7*) and in vivo by observational studies in the case of the Beta variant (*8*,*9*). However, such breakthrough infections, even those caused by Beta variant, remain rare in fully vaccinated populations and are mostly asymptomatic or moderately symptomatic (*8*–*10*).

Conclusions

We describe a COVID-19 Gamma variant cluster with a high attack rate even in fully vaccinated persons. The Gamma variant is the predominant variant in French Guiana which, as of July 2021, caused a third epidemic wave, threatening to overwhelm the hospital capacity (*11*). Such a low vaccine efficiency against infection by the Gamma variant was not expected because in vitro studies have shown a similar reduction of neutralization for Beta or Gamma variants by BNT162b2-elicited antibodies (*5*) and a conserved CD4+ T-cell response against spike proteins

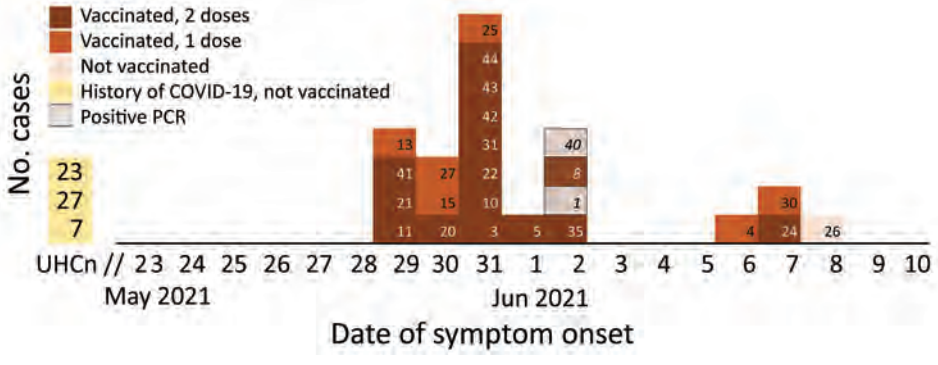

Figure. Epidemic curve for symptomatic and asymptomatic COVID-19 case-patients, by date of symptom onset or date of PCR, during an outbreak in gold-mine workers in French Guiana, May 29–June 8, 2021. Of the case-patients with undated history of COVID-19, case-patient 7 had a high level of severe acute respiratory syndrome coronavirus 2 (SARS-CoV-2) antibodies, probably from an old infection. Case-patients 23 and 26 had low levels of antibodies, indicating either recent or very old infection. Case-patient 40 was positive by PCR with cycle threshold = 33 on June 2 and had a high level of SARS-CoV-2 antibodies, indicating possible semi-recent infection dating back a few days or weeks. COVID-19, coronavirus disease; UHCn, undated history of COVID-19 (positive serology) with negative PCR, not vaccinated.

from the Beta variant (*6*). Of the 10,262 COVID-19 vaccine breakthrough infections identified in the United States during January–April 2021, for which 555 had available sequencing, only 28 were caused by the Gamma variant (*12*). Furthermore, real-world effectiveness against any infection by a Beta variant, which shares a similar E484K mutation on the gene coding for the spike protein, was estimated at 75.0% (*9*). Given the surprisingly high attack rate, we hypothesized potential dysfunctions of conservation or administration of vaccines, but the absence of traceable cold-chain interruption and the use of different batches seemed to refute this hypothesis. The relative isolation of the mining site and careful contact tracing suggested limited numbers of viral introductions inside this community. The low C_t of positive PCR for SARS-CoV-2 despite prior vaccination suggested that a complete vaccination scheme with BNT162b2 vaccine was not sufficient to prevent symptomatic SARS-CoV-2 infection and its transmission in this context of communal life without masks. The working conditions of some miners (heat, humidity, aerosol) and the sharing of machine cabs for others could also have contributed to transmission. The absence of severe COVID-19 in a high-risk population (*13*) suggests but does not prove protection against severe disease, as reported for the Beta variant in another context (*14*).

In conclusion, we describe a VOC Gamma COVID-19 outbreak with a strikingly high attack rate among persons fully vaccinated with BNT162b2 vaccine. Our observation suggested that BNT162b2 protected from severe COVID-19. However, this single

Table. Characteristics of gold miners by active SARS-CoV-2 infection status, Cacao, French Guiana, May–June 2021*

Characteristic	Total, no. (%)	Acute SARS-CoV-2 infection			
		No	Yes	Total %	p value
All participants	44	20	24	54.6	
Mean age	44	51.9	54.5		0.88
Immune status					
Fully vaccinated, 2 doses	25 (56.8)	10	15	60.0	0.20
Vaccinated, 1 dose	9 (20.5)	3	6	66.7	
History of COVID-19, vaccinated 1 dose	3 (6.8)	3	0	0.00	
History of COVID-19, not vaccinated	3 (6.8)	3	0	0.00	
Neither vaccinated nor history	4 (9.1)	1	3	75.0	
History of previous COVID-19					
Y	6 (8.9)	6	0	0.00	0.004
N	38 (86.4)	14	24	63.2	
Sex					
M	42 (95.4)	18	24	57.1	0,11
F	2 (4.5)	2	0	0.0	
Age, y					
<55	24 (54.5)	11	12	52.2	0.74
≥55	20 (45.4)	9	12	57.1	
Country of birth					
Brazil	34 (77.3)	16	18	52.9	
Surinam	6 (13.6)	2	4	66.7	
Haiti	2 (4.5)	1	1		
Guyana	1 (2.3)	0	1		
France	1 (2.3)	1	0		
Occupation					
Laborer	20 (45.4)	8	12	60.0	0.73
Operator	17 (38.6)	8	9	52.9	
Other	7 (15.9)	4	3	42.9	
Eat alone					
Y	7 (15.9)	5	2	28.6	0.13
N	37 (84.1)	15	22	59.5	
Live alone					
Y	28 (63.6)	15	13	46.4	0.13
N	16 (36.4)	5	11	68.8	
Contact outside the mine in the previous 2 weeks					
Y	26 (60.5)	10	16	61.5	0.35
N	17 (39.5)	9	8	47.1	
Underlying conditions					
Hypertension	11 (25.0)	5	6	54.6	1.00
Diabetes	4 (9.1)	2	2	50.0	0.85
Obesity	4 (9.1)	2	2	50,0	0.85
Cardiac insufficiency	3 (8.3)	1	2	66.7	0.62

*We defined acute SARS-CoV-2 infection in participants as having a positive SARS-CoV-2 antigenic or PCR test in June 2021, symptomatic or not. Of the 24 with acute infection, 21 were symptomatic and 3 asymptomatic infections. p value indicates degree of significance. COVID-19, coronavirus disease; SARS-CoV-2, severe acute respiratory syndrome coronavirus 2.

unexpected outbreak in a small and isolated vaccinated population requires further real-life studies on BNT162b2 vaccine effectiveness against the VOC Gamma. Masking and social distancing, even among those fully vaccinated, may be necessary among persons with frequent exposure in Gamma variant–endemic zones.

Acknowledgments

We acknowledge the contribution of Julien Tedi, Flore Lapauw, and Laura Verger; the Regional Health Agency of French Guiana (Agence régionale de la Santé de Guyane); the Public Health Agency in French Guiana (Santé Publique France Guyane); the logistics of the delocalized prevention and care centers (CDPS); Sébastien Teissier and his team; the CDPS team of Cacao and Regina, especially Malika Miguel and Solenn Ferelloc; the coordinators of CDPS; the directors of Cayenne Hospital; the laboratory team of Cayenne Hospital; and the Pasteur Institute of French Guiana. Moreover, we thank the mine manager and all his employees for their help in the investigation of this cluster.

About the Authors

Dr. Vignier is a public health and infectious disease physician in the Department of Research, Innovation and Public Health (Centre Investigation Clinique Antilles Guyane) and Infectious Disease Department of the Cayenne Hospital in French Guiana. His primary research interests include tropical medicine, migrant health, and social epidemiology. Dr. Bérot is a dermatology and infectious disease physician in the Infectious Disease Department of the Ouest Guyanais Hospital in French Guiana. His primary research interests include tropical disease and skin infections.

References

1. National Institutes of Health COVID-19 Treatment Guidelines Panel. Coronavirus disease 2019 (COVID-19) treatment guidelines. 2021 [cited 2021 Jun 18]. https://www.covid19treatmentguidelines.nih.gov
2. Haute Autorité de Santé. Vaccination strategy against SARS-CoV-2: vaccination of people with a history of Covid-19 [in French]. 2021 Feb 11 [cited 2021 Jun 28]. https://www.has-sante.fr/upload/docs/application/pdf/2021-02/strategie_de_vaccination_contre_le_sars-cov-2___vaccination_des_personnes_ayant_un_antecedent_de_covid-19_-_synthese.pdf
3. Polack FP, Thomas SJ, Kitchin N, Absalon J, Gurtman A, Lockhart S, et al.; C4591001 Clinical Trial Group. Safety and efficacy of the BNT162b2 mRNA COVID-19 vaccine. N Engl J Med. 2020;383:2603–15. https://doi.org/10.1056/NEJMoa2034577
4. Haas EJ, Angulo FJ, McLaughlin JM, Anis E, Singer SR, Khan F, et al. Impact and effectiveness of mRNA BNT162b2 vaccine against SARS-CoV-2 infections and COVID-19 cases, hospitalizations, and deaths following a nationwide vaccination campaign in Israel: an observational study using national surveillance data. Lancet. 2021;397:1819–29. https://doi.org/10.1016/S0140-6736(21)00947-8
5. Hoffmann M, Arora P, Groß R, Seidel A, Hörnich BF, Hahn AS, et al. SARS-CoV-2 variants B.1.351 and P.1 escape from neutralizing antibodies. Cell. 2021;184:2384–2393.e12. https://doi.org/10.1016/j.cell.2021.03.036
6. Geers D, Shamier MC, Bogers S, den Hartog G, Gommers L, Nieuwkoop NN, et al. SARS-CoV-2 variants of concern partially escape humoral but not T-cell responses in COVID-19 convalescent donors and vaccinees. Sci Immunol. 2021 May 25;6:eabj1750.
7. Liu Y, Liu J, Xia H, Zhang X, Fontes-Garfias CR, Swanson KA, et al. Neutralizing activity of BNT162b2-elicited serum. N Engl J Med. 2021;384:1466–8. https://doi.org/10.1056/NEJMc2102017
8. Kustin T, Harel N, Finkel U, Perchik S, Harari S, Tahor M, et al. Evidence for increased breakthrough rates of SARS-CoV-2 variants of concern in BNT162b2-mRNA-vaccinated individuals. Nat Med. 2021 Jun 14 [Epub ahead of print.]
9. Abu-Raddad LJ, Chemaitelly H, Butt AA; National Study Group for COVID-19 Vaccination. Effectiveness of the BNT162b2 COVID-19 vaccine against the B.1.1.7 and B.1.351 variants. N Engl J Med. 2021 May 5 [Epub ahead of print]. https://doi.org/10.1056/NEJMc2104974
10. Swift MD, Breeher LE, Tande AJ, Tommaso CP, Hainy CM, Chu H, et al. Effectiveness of mRNA COVID-19 vaccines against SARS-CoV-2 infection in a cohort of healthcare personnel. Clin Infect Dis 2021 Apr 26 [Epub ahead of print.] https://doi.org/10.1093/cid/ciab361
11. Santé Publique France. Regional epidemiological point: special COVID-19 [in French]. 2021 Jun 17 [cited 2021 Jun 18]. https://www.guyane.ars.sante.fr/system/files/2021-06/Num63_Guyane_PER_COVID19_20210617.pdf
12. CDC COVID-19 Vaccine Breakthrough Case Investigations Team. COVID-19 vaccine breakthrough infections reported to CDC—United States, January 1–April 30, 2021. MMWR Morb Mortal Wkly Rep. 2021;70:792–3.
13. Gao YD, Ding M, Dong X, Zhang JJ, Kursat Azkur A, Azkur D, et al. Risk factors for severe and critically ill COVID-19 patients: a review. Allergy. 2021;76:428–55. https://doi.org/10.1111/all.14657
14. Bailly B, Guilpain L, Bouiller K, Chirouze C, N'Debi M, Soulier A, et al. BNT162b2 mRNA vaccination did not prevent an outbreak of SARS COV-2 variant 501Y.V2 in an elderly nursing home but reduced transmission and disease severity. Clin Infect Dis. 2021 2021 May 16 [Epub ahead of print]. https://doi.org/10.1093/cid/ciab446

Address for correspondence: Nicolas Vignier, Centre d'Investigation Clinique Antilles Guyane Inserm 1424, Centre hospitalier de Cayenne, Av. des flamboyants, BP 6006, 97306 Cayenne CEDEX, French Guiana; email: dr.vignier@gmail.com

Seoul Virus Associated with Pet Rats, Scotland, UK, 2019

James G. Shepherd, Andrew E. Blunsum, Stephen Carmichael, Katherine Smollett, Hector Maxwell-Scott, Eoghan C.W. Farmer, Jane Osborne, Alasdair MacLean, Shirin Ashraf, Rajiv Shah, Rory Gunson, Ana da Silva Filipe, Emma J. Aarons, Emma C. Thomson

We describe a case of hemorrhagic fever with renal syndrome caused by Seoul virus in a woman in Scotland, UK. Whole-genome sequencing showed the virus belonged to a lineage characterized by recent international expansion, probably driven by trade in pet rats.

Hantaviruses (genus *Orthohantavirus*, family *Hantaviridae*) are segmented, single-stranded RNA viruses maintained by chronic subclinical infection of rodent and insectivore hosts. Human infection occurs after exposure to the saliva, urine, or feces of infected animals. The infecting viral species determines syndromic manifestation in humans. Hantaviruses endemic to the Americas, such as Sin Nombre virus and Andes virus, cause hantavirus pulmonary syndrome, whereas Old World hantaviruses, mainly Hantaan virus, Dobrava virus, and Seoul virus (SEOV), cause hemorrhagic fever with renal syndrome (HFRS). We identified and treated HFRS in a woman in Scotland, UK.

The Study

In 2019, a woman 51 years of age sought treatment at Queen Elizabeth University Hospital (Glasgow, Scotland, UK) for fever, diarrhea, vomiting, and malaise that had developed 5 days earlier. A teacher in Glasgow, she lived with her husband and 3 teenage children. Her 12-year-old daughter had experienced a febrile illness associated with myalgia the previous week but recovered without seeking medical attention. There was no notable travel history.

Author affiliations: MRC–University of Glasgow Centre for Virus Research, Glasgow, Scotland, UK (J.G. Shepherd, S. Carmichael, K. Smollett, S. Ashraf, R. Shah, A. da Silva Filipe, E.C. Thomson); National Health Service Greater Glasgow and Clyde, Glasgow (A.E. Blunsum, E.C.W. Farmer); Public Health England, London, UK (H. Maxwell-Scott, J. Osborne, E.J. Aarons); West of Scotland Specialist Virology Centre, Glasgow (A. MacLean, R. Gunson); London School of Hygiene and Tropical Medicine, London (E.C. Thomson)

DOI: https://doi.org/10.3201/eid2710.211298

The patient had bred fancy rats (*Rattus norvegicus domestica*) for the previous 2 years. She owned 37 rats, which were housed in cages in her bedroom. Three months before, she had acquired 4 stud rats from a local breeder. She had overseen several recent litters; 27 of her rats were newborn or juvenile. The patient and her 12-year-old daughter cared for the rats, whereas her husband and other children had little contact with the animals.

At admission, the patient had conjunctival suffusion, pallor, and temperature of 38.9°C. We found evidence of mild perioral bleeding. She had a blood pressure of 91/66 mm Hg and a heart rate of 125 bpm.

Blood tests revealed mild lymphopenia, hemoglobin levels within reference levels, and a platelet count of 70 $\times 10^9$/L (reference range 150–410 × 10^9/L) (Table 1). Her serum creatinine was 87 mmol/L (reference range 40–130 mmol/L). She had transaminitis, but her bilirubin and coagulation results were within reference ranges. She had elevated levels of C-reactive protein (58 mg/L [reference range 1–10 mg/L]). Urine dipstick showed microhematuria and proteinuria. An abdominal ultrasound showed no abnormalities. She had negative serologic results for viral hepatitis and HIV.

Our differential diagnosis included leptospirosis, rat-bite fever, and hantavirus infection. We prescribed oral doxycycline and intravenous benzylpenicillin. Her hemodynamic condition stabilized with intravenous fluids during the next 48 hours. However, oliguria and acute kidney injury developed; creatinine levels peaked at 182 mmol/L. Polyuria also developed, and she required intravenous fluid therapy before her renal function began to recover.

Blood and urine cultures yielded no growth. Samples sent to the Rare and Imported Pathogens Laboratory (Porton Down, UK) tested negative for *Leptospira* by enzyme immunoassay and PCR but positive for hantavirus IgG by serologic assay (Table 2). Reverse transcription PCR found hantavirus RNA in patient

Table 1. Hematologic and biochemical markers in patient with Seoul virus infection, Scotland, UK, 2019*

Parameter (reference range)	Day 1	Day 2	Day 4	Day 6	Day 8	Day 12	Day 29
Hemoglobin (115–165 × 10^9/L)	136	144	114	133	112	122	128
Platelets (150–410 × 10^9/L)	70	38	46	111	180	244	257
Neutrophils (2.0–7.0 × 10^9 cells/L)	2.3	2.4	2.1	3.6	3.2	3.2	3.5
Lymphocytes (1.1–5.0 × 10^9 cells/L)	0.7	1.2	1.4	4	2.4	2.5	3
Sodium (133–146 mmol/L)	131	133	143	144	145	142	141
Urea (2.5–7.8 mmol/L)	6.4	6.4	7.4	9.1	9.6	7.4	5.2
Creatinine (40–130 mmol/L)	87	92	158	182	134	97	83
Estimated glomerular filtration rate (>60 mL/min)	>60	56	30	25	36	53	>60
Alanine aminotransferase (<50 U/L)	NA	282	101	108	71	70	17
Aspartate aminotransferase (<40 U/L)	NA	341	73	84	41	35	18
Albumin (35–50 g/L)	NA	35	24	27	26	32	38
C-reactive protein (1–10 mg/L)	58	104	50	30	14	3	NA

*NA, not available.

blood samples. Genomic sequencing matched SEOV small segments in GenBank.

The patient's condition improved with supportive therapy, and she was discharged after a 12-day inpatient stay. A public health team inspected her property and recommended that the rats be euthanized, to which she agreed. However, the breeder who supplied the animals removed the rats from the property and refused to cooperate further.

At a clinic appointment 28 days after seeking treatment, the patient had no symptoms. Renal function, liver enzymes, and platelets had normalized, and proteinuria had resolved. Serologic assays demonstrated an increase in IgG titer against Old World hantaviruses (Table 2). We determined the genomic sequences of SEOV small, medium, and large segments by metagenomic sequencing of a stored blood sample from time of admission.

Conclusions

HFRS is characterized by fever, renal impairment, and thrombocytopenia. HFRS, especially cases associated with Hantaan virus, is responsible for many deaths in Southeast Asia (*1*), whereas HFRS associated with SEOV causes relatively mild disease with a case-fatality rate of <1% (*2*). SEOV cases often begin with fever, malaise, and gastrointestinal symptoms before progressing to shock and acute kidney injury of varying severity (*3*,*4*). Associated transaminitis is suggestive of HFRS caused by SEOV (*2*), as illustrated in this case. Most infections are probably subclinical or mild, as demonstrated by this patient's daughter, who had experienced mild symptoms suggestive of SEOV infection. However, we were unable to obtain a sample for serologic confirmation.

SEOV is widely distributed because of the ubiquity of its principal host, the *R. norvegicus* rat (*5*). In the United Kingdom, where the virus is established in wild rodents, cases of human disease have been associated with occupational exposure in agricultural workers (*6*,*7*). However, growing evidence exists of SEOV circulation among pet rats. The United Kingdom has a network of pet rat owners who trade rats for breeding. In 2013, SEOV was isolated from pet rats in a breeding colony linked to cases of human infection in the United Kingdom (*4*,*8*). Later, human cases of SEOV associated with ratteries were reported in France (*9*) and the Netherlands (*10*). In 2017, a large SEOV outbreak among pet rat owners was linked to in-home ratteries in the United States and Canada (*11*). We used RAxML (https://github.com/stamatak/standard-RAxML) to conduct a phylogenetic analysis of SEOV sequences derived from rats associated with these outbreaks (*4*,*8*,*9*,*10*,*11*) in addition to the virus sequence from the patient described in this report; these isolates formed a well-supported monophyletic clade (Figure). This clade is distinct from SEOV sequences recovered from wild rodents in Europe and the Americas, suggesting a single introduction and international expansion of this lineage into domesticated rat populations, rather than separate local introductions from wild rats. A

Table 2. IgG against hantaviruses in patient with Seoul virus infection, Scotland, United Kingdom, 2019

Virus	IgG titer	
	Day 0 (admission)	Day 29 (convalescent)
Dobrava virus	Negative	>1:10,000
Hantaan virus	>1:10,000	>1:10,000
Puumala virus	Negative	>1:10,000
Saaremaa virus	1:1,000	>1:10,000
Seoul virus	1:3,200	>1:10,000
Sin Nombre virus	Negative	Negative

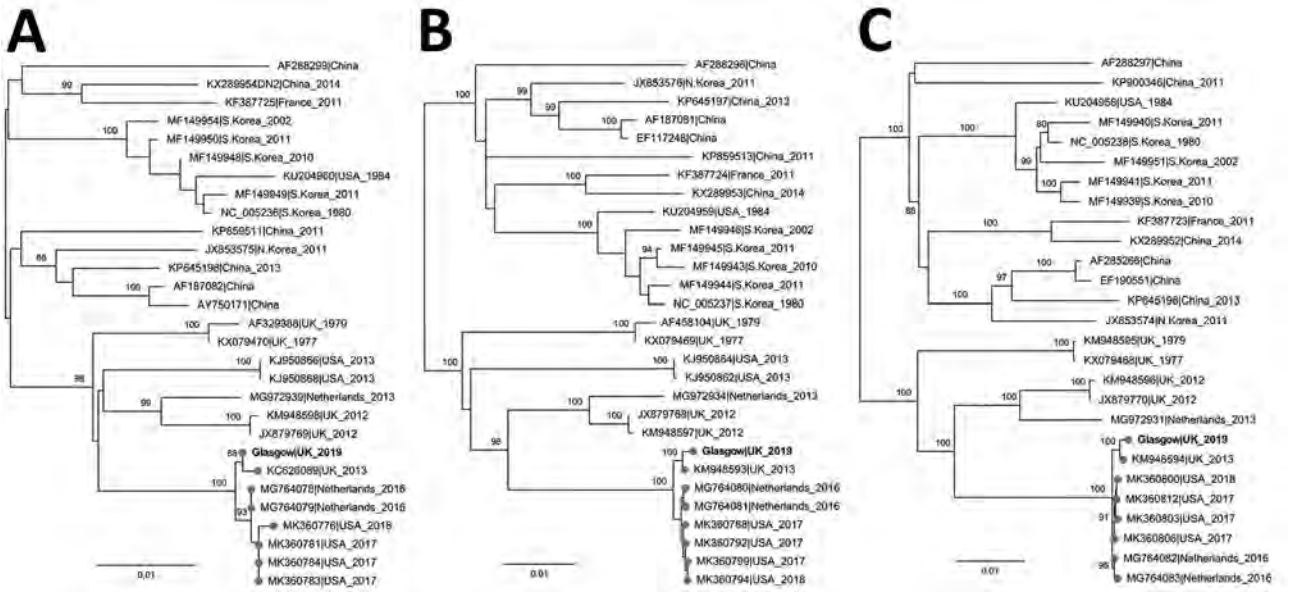

Figure. Maximum-likelihood phylogenetic tree based on the small (A), medium (B), and large (C) segments of Seoul virus isolated from a patient in Scotland, United Kingdom, 2020 (bold text; GenBank accession nos. MZ343375–7), and reference sequences. Isolate names indicate GenBank accession number as well as location and date of isolate. Phylogenetic relationships inferred by RAxML (https://github.com/stamatak/standard-RAxML) using the general time-reversible plus gamma distribution plus invariable site model as determined by jModeltest (https://github.com/ddarriba/jmodeltest2). The tree was rooted at midpoint. Numbers to the left of nodes indicate bootstrap values based on 1,000 replicates. Gray circles indicate sequences associated with domesticated rats. Scale bar indicates substitutions per site.

recent study from the Netherlands revealed evidence of international trading of rats by breeding farms and private persons, a practice that might promote cross-border dispersal of this lineage (*12*).

The risk for SEOV transmission from domesticated rats might be greater than that posed by wild rodents. A seroprevalence study performed in 2014 revealed that 34.1% of owners of fancy rat in the United Kingdom had antibodies against SEOV, compared with 3.3% of healthy blood donors and 1.7% of farmers (*13*). These findings might reflect the behaviors of fancy rat owners, who often view their pets as valued companion animals. In our study, the patient and her daughter reported kissing the rats and housing them in bedrooms. Owners might not follow public health advice on preventive measures such as avoiding kissing or holding small mammals near the face and keeping rodents out of sleeping and eating areas; public health messaging should be tailored to address the specific health beliefs of this community (*14*). Although the patient in this study agreed to the proposed euthanasia of her rats, the breeder preemptively removed them from the property and refused to cooperate further, mirroring the behavior of breeders in other outbreaks (*10*,*15*). This pattern suggests breeders' rejection of SEOV as a major pathogen (*10*,*15*). A holistic response to future outbreaks might prevent similar situations. For example, an outbreak in the United States was effectively controlled by a mixture of methods including euthanasia, intensive owner education, and test and quarantine approaches that enabled the protection of uninfected rats (*11*).

In summary, we report the persistence of a SEOV lineage associated with pet rats in the United Kingdom, highlighting the ongoing risk for HFRS among pet rat owners. This lineage has undergone recent international dissemination, probably driven by trade of pet rats. Engagement and education within the community of owners and breeders will be crucial to limiting further SEOV infections transmitted from pet rats. Physicians should consider SEOV in any febrile patient with a recent history of rat exposure.

J.G.S., S.C., K.S., S.A., R.S., A.S.F., and E.C.T. are supported by the Medical Research Council (grant no. MC_UU_1201412).

About the Author

Dr. Shepherd is a clinical research fellow at the University of Glasgow, Glasgow, Scotland, UK. His research interests include the use of next-generation sequencing for the detection of novel and emerging viruses.

References

1. Clement J, LeDuc JW, Lloyd G, Reynes JM, McElhinney L, Van Ranst M, et al. Wild rats, laboratory rats, pet rats: global Seoul hantavirus disease revisited. Viruses. 2019;11:652. https://doi.org/10.3390/v11070652
2. Clement J, LeDuc JW, McElhinney LM, Reynes JM, Van Ranst M, Calisher CH. Clinical characteristics of ratborne Seoul hantavirus disease. Emerg Infect Dis. 2019;25:387–8. https://doi.org/10.3201/eid2502.181643
3. Woods C, Palekar R, Kim P, Blythe D, de Senarclens O, Feldman K, et al. Domestically acquired Seoul virus causing hemorrhagic fever with renal syndrome—Maryland, 2008. Clin Infect Dis. 2009;49:e109–12. https://doi.org/10.1086/644742
4. Taori SK, Jameson LJ, Campbell A, Drew PJ, McCarthy ND, Hart J, et al. UK hantavirus, renal failure, and pet rats. Lancet. 2013;381:1070. https://doi.org/10.1016/S0140-6736(13)60599-1
5. Lin XD, Guo WP, Wang W, Zou Y, Hao ZY, Zhou DJ, et al. Migration of Norway rats resulted in the worldwide distribution of Seoul hantavirus today. J Virol. 2012;86:972–81. https://doi.org/10.1128/JVI.00725-11
6. McKenna P, Clement J, Matthys P, Coyle PV, McCaughey C. Serological evidence of hantavirus disease in Northern Ireland. J Med Virol. 1994;43:33–8. https://doi.org/10.1002/jmv.1890430107
7. Jameson LJ, Logue CH, Atkinson B, Baker N, Galbraith SE, Carroll MW, et al. The continued emergence of hantaviruses: isolation of a Seoul virus implicated in human disease, United Kingdom, October 2012. Euro Surveill. 2013;18:4–7. https://doi.org/10.2807/ese.18.01.20344-en
8. McElhinney LM, Marston DA, Pounder KC, Goharriz H, Wise EL, Verner-Carlsson J, et al. High prevalence of Seoul hantavirus in a breeding colony of pet rats. Epidemiol Infect. 2017;145:3115–24. https://doi.org/10.1017/S0950268817001819
9. Reynes J-M, Carli D, Bour J-B, Boudjeltia S, Dewilde A, Gerbier G, et al. Seoul virus infection in humans, France, 2014–2016. Emerg Infect Dis. 2017;23:973–7. https://doi.org/10.3201/eid2306.160927
10. Swanink C, Reimerink J, Gisolf J, de Vries A, Claassen M, Martens L, et al. Autochthonous human case of Seoul virus infection, the Netherlands. Emerg Infect Dis. 2018;24:2158–63. https://doi.org/10.3201/eid2412.180229
11. Knust B, Brown S, de St Maurice A, Whitmer S, Koske SE, Ervin E, et al.; Multistate Seoul Virus Outbreak Investigation Team. Seoul virus infection and spread in United States home-based ratteries: rat and human testing results from a multistate outbreak investigation. J Infect Dis. 2020;222:1311–9. https://doi.org/10.1093/infdis/jiaa307
12. Cuperus T, de Vries A, Hoornweg TE, Fonville M, Jaarsma RI, Opsteegh M, et al. Seoul virus in pet and feeder rats in the Netherlands. Viruses. 2021;13:443. https://doi.org/10.3390/v13030443
13. Duggan JM, Close R, McCann L, Wright D, Keys M, McCarthy N, et al. A seroprevalence study to determine the frequency of hantavirus infection in people exposed to wild and pet fancy rats in England. Epidemiol Infect. 2017;145:2458–65. https://doi.org/10.1017/S0950268817001480
14. Robin C, Perkins E, Watkins F, Christley R. Pets, purity and pollution: why conventional models of disease transmission do not work for pet rat owners. Int J Environ Res Public Health. 2017;14:1526. https://doi.org/10.3390/ijerph14121526
15. Fill M-MA, Mullins H, May AS, Henderson H, Brown SM, Chiang C-F, et al. Notes from the field: multiple cases of Seoul virus infection in a household with infected pet rats—Tennessee, December 2016–April 2017. MMWR Morb Mortal Wkly Rep. 2017;66:1081–2. https://doi.org/10.15585/mmwr.mm6640a4

Address for correspondence: Emma Thomson, University of Glasgow Centre for Virus Research, Stoker Bldg Rm 302, 464 Bearsden Rd, Glasgow, Scotland G61 1QH, UK; email: emma.thomson@glasgow.ac.uk

Relapsing Fever Infection Manifesting as Aseptic Meningitis, Texas, USA

Lisa Ellis, Michael W. Curtis, Sarah M. Gunter, Job E. Lopez

Medscape EDUCATION ACTIVITY

In support of improving patient care, this activity has been planned and implemented by Medscape, LLC and Emerging Infectious Diseases. Medscape, LLC is jointly accredited by the Accreditation Council for Continuing Medical Education (ACCME), the Accreditation Council for Pharmacy Education (ACPE), and the American Nurses Credentialing Center (ANCC), to provide continuing education for the healthcare team.

Medscape, LLC designates this Journal-based CME activity for a maximum of 1.00 ***AMA PRA Category 1 Credit(s)™***. Physicians should claim only the credit commensurate with the extent of their participation in the activity.

Successful completion of this CME activity, which includes participation in the evaluation component, enables the participant to earn up to 1.0 MOC points in the American Board of Internal Medicine's (ABIM) Maintenance of Certification (MOC) program. Participants will earn MOC points equivalent to the amount of CME credits claimed for the activity. It is the CME activity provider's responsibility to submit participant completion information to ACCME for the purpose of granting ABIM MOC credit.

All other clinicians completing this activity will be issued a certificate of participation. To participate in this journal CME activity: (1) review the learning objectives and author disclosures; (2) study the education content; (3) take the post-test with a 75% minimum passing score and complete the evaluation at http://www.medscape.org/journal/eid; and (4) view/print certificate. For CME questions, see page 2751.

Release date: September 20, 2021; Expiration date: September 20, 2022

Learning Objectives

Upon completion of this activity, participants will be able to:

- Describe clinical presentation and course in a case of neuroborreliosis in Austin, Texas, that was initially thought to be Lyme disease (LD)
- Determine retrospective serological analysis and other laboratory findings in a case of neuroborreliosis in Austin, Texas, that was initially thought to be LD
- Identify clinical and public health implications of findings in this case of neuroborreliosis in Austin, Texas, that was initially thought to be LD.

CME Editor

Terie A. Grant, BS, Copyeditor, Emerging Infectious Diseases. *Disclosure: Terie A. Grant, BS, has disclosed no relevant financial relationships.*

CME Author

Laurie Barclay, MD, freelance writer and reviewer, Medscape, LLC. *Disclosure: Laurie Barclay, MD, has disclosed no relevant financial relationships.*

Authors

Disclosures: ***Lisa C. Ellis, MD; Michael W. Curtis, PhD; Sarah M. Gunter, PhD, MPH;*** *and* ***Job E. Lopez, PhD,*** *have disclosed no relevant financial relationships.*

Author affiliations: Austin Infectious Disease Consultants, Austin, Texas, USA (L. Ellis); Baylor College of Medicine, Houston, Texas (M.W. Curtis, S.M. Gunter, J.E. Lopez)

DOI: https://doi.org/10.3201/eid2710.210189

Tickborne relapsing fever spirochetes are an overlooked cause of disease around the globe. We report a case of tickborne relapsing fever in a patient in Texas, USA, who had a single febrile episode and gastrointestinal and neurologic symptoms. Immunoblot analysis using recombinant *Borrelia* immunogenic protein A implicated *Borrelia turicatae* as the causative agent.

Tickborne relapsing fever (TBRF) spirochetes are globally neglected pathogens. *Borrelia turicatae* is found in the southwestern and eastern United States into Latin America (*1*), and high-risk populations include military personnel, outdoor enthusiasts, and impoverished undocumented immigrants (*2*–*4*). However, evidence indicates the presence of endemic foci of *B. turicatae* in metropolitan cities of Texas, USA (*4*,*5*).

TBRF is often misdiagnosed because of the nonspecific manifestations of the disease. More than 90% of patients experience recurrent febrile episodes, rigors, headache, and myalgia (*6*). Previous work suggests that *B. turicatae* is similar to Old World species, manifesting with neurologic complications (*7*). However, these diagnoses were made on the basis of a priori assumptions, and the causative agents were never confirmed.

We report a case of neuroborreliosis in Austin, Texas, USA, that was initially suspected to be Lyme disease (LD). A retrospective serologic analysis was performed using the diagnostic antigen, *Borrelia* immunogenic protein A (BipA). This antigen is absent from LD-causing spirochetes and might be a species-specific antigen for North American TBRF *Borrelia* (*8*,*9*).

The Study

The patient was a previously healthy 30-year-old man residing in Austin near a creek greenbelt that he frequented (Figure 1); he had no recent travel outside the city. On March 5, 2020, he experienced acute dizziness, headache, myalgia, vomiting, chills, and fever of 37.8°C (reference 36.1°C–37.2°C). Symptoms were attributed to a foodborne illness, and he improved after several days. However, he continued to experience dizziness, headache, fatigue, myalgia, and intermittent severe night sweats, with no report of further fever.

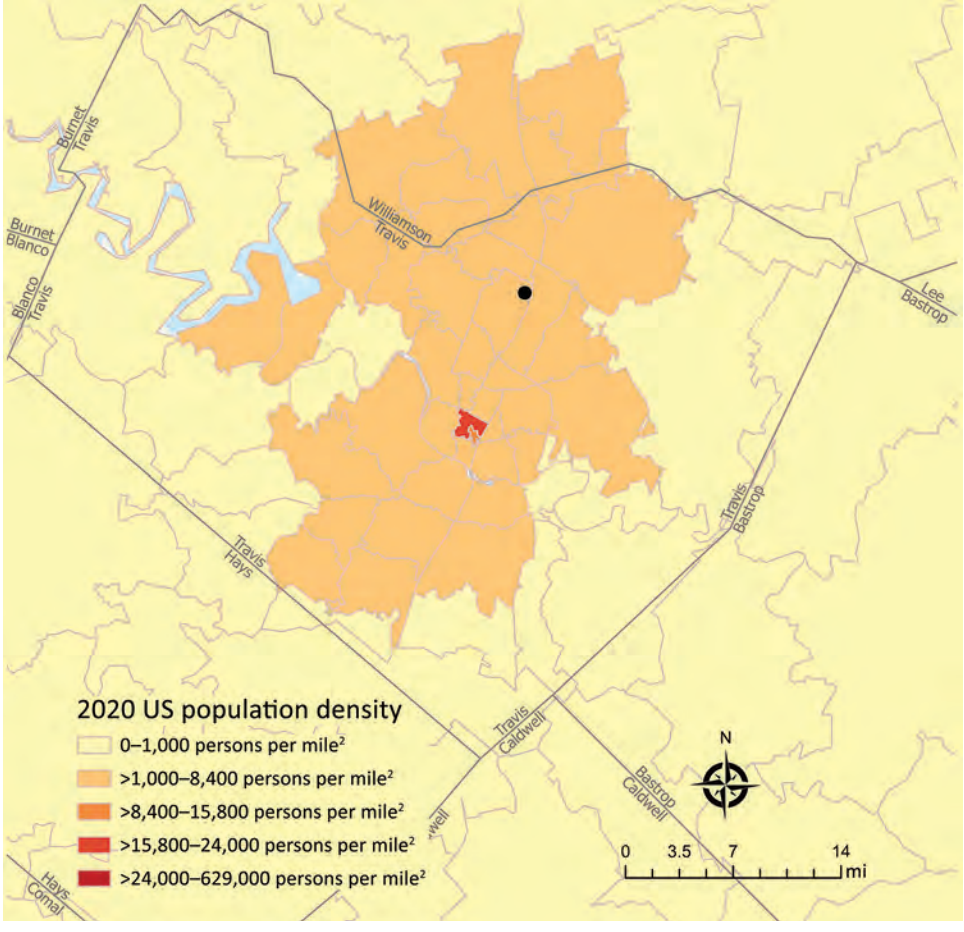

Figure 1. Suspected *Borrelia* exposure site within city limits for a patient in Austin, Texas, USA. The patient's suspected exposure location (black circle, Walnut Creek Metropolitan Park) was overlayed on a population density by ZIP code map. County boundaries are displayed as gray lines. Population density data was sourced from Esri's U.S. Updated Demographic (2020/2025) Data (https://www.esri.com).

Within 2 weeks, he had Bell's palsy on his left side, and the primary care physician ordered a blood analysis. Results for complete blood count, electrolytes, blood urea nitrogen, creatinine, and liver enzymes were unremarkable. Erythrocyte sedimentation rate was 62 mm/h (reference <15 mm/h), and C-reactive protein was 97.5 mg/L (reference <8.0 mg/L). Valacyclovir (1 g orally 3×/d for 7 d) and prednisone (20 mg orally 2×/d for 5 d) were prescribed, with partial improvement. Subsequent blood testing showed the erythrocyte sedimentation rate declined to 41 mm/h, and C-reactive protein declined to 43.2 mg/L.

Two weeks later, he had Bell's palsy on his right side, blurred vision, tinnitus, and cervical lymph node enlargement. Dizziness, headache, and fatigue continued. Results of complete blood count and metabolic panel were unremarkable. The patient underwent magnetic resonance imaging of the brain with contrast, which revealed faint nonspecific enhancement in the right internal auditory canal. High-resolution imaging of the 7th and 8th cranial nerves was not performed.

The patient's wife reported removing ticks from herself and a pet 4 weeks before the patient's illness began, and LD was suspected. A 2-tiered antibody test was performed. The enzyme immunoassay result was 2.43 (>1.09 considered positive). The LD IgM immunoblot was positive for the 23 kDa and 39 kDa bands, but the IgG immunoblot was negative.

The patient was referred to an infectious disease specialist who suspected TBRF and ordered a lumbar puncture. Clear, colorless cerebrospinal fluid (CSF) was recovered, and the analysis revealed 124 leukocytes/UL (reference <5 leukocytes/UL) with 85% lymphocytes, 10% monocytes, 5% large mononuclear cells, and 0% erythrocytes/UL. CSF protein was 103 mg/dL (reference 15.0–45.0 mg/dL), and glucose was 52 mg/dL (reference 40–70 mg/dL). CSF was analyzed by the Associated Regional and University Pathologists laboratory for LD and TBRF spirochete DNA, the Venereal Disease Research Laboratory test for neurosyphilis, and the Biofire Filmarray Meningitis/Encephalitis (bioMérieux, https://www.biomerieux-usa.com) panel that detects 6 bacterial and 7 viral pathogens. All test results were negative.

Given the patient's clinical history, intravenous ceftriaxone was administered (2 g/d for 14 d), and he showed considerable improvement within 4 days of treatment. Upon completion of antibiotics, all symptoms were resolved except for minimal lower right facial weakness. Deidentified serum samples and CSF collected 5 weeks after the onset of illness were sent to Baylor College of Medicine (Houston, TX, USA) for additional testing.

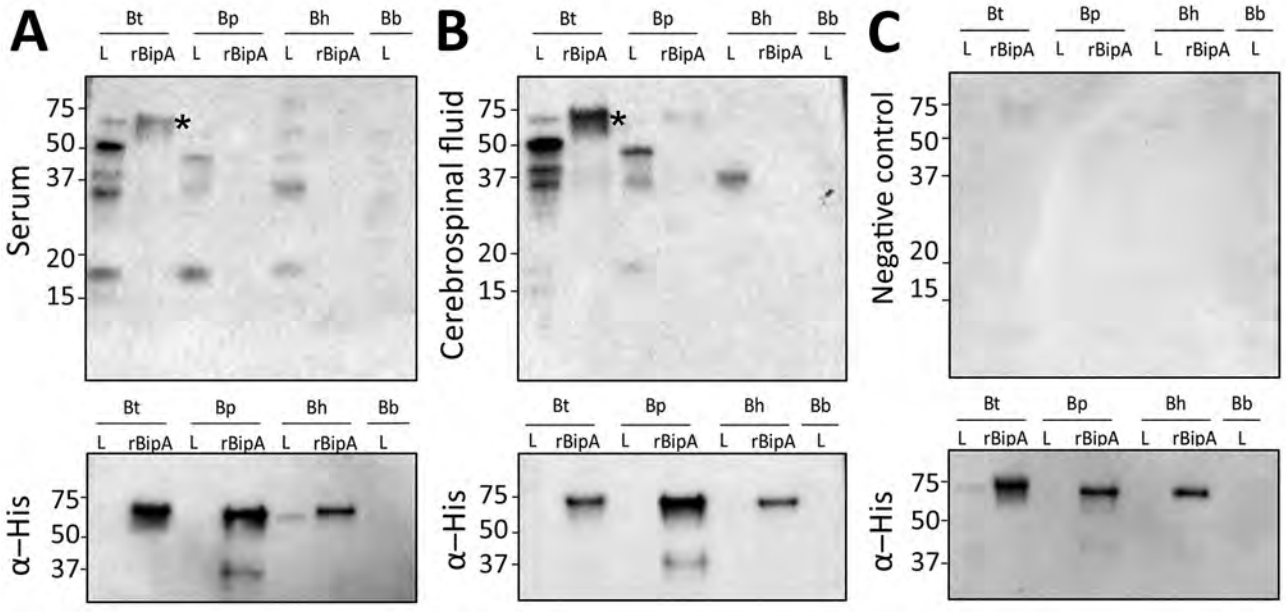

Figure 2. Immunoblots assessing antibody responses to *Borrelia* protein lysates and rBipA in samples from a patient in Texas, USA, and a control sample. A, B) Serum (A, upper panel) and cerebrospinal fluid (B, upper panel) samples were used to detect reactivity to *Borrelia* protein lysates and to rBipA from each species of tickborne relapsing fever spirochete. C) Negative human serum sample (upper panel) and immunoblots (bottom panel) that were reprobed with a monoclonal antibody for the histidine residues fused on the N terminus of each recombinant protein. Asterisks (*) indicates rBipA, which is ≈65 kDa. Molecular masses in kDa are indicated on the left of each immunoblot. Bb, *Borreliela* (*Borrelia*) *burgdorferi*; Bh, *B. hermsii*; BipA, *Borrelia* immunogenic protein A; Bp, *B. parkeri*; Bt, *B. turicatae*; rBipA, recombinant BipA.

No spirochetes were recovered from the CSF nor was DNA detected; therefore, we performed serologic tests using recombinant BipA (rBipA) (*8*,*9*). We generated expression constructs for *B. turicatae*, *B. parkeri*, and *B. hermsii* rBipA by using GenScript (GenScript, https://www.genscript.com) in the pET19b vector. We purified recombinant proteins and performed immunoblotting and ELISA, as previously described (*8*). For immunoblots, we used protein lysates from *B. turicatae* 91E135, *B. hermsii* DAH, and *B. parkeri* SLO. We probed immunoblots with the patient's serum sample and CSF diluted 1:200. Only the serum sample was diluted 2-fold from 1:200 to 1:256,000 for the ELISA because the CSF was depleted in prior assays. The secondary antibody was goat anti-human IgA, IgG, and IgM (Millipore, https://www.emdmillipore.com). We repeated serologic assays twice.

Serologic assays indicated likely exposure to *B. turicatae.* Strong responses were detected with the serum sample and CSF to *B. turicatae* protein lysates and rBipA (Figure 2, panels A and B upper). Antibodies in the patient's serum and CSF cross-reacted with protein lysates from *B. parkeri* and *B. hermsii*, but reactivity to rBipA from these species was undetectable (Figure 2, panels A, B, top images). In addition, reactivity to *B. burgdorferi* protein lysates was undetectable (Figure 2, panels A, B, top images). A negative control serum sample from a subject without history of TBRF failed to detect proteins (Figure 2, panel C, top image). Reprobing immunoblots with a monoclonal antibody for the histidine residues fused to rBipA demonstrated that protein was electrophoresed and transferred to membranes (Figure 2, bottom images). ELISA further indicated infection attributable to *B. turicatae* with antibody titers to *B. turicatae* rBipA between 1:400 to 1:800, and responses to *B. parkeri* and *B. hermsii* rBipA were undetectable.

Conclusions

This study reports a case of neurologic TBRF likely caused by *B. turicatae*. The hallmark of TBRF is recurrent febrile episodes (*6*), but this patient had a single febrile episode, nausea, and predominantly neurologic symptoms. *B. turicatae* has been suspected to cause neurologic symptoms including facial paralysis, vertigo, hearing loss, delirium, and hallucinations (*10*). However, past diagnoses were attributed solely on the basis of the geographic range of the probable pathogen and were not empirically confirmed.

This study demonstrated that rBipA could aid in identifying the TBRF species causing infection. It was unlikely that the patient was exposed to *B. hermsii* and *B. parkeri* because of his travel history, but we used this opportunity to assess serologic crossreactivity to rBipA from these 2 species. Similar to prior work with *B. turicatae*–infected laboratory animals (*8*), we detected no crossreactive patient antibodies to *B. hermsii* rBipA. This finding was expected given that the proteins share ≈35% amino acid identity (*11*). Of note, rBipA could differentiate between infections caused by *B. parkeri* and *B. turicatae,* which share ≈75% amino acid identity (*11*).

In summary, *B. turicatae* is often misdiagnosed, and healthcare providers should understand the pathogen's circulation (*2*,*5*,*11*). Endemic foci have been identified in Florida, USA, and within and around the 4 largest cities of Texas (Austin, San Antonio, Dallas, and Houston) (*1*–*3*,*5*,*7*). With urban expansion and the incorporation of greenbelts into metropolitan areas, *B. turicatae* should be considered in cases of fever with neurologic symptoms when the Lyme antibody test is positive but prevalence of LD is not epidemiologically supported.

Acknowledgments

We thank Aparna Krishnavajhala and Alexander Kneubehl for critical review of this manuscript and Tom Schwan for originally providing *B. hermsii*, *B. turicatae*, and *B. parkeri* isolates for serology.

This work was supported by funding from National Institutes of Health grant no. AI144187 (JEL). Michael W. Curtis was supported through the Infection and Immunity T32 Fellowship at Baylor College of Medicine (grant no. T32AI055413).

About the Author

Dr. Ellis is an infectious disease specialist in Austin, Texas, USA, in clinical practice with Austin Infectious Disease Consultants. Her research interests include HIV and atypical mycobacterium infections.

References

1. Lopez JE, Krishnavahjala A, Garcia MN, Bermudez S. Tick-borne relapsing fever spirochetes in the Americas. Vet Sci. 2016;3:1–18. https://doi.org/10.3390/vetsci3030016
2. Rawlings JA. An overview of tick-borne relapsing fever with emphasis on outbreaks in Texas. Tex Med. 1995;91:56–9.
3. Christensen AM, Pietralczyk E, Lopez JE, Brooks C, Schriefer ME, Wozniak E, et al. Diagnosis and management of *Borrelia turicatae* infection in febrile soldier, Texas, USA. Emerg Infect Dis. 2017;23:883–4. https://doi.org/10.3201/eid2305.162069
4. Campbell SB, Kliioueva A, Taylor J, Nelson C, Tomasi S, Replogle A, et al. Evaluating the risk of tick-borne relapsing fever among occupational cavers—Austin, TX, 2017. Zoonoses Public Health. 2019;66:579–86. https://doi.org/10.1111/zph.12588

5. Bissett JD, Ledet S, Krishnavajhala A, Armstrong BA, Kliioueva A, Sexton C, et al. Detection of tickborne relapsing fever spirochete, Austin, Texas, USA. Emerg Infect Dis. 2018;24:2003–9. https://doi.org/10.3201/eid2411.172033
6. Dworkin MS, Schwan TG, Anderson DE Jr, Borchardt SM. Tick-borne relapsing fever. Infect Dis Clin North Am. 2008;22:449–68, viii. https://doi.org/10.1016/j.idc.2008.03.006
7. Gillespie JO. Relapsing fever in the United States. JAMA. 1935;104:1878–81. https://doi.org/10.1001/jama.1935.02760210010003
8. Lopez JE, Wilder HK, Boyle W, Drumheller LB, Thornton JA, Willeford B, et al. Sequence analysis and serological responses against *Borrelia turicatae* BipA, a putative species-specific antigen. PLoS Negl Trop Dis. 2013;7:e2454. https://doi.org/10.1371/journal.pntd.0002454
9. Lopez JE, Schrumpf ME, Nagarajan V, Raffel SJ, McCoy BN, Schwan TG. A novel surface antigen of relapsing fever spirochetes can discriminate between relapsing fever and Lyme borreliosis. Clin Vaccine Immunol. 2010;17:564–71. https://doi.org/10.1128/CVI.00518-09
10. Cadavid D, Barbour AG. Neuroborreliosis during relapsing fever: review of the clinical manifestations, pathology, and treatment of infections in humans and experimental animals. Clin Infect Dis. 1998;26:151–64. https://doi.org/10.1086/516276
11. Wilder HK, Wozniak E, Huddleston E, Tata SR, Fitzkee NC, Lopez JE. Case report: a retrospective serological analysis indicating human exposure to tick-borne relapsing fever spirochetes in Texas. PLoS Negl Trop Dis. 2015;9:e0003617. https://doi.org/10.1371/journal.pntd.0003617

Address for correspondence: Job Lopez, Baylor College of Medicine, One Baylor Plaza, Houston, TX 77030, USA; email: job.lopez@bcm.edu

Widespread Disease in Hedgehogs (*Erinaceus europaeus*) Caused by Toxigenic *Corynebacterium ulcerans*

An Martel, Filip Boyen, Jörg Rau, Tobias Eisenberg, Andreas Sing, Anja Berger, Koen Chiers, Sarah Van Praet, Serge Verbanck, Muriel Vervaeke, Frank Pasmans

Toxin-producing *Corynebacterium ulcerans*, a causative agent of diphtheria in humans, was isolated from 53 hedgehogs in Belgium during the spring of 2020. Isolates showed low levels of acquired antimicrobial drug resistance. Strain diversity suggests emergence from an endemic situation. These findings stress the need for raising public awareness and improved wildlife disease surveillance.

Hedgehogs across northern Belgium are currently being affected by an ulcerative skin disease. The purpose of this study was to identify the cause of these skin lesions.

The Study

During May and June 2020, we tested 81 hedgehogs (*Erinaceus europaeus*) that had ulcerative skin lesions and were provided by the public to 4 animal rescue centers across northern Belgium (Figure 1). Cases derived from 3 provinces in Flanders (East Flanders, Antwerp, and Limburg); total surface area of these provinces is 8,310 km^2. All hedgehogs were individually housed, and we conducted sampling after euthanasia or natural death. We obtained 60 *Corynebacterium ulcerans* isolates from ulcers or abscesses on the head or limbs from 53 of 81 investigated hedgehogs; all were adult males. For 6 animals, we obtained >1 isolate from different lesions.

Although *C. ulcerans* was isolated most often, lesions yielded abundant, polybacterial growth (Table 1). We showed by systematic postmortem examinations that 9 animals had a good body condition generally but had multiple cutaneous ulcers on the head and limbs. Histopathologic analysis of skin of these animals showed subacute, extensive, ulcerative dermatitis and suppurative exudation and crusting. Inflammation sometimes extended to the subcutis and even to underlying skeletal muscles.

In some instances, we observed nodular inflammation consisting of central necrosis admixed with degenerated neutrophils and bordered by a small rim of macrophages (abscess formation) and fistulation. We observed intralesional microcolonies of gram-positive bacilli. We subjected organs that showed macroscopic abnormalities to histopathologic analysis. Four animals had interstitial pneumonia, 1 animal had ascending hepatitis, and 1 animal had fibrinosuppurative epicarditis and intralesional gram-positive bacteria.

Despite presence of parasites related to skin disease (fly maggots; myiasis, n = 5; *Sarcoptes scabiei*, n = 1; and *Caparinia* spp., (n = 1) and pathogens related to systemic disease (herpesvirus, n = 2 [*3*] and lungworms; *Crenosoma striatum*, n = 2), we found no consistent evidence for other causes of primary disease. Although evidence is insufficient to conclusively attribute the observed lesions to *C. ulcerans*, its widespread and high-level occurrence in diseased male hedgehogs is a serious concern, given frequent exposure of humans to hedgehogs and because *C. ulcerans* is the predominant cause of human diphtheria in many countries in Europe (*4*).

C. ulcerans isolates from hedgehogs belong to several clusters. We identified 56 isolates of *C. ulcerans* to the species level by using matrix-assisted laser desorption/ionization time-of-flight mass spectrometry (*5*) and sequencing of the *rpoB* gene (*6*). We also typed isolates by analysis of infrared spectra (*7*). Isolates grouped with *C. ulcerans* strains from humans and other animals (hedgehogs and red foxes [*Vulpes vulpes*] from Germany) (*1*) and clustered in 3 sublineages (Figure 2). The

Author affiliations: Ghent University, Merelbeke, Belgium (A. Martel, F. Boyen, K. Chiers, S. Van Praet, S. Verbanck, F. Pasmans); Chemical and Veterinary Analysis Agency Stuttgart, Fellbach, Germany (J. Rau); Hessian State Laboratory, Giessen, Germany (T. Eisenberg); Bavarian Health and Food Safety Authority, Oberschleißheim, Germany (A. Sing, A. Berger); Agency for Nature and Forests, Brussels, Belgium (M. Vervaeke)

DOI: https://doi.org/10.3201/eid2710.203335

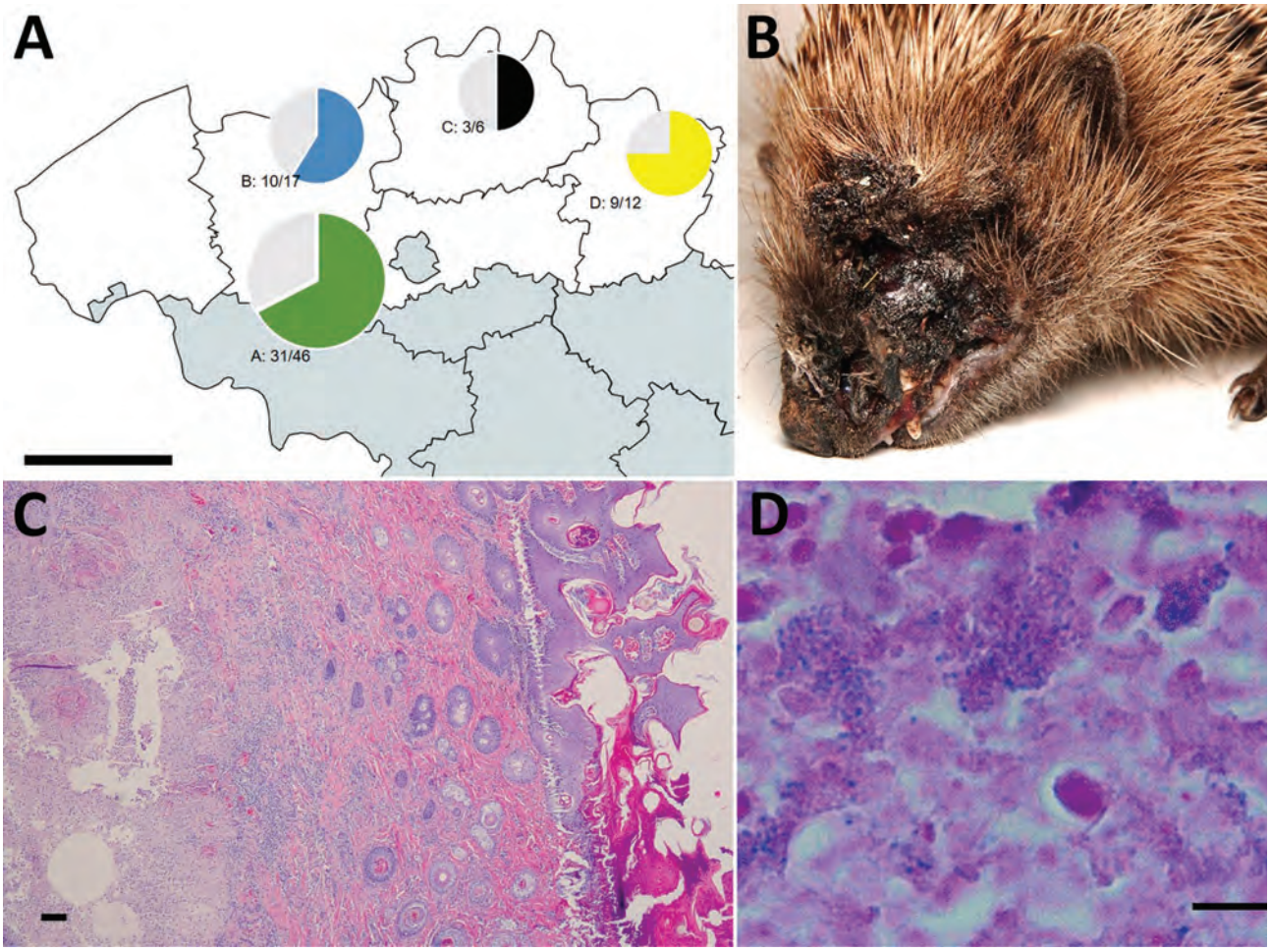

Figure 1. Toxigenic *Corynebacterium ulcerans* as cause of widespread disease in hedgehogs (*Erinaceus europaeus*), Flanders, Belgium. A) Locations of 81 hedgehogs with lesions on the head or limbs from 4 regions in Flanders, Belgium, who were tested for *C. ulcerans*. Green, blue, black, and yellow indicate proportion of positive animals; gray indicates proportion of negative animals. Regions: A, Geraardsbergen; B, Merelbeke; C, Herenthout; D, Oudsbergen. Scale bar = 50 km. B) Representative clinical state with necrotizing facial dermatitis in 1 male hedgehog from Merelbeke. C) Ulcerative dermatitis with suppurative exudation and inflammation extending into the subcutis and underlying skeletal muscles. Hematoxylin and eosin stained; scale bar = 100 μm. D) Microcolonies of gram-positive bacilli in suppurative exudate. Gram stain; scale bar = 10 μm.

high diversity is similar to that reported by Berger et al. (*1*), and results argue against nocosomial infections and emergence and spread of a single *C. ulcerans* clone in the hedgehog population in Flanders. Instead, the high diversity of the isolates suggests *C. ulcerans* endemicity in the hedgehog population.

We found limited acquired antimicrobial resistance in *C. ulcerans* isolates from hedgehogs. We compiled MIC data for all *C. ulcerans* isolates (Table 2). Acquired resistance against enrofloxacin was detected in 4 isolates.

Most *C. ulcerans* isolates from hedgehogs produce toxins. We evaluated presence and expression of toxins by detection of the diphtheria toxin gene (*toxE*) by using a duplex PCR (*6*) and the Elek test (*11*). Results showed a positive result for this gene in 50/56 isolates by PCR and positive (26/56 isolates) or weak positive (16/56 isolates) results by Elek test. One animal was positive for the *toxE* gene in 1 location (*C. ulcerans* isolate from a head lesion) and negative for the gene in another location (isolate from a foot lesion).

Although diphtheria vaccination coverage in humans is high in Belgium, since 2010, sporadic cases (14 cases during 2010–2017) of infection by toxigenic corynebacteria have occurred (*6*). Because presence of the *toxE* gene and toxin production are associated with pathogenicity in humans, these results suggest a zoonotic potential of most hedgehog-derived *C. ulcerans* isolates.

Table 1. Bacterial isolates obtained from 81 diseased hedgehogs, Flanders, Belgium*

Bacterial species obtained from lesions	No. positive animals
Corynebacterium ulcerans	53
Staphylococcus aureus	25
Enterococcus faecalis	23
Streptococcus canis	18
Streptococcus dysgalactiae	18
Proteus vulgaris/P. hauseri	17
Staphylococcus rostri	15
Proteus mirabilis	14
Streptococcus pyogenes†	13
Staphylococcus xylosus	10
Staphylococcus microti	8
Staphylococcus sciuri	8
Vagococcus fluvialis	8
Enterococcus avium	7
Escherichia coli	7
Staphylococcus pettenkoferi	7
Morganella morganii	6
Staphylococcus fleurettii	6
Pasteurella multocida	4
Corynebacterium amycolatum	3
Bacteroides fragilis	3
Staphylococcus simulans	3
Trueperella pyogenes	3
Vagococcus lutrae	2
Arcanobacterium haemolyticum	1
Bacillus sp.	1
Bacteroides pyogenes	1
Corynebacterium confusum	1
Corynebacterium rouxii	1
Enterococcus hirae	1
Enterobacter hormaechei	1
Gemella haemolysans	1
Lactococcus garvieae	1
Streptococcus gallinaceus	1
Streptococcus thoraltensis	1

*Bacteria were identified by using matrix-assisted laser desorption/ionization time-of-flight mass spectrometry. Biovar identification for the *C. diphtheriae* isolate was performed by using the Api Coryne System (bioMérieux, https://www.biomerieux.com).
†Also detected by Berger et al. (*1*) and Franklinos et al. (*2*).

Conclusions

Hedgehogs are mammals that are abundant in Europe and are frequently observed in nature reserves and urbanized areas. Because of their defensive behavior, sick animals are easily brought to animal rescue centers by the public, as testified by the large number of animals we examined in a short time frame during this study. The nature of their spiny defense promotes breaching and inoculating of the human epidermis with bacteria during handling. Other potential routes of transmission might include bite wounds or contact with the contaminated environment of the hedgehogs. Several potentially zoonotic or anthroponotic bacterial species, including *C. rouxii* and *Streptococcus pyogenes*, are associated with ulcerative lesions in diseased hedgehogs (Table 1).

Although Gower et al. (*12*) showed that the major risk factor for *C. ulcerans* infection in humans is exposure to domestic animals (e.g., dogs, cats), widespread occurrence of toxigenic *C. ulcerans* in most diseased hedgehogs across Flanders should prompt authorities to alert all stakeholders, including members of the public and staff at animal rescue centers, to take precautionary measures when handling hedgehogs. Although vaccination against *C. diphtheriae* protects against *C. ulcerans* disease, exposure to *C. ulcerans* from susceptible persons might result in severe disease (*12*). Recommendations should include wearing protective gloves and cleaning and disinfecting hands and fomites after contact with a hedgehog, as well as vaccination of persons who are frequently exposed to hedgehogs.

Treatment of infections with pyogenic coryneform bacteria in animals is challenging, and the 4 rescue centers involved in this study reported poor treatment success. Results of antimicrobial susceptibility testing suggest that this finding is not caused by acquired antimicrobial drug resistance but probably by insufficiently high antimicrobial drug concentrations reaching the *C. ulcerans* bacteria inside pus. Therefore, debriding the lesions should be included in any treatment. Euthanasia should be considered for severe cases.

Emergence of *C. ulcerans* infection in hedgehogs is consistent with an increasing number of reports of *C. ulcerans* infections in wildlife across Europe and warrants attention across the continent (*1,13,14*). Reports dating back from the 1950s and the presence of several distantly related clusters of *C. ulcerans* in this study argue against a recent introduction of this pathogen in wildlife populations in Europe and favors the hypothesis that the observed and previously unreported high numbers of diseased hedgehogs result from pathogen emergence from a disease-endemic state. Although most wild animals affected with *C. ulcerans* have systemic infections (*1*), in our study, the manifestations of cutaneous disease dominated.

The finding that only male hedgehogs had this disease and that lesions are found mostly on body parts not covered with spines suggests the *C. ulcerans* infections might be opportunistic infections of wounds, arising from male-specific behavior during the mating season. Bite wounds are well known to be susceptible to infection with opportunistic pathogens that are part of the oral microbiota (*15*). Strain typing suggests that hedgehogs are a major reservoir of highly diverse *C. ulcerans* isolates. Active surveillance should elucidate the magnitude of this reservoir in healthy hedgehogs and the impact on the population level. Until the mechanisms underpinning the observed emergence of this potentially zoonotic wildlife disease from its disease-endemic state can be clarified, persons handling hedgehogs should take precautions to prevent possible transmission of *C. ulcerans*.

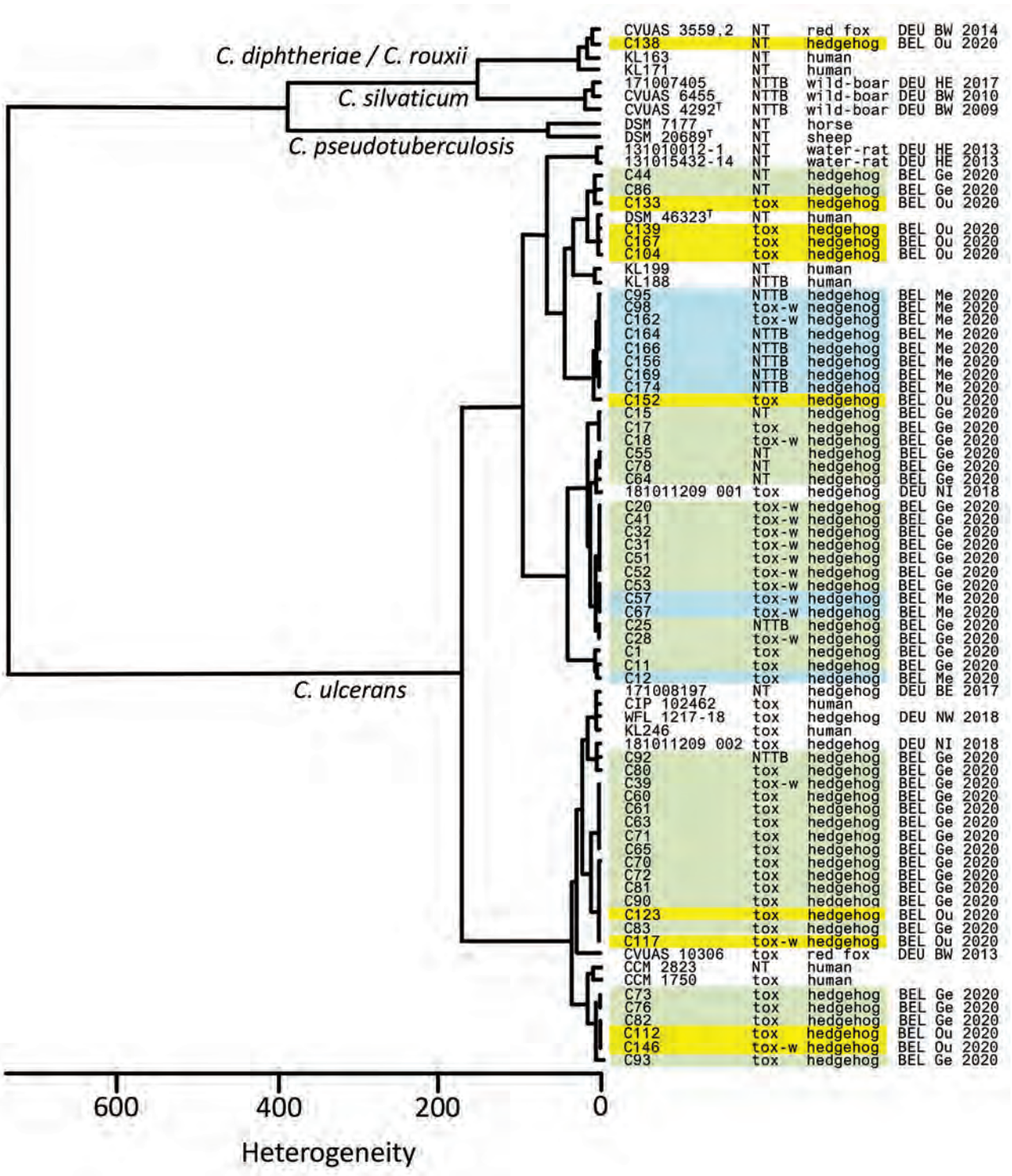

Figure 2. Dendrogram of Fourier-transformed infrared spectra of *Corynebacterium* spp. strains obtained from hedgehogs (*Erinaceus europaeus*), Flanders, Belgium, compared with spectra from several *C. ulcerans* isolates, including isolates from free-roaming red foxes (*Vulpes vulpes*) and wild boars *(Sus scrofa scrofa*) (*1*) and other well characterized and available isolates from animals and humans. Additional details for isolates were determined by using matrix-assisted laser desorption/ionization time-of-flight mass spectrometry (*8*). Country of origin: BEL, Belgium (region: Ge, Geraardsbergen [green]; Me, Merelbeke [blue]; Ou, Oudsbergen [yellow]); BE, Berlin; BY, Bavaria; DEU, Germany. NT, no tox gene; NTTB, nontoxic but tox-bearing (these are isolates that have the toxin gene, but do not produce toxins); T, type strain; Tox, toxigenic; tox-w, toxigenic (weak).

Table 2. Distribution of MIC values for 60 isolates of *Corynebacterium ulcerans* isolates from hedgehogs, Flanders, Belgium*

Drug	MIC, μg/mL											
	<0.016	0.016	0.032	0.064	0.12	0.25	0.5	1	2	4	8	16
Amoxicillin	1	10	6	8	25	10	0	0	0	0	0	0
Amoxicillin/clavulanate	2	2	2	12	18	22	2	0	0	0	0	0
Clindamycin	0	0	0	0	0	0	0	34	26	0	0	0
Doxycycline	0	0	0	0	5	27	13	13	2	0	0	0
Enrofloxacin	0	4	33	19	0	0	0	4	0	0	0	0
Erythromycin	0	1	50	9	0	0	0	0	0	0	0	0
Penicillin	1	1	4	6	17	20	11	0	0	0	0	0
Spiramycin	0	0	0	43	17	0	0	0	0	0	0	0
Tetracycline	0	0	0	0	0	11	29	19	1	0	0	0
Tilmicosin	0	0	0	0	0	0	1	29	29	1	0	0
Trimethoprim/sulfamethoxazole	0	0	9	43	8	0	0	0	0	0	0	0

*Values are no. isolates, which were obtained by using an epsilometer (ETEST; bioMérieux, https://www.biomerieux.com) on Mueller–Hinton agar plates containing 5% horse blood and 20 mg/L of β-NAD (bioMérieux), according to European Committee on Antimicrobial Susceptibility Testing (*9*) and Clinical and Laboratory Standards Institute (*10*) guidelines.

Acknowledgments

We thank Nancy Van Liefferinge, Filip Berlengee, Nick De Meulemeester, Frederick Thoelen, and Tom Verbeek for the participating in this study.

This study was supported by the Agency for Nature and forests of the Flemish government. Matrix-assisted laser desorption/ionization time-of-flight mass spectrometry was supported by the Research Foundation Flanders (FWO-Vlaanderen) as a Hercules project (G0H2516N, AUGE/15/05), Bijzonder Onderzoeksfonds research as a professorial staff mandate to A.M., the Bavarian State Ministry of Health and Care, and the German Federal Ministry of Health through the Robert Koch-Institute (09-47, FKZ 1369-359).

About the Author

Dr. Martel is a research professor at Wildlife Health Ghent, Ghent University, Ghent, Belgium. Her primary research interest is host–pathogen interactions in wildlife diseases.

References

1. Berger A, Dangel A, Peters M, Mühldorfer K, Braune S, Eisenberg T, et al. Tox-positive *Corynebacterium ulcerans* in hedgehogs, Germany. Emerg Microbes Infect. 2019;8:211–7. https://doi.org/10.1080/22221751.2018.1562312
2. Franklinos LH, Efstratiou A, Macgregor SK, John SK, Hopkins T, Cunningham AA, et al. *Streptococcus pyogenes* infection in a free-living European hedgehog (*Erinaceus europaeus*). EcoHealth. 2015;12:689–92. https://doi.org/10.1007/s10393-015-1051-2
3. Hydeskov HB, Dastjerdi A, Hopkins KP, Ryser-Degiorgis MP, Widén F, Cunningham AA, et al. Detection and characterisation of multiple herpesviruses in free-living Western European hedgehogs (*Erinaceus europaeus*). Sci Rep. 2018;8:13942. https://doi.org/10.1038/s41598-018-31900-w
4. Wagner KS, White JM, Lucenko I, Mercer D, Crowcroft NS, Neal S, et al.; Diphtheria Surveillance Network. Diphtheria in the postepidemic period, Europe, 2000–2009. Emerg Infect Dis. 2012;18:217–25. https://doi.org/10.3201/eid1802.110987
5. Rau J, Eisenberg T, Peters M, Berger A, Kutzer P, Lassnig H, et al. Reliable differentiation of a non-toxigenic *tox* gene-bearing *Corynebacterium ulcerans* variant frequently isolated from game animals using MALDI-TOF MS. Vet Microbiol. 2019;237:108399. https://doi.org/10.1016/j.vetmic.2019.108399
6. Martini H, Soetens O, Litt D, Fry NK, Detemmerman L, Wybo I, et al. Diphtheria in Belgium: 2010–2017. J Med Microbiol. 2019;68:1517–25. https://doi.org/10.1099/jmm.0.001039
7. Eisenberg T, Kutzer P, Peters M, Sing A, Contzen M, Rau J. Nontoxigenic tox-bearing *Corynebacterium ulcerans* infection among game animals, Germany. Emerg Infect Dis. 2014;20:448–52. https://doi.org/10.3201/eid2003.130423
8. Rau J, Eisenberg T, Sting R. MALDI-User Platform MALDI-UP [cited 2020 Jun 7]. https://maldi-up.ua-bw.de
9. The European Committee on Antimicrobial Susceptibility Testing, 2016. Breakpoint tables for interpretation of MICs and zone diameters, version 6.0 [cited 2021 Jun 25]. http://www.eucast. org/fileadmin/src/ media/PDFs/EUCAST_files/Breakpoint_tables/v_6. 0_Breakpoint_table
10. Clinical and Laboratory Standards Institute. Performance standards for antimicrobial susceptibility testing (supplement M100). 30th ed. Wayne (PA): The Institute; 2020.
11. Engler KH, Glushkevich T, Mazurova IK, George RC, Efstratiou A. A modified Elek test for detection of toxigenic corynebacteria in the diagnostic laboratory. J Clin Microbiol. 1997;35:495–8. https://doi.org/10.1128/jcm.35.2.495-498.1997
12. Gower CM, Scobie A, Fry NK, Litt DJ, Cameron JC, Chand MA, et al. The changing epidemiology of diphtheria in the United Kingdom, 2009 to 2017. Euro Surveill. 2020;25:1900462. https://doi.org/10.2807/1560-7917.ES.2020.25.11.1900462
13. Hirai-Yuki A, Komiya T, Suzaki Y, Ami Y, Katsukawa C, Takahashi M, et al. Isolation and characterization of toxigenic *Corynebacterium ulcerans* from 2 closed colonies of cynomolgus macaques (*Macaca fascicularis*) in Japan. Comp Med. 2013;63:272–8.
14. Olson ME, Goemans I, Bolingbroke D, Lundberg S. Gangrenous dermatitis caused by *Corynebacterium ulcerans* in Richardson ground squirrels. J Am Vet Med Assoc. 1988;193:367–8.
15. Abrahamian FM, Goldstein EJ. Microbiology of animal bite wound infections. Clin Microbiol Rev. 2011;24:231–46. https://doi.org/10.1128/CMR.00041-10

Address for correspondence: An Martel, Wildlife Health Ghent, Department of Pathology, Bacteriology and Avian Diseases, Faculty of Veterinary Medicine, Ghent University, Salisburylaan 133, 9820 Merelbeke, Belgium; email: an.martel@ugent.be

Confirmation of *Rickettsia conorii* Subspecies *indica* Infection by Next-Generation Sequencing, Shandong, China

Nannan Xu,[1] Wei Gai,[1] Yan Zhang, Wei Wang, Gang Wang, Gregory A. Dasch, Marina E. Eremeeva

We describe 3 similar cases of rickettsial disease that occurred after tick bites in a mountainous rural area of Shandong Province, China. Next-generation sequencing indicated the etiologic agent of 1 patient was *Rickettsia conorii* subspecies *indica*. This agent may be more widely distributed across China than previously thought.

Shandong is an eastern coastal province of China. Four natural-focal diseases—severe fever with thrombocytopenia syndrome, human granulocytic anaplasmosis, endemic typhus, and scrub typhus—are thought to have the most severe effects on human health in Shandong Province (*1*). However, as in other parts of China, exposure to rickettsial pathogens in eastern provinces is expected because of the prevalence of human-biting ticks (*2*,*3*). Specifically, Japanese spotted fever caused by *Rickettsia japonica* is endemic to Shandong; *R. japonica* and 2 other novel *Rickettsia* spp. were found in the Asian longhorned tick (*Haemaphysalis longicornis*) (*2*). Because rickettsioses have similar clinical manifestations but vary in severity (i.e., incidence of illness and death), laboratory investigation is essential for understanding the epidemiology of tick-borne diseases. We obtained sequences of *Rickettsia conorii* subspecies *indica* (ITTR) infection from 1 case; 2 other cases of spotted fever rickettsiosis (SFGR) with similar epidemiologic history and clinical features were treated at the same hospital (Appendix Table 1, Figure 1, https://wwwnc.cdc.gov/EID/article/27/10/20-4764-App1.pdf). This study was approved by the ethics committee of Qilu Hospital, of Shandong University, Jinan, Shandong, China. All patients signed consent forms.

Author affiliations: Qilu Hospital of Shandong University, Jinan, Shandong, China (N. Xu, G. Wang); Gene Research Institute, WillingMed Technology (Beijing) Co. Ltd., Beijing, China (W. Gai, Y. Zhang); The University of Texas MD Anderson Cancer Center, Houston, Texas, USA (W. Wang); Centers for Disease Control and Prevention, Atlanta, Georgia, USA (G.A. Dasch); Georgia Southern University, Statesboro, Georgia, USA (M.E. Eremeeva)

DOI: https://doi.org/10.3201/eid2710.204764

The Study

In the summer of 2019, a 53-year-old man (patient 1) was hospitalized with a 5-day history of fever (41°C), influenza-like symptoms, and generalized maculopapular rash (Figure 1, panel A). A farmer working in a rural mountainous area of Zibo, Shandong Province, he was bitten by a tick 6 days before onset of illness. At admission, clinical blood tests revealed elevated leukocyte count (12.91×10^9 cells/L) with neutrophilia (90.5%) and thrombocytopenia (73×10^9/L), as well as increased procalcitonin (3.870 ng/mL) and C-reactive protein (38.31 mg/mL). Rickettsiosis was suspected, and oral minocycline was prescribed on the second day after admission. Symptoms subsided after 2 days of treatment; the patient was discharged from the hospital 6 days later. Serum samples collected on days 8 and 24 after onset of illness tested positive for *Rickettsia conorii* IgG (titers 1,024 at day 8 and 16,384 at day 24) by immunofluorescence assay (IFA) (Fuller Laboratories, http://www.fullerlaboratories.com).

Patient 2, a 41-year-old female agriculture worker from Jinan, the capital of Shandong Province, came from an environment similar to that of patient 1. Patient 2 was hospitalized 18 days after a tick bite; symptoms were an 8-day history of fever (39°C), meningitis, and a sparsely spread purpuric rash (Figure 1, panel B). Intravenous doxycycline treatment was initiated 1 day after admission. Four days after admission, despite 2 days of treatment, the patient experienced seizures, coma, and cardiac arrhythmia. After 2 more days of intravenous doxycycline treatment, the patient improved and was discharged 4

[1]These authors contributed equally to this article.

days later. Serum samples collected on days 9 and 22 after onset of illness tested positive for *R. conorii* IgG by IFA (titers 128 at day 9 and 1,024 at day 22).

Patient 3, a 45-year-old woman, had a history of travel to a farming area in Tai'an, Shandong Province, and was bitten by a tick 8 days before onset of illness. At admission, she had a 5-day history of fever (39°C). She did not have rash but had an ulcerated eschar on her right foot (Figure 1, panel C). Blood tests at hospital admission revealed elevated leukocyte count (10.12×10^9 cells/L), procalcitonin (0.108 ng/mL), and C-reactive protein (46.39 mg/mL). The patient was treated with minocycline beginning the next day after admission; she began to improve on day 3 of treatment and was discharged after 3 more days. Serum samples collected on days 9 and 20 after onset of illness tested positive for *R. conorii* IgG by IFA (titers 64 at day 9 and 1,024 at day 20).

Conventional bacterial cultures of blood samples collected at admission yielded negative results for all 3 patients, as did viral nucleic acid detection of pharyngeal swab samples. Results of serologic ELISA tests for *Coxiella burnetii* phase II IgG (IBL International GmbH, https://www.ibl-international.com), *Rickettsia typhi* IgM (Fuller Laboratories), and *Orientia tsutsugamushi* IgM (InBios International, Inc., https://inbios.com) were all negative.

To identify the potential causative pathogen, we performed next-generation sequencing (NGS) on the Ion Torrent platform (Thermo Fisher Scientific, https://www.thermofisher.com) by using DNA extracted from the peripheral blood of patient 1, collected on day 7 after onset of fever and before administration of antimicrobial drugs. The sequencing data are deposited at the National Center for Biotechnology Information Sequence Read Archive (accession no. SRR10855057). We mapped those sequences to *R. conorii* ITTR (Appendix Figure 2). Coverage was low except for 16S and 23S rRNA genes, but matching sequences were found across the ITTR genome and to other *Rickettsia* genomes (data not shown). We identified reads mapping to specific *Rickettsia* genomes by using BLAST (https://blast.ncbi.nlm.nih.gov/Blast.cgi) (Appendix Table 2). We identified the *Rickettsia*-specific 16S rRNA gene sequences with the Ribosomal Database Project Classifier by using Geneious Prime 19 (Geneious, https://www.geneious.com) (Appendix Table 2). Moreover, we identified sequence reads matching 3 genes commonly used for speciation of *Rickettsia* (*glt*A, *omp*A, *omp*B); 6 other proteins; and 1 pseudogene, *rnp*B, and containing or flanking 20 of the 33 rickettsial tRNAs (33 reads) (Figure 2; Appendix Table 2). Many sequence reads mapped most closely to ITTR or to ITTR and its closest relative, *R. conorii conorii* Malish 7; sequence reads mapped less frequently to the other subspecies, *R. conorii caspia* and *R. conorii israelensis.*

Conclusions

Many tickborne rickettsiae have been described from China, including *R. heilongjiangiensis*, *R. sibirica* BJ-90, *R. sibirica mongolotimonae*, *R. monacensis*, *R. raoultii*, *R. slovaca*, *R. japonica*, *Candidatus* R. tarasevichiae, and other *Rickettsia* spp. of unknown pathogenicity (*2*,*4*). We molecularly confirmed a case of SFGR disease in eastern China caused by *R. conorii* subsp. *indica*. We identified 2 other serologically confirmed cases of SFGR with similar history of tick bite, similar clinical manifestations, and shared epidemiologic features.

NGS technology provided the specific etiology of SFGR in 1 of these patients. The single NGS read length exceeded the size of tRNAs, so they were informative for identification, but diagnostic sites were also obtained for protein fragments (Appendix Table 2). The sensitivity of NGS depends on the type of the clinical sample, the timing of collection, and desirability for depleting human DNA to improve sensitivity of pathogen detection by increasing the number of agent sequences (*5*).

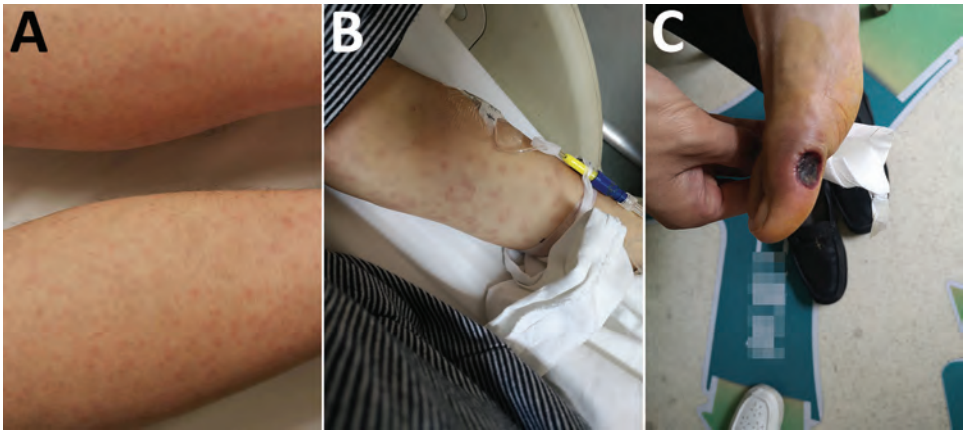

Figure 1. Skin manifestations of patients in study of confirmation of *Rickettsia conorii* subspecies *indica* infection by next-generation sequencing, Shandong, China. A) Rash in patient 1; B) rash in patient 2; C) eschar in patient 3

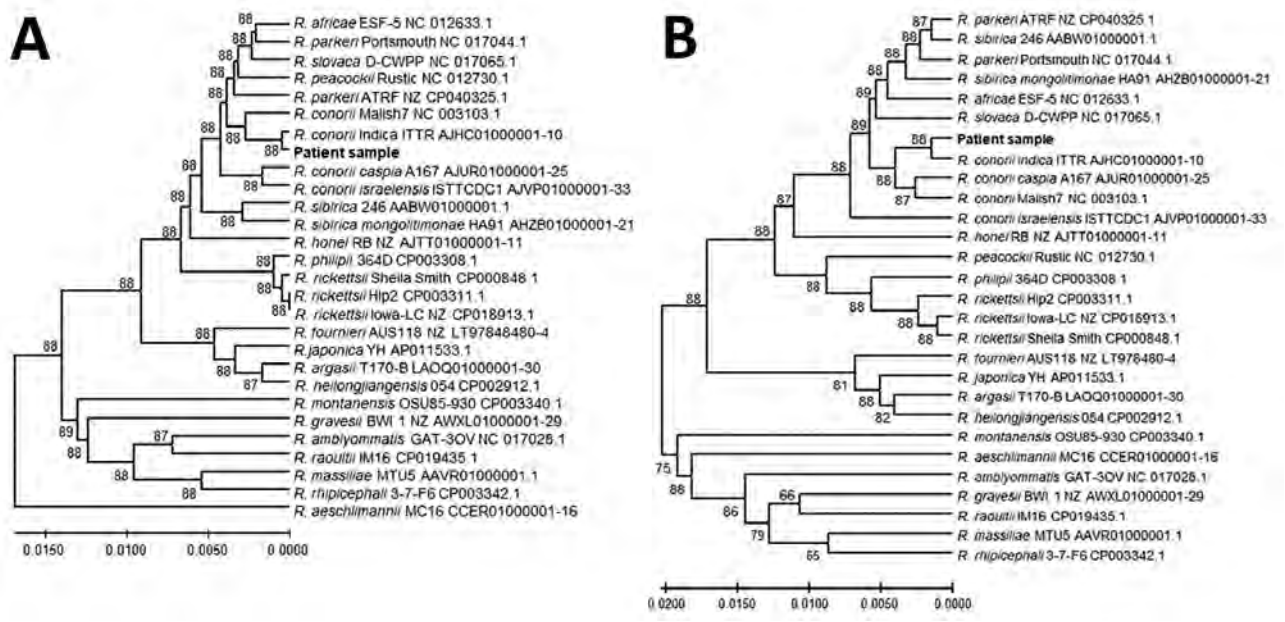

Figure 2. Genetic relationships of the spotted fever group rickettsia detected in blood of patient 1 in study of confirmation of *Rickettsia conorii* subspecies *indica* infection by next-generation sequencing, Shandong, China. This analysis used concatenated sequences from 27 spotted fever rickettsial genomes homologous to the patient sequences (shown in bold text). A) Analysis of 1,379 positions in the tRNA-associated sequences; B) analysis of 1,519 positions in the protein gene–associated sequences. Each tree was constructed upon concatenation of 6 different genome sites (Appendix Table 2, https://wwwnc.cdc.gov/EID/article/27/10/20-4764-App1.pdf); the consensus of reads from sites with overlapping reads was used. The evolutionary relationships were inferred by using UPGMA implemented in MEGA X (*15*). The optimal trees are shown. The percentage of replicate trees in which the taxa clustered together in the bootstrap test (500 replicates) are shown next to the branches. The evolutionary distances computed by using the Kimura 2-parameter method are in the units of the number of base substitutions per site. The proportion of sites where ≥1 unambiguous base is present in ≥1 sequence for each descendent clade is shown next each internal node in the tree. All ambiguous positions were removed for each sequence pair (pairwise deletion option). Scale bars indicate the percentage of nucleotide variation between the sequences.

R. conorii is divided taxonomically into 4 subspecies: *R. conorii conorii*, *R. conorii caspia*, *R. conorii israelensis*, and *R. conorii indica* (*6*). The members of this group exhibit substantial genome sequence similarity and shared antigenic makeup; however, the diseases they cause might be distinguished by specific clinical manifestations, rates of illness or death, and the areas of their endemicity and predominant tick vectors (*6*). PCR-confirmed clinical cases caused by ITTR have been diagnosed in India (*7*), Sicily (*8*) and Xinjiang Uygur Autonomous Region, China (GenBank accession nos. MG190327–9). Well-documented entomologic surveys indicate a broader area of circulation of this etiologic agent, extending beyond India and Pakistan (*9*) to Laos (*10*) and western provinces of China (*11*,*12*). In those areas, ITTR is associated either with *Rhipicephalus turanicus* (sheep tick) or *Rh. sanguineus* (brown dog tick) collected from pet dogs (*12*,*13*), suggesting a high probability of human exposure, given the proximity of these animals to human habitats. Our findings indicate that circulation of ITTR in Shandong Province and transmission to humans occurs in rural mountainous areas where the presence of both tick species has been documented (*3*,*14*). These findings suggest transmission of 1 or several SFGRs to humans might occur across China, thus requiring additional diagnostic and surveillance efforts that could lead to improved identification and management of patients with these infections.

Acknowledgments

We thank National Engineering Research Center for Beijing Biochip Technology for technical support.

About the Author

Dr. Xu is an infectious disease doctor in Qilu Hospital of Shandong University. Her research interests include early detection and differential diagnosis of diseases with febrile syndrome. Dr. Gai is working to explore novel pathogen detection methods and products based on NGS technology. He is interested in improving application of next-generation sequencing for routine clinical diagnostics.

References

1. Chen R, Kou Z, Xu L, Cao J, Liu Z, Wen X, et al. Analysis of epidemiological characteristics of four natural-focal diseases in Shandong Province, China in 2009–2017: a descriptive analysis. PLoS One. 2019;14:e0221677. https://doi.org/10.1371/journal.pone.0221677
2. Qin XR, Han HJ, Han FJ, Zhao FM, Zhang ZT, Xue ZF, et al. *Rickettsia japonica* and novel *Rickettsia* species in ticks, China. Emerg Infect Dis. 2019;25:992–5. https://doi.org/10.3201/eid2505.171745
3. Zhang R, Zhao A, Wang X, Zhang Z. Diversity of tick species on domestic animals in Shandong Province, China, using DNA barcoding. Exp Appl Acarol. 2017;73:79–89. https://doi.org/10.1007/s10493-017-0161-7
4. Fang LQ, Liu K, Li XL, Liang S, Yang Y, Yao HW, et al. Emerging tick-borne infections in mainland China: an increasing public health threat. Lancet Infect Dis. 2015;15:1467–79. https://doi.org/10.1016/S1473-3099(15)00177-2
5. Schlaberg R, Chiu CY, Miller S, Procop GW, Weinstock G; Professional Practice Committee and Committee on Laboratory Practices of the American Society for Microbiology; Microbiology Resource Committee of the College of American Pathologists. Validation of metagenomic next-generation sequencing tests for universal pathogen detection. Arch Pathol Lab Med. 2017;141:776–86. https://doi.org/10.5858/arpa.2016-0539-RA
6. Zhu Y, Fournier PE, Eremeeva M, Raoult D. Proposal to create subspecies of *Rickettsia conorii* based on multi-locus sequence typing and an emended description of *Rickettsia conorii*. BMC Microbiol. 2005;5:11. https://doi.org/10.1186/1471-2180-5-11
7. Biswal M, Zaman K, Suri V, Gopi S, Kumar A, Gopi T, et al. Molecular confirmation & characterization of *Rickettsia conorii* in north India: a report of three cases. Indian J Med Res. 2020;151:59–64. https://doi.org/10.4103/ijmr.IJMR_92_18
8. Torina A, Fernández de Mera IG, Alongi A, Mangold AJ, Blanda V, Scarlata F, et al. *Rickettsia conorii* Indian tick typhus strain and *R. slovaca* in humans, Sicily. Emerg Infect Dis. 2012;18:1008–10. https://doi.org/10.3201/eid1806.110966
9. Ghafar A, Khan A, Cabezas-Cruz A, Gauci CG, Niaz S, Ayaz S, et al. An assessment of the molecular diversity of ticks and tick-borne microorganisms of small ruminants in Pakistan. Microorganisms. 2020;8:E1428. https://doi.org/10.3390/microorganisms8091428
10. Phongmany S, Rolain JM, Phetsouvanh R, Blacksell SD, Soukkhaseum V, Rasachack B, et al. Rickettsial infections and fever, Vientiane, Laos. Emerg Infect Dis. 2006;12:256–62. https://doi.org/10.3201/eid1202.050900
11. Guo LP, Jiang SH, Liu D, Wang SW, Chen CF, Wang YZ. Emerging spotted fever group rickettsiae in ticks, northwestern China. Ticks Tick Borne Dis. 2016;7:1146–50. https://doi.org/10.1016/j.ttbdis.2016.08.006
12. Song S, Chen C, Yang M, Zhao S, Wang B, Hornok S, et al. Diversity of *Rickettsia* species in border regions of northwestern China. Parasit Vectors. 2018;11:634. https://doi.org/10.1186/s13071-018-3233-6
13. Hazihan W, Dong Z, Guo L, Rizabek K, Askar D, Gulzhan K, et al. Molecular detection of spotted fever group rickettsiae in ticks parasitizing pet dogs in Shihezi City, northwestern China. Exp Appl Acarol. 2019;77:73–81. https://doi.org/10.1007/s10493-018-00337-1
14. Zhang G, Zheng D, Tian Y, Li S. A dataset of distribution and diversity of ticks in China. Sci Data. 2019;6:105. https://doi.org/10.1038/s41597-019-0115-5
15. Kumar S, Stecher G, Li M, Knyaz C, Tamura K. MEGA X: Molecular Evolutionary Genetics Analysis across computing platforms. Mol Biol Evol. 2018;35:1547–9. https://doi.org/10.1093/molbev/msy096

Address for correspondence: Gang Wang, Department of Infectious Diseases, Qilu Hospital of Shandong University, 107 Wenhua Xilu, Jinan, Shandong, 250012, China; email: wangg1975@hotmail.com; Marina Eremeeva, Jiann-Ping Hsu College of Public Health, Georgia Southern University, 501 Forest Dr, Statesboro, GA 30458, USA; email: meremeeva@georgiasouthern.edu

Rapid Increase in Lymphogranuloma Venereum among HIV-Negative Men Who Have Sex with Men, England, 2019

Mateo Prochazka, Hannah Charles, Hester Allen, Michelle Cole, Gwenda Hughes, Katy Sinka

Incidence of lymphogranuloma venereum increased in England during 2018–2019, after a period of decline. Our retrospective analysis of national surveillance data identified a rapid increase in diagnoses among HIV-negative men who have sex with men. These findings indicate a need for sustained surveillance and targeted public health action.

Lymphogranuloma venereum (LGV) is an invasive form of *Chlamydia trachomatis* infection. In high-income countries, LGV is concentrated among gay, bisexual, and other men who have sex with men (MSM) (*1*). Although LGM was initially characterized as affecting predominantly MSM living with HIV who have symptomatic proctitis (*2*,*3*), recent evidence suggests considerable underestimation of the actual extent of LGV among MSM in Europe because of insufficient testing of asymptomatic persons (*4*). Changes to UK guidelines (*5*) and testing practices of several large London clinics have led to expanded testing in MSM regardless of HIV status, leading to increased diagnoses among HIV-negative MSM and those without symptoms of proctitis (*6*–*9*). Expanded testing may have precipitated a decline in incidence during 2016–2018 (*9*); however, 2019 saw the highest number of LGV diagnoses reported in England since routine testing began in 2004, and test positivity increased from 8.2% in 2018 to 9.0% in 2019 (*10*). In this study, we investigated the changing epidemiology of LGV among MSM in England during 2015–2019 and risk factors associated with recent cases.

The Study

We conducted a retrospective analysis of adult (≥16 years of age) MSM in England who visited sexual health service (SHS) sites during January 1, 2015–December 31, 2019. We obtained data from the Genitourinary Medicine Clinic Activity Dataset Sexually Transmitted Infection (STI) Surveillance System, which has recorded LGV diagnoses, obtained through multiplex reverse transcription PCR (*4*), since 2011. We included all SHS site visits by men who self-reported as MSM in England during 2015–2019. We cleaned and deduplicated data according to a routine practice described previously (*11*). We described the number of annual LGV diagnoses during 2015–2019 by age group, race (White [e.g., White British, White Irish, or White other background] and non-White), place of residence (London or rest of England), region of birth (United Kingdom, Europe, Asia, Oceania, Latin America and the Caribbean [LAC], North America, and Africa), history of a bacterial STI in the previous year (defined as having a recorded diagnoses of chlamydia, gonorrhea, or syphilis in the 365 days before attendance), and HIV status at time of LGV diagnosis. We used quarterly data on LGV diagnoses stratified by HIV status to examine changes over time in the proportion of diagnoses that were made among MSM who are HIV-negative or with unknown HIV status. We used generalized linear models with logarithmic function, Poisson distribution, and robust variances to identify the changes in risk for LGV in 2019 by quarter. We included covariates in the model if they showed strong association with an LGV diagnosis in the bivariate analyses ($p<0.05$). We adjusted the final model for HIV status, history of a previous bacterial STI, region of birth, and age group. We performed all data analyses using Stata 15.1 (https://www.stata.com).

Public Health England collects pseudonymized, electronic data on all STI tests and diagnoses from all commissioned SHS sites in England (*11*). Public

Author affiliation: Public Health England, London, UK

DOI: https://doi.org/10.3201/eid2710.210309

Health England has approval to handle data obtained by the Genitourinary Medicine Clinic Activity Dataset STI Surveillance System under Regulation 3 of the Health Service (Control of Patient Information) Regulations 2002 (https://www.gov.uk/government/publications/hiv-and-sti-data-sharing-policy).

Of 2,116,345 SHS visits by MSM during 2015–2019, we identified 3,461 diagnoses of LGV (Table 1). The highest number of LGV diagnoses was recorded in 2019 (n = 1,018); this increase was mainly attributed to increases in diagnoses in the third and fourth quarter of the year (Figure 1). The proportion of diagnoses among MSM who are HIV-negative or with unknown HIV status increased from 31.4% in 2015 to 58.4% in 2019 (Table 1). In 2019, most LGV diagnoses in MSM were among White MSM (72.7%) and MSM residing in London (79.1%). A total of 614 (60.3%) LGV diagnoses in 2019 were made among those who had a bacterial STI diagnosis in the previous year (Table 1).

Our regression analyses included 526,102 visits and 1,018 LGV diagnoses among MSM in England in 2019 (Table 2). Compared with quarter 1 of 2019, the risk for having LGV diagnosed was 73% higher in quarter 3 and 66% higher in quarter 4. Living with HIV, residing in London, and having a previous bacterial STI were strongly associated with an LGV diagnosis in the crude and adjusted models (Table 2). Being born in LAC or in Europe outside of the UK were also associated with increased risk for LGV (Figure 2).

Conclusions

We show that a rapid increase occurred in LGV diagnoses in England in 2019, particularly affecting MSM who are HIV-negative or with unknown HIV status, such that nearly 60% of all LGV diagnoses are now in this group. This trend represents a major shift in the epidemiology of LGV; infection was previously associated with MSM living with HIV (*2*). However, having LGV diagnosed continues to be associated with living with HIV, as well as having a previous STI diagnosis, residing in London, and being born in LAC or Europe outside the United Kingdom.

An earlier decline in LGV diagnoses (*9*) has been attributed to revisions to LGV testing guidelines that led to expanded testing (*5*,*12*). However, because no revisions have been made since 2015, changes to testing practice are unlikely to explain the recent increase, which is concurrent with increases in test positivity (*10*). Of note, use of HIV preexposure prophylaxis (PrEP) in England may have contributed to increased

Table 1. Characteristics of men who have sex with men who had lymphogranuloma venereum diagnosed, England, 2015–2019*

Characteristic	No. (%) patients				
	2015	2016	2017	2018	2019
Total no. patients	663	620	505	655	1,018
Age group, y					
16–24	45 (6.8)	31 (5.0)	40 (7.9)	27 (4.1)	81 (8.0)
25–34	250 (37.7)	234 (37.7)	166 (32.9)	243 (37.1)	377 (37.0)
35–44	229 (34.5)	208 (33.6)	141 (27.9)	219 (33.4)	301 (29.6)
45–54	103 (15.5)	115 (18.6)	124 (24.6)	122 (18.6)	180 (17.7)
55–64	26 (3.9)	24 (3.9)	25 (5.0)	32 (4.9)	68 (6.7)
≥65	4 (0.6)	5 (0.8)	5 (1.0)	11 (1.7)	7 (0.7)
Unknown	6 (0.9)	3 (0.5)	4 (0.8)	1 (0.2)	4 (0.4)
Residence					
London	512 (77.2)	469 (75.7)	362 (71.7)	507 (77.4)	806 (79.1)
Rest of England	151 (22.8)	151 (24.4)	143 (28.3)	148 (22.6)	212 (20.8)
Race					
White	499 (75.3)	479 (77.3)	383 (75.8)	485 (74.0)	740 (72.7)
Non-White	124 (18.7)	121 (19.5)	99 (19.6)	125 (19.1)	208 (20.4)
Unknown	40 (6.0)	20 (3.2)	23 (4.6)	45 (6.9)	70 (6.9)
Region of birth					
United Kingdom	333 (50.2)	317 (51.1)	248 (49.1)	300 (45.8)	443 (43.5)
Europe	159 (24.0)	139 (22.4)	112 (22.2)	172 (26.3)	256 (25.2)
Asia	38 (5.7)	33 (5.3)	25 (5.0)	38 (5.8)	50 (4.9)
Oceania	10 (1.5)	13 (2.1)	7 (1.4)	18 (2.8)	28 (2.8)
Latin America and Caribbean	51 (7.7)	41 (6.6)	45 (8.9)	44 (6.7)	111 (10.9)
Northern America	9 (1.4)	7 (1.1)	22 (4.4)	18 (2.8)	18 (1.8)
Africa	14 (2.1)	23 (3.7)	13 (2.6)	25 (3.8)	31 (3.1)
Unknown	49 (7.4)	47 (7.6)	33 (6.5)	40 (6.1)	81 (8.0)
Bacterial STI in previous year					
Yes	310 (46.8)	276 (44.5)	217 (43.0)	356 (54.4)	614 (60.3)
No	353 (53.2)	344 (55.5)	288 (57.0)	299 (45.7)	404 (39.7)
HIV status					
Living with HIV	455 (68.6)	420 (67.7)	299 (59.2)	302 (46.1)	424 (41.7)
Negative or unknown status	208 (31.4)	200 (32.7)	206 (40.8)	353 (53.9)	594 (58.4)

*STI, sexually transmitted infection.

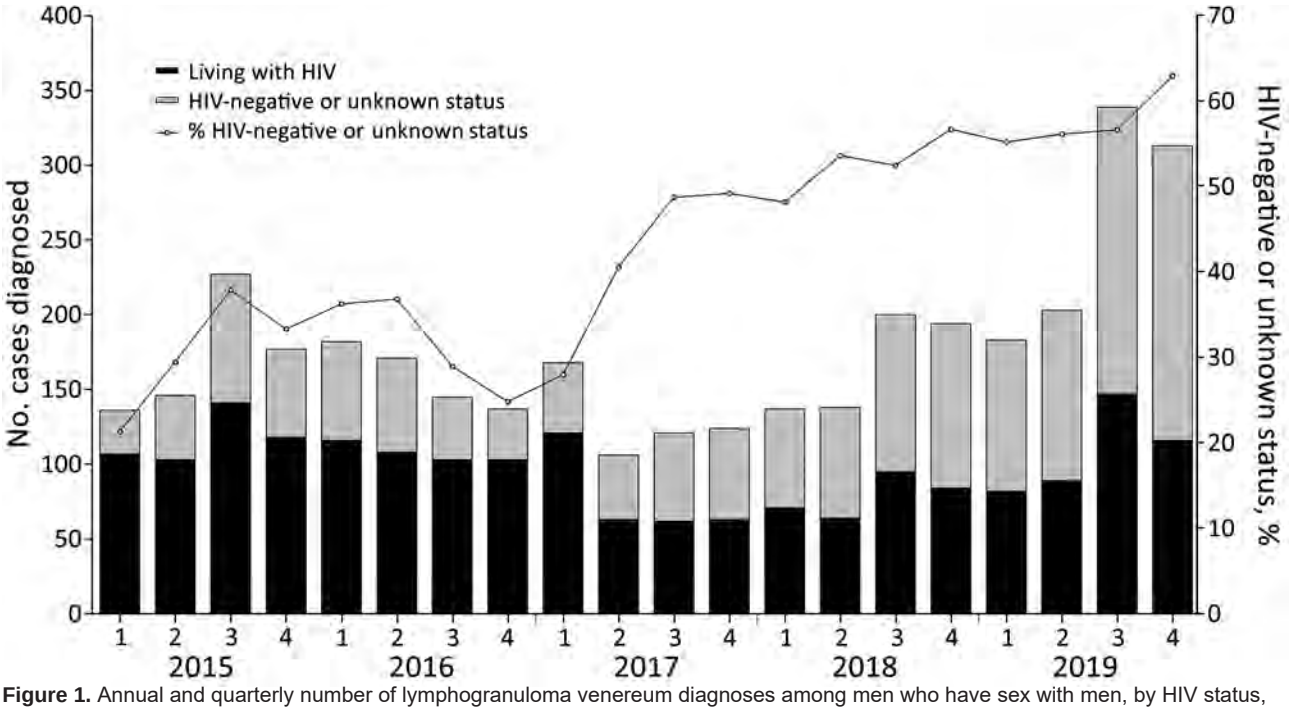

Figure 1. Annual and quarterly number of lymphogranuloma venereum diagnoses among men who have sex with men, by HIV status, England, 2015–2019.

testing for *C. trachomatis* and subsequent detection of LGV. Increased access to HIV prevention, including PrEP, in HIV-negative MSM engaging in high-risk sexual activities may have facilitated the change in the epidemiology of LGV and led to the observed increase in incidence among this group (*13*); the

Table 2. Crude and adjusted incidence rate ratios for lymphogranuloma venereum among men who have sex with men, England, 2019*

Characteristic	Crude incidence rate ratio (95% CI)	Adjusted† incidence rate ratio (95% CI)
Year		
Quarter 1	Referent	Referent
Quarter 2	1.10 (0.90–1.35)	1.13 (0.92–1.40)
Quarter 3	1.68 (1.40–2.02)	1.73 (1.43–2.10)
Quarter 4	1.49 (1.24–1.80)	1.66 (1.36–2.01)
HIV		
Negative or unknown status	Referent	Referent
Living with HIV	2.55 (2.26–2.90)	2.23 (1.93–2.57)
Bacterial STI in previous year		
No	Referent	Referent
Yes	4.01 (3.54–4.55)	3.17 (2.77–3.63)
Residence		
Rest of England	Referent	Referent
London	4.28 (3.68–4.98)	3.62 (3.06–4.28)
Region of birth		
United Kingdom	Referent	Referent
Europe	2.42 (2.07–2.82)	1.30 (1.10–1.53)
Asia	1.27 (0.95–1.70)	0.82 (0.61–1.10)
Oceania	2.96 (2.02–4.33)	1.44 (0.98–2.12)
Latin America and Caribbean	3.78 (3.07–4.65)	1.59 (1.27–1.98)
North America	1.89 (1.18–3.02)	1.09 (0.68–1.75)
Africa	1.60 (1.11–2.30)	0.90 (0.62–1.30)
Age group, y		
16–24	Referent	Referent
25–34	2.16 (1.70–2.75)	1.40 (1.09–1.81)
35–44	2.67 (2.09–3.42)	1.49 (1.14–1.94)
45–54	2.48 (1.91–3.22)	1.47 (1.10–1.96)
55–64	2.00 (1.45–2.76)	1.60 (1.13–2.26)
≥65	0.58 (0.27–1.25)	0.55 (0.23–1.28)

*Ratios determined by using generalized linear models using a logarithmic linking function and Poisson distribution with robust variances.
†Adjusted for all the covariates shown in the table.

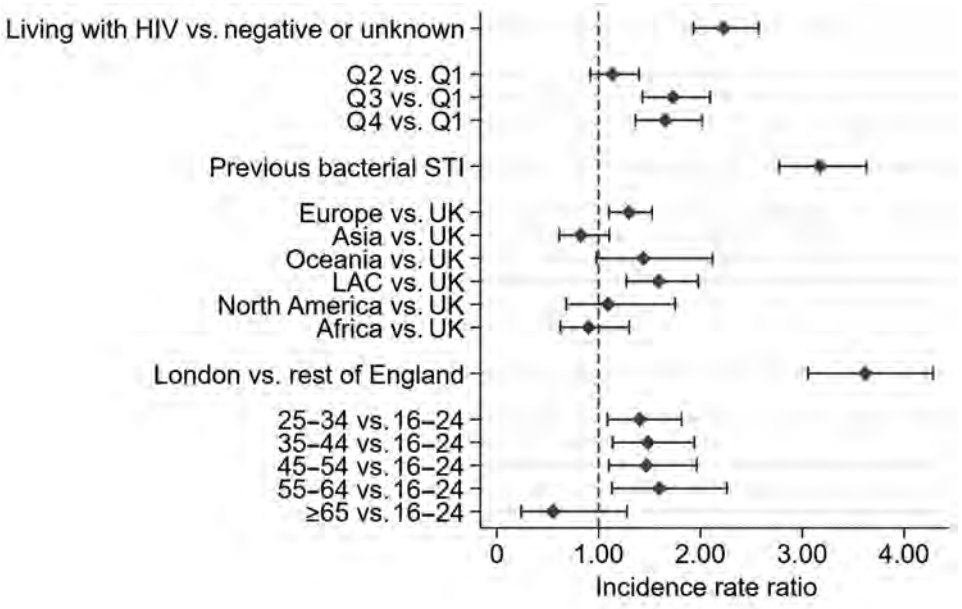

Figure 2. Adjusted incidence rate ratios for lymphogranuloma venereum among men who have sex with men, England, 2019. Diamonds indicate effect estimates (incidence rate ratio); error bars indicate 95% CIs for those estimates. LAC, Latin America and the Caribbean; Q, quarter; STI, sexually transmitted infection; UK, United Kingdom.

association with previous STI diagnosis further supports this hypothesis. Further investigation will be needed to understand the impact of HIV prevention on transmission of bacterial STIs. However, the increasing proportion of LGV diagnoses among HIV-negative MSM during 2017–2019 is in line with reports from other countries in Europe (*6*,*8*,*14*,*15*).

The first limitation of this study is that unmeasured behavioral covariates (e.g., number of partners, PrEP use, drug use, group sex, and venue-based activities) were not available. Inclusion of behavioral covariates in routine STI surveillance in England is underway and will be examined in future iterations of these analyses. Second, the risk among some groups, such as those not born in the United Kingdom, could be overestimated because of differing patterns of healthcare access and barriers to access.

In summary, we report a steep increase in the number of LGV diagnoses identified in SHS sites after a period of decline, which indicates the need for sustained surveillance and public health action. Our findings indicate that the epidemiology of LGV has changed, and an increased number of diagnoses are occurring among MSM who are HIV-negative or with unknown HIV status, highlighting the need to integrate health promotion and increase LGV testing within HIV prevention delivery. In addition, increased LGV risk among MSM born in LAC and in countries in Europe that are outside the United Kingdom indicates the need for increased accessibility of health promotion materials and wider engagement with these communities.

About the Author

Dr. Prochazka is a medical doctor and epidemiologist focused on control of infectious diseases. He is a consultant epidemiology scientist supporting STI and COVID-19 surveillance at Public Health England.

References

1. Childs T, Simms I, Alexander S, Eastick K, Hughes G, Field N. Rapid increase in lymphogranuloma venereum in men who have sex with men, United Kingdom, 2003 to September 2015. Euro Surveill. 2015;20:30076. https://doi.org/10.2807/1560-7917.ES.2015.20.48.30076
2. Hughes G, Alexander S, Simms I, Conti S, Ward H, Powers C, et al.; LGV Incident Group. Lymphogranuloma venereum diagnoses among men who have sex with men in the U.K.: interpreting a cross-sectional study using an epidemic phase-specific framework. Sex Transm Infect. 2013;89:542–7. https://doi.org/10.1136/sextrans-2013-051051
3. Saxon C, Hughes G, Ison C; UK LGV Case-Finding Group. Asymptomatic lymphogranuloma venereum in men who have sex with men, United Kingdom. Emerg Infect Dis. 2016;22:112–6. https://doi.org/10.3201/EID2201.141867
4. Cole MJ, Field N, Pitt R, Amato-Gauci AJ, Begovac J, French PD, et al. Substantial underdiagnosis of lymphogranuloma venereum in men who have sex with men in Europe: preliminary findings from a multicentre surveillance pilot. Sex Transm Infect. 2020;96:137–42. https://doi.org/10.1136/sextrans-2019-053972
5. Nwokolo NC, Dragovic B, Patel S, Tong CY, Barker G, Radcliffe K. 2015 UK national guideline for the management of infection with *Chlamydia trachomatis*. Int J STD AIDS. 2016;27:251–67. https://doi.org/10.1177/0956462415615443
6. van Aar F, Kroone MM, de Vries HJ, Götz HM, van Benthem BH. Increasing trends of lymphogranuloma venereum among HIV-negative and asymptomatic men who have sex with men, the Netherlands, 2011 to 2017. Euro Surveill. 2020;25. https://doi.org/10.2807/1560-7917.ES.2020.25.14.1900377

7. Peuchant O, Touati A, Laurier-Nadalié C, Hénin N, Cazanave C, Bébéar C, et al. Prevalence of lymphogranuloma venereum among anorectal *Chlamydia trachomatis*-positive MSM using pre-exposure prophylaxis for HIV. Sex Transm Infect. 2020;96:615–7. https://doi.org/10.1136/sextrans-2019-054346
8. De Baetselier I, Tsoumanis A, Verbrugge R, De Deken B, Smet H, Abdellati S, et al. Lymphogranuloma venereum is on the rise in Belgium among HIV negative men who have sex with men: surveillance data from 2011 until the end of June 2017. BMC Infect Dis. 2018;18:689. https://doi.org/10.1186/s12879-018-3600-0
9. Allen H, Pitt R, Bardsley M, Smolarchuk C, Sullivan A, Mohammed H, et al. Investigating the decline in lymphogranuloma venereum diagnoses in men who have sex with men in the United Kingdom since 2016: an analysis of surveillance data. Sex Health. 2020;17:344–51. https://doi.org/10.1071/SH20001
10. Charles H, Prochazka M, Sinka K. Trends of lymphogranuloma venereum in England: 2019. Health Protection Report. 2020;14 [cited 2021 Feb 9]. https://assets.publishing.service.gov.uk/government/uploads/system/uploads/attachment_data/file/942751/hpr2320_LGV-10.pdf
11. Public Health England. GUMCAD STI Surveillance System: data specification and technical guidance. 2020 Apr [cited 2021 Feb 9]. https://assets.publishing.service.gov.uk/government/uploads/system/uploads/attachment_data/file/879785/GUMCAD_Data_Specification_and_Technical_Guidance.pdf
12. White J, O'Farrell N, Daniels D; British Association for Sexual Health and HIV. 2013 UK national guideline for the management of lymphogranuloma venereum. Int J STD AIDS. 2013;24:593–601. https://doi.org/10.1177/0956462413482811
13. Gafos M, Horne R, Nutland W, Bell G, Rae C, Wayal S, et al. The context of sexual risk behaviour among men who have sex with men seeking PrEP, and the impact of PrEP on sexual behaviour. AIDS Behav. 2019;23:1708–20. https://doi.org/10.1007/s10461-018-2300-5
14. Marangoni A, Foschi C, Tartari F, Gaspari V, Re MC. Lymphogranuloma venereum genovariants in men having sex with men in Italy. Sex Transm Infect. Sex Transm Infect. 2020 Oct 26 [Epub ahead of print]. https://doi.org/10.1136/sextrans-2020-054700
15. Martínez-García L, Rodríguez-Domínguez M, Lejarraga C, Rodríguez-Jiménez MC, González-Alba JM, Puerta T, et al. The silent epidemic of lymphogranuloma venereum inside the COVID-19 pandemic in Madrid, Spain, March 2020 to February 2021. Euro Surveill. 2021;26:2100422. https://doi.org/10.2807/1560-7917.ES.2021.26.18.2100422

Address for corresponding: Hannah Charles, Public Health England, 61 Colindale Ave, London, NW9 5EQ, UK; email hannah.charles@phe.gov.uk

etymologia revisited

Originally published in June 2019

***Neospora caninum* [ne-os' pə-rə ca-nin' um]**

From the *neo-* (Latin, "new") + *spora* (Greek, "seed") and *canis* (Latin, "dog"), *Neospora caninum* is a sporozoan parasite that was first described in 1984. It is a major pathogen of cattle and dogs but can also infect horses, goats, sheep, and deer. Antibodies to *N. caninum* have been found in humans, predominantly in those with HIV infection, although the role of this parasite in causing or exacerbating illness is unclear.

Sources:

1. Bjerkås I, Mohn SF, Presthus J. Unidentified cyst-forming sporozoon causing encephalomyelitis and myositis in dogs. Z Parasitenkd. 1984;70:271–4. http://dx.doi.org/10.1007/BF00942230
2. Dubey JP. Review of *Neospora caninum* and neosporosis in animals. Korean J Parasitol. 2003; 41:1–16. http://dx.doi.org/10.3347/kjp.2003.41.1.1
3. Lobato J, Silva DA, Mineo TW, Amaral JD, Segundo GR, Costa-Cruz JM, et al. Detection of immunoglobulin G antibodies to *Neospora caninum* in humans: high seropositivity rates in patients who are infected by human immunodeficiency virus or have neurological disorders. Clin Vaccine Immunol. 2006;13:84–9. http://dx.doi.org/10.1128/CVI.13.1.84-89.2006

https://wwwnc.cdc.gov/eid/article/25/6/et-2506_article

Natural *Plasmodium inui* Infections in Humans and *Anopheles cracens* Mosquito, Malaysia

Jonathan W.K. Liew, Fatma D. Mohd Bukhari, Nantha Kumar Jeyaprakasam, Wei Kit Phang, Indra Vythilingam, Yee Ling Lau

We detected 2 natural, asymptomatic *Plasmodium inui* monoinfections in humans in Malaysia by using nested PCR on concentrated high-volume blood samples. We found a *P. inui*–positive *Anopheles cracens* mosquito in the same site as the human infections. Investigators should use ultrasensitive detection methods to identify simian malaria parasite transmission in humans.

Zoonotic transmission of simian malaria parasites to humans have been occurring in Southeast Asia and South America. Among the 3 simian malaria parasites in Southeast Asia experimentally shown to infect humans (*1*), *Plasmodium knowlesi*, *P. cynomolgi*, and *P. inui*, only *P. knowlesi* and *P. cynomolgi* have been reported in cases of natural infection (*2*). We report 2 natural, asymptomatic *P. inui* human infections detected by using nested PCR (nPCR) on concentrated high-volume blood.

The Study

We conducted an epidemiologic and entomological study at a campsite in Kem Sri Gading, Pahang, Malaysia (3°45′46.24″N, 102°34′20.32″E), because of frequent reports of human *P. knowlesi* infections acquired from this area. Kem Sri Gading is a receptive area, a location in which the ecosystem permits malaria transmission because vector and reservoir host populations both inhabit it.

On March 2, 2020, we obtained ≤3 mL of venous blood from 71 persons at the camp who provided consent. Participants had undergone training in the forest at Kem Sri Gading during January 27–28, 2020. The Medical Research and Ethics Committee, Ministry of Health Malaysia, approved this study (approval no. NMRR-15-672-23975 for the human study and approval no. NMRR-19-962-47606 for the mosquito study).

The 2 case-patients we report, PMAR0041, a 20-year-old woman, and PMAR0052, a 19-year-old woman, had no previous history of malaria. Before our study, PMAR0041 was in a nonreceptive city in Selangor 1–2 weeks before training at the camp; PMAR0052 regularly entered forested areas ≥2 times per month. During January 29–March 2, 2020, neither case-patient visited any potentially receptive areas. Both persons reported they were healthy before, during, and after blood collection.

Using the amount of DNA equivalent to 500 μL of whole blood (*3*), we detected *Plasmodium* in the 2 cases in separate nPCR assays (Appendix, https://wwwnc.cdc.gov/EID/article/27/10/21-0412-App1.pdf). We used primers targeting both the asexual and sexual 18S rRNA genes of *Plasmodium* (*4*). Sequence analysis of the cloned genus PCR products confirmed *P. inui* (Table). We performed species-specific nPCR assays to detect 5 known human malaria parasites, including *P. knowlesi*, and to detect *P. cynomolgi* and *P. inui*, by using previously published primers (*4*–*6*). However, the species-specific PCR amplification demonstrated spurious results; we were unable to produce consistent results over repeated tests. Thus, *P. inui* was detected only in case-patient PMAR0041 (Figure 1) because the protocol produced insufficient DNA, which hampered further analyses. However, we found likely trophozoites in thick blood smears of each case during 2 hours of observation (Figure 2).

On October 9, 2020, we obtained a second blood sample from case-patient PMAR0041; case-patient PMAR0052 did not consent to a second blood collection. Between the first and follow-up blood collections, PMAR0041 did not travel to any receptive areas. We did not detect any *Plasmodium* DNA in the second blood sample from PMAR0041 after repeated tests.

Authors affiliation: Universiti Malaya, Kuala Lumpur, Malaysia

DOI: https://doi.org/10.3201/eid2710.210412

Table. Nucleotide BLAST results of the PCR products sequenced in a study of natural transmission of *Plasmodium inui* in 2 humans and in *Anopheles cracens* mosquitoes, Malaysia*

Sequence source and length, bp (GenBank accession no.)	Description of sequence (GenBank accession no.)	% Identity	% Query cover
Patient PMAR0041, 234 (MW555281)	*Plasmodium inui* asexual type 18S rRNA, Celebes (AB287276)	99.57†	100
	P. inui asexual type, 18S rRNA, Thailand (EU400385)	99.57	100
	P. inui asexual type, 18S rRNA, Taiwan I (FN430724)	99.57	100
Patient PMAR0052, 243 (MW555282)	*P. inui* sexual type, 18S rRNA, Taiwan I (FN429982)	99.59†	100
	P. inui 18S rRNA, *Anopheles latens* mosquito, Sarawak (MN535358)	99.18‡	100
	P. inui sexual type, 18S rRNA from monkey (FJ619103)	99.18	100
	P. inui 18S rRNA, wild monkey, Thailand (EU400386)	99.18	100
An. cracens, 986 (MW555286)	*P. inui* asexual type, 18S rRNA, Celebes (AB287276)	99.90†	100
	P. inui 18S rRNA, *An. latens*, Sarawak (MN535320)	99.80‡	100
	P. inui asexual type 18S rRNA, wild monkey, Thailand (EU400385)	99.70	100
	P. inui asexual type 18S rRNA, South China (HM032051)	99.49	100
	P. inui asexual type 18S rRNA, Taiwan II (FN430725)	99.49	100

*BLAST, https://blast.ncbi.nlm.nih.gov. bp, base pair.
†This sequence had only a 1 single-nucleotide mismatch at the forward primer priming site.
‡This sequence had 2 single-nucleotide mismatches, 1 at the forward primer priming site.

We collected *Anopheles cracens*, *An. introlatus*, and *An. barbirostris* sensu lato mosquitoes at the camp by using human landing catches and Mosquito Magnet Independence Trap (Woodstream Corp., https://www.woodstream.com). *An. cracens* was the predominant mosquito species collected. Only 1 nonblood fed *An. cracens* mosquito, caught on August 24, 2020, was *Plasmodium*-positive in its head and thorax by nPCR (*4*). We found no oocysts upon dissection of the mosquito gut. We were unable to successfully dissect the salivary glands because the mosquito was dead. We used published primers (*7*) to amplify the *P. inui* 18S rRNA gene and confirmed *P. inui* by sequencing the PCR product (Table). We tested the entomological team by using the same PCR methods described for the case-patients but detected no *Plasmodium*.

Our analyses showed that the *P. inui* sequence obtained from case-patient PMAR0041 was identical to the corresponding region on the asexual type 18S rRNA sequence obtained from the *An. cracens* mosquito (Appendix Figure 2), but the *P. inui* sequence obtained from case-patient PMAR0052 was of the sexual type 18S rRNA (Table). The human *P. inui*–positive cases we detected originated from separate DNA extractions and PCR assays on different days by using dedicated benchtops for different procedures. The case-patients had the only *P. inui*–positive samples, but we identified a few *P. knowlesi*–positive samples among the 71 persons screened at the camp (Appendix Figure 1). The *An. cracens* mosquito was the only *Plasmodium*-positive mosquito we detected. We hypothesize that PMAR0041, PMAR0052, and the *Plasmodium*-positive mosquito were monoinfected

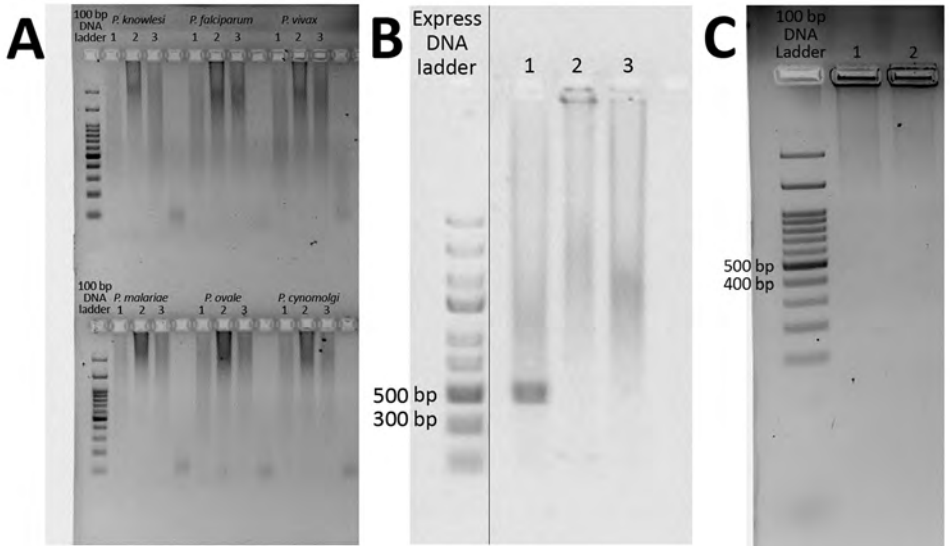

Figure 1. Species-specific nested PCR amplification products for a study of *Plasmodium inui* infections among humans, Malaysia. Samples were subjected to electrophoresis on a 1.5% agarose gel. A) Results for detection of *P. knowlesi*, *P. falciparum*, *P. vivax*, *P. malariae*, *P. ovale*, and *P. cynomolgi*. Lane 1, human case-patient PMAR0041; lane 2, human case-patient PMAR0052; lane 3, no-template control. B) Results for the detection of *P. inui* in human case-patient PMAR0041. Lane 1, case-patient PMAR0041; lane 2, negative control; lane 3, no-template control. The solid vertical line indicates these are separate parts of the same image. C) Results for the detection of *P. inui* in human case-patient PMAR0052. Lane 1, case-patient PMAR0052; lane 2, no-template control.

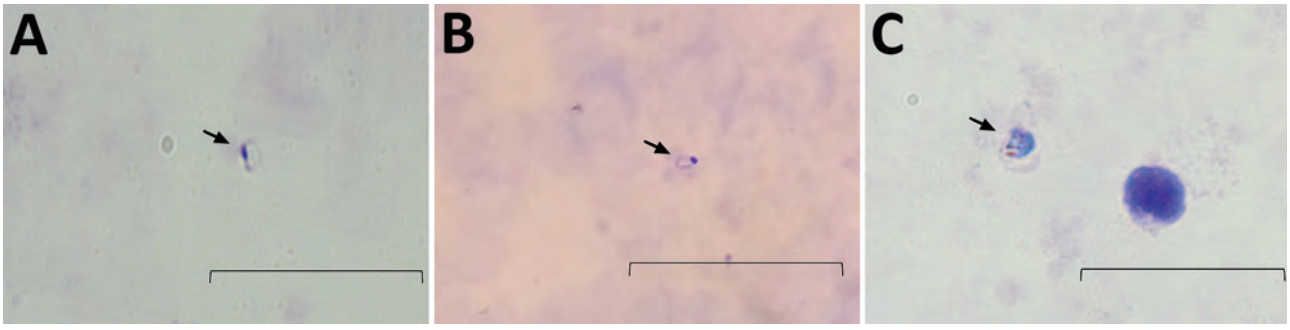

Figure 2. Micrographs of the thick blood smears showing *Plasmodium* trophozoites in 2 human cases of *Plamodium inui* infection, Malaysia. A) Smear from case-patient PMAR0041, taken by using an Olympus BX51 microscope (Olympus Corporation, https://www.olympus-lifescience.com). B) Smear from case-patient PMAR0041, taken by using Redmi Note 4 (Xiaomi Corporation, https://www.mi.com) smartphone camera. C) Smear from case-patient PMAR0052, taken by using an Olympus BX51 microscope. Arrows indicate *P. inui* trophozoites in each image. Scale bars indicate 20 μm.

with *P. inui* because we found no other *Plasmodium* species in any of them.

Conclusions

In experimentally infected humans, patent *P. inui* infections appeared ≥31 days after infectious mosquito bites (*8*). Similarly, both cases we report show a patent infection ≈30 days after alleged exposure. *P. inui* undergoes a 72-hour erythrocytic cycle, causing quartan fever (*8*). Infection by the quartan *P. inui* could be self-limiting in humans because the parasite was not detected in case-patient PMAR0041 ≈8 months after exposure. Indeed, *P. inui* infections in monkeys are usually low-grade and chronic and can be self-limiting (*9*,*10*). In addition, the *P. inui* OS strain parasite count in experimentally infected humans was <2,520/μL blood. Symptoms were mild, and parasitemia could be submicroscopic or undetectable for certain periods. Antimalarial intervention was deemed unnecessary in these experimental infections (*8*).

Natural human *P. inui* infection seems possible, but because of the very low number of parasites and sharp fluctuations between negative and moderate parasitemia by microscopy (*8*,*10*), previous studies that used less sensitive methods, including standard PCR, were not able to detect it (*11*). We show that nPCR on concentrated, high-volume blood was more sensitive at detecting low-grade infection than standard PCR (*12*), which highlights the need for ultrasensitive detection tools.

We found 2 forms of *Plasmodium* 18S rRNA genes: the asexual type, which is expressed during the parasite's asexual life cycle in the vertebrate host; and the sexual type, which is expressed during its sexual life cycle in the mosquito vector. The *Plasmodium*-genus PCR primers we used amplify asexual and sexual 18S rRNA, but the *P. inui*–specific primers only amplify the asexual type, which explains the negative results from the species-specific nPCR despite the positive amplifications in the *Plasmodium*-genus PCR. Nonetheless, successful PCR amplification is compounded by low levels of parasites and the subsequent chance effect that can lead to occasional spurious results, as we experienced.

P. inui sporozoites have been found naturally occurring in *An. cracens* mosquitoes (*2*). Other mosquito species from the Leucosphyrus group can transmit *P. inui* naturally (*2*). In addition, laboratory experiments showed *P. inui* adapted to co-indigenous *Anopheles* mosquito species (*13*).

P. inui has a wide geographic range in Asia, including southern India, Southeast Asia, and Taiwan (*13*). A surveillance study reported that the prevalence of *P. inui* among wild macaques in Pahang was 66.7% (26/39 macaques sampled); 76.9% of these infections were co-infections with other *Plasmodium* species (*14*). Given the high prevalence of *P. inui* among macaques and natural *Anopheles* mosquito vectors (*2*), humans could be exposed to *P. inui* via vectorborne transmission from infected macaques, particularly at a location where humans, macaque hosts, and mosquito vectors co-exist. Furthermore, studies report that *P. inui* often occurs in co-infections with *P. knowlesi* and *P. cynomolgi* in monkeys and mosquitoes (*2*), and that humans frequently can be exposed to a mix of non-human primate malaria sporozoites (*15*). Because human *P. inui* infections can be asymptomatic, *P. inui* could evolve to efficiently infect humans (*2*), especially considering patent human infection can be established by just a few parasites (*8*). Strains from different geographic locations might even exhibit different infection patterns. Investigators should use ultrasensitive methods for epidemiologic and entomological studies of simian malaria transmissions in Malaysia and other countries in malaria elimination efforts.

Acknowledgments

We thank the volunteers for their willingness to provide blood samples and especially thank the 2 patients for their cooperation.

This study was supported by the Long Term Research Grant Scheme awarded to Y.L.L. (grant no. LRGS/1/2018/UM/01/1/4) and I.V. (grant no. LRGS/1/2018/UM/01/1/3) by the Ministry of Higher Education Malaysia.

About the Author

Dr. Liew is a post-doctoral researcher at Universiti Malaya, Kuala Lumpur, Malaysia. His research interest is in vectorborne diseases especially malaria and dengue. His research work includes the entomological and epidemiological, as well as fundamental aspects of these diseases.

References

1. Coatney GR, Collins WE, Warren M, Contacos PG. The primate malarias. Washington DC: National Institutes of Health; 1971.
2. Jeyaprakasam NK, Liew JWK, Low VL, Wan-Sulaiman W-Y, Vythilingam I. *Plasmodium knowlesi* infecting humans in Southeast Asia: what's next? PLoS Negl Trop Dis. 2020;14:e0008900. https://doi.org/10.1371/journal.pntd.0008900
3. Imwong M, Hanchana S, Malleret B, Rénia L, Day NPJ, Dondorp A, et al. High-throughput ultrasensitive molecular techniques for quantifying low-density malaria parasitemias. J Clin Microbiol. 2014;52:3303–9. https://doi.org/10.1128/JCM.01057-14
4. Singh B, Bobogare A, Cox-Singh J, Snounou G, Abdullah MS, Rahman HA. A genus- and species-specific nested polymerase chain reaction malaria detection assay for epidemiologic studies. Am J Trop Med Hyg. 1999;60:687–92. https://doi.org/10.4269/ajtmh.1999.60.687
5. Imwong M, Tanomsing N, Pukrittayakamee S, Day NP, White NJ, Snounou G. Spurious amplification of a *Plasmodium vivax* small-subunit RNA gene by use of primers currently used to detect *P. knowlesi*. J Clin Microbiol. 2009;47:4173–5. https://doi.org/10.1128/JCM.00811-09
6. Lee KS, Divis PCS, Zakaria SK, Matusop A, Julin RA, Conway DJ, et al. *Plasmodium knowlesi*: reservoir hosts and tracking the emergence in humans and macaques. PLoS Pathog. 2011;7:e1002015. https://doi.org/10.1371/journal.ppat.1002015
7. Chua TH, Manin BO, Daim S, Vythilingam I, Drakeley C. Phylogenetic analysis of simian Plasmodium spp. infecting Anopheles balabacensis Baisas in Sabah, Malaysia. PLoS Negl Trop Dis. 2017;11:e0005991. https://doi.org/10.1371/journal.pntd.0005991
8. Coatney GR, Chin W, Contacos PG, King HK. *Plasmodium inui*, a quartan-type malaria parasite of Old World monkeys transmissible to man. J Parasitol. 1966;52:660–3. https://doi.org/10.2307/3276423
9. Garnham PCC. The mosquito transmission of *Plasmodium inui* Halberstaedter and Prowazek, and its pre-erythrocytic development in the liver of the rhesus monkey. Trans R Soc Trop Med Hyg. 1951;45:45–52. https://doi.org/10.1016/S0035-9203(51)90524-X
10. Schmidt LH, Fradkin R, Harrison J, Rossan RN, Squires W. The course of untreated *Plasmodium inui* infections in the rhesus monkey (*Macaca mulatta*). Am J Trop Med Hyg. 1980;29:158–69. https://doi.org/10.4269/ajtmh.1980.29.158
11. Siner A, Liew ST, Kadir KA, Mohamad DSA, Thomas FK, Zulkarnaen M, et al. Absence of *Plasmodium inui* and *Plasmodium cynomolgi*, but detection of *Plasmodium knowlesi* and *Plasmodium vivax* infections in asymptomatic humans in the Betong division of Sarawak, Malaysian Borneo. Malar J. 2017;16:417. https://doi.org/10.1186/s12936-017-2064-9
12. Hofmann NE, Gruenberg M, Nate E, Ura A, Rodriguez-Rodriguez D, Salib M, et al. Assessment of ultra-sensitive malaria diagnosis versus standard molecular diagnostics for malaria elimination: an in-depth molecular community cross-sectional study. Lancet Infect Dis. 2018;18:1108–16. https://doi.org/10.1016/S1473-3099(18)30411-0
13. Collins WE, Sullivan JS, Galland GG, Nace D, Williams A, Williams T, et al. Isolates of *Plasmodium inui* adapted to *Macaca mulatta* monkeys and laboratory-reared anopheline mosquitoes for experimental study. J Parasitol. 2007;93:1061–9. https://doi.org/10.1645/GE-1035R.1
14. Amir A, Shahari S, Liew JWK, de Silva JR, Khan MB, Lai MY, et al. Natural *Plasmodium* infection in wild macaques of three states in peninsular Malaysia. Acta Trop. 2020;211:105596. https://doi.org/10.1016/j.actatropica.2020.105596
15. Maeno Y, Quang NT, Culleton R, Kawai S, Masuda G, Nakazawa S, et al. Humans frequently exposed to a range of non-human primate malaria parasite species through the bites of *Anopheles dirus* mosquitoes in south-central Vietnam. Parasit Vectors. 2015;8:376. https://doi.org/10.1186/s13071-015-0995-y

Address for correspondence: Yee Ling Lau, Department of Parasitology, Faculty of Medicine, Universiti Malaya, 50603, Kuala Lumpur, Malaysia; email: lauyeeling@um.edu.my

Genetic Characterization of Seoul Virus in the Seaport of Cotonou, Benin

Guillaume Castel, Ravi Kant, Sylvestre Badou, Jonas Etougbétché, Henri-Joël Dossou, Philippe Gauthier, Gualbert Houéménou, Teemu Smura, Tarja Sironen, Gauthier Dobigny

Seoul virus is a zoonotic pathogen carried by the brown rat *Rattus norvegicus*. Information on its circulation in Africa is limited. In this study, the virus was detected in 37.5% of brown rats captured in the Autonomous Port of Cotonou, Benin. Phylogenetic analyses place this virus in Seoul virus lineage 7.

Rodents are the most diversified order of wild mammals and are also the prevailing mammal lineage associated with human-inhabited socioecosystems. In addition to their destructive behaviors, rodents are involved in maintaining, disseminating, and transmitting zoonotic pathogens, impacting both animal and human health (*1*).

Hantaviruses are transmitted to humans by inhalation of aerosols contaminated by rodent excreta, including urine, feces, and saliva. They are the causative agents of hemorrhagic fevers and are considered emerging pathogens that impact public health worldwide. Hantaviruses are enveloped with a tripartite single-stranded RNA genome of negative polarity comprising small (S), medium (M), and large (L) segments.

Author affiliations: CBGP, INRAE, CIRAD, IRD, Institut Agro, Univ Montpellier, Montpellier, France (G. Castel, S. Badou, J. Etougbétché, H.-J. Dossou, P. Gauthier, G. Dobigny); University of Helsinki, Haartmaninkatu 3, Helsinki FI-00290, Finland (R. Kant, T. Smura, T. Sironen); University of Helsinki, Agnes Sjöbergin katu 2, Helsinki FI-00790 (R. Kant, T. Sironen); Laboratoire de Recherche en Biologie Appliquée, Unité de Recherche sur les Invasions Biologiques, Ecole Polytechnique d'Abomey-Calavi, Université d'Abomey-Calavi, Cotonou, Benin (S. Badou, HJ. Dossou, J. Etougbétché, G. Houéménou); Laboratoire de Génétique Moléculaire et d'Analyse des Génomes, Faculté des Sciences et Techniques,Université d'Abomey-Calavi, Cotonou (S. Badou); Institut de Géographie, d'Aménagement du Territoire et d'Environnement, Université d'Abomey-Calavi, Cotonou (H.-J. Dossou).

DOI: https://doi.org/10.3201/eid2710.210268

Because hantaviruses are host-specific, their geographic distribution is tightly linked to that of their host. However, the emergence of hantaviruses in new geographic regions is still possible by the spread of the rodent reservoir (*2*). Transport-mediated dissemination of rodent-borne hantaviruses is of critical importance in their distribution and constitutes a critical health concern (*3*). Seoul virus (SEOV), an orthohantavirus first identified in South Korea in 1982, has had a particular impact on global human health attributable to its worldwide dispersal (*2,4*). Some outbreaks are hypothesized to be driven by the sporadic introduction of its now cosmopolitan host, the Norway or brown rat (*Rattus norvegicus*), at seaports or from pet and laboratory rats (*5,6*). Little is known concerning the circulation of SEOV in Africa, although a recent study reported its presence in southeastern Senegal (*7*). We screened rats in the Autonomous Port of Cotonou, Benin, to determine the presence of SEOV in these rodents.

The Study

We trapped rodents in the seaport of Cotonou using Sherman line capture traps and locally made wide mesh traps that were set for 3 consecutive nights in April 2018. We transported the animals to the Laboratoire de Recherche en Biologie Appliquée laboratory in closed containers and processed them the same day. We anesthetized the rodents with diethyl ether and subsequently euthanized them by cervical dislocation.

We screened blood samples from 32 brown rats and 37 house mice (*Mus musculus*) for the presence of hantavirus-reactive antibodies by using an immunofluorescence assay as previously described (*8*). A total of 12 (37.5%) rats were seropositive, and the lungs of 2 rats were confirmed positive by reverse transcription PCR as previously described (*9*). This discrepancy cannot be explained by the presence of maternal antibodies because all seropositive rats were adults except for 1 subadult. However, the difference could be because of

the limited sensitivity of the panhantavirus PCR or to a viral load decrease over time that fell below detection limits in rats that were infected several months earlier.

We treated reverse transcription PCR–positive samples with DNase I (Thermo Fisher Scientific, https://www.thermofisher.com), and purified samples with Agencourt RNA Clean XP magnetic beads (Beckman Life Sciences, https://www.beckmancoulter.com). We removed ribosomal RNA using a NEBNext rRNA depletion kit (New England BioLabs, https://www.neb.com). We prepared the sequencing library with a NEBNext Ultra II RNA library prep kit and quantified it using a NEBNext Library Quant kit for Illumina (Illumina, https://www.illumina.com). We sequenced pooled libraries on a MiSeq platform using a MiSeq v3 reagent kit with 300 bp paired-end reads. Raw sequence reads were trimmed and low-quality (quality score <15) or short (<36 nt) sequences were removed using Trimmomatic (*10*). The trimmed sequence reads were assembled against reference sequences (GenBank accession nos. NC_005237.1, NC_005236.1, NC_005238.1) using Bowtie2 algorithm (*11*) and some in-house scripts.

We deposited S, M, and L segment sequences of strain Benin1368 into GenBank (accession nos. MW561221–3) and analyzed them by using BLAST (https://blast.ncbi.nlm.nih.gov). BLAST revealed that the best matches were with SEOV strain CSG5 (accession nos. AB618112–30) from Vietnam for the S segment (97.51% nt identity) and the M segment (97.70% nt identity) and with SEOV strain Lyon/Rn/FRA/2013/LYO852 (accession no. KF387723) from France for the L segment (96.82% nt identity).

We performed phylogenetic analyses on 3 datasets composed of complete or nearly complete coding regions of S, M, and L segment sequences of SEOV from different geographic areas available in GenBank. We used sequences of Hantaan and Anjozorobe viruses as outgroups in all analyses. We performed phylogenetic analyses as previously described (*12*) using the general time-reversible plus gamma distribution plus invariant sites model (S and M segment) or the general time-reversible plus gamma distribution model (L segment).

The 3 datasets produced broadly concordant phylogenetic topologies (Figure 1, https://wwwncd.cdc.gov/EID/article/27/10/21-0268-F1.htm). All datasets grouped the SEOV strains from Cotonou within a cluster that included strains from Europe (France and Belgium) and from Southeast Asia (Indonesia, Singapore, Vietnam, and Cambodia), referred to as SEOV lineage 7 (*13*). Variants of this lineage belonged to SEOV phylogroup A; this group originated in China and subsequently spread to other parts of the world (*2*). More specifically, SEOV lineage 7 may reflect the historical connections between regions of Southeast Asia and France through critical trade routes (*14*).

From Africa, only short SEOV sequences from conserved parts of S (226 nt) and L (347 nt) segments were available from wild black rats (*R. rattus*) from Senegal (*7*). For this reason, we did not include them in our datasets using complete segments. However, phylogenetic analyses on the basis of datasets including these short sequences place them in SEOV lineage 4 (S segment) or 3 (L segment), with low branch support (Figure 2, https://wwwncd.cdc.gov/EID/article/27/10/21-0268-F2.htm). This inconsistency is potentially attributable to the short length and high conservation of these sequences; although it could indicate a distinct introduction event from Benin, this interpretation must be considered with caution because of the low level of phylogenetic information provided by these sequences. We calculated estimates of evolutionary divergence between strains from Senegal and Benin using MEGAX (http://www.megasoftware.net). Analyses showed 95.7% nt homology for the S segment and 94.8% nt homology for the L segment. Analyses showed 97.85% amino acid-level homology for the nucleocapsid protein and 100% amino acid-level homology for the RNA polymerase.

Conclusion

Because of insufficient testing for hantavirus infections and unreported mild cases (*14*), the exact circulation of hantaviruses on the continent of Africa is unknown. Whereas SEOV is not widely considered a public health issue in Africa by local health authorities, the presence of SEOV-like agents in humans and wild rats is strongly suspected in at least 17 different countries (*4*). Recent and unambiguous sequencing-based identification of SEOV in Senegal (*7*) and in Benin with our study confirms that SEOV should be anticipated as a possible cause of illness, such as hemorrhagic fever with renal syndrome. Seaports and ships have already been identified as potential entry points for hantaviruses (*2*,*15*), which is a likely cause in Africa, as our study shows. SEOV strains recovered from brown rats from the Cotonou seaport are phylogenetically similar to strains from Southeast Asia and Europe, regions where many maritime trade exchanges occur that could explain the presence of these strains in Cotonou. The accidental transportation of SEOV-carrying rats at seaports could lead to local emergence of SEOV infections among port workers. Regular sanitary control of rats within seaports could prevent rodentborne and arthropodborne pathogen dissemination through sea trade.

Acknowledgments

We thank the Autonomous Port of Cotonou authorities and staff who facilitated our access to their infrastructures. We also thank Serenal Dool for editing the manuscript.

This study was supported by the VEO European Union's Horizon 2020 (grant no. 874735), Academy of Finland (grant no. 318726), and the Jane and Aatos Erkko Foundation. Field and laboratory work was conducted under the research agreement between the Republic of Benin and the French Institute of Research for Sustainable Development (September 30, 2010) and the Scientific and Technical Cooperation Agreement (July 3, 2019) between the University of Abomey-Calavi and the Institut de Recherche et de Développement. The collection and use of tissue samples (spleen, lung, kidney, brain, dried blood spots) and genetic data was authorized under the Access and Benefit Sharing, Nagoya protocol (permit no. 608/DGEFC/DCPRNF/PF-APA/SA) (December 2019).

This study is part of a long-term partnership between Cotonou Autonomous Seaport, Port of Antwerp International, the Polytechnic School of Abomey-Calavi, the French Institute of Research for Sustainable Development, and the International Institute of Tropical Agriculture on maritime trade-associated biological invasions.

About the Author

Dr. Castel is a researcher in virology at the French National Research Institute for Agriculture, Food and Environment. His research interests include the diversity of hantaviruses and the evolutionary processes that shape it using phylogenetic and phylogeographic approaches.

References

1. Colombe S, Jancloes M, Rivière A, Bertherat E. A new approach to rodent control to better protect human health: first international meeting of experts under the auspices of WHO and the Pan American Health Organization. Weekly Epidemiological Record. 2019;–17:197–203.
2. Lin XD, Guo WP, Wang W, Zou Y, Hao ZY, Zhou DJ, et al. Migration of Norway rats resulted in the worldwide distribution of Seoul hantavirus today. J Virol. 2012;86:972–81. https://doi.org/10.1128/JVI.00725-11
3. Klempa B. Hantaviruses and climate change. Clin Microbiol Infect. 2009;15:518–23. https://doi.org/10.1111/j.1469-0691.2009.02848.x
4. Clement J, LeDuc JW, Lloyd G, Reynes JM, McElhinney L, Van Ranst M, et al. Wild rats, laboratory rats, pet rats: global Seoul hantavirus disease revisited. Viruses. 2019;11:652. https://doi.org/10.3390/v11070652
5. Childs JE, Klein SL, Glass GE. A case study of two rodent-borne viruses: not always the same old suspects. Front Ecol Evol. 2019;7:35. https://doi.org/10.3389/fevo.2019.00035
6. Dupinay T, Pounder KC, Ayral F, Laaberki MH, Marston DA, Lacôte S, et al. Detection and genetic characterization of Seoul virus from commensal brown rats in France. Virol J. 2014;11:32. https://doi.org/10.1186/1743-422X-11-32
7. Diagne MM, Dieng I, Granjon L, Lucaccioni H, Sow A, Ndiaye O, et al. Seoul orthohantavirus in wild black rats, Senegal, 2012–2013. Emerg Infect Dis. 2020;26:2460–4. https://doi.org/10.3201/eid2610.201306
8. Van Cuong N, Carrique-Mas J, Vo Be H, An NN, Tue NT, Anh NL, et al. Rodents and risk in the Mekong Delta of Vietnam: seroprevalence of selected zoonotic viruses in rodents and humans. Vector Borne Zoonotic Dis. 2015;15:65–72. https://doi.org/10.1089/vbz.2014.1603
9. Klempa B, Fichet-Calvet E, Lecompte E, Auste B, Aniskin V, Meisel H, et al. Hantavirus in African wood mouse, Guinea. Emerg Infect Dis. 2006;12:838–40. https://doi.org/10.3201/eid1205.051487
10. Bolger AM, Lohse M, Usadel B. Trimmomatic: a flexible trimmer for Illumina sequence data. Bioinformatics. 2014;30:2114–20. https://doi.org/10.1093/bioinformatics/btu170
11. Langmead B, Salzberg SL. Fast gapped-read alignment with Bowtie 2. Nat Methods. 2012;9:357–359. https://doi.org/10.1038/nmeth.1923
12. Murri S, Madrières S, Tatard C, Piry S, Benoit L, Loiseau A, et al. Detection and genetic characterization of Puumala Orthohantavirus S-segment in areas of France non-endemic for nephropathia epidemica. Pathogens. 2020;9:721. https://doi.org/10.3390/pathogens9090721
13. Ling J, Verner-Carlsson J, Eriksson P, Plyusnina A, Löhmus M, Järhult JD, et al. Genetic analyses of Seoul hantavirus genome recovered from rats (*Rattus norvegicus*) in the Netherlands unveils diverse routes of spread into Europe. J Med Virol. 2019;91:724–30. https://doi.org/10.1002/jmv.25390
14. Heyman P, Plyusnina A, Berny P, Cochez C, Artois M, Zizi M, et al. Seoul hantavirus in Europe: first demonstration of the virus genome in wild *Rattus norvegicus* captured in France. Eur J Clin Microbiol Infect Dis. 2004;23:711–7. https://doi.org/10.1007/s10096-004-1196-3
15. Lokugamage N, Kariwa H, Lokugamage K, Iwasa MA, Hagiya T, Yoshii K, et al. Epizootiological and epidemiological study of hantavirus infection in Japan. Microbiol Immunol. 2004;48:843–51. https://doi.org/10.1111/j.1348-0421.2004.tb03616.x

Address for correspondence: Gauthier Dobigny, Centre de Biologie pour la Gestion des Populations, 755, avenue du Campus Agropolis, 34988 Montferrier sur Lez, Montpellier, France; email: gauthier.dobigny@ird.fr

Therapeutic Efficacy of Human Monoclonal Antibodies against Andes Virus Infection in Syrian Hamsters

Brandi N. Williamson,[1] Joseph Prescott,[1] Jose L. Garrido, Raymond A. Alvarez, Heinz Feldmann, Maria I. Barría

Andes virus, an orthohantavirus endemic to South America, causes severe hantavirus cardiopulmonary syndrome associated with human-to-human transmission. No approved treatments or vaccines against this virus are available. We show that a combined treatment with 2 monoclonal antibodies protected Syrian hamsters when administered at midstage or late-stage disease.

Hantavirus cardiopulmonary syndrome (HCPS) is a severe disease caused by infection with pathogenic New World orthohantaviruses, including Andes virus (ANDV). ANDV is transmitted to humans via the aerosolized excrement of the rodent reservoir and vector, the *Oligoryzomys longicaudatus* long-tailed pygmy rice rat (*1*). Unlike other orthohantaviruses, ANDV has been associated with human-to-human transmission and is associated with a high case fatality rate of 35%–40% (*2*–*5*). The large 2018 ANDV outbreak in the Austral Patagonian region at Epuyén village (Chubut Province, Argentina) reemphasized the probability of person-to-person transmission, highlighting the urgent need for specific therapies and vaccines (*5*).

ANDV infection has a long incubation period of 2–3 weeks, followed by a 3- to 5-day prodrome phase characterized by fever, headache and gastrointestinal symptoms. HCPS develops over a 2–7 day period characterized by falling blood pressure, lung edema or failure, cardiac shock, and death in a substantial number of patients (*6*). As of August 2021, treatment for HCPS remains supportive, requiring interventions such as oxygenation, mechanical ventilation, extracorporeal membrane oxygenation, and fluid balancing (*6*). No licensed specific treatment options or vaccine are available. In HCPS patients, high hantavirus-specific neutralizing antibodies correlate strongly with survival, milder disease outcomes, and faster recovery (*7*,*8*). Passive transfusion of specific monoclonal antibodies (mAbs) protected animals from ANDV challenge in the lethal Syrian hamster disease model (*9*–*11*). All of these data suggest an important role for neutralizing antibodies in controlling orthohantavirus infections in vivo.

Our group has previously reported that mAbs isolated from HCPS survivors (clones JL16 and MIB22) protected hamsters from lethal ANDV challenge when mAb treatment was initiated early postinfection, suggesting potent postexposure efficacy (*11*). We sought to develop a late-stage disease treatment schedule for mAb treatment in the Syrian hamster model of ANDV disease.

The Study

The Syrian hamster model of lethal ANDV infection has been well established as the only animal model recapitulating many characteristics of HCPS (*12*,*13*). All infectious ANDV work was conducted in the Biosafety Level 4 facility at Rocky Mountain Laboratories (National Institutes for Health, National Institute of Allergy and Infectious Disease, Hamilton, MT, USA), according to standard operating protocols approved by the Institutional Biosafety Committee. All animal experiments were approved by the institutional Animal Care and Use Committee.

Author affiliations: National Institutes of Health, National Institute of Allergy and Infectious Diseases, Hamilton, Montana, USA (B.N. Williamson, J. Prescott, H. Feldmann); Robert Koch Institute, Berlin, Germany (J. Prescott); Ichor Biologics LLC, New York, New York, USA (J.L. Garrido, R.A. Alvarez); Universidad de Concepción, Concepción, Chile (J.L. Garrido, M.I. Barría); Universidad San Sebastián, Puerto Montt, Chile (M.I. Barría)

DOI: https://doi.org/10.3201/eid2710.210735

[1]These first authors contributed equally to this article.

We inoculated hamsters intranasally with 200 focus-forming units of ANDV (Chile-9717869) and administered mAbs (MIB22 + JL16) directed against ANDV glycoprotein (*11*) twice by the intraperitoneal route as a cocktail therapy. The study comprised 2 sets of experiments addressing treatment at midstage and late-stage disease. Both sets included control and treatment groups. The treatment group (n = 18) received an injection of the 2 mAbs (25 mg/kg of each mAb), and the control group (n = 18) received an isotype control mAb (50 mg/kg). To determine differences in ANDV replication, we euthanized 6 animals of each group at a predetermined time point (10 days postinfection [dpi]) and kept 12 animals in each group to monitor survival.

First, we determined the efficacy of the mAb cocktail administered at 5 and 9 days dpi (5+9) to a treatment group (n = 12), compared with a control group (n = 12) treated with isotype antibody (Figure 1, panel A). The control animals had a median time to death of 13 dpi, as previously observed (*12*). We monitored the animals and performed weight and physical examinations daily until euthanasia or until no clinical signs of illness were observed for 2 consecutive days (treatment group; day 18) (Figure 1, panel B). Human mAb cocktail treatment was well tolerated and resulted in 100% protection from ANDV challenge (Figure 1, panel C; p<0.0001). We necropsied 6 animals at 10 dpi to determine lung viral loads by quantitative reverse transcription PCR as previously described (*11*). Results showed that the group treated with the mAb cocktail had significantly reduced lung viral RNA copy numbers compared with those for the isotype control group (Figure 1, panel D; p = 0.04). We also measured viral RNA in animals at 42 dpi. Although we detected viral RNA in lung tissue, the amount of viral RNA was significantly lower compared with that in animals necropsied at 10 dpi (Figure 1, panel D; p = 0.0037); this finding resembles the pathology seen in humans in which viral RNA can be detectable even months after resolution of acute infection. Although detectable viral RNA does not translate necessarily into infectious virus, this finding suggests that disease manifestation and outcome are not directly associated with the presence of viral RNA (*14*).

To further assess the efficacy of the mAb cocktail against ANDV, we evaluated the mAb cocktail treatment at an advanced stage of ANDV infection by treating the animals at 8 and 10 dpi (8+10) (Figure 2, panel A) (n = 12). We monitored these animals and recorded weight changes (Figure 2, panel B). Eleven of the 12 control-group animals treated with isotype antibody succumbed to disease or met the euthanasia criteria. The single surviving control animal showed clinical signs of disease that scored

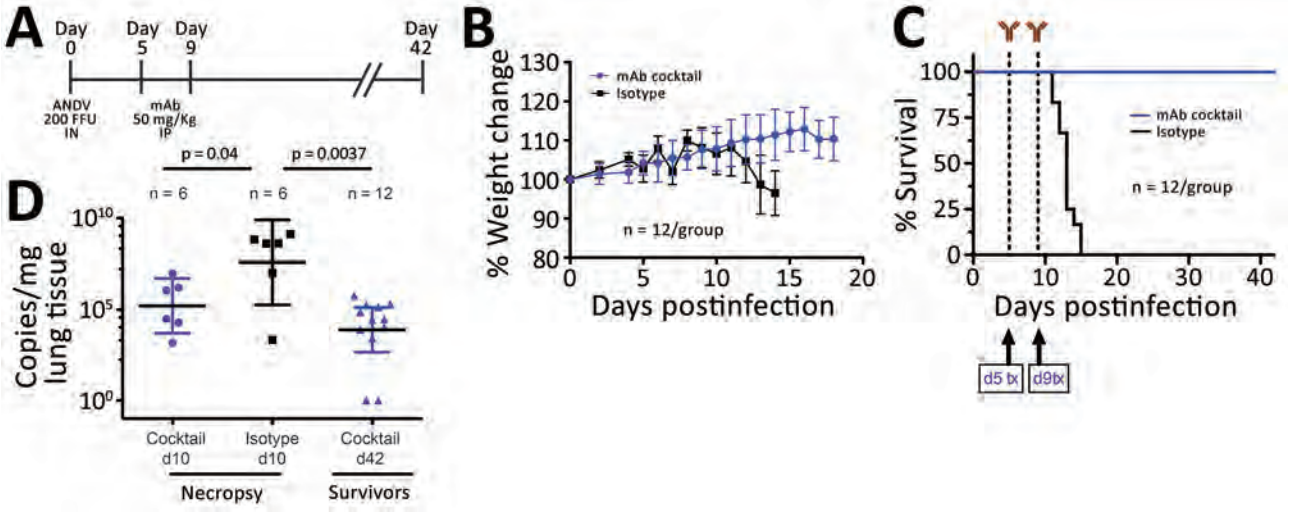

Figure 1. In vivo efficacy of a cocktail of human mAbs specific for ANDV glycoprotein administered at days 5 and 9 postinfection in the Syrian hamster model of hantavirus cardiopulmonary syndrome. A) Syrian hamsters were inoculated intranasally with 200 FFU of ANDV and then administered intraperitoneally a cocktail of mAb (JL16 + MIB22, 25 mg/kg each) or isotype control (50 mg/kg) on day 5 and day 9 postinfection. B) Percentage of weight change monitored until 18 days postinfection, represented as the average per group. Error bars indicate 95% CIs. C) Statistical evaluation of survival by group. Survival was evaluated at p<0.0001 by Mantel-Cox log-rank test using GraphPad Prism (GraphPad Software, Inc., https://www.graphpad.com); p<0.05 was significant. d5 tx and d9 tx indicate treatment schedule (5 and 9 days postinfection). D) ANDV RNA copies per milligram of lung tissue on day 10 postinfection (d10) and 42 days postinfection (d42). Samples were compared to a standard curve using an in vitro transcribed ANDV RNA fragment of known small segment copy number. p values by unpaired t-test using GraphPad Prism. Symbols indicate geometric means; horizontal line indicates median; error bars indicate 95% CIs. ANDV, Andes virus; FFU, focus-forming units; mAbs, monoclonal antibodies.

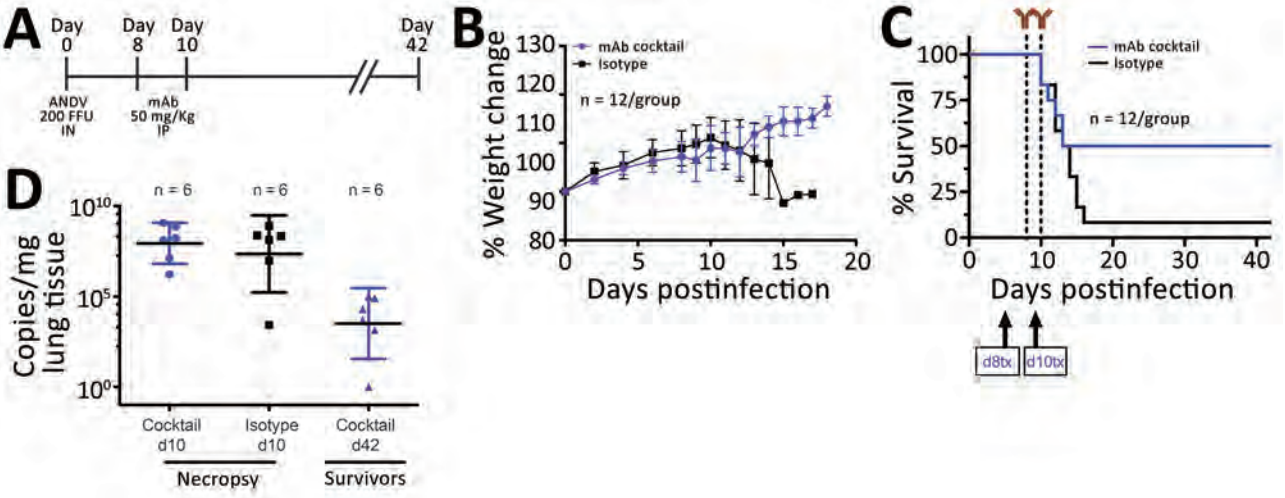

Figure 2. In vivo efficacy of a cocktail of human mAbs specific for ANDV glycoprotein administered at days 8 and 10 postinfection in the Syrian hamster model of hantavirus cardiopulmonary syndrome. A) Syrian hamsters were inoculated intranasally with 200 FFU of ANDV and then administered intraperitoneally a cocktail of mAbs (JL16 + MIB22; 25 mg/kg each) or isotype control (50 mg/kg) on day 8 and day 10 postinfection. B) Percentage of weight change monitored until 18 days postinfection, represented as the average per group. Error bars indicate 95% CIs. C) Statistical evaluation of survival by group. Survival was evaluated at p = 0.123 by Mantel-Cox log-rank test using GraphPad Prism (GraphPad Software, Inc., https://www.graphpad.com); p<0.05 was significant. d8 tx and d10 tx indicate treatment schedule (8 and 10 days postinfection). D) ANDV RNA copies per milligram of lung tissue on day 10 (d10) and day 42 (d42) postinfection. Samples were compared to a standard curve using an in vitro transcribed ANDV RNA fragment of known small segment copy number. Symbols indicate geometric means; horizontal line indicates median; error bars indicate 95% CIs. ANDV, Andes virus; FFU, focus-forming units; mAbs, monoclonal antibodies.

just below the euthanasia criteria, which include signs of moribundity: ataxia, reluctancy to move, bleeding from any orifice, tachypnea, or paralysis. The isotype control group showed a median survival time of 12 dpi. In the mAb cocktail treatment group, 6 hamsters survived; although our results (p = 0.123) were not statistically significant (at a p<0.05 level), the mAb cocktail showed 50% efficacy when administered at the time points of 8 and 10 dpi (Figure 2, panel C). As before, we necropsied 6 animals at 10 dpi to determine ANDV RNA loads in the lungs. We observed no significant differences in viral RNA loads between the mAb cocktail–treated group and control groups (Figure 2, panel D). Finally, the 6 surviving hamsters that were necropsied at 42 dpi showed a decrease in lung viral loads, compared with the group that was necropsied at 10 dpi (Figure 2, panel D). Ultimately, we measured the concentration of human IgG in serum samples from animals necropsied at 10 dpi (Appendix Figure 1, https://wwwnc.cdc.gov/EID/article/27/10/21-0735-App1.pdf).

Conclusions

Our results demonstrate that the human mAb cocktail containing JL16 and MIB22 is able to completely or partially protect Syrian hamsters against lethal ANDV challenge when administered as a 2-dose regimen at midstage (5 and 9 dpi) and late-stage (8 and 10 dpi) disease. To date, the Syrian hamster is the only ANDV preclinical disease model that is appropriate to evaluate the efficacy of therapeutic and prophylactic countermeasures. Thus, our antibody cocktail study meets the Food and Drug Administration animal rule, which requires evidence of efficacy of a countermeasure in a well-established and evaluated animal model indicating potential benefit for human use (*13*). Our results highlight the potential of recombinant human mAbs JL16 and MIB22 to be used as postexposure countermeasure, even at later stages of infection. This finding is supported by a previous study (*15*) showing that immune plasma containing neutralizing antibodies decreases the case-fatality rate in HCPS patients who had mild to severe disease at hospitalization, highlighting the potential of human antibodies to alter the clinical outcome.

Fine-tuning the dosing and more effective combinations of mAbs will likely extend the therapeutic window even further. However, the 100% midstage and 50% late-stage protection observed in these experiments are very encouraging in the endeavor to find a specific treatment for human HCPS caused by ANDV infection.

Acknowledgments

We thank the Rocky Mountain Veterinary Branch for animal care and veterinary oversight.

This work was partially funded by the Intramural Research Program of the National Institute of Allergy and Infectious Diseases (NIAID), National Institutes of Health. M.I.B. was partially supported by the National Agency for Research and Development/FONDEF (ID14I20084) in collaboration with Ichor Biologics. J.L.G. and R.A. were partially supported by a Small Business Innovation Research grant through the NIAID (grant R43 AI138740-01A1).

About the Authors

Dr. Williamson is a microbiologist in the molecular pathogenesis unit of the laboratory of virology at Rocky Mountain Laboratory, National Institute of Allergy and Infectious Diseases, National Institutes of Health, Hamilton, MT, USA. Her research interests include a wide range of organisms, including *Borrelia hermsii*, *Oropouche orthobunyavirus*, Colorado tick fever virus, and hantaviruses; she also studies the molecular determinants of pathogenesis for emerging respiratory viruses. Dr. Prescott is the group leader of the comparative immunology or risk group 4 viruses section at the Robert Koch Institute, Berlin, Germany. His research interests include the immune responses to hemorrhagic fever viruses in their natural reservoirs and in animal models of disease.

References

1. Figueiredo LT, Souza WM, Ferrés M, Enria DA. Hantaviruses and cardiopulmonary syndrome in South America. Virus Res. 2014;187:43–54. https://doi.org/10.1016/j.virusres.2014.01.015
2. Martinez VP, Bellomo C, San Juan J, Pinna D, Forlenza R, Elder M, et al. Person-to-person transmission of Andes virus. Emerg Infect Dis. 2005;11:1848–53. https://doi.org/10.3201/eid1112.050501
3. Padula PJ, Edelstein A, Miguel SD, López NM, Rossi CM, Rabinovich RD. Hantavirus pulmonary syndrome outbreak in Argentina: molecular evidence for person-to-person transmission of Andes virus. Virology. 1998;241:323–30. https://doi.org/10.1006/viro.1997.8976
4. Ferrés M, Vial P, Marco C, Yanez L, Godoy P, Castillo C, et al.; Andes Virus Household Contacts Study Group. Prospective evaluation of household contacts of persons with hantavirus cardiopulmonary syndrome in Chile. J Infect Dis. 2007;195:1563–71. https://doi.org/10.1086/516786
5. Martínez VP, Di Paola N, Alonso DO, Pérez-Sautu U, Bellomo CM, Iglesias AA, et al. "Super-spreaders" and person-to-person transmission of Andes virus in Argentina. N Engl J Med. 2020;383:2230–41. https://doi.org/10.1056/NEJMoa2009040
6. Jonsson CB, Hooper J, Mertz G. Treatment of hantavirus pulmonary syndrome. Antiviral Res. 2008;78:162–9. https://doi.org/10.1016/j.antiviral.2007.10.012
7. Valdivieso F, Vial P, Ferres M, Ye C, Goade D, Cuiza A, et al. Neutralizing antibodies in survivors of Sin Nombre and Andes hantavirus infection. Emerg Infect Dis. 2006;12:166–8. https://doi.org/10.3201/eid1201.050930
8. MacNeil A, Comer JA, Ksiazek TG, Rollin PE. Sin Nombre virus–specific immunoglobulin M and G kinetics in hantavirus pulmonary syndrome and the role played by serologic responses in predicting disease outcome. J Infect Dis. 2010;202:242–6. https://doi.org/10.1086/653482
9. Hooper JW, Brocato RL, Kwilas SA, Hammerbeck CD, Josleyn MD, Royals M, et al. DNA vaccine-derived human IgG produced in transchromosomal bovines protect in lethal models of hantavirus pulmonary syndrome. Sci Transl Med. 2014;6:264ra162. https://doi.org/10.1126/scitranslmed.3010082
10. Duehr J, McMahon M, Williamson B, Amanat F, Durbin A, Hawman DW, et al. Neutralizing monoclonal antibodies against the Gn and the Gc of the Andes virus glycoprotein spike complex protect from virus challenge in a preclinical hamster model. MBio. 2020;11:e00028–20. https://doi.org/10.1128/mBio.00028-20
11. Garrido JL, Prescott J, Calvo M, Bravo F, Alvarez R, Salas A, et al. Two recombinant human monoclonal antibodies that protect against lethal Andes hantavirus infection in vivo. Sci Transl Med. 2018;10:eaat6420. https://doi.org/10.1126/scitranslmed.aat6420
12. Safronetz D, Zivcec M, Lacasse R, Feldmann F, Rosenke R, Long D, et al. Pathogenesis and host response in Syrian hamsters following intranasal infection with Andes virus. PLoS Pathog. 2011;7:e1002426. https://doi.org/10.1371/journal.ppat.1002426
13. Safronetz D, Ebihara H, Feldmann H, Hooper JW. The Syrian hamster model of hantavirus pulmonary syndrome. Antiviral Res. 2012;95:282–92. https://doi.org/10.1016/j.antiviral.2012.06.002
14. Kuenzli AB, Marschall J, Schefold JC, Schafer M, Engler OB, Ackermann-Gäumann R, et al. Hantavirus cardiopulmonary syndrome due to imported Andes hantavirus infection in Switzerland: a multidisciplinary challenge, two cases and a literature review. Clin Infect Dis. 2018;67:1788–95. https://doi.org/10.1093/cid/ciy443
15. Vial PA, Valdivieso F, Calvo M, Rioseco ML, Riquelme R, Araneda A, et al.; Hantavirus Study Group in Chile. A non-randomized multicentre trial of human immune plasma for treatment of hantavirus cardiopulmonary syndrome caused by Andes virus. Antivir Ther. 2015;20:377–86. https://doi.org/10.3851/IMP2875

Address for correspondence: María Inés Barría, Translational Virology, Facultad de Medicina y Ciencia, Universidad San Sebastián, Puerto Montt, Chile; email: maria.barriac@uss.cl

Outbreak of Oropouche Virus in French Guiana

Mélanie Gaillet, Clara Pichard, Johana Restrepo, Anne Lavergne, Lucas Perez, Antoine Enfissi, Philippe Abboud, Yann Lambert, Laurence Ma, Marc Monot, Magalie Demar, Felix Djossou, Véronique Servas, Mathieu Nacher, Audrey Andrieu, Julie Prudhomme, Céline Michaud, Cyril Rousseau, Isabelle Jeanne, Jean-Bernard Duchemin, Loïc Epelboin,[1] Dominique Rousset[1]

Oropouche fever is a zoonotic dengue-like syndrome caused by Oropouche virus. In August–September 2020, dengue-like syndrome developed in 28 of 41 patients in a remote rainforest village in French Guiana. By PCR or microneutralization, 23 (82.1%) of 28 tested patients were positive for Oropouche virus, documenting its emergence in French Guiana.

French Guiana is an overseas territory of France in northern South America; 95% of the country is covered by Amazon rainforest. The remote village of Saül, deep in the rainforest, had 152 permanent inhabitants in 2017 (INSEE, https://www.insee.fr/fr/statistiques/4271842), but the actual population in 2020 was 95. The nurse of the health center keeps an updated count of inhabitants in the village, a number that was stable because of isolation during the coronavirus disease (COVID-19) pandemic. In August and September 2020, French Guiana was experiencing simultaneous COVID-19 and dengue outbreaks. Several inhabitants of Saül were treated for dengue-like symptoms, including fever and diffuse muscle pain, but rapid diagnostic testing for dengue was negative.

The Study

Saül houses 1 of 17 remote centers for prevention and care (RCPC) distributed throughout the inner territories of French Guiana (Figure 1). On August 11, 2020, a 55-year-old patient from Saül sought treatment with a dengue-like syndrome (DLS) including a marked meningeal component but tested negative for dengue. The patient was hospitalized on August 22 in Cayenne, the territorial capital. Bacteriologic, virologic, and parasitologic investigations were inconclusive. The Saül RCPC reported 15 additional patients with dengue-negative DLS during August 22–September 7. Consequently, an investigation was scheduled to begin in Saül on September 16. Sociodemographic data, clinical manifestations and evolution, and biological samples were systematically collected for each new case and, when possible, retrospectively for patients who sought treatment for DLS symptoms during August 11–September 16 (Appendix, https://wwwnc.cdc.gov/EID/article/27/10/20-4760-App1.pdf).

On September 22, because results of serologic testing for common locally circulating arboviruses were negative, we performed real-time PCR for Oropouche-like virus on all available samples collected ≤5 days after the onset of symptoms (*1*). We performed viral isolations on Vero cells from PCR-positive samples and sequenced 1 isolate. Later, we performed microneutralization tests to complete biologic investigations on late serum samples. We collected clinical, biological, and anamnestic data, including localization (Figure 2), from medical and laboratory records (Appendix).

As part of the entomologic investigation, over a 48-hour period during September 30–October 2, we captured potential vectors by using 11 BG-Sentinel traps (Biogents, https://biogents.com), 5 CDC light traps (BioQuip, https://www.bioquip.com), and 1 Woodstream Mosquito Magnet trap (https://www.woodstream.com). Vector control measures, mostly aerial insecticide spraying and larval treatment, were

Author affiliations: Cayenne Hospital Center, Cayenne, French Guiana (M. Gaillet, C. Pichard, L. Perez, P. Abboud, Y. Lambert, M. Demar, F. Djossou, V. Servas, M. Nacher, C. Michaud, L. Epelboin); Collectivité Territoriale de Guyane, Cayenne (J. Restrepo); Institut Pasteur de la Guyane, Cayenne (A. Lavergne, A. Enfissi, J.-B. Duchemin, D. Rousset); Institut Pasteur, Paris, France (L. Ma, M. Monot); Santé Publique France, Cellule Régionale Guyane, Cayenne (A. Andrieu, J. Prudhomme, C. Rousseau); Health Regional Agency of French Guiana, Cayenne (I. Jeanne)

DOI: https://doi.org/10.3201/eid2710.204760

[1]These authors contributed equally to the work.

only implemented 1 week later because of logistical constraints (lack of necessary aerial resources).

We obtained oral consent from patients to participate in the study and collected the biological samples as part of the care process. All data were collected on a standardized form and kept confidential to prevent disclosure of any personally identifiable information according to the requirements of the Commission Nationale de l'Informatique et des Libertés (https://www.cnil.fr).

During August 11–October 15, 2020, DLS was diagnosed in 41 (of 95 total) residents of Saül who sought treatment at an RCPC. Median age was 38 years (range 3–82 years, interquartile range 16–51 years) (Appendix Table 1); male-to-female ratio was 1.6:1 (Appendix Table 2). We tested blood samples from 28 patients; 23 were confirmed positive for Oropouche virus (OROV), 7 by PCR alone, 12 by microneutralization alone, and 4 by both. For the other 5 patients sampled, we were unable to confirm the diagnosis in the absence of a later sample to test for seroconversion. In addition, 17 residents, including 8 children, later reported having experienced DLS during the study period but did not visit the RPCP and therefore were not included in the study.

We obtained 5 viral isolates on Vero cells from PCR-positive serum samples; sequencing 1 of these isolates confirmed OROV infection. The attack rate in the village population was 43.2% (41/95); however, including residents with DLS symptoms who did not seek medical help would make the actual attack

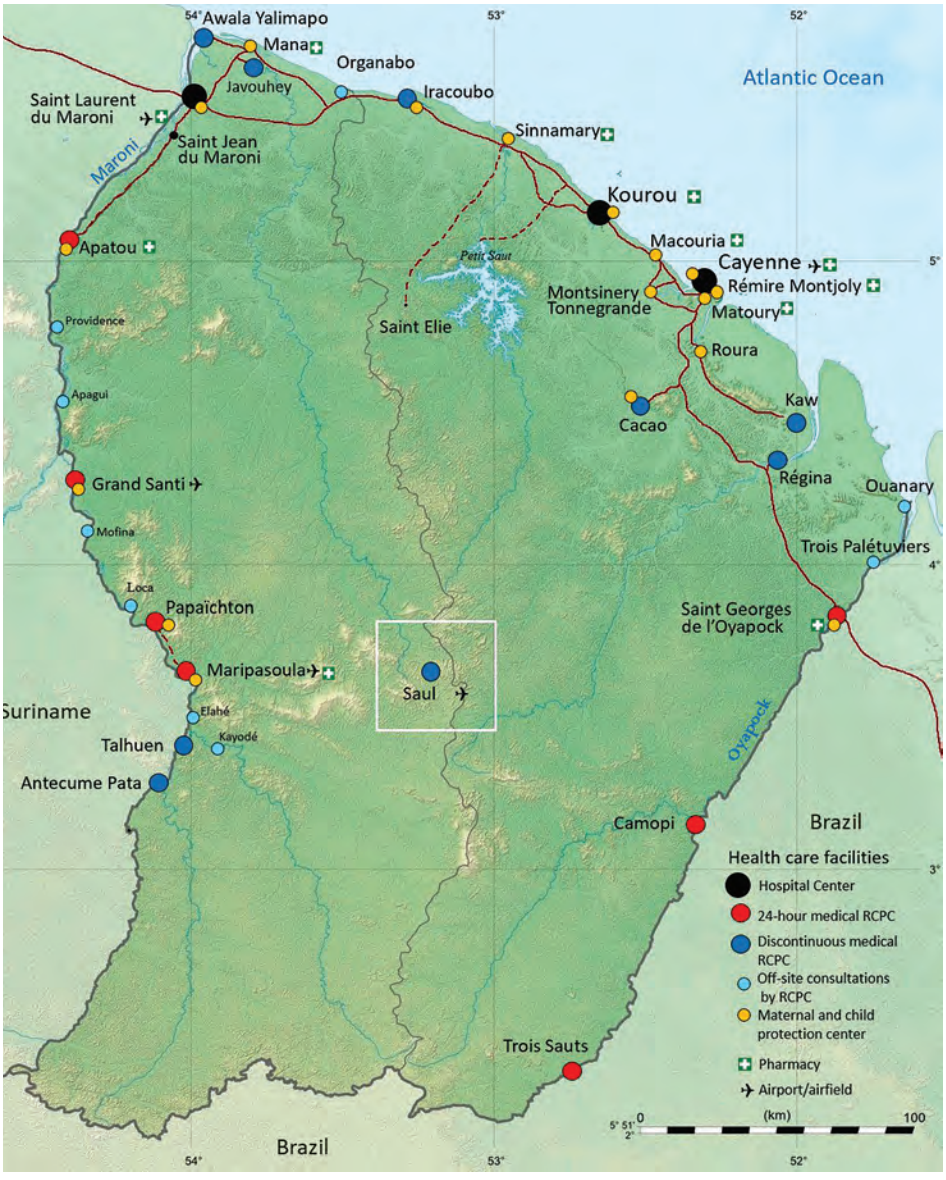

Figure 1. Locations of the town of Saül and 17 remote centers for prevention and care in French Guiana. Black circles: hospital centers; red circles: 24-hour remote centers for prevention and care; dark blue circles: remote centers for prevention and care (not 24-hour); light blue circles: off-site consultations with remote center for prevention and care; orange circles: maternal and child protection centers. Source: Dr. Elise Martin, Centre Hospitalier de Cayenne, French Guiana.

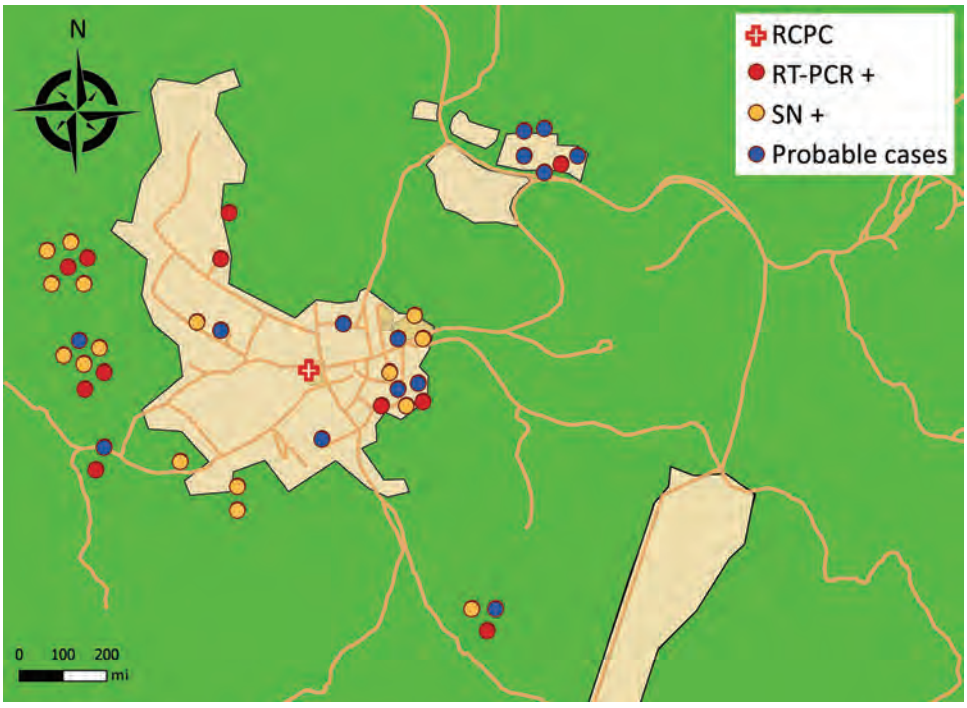

Figure 2. Spatial distribution of patient settlement around the town of Saül, French Guiana, and results of biologic testing for Oropouche virus by testing method. Geolocation is approximate to preserve patient anonymity. For probable cases (N = 18), samples were not taken. Green area, rainforest; light orange area, main districts of Saül; dark orange lines, forest trails. RCPC, remote centers for prevention and care; RT-PCR+, diagnosed with real-time PCR alone (N = 11); SN+, diagnosed with seroneutralization alone (N = 12).

rate 61.1% (58/95). Few patients had underlying conditions. Symptoms by order of frequency were fever, headache, myalgia, and asthenia (Appendix Table 2). The illness followed 3 successive phases: a 2–4-day acute phase, followed by a remission phase, then a rebound of symptoms ≈7–10 days after onset. Symptom intensity decreased by the end of the second week. Persistent tiredness was reported by 73.2% patients (30/41). Elevated CRP levels of up to 10 mg/L were observed in 5 (23%) of 22 patients and lymphopenia in 10 (42%) of 24. The outbreak peaked on September 16 (Figure 2), suggesting that transmission was slowing toward the end of September. The environmental vector control intervention was first applied on September 23 and then again the week of October 6–13. The disease affected all areas of the village of Saül; the index case-patient lived on the forest edge (Appendix Figure).

In total, during 36 nighttime trapping efforts, we collected 254 mosquitoes, 242 (95%) *Culex quinquefasciatus*, and 31 *Culicoides* (biting midges), only 1 of which was *C. paraensis*, which we trapped indoors with a BG trap. We captured the other midge specimens, mostly members of the *C. guttatus* group of subgenus *Hoffmania*, near a cocoa tree orchard close to the village.

Conclusions

Since the early 1960s, >30 OROV outbreaks have been reported, mainly in the northern states of Brazil (*2*,*3*), Peru, Ecuador (*4*), and Trinidad and Tobago, where OROV was first reported in 1955 (*5*). We report an outbreak of OROV fever in French Guiana. OROV is an arbovirus (genus *Orthobunyavirus*), transmitted through several vectors, including *C. paraensis* midges and *Cx. quinquefasciatus* mosquitoes in the urban cycle and *Aedes serratus* and *Coquillettidia venezuelensis* mosquitoes in the sylvatic cycle (*6*). Vertebrate hosts include sloths (*Bradypus tridactylus*) and monkeys (*Saguinus* spp., *Saimiri* spp., *Alouatta* spp.) (*7*). Because vectors and hosts both exist in French Guiana, the report of an OROV outbreak in this country was not unexpected.

OROV PCR is not routinely performed and serodiagnosis is not available in French Guiana; therefore, some individual cases of OROV infection not associated with an outbreak may have gone undetected. However, it is unlikely that many cases from past outbreaks went undiagnosed. Indeed, French Guiana is familiar with arbovirus outbreaks and has the resources to investigate them (*8*–*10*). Moreover, the high attack rate, homogeneous distribution of cases across the village, and different age groups affected in this outbreak imply the population had no immunity against OROV. The high attack rate could be explained by Saül's remoteness together with factors related to the COVID-19 pandemic. The village, which is accessible only by air, has been especially affected by the COVID-19 lockdown and subsequent

movement restrictions, which have isolated it even further. Also, a decrease in army presence in the surrounding forest has led to a substantial increase in illegal gold miners passing through from Brazil, which could have resulted in imported OROV. In addition, unmaintained forest trails around the village may have changed the vector density, but further entomologic studies are needed to test this hypothesis. We captured an abundance of potential vectors, especially *Cx. quinquefasciatus* mosquitoes, within the village itself. The low capture yield of local *Culicoides* spp. midges might have been linked to seasonal trends.

As described in the literature, clinical manifestations were moderately severe, and symptoms recurred among most of the patients studied (*11*). After the entomologic investigation, vector control measures were implemented in week 40. The near-exclusive presence in the village of *Cx. quinquefasciatus* mosquitoes among possible vectors suggests this species as the most plausible vector for this outbreak. However, because vectors were captured and sampled near the end of the outbreak, other potential vectors active earlier cannot be excluded. The presence of *Cx. quinquefasciatus* mosquitoes on the coast and in main cities of French Guiana and the geographic expansion of OROV in South America in recent years call for increased epidemiologic surveillance in this region (*12*).

Acknowledgments

We thank Séverine Timane Reillon, Frédéric Bouteille, Jean Yves Cattin, Fabien Rogalle, Fanny Gras, Sylvain Fradin, Romuald Carinci, Jean Issaly, Florence Jean Dit Gautier, Antonio Lopez, Mathilde Boutrou, Laure Lemée, David Moua, Laetitia Bremand, Bhety Labeau, Vincent Robert, Solène Wiedner-Papin for their involvement and willingness to help in the composition of this article.

About the Author

Dr. Gaillet is an infectious diseases specialist and epidemiologist. She created a mobile public health team in isolated communities in the most inaccessible villages of French Guiana, which intervenes on a wide range of public health issues, including the investigation of epidemics and increasing awareness of the prevention of coronavirus disease and many other topics.

References

1. Naveca FG, Nascimento VAD, Souza VC, Nunes BTD, Rodrigues DSG, Vasconcelos PFDC. Multiplexed reverse transcription real-time polymerase chain reaction for simultaneous detection of Mayaro, Oropouche, and Oropouche-like viruses. Mem Inst Oswaldo Cruz. 2017;112:510–3. https://doi.org/10.1590/0074-02760160062
2. Tilston-Lunel NL, Hughes J, Acrani GO, da Silva DE, Azevedo RS, Rodrigues SG, et al. Genetic analysis of members of the species Oropouche virus and identification of a novel M segment sequence. J Gen Virol. 2015;96:1636–50. https://doi.org/10.1099/vir.0.000108
3. Sakkas H, Bozidis P, Franks A, Papadopoulou C. Oropouche fever: a review. Viruses. 2018;10:10. https://doi.org/10.3390/v10040175
4. Wise EL, Pullan ST, Márquez S, Paz V, Mosquera JD, Zapata S, et al. Isolation of Oropouche virus from febrile patient, Ecuador. Emerg Infect Dis. 2018;24:935–7. https://doi.org/10.3201/eid2405.171569
5. Anderson CR, Spence L, Downs WG, Aitken TH. Oropouche virus: a new human disease agent from Trinidad, West Indies. Am J Trop Med Hyg. 1961;10:574–8. https://doi.org/10.4269/ajtmh.1961.10.574
6. Smith GC, Francy DB. Laboratory studies of a Brazilian strain of *Aedes albopictus* as a potential vector of Mayaro and Oropouche viruses. J Am Mosq Control Assoc. 1991;7:89–93.
7. Pinheiro FP, Travassos da Rosa AP, Travassos da Rosa JF, Ishak R, Freitas RB, Gomes ML, et al. Oropouche virus. I. A review of clinical, epidemiological, and ecological findings. Am J Trop Med Hyg. 1981;30:149–60. https://doi.org/10.4269/ajtmh.1981.30.149
8. Mutricy R, Djossou F, Matheus S, Lorenzi-Martinez E, De Laval F, Demar M, et al. Discriminating Tonate virus from dengue virus infection: a matched case-control study in French Guiana, 2003–2016. Am J Trop Med Hyg. 2020;102:195–201. https://doi.org/10.4269/ajtmh.19-0156
9. Epelboin L, Boullé C, Ouar-Epelboin S, Hanf M, Dussart P, Djossou F, et al. Discriminating malaria from dengue fever in endemic areas: clinical and biological criteria, prognostic score and utility of the C-reactive protein: a retrospective matched-pair study in French Guiana. PLoS Negl Trop Dis. 2013;7:e2420. https://doi.org/10.1371/journal.pntd.0002420
10. Bonifay T, Prince C, Neyra C, Demar M, Rousset D, Kallel H, et al.; Char Chik Working group. Atypical and severe manifestations of chikungunya virus infection in French Guiana: A hospital-based study. PLoS One. 2018;13:e0207406. https://doi.org/10.1371/journal.pone.0207406
11. Travassos da Rosa JF, de Souza WM, Pinheiro FP, Figueiredo ML, Cardoso JF, Acrani GO, et al. Oropouche virus: clinical, epidemiological, and molecular aspects of a neglected *Orthobunyavirus*. Am J Trop Med Hyg. 2017;96:1019–30.
12. Talaga S, Duchemin JB, Girod R, Dusfour I. The *Culex* mosquitoes (Diptera: Culicidae) of French Guiana: a comprehensive review with the description of three new species. J Med Entomol. 2021;58:182–221.

Address for correspondence: Loïc Epelboin, Unité des Maladies Infectieuses et Tropicales, Centre Hospitalier Andrée Rosemon et Université de la Guyane, Av des Flamboyants, F-97300, Cayenne, French Guiana, France; email: epelboincrh@hotmail.fr

Effects of COVID-19 Pandemic on Reported Lyme Disease, United States, 2020

David W. McCormick, Kiersten J. Kugeler, Grace E. Marx, Praveena Jayanthi, Stephanie Dietz, Paul Mead, Alison F. Hinckley

Author affiliations: Centers for Disease Control and Prevention, Fort Collins, Colorado, USA. (D.W. McCormick, K.J. Kugeler, G.E. Marx, P. Mead, A.F. Hinckley); ICF International Inc., Atlanta, Georgia, USA (P. Jayanthi); Centers for Disease Control and Prevention, Atlanta (P. Jayanthi, S. Dietz)

DOI: https://doi.org/10.3201/eid2710.210903

Surveys indicate US residents spent more time outdoors in 2020 than in 2019, but fewer tick bite–related emergency department visits and Lyme disease laboratory tests were reported. Despite ongoing exposure, Lyme disease case reporting for 2020 might be artificially reduced due to coronavirus disease–associated changes in healthcare-seeking behavior.

The coronavirus disease (COVID-19) pandemic has altered how humans interact with their environment and the healthcare system (*1*,*2*), and strained resources have limited the ability of state and local health departments to respond to reports of notifiable diseases (*3*). The Centers for Disease Control and Prevention (CDC) typically is notified of 30,000–40,000 Lyme disease cases annually (*4*), but the COVID-19 pandemic likely will affect the case counts. Most Lyme disease cases are acquired in spring and early summer (*5*); in 2020, these seasons coincided with the initial spread of COVID-19 and widespread stay-at-home orders. We explored 4 data sources to assess how the COVID-19 pandemic might have influenced tick bite risk and associated healthcare-seeking practices and affected reported Lyme disease cases for 2020.

The pathway for Lyme disease case reporting begins with environmental risk and culminates with case notification to CDC (Appendix Figure, https://wwwnc.cdc.gov/EID/article/27/10/21-0903-App1.pdf). Environmental risk is relatively stable in high-incidence areas and driven by ecologic factors unaffected by COVID-19 (*6*). The pandemic might have altered the frequency of outdoor activities and probability of encountering ticks, healthcare-seeking and provider services patterns, and case investigation and reporting. The data sources we used measure changes in time spent outdoors, information-seeking patterns for tick removal, emergency department (ED) visits for tick bites, and laboratory testing for Lyme disease. This analysis was considered nonhuman subjects research by CDC.

To assess potential behavior shifts that might have increased risk for tick encounters, we analyzed data from Porter Novelli's PN View 360+ consumer survey (*7*). Among 4,013 participants who responded to the survey distributed during July 31–August 9, 2020, approximately half (49.9%) reported that they had spent a lot more time or slightly more time outdoors by that point in 2020 compared with prior years. Only 20.9% of respondents reported spending less time outdoors in 2020.

To indirectly assess frequency of tick encounters in 2020 compared with prior years, we evaluated total monthly visits during 2018–2020 to a CDC website describing tick removal (*8*). Visits to this website typically increase during late spring and summer and again in October, when most bites from blacklegged ticks (*Ixodes scapularis* and *Ixodes pacificus*) occur (*5*). We observed 818,167 website visits during 2020, ≈25% more than in 2019 (681,021) and 2018 (630,839) (Figure).

To assess patterns related to healthcare-seeking for tick encounters, we identified ED visits for tick bites by using the National Syndromic Surveillance Program (NSSP) BioSense platform (*9*). ED visits for tick bites decreased in 2020 from 2019 in both total number and rate per 100,000 ED visits (Figure). The largest relative decreases were observed in May. During 2017–2019, the average number of ED visits for tick bites during the month of May was 12,693, an average rate of 145/100,000 ED visits. During May 2020, only 5,845 ED visits for tick bites occurred, a rate of 89/100,000 ED visits.

We quantified cumulative counts and percent positivity of serologic tests for Lyme disease performed by an independent clinical laboratory. Lyme disease testing volume decreased from 2019 to 2020; 25.0% fewer tests were performed, and test positivity decreased slightly to <1% (Table).

During the first wave of the COVID-19 pandemic in 2020, the US population spent more time outdoors and visited a CDC website describing safe tick removal more frequently than during prior years. However, fewer persons sought care for tick bites, and substantially fewer laboratory tests for Lyme disease were ordered. These findings suggest that the risk of acquiring Lyme disease was similar or potentially higher in 2020 compared with risk during prior years, but fewer persons sought care, and fewer positive laboratory reports were referred for case investigation.

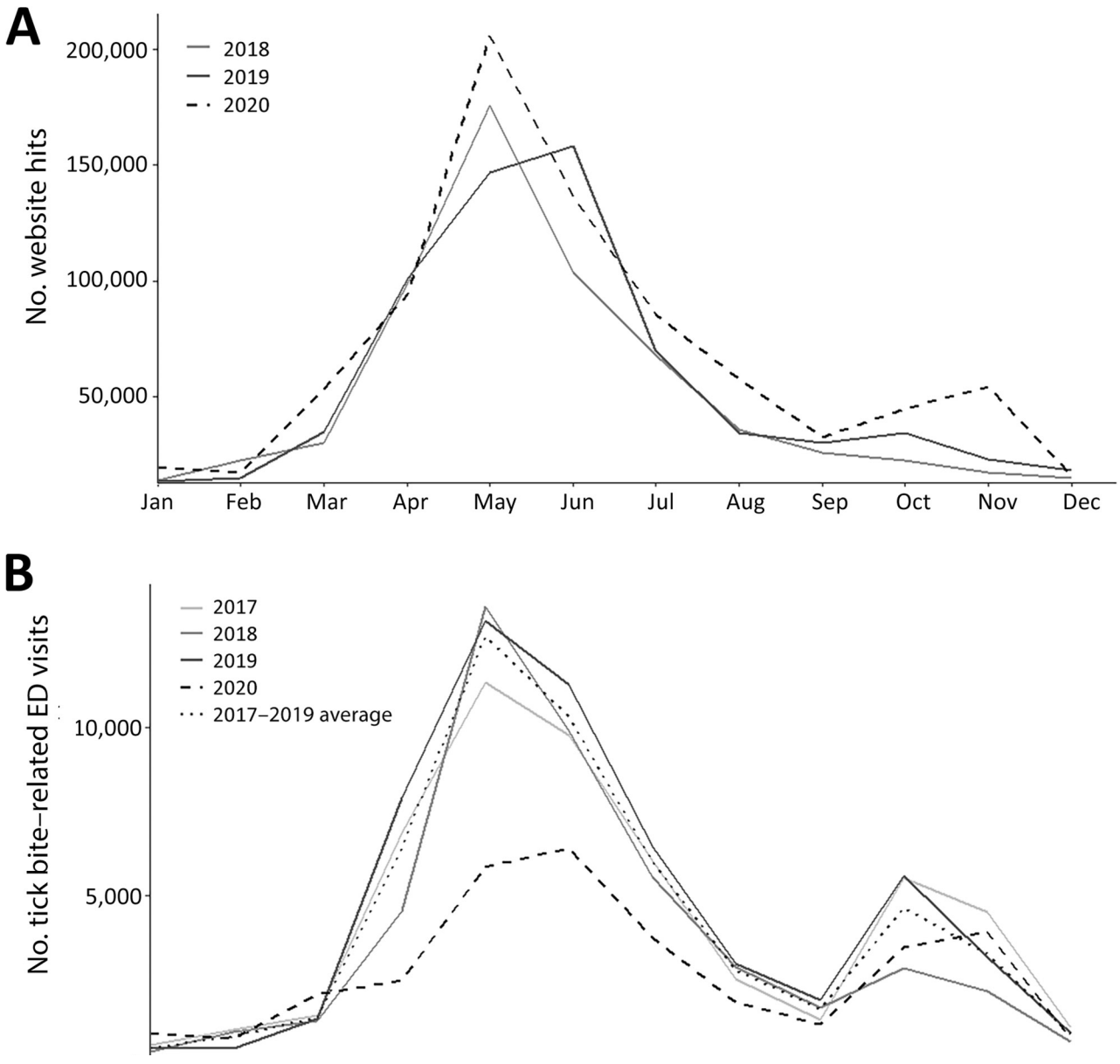

Figure. Comparison of visits to the Centers for Disease Control and Prevention (CDC) website on tick removal, 2018–2020, and to the ED for tick-bite related chief complaints, 2017–2020, United States. A) Website visits per month for https://www.cdc.gov/ticks/removing_a_tick.html. B) ED visits by month in which the chief health complaint was tick bite. Comparison of 2020 to the average of the previous 4 years is shown. ED, emergency department.

Table. Number and percent positive for Lyme disease tests performed by a large commercial laboratory and percent decrease in 2020 compared with 2019, United States*

	2019		2020		% Decrease in testing	Absolute difference in
Testing tier	Total tests	% Positive	Total tests	% Positive	volume (95% CI)	% positive (95% CI)
First tier†	925,939	9.6	691,453	9.2	25.3 (25.2–25.4)	0.3 (0.2–0.4)
Second tier‡	422,801	11.0	320,616	10.2	24.2 (24.1–24.3)	0.8 (0.6–0.9)
Total	1,348,740	10.0	1,012,069	9.5	25.0 (25.1–24.9)	0.5 (0.4–0.6)

*Percent positive indicates the percentage of the total laboratory tests that were positive for each test tier and overall. The percent decrease in testing volume shows the percentage decrease in total tests performed by tier and overall for 2020 compared with 2019. Two-tier testing for Lyme disease is recommended, whereby specimens positive or equivocal on the first tier are subjected to the second tier. Additional details about testing tiers are available at https://www.cdc.gov/lyme/diagnosistesting/index.html.
†First-tier tests include enzyme immunoassays for IgM/IgG combined, IgM alone, and C6 antigen.
‡Second-tier tests include immunoblot for IgM or IgG.

Consequently, we anticipate that, once ultimately finalized, the official number of confirmed and probable Lyme disease cases in 2020 will be substantially lower than that for prior years.

One limitation of our study is that data sources we examined represent national trends and are indirect surrogates for Lyme disease risk and reporting, which vary geographically. Visits to a website describing tick removal might not correspond with finding an attached tick. Available data on laboratory testing represents 1 independent clinical laboratory; other commercial or academic laboratories might not have experienced a similar decrease in testing. Data sources associated with telehealth utilization and prescription claims could provide additional insights into the diagnosis and treatment for Lyme disease in 2020.

Already an issue in high-incidence states, the pandemic has highlighted the need for alternative Lyme disease surveillance strategies that rely less on human resources. An anticipated and potentially substantial decrease in reported Lyme disease in 2020 likely reflects the effects of the COVID-19 pandemic rather than a true change in Lyme disease incidence. Decreased reporting also could render 2020 inconsistent with long-term trends and changes in the epidemiology of the disease. Although nonpharmaceutical interventions for COVID-19 have mitigated the transmission of respiratory pathogens (*10*), these results suggest the behavioral and reporting changes seen for Lyme disease might extend to other nonrespiratory diseases.

Acknowledgments

We thank Melanie Spillane for her assistance with collating data from National Syndromic Surveillance Program and Anna Perea for assistance with Porter Novelli's PN View 360+ consumer survey data.

About the Author

Dr. McCormick is an Epidemic Intelligence Service Officer in the Bacterial Diseases Branch, Division of Vector-Borne Diseases, National Center for Emerging and Zoonotic Infectious Diseases, Centers for Disease Control and Prevention, Fort Collins, Colorado. His primary research interests are the epidemiology and prevention of bacterial vectorborne diseases.

References

1. Hartnett KP, Kite-Powell A, DeVies J, Coletta MA, Boehmer TK, Adjemian J, et al.; National Syndromic Surveillance Program Community of Practice. Impact of the COVID-19 pandemic on emergency department visits—United States, January 1, 2019–May 30, 2020. MMWR Morb Mortal Wkly Rep. 2020;69:699–704. https://doi.org/10.15585/mmwr.mm6923e1
2. Czeisler MÉ, Marynak K, Clarke KEN, Salah Z, Shakya I, Thierry JM, et al. Delay or avoidance of medical care because of COVID-19–related concerns—United States, June 2020. MMWR Morb Mortal Wkly Rep. 2020;69:1250–7. https://doi.org/10.15585/mmwr.mm6936a4
3. Weber L, Ungar L, Smith MR, Recht H, Barry-Jester AM. Hollowed out public health system faces more cuts amid virus. Associated Press. 2020 Jul 1 [cited 2021 Apr 20]. https://apnews.com/article/b4c4bb2731da9611e6da5b6f9a52717a
4. Schwartz AM, Hinckley AF, Mead PS, Hook SA, Kugeler KJ. Surveillance for Lyme disease—United States, 2008–2015. MMWR Surveill Summ. 2017;66:1–12. https://doi.org/10.15585/mmwr.ss6622a1
5. Mead PS. Epidemiology of Lyme disease. Infect Dis Clin North Am. 2015;29:187–210. https://doi.org/10.1016/j.idc.2015.02.010
6. Burtis JC, Sullivan P, Levi T, Oggenfuss K, Fahey TJ, Ostfeld RS. The impact of temperature and precipitation on blacklegged tick activity and Lyme disease incidence in endemic and emerging regions. Parasit Vectors. 2016;9:606. https://doi.org/10.1186/s13071-016-1894-6
7. Porter Novelli. ConsumerStyles & YouthStyles 2021 [cited 2021 Apr 20]. http://styles.porternovelli.com/consumer-youthstyles
8. Centers for Disease Control and Prevention. Tick removal [cited 2021 Apr 20]. https://www.cdc.gov/ticks/removing_a_tick.html
9. Marx GE, Spillane M, Beck A, Stein Z, Powell AK, Hinckley AF. Emergency department visits for tick bites—United States, January 2017–December 2019. MMWR Morb Mortal Wkly Rep. 2021;70:612–6. https://doi.org/10.15585/mmwr.mm7017a2
10. Olsen SJ, Azziz-Baumgartner E, Budd AP, Brammer L, Sullivan S, Pineda RF, et al. Decreased influenza activity during the COVID-19 pandemic–United States, Australia, Chile, and South Africa, 2020. Am J Transplant. 2020;20:3681–5. https://doi.org/10.1111/ajt.16381

Address for correspondence: David McCormick, Centers for Disease Control and Prevention, 3156 Rampart Rd, Mailstop P02, Fort Collins, CO 80521, USA; email: yup1@cdc.gov

Genomic Sequencing of SARS-CoV-2 E484K Variant B.1.243.1, Arizona, USA

Peter T. Skidmore, Emily A. Kaelin, LaRinda A. Holland, Rabia Maqsood, Lily I. Wu, Nicholas J. Mellor, Joy M. Blain, Valerie Harris, Joshua LaBaer, Vel Murugan, Efrem S. Lim

Author affiliation: Arizona State University, Tempe, Arizona, USA

DOI: https://doi.org/10.3201/eid2710.211189

Genomic surveillance can provide early insights into new circulating severe acute respiratory syndrome coronavirus 2 (SARS-CoV-2) variants. While conducting genomic surveillance (1,663 cases) from December 2020–April 2021 in Arizona, USA, we detected an emergent E484K-harboring variant, B.1.243.1. This finding demonstrates the importance of real-time SARS-CoV-2 surveillance to better inform public health responses.

Genomic sequencing surveillance tracks the evolution of severe acute respiratory syndrome coronavirus 2 (SARS-CoV-2) and can provide early-warning insight of new variants circulating in communities. SARS-CoV-2 continues to acquire mutations in its genome as it spreads around the world. Although many mutations have little or no consequence on virus fitness, some mutations affect receptor binding or reduce antibody neutralization (*1*,*2*). Other mutations have been associated with increased transmission and clinical disease severity (*3*; Y. Liu et al., unpub. data, https://doi.org/10.1101/2021.03.08.434499). As of July 2021, the US SARS-CoV-2 Interagency Group has designated 4 variants of concern (VOC) and 7 variants of interest (VOI) in the United States based on the combination of mutations and associated attributes (*5*). Several of these VOCs and VOIs (e.g., Beta/B.1.351, Gamma/P.1, Delta/B.1.617.2) harbor the E484K mutation in the spike glycoprotein gene (*4*). Studies have demonstrated that the E484K mutation reduces antibody neutralization (*2*,*5*,*6*). E484K variants have also been identified in reinfection cases, suggesting a role in breakthrough infections (*2*,*5*–*7*); these findings indicate the need to monitor for SARS-CoV-2 variants in real time.

In an effort to provide statewide genomic surveillance, we sequenced the SARS-CoV-2 genome from 1,663 positive samples collected December 28, 2020–April 12, 2021 in Arizona, United States. Samples were primarily from Maricopa (56.9%), Coconino (26.4%), and Pima (8.5%) Counties. Study participants were 53.8% male, 46.2% female; age range was 5–81 years (median of 25 years). We successfully sequenced 1,538 (92.5%) high-quality complete genomes and found VOCs Alpha/B.1.1.7 (n = 336, 21.8%), Gamma/P.1 (n = 5, 0.33%), Beta/B.1.351 (n = 1, 0.07%), and Delta/B.1.617.2 (n = 1, 0.07%) and VOIs Epsilon/B.1.427/B.1.429 (n = 416, 27.0%), Iota/B.1.526 (n = 7, 0.5%), and Zeta/P.2 (n = 8, 0.5%) (Appendix Table 1, https://wwwnc.cdc.gov/EID/article/27/10/21-1189-App1.pdf). We detected 8 genomes associated with a common B.1.243 variant that had acquired an E484K mutation in the spike protein. The novel variant had 11 lineage-defining mutations, including V213G and E484K in the spike gene, a 9-nt deletion in open reading frame (ORF) 1ab (ΔSGF3675–77), a 3-nt insertion in the noncoding intergenic region upstream of the N gene, and other synonymous substitutions (Appendix Table 2, Figure 1). These 11 conserved mutations are distinct from the mutations associated with the parent lineage, B.1.243. The parent B.1.243 lineage is a common variant circulating in the United States that was observed in March 2020, early in the pandemic (Figure, panels A–C). The B.1.243 parent lineage encodes the spike gene D614G substitution but none of the other concerning mutations (Appendix Table 3, Figure 1). This new E484K-harboring variant has been officially designated as B.1.243.1 using the pangolin nomenclature system (*8*).

We examined the GISAID repository (https://www.gisaid.org) for additional B.1.243.1 genomes to determine its prevalence and geographic distribution. We found that B.1.243.1 is predominantly established in Arizona. Of 24 cases of B.1.243.1 sequenced during February 1–April 14, a total of 21 cases were from Arizona (Figure, panel C; Appendix Table 4). Two cases were sequenced from samples collected in Texas on February 24 and March 20 and another from a sample collected in New Mexico on March 8, suggesting that B.1.243.1 had spread to other states. We also identified 2 instances in which the parent B.1.243 lineage independently acquired the E484K mutation. However, both genomes lacked the other B.1.243.1 lineage-defining mutations and appear to be dead-end transmission events. Phylogenetic analyses indicate that the B.1.243.1 sequences form a monophyletic clade within the B.1.243 clade (Appendix Figure 2). Multiple internal branching observed in the B.1.243.1 clade indicates continued diversification of the lineage sequences, which suggests that B.1.243.1 was being established in circulation within Arizona. In contrast, the 2 additional

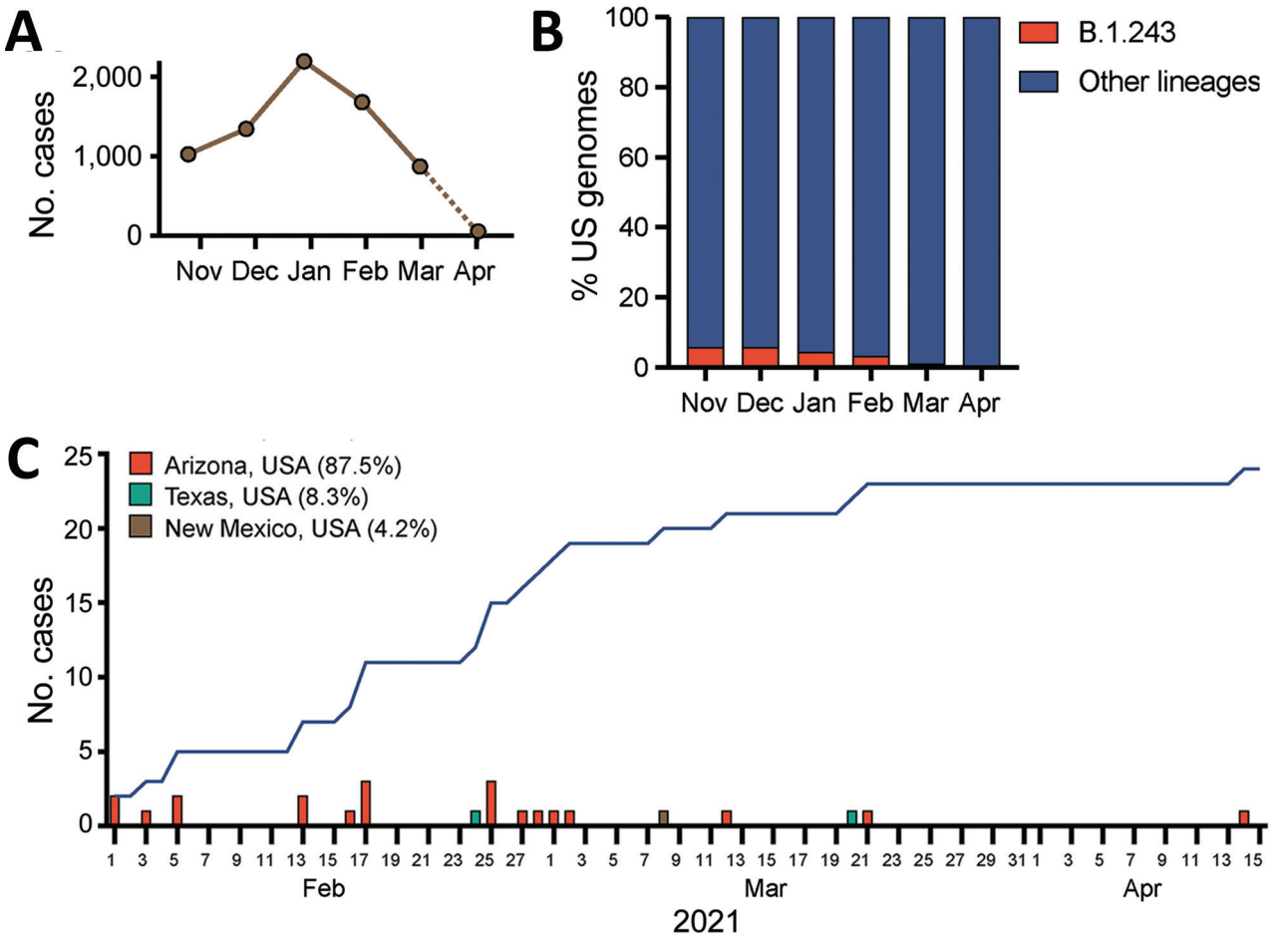

Figure. Emergence of E484K-harboring B.1.243.1 variant of severe acute respiratory syndrome coronavirus 2 (SARS-CoV-2) in Arizona, United States. A) Prevalence of B.1.243 parental lineage in the United States by number of cases per month, November 2020–April 2021. Dashed line indicates incomplete reporting of sequences from April 2021. B) Prevalence of B.1.243 parental lineage in the United States by proportion of sequenced genomes per month, November 2020–April 2021. C) Total B.1.243.1 cases reported February–April 2021. Blue curve indicates cumulative case incidence.

B.1.243 cases bearing the E484K mutation alone were phylogenetically distinct from the B.1.243.1 clade, suggesting that those isolates had evolved independently.

Genomic sequencing surveillance can provide early warnings of emergent variants. Because phylogenetic evidence suggested that B.1.243.1 was beginning to circulate in Arizona, the Arizona Department of Health Services (ADHS) was notified on March 18, 2021, and contact tracing was performed for the early B.1.243.1 cases. Of the case-patients who were interviewed, none reported connection to other patients. At the time of reporting (May 2021), the most recent case of B.1.243.1 had been reported on April 14, 2021 (Appendix Table 4). The limited spread of B.1.243.1 coincides with competition from the rapid rise in transmission of the Alpha (B.1.1.7) variant in the United States (*9*).

A limitation of this study is that the sequencing surveillance represented 0.31% of 503,825 total SARS-CoV-2 cases in Arizona during the study period. Targeted sampling efforts, such as prescreening samples for the E484K mutation by PCR-based assays, would complement random sampling for genomic sequencing surveillance. Our study highlights the need for sustained genomic surveillance in public health strategies and responses.

Acknowledgments

We thank the authors from originating laboratories responsible for obtaining the specimens and the submitting laboratories where genetic sequence data were generated and shared via the GISAID initiative, on which part of the research is based. We thank Brenna Garrett, Kenneth Komatsu and the Arizona Department of Health Services, and local health departments for contact tracing.

This research was supported in part by the Arizona State University Knowledge Enterprise and Arizona Department of Health Services. E.S.L. is supported in part by NIH grant R00DK107923.

Author contributions: methodology, P.T.S., E.A.K., L.A.H., R.M., L.I.W., N.J.M., J.M.B., V.H., E.S.L.; investigation, P.T.S., E.A.K., R.M., E.S.L.; resources, L.I.W., V.H., J.L., V.M.; data curation, P.T.S., E.A.K., R.M.; original draft of manuscript, P.T.S., E.A.K., R.M., E.S.L.; review and editing of manuscript, P.T.S., E.A.K., L.A.H., R.M., E.S.L.; supervision, J.L., V.M., E.S.L.; conceptualization, E.S.L.; funding acquisition, E.S.L. All authors reviewed and approved the final manuscript.

About the Author

Mr. Skidmore is a bioinformatician at Arizona State University under the supervision of Efrem Lim. His primary research interests include the role of the microbiome in health and disease and tracking the spread of infectious diseases.

References

1. Starr TN, Greaney AJ, Hilton SK, Ellis D, Crawford KHD, Dingens AS, et al. Deep mutational scanning of SARS-CoV-2 receptor binding domain reveals constraints on folding and ACE2 binding. Cell. 2020;182:1295–1310.e20. https://doi.org/10.1016/j.cell.2020.08.012
2. Garcia-Beltran WF, Lam EC, St. Denis K, Nitido AD, Garcia ZH, Hauser BM, et al. Multiple SARS-CoV-2 variants escape neutralization by vaccine-induced humoral immunity. Cell. 2021;184:2372–83.
3. Challen R, Brooks-Pollock E, Read JM, Dyson L, Tsaneva-Atanasova K, Danon L. Risk of mortality in patients infected with SARS-CoV-2 variant of concern 202012/1: matched cohort study. BMJ. 2021;372:n579. https://doi.org/10.1136/bmj.n579
4. Centers for Disease Control and Prevention. SARS-CoV-2 variant classifications and definitions. 2021 [cited 2021 Mar 22]. https://www.cdc.gov/coronavirus/2019-ncov/cases-updates/variant-surveillance/variant-info.html
5. Liu Z, VanBlargan LA, Bloyet L-M, Rothlauf PW, Chen RE, Stumpf S, et al. Identification of SARS-CoV-2 spike mutations that attenuate monoclonal and serum antibody neutralization. Cell Host Microbe. 2021 Mar 10;29:477–88.e4.
6. Chen RE, Zhang X, Case JB, Winkler ES, Liu Y, VanBlargan LA, et al. Resistance of SARS-CoV-2 variants to neutralization by monoclonal and serum-derived polyclonal antibodies. Nat Med. 2021;27:717–26. https://doi.org/10.1038/s41591-021-01294-w
7. Nonaka CKV, Franco MM, Gräf T, de Lorenzo Barcia CA, de Ávila Mendonça RN, de Sousa KAF, et al. Genomic evidence of SARS-CoV-2 reinfection involving E484K spike mutation, Brazil. Emerg Infect Dis. 2021;27:1522–4. https://doi.org/10.3201/eid2705.210191
8. Rambaut A, Holmes EC, O'Toole Á, Hill V, McCrone JT, Ruis C, et al. A dynamic nomenclature proposal for SARS-CoV-2 lineages to assist genomic epidemiology. Nat Microbiol. 2020;5:1403–7. https://doi.org/10.1038/s41564-020-0770-5
9. Centers for Disease Control and Prevention. Variant proportions.2021 May 18 [cited 2021 May 19]. https://covid.cdc.gov/covid-data-tracker/?CDC_AA_refVal=https%3A%2F%2Fwww.cdc.gov%2Fcoronavirus%2F2019-ncov%2Fcases-updates%2Fvariant-proportions.html#variant-proportions

Address for correspondence: Efrem S. Lim, Arizona State University, PO Box 876101, Tempe, AZ 85287, USA; email: Efrem.Lim@asu.edu

SARS-CoV-2 Neutralization Resistance Mutations in Patient with HIV/AIDS, California, USA

Seth A. Hoffman, Cristina Costales, Malaya K. Sahoo, Srikanth Palanisamy, Fumiko Yamamoto, ChunHong Huang, Michelle Verghese, Daniel A. Solis, Mamdouh Sibai, Aruna Subramanian, Lucy S. Tompkins, Philip Grant, Robert W. Shafer, Benjamin A. Pinsky

Author affiliation: Stanford University School of Medicine, Stanford, California, USA

DOI: https://doi.org/10.3201/eid2710.211461

We report persistent severe acute respiratory syndrome coronavirus 2 infection in a patient with HIV/AIDS; the virus developed spike N terminal domain and receptor binding domain neutralization resistance mutations. Our findings suggest that immunocompromised patients can harbor emerging variants of severe acute respiratory syndrome coronavirus 2.

In December 2020, a 61-year-old woman living with HIV/AIDS was tested for severe acute respiratory syndrome coronavirus 2 (SARS-CoV-2) infection at a community testing center in California, USA; she produced an anterior nasal swab sample that tested positive by reverse transcription PCR (RT-PCR). At the time of sample collection, she had a 10-day history of nonproductive cough, and was not receiving antiretroviral therapy (Figure). Her CD4 count was

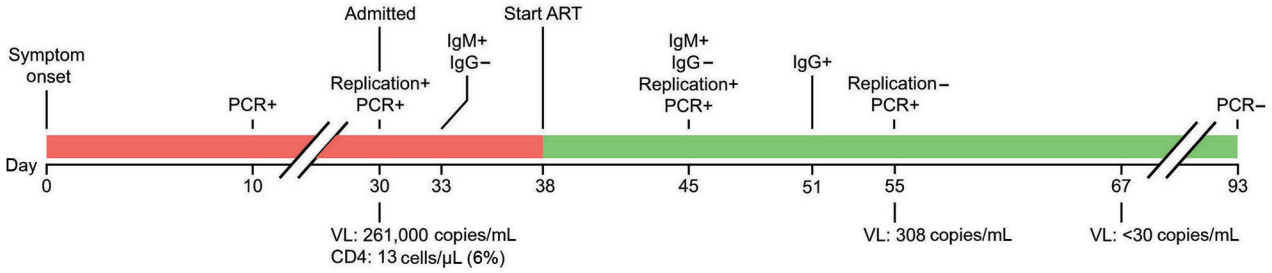

Figure. Timeline of SARS-CoV-2 infection in a patient with HIV/AIDS, California, USA. Line breaks indicate separation in time intervals. Replication indicates detection of minus-strand RNA. ART, antiretroviral therapy; IgG, spike S1 domain IgG; IgM, spike receptor binding domain IgM; VL, HIV viral load; +, positive; –, negative.

13 cells/μL and HIV-1 viral load was 262,000 copies/mL. She never required hospitalization for SARS-CoV-2 infection. Thirty days after symptom onset, she no longer had respiratory symptoms and underwent SARS-CoV-2 screening upon admission to Stanford Hospital (Stanford, CA, USA) for treatment of a severe decubitus ulcer. Her nasopharyngeal swab (NPS) sample tested positive for SARS-CoV-2 by RT-PCR (cycle threshold [C_t] value 17.6). We detected minus-strand viral RNA, indicating active viral replication (*1*). On day 33, three days after admission to Stanford Hospital, antibody testing showed plasma positive for IgM against SARS-CoV-2 spike receptor binding domain (RBD) but negative for IgG against SARS-CoV-2 spike S1 (*2*,*3*). She began antiretroviral therapy (ART) 38 days after symptom onset. On day 45, an NPS sample tested positive (C_t 16.6) for SARS-CoV-2 with detectable minus-strand RNA.

Because the patient had ongoing viral replication, we conducted whole-genome sequencing using archived nucleic acids from the NPS samples collected on days 30 and 45. We enriched the viral genome using laboratory-developed multiplex RT-PCR reactions that generated multiple overlapping amplicons of ≈1,200 bp. We prepared fragment libraries using NEBNext DNA Library Prep reagents (New England Biolabs, https://www.neb.com) according to the manufacturer's instructions; we sequenced the libraries on Illumina MiSeq with single-end 150-cycle sequencing using MiSeq Reagent Kit v3 (https://www.illumina.com). We assembled the consensus sequences and identified mutations using a custom bioinformatics pipeline and SARS-CoV-2 isolate Wuhan-Hu-1 (GenBank accession no. NC_45512.2) as reference. For these 2 samples we observed mean whole-genome coverage of 963× (day 30) and 894× (day 45). We used the consensus sequences from the day 30 (GISAID accession no. EPI_ISL_2009056) and day 45 (GISAID accession no. EPI_ISL_2009057) samples to query the GISAID CoVserver (https://www.gisaid.org) and Phylogenetic Assignment of Named Global Outbreak LINeages (PANGOLIN, https://pangolin.cog-uk.io) to determine clade and lineage.

The sequence from the sample taken on day 30 revealed a G clade, B.1.234 lineage virus (Table). Because the day 45 sequence shares 18 mutations (8 synonymous and 10 nonsynonynmous) with the day 30 sequence and is the most closely related sequence to the day 30 sequence in GISAID, we believe the day 45 sequence probably evolved from the day 30 sequence. The day 45 sequence contained additional spike mutations, including C15F (variant percent 44.3%), del141_144 (17.5%), Y248N (13.4%), ins248_Y/LLSFN (44.5%), and E484Q (67.7%) (Table). The cysteine residue at position 15 (C15) in the spike N terminal domain (NTD) is linked by a disulfide bond to C136; mutations at either of these positions alter this bond and reduce neutralization by monoclonal antibodies (*4*). Deletions and insertions in the NTD are also involved in immune escape, including the common del141_144 mutation and insertions at position Y248 (*5*). The E484Q mutation is located in the RBD domain of the spike gene and is also found in the Kappa variant of interest (i.e., B.1.617.1) (*6*). Viruses harboring E484Q have reduced susceptibility to monoclonal antibodies, convalescent plasma, and vaccinee plasma (*7*,*8*).

The patient showed SARS-CoV-2 IgG seroconversion on day 51, thirteen days after initiating ART. SARS-CoV-2 antibody isotypes typically follow a similar time-course; IgM, IgA, and IgG usually become detectable ≈14 days after illness onset (*2*). This patient's delayed IgG class switch was probably caused by HIV/AIDS-associated B-cell dysfunction; we hypothesize that the ineffective IgM response might have selected for the observed spike mutations (*9*). On day 55, seventeen days after initiating ART, the patient's HIV-1 viral load was 330 copies/mL. An NPS sample collected that day was negative for minus-strand SARS-CoV-2 RNA, and the viral load had

Table. Mutations in severe acure respiratory syndrome coronavirus 2 sequences from a patient with HIV/AIDS, California, USA*

Nucleotide mutation	Translation	Variant reads/read depth (%)	
		Day 30	Day 45
Day 45 sample only			
21606G>T	S: C15F	ND	661/1,493 (44.3)
d21982_12	S: del_141–144	ND	248/1,420 (17.5)
22304T>A	S: Y248N	ND	333/2,488 (13.4)
ins_22304_12 (TAT>TTACTCAGTTTTAAT)	S: ins_248_Y->LLSFN	ND	919/2,065 (44.5)
23012G>C	S: E484Q	ND	1,088/1,607 (67.7)
Day 30 sample only			
26801C>T	Membrane protein: L93L	753/2,196 (34.3)	ND
27146A>G	Membrane protein: T208T	567/1,843 (30.8)	ND
Both samples			
241C>T	5′ untranslated region	1,206/1,213 (99.4)	848/851 (99.6)
829C>T	NSP2: N8N	862/866 (99.5)	652/653 (99.8)
2258G>A	NSP2: V485I	3,280/3,293 (99.6)	1,524/1,528 (99.7)
3037C>T	NSP3: F106F	1,781/1,783 (99.9)	1,139/1,142 (99.7)
6441A>G	NSP3: K1241R	2,385/2,389 (99.8)	1,499/1,500 (99.9)
8140C>T	NSP3: S1807S	2,491/2,505 (99.4)	1,399/1,410 (99.2)
9204A>G	NSP4: D217G	1,395/1,401 (99.6)	651/653 (99.7)
10015C>T	NSP4: Y487Y	527/530 (99.4)	244/245 (99.6)
10641C>T	NSP5: T196M	516/517 (99.8)	176/179 (98.3)
13858G>T	NSP12: D131Y (or RdRp D140Y)	3,814/3,832 (99.5)	3,081/3,100 (99.4)
14408C>T	NSP12: P314L (or RdRp P323L)	3,923/3,938 (99.6)	2,872/2,890 (99.4)
18288A>G	NSP14: V83V	2,498/2,521 (99.1)	1,868/1,886 (99.0)
20268A>G	NSP15: L216L	1,655/1,662 (99.6)	873/885 (98.6)
23403A>G	S: D614G	2,991/3,018 (99.1)	1,792/1,800 (99.6)
28744C>T	NP: I157I	5,669/5,704 (99.4)	4,311/4,343 (99.3)
28854C>T	NP: S194L	5,681/5,706 (99.6)	4,477/4,498 (99.5)
29384G>T	NP: D371Y	5,843/5,889 (99.2)	4,779/4,807 (99.4)
29445C>T	NP: T391I	5,928/6,006 (98.7)	4,641/4,670 (99.4)

*Compared with the reference Wuhan-Hu-1 (GenBank accession no. NC_045512.2) sequence. Patient samples collected 30 (hCoV-19/USA/CA-Stanford-07_S25/2021, GISAID accession no. EPI_ISL_2009057) and 45 (hCoV-19/USA/CA-Stanford-07_S24/2021, GISAID accession no. EPI_ISL_2009056) days after symptom onset. ND, not detected; NP, nucleoprotein; NSP, nonstructural protein; RdRp, RNA-dependent RNA polymerase; S, spike protein.

decreased >1,000-fold (C_t 27.2). The patient's SARS-CoV-2 infection remained asymptomatic throughout her hospitalization. On day 93, she produced an NPS sample that tested negative for SARS-CoV-2 RNA.

In summary, we describe an HIV-positive patient who had a prolonged course of asymptomatic, active SARS-CoV-2 infection leading to the emergence of NTD and RBD mutations associated with reduced antibody neutralization. Our findings add to the accumulating evidence that immunocompromised persons, including persons living with HIV/AIDS, might host ongoing SARS-CoV-2 replication that could enable the development of variants of concern/interest (F. Karim, unpub. data, https://www.medrxiv.org/content/10.1101/2021.06.03.21258228v1). The emergence of multiple spike mutations in this patient over a relatively short timeframe (i.e., 15 days) further highlights the potential role of persons living with uncontrolled HIV as possible sources of SARS-CoV-2 variants. Finally, these findings emphasize the need to diagnose HIV in the >6 million infected persons worldwide who are unaware of their status and provide them with accessible ART. These interventions are critical for overall global health and might also contribute to controlling the COVID-19 pandemic.

Acknowledgments

We thank the healthcare providers and laboratory staff at Stanford Health Care for their high-quality work and dedication to patient care.

About the Author

Dr. Hoffman is an infectious diseases fellow at the Stanford University School of Medicine, Stanford, California, USA. His research interests include global health equity and clinical research to benefit underserved populations.

References

1. Hogan CA, Huang C, Sahoo MK, Wang H, Jiang B, Sibai M, et al. Strand-specific reverse transcription PCR for detection of replicating SARS-CoV-2. Emerg Infect Dis. 2021;27:632–5. https://doi.org/10.3201/eid2702.204168
2. Röltgen K, Powell AE, Wirz OF, Stevens BA, Hogan CA, Najeeb J, et al. Defining the features and duration of antibody responses to SARS-CoV-2 infection associated with disease severity and outcome. Sci Immunol. 2020;5:eabe0240. https://doi.org/10.1126/sciimmunol.abe0240
3. Wang H, Wiredja D, Yang L, Bulterys PL, Costales C, Röltgen K, et al. Case-control study of individuals with discrepant nucleocapsid and spike protein SARS-CoV-2 IgG results. Clin Chem. 2021;67:977–86. https://doi.org/10.1093/clinchem/hvab045

4. McCallum M, De Marco A, Lempp FA, Tortorici MA, Pinto D, Walls AC, et al. N-terminal domain antigenic mapping reveals a site of vulnerability for SARS-CoV-2. Cell. 2021;184:2332–2347.e16. https://doi.org/10.1016/j.cell.2021.03.028
5. Harvey WT, Carabelli AM, Jackson B, Gupta RK, Thomson EC, Harrison EM, et al.; COVID-19 Genomics UK (COG-UK) Consortium. SARS-CoV-2 variants, spike mutations and immune escape. Nat Rev Microbiol. 2021;19:409–24. https://doi.org/10.1038/s41579-021-00573-0
6. Verghese M, Jiang B, Iwai N, Mar M, Sahoo MK, Yamamoto F, et al. A SARS-CoV-2 variant with L452R and E484Q neutralization resistance mutations. J Clin Microbiol. 2021;59:e0074121. https://doi.org/10.1128/JCM.00741-21
7. Edara VV, Pinsky BA, Suthar MS, Lai L, Davis-Gardner ME, Floyd K, et al. Infection and vaccine-induced neutralizing-antibody responses to the SARS-CoV-2 B.1.617 variants. N Engl J Med. 2021;NEJMc2107799. https://doi.org/10.1056/NEJMc2107799
8. Greaney AJ, Loes AN, Crawford KHD, Starr TN, Malone KD, Chu HY, et al. Comprehensive mapping of mutations in the SARS-CoV-2 receptor-binding domain that affect recognition by polyclonal human plasma antibodies. Cell Host Microbe. 2021;29:463–476.e6. https://doi.org/10.1016/j.chom.2021.02.003
9. Moir S, Fauci AS. B cells in HIV infection and disease. Nat Rev Immunol. 2009;9:235–45. https://doi.org/10.1038/nri2524

Address for correspondence: Benjamin A. Pinsky, Stanford University School of Medicine, 3375 Hillview Ave, Rm 2913, Palo Alto, CA 94304, USA; email: bpinsky@stanford.edu

SARS-CoV-2 Delta Variant among Asiatic Lions, India

Anamika Mishra, Naveen Kumar, Sandeep Bhatia, Ashutosh Aasdev, Sridhar Kanniappan, Abelraj Thaya Sekhar, Aparna Gopinadhan, Ramu Silambarasan, Chirukandoth Sreekumar, Chandan Kumar Dubey, Meghna Tripathi, Ashwin Ashok Raut, Vijendra Pal Singh

Author affiliations: ICAR–National Institute of High Security Animal Disease, Bhopal, India (A. Mishra, N. Kumar, S. Bhatia, A. Aasdev, C.K. Dubey, M. Tripathi, A.A. Raut, V.P. Singh); Arignar Anna Zoological Park, Chennai, India (S. Kanniappan, A.T. Sekhar, A. Gopinadhan, R. Silambarasan); Madras Veterinary College, Chennai (C. Sreekumar); All India Institute of Medical Sciences, Bhopal (A.A. Raut)

DOI: https://doi.org/10.3201/eid2710.211500

In May 2021, severe acute respiratory syndrome coronavirus 2 (SARS-CoV-2) was detected in Asiatic lions in a zoological park in India. Sequence and phylogenetic analyses showed the SARS-CoV-2 strains were the B.1.617.2 (Delta) variant. To reduce transmission of variants of concern, surveillance of SARS-CoV-2 in wild animal populations should be increased.

Severe acute respiratory syndrome coronavirus 2 (SARS-CoV-2), in natural conditions, has shown a broad host susceptibility range (*1*). Identifying susceptible animal species, reservoirs, and cross-species transmission is a global scientific and public health concern. We found evidence of natural SARS-CoV-2 infection in Asiatic lions (*Panthera leo persica*) caused by the lineage B.1.617.2 (Delta) variant (World Health Organization nomenclature). We provide coronavirus disease (COVID-19) case information and detailed genomic characterization.

Arignar Anna Zoological Park in Chennai, India, houses 13 Asiatic lions, 9 in a lion safari and 2 each in separate moat enclosures. Beginning May 21, 2021, four of the safari lions started showing signs of loss of appetite, nasal discharge, and occasional coughing. Nasal swab, rectal swab, and fecal samples were collected from 11 lions during May 24–29, 2021, and sent to the Indian Council of Agricultural Research–National Institute of High Security Animal Diseases (Bhopal, India) for molecular investigations (Appendix Table 1, https://wwwnc.cdc.gov/EID/article/27/10/21-1500-App1.pdf).

We used the VIRALDTECT II Multiplex Real Time PCR Kit for COVID-19 (Genes2Me, https://genes2me.com) to confirm SARS-CoV-2 in 9/11 lions. The other 2 lions were sampled on June 19, 2021, and tested negative for SARS-CoV-2. We also used a World Organisation for Animal Health–recommended reverse transcription PCR (RT-PCR) method to test for canine distemper virus on samples from all 13 lions; all tested negative (*2*). Two of the infected lions died of COVID-19, one on June 3 and the other on June 16, 2021.

After we confirmed SARS-CoV-2 infection, we performed whole-genome sequencing directly from nasal swab specimens of 4 lions that initially showed symptoms by using the MinION sequencing platform (Oxford Nanopore Technologies, https://nanoporetech.com) (Appendix). We deposited sequences in GenBank (accession nos. MZ363851–4) and GISAID (https://www.gisaid.org; accession nos. EPI_ISL_2821077–80).

To elucidate the temporal dynamics of SARS-CoV-2 among the lions, we downloaded 310 complete SARS-CoV-2 genomes from GISAID (*3*) that had high coverage and were sequenced from the Tamil Nadu state of

India, where the zoological park is located, during January 1–June 11, 2021. To generate a set of representative sequences, we used a UCLUST algorithm (*4*) to select sequences that clustered at the 99.9% identity threshold. We used MAFFT version 7.475 (*5*) to align representative SARS-CoV-2 sequences from GISAID with sequences from the lions; then we constructed a phylogenetic tree by using the general time reversible plus gamma model in RAxML version 8.2.12 (*6*) (Figure).

The amino acid substitutions and deletions in the spike protein of SARS-CoV-2 in lions typically matched with the SARS-CoV-2 Delta variant (Appendix Table 2). We noted amino acid changes in the N terminal domain (NTD), including T19R, G142D, E156del, F157del, R158G; in the receptor binding motif (RBM), including L452R and T478K; and in D614G of subdomain 2. We also noted a substitution close to S1/S2 protease cleavage site at P681R and heptad repeat 1 at D950N (Appendix Figures 1, 2). In addition, the lion sequences had the K77T substitution in the NTD, which has been detected in SARS-CoV-2 genomes from 24 countries. In India, frequency of the K77T substitution generally is low (0.44%) but occurred in 27.42% (65/237) of sequences in the B.1.167.2 lineage collected in Tamil Nadu state (Appendix Table 2).

The changes in the spike protein, including E156del, F157del, and R158G, of lion sequences were not found in human SARS-CoV-2 sequences from the same geographic area, nor were changes in nonstructural protein 3 (NS3) V88I, possibly because SARS-CoV-2 sequencing is limited in the region. Furthermore, these changes in spike and NS3 were not seen in previously reported lion SARS-CoV-2 sequences, ruling out the possibility that these are host-adapted mutations (*7*) (Appendix Figure 3). Further investigations could delineate whether changes in the spike protein, namely E156del, F157del, R158G, and K77T, are escape mutants or are associated with increased transmissibility or pathogenicity.

A nucleotide similarity comparison of the 4 lion SARS-CoV-2 sequences against the sequences available in GISAID and phylogenetic analysis revealed that the lion sequences closely matched with a representative human SARS-CoV-2 sequence of B.1.617.2 lineage, GISAID accession no. EPI_ISL_2463770, that comprises 152 viral genome pools collected from the same geographic region during the same month that the lions' samples were collected (Figure; Appendix Figure 4). The park's management strictly adhered to COVID-19 guidelines and did not introduce any new animals to the zoo during India's widespread COVID-19 pandemic. The primary source of SARS-CoV-2 infection in the lions might have been an asymptomatic or paucisymptomatic person. Among the 9 infected lions, 7 were in the lion safari and shared a common habitat, shelter, feeding spaces, and water sources. The other 2 infected lions were on display in separate enclosures that shared a common moat. Because shared habitats offered opportunities for close physical contact, identifying genetically identical SARS-CoV-2 infections in these lions in a short period of time indicates the possibility of lion-to-lion transmission.

In conclusion, evidence of confirmed natural SARS-CoV-2 Delta variant infections in Asiatic lions in India justifies need for increased SARS-CoV-2 surveillance in wild animal species. In addition, strict biosecurity measures should be implemented for wild animals kept in captivity.

This article was preprinted at https://doi.org/10.1101/2021.07.02.450663.

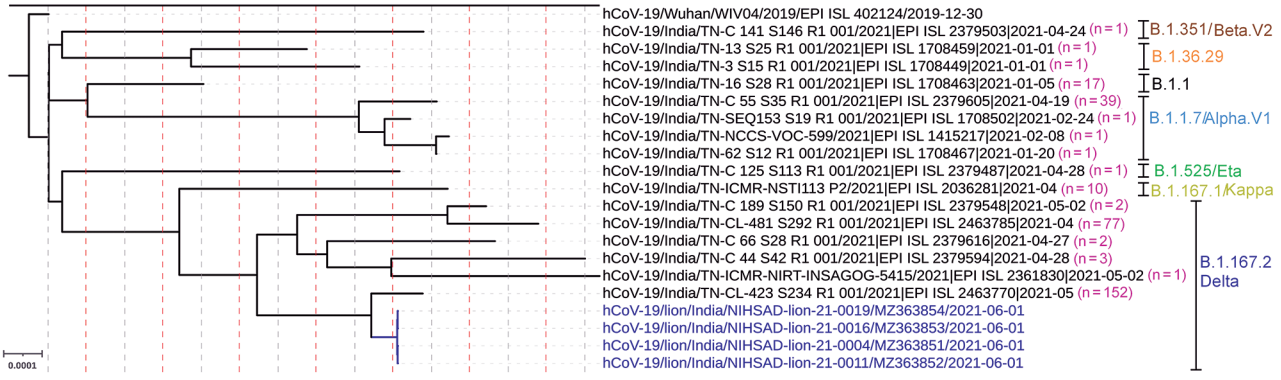

Figure. Complete genome phylogenetic analysis of severe acute respiratory syndrome coronavirus 2 (SARS-CoV-2) detected in Asiatic lions (*Panthera leo persica*), India (blue text), and representative sequences of different clusters generated at 99.9% identity threshold from the available SARS-COV-2 sequences from Tamil Nadu, India, in the GISAID. The maximum-likelihood tree was rooted to Wuhan-Hu-1 reference sequence (GISAID accession no. EPI_ISL_402124). GenBank accession numbers are provided for the sequences from this study. Pink numbers in parentheses indicate the number of SARS-CoV-2 genome sequences clustered at 99.9% identity threshold. Other text colors represent SARS-CoV-2 variants. Scale bar indicates nucleotide substitutions per site.

Acknowledgments

We thank Debasis Jana (Arignar Anna Zoological Park, Chennai, India) for providing the clinical information and for sending samples for SARS-CoV-2 molecular investigations for the lions. We also thank V.P. Singh for providing infrastructure facilities to carry out this study, Atul Kumar Pateriya for assistance with quantitative reverse transcription PCR, and the originating and submitting laboratories for sharing SARS-CoV-2 genomic sequence data via GISAID.

This study was funded by the service project of ICAR-National Institute of High Security Animal Diseases (ICAR-NIHSAD), Bhopal, India, and ICAR-National Agricultural Science Fund (grant no. NASF/ABA-8027/2020-21).

About the Author

Dr. Mishra holds a senior scientist position in the Zoonotic Diseases Group, ICAR-National Institute of High Security Animal Diseases, Bhopal, India. Her primary research interests are the pathogenomics and host-pathogen interactions of high-risk zoonotic viruses.

References

1. World Organisation for Animal Health. SARS-COV-2 in animals—situation report 1 [cited 2021 Jun 16]. https://www.oie.int/app/uploads/2021/06/sars-cov-2-situation-report-1.pdf
2. Frisk AL, König M, Moritz A, Baumgärtner W. Detection of canine distemper virus nucleoprotein RNA by reverse transcription-PCR using serum, whole blood, and cerebrospinal fluid from dogs with distemper. J Clin Microbiol. 1999;37:3634–43. https://doi.org/10.1128/JCM.37.11.3634-3643.1999
3. Elbe S, Buckland-Merrett G. Data, disease and diplomacy: GISAID's innovative contribution to global health. Glob Chall. 2017;1:33–46. https://doi.org/10.1002/gch2.1018
4. Edgar RC. Search and clustering orders of magnitude faster than BLAST. Bioinformatics. 2010;26:2460–1. https://doi.org/10.1093/bioinformatics/btq461
5. Katoh K, Standley DM. MAFFT multiple sequence alignment software version 7: improvements in performance and usability. Mol Biol Evol. 2013;30:772–80. https://doi.org/10.1093/molbev/mst010
6. Stamatakis A. RAxML version 8: a tool for phylogenetic analysis and post-analysis of large phylogenies. Bioinformatics. 2014;30:1312–3. https://doi.org/10.1093/bioinformatics/btu033
7. McAloose D, Laverack M, Wang L, Killian ML, Caserta LC, Yuan F, et al. From People to *Panthera*: natural SARS-CoV-2 infection in tigers and lions at the Bronx Zoo. MBio. 2020;11:e02220–20. https://doi.org/10.1128/mBio.02220-20

Address for correspondence: Anamika Mishra, Pathogenomics Lab, Zoonotic Diseases Group, ICAR-National Institute of High Security Animal Disease, Bhopal 462022, India; email: reach2anamika@yahoo.com

SARS-CoV-2 Variants in Immunocompromised Patient Given Antibody Monotherapy

Aurélie Truffot, Julien Andréani, Marion Le Maréchal, Alban Caporossi, Olivier Epaulard, Raphaele Germi, Pascal Poignard, Sylvie Larrat

Author affiliation: Centre Hospitalier Universitaire Grenoble Alpes, Grenoble, France

DOI: https://doi.org/10.3201/eid2710.211509

A 72-year-old immunocompromised man infected with severe acute respiratory syndrome coronavirus 2 received bamlanivimab monotherapy. Viral evolution was monitored in nasopharyngeal and blood samples by melting curve analysis of single-nucleotide polymorphisms and whole-genome sequencing. Rapid emergence of spike receptor binding domain mutations was found, associated with a compartmentalization of viral populations.

A 72-year-old immunocompromised man in France who had chronic lymphocytic leukemia associated with hypogammaglobinemia for 4 years experienced diarrhea, asthenia, fever, and cough associated with coronavirus disease (COVID-19). Although he had received 1 injection of severe acute respiratory syndrome coronavirus 2 (SARS-CoV-2) mRNA vaccine (BNT162b2; Pfizer/BioNTech, https://www.pfizer.com) 20 days earlier, we confirmed a diagnosis of COVID-19 by using a semiquantitative SARS-CoV-2 reverse transcription PCR (RT-PCR) viral load assay. This assay showed a cycle threshold (C_t) value of 27 for a nasopharyngeal swab specimen. His most recent monoclonal antibody (mAb) chemotherapy treatment (venetoclax and rituximab) had been conducted 17 days earlier. Because of his immunocompromised status, treatment with bamlanivimab (LY-CoV555), a neutralizing IgG1 mAb, was initiated at day 0, 4 days after onset of symptoms (Table). The patient received an infusion of 700 mg in a single dose and was discharged.

Analysis of samples showed a high viral load in a nasopharyngeal swab specimen (C_t 20) and a blood sample (C_t 37) (Table). Three days after the mAb infusion, the patient's symptoms worsened, and he was hospitalized in the Infectious Diseases Department at Grenoble Hospital (Grenoble, France) on day 6. The condition of the patient had deteriorated; he had an additional need for oxygen, which resulted in a convalescent-phase plasma transfusion on day 10.

After this treatment, the condition of the patient continued to deteriorate, and he was transferred to

the intensive care unit on day 13. A high dose of corticosteroids was given on days 21–26. This treatment resulted in an improvement of his respiratory condition, but the patient remained dependent on supplemental oxygen (6 L/min). The patient was discharged from the intensive care unit and returned

Table. Clinical and biological characteristics of immunocompromised patient given bamlanivimab for COVID-19, France*

Disease course, day†	Clinical manifestations	Treatment/action	Clinical samples‡	RT-PCR results (mean C_t value)	VirSNIP Kit results	NGS clade
–20		First dose mRNA vaccine§				
–17		Venetoclax, rituximab				
–4	Cough, fever, diarrhea, asthenia	NA				
–3			NP	Positive (27)¶	NA	NA
0		Bamlanivimab (700 mg)				
3			NP	Positive (20)	E484, N501Y	20I/501Y.V1
			Blood	Positive (37)	NA	NA
			Serum (30.7)			
6		Hospitalized at infectious diseases department	NP	Positive (21)	E484Q, N501Y	20I/501Y.V1 + E484Q
			Blood	Negative	NA	NA
7			Serum (23.2)			
10		Convalescent-phase plasma	NP	Positive (17)	E484Q, N501Y	20I/501Y.V1 + E484Q
11			NP	Positive (19)	E484Q, N501Y	20I/501Y.V1 + E484Q
			Blood	Positive (30)	E484, N501Y	20I/501Y.V1 ± 493R
		High-flow nasal oxygen	Serum (26.5)			
13		Transferred to ICU				
15			NP	Positive (21)	E484Q, N501Y	20I/501Y.V1+E484Q
17			Blood	Positive (31)	E484, N501Y	20I/501Y.V1 ± 493R ± 484K ± 484Q
			Serum (22.9)			
21		High-dose corticotherapy protocol				
26		High-dose corticotherapy protocol				
33		Transferred to infectious disease department	NP	Positive (17)	E484Q, N501Y	20I/501Y.V1 + E484Q
	Improvement in respiratory condition	NA	Blood	Positive (37)	NA	NA
			Serum (30.8)			
39			NP	Positive (17)	E484Q, N501Y	20I/501Y.V1 + E484Q
			Blood	Negative		
			Serum (18.6)			
45			NP	Positive (20)	E484Q, N501Y	20I/501Y.V1 + E484Q
47		Treatment with remdesivir (10 d)				
52			NP	Positive (31)	E484Q, N501Y	20I/501Y.V1 + E484Q
54			NP	Positive (30)	E484Q, N501Y	20I/501Y.V1 + E484Q
56		Hospitalization for follow-up care				
61			NP	Negative	NA	NA
80			NP	Negative	NA	NA

*Blank cells indicate that clinical status was stable on that day, and no treatment was given. COVID-19, coronavirus disease; C_t, cycle threshold; D, day; ICU, intensive care unit; NA, not available; NP, nasopharyngeal swab specimen; NGS, next-generation sequencing; RT-PCR, reverse transcription PCR.
†Day 0 indicates first day of follow-up care at hospital.
‡Serologic results given by using the Wantai antibody test (index of positivity = 1).
§Vaccine BNT162b2 (Pfizer/BioNTech, https://www.pfizer.com).
¶Test was performed in an external laboratory (no sample was available for further analysis).

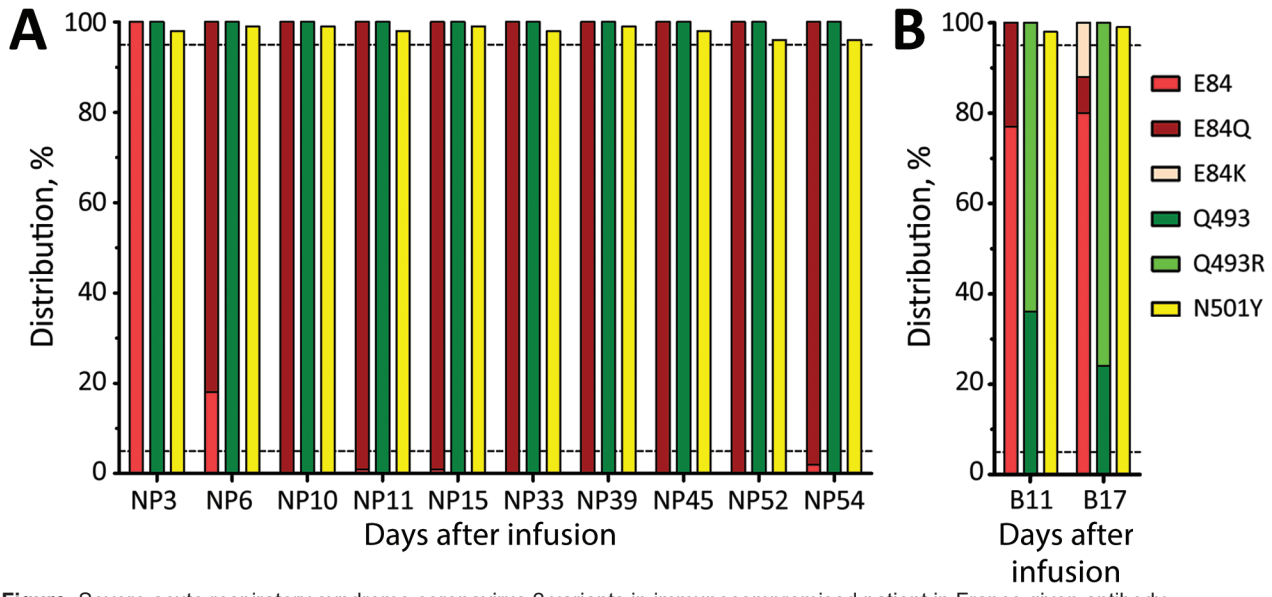

Figure. Severe acute respiratory syndrome coronavirus 2 variants in immunocompromised patient in France given antibody monotherapy showing compartmentalization and variation of mutation frequency for the spike protein. Mutations of interest are indicated by days after bamlanivimab infusion. A) NP samples; B) blood samples. The upper dashed horizontal line indicates 95% and the lower dashed horizontal line indicates 5%. B, blood; NP, nasopharyngeal.

to the infectious disease department on day 33, but still had a high viral load in nasopharyngeal swab specimens (C_t v20 on day 45).

Because of this persistent viral replication, the patient was given remdesivir on day 47 and this treatment was continued for 10 days (200 mg for 1 day, followed by 100 mg/d for 9 days). SARS-CoV-2 carriage in a nasopharyngeal swab specimen decreased during treatment, and the patient was discharged from the infectious disease department and transferred to a rehabilitation center. The nasopharyngeal swab specimen viral load became negative on day 61.

To monitor viral evolution, we performed a multiplex RT-PCR based on melting curve analyses with VirSNIP Kits (TIB Molbiol, https://www.tib-molbiol.de) to evaluate the presence of the S: E484K and S: N501Y mutations in SARS-CoV-2 variants. Three days after mAb treatment (day 3), RT-PCR results suggested the presence of S: N501Y and an absence of S:E484K on an nasopharyngeal swab specimen. On day 6, the S:N501Y mutation was still present but was also found associated with an undetermined mutation at position 484 (melting temperatures different from those of wild-type E and the mutated strain K). On day 11, we detected the S: N501Y mutation in a blood sample but found no mutation at position 484. No nasopharyngeal swab specimen or blood sample from before mAb administration was available for analysis and comparison.

We performed whole-genome sequencing on 12 clinical samples by using amplicon-based technology on the Ion Torrent Platform (ThermoFisher, https://www.thermofisher.com) according to the protocol of and plug-ins used by Sjaarda et al. (*1*). We confirmed results of this analysis by using the minimap2 program (*2*). This analysis detected clade 20I/501Y.V1, Alpha variant (Pangolin: B.1.1.7), on day 3 in nasopharyngeal swab specimens. Three days later (day 6), a novel mutation (G23012C, S: E484Q) appeared in nasopharyngeal swab specimens at frequency of 82%, which rapidly reached >99% (S: E484Q) 10 days after mAb treatment (Table; Figure). Eleven days after the mAb infusion, we detected an additional nucleotide mutation A23040G (S: Q493R) in only a blood sample at a frequency of 64%. This rate reached 76% at day 17 without any detection in nasopharyngeal swab specimens.

Clinical trials of monotherapy treatment for SARS-CoV-2 infection have shown that subsequent dynamic shifts in the viral population appear to be frequent (*3*,*4*). An in vitro model showed that E484 and Q493 are 2 amino acid mutations of the spike protein that are known to be critical for bamlanivimab binding (*5*,*6*). The S: E484Q mutation is a hotspot of escape and could reduce susceptibility to bamlanivimab by >1,000-fold (*6*) and S: Q493R by >6,666-fold (*7*). Use of bitherapy with bamlanivimab and etesevimab decreases the risk for emergence of drug-resistant variants (*5*,*8*). However, an escape mutation after use of this drug combination was recently described (*7*).

Our analysis identified signs of compartmentalized viral populations on the basis of sequences

recovered in blood and nasopharyngeal swab samples (notably on day 17). Such a phenomenon has been reported in clinical trials (*9*,*10*). Further analysis is needed to distinguish genetic changes that occur in the primary viral population from apparent changes to clarify whether such escape mutants are enough to spread and persist in humans and how SARS-CoV-2 displays compartmentalized replication. Genomic surveillance for SARS-CoV-2 variants is encouraged for COVID-19 patients given mAbs as monotherapy or biotherapy.

About the Author

Dr. Truffot is a physician in the Department of Virology, University Hospital of Grenoble, Grenoble, France. Her research interests include novel sequencing technologies for genome diagnosis and follow-up of major pathogens, including SARS-CoV-2, and quantification of monoclonal antibodies by high-performance liquid chromatography/mass spectrometry.

References

1. Sjaarda CP, Rustom N, Evans GA, Huang D, Perez-Patrigeon S, Hudson ML, et al. Phylogenomics reveals viral sources, transmission, and potential superinfection in early-stage COVID-19 patients in Ontario, Canada. Sci Rep. 2021;11:3697. https://doi.org/10.1038/s41598-021-83355-1
2. Li H. Minimap2: pairwise alignment for nucleotide sequences. Bioinformatics. 2018;34:3094–100. https://doi.org/10.1093/bioinformatics/bty191
3. Gottlieb RL, Nirula A, Chen P, Boscia J, Heller B, Morris J, et al. Effect of bamlanivimab as monotherapy or in combination with etesevimab on viral load in patients with mild to moderate COVID-19: a randomized clinical trial. JAMA. 2021;325:632–44. https://doi.org/10.1001/jama.2021.0202
4. Lohr B, Niemann D, Verheyen J. Bamlanivimab treatment leads to rapid selection of immune escape variant carrying E484K mutation in a B.1.1.7 infected and immunocompromised patient. Clin Infect Dis. 2021 May 1 [Epub ahead of print]. https://doi.org/10.1093/cid/ciab392
5. Baum A, Fulton BO, Wloga E, Copin R, Pascal KE, Russo V, et al. Antibody cocktail to SARS-CoV-2 spike protein prevents rapid mutational escape seen with individual antibodies. Science. 2020;369:1014–8. https://doi.org/10.1126/science.abd0831
6. Starr TN, Greaney AJ, Dingens AS, Bloom JD. Complete map of SARS-CoV-2 RBD mutations that escape the monoclonal antibody LY-CoV555 and its cocktail with LY-CoV016. Cell Rep Med. 2021;2:100255. https://doi.org/10.1016/j.xcrm.2021.100255
7. Focosi D, Novazzi F, Genoni A, Dentali F, Dalla Gasperina D, Baj A, et al. Emergence of SARS-CoV-2 spike protein escape mutation Q493R after treatment for COVID-19. Emerg Infect Dis. 2021;27: 2728–31. https://doi.org/10.3201/eid2710.211538
8. Copin R, Baum A, Wloga E, Pascal KE, Giordano S, Fulton BO, et al. The monoclonal antibody combination REGEN-COV protects against SARS-CoV-2 mutational escape in preclinical and human studies. Cell. 2021;184:3949–3961.e11. https://doi.org/10.1016/j.cell.2021.06.002
9. Jary A, Leducq V, Malet I, Marot S, Klement-Frutos E, Teyssou E, et al. Evolution of viral quasispecies during SARS-CoV-2 infection. Clin Microbiol Infect. 2020;26:1560.e1–4. https://doi.org/10.1016/j.cmi.2020.07.032
10. Rueca M, Bartolini B, Gruber CE, Piralla A, Baldanti F, Giombini E, et al. Compartmentalized replication of SARS-Cov-2 in upper vs. lower respiratory tract assessed by whole genome quasispecies analysis. Microorganisms. 2020;8:1302. https://doi.org/10.3390/microorganisms8091302

Address for correspondence: Sylvie Larrat, Laboratoire de Virologie, Centre Hospitalier Universitaire, Grenoble Alpes¸ L'Institut de Biologie et de Pathologie, Blvd de la Chantourne Grenoble, Grenoble 38043, France; email: slarrat@chu-grenoble.fr

Emergence of SARS-COV-2 Spike Protein Escape Mutation Q493R after Treatment for COVID-19

Daniele Focosi, Federica Novazzi, Angelo Genoni, Francesco Dentali, Daniela Dalla Gasperina, Andreina Baj, Fabrizio Maggi

Author affiliations: Pisa University Hospital, Pisa, Italy (D. Focosi); Azienda Socio-Sanitaria Territoriale, Varese, Italy (F. Novazzi, F. Dentali, A. D. Dalla Gasperina, A. Baj, F. Maggi); University of Insubria, Varese, (A. Genoni, F. Dentali, D. Dalla Gasperina, A. Baj, F. Maggi)

DOI: https://doi.org/10.3201/eid2710.211538

We report in vivo selection of a severe acute respiratory syndrome coronavirus 2 spike mutation (Q493R) conferring simultaneous resistance to bamlanivimab and etesivimab. This mutation was isolated from a patient who had coronavirus disease and was treated with these drugs.

Variants of severe acute respiratory syndrome coronavirus 2 (SARS-CoV-2) usually result from random mutations in humans or other hosts, but accelerated evolution can also occur under selective pressure from therapeutic interventions using

neutralizing antibodies (*1*). Bamlanivimab has been recently withdrawn as a monotherapy because of treatment failure against E484K SARS-CoV-2 virus variants. Emergency use remains authorized for the bamlanivimab/etesevimab cocktail, targeting overlapping epitopes (*2*), for which no completely resistant variant has been reported to date. This cocktail has been effective in reducing hospitalizations when administered early after infection (*3*).

Given increasing reports of accelerated intrahost evolution of drug-resistant SARS-CoV-2 clades after neutralizing antibody–based treatments (*4*,*5*), we began screening patients who failed to show virus-negative results for nasopharyngeal swab (NPS) specimens after they were given bamlanivimab/etesevimab. We report an in vivo case of a spike protein escape mutation conferring combined resistance to bamlanivimab and etesevimab.

A 73-year-old man had cholangiocarcinoma diagnosed during February 2021. While he was waiting for chemotherapy, sepsis developed, and he was admitted to Varese Hospital (Varese, Italy) on April 12 and given a steroid and antimicrobial drugs. At admission, reverse transcription PCR (RT-PCR) for SARS CoV-2 in an NPS specimen showed a negative result, but the same test showed a positive result on April 24.

Given that he had recovered from sepsis, the patient was moved to the coronavirus disease unit of the hospital on April 25. He satisfied 1 of the frail-patient categories for emergency use of spike protein monoclonal antibodies approved by the Italian Drug Agency. The patient was also seronegative for S1/S2 IgG against spike protein (Diasorin, https://www.diasorin.com).

On April 26, the patient received a single intravenous infusion of bamlanivimab (700 mg) and etesevimab (400 mg) at the hospital. RT-PCR performed on an NPS specimen collected before the infusion was positive for SARS-CoV-2 and showed a cycle threshold (C_t) of 12 (Alinity Analyzer; Abbott Laboratories, https://www abbott.com).

Follow-up analysis of NPS specimens showed positive results on Apr 28 (C_t 15) and May 3 (C_t 24). Chest computed tomography on April 30 showed progression to interstitial pneumonia, and the patient was given noninvasive ventilation. No additional bamlanivimab/etesevimab infusion was performed, and the patient died on May 14.

According to national guidelines for breakthrough infections, we sequenced SARS-CoV-2–positive samples. We performed a SARS CoV-2 RT-PCR on NPS specimens by using the Alinity Platform (Abbott Laboratories), and measured S1/S2 IgG by using a chemiluminescent immunoassay (Diasorin). We used the Sanger method to sequence the spike gene as reported (*6*), analyzed sequences by using NextStrain (https://nextstrain.org), and deposited sequences in GenBank.

Spike gene sequencing of the NPS specimen obtained on April 24 clade B.1.1.7 (Alpha; NextStrain clade 20I/501Y.V1; GenBank accession no. MZ157261), which was 94% prevalent in Italy at that time. However, the May 3 specimen showed a secondary A1478G peak in the spike protein gene, corresponding to the spike Q493R mutation, which became predominant by May 8 (C_t 18; GenBank accession no. MZ157275) (Figure).

E484, F490, Q493, and S494 are the 4 aa residues within the spike protein receptor-binding motif that are known to be critical for bamlanivimab binding. Q493 is also among the many more receptor-binding motif residues crucial for interactions with etesivimab. Q493R/K (which can be selected in vitro by bamlanivimab [*7*,*8*]) is to date the only mutation that causes resistance to bamlanivimab and etesivimab. This residue also causes resistance to other class 3 monoclonal antibodies (*8*) (i.e., those that do not overlap with the angiotensin-converting enzyme 2 binding site and have accessibility to the receptor-binding domain epitope in the up and down conformations).

In pseudoviral neutralization assays, Q493R reduces susceptibility to bamlanivimab by >6,666-fold, to etesevimab by 232-fold, and to the combination of both drugs by >100-fold (*2*). In a flow cytometry competitive assay, Q493R reduces the 50% inhibitory concentration >100-fold for bamlanivimab and 42-fold for etesivimab (*7*). Q493R has a frequency of 0.006% in the GISAID database (https://www.gisaid.org; 85 of 1,424,998 deposited sequences as of May 8, 2021; https://covid19dashboard.regeneron.com/?tab=Mutation_Details&subTab=Spike), making the occurrence of co-infection with a Q493R-positive strain extremely unlikely in our patient.

It remains unclear how such risk extends to different spike protein monoclonal antibody cocktails targeting nonoverlapping epitopes. Although different mutations can similarly cause immune escape by the nonoverlapping REGN-CoV-2 (imdevimab plus casirivimab) cocktail, hamster models and clinical trials showed no increased emergence of variants (R. Copin et al., Regeneron Pharamaceuticals Inc., pers. comm., 2021 Jun 22). Nevertheless, Choi et al. reported a patient having detectable SARS-CoV-2 for 154 days, and accelerated viral evolution in the spike protein after being given remdesivir and REGN-CoV-2 (*4*).

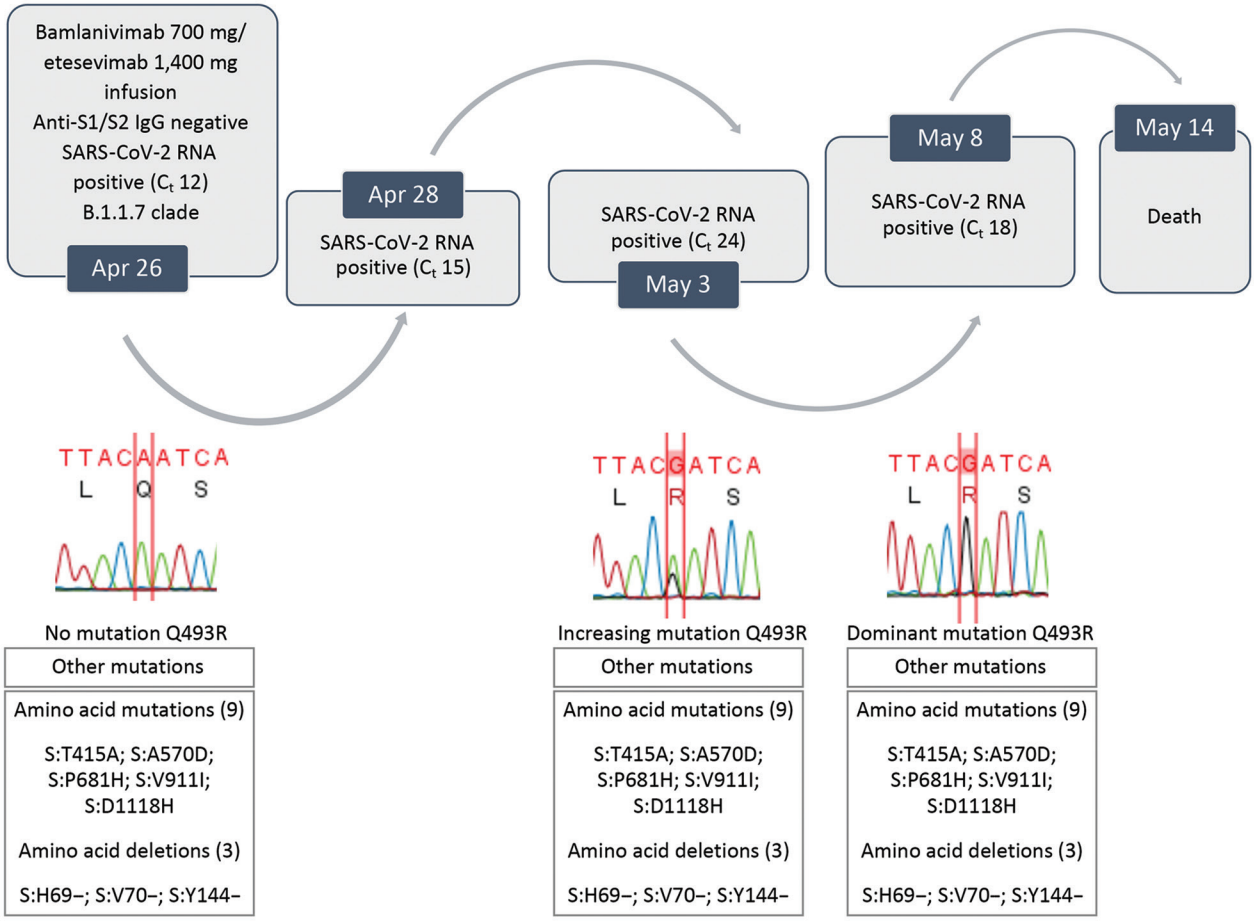

Figure. Evolution of SARS-CoV-2 variants in a patient who had coronavirus disease who was given bamlanivimab and etesivimab, Italy. C_t, cycle threshold; SARS-CoV-2, severe acute respiratory syndrome coronavirus 2.

The nonoverlapping AZD7442 (COV2–2130 and COV2–2196) cocktail also seems resistant to rapid escape (J. Dong et al., Huazhong University of Science and Technology, pers. comm., 2021 Jun 21), but again, such in vitro or animal models could miss rare in vivo events.

In conclusion, SARS-CoV-2 mutations conferring resistance to bamlanivimab and etesevimab can arise in vivo after specific selective pressure; Q493 mutations increase binding affinity to the angiotensin-converting enzyme 2. Additional studies are needed to clarify whether such escape mutations can spread and persist in humans. Genomic surveillance for SARS-CoV-2 variants is encouraged for coronavirus disease patients who do not respond well to treatment with spike protein monoclonal antibodies.

About the Author

Dr. Focosi is a medical research scientist at Pisa University Hospital, Pisa, Italy. His research interests are clinical immunology and emerging viral infections, including diagnostics and neutralizing antibody-based therapeutics.

References

1. Jensen B, Luebke N, Feldt T, Keitel V, Brandenburger T, Kindgen-Milles D, et al. Emergence of the E484K mutation in SARS-COV-2-infected immunocompromised patients treated with bamlanivimab in Germany. Lancet Reg Health Eur. 2021;8:100164. https://doi.org/10.1016/j.lanepe.2021.100164
2. US Food and Drug Administration. Emergency use authorization (EUA) for bamlanivimab 700 mg and estevimab 1,400 mg IV administered together. Center for Drug Use and Evaluation (CDER), 2021 [cited 2021 Jul 22]. https://www.fda.gov/media/145802/download
3. Matthews DB. A cocktail of antibodies for COVID-19 therapy. Nat Rev Immunol. 2020;20:591. https://doi.org/10.1038/s41577-020-00431-9
4. Choi B, Choudhary MC, Regan J, Sparks JA, Padera RF, Qiu X, et al. Persistence and evolution of SARS-CoV-2 in an immunocompromised host. N Engl J Med. 2020;383:2291–3. https://doi.org/10.1056/NEJMc2031364
5. Hensley MK, Bain WG, Jacobs J, Nambulli S, Parikh U, Cillo A, et al. Intractable COVID-19 and prolonged SARS-CoV-2 replication in a CAR-T-cell therapy

recipient: a case study. Clin Infect Dis. 2021;ciab072. https://doi.org/10.1093/cid/ciab072
6. Maggi F, Novazzi F, Genoni A, Baj A, Spezia PG, Focosi D, et al. Imported SARS-COV-2 variant P.1 detected in traveler returning from Brazil to Italy. Emerg Infect Dis. 2021;27:1249–51. https://doi.org/10.3201/eid2704.210183
7. European Medicines Agency. Assessment report Eli Lilly. Company Limited use of bamlanivimab and etesevimab for the treatment of COVID-19, 2021 [cited 2021 Jun 2]. https://www.ema.europa.eu/en/documents/referral/eli-lilly-company-limited-antibody-combination-bamlanivimab/etesevimab-covid19-article-53-procedure-assessment-report_en.pdf
8. Starr TN, Greaney AJ, Dingens AS, Bloom JD. Complete map of SARS-CoV-2 RBD mutations that escape the monoclonal antibody LY-CoV555 and its cocktail with LY-CoV016. Cell Rep Med. 2021;2:100255. https://doi.org/10.1016/j.xcrm.2021.100255

Address for correspondence: Andreina Baj, University of Insubria, Via Dunant 5, Varese 21100, Italy; email: andreina.baj@uninsubria.it

Indoor and Outdoor Rodent Hosts of *Orientia tsutsugamushi*, Shandong Province, China

Fei Li, Zhen-Tang Zhang, Li-Zhu Fang, Hao Yu, Xiang-Rong Qin, Xue-Jie Yu

Author affiliations: Shandong University, Jinan, China (F. Li); Huangdao District Center for Disease Control and Prevention, Qingdao, China (Z.-T. Zhang); Wuhan University, Wuhan, China (L.-Z. Fang, H. Yu, X.-J. Yu); The Second Hospital of Shandong University, Jinan (X.-R. Qin)

DOI: https://doi.org/10.3201/eid2710.210393

During December 2012–July 2016, we tested small indoor and outdoor mammals in Qingdao, China, for *Orientia tsutsugamushi* infection. We found that outdoor *Apodemus agrarius* mice, *Cricetulus barabensis* hamsters, and *Niviventer confucianus* rats, as well as indoor *Mus musculus* mice, tested positive for *O. tsutsugamushi* by PCR.

Scrub typhus is an emerging infectious disease caused by *Orientia tsutsugamushi* (*1*), which is transmitted through the bites of infected chiggers, the larvae of trombiculid mites of the genus *Leptotrombidium*. Scrub typhus has been documented in southern China for thousands of years (*2*) and emerged in northern China during the 1990s (*3*). Several studies have investigated the animal hosts of *O. tsutsugamushi* (*4*,*5*), but the major hosts and seasonality of *O. tsutsugamushi* in northern China remain unclear. We collected small animals in Qingdao, a city in eastern China, to investigate the hosts and seasonality of *O. tsutsugamushi*.

During December 2012–July 2016, we used indoor and outdoor mousetraps to capture 162 small mammals (154 rodents and 8 shrews) in 2 villages in Huangdao District, Qingdao (119°30′–121°00′E, 35°35′–37°09′N) (Figure). All animal samples were obtained in accordance with the Implementation Regulations of the People's Republic of China on the Protection of Terrestrial Wild Animals (http://www.gov.cn/zhengce/2020-12/25/content_5574749.htm). The collection of rodents for microbiological studies was approved by the Ethics Committee of Prevention Medicine of Shandong University (Jinan, China; approval no. 20150501).

We classified samples by morphologic characteristics. We captured all 7 *Cricetulus barabensis* hamsters, 18 *Tscherskia triton* hamsters, and 8 *Niviventer confucianus* rats in the fields, as well as 98.6% (69/70) of *Apodemus agrarius* mice. We captured most *Rattus norvegicus* rats (22/24; 92%) and *Mus musculus* mice (18/27; 67%) in indoor settings, as well as 25% (2/8) of *Crocidura lasiura* shrews.

We extracted and screened DNA from rodent spleens for *O. tsutsugamushi* by nested PCR selective for the 56-kDa type-specific antigen gene with outer primers (5′- TCAAGCTTATTGCTAGTGCAATGTCTGC-3′ and 5′-AGGGATCCCTGCTGCTGTGCTTGCTGCG-3′) and inner primers (5′-GATCAAGCTTCCTCAGCCTACTATAATGCC-3′ and 5′-CTAGGGATCCCGACAGATGCACTATTAGGC-3′) (*6*,*7*). Overall, 4.5% of 154 rodents but none of the 8 shrews were positive for *O. tsutsugamushi*.

All infected rodents were captured during autumn (i.e., September–November); among rodents captured in autumn, the infection rate was 8.1% (7/86; $p>0.05$ by 1-sided Fisher exact test). None of the 68 rodents captured during spring, summer, and winter tested positive for *O. tsutsugamushi* (Table). The absence of *O. tsutsugamushi* infection among rodents collected during spring, summer, and winter indicated that these rodents were not reservoirs but temporary amplifying hosts for *O. tsutsugamushi*. The presence of *O. tsutsugamushi* among rodents during autumn months is consistent with the seasonality of

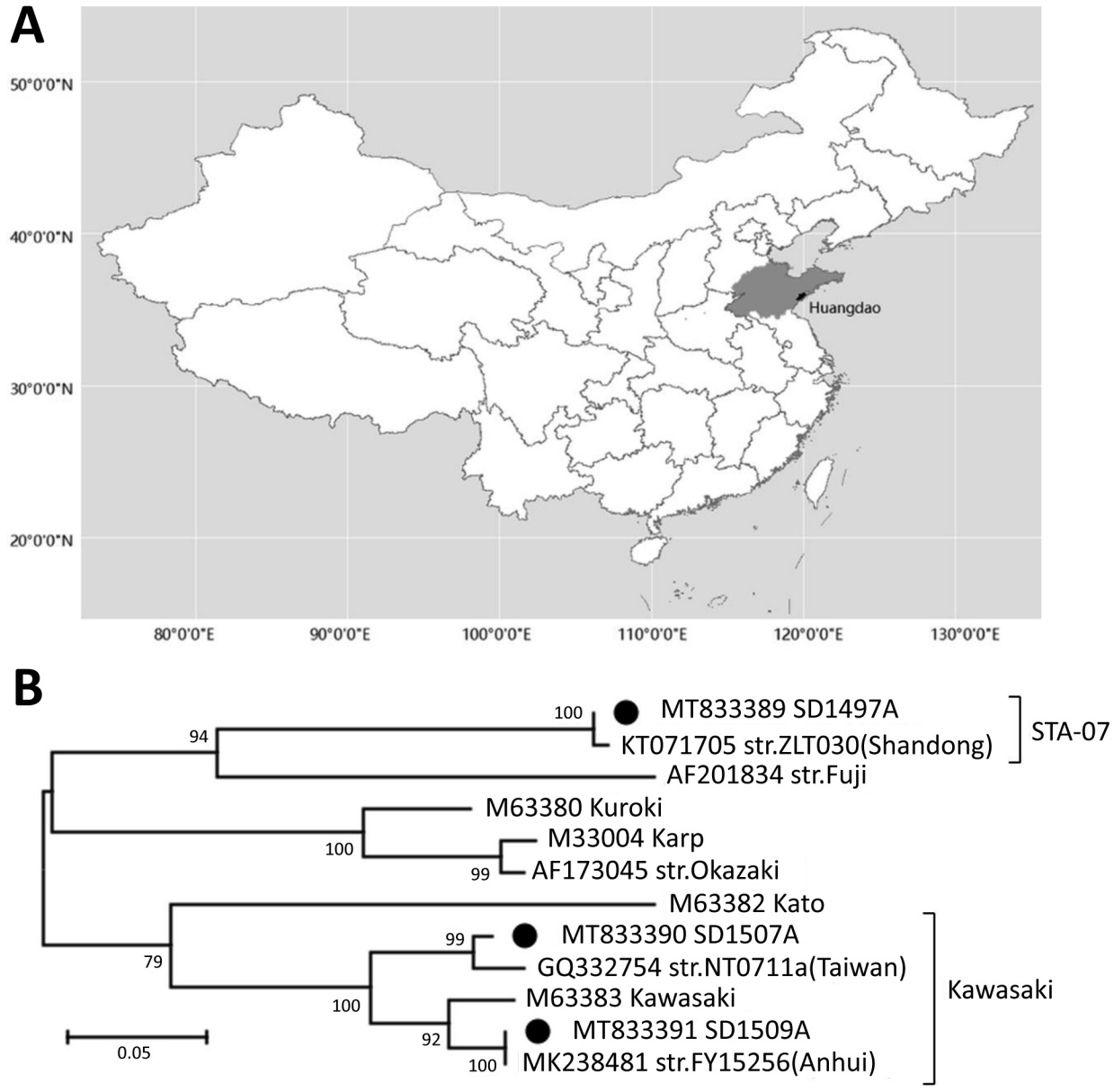

Figure. *Orientia tsutsugamushi* in small mammals, Qingdao, Shandong Province, China, December 2012–July 2016. A) Location of Shandong Province in China. B) Maximum-likelihood phylogenetic tree of *O. tsutsugamushi* constructed by MEGA version 7.0 (http://www.megasoftware.net). Black circles indicate strains isolated in this study. Numbers to the left of nodes indicate bootstrap values based on 1,000 replicates. Scale bar indicates number of nucleotide substitutions per site.

scrub typhus among patients in Shandong Province. Among humans, *O. tsutsugamushi* infections occur during September–December and peak in October (*8*), in alignment with the reproductive season of *Leptotrombidium scutellare* mites (*3*).

Overall, we found that 4.3% of *A. agrarius* mice, 7.4% of *M. musculus* mice, 12.5% of *N. confucianus* rats, and 14.3% of *C. barabensis* hamsters tested positive for *O. tsutsugamushi*; these results indicate the potential role of these rodents as animal hosts for *O. tsutsugamushi*. None of the 24 *R. norvegicus* rats, 18 *T. triton* hamsters, or 8 *C. lasiura* shrews tested positive, suggesting that these animals are not major hosts for *O. tsutsugamushi*. *R. norvegicus* rats, which were mainly captured indoors, were all negative for *O. tsutsugamushi*; these findings suggest that these rats might primarily stay indoors, thereby avoiding exposure to chiggers in the fields. We found 2 (11.1%) *O. tsutsugamushi*–positive indoor house mice, possibly reflecting their travels between house and field.

Table. Prevalence of *Orientia tsutsugamushi* in small mammals, Qingdao, Shandong Province, China, December 2012–July 2016

Species	Season, no. positive/no. tested (%)				
	Spring	Summer	Autumn	Winter	Total
Rodent					
Apodemus agrarius	0/2 (0)	0/28 (0)	3/39 (7.7)	0/1 (0)	3/70 (4.3)
Mus musculus	0/2 (0)	0/14 (0)	2/9 (22.2)	0/2 (0)	2/27 (7.4)
Rattus norvegicus	0/4 (0)	0/8 (0)	0/9 (0)	0/3 (0)	0/24 (0)
Tscherskia triton	0/1 (0)	0/1 (0)	0/15 (0)	0/1 (0)	0/18 (0)
Niviventer confucianus	0	0	1/8 (12.5)	0	1/8 (12.5)
Cricetulus barabensis	0/1 (0)	0	1/6 (16.7)	0	1/7 (14.3)
Shrew					
Crocidura lasiura	0	0	0/8 (0)	0	0/8 (0)
Total	0/10 (0)	0/51 (0)	7/94 (7.4)	0/7 (0)	7/162 (4.3)

The sequences of *O. tsutsugamushi* from rodents identified belonged to 2 lineages, Kawasaki and STA-07 (Figure). We identified the Kawasaki strain in 4 rodent species collected in the same village during the autumns of 2013 and 2014 and the STA-07 strain in *A. agrarius* mice in a village 20 km away during the autumn of 2014. These results suggest that *O. tsutsugamushi* isolates from same geographic area are highly homologous regardless of host species. We deposited the 56-kDa type-specific antigen gene sequences obtained in this study in GenBank (accession nos. MT833389–95).

In conclusion, we documented *O. tsutsugamushi* infection among outdoor *A. agrarius* mice, *N. confucianus* rats, and *C. barabensis* hamsters, as well as indoor *M. musculus* mice, in Shandong Province; these rodents might serve as animal hosts for *O. tsutsugamushi*. The finding of *O. tsutsugamushi* infection among indoor mice suggest that persons might be exposed to chiggers and *O. tsutsugamushi* at home. Further study is needed to investigate whether scrub typhus patients in the area had a history of working or traveling in the fields and whether their houses were infested with mice and chiggers. Our results indicate that physicians should be attentive to patients who might have *O. tsutsugamushi* infection, even if those patients have not worked in the field.

About the Author

Ms. Li is a doctoral candidate at Shandong University, Jinan, China. Her research interests include emerging infectious disease and vector-borne disease.

References

1. Walker DH. *Rickettsiae*. In: Baron S, editor. Medical Microbiology. 4th ed. Galveston (TX): University of Texas Medical Branch at Galveston; 1996.
2. Fan MY, Walker DH, Yu SR, Liu QH. Epidemiology and ecology of rickettsial diseases in the People's Republic of China. Rev Infect Dis. 1987;9:823–40. https://doi.org/10.1093/clinids/9.4.823
3. Zhang S, Song H, Liu Y, Li Q, Wang Y, Wu J, et al. Scrub typhus in previously unrecognized areas of endemicity in China. J Clin Microbiol. 2010;48:1241–4. https://doi.org/10.1128/JCM.01784-09
4. Liu YX, Jia N, Xing YB, Suo JJ, Du MM, Jia N, et al. Consistency of the key genotypes of *Orientia tsutsugamushi* in scrub typhus patients, rodents, and chiggers from a new endemic focus of northern China. Cell Biochem Biophys. 2013;67:1461–6. https://doi.org/10.1007/s12013-013-9646-0
5. Wu G-H,Wang C-J, Li B-J, Jiang Z-K, Ding L-Y,Wang L. General situation on studies of animal hosts of tsutsugamushi disease in China. Chinese Journal of Hygienic Insecticides of Equipments. 2013;19:370–3.
6. Tamura A, Yamamoto N, Koyama S, Makisaka Y, Takahashi M, Urabe K, et al. Epidemiological survey of *Orientia tsutsugamushi* distribution in field rodents in Saitama Prefecture, Japan, and discovery of a new type. Microbiol Immunol. 2001;45:439–46. https://doi.org/10.1111/j.1348-0421.2001.tb02643.x
7. Furuya Y, Yoshida Y, Katayama T, Yamamoto S, Kawamura A Jr. Serotype-specific amplification of *Rickettsia tsutsugamushi* DNA by nested polymerase chain reaction. J Clin Microbiol. 1993;31:1637–40. https://doi.org/10.1128/jcm.31.6.1637-1640.1993
8. Wu GH. The epidemiological characteristics and prevention and cure of scrub typhus in China. China Public Health. 2000;16:777–9.

Address for correspondence: Xiang-rong Qin, 247 Beiyuandajie, Jinan, Shandong Province 250033, China; email: qinxiangrong07@qq.com; Xue-jie Yu, 115 Donghu Rd, Wuhan, Hubei 430071, China; email: yuxuejie@whu.edu.cn

Nocardiosis in Immunocompromised Patients on Alternative *Pneumocystis* Prophylaxis

Alfredo G. Puing, David J. Epstein, Niaz Banaei, Aruna K. Subramanian, Anne Y. Liu

Author affiliations: City of Hope National Medical Center, Duarte, California, USA (A.G. Puing); Stanford University School of Medicine, Stanford, California, USA (A.G. Puing, D.J. Epstein, N. Banaei, A.K. Subramanian, A.Y. Liu)

DOI: https://doi.org/10.3201/eid2710.210620

Prophylactic trimethoprim/sulfamethoxazole (TMP/SMX) prevents *Pneumocystis jirovecii* pneumonia and nocardiosis in immunocompromised patients but sometimes is avoided because of purported allergies or side effects. Of 25 immunocompromised patients receiving alternative prophylaxis in whom nocardiosis developed, 16 subsequently tolerated TMP/SMX treatment. Clinicians should consider TMP/SMX allergy evaluation and rechallenging to assess patient tolerance.

Trimethoprim/sulfamethoxazole (TMP/SMX) is the drug of choice for *Pneumocystis jirovecii* pneumonia (PJP) prophylaxis in immunocompromised patients (*1*). Second-line prophylactic agents include atovaquone, dapsone, pentamidine, and clindamycin with pyrimethamine. Alternative agents can be less effective than TMP/SMX at preventing PJP and opportunistic infections caused by *Listeria monocytogenes*, *Toxoplasma gondii*, and *Nocardia* spp. Prophylactic TMP/SMX is sometimes avoided because of a prior adverse drug reaction or when patients are receiving drugs that have potentially overlapping toxicities. Nonetheless, second-line PJP prophylaxis regimens can increase the risk for opportunistic infections, such as nocardiosis (*2*). Most nocardiosis occurs in patients with impaired cell-mediated immunity; TMP/SMX is the cornerstone of standard therapy (*3*). We describe a series of nocardiosis cases in immunocompromised patients who were receiving alternative or no PJP prophylaxis because of TMP/SMX avoidance. We provide the reasons for TMP/SMX avoidance and proportion of patients who subsequently tolerated TMP/SMX.

We conducted a retrospective chart review at Stanford Hospital (Stanford, CA, USA) for patients with nocardiosis diagnosed during January 1, 1998–January 28, 2020. We included patients avoiding TMP/SMX for PJP prophylaxis in whom nocardiosis was identified on culture or by molecular techniques, such as 16S rRNA PCR-based assay. We used Stanford Hospital's protocols for defining immunocompromised status requiring PJP prophylaxis. We collected baseline demographic, clinical, microbiological, and outcome information, including immunocompromising condition, PJP prophylaxis indication and agent, reason for TMP/SMX avoidance, and TMP/SMX rechallenge outcome, if performed. This study was approved by Stanford University's Institutional Review Board (approval no. 54959).

During the study period, nocardiosis developed among 25 immunocompromised patients deliberately avoiding TMP/SMX. Most (68%) patients were female; median age of patients was 55 years. Among the 25 patients, 7 (28%) were lung transplant recipients, 6 (24%) had undergone allogeneic hematopoietic cell transplantation (HCT), 5 (20%) were heart transplant recipients, and 7 (28%) had other immunocompromising conditions (Appendix Table, https://wwwnc.cdc.gov/EID/article/27/10/21-0620.App1.pdf). At diagnosis, 15 (60%) patients were taking atovaquone, 4 (16%) inhaled pentamidine, 3 (12%) dapsone, and 3 (12%) no antimicrobial drug prophylaxis.

Thirteen (52%) patients were not taking TMP/SMX because of a reported history of allergy, 6 because of concern for cytopenia (24%), and 3 because of elevated creatinine (12%). TMP/SMX was avoided in 1 patient for elevated transaminases, 1 for gastrointestinal intolerance, and 1 for unstated reasons. Among 10 patients with a TMP/SMX allergy label who attempted challenge or desensitization, 7 (70%) tolerated the drug; nonsevere rash developed in the other 3 patients. Among 10 patients avoiding TMP/SMX prophylaxis for nonallergy reasons, 9 (90%) tolerated TMP/SMX when rechallenged. Overall, TMP/SMX introduction was attempted in 20/25 patients; 80% successfully tolerated the drug, and 20% had mild, reversible adverse effects (Figure).

In this retrospective case series, 16/25 (64%) patients who had nocardiosis while deliberately avoiding TMP/SMX prophylaxis ultimately were treated with TMP/SMX. Immunocompromised patients often are prescribed alternative drugs to TMP/SMX prophylaxis because of concerns over side effects or allergic reactions (*4*). However, desensitization or rechallenge could enable a substantial proportion of patients to safely take TMP/SMX for prophylaxis. In our study, 70% of patients with a history of TMP/

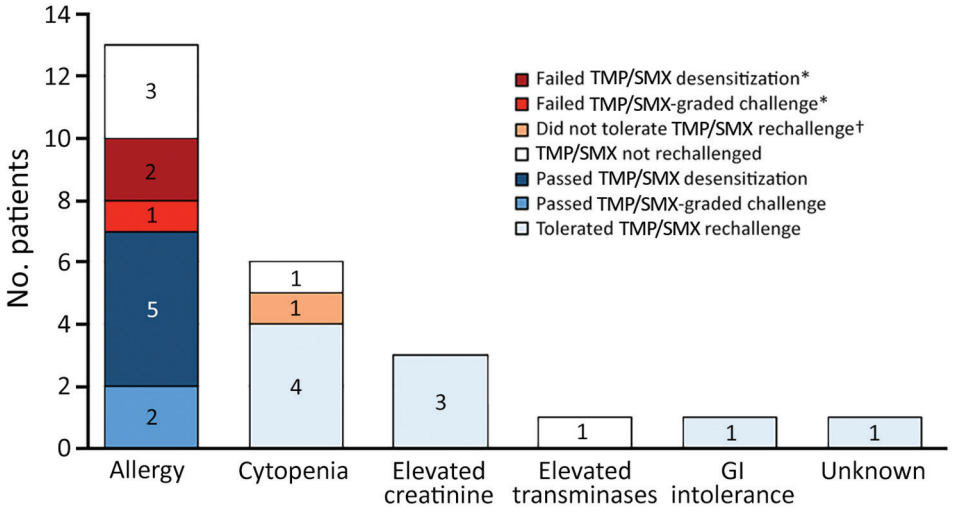

Figure. Reasons for TMP/SMX avoidance and TMP/SMX rechallenge outcomes among immunocompromised patients in whom TMP/SMX prophylaxis for *Pneumocystis jirovecii* pneumonia prophylaxis was avoided, Stanford, California, USA. *Failed TMP/SMX introduction because of rash or GI symptoms that were not severe. †Developed intractable nausea and vomiting after TMP/SMX was introduced and did not tolerate rechallenge. GI, gastrointestinal; TMP/SMX, trimethoprim/sulfamethoxazole

SMX allergy tolerated a TMP/SMX graded challenge or desensitization when attempted, and 90% of patients avoiding TMP/SMX prophylaxis for nonallergy reasons tolerated TMP/SMX when rechallenged. Our results concur with findings from a study that showed 74% of kidney transplant recipients who underwent TMP/SMX rechallenge had no recurrence of adverse drug reactions (*5*).

TMP/SMX prophylaxis might decrease the incidence of nocardiosis in immunocompromised patients. In a retrospective review of HCT recipients with nocardiosis, most (12/15) cases occurred in patients receiving alternate PJP prophylaxis (*2*). Other studies have questioned the efficacy of TMP/SMX prophylaxis in preventing nocardiosis in HCT or solid organ transplant recipients (*6*–*8*).

Taken together, these findings suggest that rates of this highly pathological infection might be reduced by systematically reevaluating TMP/SMX avoidance and reconsidering prophylactic TMP/SMX. Consulting with an allergist can detect contraindications, such as severe cutaneous adverse reactions, and opportunities for challenge or desensitization. Patients with a history of maculopapular rash, cytopenia, or increased creatinine with TMP/SMX might tolerate reintroduction. Electronic medical records can be designed to prompt revisiting whether TMP/SMX avoidance is appropriate (*9*).

The first limitation of our study is that we only included immunocompromised patients from a single healthcare system; our findings might not be generalizable to other settings. Second, some immunocompromised patients with nocardiosis possibly were not included in our cohort; although defining the incidence of nocardiosis would be informative, the intent of our study was to describe consequences of unnecessary TMP/SMX avoidance. Third, specifics of desensitization or graded challenge protocols were not consistently documented and thus might not be uniform.

Despite these limitations, our study shows that most patients in whom nocardiosis developed while avoiding TMP/SMX prophylaxis later tolerated TMP/SMX treatment. Future research should prospectively evaluate the risks and benefits of TMP/SMX reintroduction in immunocompromised patients who have had a prior adverse reaction. In conclusion, our findings suggest that revisiting TMP/SMX avoidance could prevent nocardiosis cases.

A.G.P. developed the research question, designed the data collection, compiled and analyzed the data, contributed to writing the manuscript, developed the figure, revised the manuscript; A.Y.L. developed the research question, designed the study, supervised data collection and cleaning, contributed to data analysis and manuscript preparation; D.J.E., N.B., and A.K.S reviewed the manuscript and provided expert input; all authors approved the final version of the manuscript to be published.

About the Author

Dr. Puing is an infectious diseases specialist at City of Hope National Medical Center. His main research interests center on evaluating the impact of infections following solid organ and hematopoietic stem cell transplantation, and the efficacy of antiinfective prophylaxis protocols.

References

1. Stern A, Green H, Paul M, Vidal L, Leibovici L. Prophylaxis for Pneumocystis pneumonia (PCP) in non-HIV

immunocompromised patients. Cochrane Database Syst Rev. 2014;2014:CD005590. https://doi.org/10.1002/14651858.CD005590.pub3
2. Shannon K, Pasikhova Y, Ibekweh Q, Ludlow S, Baluch A. Nocardiosis following hematopoietic stem cell transplantation. Transpl Infect Dis. 2016;18:169–75. https://doi.org/10.1111/tid.12499
3. Wallace RJ, Septimus EJ, Williams TW, Conklin RH, Satterwhite TK, Bushby MB, et al. Use of trimethoprim-sulfamethoxazole for treatment of infections due to *Nocardia*. Rev Infect Dis. 1982;4:315–25. https://doi.org/10.1093/clinids/4.2.315
4. Epstein DJ, Benamu E, Subramanian AK. Use of alternative agents for prevention of opportunistic infections in heart and lung transplant recipients. Clin Infect Dis. 2018;67:1637–9. PubMed https://doi.org/10.1093/cid/ciy397
5. Urbancic KF, Ierino F, Phillips E, Mount PF, Mahony A, Trubiano JA. Taking the challenge: A protocolized approach to optimize *Pneumocystis* pneumonia prophylaxis in renal transplant recipients. Am J Transplant. 2018;18:462–6. PubMed https://doi.org/10.1111/ajt.14498
6. Coussement J, Lebeaux D, van Delden C, Guillot H, Freund R, Marbus S, et al. *Nocardia* infection in solid organ transplant recipients: a multicenter European case-control study. Clin Infect Dis. 2016;63:338–45. https://doi.org/10.1093/cid/ciw241
7. Hemmersbach-Miller M, Stout JE, Woodworth MH, Cox GM, Saullo JL. *Nocardia* infections in the transplanted host. Transpl Infect Dis. 2018;20:e12902. https://doi.org/10.1111/tid.12902
8. Filice GA. Nocardiosis in persons with human immunodeficiency virus infection, transplant recipients, and large, geographically defined populations. J Lab Clin Med. 2005;145:156–62. https://doi.org/10.1016/j.lab.2005.01.002
9. Baneman E, Kim N, Rana M, Renteria AS, Steinberg AS, Jakubowski RM, et al. Optimizing the use of trimethoprim-sulfamethoxazole for prevention of PCP and opportunistic infections in allogeneic hematopoietic cell transplant recipients. J Clin Oncol. 2018;36:138. https://doi.org/10.1200/JCO.2018.36.30_suppl.138

Address for correspondence: Alfredo G. Puing, Division of Infectious Diseases, Department of Medicine, City of Hope National Medical Center, 1500 E Duarte Rd, Modular 1 West, Duarte, CA 91010, USA; email: apuing@coh.org

Autochthonous Case of *Rickettsia slovaca* Infection in Russia

Ruslan F. Sayfullin, Nadezhda E. Perekopskaya, Ludmila S. Karan, Nadezhda N. Zvereva, Muhammad A. Sayfullin

Author affiliations: Municipal Clinical Hospital No 52, Moscow, Russia (R.F. Sayfullin); Pirogov Russian National Research Medical University, Moscow (R.F. Sayfullin, N.N. Zvereva, M.A. Sayfullin); Infectious Clinical Hospital No. 1, Moscow (N.E. Perekopskaya); Central Scientific Research Institute of Epidemiology, Moscow (L.S. Karan); Gamaleya Institute of Epidemiology and Microbiology, Moscow (M.A. Sayfullin).

DOI: https://doi.org/10.3201/eid2710.204621

We describe an autochthonous case of *Rickettsia slovaca* infection in a man 35 years of age from Russia who had tickborne lymphadenopathy. We used ELISA and quantitative PCR testing to further identify DNA and confirm diagnosis. Physicians in Russia should consider similar diseases in differential diagnoses after tick bites.

Rickettsia slovaca was isolated in *Dermacentor marginatus* ticks in 1968 in Slovakia and recognized as a *Rickettsia* species with unknown pathogenicity. In 1997, a study described the first laboratory-confirmed case of *Rickettsia slovaca* infection in a human (*1*). *R. slovaca* has been detected in ticks in many countries in Europe, including the Mediterranean region. Human cases of syndromes that can be caused by *R. slovaca*, including tickborne lymphadenopathy (TIBOLA), *Dermacentor*-borne necrosis-erythema-lymphadenopathy (DEBONEL), and scalp eschar and neck lymphadenopathy after tick bite (SENLAT) have been reported (*2*,*3*). *R. slovaca* has been detected in ticks in 4 of 85 regions of Russia (Figure), and 1 imported case of *R. slovaca* infection was reported (*4*–*7*). The aim of our study was to describe an autochthonous case of *R. slovaca* infection in a man in Russia.

In May 2019, a 35-year-old male resident of Russia with an unremarkable medical history sought treatment for eschar on the skin of his right shin, painful and enlarged inguinal lymph nodes, rash, pain in his right knee, and severe fatigue. Before onset, he was in a rural village in the Voronezh region of Russia for 8 days, where he had contact with domestic animals and later noticed an insect bite near the location of the eschar. He reported no history of foreign travel in the previous 6 months.

Disease onset began with an ulcer, 2–3 cm in diameter, on his right shin. By days 3–4, the ulcer became an eschar, and the patient experienced chills and sweats at night. By days 5–6, chills and sweats remained, and an erythema up to 5 cm in diameter appeared around the eschar. The patient also noticed pain in his right knee, papular rash on his right leg and the right side of his trunk and neck, and enlarged and painful inguinal and axillary lymph nodes. On day 6, he was examined by a surgeon, who suspected a skin infection and initiated amoxicillin (1.5 g/d). On days 7–8, the rash spread to other limbs, lymph nodes in his neck became painful and enlarged, the pain in his right knee worsened, and low-grade fever (37.4°C–37.6°C) developed.

On day 8 after symptom onset, he was hospitalized at Infectious Clinical Hospital No. 1 in Moscow. At admission, he had a black eschar surrounded by erythema on the upper part of his right shin and vesiculopapular rash on his limbs and trunk concentrated around the eschar and on the skin of the right knee; in addition, there was bright hyperemia of previously existing scratches. Inguinal, axillary, and neck lymph nodes were painful by palpation and enlarged to 1.5–2.0 cm; his right knee was enlarged and painful by palpation and had impaired range of motion. We found no abnormalities from complete blood count and urinalysis on admission. We suspected skin and soft tissue infection with knee arthritis and changed antimicrobial therapy to ceftriaxone (2.0 g/d) and metronidazole (1.5 g/d).

On day 10, his body temperature normalized and the erythema around the eschar faded, but the rash continued to spread (Appendix, https://wwwnc.cdc.gov/EID/article/27/10/20-4621-App1.pdf) and the pain in his knee worsened. He had slightly elevated C-reactive protein (12 mg/L; reference <5 mg/L), but urine and blood cultures showed no growths. Taking into account anamnesis and a black eschar typical of TIBOLA, DEBONEL, and SENLAT syndromes, we suspected rickettsiosis. We detected *Rickettsia* DNA, but only in the sample from the eschar swab sample. We confirmed *R. slovaca* infection by molecular assay on blood and the eschar swab samples, collected on day 10 after disease onset (Appendix). We extracted DNA using a QIAGEN DNeasy blood and tissue kit (https://www.qiagen.com) and tested it with an AmpliSens *Rickettsia* spp. SFG-FL real-time PCR kit (https://www.amplisens.ru). For further confirmation, we used DNA isolated from the swab to sequence partial OmpA (primers Rr190.70p, Rr190.701n) and gltA (primers RpCS.877p, RpCS.1258n) genes (*8*).

We changed the patient's antimicrobial therapy to doxycycline (0.2 g/d), and his health improved rapidly. By day 15, pain and edema in his right knee had regressed, the rash had faded, and the eschar had begun to heal. The patient was discharged, but continued taking doxycycline for 10 additional days.

By 2 months after disease onset, the eschar and a few elements of papular rash around it had completely disappeared, but substantial fatigue remained for up to 5 months. For serologic assays, we collected serum samples on days 10, 30, and 160 after disease onset and tested for *Rickettsia* IgM and IgG using a Vircell *Rickettsia conorii* ELISA IgG/IgM kit (https://www.vircell.com). The lack of serologic response that we observed may have been related to the sensitivity of

Figure. Regions in Russia where *Rickettsia slovaca* was detected only in ticks and the region where an autochthonous human case of *R. slovaca* infection was registered.

the ELISA test we used (*9*). On the basis of our findings, physicians should consider TIBOLA, DEBONEL, and SENLAT syndromes in differential diagnoses after tick bites occurring in Russia.

About the Author

Dr. R.F. Sayfullin is an assistant professor of children's infectious diseases at the Pirogov Russian National Research Medical University and a pathologist in Municipal Clinical Hospital No. 52 in Moscow, Russia. His research interests include tick-borne infections, tropical diseases, and travel medicine.

References

1. Raoult D, Berbis P, Roux V, Xu W, Maurin M. A new tick-transmitted disease due to Rickettsia slovaca. Lancet. 1997;350:112–3. https://doi.org/10.1016/S0140-6736(05)61814-4
2. Parola P, Paddock CD, Socolovschi C, Labruna MB, Mediannikov O, Kernif T, et al. Update on tick-borne rickettsioses around the world: a geographic approach. Clin Microbiol Rev. 2013;26:657–702. https://doi.org/10.1128/CMR.00032-13
3. Oteo JA, Portillo A. Tick-borne rickettsioses in Europe. Ticks Tick Borne Dis. 2012;3:271–8. https://doi.org/10.1016/j.ttbdis.2012.10.035
4. Rudakov NV, Shpynov SN, Yastrebov VK, Samoylenko IE, Kumpan LV, Reshetnikova TA, et al. The present state of the problem of rickettsioses in Russia and new approaches to the classification of diseases caused by spotted fever group Rickettsiae [in Russian]. Acta Biomedica Scientifica. 2012;5:109–13.
5. Shpynov SN, Rudakov NV, Fournier PE, Raoult D. Molecular typing of Rickettsiae, Anaplasmae, and Ehrlichiae in ticks in the Russian Federation and the Republic of Kazakhstan [in Russian]. Zdorov'e Naseleniya i Sreda Obitaniya. 2012;1:33–5.
6. Igolkina YP, Fomenko NV, Livanova NN, Astanin VB, Gosteeva LA, Chernousova NY, et al. Identification of various types of Rickettsia in Ixodes mites, in the blood of humans and small mammals in the south of western Siberia and the Urals [in Russian]. Bulletin of Siberian Medicine. 2006;5:121–5. https://doi.org/10.20538/1682-0363-2006--121-125
7. Tarasevich IV, Saifullin MA, Luchshev AV, Pantyukhina AN, Mazankova LN, Dudina KR, et al. Imported rickettsial diseases detected in Moscow among tourists from endemic foci [in Russian]. Epidemiology and Infectious Diseases. 2015:55–61.
8. Portillo A, de Sousa R, Santibáñez S, Duarte A, Edouard S, Fonseca IP, et al. Guidelines for the detection of Rickettsia spp. Vector Borne Zoonotic Dis. 2017;17:23–32. https://doi.org/10.1089/vbz.2016.1966
9. Santibáñez S, Ibarra V, Portillo A, Blanco JR, Martínez de Artola V, Guerrero A, et al. Evaluation of IgG antibody response against Rickettsia conorii and Rickettsia slovaca in patients with DEBONEL/TIBOLA. Ann N Y Acad Sci. 2006;1078:570–2. https://doi.org/10.1196/annals.1374.113

Address for correspondence: Ruslan Sayfullin, Pirogov Russian National Research Medical University, Ostrityanova, 1, 117997, Moscow, Russia; email: ppsaifullin@rambler.ru

Equine Herpesvirus 1 Variant and New Marker for Epidemiologic Surveillance, Europe, 2021

Gabrielle Sutton, Camille Normand, Flora Carnet, Anne Couroucé, Marie Garvey, Sophie Castagnet, Christine I. Fortier, Erika S. Hue, Christel Marcillaud-Pitel, Loïc Legrand, Romain Paillot, Pierre-Hugues Pitel, Ann Cullinane, Stéphane Pronost

Author affiliations: University of Caen Normandy, Caen, France (G. Sutton, C. Normand, F. Carnet, A. Couroucé, C.I. Fortier, E.S. Hue, L. Legrand, S. Pronost); LABÉO Frank Duncombe, Saint-Contest, France (G. Sutton, C. Normand, F. Carnet, S. Castagnet, C.I. Fortier, E.S. Hue, L. Legrand, R. Paillot, P.-H. Pitel, S. Pronost); Cisco-Oniris, Nantes, France (A. Couroucé); Irish Equine Centre, Johnstown, Naas, Ireland (M. Garvey, A. Cullinane); Réseau d'Épidémio-Surveillance en Pathologie Équine, Saint-Contest (C. Marcillaud-Pitel, L. Legrand, P.-H. Pitel, S. Pronost); Writtle University College, Chelmsford, UK (R. Paillot)

DOI: https://doi.org/10.3201/eid2710.210704

Equine herpesvirus 1 isolates from a 2021 outbreak of neurologic disease in Europe have a mutation, A713G, in open reading frame 11 not detected in 249 other sequences from equine herpesvirus 1 isolates. This single-nucleotide polymorphism could help identify horses infected with the virus strain linked to this outbreak.

Equine herpesvirus 1 (EHV-1) is a threat to the equine industry, as demonstrated by the ongoing outbreak of neurologic disease initially reported at a large equestrian event in Valencia, Spain. EHV-1 infection is associated with respiratory disease, abortion in mares, neonatal death of foals, ocular disease, and, more rarely, encephalomyelopathy. As of March 26, 2021, a total of 18 horses had died during the outbreak: 11 in Spain, 5 in Germany, and 2 in Belgium. As the horses have returned from Spain to their training yards, the virus has spread to 9 other countries in Europe and to Qatar.

EHV-1 is endemic in horse populations worldwide. Reactivation of latent virus can occur at any time, but infected horses are more vulnerable when exposed to stress. When an outbreak occurs during an equestrian event and horses return to their respective countries or regions, the emergence of new cases of EHV-1 in the weeks and months after often elicits questions regarding the involvement of the strain from the original outbreak.

A total of 850 horses from many different countries were in attendance at the CES Valencia Spring Tour competition in February 2021; of those, 180 horses stayed in Valencia after the venue was closed by authorities in Spain. Most of these horses were pyrexic, and some developed neurologic disease. Nasopharyngeal swab samples were collected from 67 horses and sent to LABÉO Frank Duncombe (Saint-Contest, France) for PCR analysis. We tested 19 positive samples by the allelic-discrimination real-time PCR for a single-nucleotide polymorphism (SNP), A2254G, within open reading frame (ORF) 30, which has been associated with the neuropathogenic phenotype of EHV-1 (*1*). However, this association is not absolute, and the 19 samples tested positive for the A2254 genotype (i.e., the genotype more commonly associated with the nonneuropathogenic phenotype of EHV-1).

Viruses (FR/Valencia1/2021 and FR/Valencia2/2021) from 2 horses from France that remained in Valencia were isolated on cell culture and characterized by multilocus sequence typing (MLST) as belonging to clade 10 (*2*–*4*). MLST demonstrated that the virus associated with the outbreak of encephalomyelopathy in Valencia was closely related to other viruses circulating for several years in Europe; however, this tool is not accurate enough to identify a specific strain. Analysis of the sequences of the different ORF fragments used for the MLST revealed a mutation at position 713 of ORF11 (A713G) in FR/Valencia1/2021 and FR/Valencia2/2021 when compared with reference strains Ab4 and V592. This A713G mutation was not identified in 103 ORF11 sequences obtained in GenBank from strains isolated in the United Kingdom, United States, China, Australia, Belgium, New Zealand, Japan, or India. Furthermore, this mutation was not identified in 131 ORF11 sequences from strains isolated in Ireland or in 15 ORF11 sequences from EHV-1 strains isolated in France. Although we cannot exclude the existence of this mutation in other strains from the field, its absence in the 249 ORF11 sequences analyzed suggests that this SNP constitutes a possible marker to identify horses infected with the virus strain linked to the Valencia outbreak.

Because the Federation Equestre Internationale (Lausanne, Switzerland), the international governing body of equestrian sports, cancelled international events in 11 countries in Europe during March 1–April 11, 2021, the detection of this SNP might be helpful for investigating the extent of virus spread in different countries. For example, the identification of this ORF11 A713G genotype in a nasopharyngeal swab specimen taken from a horse with no known link to the event in Valencia triggered further investigations. These investigations revealed that the horse had stayed in a stable that, just a day before, had lodged a sick horse that had returned from Valencia.

Further investigations are warranted to determine the role of this mutation, which induces a change of lysine to arginine (K238R) in ORF11 (tegument protein). This SNP is helpful for differentiating EHV-1 cases linked to the recent epizootic in Spain from the many other strains of EHV-1 circulating in different countries. It might also help identify, in the future, abortions linked to the Valencia strain. A sensitive real-time PCR for the routine detection of this variant in clinical samples is under development and will be extremely useful in tracking the virus and in performing molecular epidemiology studies at the European level. Unlike MLST or whole-genome sequencing, such an assay could be readily deployed in a diagnostic laboratory.

About the Author

Dr. Sutton holds a postdoctoral position at LABÉO, focusing on antiviral strategies against EHV-1. She completed her PhD in virology at the University of Caen Normandy, focusing on the molecular characterization of equine herpesvirus 1 strains collected in France and the development of an EHV-1 real-time neutralization assay on the xCELLigence technology.

References

1. Nugent J, Birch-Machin I, Smith KC, Mumford JA, Swann Z, Newton JR, et al. Analysis of equid herpesvirus 1 strain variation reveals a point mutation of the DNA polymerase strongly associated with neuropathogenic versus nonneuropathogenic disease outbreaks. J Virol. 2006;80:4047–60. https://doi.org/10.1128/JVI.80.8.4047-4060.2006
2. Sutton G, Garvey M, Cullinane A, Jourdan M, Fortier C, Moreau P, et al. Molecular surveillance of EHV-1 strains circulating in France during and after the major 2009 outbreak in Normandy involving respiratory infection, neurological disorder, and abortion. Viruses. 2019;11:916–34. https://doi.org/10.3390/v11100916
3. Garvey M, Lyons R, He=ctor RD, Walsh C, Arkins S, Cullinane A. Molecular characterisation of equine Herpesvirus 1 isolates from cases of abortion, respiratory and neurological disease in Ireland between 1990 and 2017. Pathogens. 2019;8:7. https://doi.org/10.3390/pathogens8010007
4. Bryant NA, Wilkie GS, Russell CA, Compston L, Grafham D, Clissold L, et al. Genetic diversity of equine herpesvirus 1 isolated from neurological, abortigenic and respiratory disease outbreaks. Transbound Emerg Dis. 2018;65:817–32. https://doi.org/10.1111/tbed.12809

Address for correspondence: Stéphane Pronost, LABÉO, 1 route de Rosel, 14053 Caen CEDEX 4, France; email: stephane.pronost@laboratoire-labeo.fr

Emergomyces orientalis Emergomycosis Diagnosed by Metagenomic Next-Generation Sequencing

Da He[1], Min Quan[1], Hongyan Zhong, Zhixing Chen, Xiaohui Wang, Fang He, Junyan Qu, Taoyou Zhou, Xiaoju Lv, Zhiyong Zong

Author affiliations: Center for Infectious Diseases, West China Hospital of Sichuan University, Chengdu, China (D. He, M. Quan, Z. Chen, X. Wang, F. He, J. Qu, T. Zhou, X. Lv, Z. Zong); Hospital of Chengdu Office of People's Government of Tibetan Autonomous Region, Chengdu (H. Zhong); West China Hospital of Sichuan University, Chengdu (Z. Chen); Center for Infectious Diseases, Yaan People's Hospital, Yaan, China (X. Wang)

DOI: https://doi.org/10.3201/eid2710.210769

Emergomyces is a newly described dimorphic fungus genus; it may cause fatal infections in immunocompromised patients, but diagnosis is often delayed. We report a case of disseminated emergomycosis caused by the novel species *Emergomyces orientalis* in a kidney transplant recipient from Tibet. Infection was diagnosed early by metagenomic next-generation sequencing.

Emergomycosis (formerly called emmonsiosis) is an emerging dimorphic fungal disease, usually caused by *Emergomyces pasteurianus* or *Es. africanus*, usually disseminated and commonly identified and fatal in immunocompromised patients, especially HIV-positive patients from South Africa (*1*,*2*). Diagnosis of emergomycosis is often delayed, and best clinical practices for diagnosing and treating organ transplant recipients are lacking. Five species with different geographic distributions have been described: *Es. pasteurianus*, *Es. africanus*, *Es. canadensis*, *Es. europaeus*, and *Es. orientalis*. Globally, the only case of *Es. orientalis* infection, reported in China in 2017, was initially misdiagnosed as disseminated cryptococcosis (*3*). We report another case of *Es. orientalis* infection involving lung and soft tissue damage that was diagnosed early and accurately and treated precisely.

A 41-year-old man from Tibet who had received a kidney transplant 6 years earlier was admitted to a hospital with a 1-month history of progressive right lower chest pain and mild cough with a small amount of sputum. He was taking tacrolimus, mycophenolate mofetil, and prednisone. He was a herder caring for sheep, horses, and dogs. We noted reduced breath sounds in his lower right lung; chest computed tomography images indicated pneumonia (Figure, panel A). A bronchoalveolar lavage fluid smear revealed yeast-like fungi on both Gram staining and Grocott-Gomori methenamine silver staining (Figure, panel B). Because pulmonary cryptococcosis was suspected, fluconazole (400 mg 1×/d) was initiated. Results of a cryptococcal antigen lateral flow immunoassay (IMMY, https://www.immy.com) was negative, but a Platelia *Aspergillus* antigen immunoenzymatic sandwich microplate assay (Bio-Rad, https://www.bio-rad.com) resulted in an unexpectedly high level (6.42 [reference 0.00–0.49] signal:cutoff ratio). After 1 week of ineffective empirically prescribed treatment, we had a lung biopsy performed. Electron microscopy revealed yeast cells in a unique form, measuring ≈3 μm, scattered in necrotizing granulomas (Figure, panel C). Metagenomic next-generation sequencing (mNGS) of fresh tissue indicated *Es. orientalis* (sequence reads 143;, Illumina NextSeq 550 platform, https://www.illumina.com; Appendix Figure 1, https://wwwnc.cdc.gov/EID/article/27/10/21-0769-App1.pdf). We initiated oral itraconazole (200 mg 2×/d) immediately and decreased tacrolimus dosage according to its plasma concentration. Finally, we isolated the pure *Es. orientalis* strain (Figure, panel D). Specific secondary, α-shaped conidiophores clearly indicated *Emergomyces* (Figure, panel E). *Es. orientalis* was confirmed by PCR amplification targeting the rDNA internal transcribed spacer region followed by BLAST sequence comparison (https://blast.ncbi.nlm.nih.gov/Blast.cgi; GenBank accession no. NR_148064.1; coverage 96%, identity 99.33%) (Appendix Figure 2).

During treatment, the patient had intermittent mild fever and an acne-like rash on his chin, and a small new pulmonary lesion developed in the right upper lobe. Repeated blood cultures were all negative. We prescribed oral posaconazole (400 mg 2×/d) after determining a MIC of 0.008 μg/mL (Appendix Table). Later, the lung lesions partially resolved, but we found a painful soft tissue abscess (55 × 15 × 30 mm) on the right side of his waist (Figure, panel F) from which we drained purulent grayish-green fluid. We again cultured *Es. orientalis*. Therefore, we added flucytosine (1,000 mg 3×/d) and withdrew tacrolimus and mycophenolate mofetil for 1 month. After 6 months of recurrent hospitalization, we discharged the

[1]These authors contributed equally to this article.

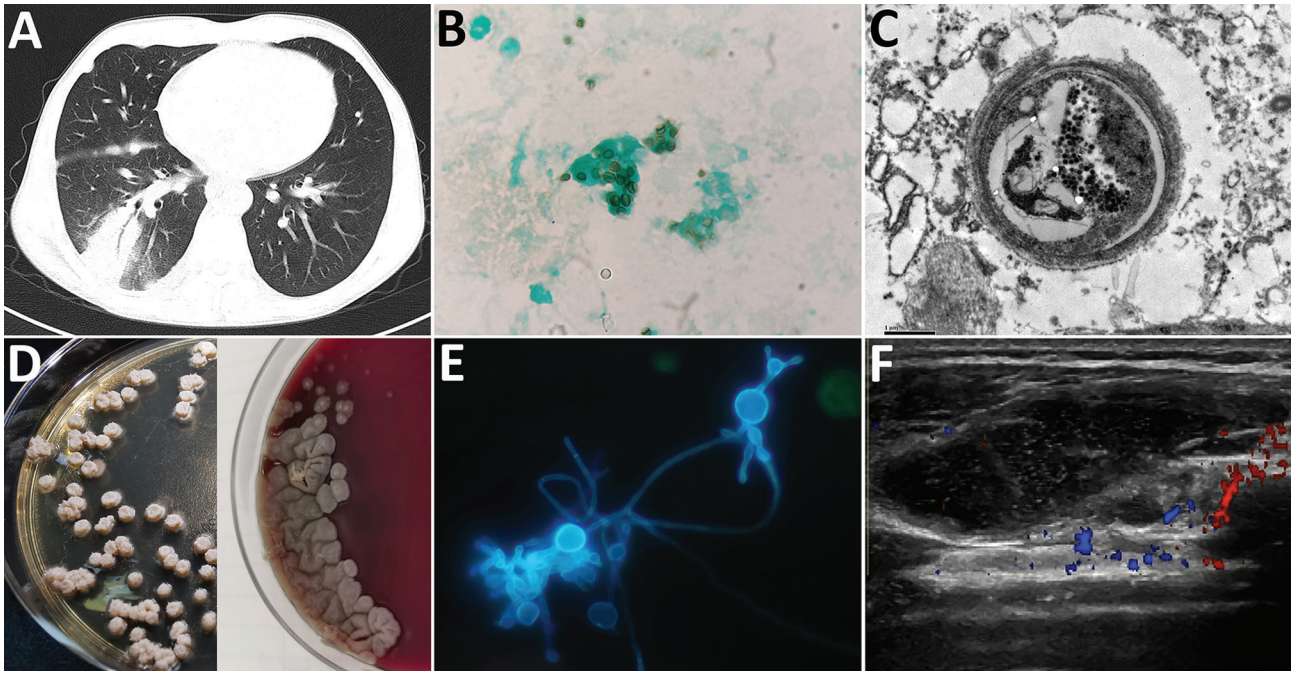

Figure. *Emergomyces orientalis* infection in a kidney transplant patient from Tibet. A) Pulmonary consolidation with the air bronchogram sign shown on a computed tomography scan. B) Microbes stained with Grocott-Gomori's methenamine silver in the bronchoalveolar lavage fluid sample (original magnification ×1,000). C) Pathological image of 1 yeast cell shown by electron microscopy in a necrotizing granuloma from paraffin-embedded pulmonary tissue (original magnification ×16,000). D) Tiny, slightly raised white colonies on Sabouraud agar on day 20 at 25°C (left) and grayish yellow furrowed colonies on blood agar on day 30 at 35°C (right) isolated from bronchoalveolar lavage fluid samples. E) Specific secondary α-shaped conidiophore shown with fluorescent calcium staining (original magnification ×1,000). F) Ultrasound revealed a soft tissue abscess in the patient's right subcostalis.

patient with a diagnosis of disseminated emergomycosis. Six months after discharge, he remained stable. We found no similarly infected or epidemiologically linked person or animal.

Previously, a retrospective study from southern Africa assessed 54 patients with disseminated emergomycosis, of whom 94% were co-infected with HIV; 96% had skin involvement, 88% had lung involvement, 44% received an incorrect diagnosis, and 48% died (*4*). In this case, we initially identified *Es. orientalis* infection using mNGS, a 1-step, culture-independent method for detecting all pathogens from 1 specimen (*5*). Although research validating mNGS assays in clinical practice is very limited, challenging cases diagnosed by mNGS have been published and expert consensus has begun to recommend mNGS for diagnosing challenging cases in immunocompromised patients (*6*,*7*). Therefore, we recommend using mNGS to diagnose challenging emergomycosis cases.

This case showed that treatment with posaconazole combined with flucytosine is effective in organ transplant recipients with disseminated emergomycosis caused by *Es. orientalis.* Although amphotericin B deoxycholate is more effective than triazoles for improving emergomycosis survival rate (71% vs. 33%) (*4*), we could not prescribe it for our patient because of nephrotoxicity. Similar to the earlier reported case of *Es. orientalis* infection, in which type 2 diabetes was the only identified cause of immunodeficiency (*3*), fluconazole was ineffective in vivo in our patient. Previously, 3 cases in China of *Es. pasteurianus* (formerly *Emmonsia pasteuriana*) infection with or without renal transplantation have also been reported (*8*–*10*).

Further research is needed to determine whether kidney transplantation is associated with *Es. orientalis* infection and risk for emergomycosis. In conclusion, clinicians need to become more aware of emergomycosis because of its common misdiagnosis and high death rate.

Acknowledgments

We thank Liubo Xiong and Yuling Xiao for their help.

This study was supported by Sichuan Science and Technology program, China (2018HH0031) and 1.3.5 project for disciplines of excellence, West China Hospital, Sichuan University (2017-046).

About the Author

Dr. He and Dr. Quan are medical students at the Center for Infectious Diseases, West China Hospital of Sichuan University in Chengdu, China. Their research interests are pathogen detection and microbial resistance.

References

1. Schwartz IS, Govender NP, Sigler L, Jiang Y, Maphanga TG, Toplis B, et al. *Emergomyces*: the global rise of new dimorphic fungal pathogens. PLoS Pathog. 2019;15:e1007977. https://doi.org/10.1371/journal.ppat.1007977
2. Rooms I, Mugisha P, Gambichler T, Hadaschik E, Esser S, Rath PM, et al. Disseminated emergomycosis in a person with HIV infection, Uganda. Emerg Infect Dis. 2019;25: 1750–1. https://doi.org/10.3201/eid2509.181234
3. Wang P, Kenyon C, de Hoog S, Guo L, Fan H, Liu H, et al. A novel dimorphic pathogen, *Emergomyces orientalis* (Onygenales), agent of disseminated infection. Mycoses. 2017;60:310–9. https://doi.org/10.1111/myc.12583
4. Schwartz IS, Govender NP, Corcoran C, Dlamini S, Prozesky H, Burton R, et al. Clinical characteristics, diagnosis, management, and outcomes of disseminated emmonsiosis: a retrospective case series. Clin Infect Dis. 2015;61:1004–12. https://doi.org/10.1093/cid/civ439
5. Simner PJ, Miller S, Carroll KC. Understanding the promises and hurdles of metagenomic next-generation sequencing as a diagnostic tool for infectious diseases. Clin Infect Dis. 2018;66:778–88. https://doi.org/10.1093/cid/cix881
6. Editorial Board of the Chinese Journal of Infectious Diseases. Clinical practice expert consensus for the application of metagenomic next generation sequencing [in Chinese]. Chin J Infect Dis. 2020;38:681–9. https://doi.org/10.3760/cma.j.cn311365-20200731-00732
7. Clinical Microbiology Group of Chinese Society of Laboratory Medicine, Clinical Microbiology Group of Chinese Society of Microbiology and Immunology, Society of Clinical Microbiology and Infection of China International Exchange and Promotion Association for Medical and Healthcare. Chinese expert consensus on metagenomics next-generation sequencing application on pathogen detection of infectious diseases [in Chinese]. Chin J Lab Med. 2021;44:107–20. https://doi.org/10.3760/cma.j.cn114452-20201026-00794
8. Feng P, Yin S, Zhu G, Li M, Wu B, Xie Y, et al. Disseminated infection caused by *Emmonsia pasteuriana* in a renal transplant recipient. J Dermatol. 2015;42:1179–82. https://doi.org/10.1111/1346-8138.12975
9. Tang XH, Zhou H, Zhang XQ, Han JD, Gao Q. Cutaneous disseminated emmonsiosis due to *Emmonsia pasteuriana* in a patient with cytomegalovirus enteritis. JAMA Dermatol. 2015; 151:1263–4. https://doi.org/10.1001/jamadermatol.2015.1792
10. Chik KK, To WK. Autochthonous *Emergomyces pasteurianus* pneumonia in an immunocompromised patient in Hong Kong: a case report. Hong Kong Med J. 2020;26:446–8. https://doi.org/10.12809/hkmj198280

Address for correspondence: Xiaohui Wang, Center for Infectious Diseases, West China Hospital of Sichuan University, Wuhouqu Guoxuexiang 37#, Chengdu 610041, China; email: wang_xiaohui@scu.edu.cn

Human Infection with Avian Influenza A(H9N2) Virus, Cambodia, February 2021

Samnang Um,[1] Jurre Y. Siegers,[1] Borann Sar, Savuth Chin, Sarika Patel, Seng Bunnary, Makara Hak, Sothy Sor, Oum Sokhen, Seng Heng, Darapheak Chau, Tum Sothyra, Asheena Khalakdina, Joshua A. Mott, Sonja J. Olsen, Filip Claes, Ly Sovann, Erik A. Karlsson

Author affiliations: National Institute of Public Health, Ministry of Health, Phnom Penh, Cambodia (S. Um, S. Chin, D. Chau); Institut Pasteur du Cambodge, Phnom Penh (J.Y. Siegers, E.A. Karlsson); US Centers for Disease Control and Prevention, Phnom Penh (B. Sar); World Health Organization Country Office, Phnom Penh (S. Patel, A. Khalakdina); National Animal Health and Production Research Institute, Phnom Penh (S. Bunnary, T. Sothyra); Food and Agriculture Organization of the United Nations Country Office, Phnom Penh (M. Hak); Prevention and Control Disease Bureau, Provincial Health Department, Siem Reap, Cambodia (S. Sor); Provincial Office of Animal Health and Production, Siem Reap (O. Sokhen); Cambodian Center for Disease Control, Ministry of Health, Phnom Penh (S. Heng, L. Sovann); US Centers for Disease Control and Prevention, Bangkok, Thailand (J.A. Mott, S.J. Olsen); Food and Agriculture Organization of the United Nations Regional Office for Asia and the Pacific, Bangkok (F. Claes)

DOI: https://doi.org/10.3201/eid2710.211039

In February 2021, routine sentinel surveillance for influenza-like illness in Cambodia detected a human avian influenza A(H9N2) virus infection. Investigations identified no recent H9N2 virus infections in 43 close contacts. One chicken sample from the infected child's house was positive for H9N2 virus and genetically similar to the human virus.

Low pathogenicity avian influenza virus subtype A(H9N2) is endemic in poultry in Asia, the Middle East, and Africa (*1*). These viruses do not cause mass mortality in poultry but can cause substantial negative economic impacts (*2*). H9N2 viruses also have zoonotic potential; 74 human infections were reported from 1998 through early 2021 (*1*,*3*,*4*), mainly in children with a history of poultry exposure. The internal gene cassettes of H9N2 viruses contribute to human adaptation of avian influenza viruses (AIV)

[1]These authors contributed equally to this article.

strains, as exemplified by the fifth wave of the H7N9 epidemic in China (*5*). Because of broad host range, global distribution, and reassortment capability, risk assessments indicate existing H9N2 viruses as a moderate pandemic risk (*2*,*6*).

H9N2 viruses circulate as they do in poultry from Cambodia endemically, in Bangladesh, Vietnam, and China (*7*,*8*). Seventy-five percent of AIVs detected in chickens in Cambodia in live bird markets (LBMs) are H9N2 (*7*). Whereas serosurveys indicate persons in Cambodia with poultry contact are exposed to H9N2, active human infections have not been detected (*9*,*10*).

On February 26, 2021, a 3-year-old boy living in Prasat Bakong, near Siem Reap, Cambodia, was taken to an outpatient clinic for influenza-like illness with onset of symptoms on February 24 (Figure). A nasopharyngeal sample obtained as part of influenza-like illness sentinel surveillance tested positive for influenza A at the National Institute of Public Health (Phnom Penh, Cambodia) but was unsubtypable for human seasonal, H5, or H7 subtypes (Appendix 1 reference *11*, https://wwwnc.cdc.gov/EID/article 27/10/21-1039-App1.pdf). The sample tested positive for H9N2 at the National Influenza Centre, Institute Pasteur du Cambodge (Phnom Penh) (*7*); a second specimen obtained on March 3 confirmed H9N2 infection. Viruses in the 2 samples were successfully isolated in embryonated chicken eggs and confirmed as H9N2; the second isolate was named A/Cambodia/21020301/2021. Hemagglutination inhibition testing confirmed infection by seroconversion. The serum sample taken on March 3 (7 days postonset) tested negative and then tested positive on March 10 (14 days postonset; hemagglutination inhibition = 240) (Appendix 1 reference *12*).

A joint One Health investigation was undertaken during March 8–11, 2021, by the Cambodia Centers for Disease Control and Ministry of Health, National Animal Health and Production Research Institute, and provincial divisions with support from the United States Centers for Disease Control and Prevention, the World Health Organization, Food and Agriculture Organization, and Institute Pasteur du Cambodge. The infected child lives in a mainly agrarian village »20 km from Siem Reap encompassing 121 households and 502 inhabitants; 80% of families conduct small-scale backyard poultry farming. The child's residence includes a chicken enclosure containing ≈50 chickens surrounded by nylon net. The child played within the enclosure and accompanied adults during feeding time. Poultry production, trading, and AIV prevalence in LBMs increase during

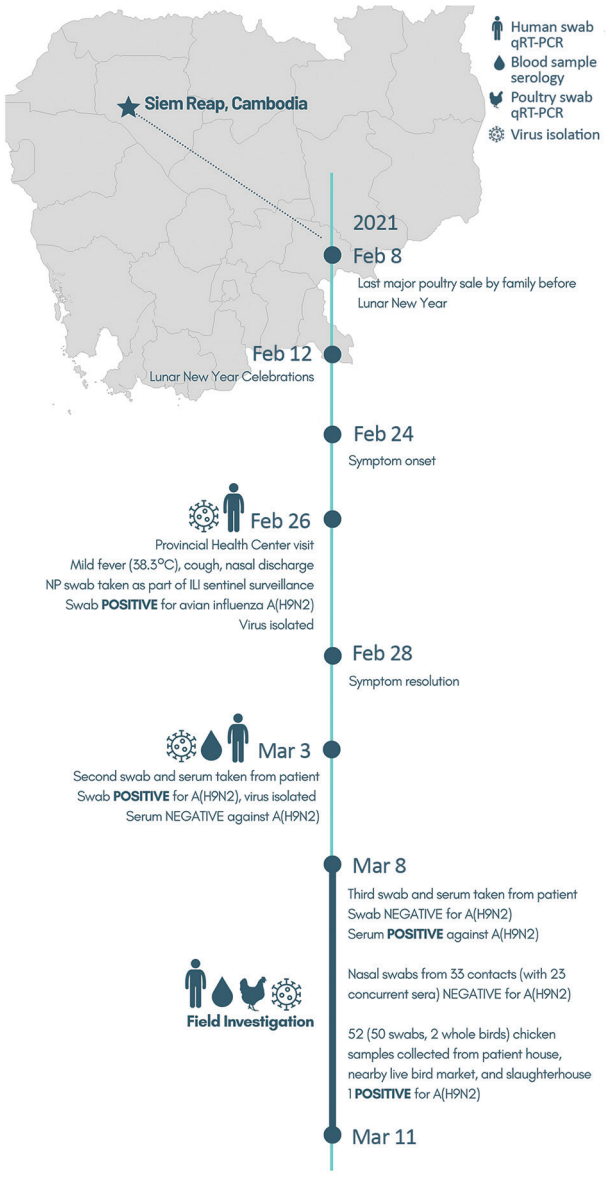

Figure. Locations of human infection and timeline of key events in the One Health investigation, Cambodia, February–March 2021. Key points and findings are indicated next to dates. Sampling and testing results are indicated by icons (in key). ILI, influenza-like illness; NP, nasopharyngeal; qRT-PCR, quantitative reverse transcription PCR.

national festival periods (*7*); a major sale took place on February 8, 2021, before Lunar New Year.

Forty-three close contacts were identified in 9 households (21 persons <15 and 22 persons ≥15 years of age; 53% female). Nine persons from 5 households reported respiratory symptoms immediately before or during the investigation. Nasal swab samples from 33/43 contacts (including all symptomatic persons), and concurrent serum samples from 23/43 contacts (including 8/9 symptomatic

persons) showed neither H9N2 infection nor seroconversion. Health education on safe poultry farming practices was provided to representatives of close contact families.

Investigations of poultry in the index house, village, local LBMs, and slaughterhouses yielded 50 tracheal/cloacal samples and 2 whole birds. One H9N2 virus was detected from a chicken at the infected child's house, isolated in embryonated chicken eggs, and subsequently named A/chicken/Cambodia/f0318251/2021. No poultry die-offs were reported in February 2021.

We sequenced the hemagglutinin and neuraminidase genes with Oxford Nanopore Technologies (Nanopore, https://nanoporetech.com) (Appendix 1 Figure). The hemagglutinin genes of A/Cambodia/21020301/2021 and A/chicken/Cambodia/f0318251/2021 (GISAID, https://www.gisaid.org; accession nos. EPI4858549, EPI1858551) clustered with G9/BJ94 lineage viruses from southern China from 2018. Neuraminidase genes (accession nos. EPI4858550, EPI1858552) clustered with G9/BJ94 lineage viruses from Laos from 2019. Overall, genetic distances between human and chicken viruses support a possible recent shared ancestor consistent with household chickens as the source of exposure.

Seroprevalence studies in rural Cambodia populations show neutralizing antibodies against H9N2 viruses of 1.1%–2.6%, indicative of undetected infections (*9*,*10*: Appendix 1 reference *13*), similar to avian-exposed persons elsewhere (Appendix 1 reference *14*). Therefore, the true burden of human H9N2 virus infections is likely higher than observed. Several human infections with H9N2 were reported in 2020, coinciding with the coronavirus pandemic (Appendix 1 reference *15*), when global human seasonal influenza declined, suggesting that sentinel surveillance systems continued to detect seasonal and zoonotic viruses (Appendix 1 reference *16*).

Endemic H9N2 and other AIVs in poultry remain a concern for zoonotic infection. An interdisciplinary One Health approach is warranted to curb continuing expansion and emergence. Early detection and control in animal populations, enhanced biosafety, candidate vaccines, and prompt antiviral treatment might mitigate the risks of reassortment and continued evolution that could result in H9N2 viruses with increased mammalian adaptation or human-to-human transmission potential.

Acknowledgments

Sequencing primer sequences were generously provided by Peter Thielen. We thank everyone involved in the investigation, including teams at the National Institute for Public Health/National Public Health Laboratory, Centers for Disease Control in Cambodia, Ministry of Health, US Centers for Disease Control and Prevention, and the Influenza Team in the Virology Unit at Institut Pasteur du Cambodge who contributed to this study. We thank all those involved in Influenza Sentinel Surveillance in Cambodia, especially Angkor Children's Hospital, Siem Reap. We thank the field teams from the National Animal Health and Production, especially Bun Chan and Chhim Vutha. We also thank all of the support teams, including the drivers and facilities personnel who made these studies possible, as well as all the local teams, epidemiologists, veterinary officers, and other staff from the Provincial Health Department in Siem Reap, the Provincial Office of Animal Health and Production, and the Applied Veterinary Epidemiology Training program, Cambodia, especially Sim Thorath, Phy Thorath, and Prum Vich. Finally, we thank all researchers who have submitted sequences to GenBank and GISAID (Appendix 2, https://wwwnc.cdc.gov/EID/article/27/10/21-1039-App2.xlsx).

This investigation was undertaken as part of a public health outbreak response and was considered a nonresearch investigation by the Cambodia Ministry of Health. Work at Institut Pasteur in Cambodia was supported by the Office of the Assistant Secretary for Preparedness and Response, US Department of Health and Human Services (grant no. IDSEP 140020-01-00; http://www.asideproject.org), and by the Food and Agriculture Organization, with funding from the United States Agency for International Development under the Emerging Pandemics Threats 2 project.

The findings and conclusions in this report are those of the author(s) and do not necessarily represent the official position of the Centers for Disease Control and Prevention or the Food and Agriculture Organization of the United Nations.

About the Author

Mr. Um is a technical officer in Influenza Surveillance and Response with the National Institute of Public Health and the Centers for Disease Control in the Ministry of Health, Phnom Penh, Cambodia; his research interests include the national influenza surveillance system in Cambodia. Mr. Siegers is a postdoctoral fellow in the Virology Unit at Institute Pasteur du Cambodge in Phnom Penh, Cambodia; his research interests include emerging and endemic infectious diseases in Southeast Asia, especially concerning spillover and exposure to avian influenza viruses.

References

1. Carnaccini S, Perez DR. H9 Influenza Viruses: An Emerging Challenge. Cold Spring Harb Perspect Med. 2020;10:a038588. https://doi.org/10.1101/cshperspect.a038588
2. Group SHW; SJCEIRS H9 Working Group. Assessing the fitness of distinct clades of influenza A (H9N2) viruses. Emerg Microbes Infect. 2013;2:e75.3. Peiris M, Yuen KY, Leung CW, Chan KH, Ip PL, Lai RW, et al. Human infection with influenza H9N2. Lancet. 1999;354:916–7. https://doi.org/10.1016/S0140-6736(99)03311-5
4. World Health Organization. Antigenic and genetic characteristics of zoonotic influenza A viruses and development of candidate vaccine viruses for pandemic preparedness; 2021. [cited 2021 March 30]; https://www.who.int/influenza/vaccines/virus/202103_zoonotic_vaccinevirusupdate.pdf
5. Pu J, Yin Y, Liu J, Wang X, Zhou Y, Wang Z, et al. Reassortment with dominant chicken H9N2 influenza virus contributed to the fifth H7N9 virus human epidemic. J Virol. 2021; JVI.01578-20.6. Centers for Disease Control and Prevention. Summary of Influenza Risk Assessment Tool (IRAT) results. 2021 [cited 2021 March 30]. https://www.cdc.gov/flu/pandemic-resources/monitoring/irat-virus-summaries.htm
7. Karlsson EA, Horm SV, Tok S, Tum S, Kalpravidh W, Claes F, et al. Avian influenza virus detection, temporality and co-infection in poultry in Cambodian border provinces, 2017–2018. Emerg Microbes Infect. 2019;8:637–9. https://doi.org/10.1080/22221751.2019.1604085
8. Suttie A, Tok S, Yann S, Keo P, Horm SV, Roe M, et al. The evolution and genetic diversity of avian influenza A(H9N2) viruses in Cambodia, 2015–2016. PLoS One. 2019;14:e0225428. https://doi.org/10.1371/journal.pone.0225428
9. Blair PJ, Putnam SD, Krueger WS, Chum C, Wierzba TF, Heil GL, et al. Evidence for avian H9N2 influenza virus infections among rural villagers in Cambodia. J Infect Public Health. 2013;6:69–79. https://doi.org/10.1016/j.jiph.2012.11.005
10. Horm SV, Tarantola A, Rith S, Ly S, Gambaretti J, Duong V, et al. Intense circulation of A/H5N1 and other avian influenza viruses in Cambodian live-bird markets with serological evidence of sub-clinical human infections. Emerg Microbes Infect. 2016;5:e70. https://doi.org/10.1038/emi.2016.69

Address for correspondence: Erik A. Karlsson, Virology Unit, Institute Pasteur du Cambodge, 5 Monivong Blvd, PO Box 983, Phnom Penh, Cambodia; email: ekarlsson@pasteur-kh.org

Antimicrobial-Resistant Nontyphoidal *Salmonella* Infections, United States, 2004–2016

Amrita Bharat, Colleen P. Murphy, Michael R. Mulvey, Saarah Hussain, Carolee A. Carson, Richard J. Reid-Smith; CIPARS Provincial Partnership[1]

Author affiliations: Public Health Agency of Canada, Winnipeg, Manitoba, Canada (A. Bharat, M.R. Mulvey); Public Health Agency of Canada, Guelph, Ontario, Canada (C.P. Murphy, S. Hussain, C.A. Carson, R.J. Reid-Smith)

DOI: https://doi.org/10.3201/eid2710.211339

To the Editor: Medalla et al. reported increased incidence of antimicrobial-resistant human infections with nontyphoidal *Salmonella* in the United States during 2004–2016 (*1*). When comparing incidence in 2004–2008 with that in 2015–2016, Bayesian hierarchical modeling estimated a 40% increase in the annual incidence of *Salmonella* infections with clinically important resistance (resistance to ampicillin or ceftriaxone or nonsusceptibility to ciprofloxacin). Most of the reported increases were attributed to serotypes I 4,[5],12:i:- and Enteritidis.

The US study used data from Laboratory-Based Enteric Disease Surveillance (https://www.cdc.gov/salmonella/reportspubs/surveillance.html) and the National Antimicrobial Resistance Monitoring System (https://www.cdc.gov/narms/index.html). The corresponding programs in Canada are the National Enteric Surveillance Program and the Canadian Integrated Program for Antimicrobial Resistance Surveillance (*2*,*3*). We used descriptive and univariable analyses without modeling for a preliminary comparison of data from these programs.

In Canada, yearly incidence (per 100,000 population) of human nontyphoidal *Salmonella* infections increased by 17% from 2004–2008 (median 18 cases) to 2015–2016 (median 21 cases). For nontyphoidal *Salmonella* (n = 20,665 isolates), resistance to ampicillin or ceftriaxone did not change substantially from 2004–2008 (ampicillin 15%; ceftriaxone 4%) to 2015–2016 (ampicillin 13%; ceftriaxone 5%). However, ciprofloxacin nonsusceptibility in nontyphoidal *Salmonella* increased from 7% in 2004–2008 to 15% in 2015–2016. For *Salmonella* Enteritidis (n = 6,694 isolates), resistance to ampicillin and ceftriaxone was uncommon (ampicillin 3%; ceftriaxone <1% for both 2004–2008 and 2015–2016). However, ciprofloxacin nonsusceptibility increased from 15% in 2004–2008 to 24% in 2015–2016. For *Salmonella* I 4, [5],12:i;- (n = 686 isolates), ampicillin resistance increased from 20% in 2004–2008 to 53% in 2015–2016, but ceftriaxone resistance decreased from 8% to 3%. Thus, increases were observed in both the United States and Canada for ciprofloxacin nonsusceptibility in *Salmonella* Enteritidis and for ampicillin resistance in *Salmonella* I 4, [5],12:i;-. Future modeling of surveillance data, enhanced by genomic analysis, will provide a more comprehensive comparison of findings for these countries.

Members of the CIPARS Provincial Partnership who contributed data: David C. Alexander (Cadham Provincial Laboratory, Winnipeg, MB, Canada), Vanessa Allen (Public Health Ontario Laboratories, Toronto, ON, Canada), Sameh El Bailey (Horizon Health Network, Saint John, NB, Canada), Sadjia Bekal (Laboratoire de Santé Publique du Québec, Sainte-Anne-de-Bellevue, QC, Canada), Greg J. German (Queen Elizabeth Hospital, Charlottetown, PEI, Canada), David Haldane (Queen Elizabeth II Health Sciences Centre, Halifax, NS, Canada), Linda Hoang (British Columbia Centre for Disease Control, Vancouver, BC, Canada), Linda Chui (Alberta Precision Laboratories-Provincial Laboratory for Public Health, Edmonton, AB, Canada), Jessica Minion (Roy Romanow Provincial Laboratory, Regina, SK, Canada), and George Zahariadis (Newfoundland and Labrador Public Health and Microbiology Laboratory, St. John's, NL, Canada)

References

1. Medalla F, Gu W, Friedman CR, Judd M, Folster J, Griffin PM, et al. Increased incidence of antimicrobial-resistant nontyphoidal *Salmonella* infections, United States, 2004–2016. Emerg Infect Dis. 2021;27:1662–72. https://doi.org/10.3201/eid2706.204486
2. Government of Canada. Canadian Integrated Program for Antimicrobial Resistance Surveillance (CIPARS) [cited 2021 Jun 1]. https://www.canada.ca/en/public-health/services/surveillance/canadian-integrated-program-antimicrobial-resistance-surveillance-cipars.html
3. Government of Canada. National Enteric Surveillance Program (NESP) [cited 2021 Jun 1]. https://www.canada.ca/en/public-health/programs/national-enteric-surveillance-program.html

Address for correspondence: Richard J. Reid-Smith, Centre for Food-borne, Environmental and Zoonotic Infectious Diseases, Public Health Agency of Canada, Ste 201, 370 Speedvale Ave W, Guelph, ON N1H 7M7, Canada; email: richard.reid-smith@canada.ca

[1]Members of the CIPARS Provincial Partnership who contributed data are listed at the end of this article.

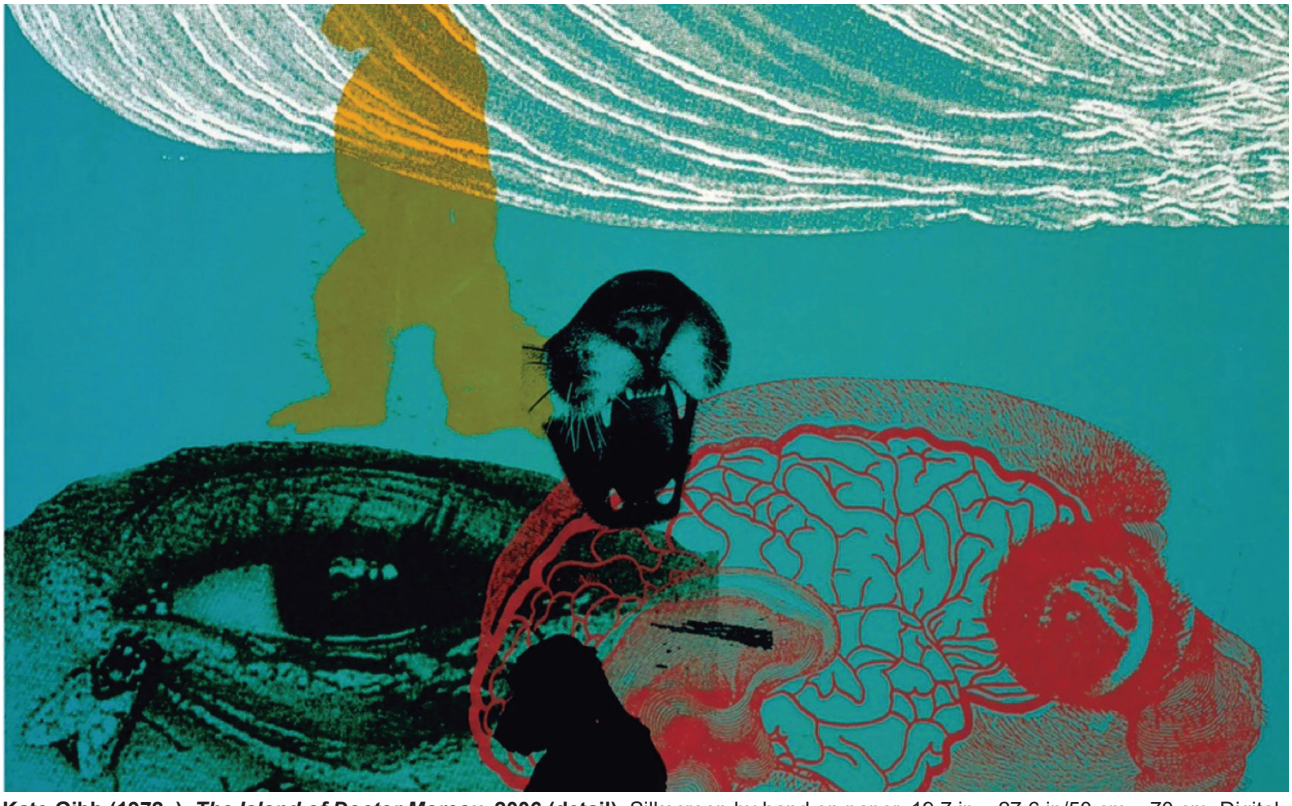

Kate Gibb (1972–), *The Island of Doctor Moreau*, 2006 (detail). Silkscreen by hand on paper, 19.7 in × 27.6 in/50 cm × 70 cm. Digital image used with permission of the artist. London, England.

Revisiting the Island of Doctor Moreau

Byron Breedlove

This month's cover art, created by contemporary English printmaker and illustrator Kate Gibb—known for her colorful, detailed screen-printed artwork developed for musicians and fashion designers—was first featured on another cover, the 2005 reissue of a classic work of early horror and science-fiction, *The Island of Doctor Moreau* by English writer H.G. Wells. Originally published in 1896, Wells's novel chronicles the story of the shipwrecked Englishman Edward Prendick. Stranded on a remote, uncharted island, Prendick is nursed back to health after his ordeal at sea only to discover he has washed up on an isle of horrors. Doctor Moreau, a mad scientist, has fled to the island from England after his experiments in vivisection were exposed. Here the doctor works without restraints, accountability, or moral guidance, performing gruesome, cruel experiments designed to transform animals into humans.

In *The Island of Doctor Moreau,* Wells intertwines several societal themes from the latter part of the 19th century, including the growing antivivisection movement, implications of Charles Darwin's research on evolution, the nature of humankind as explored in Robert Louis Stevenson's 1886 novel *The Strange Case of Dr. Jekyll and Mr. Hyde*, and the notion of humans creating chimeras, an idea articulated earlier in Mary Shelley's 1818 novel *Frankenstein*. Moreau's horrific surgical procedures triggered ethical questions and concerns about cruelty, morals, and human–animal relationships that still resonate with contemporary readers. Literature professor Roger Luckhurst notes, "In the 21st century, with genetic splicing making animal–human hybrids an actual possibility, Wells's queasy exploration of the limits of the human in this provocative satire keeps the book incredibly relevant today." Moreau's efforts to control the behaviors of

Author affiliation: Centers for Disease Control and Prevention, Atlanta, Georgia, USA

DOI: https://doi.org/10.3201/eid2710.AC2710

his menagerie of engineered creations through "The Law," a list of prohibitions recited to the island's "Beast Folk" to keep them from reverting to their animalistic selves, are also troubling.

Those who have read the novel will recall that after Moreau and his assistant Montgomery are killed, as are a number of the altered creatures, Prendick eventually escapes from the island and returns to London. He discovers, however, that he can no longer live among humans, fearing they, too, will revert to animalistic beings, and so he seeks solitude in the countryside, devoting himself to scientific studies. Gibb's collage, which draws from the interconnected themes in the novel, features silhouettes of simians, the maw of a felid, and a lacey cross-section of a brain superimposed over a soothing blue-gray background, plus a pair of flies disturbingly close to a human eye peering at the viewer.

As readers of this journal know, the xenotransplantation and surgeries, close interactions of humans and animals, and coerced association of myriad animal species on Moreau's island could potentially have led to the spread of zoonotic infections, perhaps even the emergence of novel pathogens. But no person or animal is ever infected with a zoonotic pathogen in the novel, unlike in Wells's next novel, *The War of the Worlds*, when invading Martians succumb to earthly pathogens to which they had no immunity, "slain, after all man's devices had failed. . . ."

Zoonotic diseases, an unavoidable consequence of human–animal interactions, are caused by microorganisms such as viruses, bacteria, parasites, and fungi. CDC's One Health website notes that more than 6 out of every 10 known infectious diseases in humans can be spread from animals. Perhaps in a contemporary reimagining of *The Island of Doctor Moreau*, existing or emerging zoonotic infections would factor into the narrative. In such a reworking, the isolated island setting and small number of people and animals might mitigate widespread transmission of such infections, in contrast with factors driving the emergence of new infectious diseases. Human encroachment into remote regions, factory farming, animal markets and trade, climate change, disruptions of natural areas and their ecosystems, and global migration all play a role.

Understanding those interconnections between humans, animals, plants, and their communal environment, a concept now known as One Health, is an important public health priority. In a 2018 article published in the *Annual Review of Animal Biosciences*, researchers Bird and Mazet warn, "We must be prepared to recognize the signs, identify the threat, and rapidly work together to reduce the spread of infections and health consequences before they harm the health of animals and people throughout the world." Gibb's silkscreened image seems applicable both to the events in Wells's 125-year-old novel and to those of the present day.

About the Artist

Kate Gibb created 17 covers for the 2006 reissues of H.G. Wells's works and explained, "There were strong themes and descriptive elements within the text which quickly inspired me to find and collage images quite spontaneously. I remember really enjoying the process and being pleasantly surprised by its outcome!" She has worked with fashion designers, publishers, and musicians, and her work has been featured in a number of contemporary publications. In addition to producing her print-based artworks and commercial illustrations, Gibb is an educator, most recently at England's University of Brighton. After studying textiles at Middlesex University, London, she shifted her focus to silkscreen printing and describes herself as "a silkscreen obsessive."

Bibliography

1. Bird BH, Mazet JA. Detection of emerging zoonotic pathogens: an integrated One Health approach. Annu Rev Anim Biosci. 2018;6:121–39. https://doi.org/10.1146/annurev-animal-030117-014628
2. Bishop A. Making sympathy "vicious" on *The Island of Dr. Moreau*. Nineteenth-Century Contexts. 2021;43:205–20. https://doi.org/10.1080/08905495.2021.1898229
3. Breedlove B, Arguin PM. Anthropomorphism to zoonoses: two inevitable consequences of human–animal relationships. Emerg Infect Dis. 2015;21:2282–3. https://doi.org/10.3201/eid2112.AC2112
4. Centers for Diseases Control and Prevention. One Health [cited 2021 Aug 17]. https://www.cdc.gov/onehealth/index.html
5. Gibb K. About [cited 2021 Aug 17]. http://kategibb.co.uk
6. Gibb R, Redding DW, Chin KQ, Donnelly CA, Blackburn TM, Newbold T, et al. Zoonotic host diversity increases in human-dominated ecosystems. Nature. 2020;584:398–402. https://doi.org/10.1038/s41586-020-2562-8
7. Jones KE, Patel NG, Levy MA, Storeygard A, Balk D, Gittleman JL, et al. Global trends in emerging infectious diseases. Nature. 2008;451:990–3. https://doi.org/10.1038/nature06536
8. Luckhurst R. An introduction to the island of Dr. Moreau: science, sensation and degeneration [cited 2021 Aug 17]. https://www.bl.uk/romantics-and-victorians/articles/an-introduction-to-the-island-of-doctor-moreau-science-sensation-and-degeneration
9. Wells HG. The island of Doctor Moreau. [cited 2021 Aug 7] https://www.gutenberg.org/files/159/159-h/159-h.htm
10. +81 Gallery. Kate Gibb: October 19–November 19, 2017 [cited 2021 Aug 25]. http://www.plus81.us/exhibition/kate-gibb

Address for correspondence: Byron Breedlove, EID Journal, Centers for Disease Control and Prevention, 1600 Clifton Rd NE, Mailstop H16-2, Atlanta, GA 30329-4027, USA; email: wbb1@cdc.gov

Earning CME Credit

To obtain credit, you should first read the journal article. After reading the article, you should be able to answer the following, related, multiple-choice questions. To complete the questions (with a minimum 75% passing score) and earn continuing medical education (CME) credit, please go to http://www.medscape.org/journal/eid. Credit cannot be obtained for tests completed on paper, although you may use the worksheet below to keep a record of your answers.

You must be a registered user on http://www.medscape.org. If you are not registered on http://www.medscape.org, please click on the "Register" link on the right hand side of the website.

Only one answer is correct for each question. Once you successfully answer all post-test questions, you will be able to view and/or print your certificate. For questions regarding this activity, contact the accredited provider, CME@medscape.net. For technical assistance, contact CME@medscape.net. American Medical Association's Physician's Recognition Award (AMA PRA) credits are accepted in the US as evidence of participation in CME activities. For further information on this award, please go to https://www.ama-assn.org. The AMA has determined that physicians not licensed in the US who participate in this CME activity are eligible for AMA PRA Category 1 Credits™. Through agreements that the AMA has made with agencies in some countries, AMA PRA credit may be acceptable as evidence of participation in CME activities. If you are not licensed in the US, please complete the questions online, print the AMA PRA CME credit certificate, and present it to your national medical association for review.

Article Title

Population-Based Study of Bloodstream Infection Incidence and Mortality Rates, Finland, 2004–2018

CME Questions

1. Your patient is a 67-year-old man with suspected bloodstream infection (BSI). According to the analysis of national, laboratory-based surveillance data by Kontula and colleagues, which of the following statements about incidence and outcome of BSIs in Finland during 2004–2018 is correct?

A. Annual incidence increased by 50% from 2004 to 2018
B. 30-day case fatality decreased from 13% to 12.6% whereas 30-day all-cause mortality rose from 20/100,000 to 39/100,000
C. The average annual incidence rate was highest among female persons aged 50 to 60 years
D. Of all BSIs, 5% were fatal within 1 month; case fatality was higher for female individuals than for male individuals

2. According to the analysis of national, laboratory-based surveillance data by Kontula and colleagues, which of the following statements about causative agents of BSIs in Finland during 2004–2018 is correct?

A. The proportion of BSIs caused by *Escherichia coli* decreased
B. The proportion of community-acquired (CA) BSIs decreased whereas hospital-acquired (HA) BSIs increased
C. The percentage of BSIs caused by multidrug-resistant (MDR) microbes rose from 0.4% to 2.8%, mostly because of extended-spectrum β-lactamase-producing (ESBL) E coli
D. *Staphylococcus aureus* was the most common causative pathogen

3. According to the analysis of national, laboratory-based surveillance data by Kontula and colleagues, wh ich of the following statements about clinical and public health implications of incidence, outcome, causative agents, and trends of BSIs in Finland during 2004–2018 is correct?

A. The increasing trend in CA BSIs and *E. coli* resistance is a challenge for disease prevention and guidance of antimicrobial treatment
B. The minimal increase in BSI incidence and mortality during 2004-2018 suggests that current preventive strategies are working well
C. BSI mortality is likely to decrease in the near future
D. The study determined possible predisposing factors for mortality that best identify high-risk patients

Earning CME Credit

To obtain credit, you should first read the journal article. After reading the article, you should be able to answer the following, related, multiple-choice questions. To complete the questions (with a minimum 75% passing score) and earn continuing medical education (CME) credit, please go to http://www.medscape.org/journal/eid. Credit cannot be obtained for tests completed on paper, although you may use the worksheet below to keep a record of your answers.

You must be a registered user on http://www.medscape.org. If you are not registered on http://www.medscape.org, please click on the "Register" link on the right hand side of the website.

Only one answer is correct for each question. Once you successfully answer all post-test questions, you will be able to view and/or print your certificate. For questions regarding this activity, contact the accredited provider, CME@medscape.net. For technical assistance, contact CME@medscape.net. American Medical Association's Physician's Recognition Award (AMA PRA) credits are accepted in the US as evidence of participation in CME activities. For further information on this award, please go to https://www.ama-assn.org. The AMA has determined that physicians not licensed in the US who participate in this CME activity are eligible for AMA PRA Category 1 Credits™. Through agreements that the AMA has made with agencies in some countries, AMA PRA credit may be acceptable as evidence of participation in CME activities. If you are not licensed in the US, please complete the questions online, print the AMA PRA CME credit certificate, and present it to your national medical association for review.

Article Title

Recurrence of Human Babesiosis Caused by Reinfection

CME Questions

1. Your patient is a previously healthy 64-year-old man diagnosed with babesiosis. According to the case report by Ho and colleagues, which of the following statements about clinical findings and course in a 62-year-old male physician with apparent babesiosis reinfection is correct?

A. The patient was immunocompromised because of rheumatoid arthritis and its treatment
B. Symptoms were fever, chills, and cough productive of purulent sputum
C. Examination findings included fever, joint swelling, and erythema around a tick bite
D. Treatment with a standard course of anti-Babesia antibiotics (atovaquone and azithromycin) for each episode led to complete recovery in each

2. According to the case report by Ho and colleagues, which of the following statements about laboratory findings in a patient with apparent babesiosis reinfection is correct?

A. Hemogram showed strikingly low white blood cell (WBC) and normal platelet count
B. Liver function tests were normal
C. In the first episode, *Babesia microti* immunoglobulin (Ig) M antibody was strongly positive (IgM ≥ 1:1024, IgG < 1:16), and *Anaplasma phagocytophilum* antibody was absent
D. Full genomic sequencing was performed in the first episode

3. According to the case report by Ho and colleagues, which of the following statements about clinical implications of a patient with apparent babesiosis reinfection is correct?

A. Healthcare providers should be aware that babesiosis reinfection may occur and that tick-borne disease prevention is needed in patients with or without a history of babesiosis
B. Clinical and laboratory evidence in this patient support relapse of infection rather than reinfection
C. Anamnestic antibody response with high titer IgG antibody early in the course of the second episode suggests relapse
D. The evidence proves that this patient was reinfected with *B. microti*

Earning CME Credit

To obtain credit, you should first read the journal article. After reading the article, you should be able to answer the following, related, multiple-choice questions. To complete the questions (with a minimum 75% passing score) and earn continuing medical education (CME) credit, please go to http://www.medscape.org/journal/eid. Credit cannot be obtained for tests completed on paper, although you may use the worksheet below to keep a record of your answers.

You must be a registered user on http://www.medscape.org. If you are not registered on http://www.medscape.org, please click on the "Register" link on the right hand side of the website.

Only one answer is correct for each question. Once you successfully answer all post-test questions, you will be able to view and/or print your certificate. For questions regarding this activity, contact the accredited provider, CME@medscape.net. For technical assistance, contact CME@medscape.net. American Medical Association's Physician's Recognition Award (AMA PRA) credits are accepted in the US as evidence of participation in CME activities. For further information on this award, please go to https://www.ama-assn.org. The AMA has determined that physicians not licensed in the US who participate in this CME activity are eligible for AMA PRA Category 1 Credits™. Through agreements that the AMA has made with agencies in some countries, AMA PRA credit may be acceptable as evidence of participation in CME activities. If you are not licensed in the US, please complete the questions online, print the AMA PRA CME credit certificate, and present it to your national medical association for review.

Article Title

Relapsing Fever Infection Manifesting as Aseptic Meningitis, Texas, USA

CME Questions

1. Your patient is a 64-year-old man presenting with fever and myalgias after possible tick exposure. According to the case report by Ellis and colleagues, which of the following statements about clinical presentation and course in a case of neuroborreliosis in Austin, Texas, that was initially thought to be Lyme disease (LD) is correct?

A. Initial symptoms were vomiting, diarrhea, chills, and fever without headache (HA) or other neurologic symptoms
B. Erythrocyte sedimentation rate (ESR) and C-reactive protein (CRP) were not elevated
C. Cerebrospinal fluid (CSF) and LD immunoglobulin (Ig) M immunoblot were negative
D. Ceftriaxone 2 g intravenous (IV) daily for 14 days led to significant improvement within 4 days and resolution of all symptoms at treatment completion except for minimal right lower facial weakness

2. According to the case report by Ellis and colleagues, which of the following statements about retrospective serologic analysis and other laboratory findings in a case of neuroborreliosis in Austin, Texas, that was initially thought to be LD is correct?

A. CSF collected 5 weeks after illness onset showed *Borrelia* spirochetes and DNA
B. Strong responses were detected to *B. turicatae* protein lysates and recombinant *Borrelia* immunogenic protein (rBipA) in serum and CSF, indicating likely exposure to B. turicatae
C. CSF was strongly reactive to rBipA from *B. parkeri* and *B. hermsii*
D. Enzyme-linked immunosorbent assay (ELISA) antibody titers to *B. hermsii* rBipA were between 1081:400 and 1:800

3. According to the case report by Ellis and colleagues, which of the following statements about clinical and public health implications of findings in this case of neuroborreliosis in Austin, Texas, that was initially thought to be LD is correct?

A. Endemic foci of *B. turicatae* have been identified in Colorado and Wyoming
B. *B. turicatae* is easy to diagnose from classical presentation and history of tick exposure
C. *B. turicatae* should be considered in cases of fever with neurologic symptoms when the Lyme antibody test is positive, but prevalence of LD is not epidemiologically supported
D. The findings suggest that BipA is not specific to North American TBRF

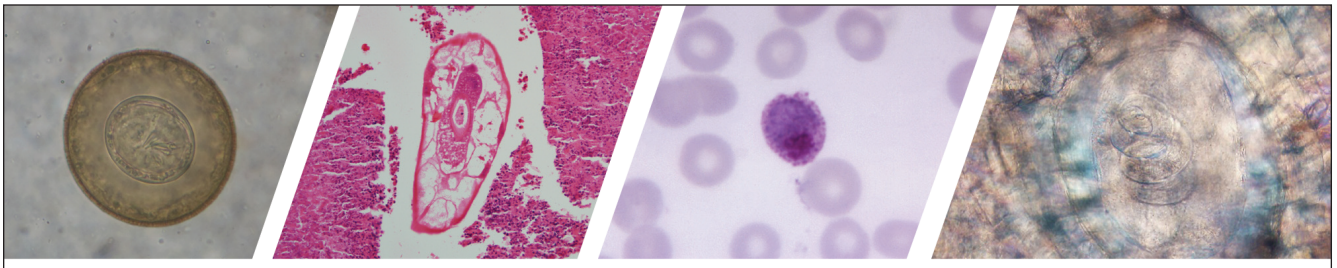

DPDx

Diagnostic Assistance and Training in Laboratory Identification of Parasites

A free service of CDC available to laboratorians, pathologists, and other health professionals in the United States and abroad

- Diagnosis from photographs of worms, histological sections, fecal, blood, and other specimen types
- Expert diagnostic review
- Formal diagnostic laboratory report
- Submission of samples via secure file share

Visit the DPDx website for information on laboratory diagnosis, geographic distribution, clinical features, parasite life cycles, and training via Monthly Case Studies of parasitic diseases.

www.cdc.gov/dpdx
dpdx@cdc.gov

U.S. Department of Health and Human Services
Centers for Disease Control and Prevention

CS272346-DE